NASA CR-134509

NASA

INTEGRATED THRUSTER ASSEMBLY PROGRAM

Aerojet Liquid Rocket Company
Sacramento, California

prepared for

NATIONAL AERONAUTICS AND SPACE ADMINISTRATION

Final Report

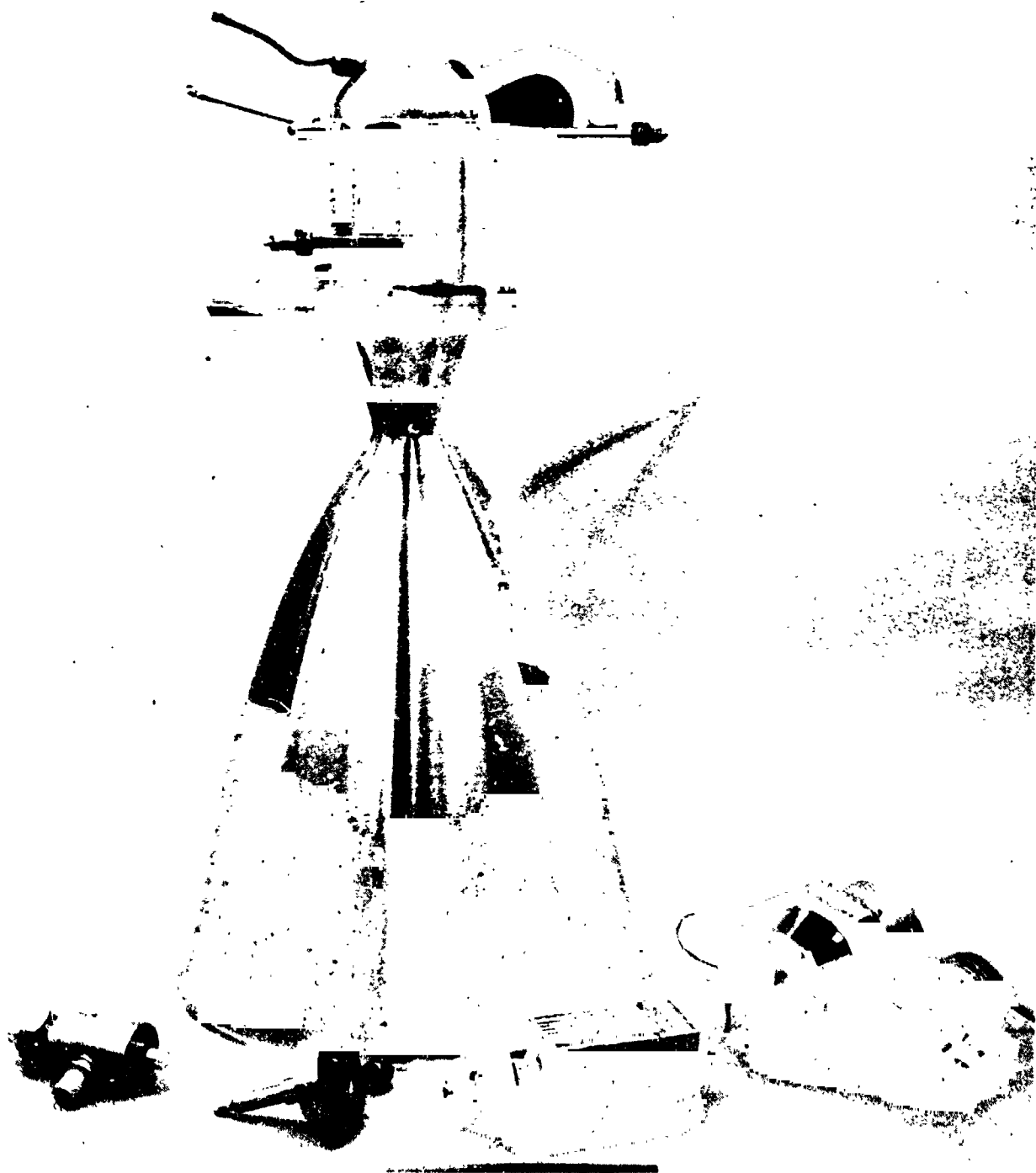INTEGRATED THRUSTER ASSEMBLY PROGRAM

30 June 1972 through 30 November 1973

Prepared Under

Contract NAS 3-15850

for

NATIONAL AERONAUTICS AND SPACE ADMINISTRATION
Lewis Research Center
Cleveland, Ohio

Paul Herr, Technical Manager

AEROJET LIQUID ROCKET COMPANY
Sacramento, California

ITA (Integrated Thruster Assembly)

The frontispiece shows the ITA chamber, an igniter valve, igniter body, integral exciter/spark plug and bracket, and a main propellant valve. The 5.62 kg (12.4 lb) flightweight chamber develops 6672 N (1500 lb_f) thrust at 207 N/cm^2 (300 psia) chamber pressure. ITA thrusters have been tested over an 3558 to 10,675 N (800 to 2400 lb_f) thrust range, over a range of mixture ratio from 2.1 to 6.8 and have been fired over 42,000 times.

FOREWORD

This is the Final Report for Contract NAS 3-15850, Integrated Thruster Assembly Investigation. The program was initiated on 30 June 1972 and completed on 30 November 1973. The program was performed by the Aerojet Liquid Rocket Company at its facility in Sacramento, California.

The NASA Lewis Research Center program managers were Paul Herr and Larry Gordon. The Aerojet Liquid Rocket Company management personnel were: R. J. LaBotz; program manager, and A. L. Blubaugh; project manager.

ABSTRACT

This program has provided technology for a long life, high performing, integrated ACPS thruster assembly suitable for use in 100 typical flights of a Space Shuttle vehicle over a ten year period. The four Integrated Thruster Assemblies (ITA) fabricated on this contract consisted of: propellant injector; a capacitive discharge, air gap torch type igniter assembly; fast response igniter and main propellant valves; and a combined regen-dump film cooled chamber. These flightweight 6672 N (1500 lb_f) thruster assemblies employed GH_2/GO_2 as propellants at a chamber pressure of 207 N/cm^2 (300 psia). Test data were obtained on thruster performance, thermal and hydraulic characteristics, dynamic response in pulsing, and cycle life. One thruster was fired in excess of 42,000 times.

SUMMARY

The Integrated Thruster Assembly (ITA) is a flightweight GH_2/GO_2 ACPS engine employing a spark initiated igniter. The nominal engine operating conditions are: 6672 N (1500 lb_f) thrust, 207 N/cm^2 (300 psia) chamber pressure, 4.0 mixture ratio 276 N/cm^2 (400 psia) valve inlet pressure, 139°K (250°R) hydrogen inlet temperature, and 208°K (375°R) oxygen inlet temperature. The thruster has demonstrated a steady state specific impulse of 4266 N sec/kg (435 sec) and a 3609 N sec/kg (368 sec) specific impulse at a 27.2 kg-sec (60 lb-sec) impulse bit. The thruster assembly, less valves, weighs 6.8 kg (15 lbs).

The objectives of the program were the investigation of chamber/injector life, pulse mode operation with cold propellants, effects of valve sequencing, and the optimization of minimum weight and cycle life relative to performance. The thruster designed to meet these objectives consisted of: a premix triplet injector (F-O-F); a regeneratively cooled chamber (79% of hydrogen), and a dump-film cooled throat and skirt; an ox rich torch type igniter; an integral exciter/spark plug (capacitive discharge type); two igniter valves; and two main propellant valves. The injector was made of stainless steel body with nickel face platelets; the chamber had a ZrCu liner with an ARMCO 22-13-5 stainless steel shell; the igniter body was nickel; the throat and nozzle were spun from Haynes 188. The materials were selected primarily for fatigue life consistent with galvanic compatibility. The thrust chamber assembly is a flightweight version of the design tested on Contract NAS 3-14354.

The SN 001 ITA was tested at simulated altitude to evaluate pulsing and steady operation, the P_c and MR operating limits, and valve sequencing. The thruster successfully demonstrated operation over a chamber pressure range of 111 to 333 N/cm^2 (160 to 482 psia), a 2.1 to 6.8 mixture ratio range, and a fuel temperature range of 118 to 318°K (213 to 572°R). The cumulative test duration on ITA SN 001 was 2513 sec, not including pulsing. ITA SN 002 was fired 42,266 times with over 4200 full thermal cycles. Testing was terminated

SUMMARY (cont.)

due to damage to the chamber in a heat streak resulting from ice formation which obstructed the film cooling ring. The ice was produced by freezing of test cell blow-back water in the cold ITA. ITA SN 003 was delivered to NASA Lewis Research Center for testing.

TABLE OF CONTENTS

TABLE OF CONTENTS (cont.)

TABLE OF CONTENTS (cont.)

APPENDIXES

TABLE LIST

TABLE LIST (cont.)

TABLE LIST (cont.)

FIGURE LIST

FIGURE LIST (cont.)

FIGURE LIST (cont.)

FIGURE LIST (cont.)

FIGURE LIST (cont.)

FIGURE LIST (Cont.)

NOMENCLATURE

A   Area

C_D Discharge coefficient

$c*$ Characteristic exhaust velocity

D_S Spark gap

E   Young's modulus

ERE   Energy Release Efficiency

FFC   Fuel Film Cooling

g   Gravitational constant

h_g Gas-side heat transfer coefficient

I_s Specific Impulse

K   Constant

k   Thermal conductivity

M   Molecular weight

MR   Mixture ratio

P   Pressure

P_c Chamber Pressure

P_d Downstream pressure

P_o Supply pressure

PN   Part number

Qs   Minimum spark discharge energy

R   Gas constant

S   Strain

SN   Serial Number

T   Temperature

t   Material thickness

TC   Thermocouple

T_{ign} Ignition temperature

T_w Wall temperature

UTS   Ultimate tensile strength

$\dot{w}$ Flow rate

NOMENCLATURE

α Coefficient of thermal expansion

γ Ratio of specific heats

ΔT Temperature difference

ε Strain due to pressure loading

γ Poisson's ratio

σ Standard deviation

τ_p Stress from pressure loading

1.0 INTRODUCTION

1.1 PURPOSE AND SCOPE OF PROGRAM

There has been considerable work in recent years on the development of hydrogen-oxygen ACPS thrusters and components for application to the Space Shuttle. Part of this effort led to the development of: a reliable ignition system on IR&D and Contract NAS 3-14348 (Ref. 1); a long life main propellant valve on Contract NAS 3-14349 (Ref. 2); a high performing, compatible injector suitable for either steady state or pulsing operation and a regeneratively-film cooled chamber, both demonstrated under Contract NAS 3-14354 (Ref. 3). Integration of these components into a flightweight thruster assembly for use in 100 flights of a Space Shuttle vehicle, introduces unresolved technical questions such as chamber/injector life, component interaction and optimization of a design to meet the often conflicting requirements of steady state performance and cooling, pulsing with cold propellants, response times, flightweight and long cycle life. The objective of this program was to develop the technology for flightweight ACPS thrusters by investigating these areas of unresolved technology.

Principal efforts on this program included review of H_2/O_2 ACPS technology, design and fabrication of an optimized flightweight Integrated Thruster Assembly (ITA), and test firing to evaluate the thruster operation over a range of operating conditions such as would be encountered in a Space Shuttle application. While specifically applicable to GH_2/GO_2 ACPS thrusters, much of the flightweight design and life cycle testing results are generally applicable to any propellant system.

The nominal design point and the operating ranges for the ITA are given in Table I. The design requirements are summarized in Table II.

The specific tasks to be accomplished on the program were:

TABLE I

ENGINE OPERATING CONDITIONS

	Nominal Design Point	Expected Operating Range
Thrust	6672 N (1500 lb)	(1)
Chamber Pressure	207 N/cm^2 (300 psia)	(1)
Mixture Ratio	4.0	(1)
Nozzle Expansion Ratio	40:1	-
Propellant Inlet Temperatures:		
Hydrogen	139°K (250°R)	111 to 334°K (200 to 600°R)
Oxygen	209°K (375°R)	Saturated gas to 334°K (600°R)
Propellant Inlet (to Valve) Pressure:		
Hydrogen	276 N/cm^2 (400 psia)	242 to 310 N/cm^2 (350 to 450 psia)
Oxygen	276 N/cm^2 (400 psia)	242 to 310 N/cm^2 (350 to 450 psia)
Specific Impulse:		
Steady State	4266 N-sec/kg (435 lb$_f$-sec/lbm)	
Pulsing (at MIB)	3923N-sec/kg (400 lb$_f$-sec/lbm) average	

---

(1) The expected operating ranges are based on predictions of the actual conditions the thruster will see on board the Space Shuttle. The inlet conditions may be anywhere within the ranges given and the chamber pressure, mixture ratio, and thrust will vary accordingly (if a mass flow controller is not employed in the propellant feed system to maintain constant thrust and mixture ratio). The actual values of these parameters are dependent upon the specific thruster design.

TABLE II

ENGINE DESIGN REQUIREMENTS

Fuel:	Gaseous hydrogen derived from the vaporization of liquid hydrogen per MIL-P-27201
Oxidizer:	Gaseous oxygen derived from the vaporization of liquid oxygen per MIL-P-25508A
Installation:	Buried within vehicle mold line
Maximum External Temperature:	260°C (500°F)
Total Life Capability:	Estimated 2500 minutes
Total Number of Firings:	Estimated 500,000 pulses, plus 25,000 deep thermal cycles (full temperature range on each component)
Maximum Single Firing Duration:	500 sec
Duty Cycle Limitations:	None
Compatibility:	Compatible with propellants, test fluids, cleaning fluids, and environmental contaminants for ten-year life requirement
Reusability:	To be reusable with minimum servicing and refurbishment
Service and Maintainability:	Design for ease of service and maintenance when required
Minimum Impulse Bit (goal):	222 N-sec (50 lb-sec)
Response:	50 millisec (time from electrical signal to 90% thrust)
Reentry Heating (goals):	30 minutes exposure per mission to the following temperatures:

At nozzle exit plane: 982°C (1800°F)
At chamber throat: 649°C (1200°F)

Nozzle Scarfing Capability:	Nozzle skirt shall be easily scarfed beyond an expansion ratio of 25:1
Weight for Complete Thruster Assembly Less Valves (goal):	6809 g (15 lb)

Page 3

1.1, Purpose and Scope of Program (cont.)

Task I:	Integrated Thruster Design
Task 11:	Thruster Hardware Fabrication
Task III:	Component Checkout
Task IV:	Integrated Thruster Assembly Testing
Task V:	Data Evaluation
Task VI:	Reporting
Task VII:	Reliability and Quality Assurance

1.2 PROGRAM GOALS

While the general objective of the program was development of tech-nology for a flightweight ACPS thruster to be accomplished through design, fabrication and experimental characterization of the ITA, some of the specific goals of this program were:

(1) High performance: 4266 N-sec/kg (435 lb_f-sec/lb_m) Isp steady state; 3923 N-sec/kg (400 lb_f-sec/lb_m) Isp minimum impulse.

(2) Minimum impulse bit: 222 N-sec (50 lb_f-sec)

(3) No duty cycle limitations.

(4) 50,000 restarts including 5000 full strain heating and cooling cycles.

(5) Thrust chamber assembly weight (exclusive of valves): 6809 g (15 lb).

(6) Operation over the range of conditions specified in Table I.

(7) Maximum single firing duration: 500 seconds.

(8) Response (time from electrical signal to 90% thrust): 50 milliseconds.

(9) Maximum exterior temperature: 260°C (500°F).

(10) Nozzle geometry: easily scarfed beyond an expansion ratio of 25:1.

1.2, Program Goals (cont.)

The thruster design requirements were 500,000 pulses and 25,000 full thermal cycles. The thruster life requirements were estimated as follows:

50 full thermal cycles/mission x 100 missions/year x 5 safety
factor = 25,000 full thermal cycles

1000 pulses/mission x 100 missions/year x 5 safety factor =
500,000 Pulses

5 minutes/mission x 100 missions/year x 5 safety factor =
2500 minute total duration

No information was available as to the duration of the pulses or the duty cycle.

1.3 ITA CONCEPT

The main components of the ITA are shown on the Frontispiece and are: thrust chamber, igniter valve, igniter body, integral exciter/spark plug and mounting bracket, and main propellant valve. A drawing of the ITA is shown in Figure 1.

The thrust chamber is composed of injector, chamber, throat section, nozzle, torus, lines and inlet line flanges that are welded together to form an integral unit. The igniter fuel manifolding and inlet line are part of the injector. The injector and chamber were tested in a workhorse version on Contract NAS 3-14354, Hydrogen-Oxygen Auxiliary Propulsion for the Space Shuttle.

The injector is a 72 element "premix I" F-O-F triplet design. The face of the injector is made from platelets that contain a fuel dump cooling circuit, the mixing cups, and the 144 "I" shaped fuel passages which discharge approximately 180° apart at right angles to the oxidizer flow (oxidizer flows
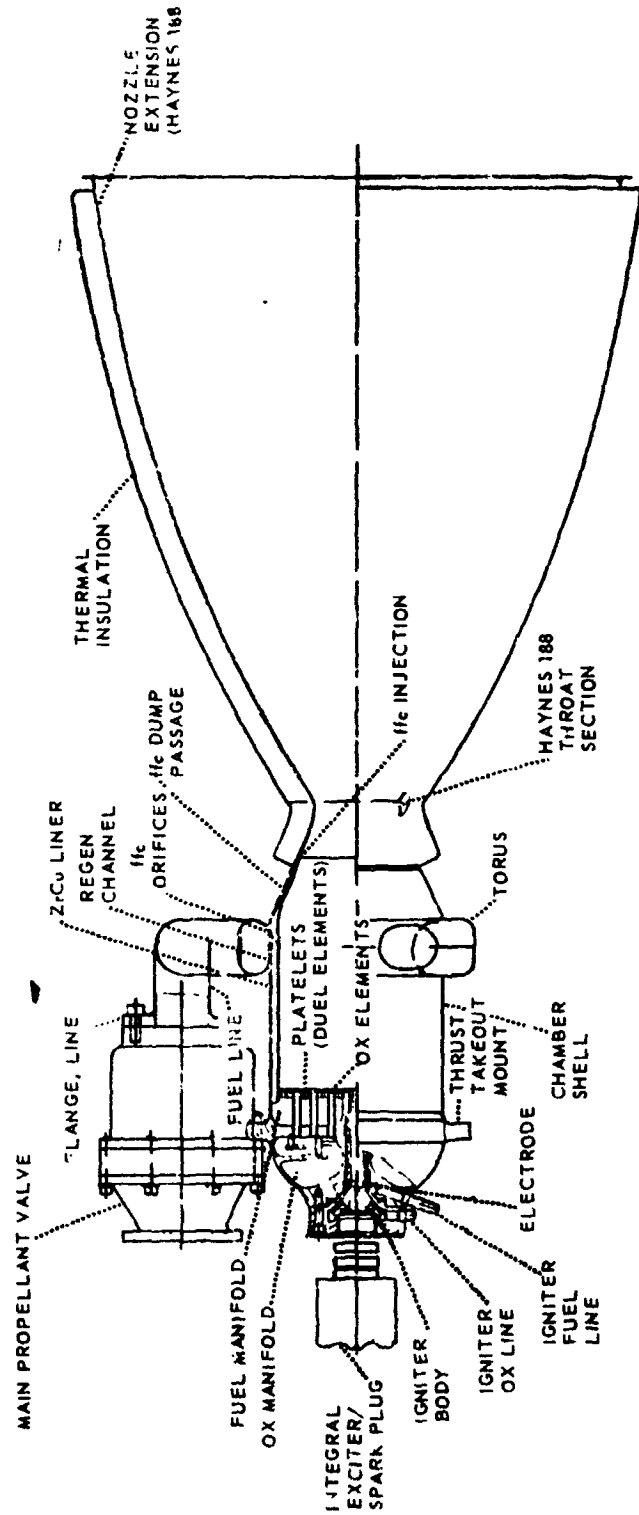
Figure 1. ITA Concept

1.2, Program Goals (cont.)

normal to the face through 72 tubes; fuel flows parallel to the face impinging
two fuel elements on each oxidizer element). The hydrogen flow into the
injector comes from the outlet of the chamber regen passages.

The chamber is a combination regen-film cooled design. By means
of orificing built into the inlet of the passages, 21% of the fuel flow is used
to dump/regen cool the convergent section and is introduced into the chamber at
a 2.4 to 1 contraction ratio to film cool the throat and skirt. The remaining
79% of the fuel flow regen cools the cylindrical section of the chamber and flows
through the injector. The chamber liner is ZrCu and the throat and nozzle are
Haynes 188 of .0762 cm (.030 inch) thickness.

The main propellant valve is a Marquardt two-way, pneumatically
actuated (vent to open) cryogenic valve. It's pilot valve is a solenoid
operated, three way valve which when de-energized, pressurizes the main valve
actuation cavity (closed configuration). Actuation of the pilot valve vents
the main valve actuation fluid causing it to open. The main propellant valve
is a flight-type version of the valve tested under Contract NAS 3-14349, Space
Shuttle APS Shutoff Valve.

The igniter employs an ALRC concept that was initially used on
Contract NAS 3-14348, Ignition System for Space Shuttle Auxiliary Propulsion
System. The igniter design is a modification of that used on Contract NAS 3-14354,
Hydrogen-Oxygen Auxiliary Propulsion for the Space Shuttle. The integral exciter/
spark plug was developed specifically for the ITA by General Laboratory Associates
(GLA). The core of the igniter is operated at a mixture ratio of 41 and is
ignited by a spark discharge from the spark plug to the igniter wall. The
igniter hydrogen film coolant and core flow are discharged coaxially at the
injector face to provide a hot (MR = 5.4) element torch in the center of the
injector for mainstage ignition. The igniter valves are normally closed, two
way, solenoid actuated, cryogenic valves.

Page 7

1.0, Introduction (cont.)

1.4 KEY ITEMS

There were four items that were considered key to the success of the program. This does not imply that other items are not important, but rather that these items were flagged for special attention because they represented a departure from the design or test experience gained on prior programs or because there were less data available on them. They are: structural life, fuel split, oxidizer distribution plate design, and igniter design.

The structural life of the ITA (cycles to failure) has been identified as a key item because that is the primary objective of the program.

The "fuel split" refers to division of the fuel flow between the fuel film cooling sleeve and the regeneratively cooled chamber. In testing a workhorse version of the ITA thrust chamber assembly on Contract NAS 3-14354, the fuel film coolant was varied by means of a separate manifold system. The fuel split between regen coolant/injector and film coolant on this program was controlled by orificing from a single manifold. The 160 orifices are drilled in the shell during fabrication and covered (inaccessible) by the fuel torus. Too much film cooling compromises performance and too little compromises throat and nozzle life.

The oxidizer distribution plate is a flow redistribution plate within the injector oxidizer manifold. During testing on Contract NAS 3-14354 and on Contract NAS 3-14379, an oxidizer distribution plate collapsed, blocking the inlet to the oxidizer elements. Obviously, the structural integrity of this part had to be improved, especially in view of the ignition sequencing and fuel lead-lag testing planned as part of the program.

The igniter was flagged as a key item because of the safety hazard of non-ignitions on testing in an altitude facility and also its impact on thruster reliability.

1.0, Introduction (cont.)

1.5 REPORT OBJECTIVES AND ORGANIZATION

This report presents the final results of the Integrated Thruster Assembly Investigation Program. The discussion of the analysis, design and fabrication is intended to present results, define the state-of-the-art and provide a detailed description of the articles that were tested. A chronology of events is provided only if it is necessary to define lessons learned or describe hardware in its final state or reworked condition. The main emphasis - consistent with the primary objective of the program - is on cycle life.

The technical discussion section of this report is composed of five sections corresponding to the five main tasks on the program, namely:

> Integrated Thruster Design
>
> Fabrication
>
> Component Checkout Testing
>
> Integrated Thruster Testing
>
> Data Analysis

The discussion under each of these headings is then categorized by component and then by discipline, except for the data analysis section in which the discussion is organized around the disciplines (performance, heat transfer, structural analysis, etc.).

The discussion section of this report has been consistently organized and numbered so that the reader, if he desires to concentrate in a given component, can easily locate the design, fabrication and checkout testing for that component. The first digit of the numbering system for the technical discussion section is 4. The second digit refers to design (4.1), fabrication (4.2), and checkout testing (4.3). The third digit of these three sections always refers to the components in this order: ITA (4.x.1), igniter (4.x.2), injector (4.x.3), chamber (4.x.4), and valves (4.x.5). By way of illustration, the sections on the injector are: design (4.1.3), fabrication (4.2.3), and checkout testing (4.3.3).

2.0   SUMMARY

The following is a summary of the program by task.   Technical discussions and a detailed description of each task is given in Section 4.0.

2.1   INTEGRATED THRUSTER DESIGN

2.1.1   ITA

The ITA design concept is shown in Figure 1 (Section 1.1). The assembly consists of four major components (injector, thrust chamber, propellant valves, and igniter assembly) which are integrated to provide a lightweight, compact, high performing thruster which meets duty cycle and cycle life requirements.   The design shown does not include igniter valves.   The ability to operate satisfactorily without these valves was investigated analytically as part of the program.

2.1.2   Injector

The injector is an "I" premix design which utilizes etched platelets to form the fuel orifices and face coolant channels.   The fuel circuit is fed directly from the thrust chamber coolant passage outlets.   The oxidizer is supplied from a dome-like manifold which covers the injector's back surface. This manifold contains distribution plates to ensure uniform oxidizer distribution.   The oxidizer orifices are contained in 72 shaped tubes which extend from the oxidize dome through the fuel plenum to the face.   The spark augmented torch igniter discharges in the center of the injector face.   The entire injector body is made from Type 304L stainless steel; the etched face plates are Nickel 200. The injector is joined to the thrust chamber by an external weld with a piston ring seal between the injector face and the chamber wall.   This injector is a flightweight version of the SN 6 and 7 premix injectors fabricated and tested on Contract NAS 3-14354.   The primary differences between the flightweight design and the SN 6 and 7 injectors are the elimination of the chamber attachment flange and the use of a structurally more optimum oxygen manifold cover. The element design and injection pattern are unchanged.

2.1, Integrated Thruster Design (cont.)

2.1.3 Thrust Chamber

The thrust chamber incorporates a composite cooling system. The major portion of the combustion chamber is regeneratively cooled (80 passages) with fuel. The convergent nozzle contains 160 orificed passages which direct 21% of the fuel flow to a station 1.50 in. upstream of the throat where it is introduced as a film coolant. The throat and entire divergent nozzle are of spun Haynes 188 material and operate at the adiabatic wall temperature. The gas-side wall material in the cooled areas forward of the fuel film coolant injection station is zirconium copper alloy which contains rectangular cross-section coolant passages. These are closed out by a 22-13-5 stainless steel shell which is brazed to the copper liner. The stainless steel shell is joined to the injector and adiabatic wall nozzle by welding. The composite cooling system results in the fuel inlet manifold (which is also made from 22-13-5 material) being located at the entrance to the convergent nozzle.

The chamber design was established in Phase II of Contract NAS 3-14354 on the basis of data obtained in contract testing. The primary differences between the ITA design and the chamber tested on Contract NAS 3-14354 are:

Change	Reason
Shallower coolant channels .381 cm (0.150) vs. .457 cm (0.180 in.)	Higher coolant density, gives lower ΔT, higher cycle life
Structural jacket material is 22-13-5 SS instead of 304L SS	Higher cycle life
Haynes 188 skirt vs. 304L skirt	Greater strength, greater oxidation resistance
Less rigid manifold	Higher cycle life

Since the above changes are primarily structural and not functional, they do not impact the operational characteristics of the unit that were established experimentally on Contract NAS 3-14354.

2.1. Integrated Thruster Design (cont.)

2.1.4 Igniter

The igniter uses an air gap spark plug with a capacitive discharge exciter. The overall mixture ratio of the igniter is 5.4 at the injector face with the ignitor designed to provide an oxidizer-rich environment (MR = 41) at the spark plug. The spark plug is integral to the capacitive discharge exciter. Propellant is supplied to the igniter from the main propellant valves. The igniter chamber is made of Nickel 201.

The basic igniter design was developed and tested under NAS 3-14348. The design for the ITA is a flightweight version of the basic design and modifications to reduce weight and improve reliability. These modifications are:

(a) Elimination of the igniter chamber flange and the igniter body to igniter chamber seal by brazing the body and chamber together into a single unit.

(b) Incorporation of the fuel manifold into the injector.

(c) Slotting of the exterior of the igniter chamber to give improved off mixture ratio cooling capability through higher coolant velocities. This also provides better centering of the igniter chamber in the injector igniter port.

(d) Relocating the igniter chamber cooling passages to provide improved cooling in the vicinity of the electrode.

(e) Incorporation of an integral, flightweight, hermetically sealed exciter package to the spark plug.

In making these modifications, care has been taken to maintain the same internal flow geometry such that mixing in the electrode area has not been altered.

2.1, Integrated Thruster Design (cont.)

The igniter operates at 100 millijoules energy level delivered
to the spark gap at a fixed gap breakdown voltage of 20,000 volts. The gap size
is 0.030 inch. Input voltage is 38 $\pm$ 4 VDC. The spark rate is 500 sparks per
second.

2.1.5 Propellant Main Valves

The valve selected for this application was designed by the
Marquardt Company. The valve is a flightweight bolted version of the X28400
valve that was designed, fabricated, and tested under Contract NAS 3-14349.
The primary differences between the flightweight valve and the Marquardt Co.
X28400 valve are the integration of the pilot valve into the main valve and
removal of static seals and flanges that were required during test evaluation.
The critical internal elements are identical. The valve envelope and weight
have been reduced without modifying the elements considered to be the heart of
the valve.

2.1.6 Others

The thrust takeout points on the ITA are located at the
injector-to-chamber interface area and consist of three machined mounting sur-
faces which are aligned with the throat-exit plane defined thrust axis.

The entire nozzle is encapsulated in a Fiberfax Lo-Con
material which ensures that the backwall temperature of the assembly does not
exceed 260°C (500°F).

2.2 FABRICATION

Four thrust chambers - consisting of injector, chamber, throat
section, skirt, torus, oxidizer and fuel inlet lines, and inlet line flanges -
were fabricated. The thrust chamber components, less flanges are shown in
Figure 2.
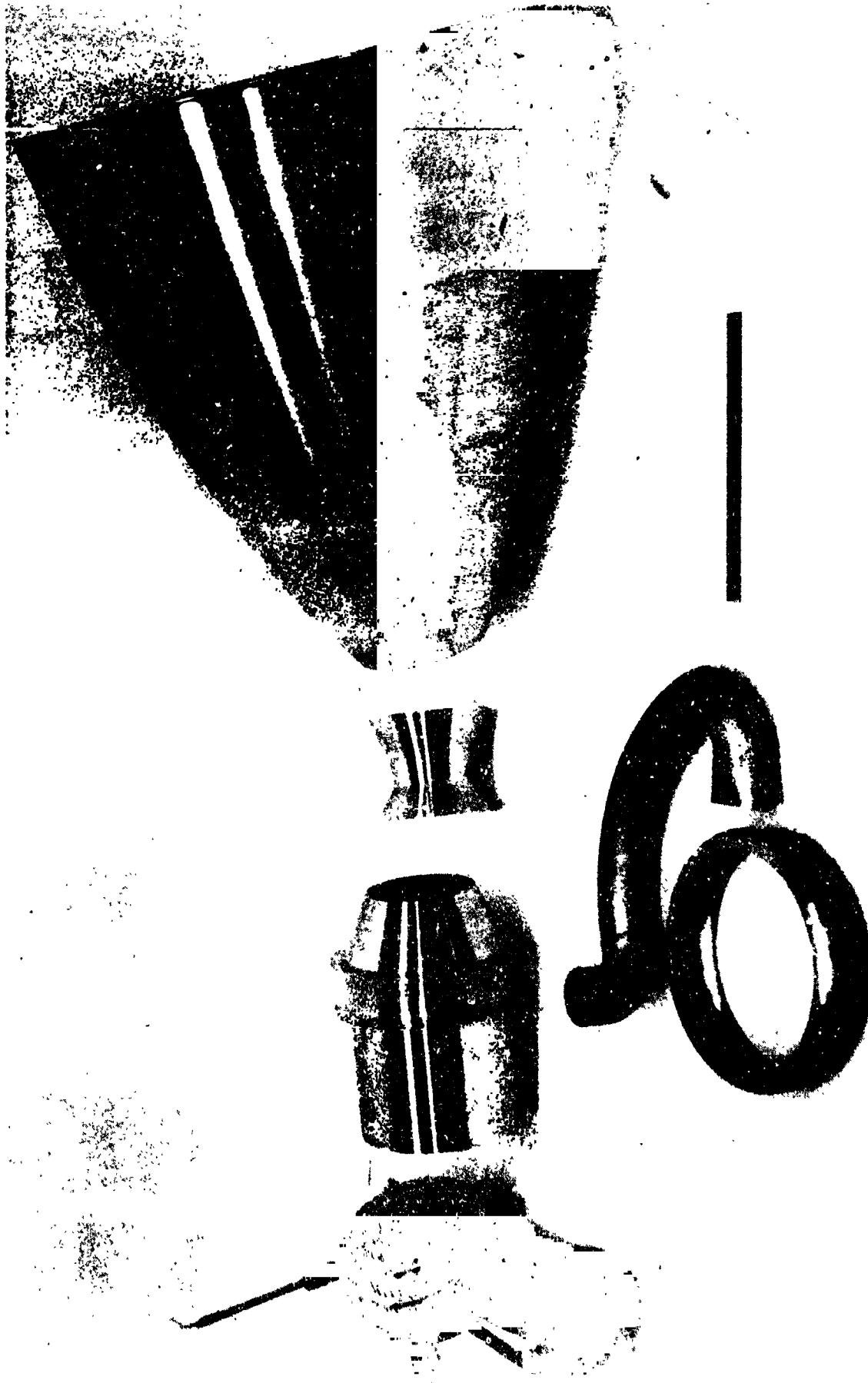
Figure 2. Thrust Chamber Components

2.2, Fabrication (cont.)

Two problems were encountered in fabrication involving spinning of the Haynes 188 nozzles and the weldment of the thin .051 to .070 cm (.020 to .030 inch) sheet metal parts. These problems were not insurmountable and the final units were quite satisfactory (see Figure 3).

Three of the thrust chambers were instrumented with thermocouples on the exterior surface. The SN 001 thrust chamber had gas-side thermocouple instrumentation in addition to the exterior thermocouples. The SN 001 thrust chamber also had a chamber P_c tap and four additional injector face thermocouples. All injectors had two face thermocouples and two thermocouples for measuring the fuel temperature in the injector manifold.

Four igniter bodies and four igniter brackets were fabricated. Six igniter valves were purchased (two spares). A total of seven integral exciters/ spark plug units (four spares) were fabricated. The igniter components are shown in Figure 4.

Two of the igniter bodies were final machined and one of them cold flow tested. The propellant orifice sizes were modified on the basis of the results from these tests to obtain the fuel split between core and coolant required to maintain a core MR of approximately 45 and to obtain the desired pressure schedule. The remaining two igniter bodies were completed to the new configuration and the initial two were reworked.

Component checkout testing of the initial integral exciter/spark plug design indicated that the design of a four diode clamp rectifier circuit was marginal. All units were refurbished to a six diode configuration that demonstrated adequate margin in acceptance testing and ITA test firings.

Five main propellant valves (Figure 5) were fabricated. Two problems were encountered during fabrication; one of which resulted in valve cycle life estimated to be approximately 60,000 cycles; the second of which resulted in an out of spec leakage rate for valve SN 011. Because of late
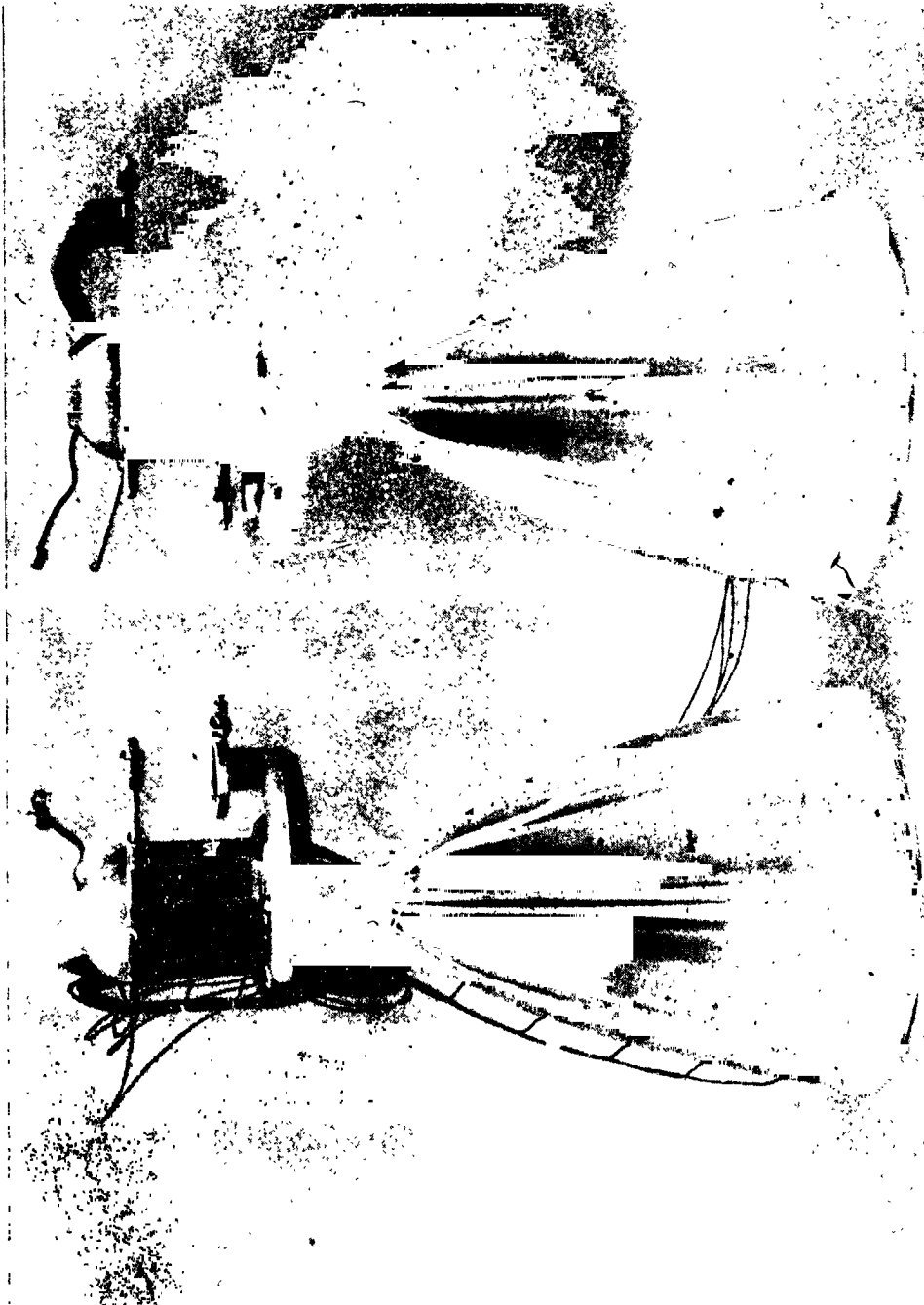
Figure 3. ITA Chamber SN 002 and SN 004

Figure 4. Igniter Components

Figure 5. Main Propellant Valve

2.2, Fabrication (cont.)

delivery of these components, they were accepted without rewor

ITA SN 001 and SN 002 were tested by ALRC. ITA SN 003 was delivered to NASA for testing at the Lewis Research Center. ITA SN 004 was a spare. The measured ITA weight was 6.895 kg (15.2 lb) exclusive of valves.

2.3 COMPONENT CHECKOUT TESTING

Component checkout testing was performed to obtain data for design verification and to ascertain that components were functioning properly before integration into the ITA. Table III is a summary of the testing performed.

The main propellant valves were acceptance tested by Marquardt at their facility. The valve timing and leakage tests were made at ALRC using ambient and cryogenic GH_2 and GO_2 at simulated altitude. The acceptance testing revealed that the pilot valve on SN 011 leaked. This same valve was used in the oxidizer circuit in the ALRC testing and exhibited considerable delay on closing with cold propellants (.5 sec, cold, versus .035 sec ambient). This valve was designated the spare.

As described above (2.2), the igniter cold flow testing and the exciter/spark plug acceptance testing were used to effect design changes that resulted in an acceptable final product.

1075 igniter functional test firings were made at simulated altitude over a wide range of operating conditions. There was not a single case of no ignition.

2.4 INTEGRATED THRUSTER TESTING

Table IV is a summary of the type of testing performed in the ALRC

TABLE III

COMPONENT CHECKOUT TEST SUMMARY

Component	Test	Purpose
Main Propellant Valve	Acceptance	Verify acceptability. Proof, leakage, pressure drop, response and electrical characteristics.
	Valve Timing and Leakage	Verify valve operating characteristics using ambient and cyrogenic operating fluids, GH_2 and GO_2.
Igniter	Cold Flow	Leak check, verify flow split, evaluate hydraulic characteristics and balance.
	Functional Test Firing	Design verification and characterization.
	Acceptance Testing	Verification of integral exciter/spark plug design at test firing conditions.
Injector	Cold Flow	1. Verify acceptability of injector body fabrication.
		2. Verify uniformity of flow distribution.
		3. Characterize hydraulics.
Chamber	Cold Flow	1. Verify regen/film cooling flow split.
		2. Verify uniformity of regen flow distribution.
		3. Characterize hydraulics of regen and ffc sections.
ITA	Cold Flow	1. Evaluation of "as built" characteristics.
		2. Balance (orifices in inlet lines).

TABLE IV

ITA TEST OBJECTIVES

Test Series	Purpose	Goals
1. Checkout	Checkout, balance, and performance and heat transfer verification at nominal propellant temperature conditions.	· 4266 N-sec/kg (435-sec) I_s steady state. · 4 MR with 276 N/cm^2 (400 psia) at valve inlet and propellants at nominal temperature. · Throat temp. <649°C (1200°F) and skirt temp. <982°C (1800°F) at nominal conditions. · External temp. <260°C (500°F). · 500-sec steady-state duration.
2. Steady-state operation	Evaluate steady-state performance over the range of propellant pressures and temperature typical of the Space Shuttle vehicle with no mass flow controller.	· Pressure at inlet to valves = 276 ± 34 N/cm^2 (400 ± 50 psia). · 111°K (200°R) ≤ T_F ≤ amb. · SAT. VAP ≤ T_o ≤ amb.
3. Valve sequencing	Evaluate valve sequencing requirements and effects of ignition delay.	· Minimize performance loss at MIB. · Determine operational limits.
4. Pulsing operation	Evaluate pulsing mode of operation, duty cycle effects, and minimum impulse bit over the anticipated range of propellant inlet temperatures and pressures.	· 3923 N-sec/kg (400-sec) I_s. · 50 mil sec response. · 222 N-sec (50 lb-sec) MIB. · No duty cycle limitations.
5. Chamber pressure and MR limits	Evaluate steady-state performance at limiting conditions of chamber pressure and mixture ratio over the range of temperatures.	· 2.5 ≤ MR ≤ 6.5. · 111°K (200°R) ≤ T_F ≤ amb. · SAT. VAP. ≤ T_o ≤ amb. · 138 (200) ≤ P_c ≤ 345 N/cm^2 (500 psia)
6. Life limits	Evaluate life capability.	· 50,000 pulses. · 5000 full thermal cycles.

2.4, Integrated Thruster Testing (cont.)

altitude facility. Test series one through five were made with ITA SN 001. The life limits tests were made with a virgin thrust chamber (SN 002). Table V is a summary of the testing performed with ITA SN 001.

The integral exciter/spark plug unit was not available at the initiation of testing. After its installation, 658 starts were attempted and made over a wide range of operating conditions including igniter and main propellant valve lead/lag tests with 100% ignition reliability.

The main problem encountered in testing was ice formation in the thruster that blocked the propellant passages. Duct coolant water spray was blown back into the thruster on shutdown. Venting of the propellants via the thrust chamber valves or the fuel valve delay on closing (which plagued the testing) resulted in ice formation on the cold hardware. Two of the ITA SN 001 tests were terminated by high throat temperatures due to ice formation in the film cooling sleeve. In one of these tests, erosion and a minor burn through occurred in the convergent section of the Haynes throat section (film cooled). The damage was repaired by welding the hole closed and polishing the inside of the throat smooth. The quantities of water introduced into the chambers and the resulting ice formation are peculiar to the test facility and will not occur in space.

A total of 86 tests were made with ITA SN 001. Of these tests, 22 were long duration runs (up to 513 sec) that resulted in over 86 data points (combinations of P_c and MR); 25 were valve and ignition sequence tests; three were flow tests and 36 were pulse tests. Over 160 of the test conditions were of sufficient duration to get either steady state performance or temperature data. ITA SN 001 was removed from the test stand to permit installation of SN 002 for the life cycle tests. ITA SN 001 after testing is shown in Figure 6.

ITA SN 002 was fired 42,266 times. The pulse train consisted of four .15 sec pulses, a .4 sec pulse and five .09 sec pulses. The fuel valve

TABLE V

TTA SN 001 TEST SUMMARY

No. of Firings	670 (84 tests including pulsing)
Total Duration	2513 sec not including pulsing
Longest Single Test	512.6 sec
Shortest Test Duration	~.04 sec
P_c Range	110/332 N/cm^2 (160/482 psia)
Fuel Temperature Range	318/109°K (572/196°R)
MR Range	6.8/2.1
Valve Inlet Pressure Range	152/434 N/cm^2 (220/630 psia)

Figure 6. ITA SN 001 After Testing

2.4, Integrated Thruster Testing (cont.)

was then opened to cool down the hardware. This basic ten pulse plus cooldown
sequence was repeated 4200+ times and resulted in a complete thermal cycle
every 10 pulses.

The ITA as a thruster assembly had a life of 20,690 pulses. At
this time, both main propellant valves had leaks in the bellows and the pilot
valve on the fuel main propellant was inoperable. The leak in the ox valve
bellows was such that an inert pressurant could not be used because of leakage
into the upstream propellant line. The demonstrated chamber life can be placed
at 30,049 to 39,514 cycles. At 30,049 pulses, a hairline crack developed in
the fuel torus. However, it was in a weld affected area adjacent to an area
that had been mechanically damaged and may not be a true measure of life. A
failure occurred in the chamber fuel inlet line at 39,514 pulses; unlike the
crack at 30,049 cycles, it rendered the chamber inoperable, but may have resulted
from deflecting the line to mate to the test stand. The crack was weld repaired
and testing resumed. Testing was terminated at 42,266 pulses because of a burn
through of the throat and nozzle in a heat streak. The heat streak, which had
not occurred up to that time, was apparently caused by ice formation during
hardware chilldown resulting from excessive delay in the main propellant fuel
valve closing. At the end of the testing there was no evidence of any failures
of the igniter body, the injector, the ZrCu chamber liner, the ARMCO 22-13-5
shell or the throat and nozzle. The igniter worked 42,266 times with 100%
reliability.

2.5 DATA ANALYSIS

2.5.1 Component Checkout Tests

Table VI is a summary of the flow coefficients that were
reduced from the igniter cold flow data. These data show that the actual hardware
hydraulic resistance was comparable to the design resistance within the part-to-
part variation and that the hardware was consistent part-to-part.

TABLE VI

IGNITER HYDRAULIC SUMMARY

$$C_D \, A^{(1)}, \; cm^2 \; (in^2)$$

Igniter SN	Ox Circuit		Fuel Circuits		Coolant	
	.101	(.0156)				
001	.109	(.0169)	.0052	(.00080)	.023	(.0036)
002	.103	(.0159)	.0050	(.00078)	.023	(.0035)
003	--		.0048	(.00075)	.024	(.0037)
004	.104	(.0161)	.0052	(.00080)	.021	(.0032
Average	.104	(.0161)	.000505	(.000782)	.0225	(.00349)
$\sigma^{(2)}$			2.91%		6.40%	
Design	(3)		.000503	(.00078)	.0206	(.0032)

(1) $\dot{w} = C_D A P \sqrt{ \dfrac{2g}{R} \cdot \dfrac{M}{T} \left(\dfrac{\gamma}{\gamma-1} \right) \left[\left(\dfrac{Pc}{P} \right)^{2/\gamma} - \left(\dfrac{Pc}{P} \right)^{\frac{\gamma+1}{\gamma}} \right] }$

(2) Standard deviation.

(3) Igniter ox manifold pressure is nominally 210 N/cm^2 (305 psia) for a Pc of 207 N/cm^2 (300 psia) at nominal propellant temperature and flow rates. The pressure difference is so low that no attempt was made to design to a given resistance. All the pressure drop in the ox igniter circuit is in the valve.

2.4, Integrated Thruster Testing (cont.)

Table VII is a summary of the test conditions encountered in the 1075 igniter functional test firings. All tests were made at simulated altitudes. The igniter assembly operated perfectly at all conditions; there were no ignition failures.

In cold flow testing the injectors and chambers the flow rate was measured for each of the 72 injector elements and the 80 regen channels of each chamber. The deviation of the flow of each channel from the average was calculated. Table VIII is a summary of the standard deviation of each chamber and injector. As indicated by the low standard deviation, the spread or variability in the data is only a few percent. This indicates no plenum (manifolding) design problems or manufacturing defects.

The cold flow test results for injector, chamber and ITA are summarized in Tables IX, X, and XI. The $C_D A$ (discharge coefficients X area) for sonic or subsonic flow correlation in the tables is the average value for each component derived from several flow rates based on Mach number simulation at 1/3 or 1/10 pressures using GN_2. The standard deviation of the $C_D A$ of all the units from the average value is approximately equal to the spread in the data. The manufacturing variation from part-to-part is, therefore small.

The most significant $C_D A$ is that of the fuel film cooling (ffs) circuit of the chamber since it determines the split of the hydrogen flow between the regen section and the ffc section. The design $C_D A$ value is .314 cm^2 (.0487 in^2). From the data in Table X the average of the four chambers is within 1.65% of the design value. Chamber SN001 is 3% low which would result in 20.4% of the hydrogen as ffc instead of 21%.

2.5.2 ITA Testing

The ITA was operated over the desired mixture ratio range (2.1 to 6.8) with propellant temperatures essentially (within 10%) varied over the desired range. Chamber pressures below the desired lower limit, 138 N/cm^2

TABLE VII
IGNITER TEST CONDITIONS

MR Range	2.7 to 7.8 overall; 14.3 to 77.4 Core
P_c Range, N/cm^2 (psia)	110 to 350 (160 to 507)
Fuel Temperature Range, °K (°R)	86 to 289 (155 to 520)
Oxidizer Temperature Range, °K (°R)	206 to 289 (370 to 520)
Propellant Inlet Pressure Range, N/cm^2 (psia)	142 to 448 (206 to 650)
Fuel Valve Lead (msec)	-20 to 10
Spark Lead (msec)	-12 to 30

TABLE VIII

FLOW UNIFORMITY
(Percent Standard Deviation)

SN	Injector Ox	Injector Fuel	Chamber Regen
001	3.08	3.56	2.57
002	2.22	3.27	2.74
003	2.54	2.20	2.93
004	2.23	2.52	3.14

TABLE IX
INJECTOR HYDRAULIC SUMMARY

Injector SN	$C_D A$, cm^2 (in^2)	
	OX	Fuel
001	2.27 (.352)	1.97 (.306)
002	2.39 (.370)	1.98 (.307)
003	2.39 (.371)	1.99 (.308)
004	2.39 (.370)	1.99 (.309)
Average	2.36 (.366)	1.98 (.307)
σ *	2.5%	.45%

TABLE X
CHAMBER HYDRAULIC SUMMARY

Chamber SN	$C_D A$, cm^2 (in^2)	
	Regen	FFC
001	1.93 (.299)	.305 (.0473)
002	1.94 (.300)	.325 (.0503)
003	1.94 (.301)	.323 (.0500)
004	1.92 (.297)	.326 (.0505)
Average	1.93 (.299)	.319 (.0495)
σ	0.59%	3.03%

TABLE XI
ITA HYDRAULIC SUMMARY

Chamber SN	$C_D A$, cm^2 (in^2)	
	OX	Fuel
001	2.31 (.358)	1.51 (.234)
002	2.46 (.382)	1.54 (.238)
003	2.34 (.362)	1.56 (.242)
004	2.39 (.370)	1.59 (.246)
Average	2.37 (.368)	1.55 (.240)
σ	2.85%	1.59%

* Standard Deviation

2.5, Data Analysis (cont.)

(200 psia), were achieved, and while the upper limit was nearly achieved (333 vs. 348 N/cm^2 (482 vs. 500 psia)). The 500 psia value was not achieved as the pressure limit on the main propellant valves precluded extensive testing at the higher pressures.

The steady state temperatures measured for the chamber gas-side and exterior, at the injector face, and on the skirt (maximum) are generally the same as those predicted on the basis of the NAS 3-14354 experimental data. The throat temperatures, however, are generally approximately 66°C (150°F) higher than predicted. The effect of mixture ratio and pressure on temperatures agreed with the predictions. However, fuel temperature caused more variation in throat temperatures than anticipated.

The agreement of measured temperatures with those used in the cycle life analysis resulted in no change in life predictions except for the throat. The higher than predicted temperatures result in a reduction in predicted design life from 100,000 to 80,000 thermal cycles. The design requirement is 25,000 cycles.

Performance was in agreement with results obtained with the injector pattern and 20% ffc on Contract NAS 3-14354. At nominal conditions the steady state specific impulse was 4266 N-sec/kg (435 lb_f-sec/lb_m). There was a problem with flow rates due to difficulties in calibration of the Ramapo flow meters. In pulsing operation, a 267 N-sec (60 lb_f-sec) M.I.B. was achieved. Specific impulse at the M.I.B. was 3609 N-sec/kg (368 lb_f-sec/lb_m.

During the valve sequence testing, the ITA was successfully operated with fuel leads (oxidizer lead desirable) up to 10 msec and with igniter delays up to 6 msec behind the opening of the lagging main propellant valve. There was no damage to the injector (ignition in the ox manifold) with the fuel lead and no damage to the chamber (chamber overpressure with delayed mainstage ignition) with the igniter lag.

2.5, Data Analysis (cont.)

The response time (time from electrical signal to 90% thrust) was approximately 59 msec (vs. 50 msec goal). There was considerable variability in valve response time with temperature and it also depended on the actuation fluid used. With self-actuation (propellants tapped off upstream of valve), the average time from electrical signal to initiation of travel was 53 msec (38 tests) for the ox valve (fuel valve faster). The ITA achieves 90% thrust 5 to 7 msec after initiation of poppet travel. Thus, with optimum valve sequencing, the response time is 53 + 6 = 59 msec. The average response time for pulses 49 thru 54 (six pulse repeated sequence used) on Test -076 was 55 msec with 52 msec being the best on any pulse.

The only component that registered any thermal response to duty cycle was the injector face, which was mildly sensitive to valve sequence on shutdown. Neither this component or any other component were adversely affected by the duty cycle (combinations of pulse widths and coast times). No combination of firing and coast times results in higher temperatures than achieved in steady state.

The Ramapo flow meters were calibrated in place with ambient and cold propellants. Only the ox ambient calibration data are without major difficulties. The cold oxidizer data were obtained with that propellant too close to the saturation temperature. The hydrogen data are not valid because the back pressure to the venturi was too high (flow was not sonic). The ox flow-meter calibration was accomplished on the basis of the ambient temperature data and data obtained with the oxidizer 13.9°C (25°F) or more above the saturation temperature. The hydrogen flow meter was not corrected on the basis of correlation between the chamber fuel circuit pressure drop (pressure upstream of the valve to the injector manifold) and early test data obtained with a venturi in the system.

3.0   CONCLUSIONS AND RECOMMENDATIONS

1.   On the basis of the fabrication and test experience, the ITA design
(less valves) is generally satisfactory. The ITA is simple (no complex parts)
with clean lines. There are no major fabrication problems that would preclude
production manufacturing. It is simple to operate and has no peculiarities that
require special consideration. The structural and fatigue life design appear
to be adequate.

2.   The igniter design is excellent. There was not a single case of
no ignition with the integral exciter/spark plug-igniter assembly over a wide
range of operating conditions (propellant temperature, MR, pressures, mainstage
valve sequencing and igniter sequencing) and with extended operation (42,266
pulses).

3.   The redesign to improve the strength of the injector oxidizer
distribution plates appears adequate.

4.   The incorporation of the orificing to split the hydrogen into regen
coolant (79%) and dump-film coolant (21%) as an integral part of the chamber was
satisfactory. There was no significant variation in hydraulic characteristics
from part-to-part, no problems were encountered in manufacture and it made
operation of the thruster very simple.

5.   The completion of 42,266 pulses is equivalent to an 8.5 year Space
Shuttle life. The failure of components that occurred were the result of mechanical
damage, were fabrication related, or were caused by ice formation due to the test
cell. No design change is recommended.

6.   The main propellant valves were unsatisfactory. They did not meet
specifications; they exhibited erratic closure times during checkout testing
and ITA testing; their cycle life was about half that required; there was no
engineering support provided to ascertain or correct the cause of the problems.

3.0, Conclusions and Recommendations (cont.)

7. With two exceptions (discussed below), the ITA fabrication generally proceeded as planned. The ITA would be easier to manufacture in quantity because of the better fixturing, tooling and process control generally possible with larger quantites.

8. The problem in fabricating the Haynes 188 nozzle resulted in program delay, but did not require design changes. Satisfactory parts were delivered. The problem was one of the vendors learning to adapt the fabrication process to the characteristics of the material.

9. The TIG weldment of the torus was not completely satisfactory. Consideration should be given to EB welding of the joint. Better fixturing is required. The part should be annealed after welding and proof tested.

10. The operating characteristics of the ITA are excellent. Its operating range meets the requirements as operating was demonstrated over the specified ranges of chamber pressure, mixture ratio, propellant temperatures, and propellant inlet pressures.

11. The component temperatures were generally as predicted so there was no compromise in predicted life. The one exception was the throat which was slightly hotter than predicted. Its thermal cycle life was still 65,000 cycles - more than two times the design requirement.

12. A fuel lead on start up can result in combustion in and damage to the oxidizer manifold. The design is less susceptible to damage with short oxidizer leads. Generally, a .010 to .020 sec oxidizer lead was used. Fuel leads up to .010 sec were demonstrated, indicating that minor changes in valve operating times could be tolerated.

3.0. Conclusions and Recommendations (cont.)

13. Shutdown was made with both oxidizer and fuel delays (generally fuel). While a fuel lag is preferred, there appears to be no more oxidation of the hot surfaces with an ox lag than there is in pulsing operation with an oxidizer lead.

14. An ox lead of .006 sec or less on start up appears to be about optimum for performance.

15. Ignition with no over-pressure damage was accomplished with the igniter delayed up to .006 after initiation of poppet travel of the lagging mainstage valve. This is the delay time predicted for operation with no igniter valves at nominal conditions.

16. The ITA operates at a 4 MR and 6672 N (1500 lb_f thrust) with 276 N/cm^2 (400 psia) at the inlet to the valves and the propellants at nominal temperature.

17. The steady state performance is 4266 N-sec/kg (435 lb_f-sec/lb_m) which meets the program goal.

18. The M.I.B. demonstrated on the program was 267 N-sec (60 lb_f-sec) which, while impressive, does not meet the 222 N-sec (50 lb_f-sec) goal. The 3609 N-sec/kg (368 lb_f-sec/lb_m) I_s at M.I.B. is less than the program goal.

19. The longest test firing duration made with the ITA was 513 sec (500 sec program goal). The only limit on the firing duration was the quantity of hydrogen in the tanks.

20. There were no thermocouples on the exterior of the aluminum foil covering the nozzle thermal insulation, so the external temperature is not known (260°C (500°F) goal).

3.0, Conclusions and Recommendations (cont.)

21. The demonstrated response time (time from electrical signal to 90% thrust) was typically .059 sec (.050 goal). The failure to meet the goal was because the main oxidizer propellant valve delay time (time from electrical signal to initiation of poppet travel) was .053 sec using the propellant as the actuation medium. The time from initiation of poppet travel of the lagging valve to 90% thrust was .006 sec. Specified valve response time was .040 sec from signal to full open.

22. The ITA weight (exclusive of valves) was 6.895 kg (15.2 lb) which is 1.33% in excess of the program goal of 6.809 kg (15 lb). The weight goal would be met by scalloping the injector at the igniter interface, reducing the thickness of the flange of the igniter body, thinning the inlet line flanges (or better yet, welding the valves to the inlet line).

23. The cycle life goal was not met due to stresses introduced in manufacturing and installation, due to mechanical damage and operational problems (icing), and because of problems with the main propellant valves. To achieve long life in fatigue as much attention must be payed to process control, inspection, protection during manufacturing and installation, operation, etc., as is payed to design.

24. The failure at 42,266 cycles was due o heat streak caused by icing. The icing resulted because of fuel valve delay on closing combined with water introduced in the chamber by blow back on shutdown.

25. The icing problem occurred on two tests with ITA SN 001. The burn through on Test-007 was caused by icing and is in the same location as the erosion of SN 002.

4.0 TECHNICAL DISCUSSION

4.1 INTEGRATED THRUSTER DESIGN

The design of the integrated thruster assembly is discussed first to provide an overview of the entire design and how the components are integrated into the assembly. The design of each component is discussed in subsequent sections.

4.1.1 ITA Design

The starting point for the ITA design and design analysis was the work done inhouse at ALRC and ultimately on Contract NAS 3-14354 (Ref. 3). Workhorse predecessors of the ITA chamber, igniter and injector were designed, built and tested on Contract NAS 3-14354. The NAS 3-14354 and ITA thrust chamber assemblies are compared in Figure 7.

The obvious major changes in the ITA versus workhorse designs are the weight reduction, the all welded construction and the incorporation of the propellant lines. There were two other changes that are not so obvious: (1) the separate ffc manifold was eliminated and (2) the oxidizer manifold was re-designed; because of the change in the flange area, to reduce ox manifold volume, and to strengthen the internal components. Other minor changes were made to improve fatigue life and will be discussed in the sections that follow. Essential features were not changed. Primarily, the injector elements are identical to the SN 006 and SN 007 Contract NAS 3-14354 injectors so that performance, heat transfer and compatibility are unaltered. The ITA design is summarized in Table XII.

4.1.1.1 Mechanical Design

As stated above, the major components of the ITA, namely: igniter, injector, chamber and valves are discussed in subsequent sections. The minor components/features that are required for completion of the

Ox Inlet

Ox Tubes

Regen (& Injector)
Fuel Inlet

ffc Inlet

Igniter Fuel
Inlet

TC

Fuel Inlet

Ox Inlet

ITA

Contract NAS 3-14354 Thrust Chamber Assembly

Figure 7. Workhorse and Flightweight TCA

TABLE XII

ITA DESIGN SUMMARY

Design Characteristics

Thrust	6672 N (150 lb$_f$)
Chamber Pressure	207 N/cm^2 (300 psia)
Mixture Ratio	4.0
Pressure at Inlet to Valves	276 N/cm^2 (400 psia)
Fuel Flow Rate	
Regen and Injector	247 g/sec (.545 lb/sec)
Fuel Film Coolant	65.8 g/sec (.145 lb/sec)
Total	313 g/sec (.69 lb/sec)
Oxidizer Flow Rate	1252 g/sec (2.76 lb/sec)
Fuel Temperature	130°C (250°R)
Oxidizer Temperature	208°C (376°R)
Igniter Fuel Flow Rate	
Core	.726 g/sec (.0016 lb/sec)
Coolant	4.26 g/sec (.0094 lb/sec)
Total	4.99 g/sec (.011 lb/sec)
Igniter Oxidizer Flow Rate	32.66 g/sec (.072 lb/sec)
Igniter Core MR	45
Igniter Overall MR	6.55

Geometry

Throat Diameter	4.88 cm (1.92 in.)
Exit Diameter	30.73 cm (12.1 in.)
Chamber Contraction Ratio	8.38 cm (3.3)
Nozzle Exit Area Ratio	40:1
Chamber L*	43.18 cm (17 in.)
Overall Length	74.68 cm (29.4 in.)
Overall Length (less exciter/spark plug)	61.37 cm (24.16 in.)
Fwd End Clearance Diameter	33.78 cm (13.3 in.)
Dimension of Cylinder Enclosing ITA	74.68 x 36.32 cm (29.4 x 14.3 in. Dia)

Weights (Design)

ITA (incl. Main Propellant Valves)	14.016 kg (30.9 lb)
Main Propellant Valves	7.257 kg (16.0 lb)
ITA (less valves)	6.758 kg (14.9 lb)
Thrust Chamber (Incl. Insulation)	3.933 kg (8.67 lb)
Injector	1.887 kg (4.16 lb)
Igniter	.939 kg (2.07 lb)

Design Performance

Specific Impulse	
Steady State	2266 N-sec/kg (435 lb$_f$-sec/lb$_m$)
Pulsing @ MIB	3923 N-sec/kg (400 lb$_f$-sec/lb$_m$)
MIB	222 N-sec (50 lb-sec)
Response (electrical signal to 90% thrust)	.050 sec

4.1, Integrated Thruster Design (cont.)

assembly (piston ring, reinforcement ribs, valve attachment, and thrust takeout mounts) are discussed in this section as part of the ITA layout.

A layout drawing of the ITA is shown in Figure 8. The oxygen inlet line is shown only in the top view.

The hydrogen enters the main propellant valve flowing from forward to aft. From the main propellant valve the fuel flows through the inlet line into the torus. There are 80 slots in the chamber shell under the torus at the entrance to each regen channel. There are also 160 orifices in the shell under the torus, one at the entrance to each dump ffc channel. The resistance of the regen-injector circuit versus the drop across the ffc orifices determines the regen versus ffc flow split. The convergent section of the chamber is convectively cooled by the flow of the hydrogen film coolant in the 160 dump cooling passages in the ZrCu liner. The throat and nozzle are film cooled.

The hydrogen in the regen circuit discharges into the injector fuel manifold at the periphery of the injector. It flows through holes in the injector face plate into circuits etched into the platelets that are bonded to the face of the injector. The platelet passages form the fuel elements and a face cooling circuit.

The GOX enters the axial flow main propellant valve flowing from aft forward. From the valve the GOX flows through the inlet line into the injector manifold. The oxidizer manifold contains flow distribution plates to ensure that the oxygen flow which is introduced into the injector manifold at a single location is uniformly distributed to the entrances of the ox elements. The oxygen enters the flow distribution passages through an annulus formed by the center spud (containing the igniter) and the hole in the center of the top distribution plate. The GOX is then allowed to expand radially outward between the two distribution plates; after a low velocity 180° turn, it then

4.1, Integrated Thruster Design (cont.)

flows radially inward from the periphery of the injector between the lower distribution plate and the flange plate containing the ox elements. The spacing between the lower distribution plate and the flange plate coupled with the reduction in flow area as the flow moves radially inward was designed to maintain a uniform velocity of the GOX as it enters the elements.

To form an integral unit the injector is welded to the chamber at the midpoint of the fuel manifold. The injector face plate contains a piston ring that is compressed by the chamber ID to seal the fuel manifold from the chamber. A small quantity of hydrogen will leak past this seal. The piston ring/seal design is identical to that used on Contract NAS 3-14354 and it resulted in no unacceptable performance degradation.

The igniter body fits into a boss in the center spud of the injector. The aft end of the igniter extends into a hole in the injector face plate and is approximately flush with the injector face. Slots for cooling passages in the igniter body are closed out by the fit of the igniter into the injector. Also, the fuel manifolding for the igniter that is machined into the injector body is completed by the placement of the igniter body in the injector. The igniter propellants are introduced through external tubes so that separate igniter valves can be used or the supply can be tapped off downstream of the main propellant valves by means of the fittings in the ITA inlet line flanges.

The integral exciter/spark plug screws into the igniter body via a slip nut and is supported by a bracket mounted on the igniter body flange. The bracket can be seen in the top view of Figure 8.

The injector flange plate is the most rigid member of the ITA. In addition to supporting the ox element-face plate assembly, the distribution plates, the center spud and the domes, it contains the thrust takeout mounts, fuel valve mount, and the ox line inlet flange is welded to it. The three
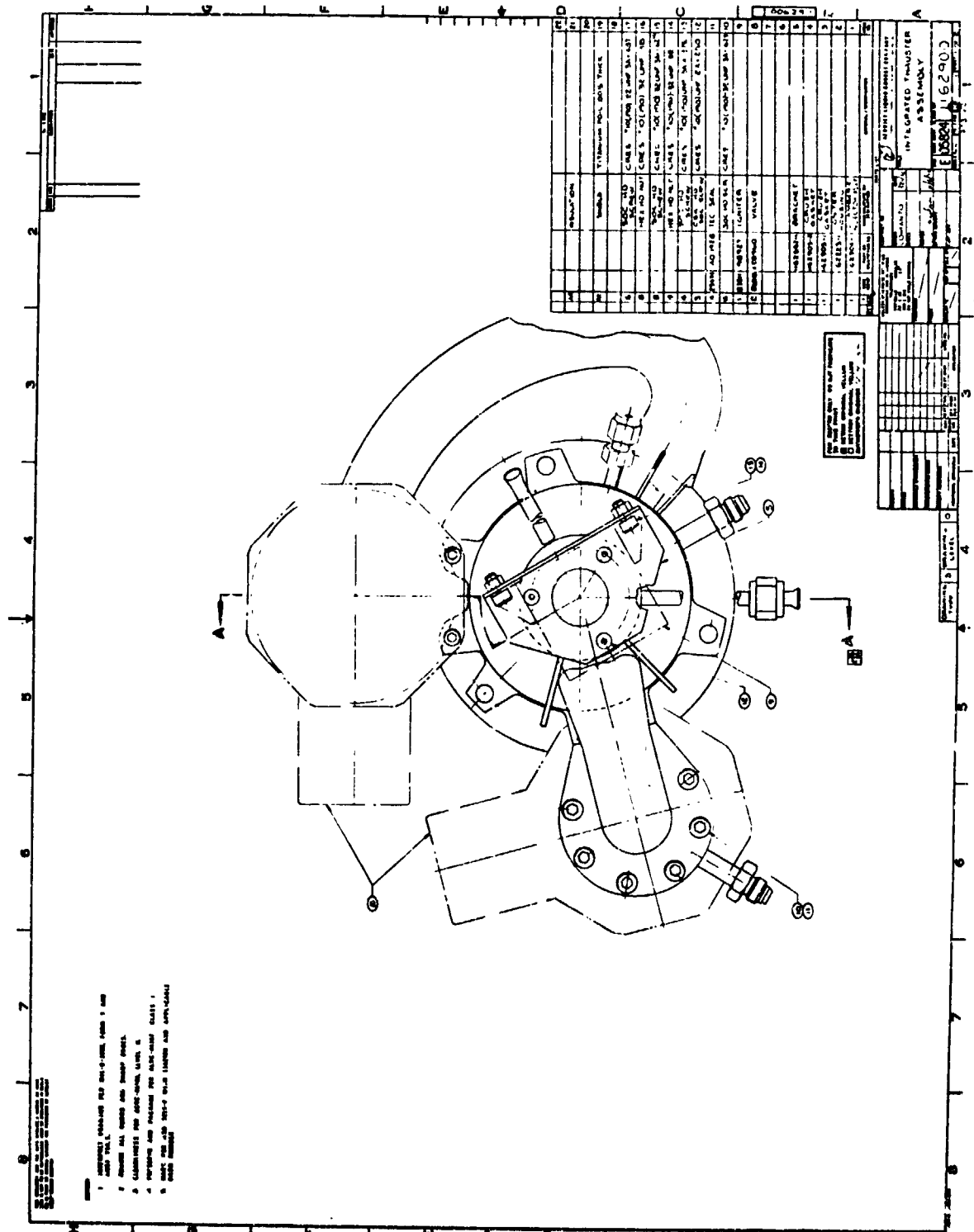
Figure 8. Integrated Thrust Assembly (Sheet 1 of 2)

Figure 8. Integrated Thrust Assembly (Sheet 2 of 2)

4.1, Integrated Thruster Design (cont.)

takeout mounts appear in tabs 120° apart with holes in them in the top view of
Figure 8. The fuel valve mounting tabs can also be seen in the top view of Figure
8. Two of the bolts in the main propellant fuel valve are no longer than the rest,
extending through the holes in the mounting tabs, and are secured to the mounting
tabs by self-locking nuts as shown in Figure 8. The incorporation of the three
thrust takeout mounts and the two fuel valve mounting tabs along with the weldment
of the ox valve flange to the injector flange plate provide good structural support,
eliminate brackets, reduce weight, reduce envelope and in general contribute to
a simple, clean configuration.

The throat section and nozzle extension are spun Haynes
88 and are .0767 cm (.030 inches) thick. The throat section is welded to the cham-
ber shell and to the nozzle extension. The weld which joins the throat section to
the chamber shell is located nominally 0.63 cm (0.25 in.) downstream for the end of
the film cooling sleeve. This weld operation is performed after the ZrCu liner has
been brazed into the steel shell so the weld location was made as far upstream of
the throat as possible without jeopardizing the film cooling sleeve.

The injector and chamber assembly are shown in Figure 9.
The cross section in this figure shows the weldment of the ox inlet line flange to
the injector flange plate and how the ox inlet line introduces the GOX into the
injector manifold.

Figure 9 also illustrates the design of the injector
center spud that accommodates the igniter housing.

Six ribs (three top and three bottom) are welded to the
torus at the location of the inlet line and two are welded to the injector dome
along side the ox inlet line. They are shown in the top view of Figure 9. The
purpose of these reinforcement ribs is to restore strength in pressure containment
members weakened by removal of material to form inlets.

The assembly shown in Figure 9 contains a dummy valve
(shown in phantom) that is used to position the fuel line during welding and to
provide support during shipment.
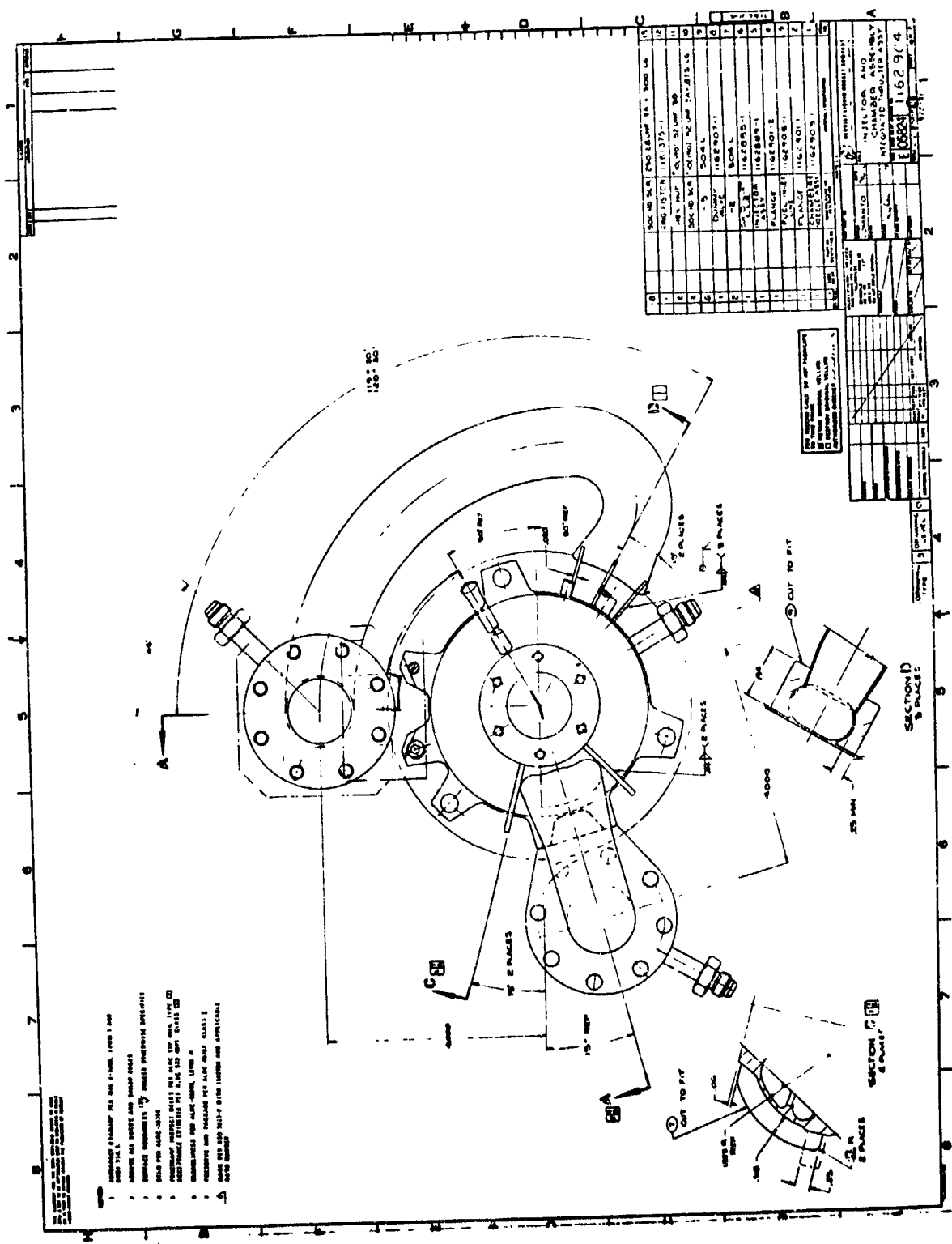
Figure 9. Injector and Chamber Assembly – Integrated Thruster Assembly (Sheet 1 of 2)

Figur 9. Injector and Chamber Assembly – Integrated Thruster Assembly (Sheet 2 of 2)

4.1, Integrated Thruster Design (cont.)

The chamber and injector assembly shown in Figure 9 is an integral assembly. All joints are welded except the following that are furnace brazed: injector center spud to flange plate and face plate; oxidizer elements (72 tubes) to flange plate and face plate; platelets to face of injector; and ZrCu liner to shell.

Two crush gasket seals are used in the igniter assembly. One seal is between the igniter flange and the injector and seals the igniter fuel manifold. The other seal is between the exciter/spark plug unit and the igniter body and seals the igniter chamber. These gaskets were .158 cm (.062 in.) thick compressed asbestos sheet packing.

4.1.1.2 Hydraulic Design

There was very little ITA hydraulic design work to be performed on this program since the ITA was based on the data and design of the thrust chamber built and tested under Contract NAS 3-14354 (Ref. 3). However, there were design analyses performed to evaluate the operational characteristics of the design.

4.1.1.2.1 Pressure Schedule

Modification of the fuel inlet to the chamber of the ITA from that tested on Contract NAS 3-14354, Reference (3), changed the pressure drop schedule and also required orificing of the inlet of the film cooling circuit for flow control. This section describes the revised pressure schedule and orifice configuration.

Coolant channel analysis of the nominal 207 N/cm^2 (300 psi) chamber pressure condition from Reference (3), using a SINDA program

4.1, Integrated Thruster Design (cont.)

subroutine which accounts for two-dimensional conduction in the rectangular coolant passage walls, shows an overall pressure drop in the regen circuit (manifold to injector) of 19.6 N/cm^2 (28.4 psid) including 6.4 N/cm^2 (9.3 psid) momentum and friction loss. Entrance, exit, and turning losses at the entrance , are calculated to be 7.51 (10.9) and 5.8 N/cm^2 (8.4 psid), respectively, including momentum losses. Based on the average of these two values the pressure drop for the passage is 26.5 N/cm^2 (38.4 psid). The total pressure drop between the manifold and the chamber is approximately 52 N/cm^2 (75 psid) including 25 N/cm^2 (36 psid) drop across the injector as measured on Contract NAS 3-14354.

The film cooling circuit dumps fuel into the chamber at an area ratio of 1.77 for which the static pressure at nominal conditions is 190 N/cm^2 (275 psid) ($\sim$.92 P_c). The pressure drop for the downstream circuit, based on SINDA Analysis, is 13.8 N/cm^2 (20 psid) with negligible entrance effects because of low fluid velocity. Since the total pressure drop in the circuit is 69 N/cm^2 (100 psid) the pressure to be dissipated at the entrance orifice mounts to 55 N/cm^2 (80 psid): manifold pressure 259 N/cm^2 (375 psia) passage pressure drop (13.8 N/cm^2 (20 psid)) less chamber static pressure at the exit (190 N/cm^2 (275 psid)).

Pressure drop in the feed line connecting the valve to the manifold totals 8.3 N/cm^2 (12 psid). This includes 1.03 N/cm^2 (1.5 psid) friction loss in the line itself -- with friction factor enhancement due to curvature effects accounted for and entrance and exit losses of 2.4 N/cm^2 (3.5) and 4.8 N/cm^2 (7.0 psid), considering the former as a standard elbow and the latter as a standard tee.

An additional point of interest is the coolant flow distribution between the regen and film cooling circuits at off-nominal propellant temperature and pressure. Ignoring second order effects -- such as changes in

4.1, Integrated Thruster Design (cont.)

friction characteristics, heat load per unit flow, etc -- a simple parametric analysis shows that the relative flow to each circuit is a function only of inlet temperature and not of pressure. There is a slight decrease in the proportion received by the film cooling circuit as fuel temperature increases -- but the variation is less than 10% over the range 111 (200) to 333°C (600°R). The ITA hydraulic analysis is summarized in Figure 10.

To determine the size of the orifice in the ffc circuit at the entrance to the ffc channels, the flow test fixture shown in Figure 11 was fabricated. This model duplicates the regen channel and film coolant channel geometry of the ITA thrust chamber. The convergent section of the chamber which introduces curvature in the film coolant channels was not duplicated as it occurs in an area where the coolant velocity is very low and, therefore, the pressure drop caused by the turning loss is small. One regen channel, two film cooling channels and inlet and outlet plenum were incorporated in the model.

The flow model and test setup are shown in Figure 12. The model was tested with ambient GN_2. Pressures were 1/10 of the actual values. The GN_2 flow rates were calculated from the design hydrogen flow rates, correcting for the difference in γ , pressure, molecular weight and temperature from the subsonic relationship:

$$\dot{w} = C_d \ A \ P_s \ \sqrt{\left(\frac{M}{T}\right) \left(\frac{2g}{R}\right) \left(\frac{\gamma}{\gamma-1}\right) \left[\left(\frac{P_d}{P_s}\right)^{2/\gamma} - \left(\frac{P_d}{P_s}\right)^{\frac{\gamma-1}{\gamma}}\right]}$$

GN_2 was applied to the model at the inlet. Flow was controlled by a 1% critical orifice. The GN_2 flow rate was determined from the pressure to the critical orifice. The GN_2 temperature was measured as was the

Ox Manifold

P = 340 psia (234 N/Cm^2)

Fuel Inlet

w = 0.69 lb/sec (313 g/sec)
T = 250°R (139°C)
P = 400 psia (276 N/Cm^2)

Orifice Outlet

P = 350 psia
(241 N/Cm^2)

Valve Outlet

P = 382 psia
(263 N/Cm^2)

Fuel Manifold

w = 0.545 lb/sec (247 g/sec)
P = 336.6 psia (232 N/Cm^2)
T = 367°R (204°C)

Chamber Pressure

P_c = 300 psia (207 N/Cm^2)

Valve Outlet

P = 391 psia
(270 N/Cm^2)

Orifice Outlet

P = 387 psia
(267 N/Cm^2)

Torus

P = 375 psia (259 N/Cm^2)

Orifice Discharge

P = 295 psia (203 N/Cm^2)
w = 0.145 lb/sec (65.8 g/sec)

Oxidizer Inlet

w = 2.76 lb/sec (1252 g/sec)
T = 375°R (208°C)
P = 400 psia (276 N/Cm^2)

FTC Injection

P = 275 psia (190 N/Cm^2)
T = 383°R (213°C)

Figure 10. ITA Pressure Schedule

Page 49
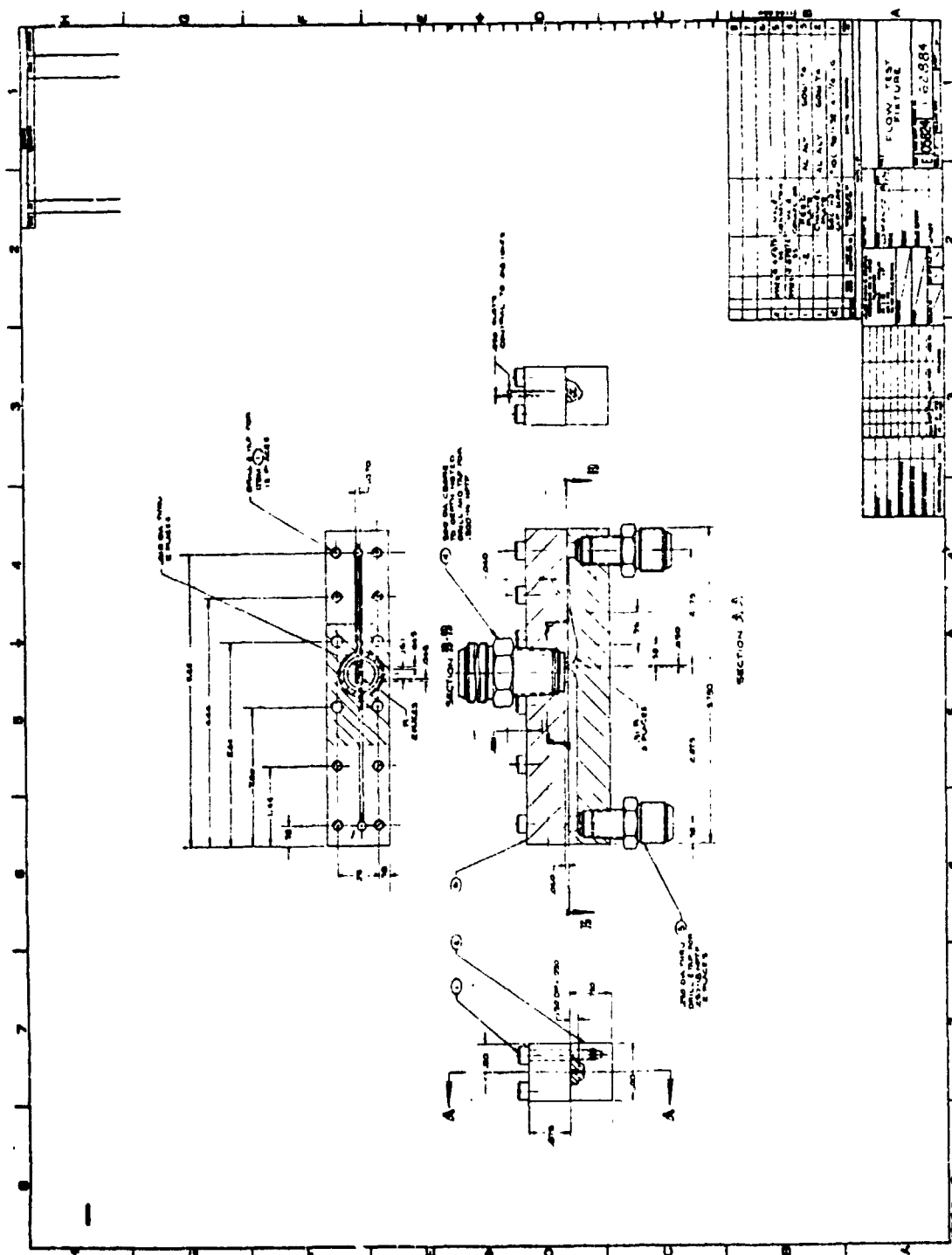
Figure 11. Flow Test Fixture

Pressure Tap

Inlet Line

Regen Channel Outlet

Film Cooling Channel Outlet

CHANNEL FLOW MODEL

Pressure Gages

Flow Model

Temperature Gages

Back Pressure Valves

Rotameters

TEST INSTALLATION
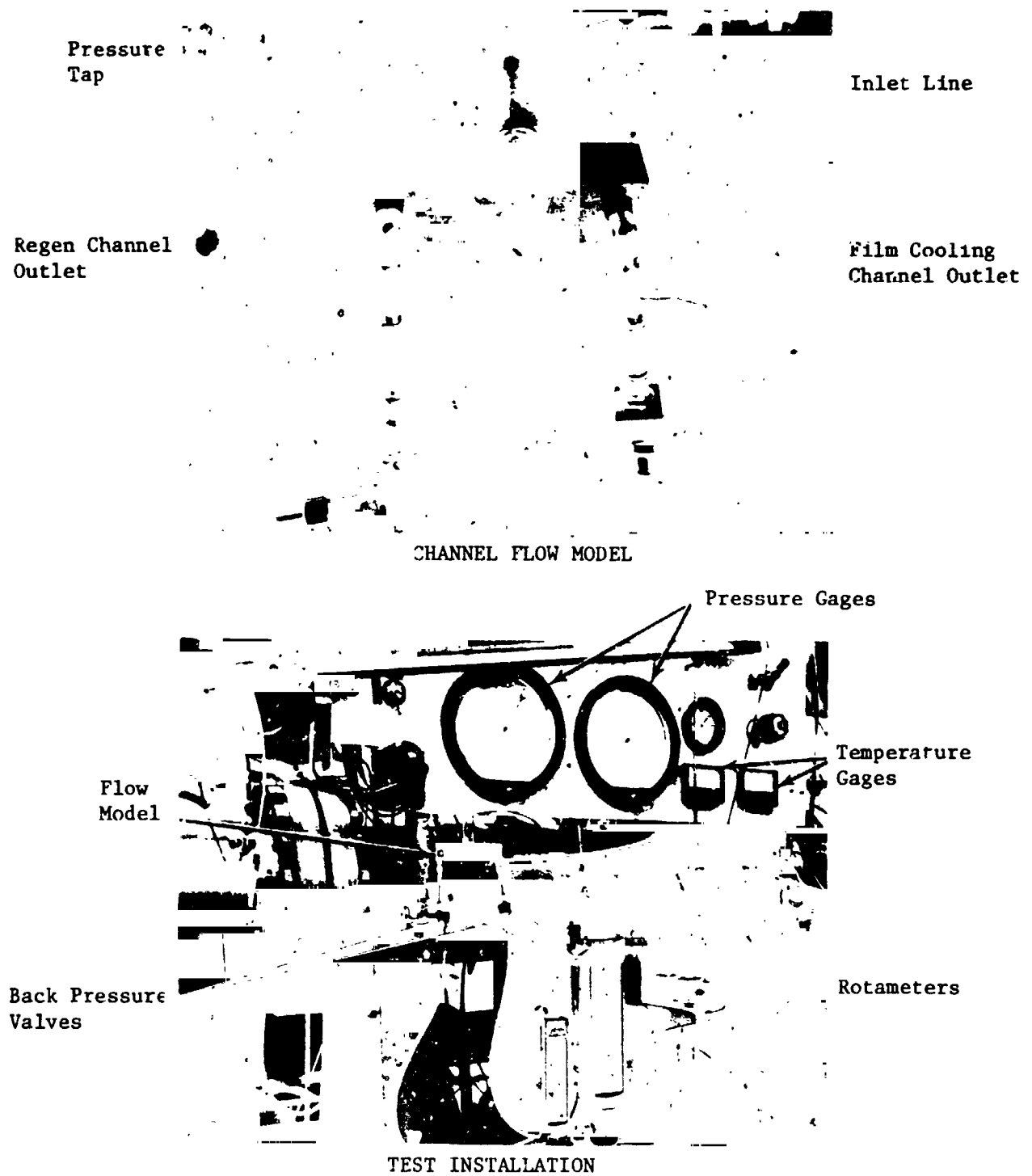
Figure 12.   Flow Model Test Setup

4.1, Integrated Thruster Design (cont.)

pressure in the inlet plenum. Flow from the discharge plenums was routed through valves, so that downstream pressure could be set, and from the valve to rotameters for flow measurement. The sum of the flows (regen channel and film coolant channels) measured with the rotameters agreed with the inlet flow rate within 1.77% (results from first six measurements).

The model was initially flowed with .0406 cm (.016 in.) and .0711 cm (.028 in.) diameter orifices at the inlet to the coolant channels. Additional testing was performed by plugging one of the film coolant channel by itself. The inlet pressure was varied to give pressure conditions both higher and lower than the actual ratio of back pressure to inlet pressure. Flow was measured via a rotameter. Hole sizes of 0.508 cm (0.020 in.) and 0.063 cm (0.025 in.) diameter were used. The flow tests were repeated with the inlet hole chamfered.

The GN_2 flow rates were plotted versus pressure ratio to permit interpolation of the data to get the flow rate for each orifice size at a pressure ratio of 0.733 which is the value of the chamber pressure at the film coolant injection point divided by the fuel manifold pressure. The flow rates thus obtained were plotted versus hole size squared as shown in Figure 13. As can be seen in the figure, the required hole size is 0.0571 cm (0.0225 in.) diameter.

Chamfering the 0.0508 cm (0.020 in.) diameter hole increased the flow rate by 8.65%. Chamfering the 0.0635 cm (0.025 in.) diameter hole increased the flow rate by 5%

4.1.1.2.2   Start Up Transient

System behavior was modeled using Aerojet's Transient Flow Computer Program. This program computes the transient flow relationships using an Adams integration technique to solve a set of simultaneous differential
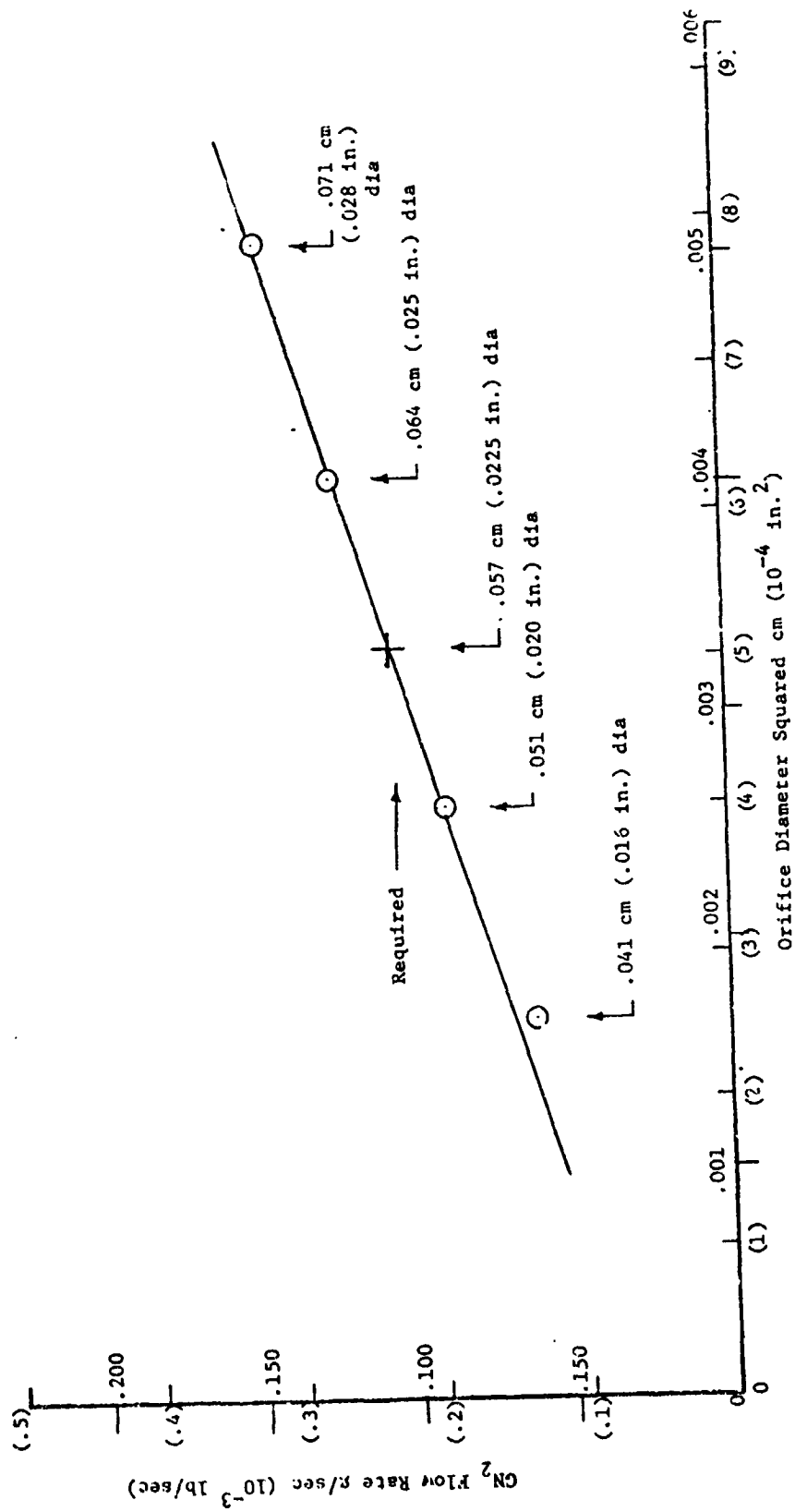
Figure 13. Flow Model Test Results

4.1, Integrated Thruster Design (cont.)

equations which describe the time-based flow and density characteristics. The program computes chamber and manifold pressure transients using ideal gas laws for the manifold filling portion of the start sequence. Complete mathematical simulation is performed on the UNIVAC 1108 high speed digital computer. System volumes and areas that were used in the study are tabulated below:

Engine System

1. Thrust Chamber Valves to Injection Orifice

Oxidizer	275 cc (16.8 in.^{3})
Fuel	442 cc (27.0 in.^{3})

2. Chamber Volume (above throat)   893 cc (54.5 in.^{3})

3. Nozzle Throat Area   16.7 cm^2 (2.90 in.^{2})

4. Valve Opening Time   6.0 millisec

Igniter System

1. Line and Manifold Volumes

Oxidizer	33 cc (2.02 in.^{2})
Fuel	20 cc (1.25 in.^{3})

2. Fuel Coolant Volume   .5 cc (0.033 in.^{3})

3. Chamber Volume to Throat   2 cc (0.12 in.^{3})

4. Throat Area   .6 cc (0.034 in.^{2})

The data desired from these studies was determination of the oxidizer lead/lag relationship and pressure buildup as a function of the valve opening sequence. The objective of these studies was to determine: the effect of igniter valve sequencing and of main propellant valve sequencing so that operation with the igniter valves removed could be evaluated and so that sequencing requirements could be determined.

4.1, Integrated Thruster Design (cont.)

The main concern in running the start transient studies was to determine conditions that could result in a hard start that would damage hardware. A hard start can result from buildup of thruster chamber pressure prior to ignition or, with a fuel lead, can result from combustion in the oxidizer manifold of the injector.

Table XIII is a summary of the conditions that were simulated by the computer transient analysis. For the thruster, two effects were investigated: the effect of oxidizer lead/lag and the effect of off-nominal operating conditions. For the igniter, several combinations of conditions were investigated: for operation with igniter valves, the effect of oxidizer volume and oxidizer lead/lag was investigated; for operation without the valves, the effect of oxidizer lead was investigated.

Some typical results are shown graphically in Figures 14 through 16. The nominal thruster cold flow (no ignition) transient is shown in Figure 14 for simultaneous opening of the fuel and oxidizer valves. Assuming the igniter is operating, thruster ignition would occur within 4.5 milliseconds after the valves start to open.

The cases run with oxidizer lead/lag are of interest to determine the amount of fuel flow into the oxidizer manifold. The fuel flow into the oxidizer manifold reached its maximum rate in about five milliseconds. In ten milliseconds, the fuel ceases to enter the oxidizer manifold because the fuel cold flow pressure in the thrust chamber has reached steady state and is not increasing. A 20-millisecond fuel lead does not result in appreciably more fuel in the oxidizer manifold than a ten-millisecond fuel lead. In five milliseconds, the accumulation of fuel in the oxidizer manifold is 1/3 of that occurring in ten milliseconds. Thus, 2/3 of the fuel that can enter the oxidizer manifold does so in the span of time corresponding to five- to ten-millisecond oxidizer lag.

TABLE XIII

ITA COLD-FLOW START TRANSIENT
SUMMARY TABLE OF ANALYSIS CONDUCTED

MAIN ENGINE SYSTEM

		POV N/cm^2 (psia)	PFV N/cm^2 (psia)	TOV ^oK (^oR)	TFV ^oK (^oR)	T.C. VALVE OXID LEAD Millisec
1.	NOMINAL	276 (400)	276 (400)	214 (385)	139 (250)	+20
		276 (400)	276 (400)	208 (375)	139 (250)	+10
		276 (400)	276 (400)	208 (375)	139 (250)	0
		276 (400)	276 (400)	208 (375)	139 (250)	-10
		276 (400)	276 (40C)	208 (375)	139 (250)	-20
2.	OFF-DESIGN	241 (350)	372 (450)	137 (246)	333 (600)	0

IGNITER SYSTEM

		POV N/cm^2 (psia)	PFV N/cm^2 (psia)	TOV ^oK(^oR)	TFV ^oK(^oR)	IGNITER VALVE OXID. LEAD Millisec	VOLUME OF OXID. SYSTEM cm^3($in.^3$)
1.	WITH VALVE	276(400)	276(400)	208(375)	139(250)	0	24.6 (1.5)
		276(400)	276(400)	208(375)	139(250)	0	16.4 (1.0)
		276(400)	276(400)	208(375)	139(250)	0	11.5 (0.7)
		276(400)	276(400)	208(375)	139(250)	+3	11.5 (0.7)
		276(400)	276(400)	208(375)	139(250)	-3	11.5 (0.7

2. WITHOUT VALVES

POV & PFV	TOV ^oK(^oR)	TFV ^oK(^oR)	T.C. VALVE OXID. LEAD Millisec	VOLUME OF OXID. SYSTEM cm^3($in.^3$)
Engine Pressure	208(375)	139(250)	0	11.5 (0.7)
Transient	208(375)	139(250)	+10	11.5 (0.7)
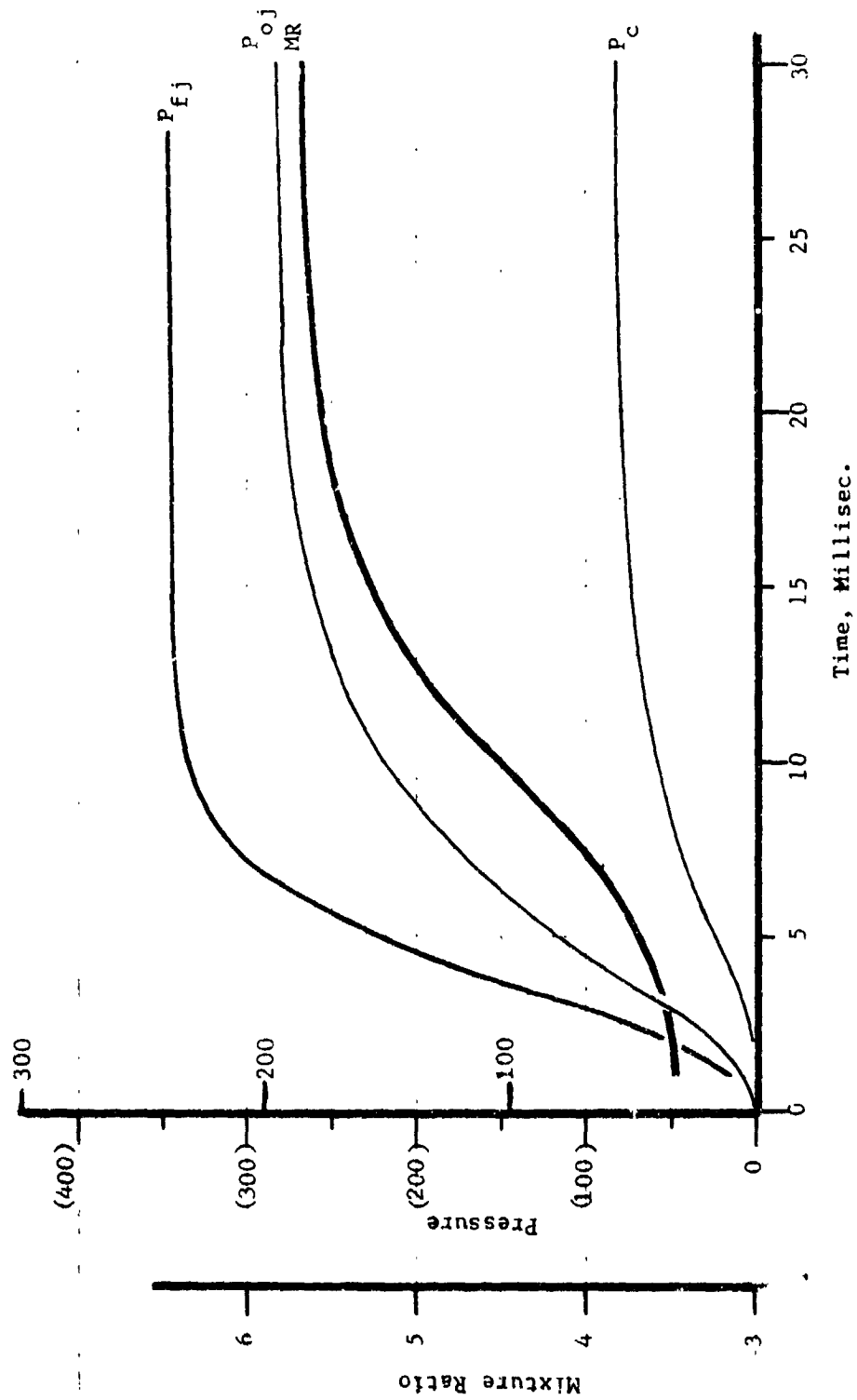
Figure 14. ITA Thruster Cold-Flow Transient - Nominal Operating Conditions
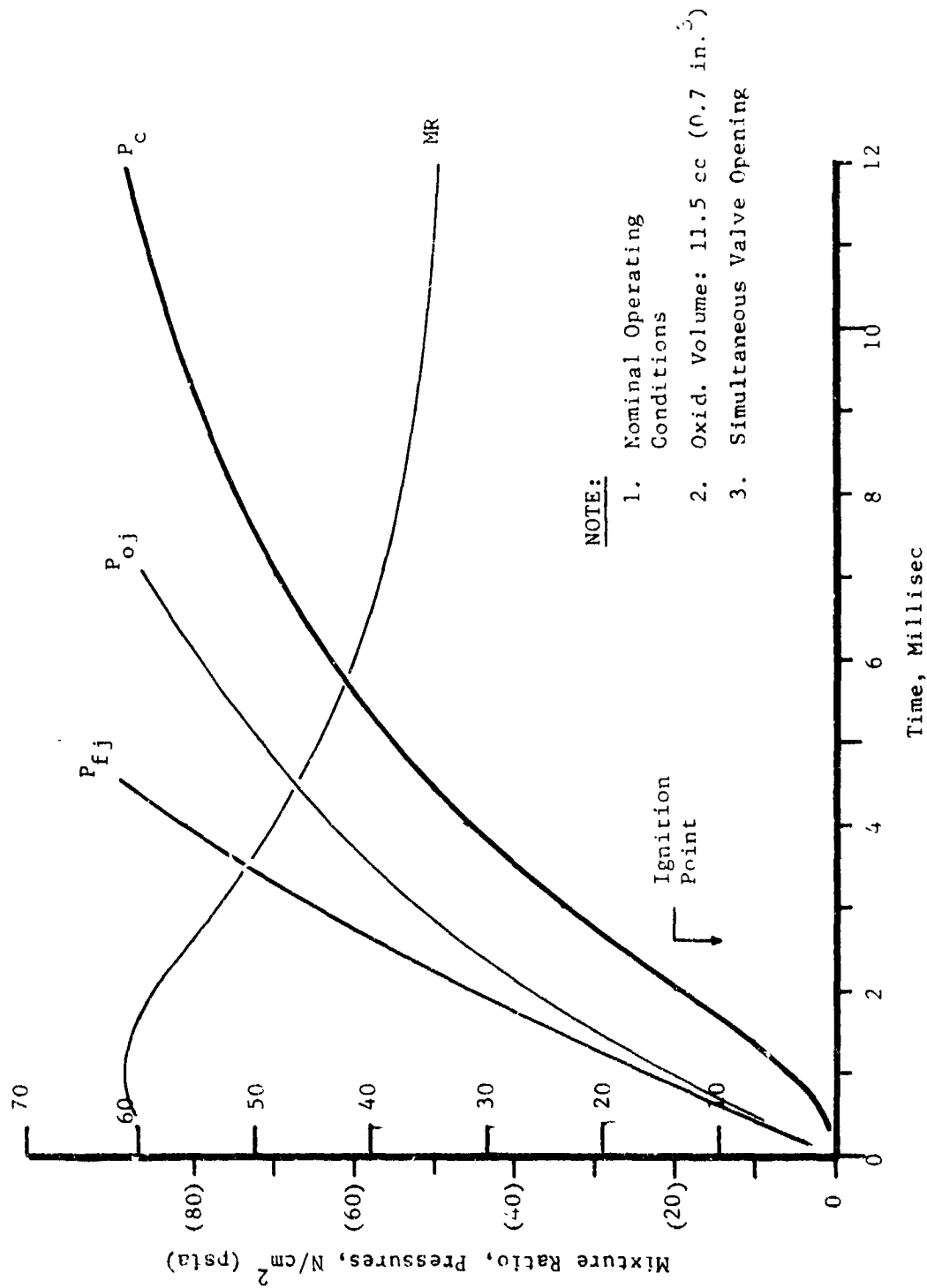
Figure 15. ITA Igniter 1d-Flow Transient – Igniter with Valves
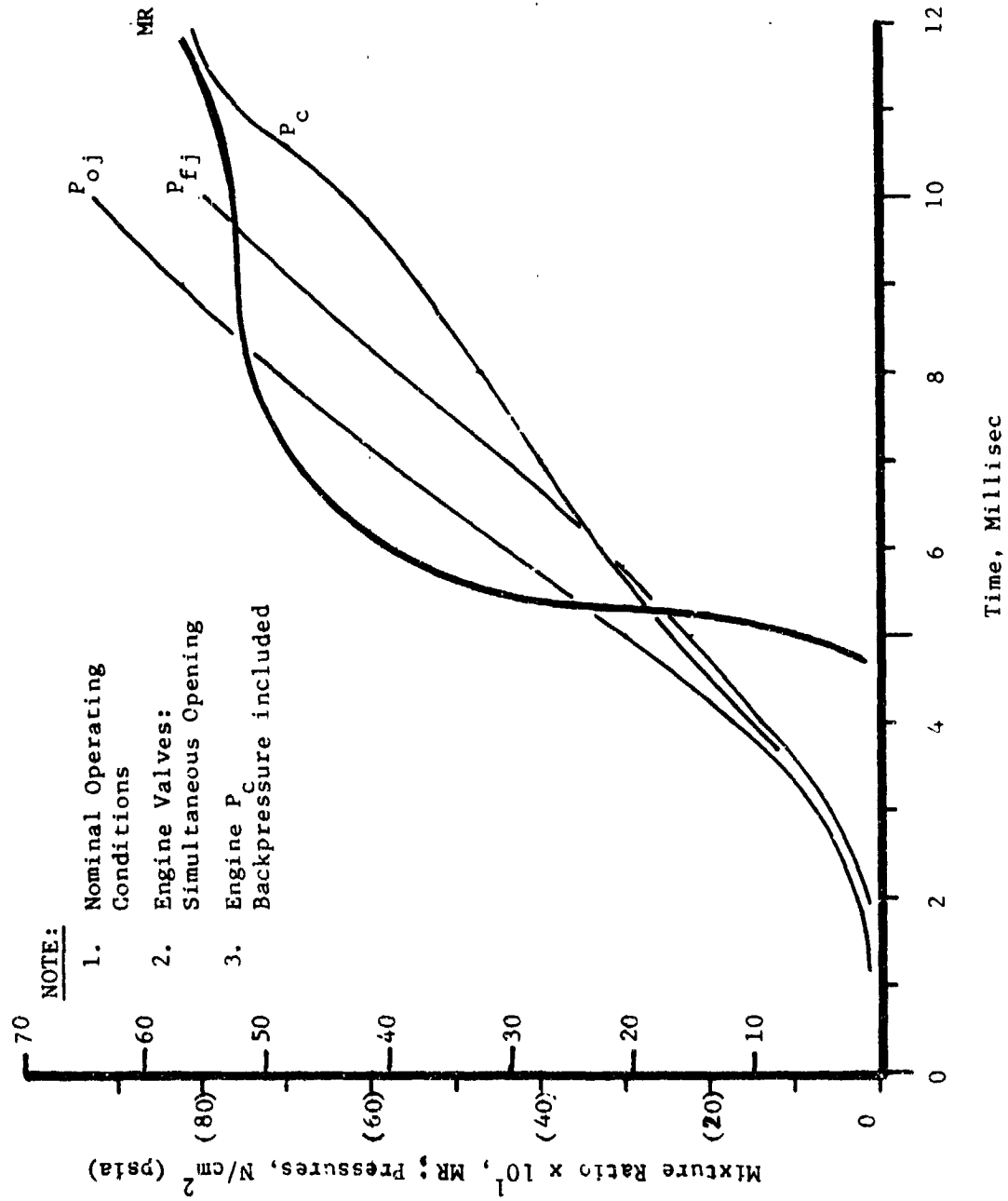
Figure 16. Igniter Cold-Flow Transient – Valveless Operation

4.1, Integrated Thruster Design (cont.)

The results of the analytical studies indicate that there will be no oxidizer manifold spikes with oxidizer leads and, with oxidizer lags of up to two milliseconds. For oxidizer lags of more than five milliseconds, the amount of fuel in the oxidizer manifold increases markedly and can potentially result in appreciable pressure spikes.

As shown in Figure 15, the igniter, when operating with valves at nominal conditions, responds much more rapidly than the thruster. Ignition should occur in less than 2.5 milliseconds after valve opening (simultaneous opening of fuel and oxidizer valve).

The igniter start transient for nominal conditions with no igniter valves is shown in Figure 16. Pressure in the thruster chamber builds up faster for the first six milliseconds than does pressure in the igniter. Igniter pressurization results from reverse flow from the thruster into the igniter. In five milliseconds, the fuel begins to flow into the igniter chamber (prior to this, the fuel flow only pressurized the manifold). Igniter ignition may not occur before six milliseconds since igniter P_c is greater than the fuel manifold pressure up to that time and, thus, prior to that time there is no flow of fuel in the igniter except for that coming in from the thruster.

For nominal conditions, igniter/thruster ignition six milliseconds after inception of valve opening is no problem. Ignition may even occur sooner because of the possible combustion of the accumulation of propellants in the igniter from the thruster. However, off-nominal conditions that result in longer delays before the inception of fuel flow could result in hard starts because of the buildup of combustible mixture (higher cold flow pressure) in the thruster prior to ignition.

The following conclusions were drawn from the start transient study and test results from Contract NAS 3-14354:

4.1, Integrated Thruster Design (cont.)

(1)   Simultaneous opening of the main propellant valves appears attractive. This mode of operation should result in a mild start transient and is optimum for I_s at the minimum impulse bit because it minimizes unreached propellant leads.

(2)   Mainstage oxidizer leads up to 0.020 sec are permissible and fuel leads less than 0.005 sec will probably not result in over-pressurization of the oxidizer dome or hard starts.

(3)   For operation with valves in the igniter system, a 0.003-sec igniter fuel lead is recommended. Contract NAS 3-14354 test experience indicated that ignition is generally more reliable with a fuel lead. Moreover, the igniter mixture ratio with a fuel lead at the time in the start transient at which the pressure is high enough to support combustion is on the order of 27 to 35 which with an oxidizer lead or with simultaneous valve opening the mixture ratio at that pressure is in excess of 80. Earlier ignition will be achieved with the lower mixture ratio.

(4)   Operation with the igniter valves removed and the igniter propellant supply tapped off downstream of the main propellant valves will result in a delay of igniter ignition 0.006 sec after initiation of travel of the main propellant valve poppets. With valves in the igniter system and the propellant supply tapped off upstream of the valves, igniter ignition will occur in less than 0.003 sec after initiation of igniter valve poppet motion.

(5)   An ignition delay of 0.006 sec will not result in a hard start transient under nominal conditions but may result in hard starts at off-design conditions.

4.1.1.2.3   ITA Sensitivity Study

The sensitivity of the ITA to propellant temperature and pressure at the valves was evaluated analytically. The study was made using

4.1, Integrated Thruster Design (cont.)

the pressure drop versus flow rate schedule of the propellant circuits and the relationship between chamber pressure versus propellant mass flow, mixture ratio and temperature. Table XIV is a summary of the results for the combinations of propellant temperatures and pressures that result in the highest and lowest mixture ratio and chamber pressure cases. The only case that appears unacceptable for extended operation is the high mixture ratio case which results in a skirt temperature in excess of the 1149°C (2100°F) design limit. The high mixture ratio results are probably optimistic as the skirt temperatures were derived from experimental data that do not account for the effect of reaction between the hydrogen film coolant and an oxidizer-rich core.

The main propellant valves were limited by the pressure that the bellows in the valve can sustain. This limit is 448 N/cm^2 (650 psia) and occurs in the open position (see Section 4.3.4.1). The sensitivity study was also applied to the limit imposed by the main propellant valves. Testing can be accomplished without exceeding the 448 N/cm^2 (650 psia) valve limit for mixture ratios of 2.5, 4 and 6.5 combined with propellant temperature from 111°K (200°F) to 333°K (600°R) for chamber pressures up to 207 N/cm^2 (300 psia). At the 345 N/cm^2 (500 psia) chamber condition, operation can be accomplished with only the cold propellant condition with mixture ratios of 6.5 and 4. Testing with nominal propellant temperatures, a 4.0 mixture ratio and 345 N/cm^2 (500 psia) chamber pressure requires 463 N/cm^2 (672 psia) at the inlet to the oxidizer valve and 461 N/cm^2 (668 psia) at the inlet to the fuel valve, which is marginal for the valve. For 345 N/cm^2 (500 psia) chamber pressure the 2.5 mixture ratio (all temperatures), the 4.0 mixture ratio (nominal temperature), and the 6.5 mixture ratio (nominal and ambient temperatures) conditions exceed the operating pressure limit for either the ox or fuel valve.

4.1.1.3   Structural Design

A strength analysis and fatigue (life) analysis was performed for each component. The basic work was done as part of Contract NAS 3-14354 (Ref. 3). Modifications that were made to the APS thruster design (Ref. 3) in the development of the ITA were analyzed as part of this program. Details of the strength analysis are given in Ref. 4. The life cycle analyses of each component is described in subsequent sections (4.1.2.5, 4.1.3.4, 4.1.4.4) for each component.

TABLE XIV

IIA SENSITIVITY TO INLET CONDITIONS AT VALVES

Case	Ox Temp °K(°R)	Ox Press. N/cm²(psia)	Fuel Temp °K(°R)	Fuel Press N/cm²(psia)	P_c N/cm²(psia)	$\dot{w}_o$ g/sec (Lb/sec)	$\dot{w}_f$ g/sec (Lb/sec)	O/F	Max Skirt* Temp °K(°F)
Nominal	209 (375)	276 (400)	139 (250)	276 (400)	207 (2.75)	1247 (0.69)	313	4	888 (1630)
High O/F	136 (245)	310 (450)	333 (600)	241 (350)	205 (297)	1905 (4.20)	132 (0.29)	14.5	1621 (2950)
Low O/F	333 (600)	241 (350)	136 (200)	310 (450)	175 (254)	875 (1.93)	487 (1.075)	1.8	677 (1290)
High P_c	136 (245)	310 (450)	136 (200)	310 (450)	255 (370)	1488 (3.28)	327 (0.72)	4.5	932 (1710)
Low P_c	333 (600)	241 (350)	333 (600)	241 (350)	155 (225)	966 (2.13)	197 (0.435)	4.9	957 (1755)

111 (200) T_{fuel} 333 (600) °K (°R)

136 (245) T_{oxid} 333 (600) °K (°R)

Pressure at valves = 276 ± N/cm² (400 ± 50 psia)

* Estimated from Contract NAS 3-14354 data

4.1, Integrated Thruster Design (cont.)

The strength and life analyses are summarized in Tables XV and XVI. Table XV is a summary of the strength analysis at various locations on the thruster at the most limiting conditions. Table XVI is a summary of the thermal cycle life analysis.

4.1.1.4 Surface Finish

One of the factors that governs fatigue life is surface finish (Ref. 5). The machining process employed to fabricate the ZrCu chamber liner and the Haynes 188 nozzle and extension could be expected to result in a surface finish between .81[1] and 3.18 (32[2] and 125). On the other hand, cycle life data used in the fatigue and life analysis were obtained with polished test specimens. This raised the question as to whether the surface finish could compromise fatigue life and what the surface finish requirement should be.

ALRC Space Shuttle fatigue design procedures utilized a factor, called the surface factor that related the endurance limit (cyclic stress, fully reversed, that specimen can withstand prior to failure) to tensile strength as a function of the fabrication process as shown in Figure 17 for steel.

In order to evaluate the effect of surface finish on cycle life, it was assumed that Figure 17 could be used to estimate the reduction in the endurance limit for the ZrCu liner and the Haynes 188 nozzle. Surface factors were obtained from Figure 17 at the tensile strength of ZrCu at 193°C (380°F) and Haynes 188 at 249°C (480°F) (average temperature at the most limiting conditions as summarized in Table XVI) for the surface conditions as defined by the figure.

The surface conditions are described in Figure 17 by production processes that result in a range of surface roughness. The surface roughness that was assigned to each process is tabulated below:

---

(1) micron (mu)
(2) micro inches (μ in.)

TABLE XV

SUMMARY OF STRENGTH ANALYSIS RESULTS
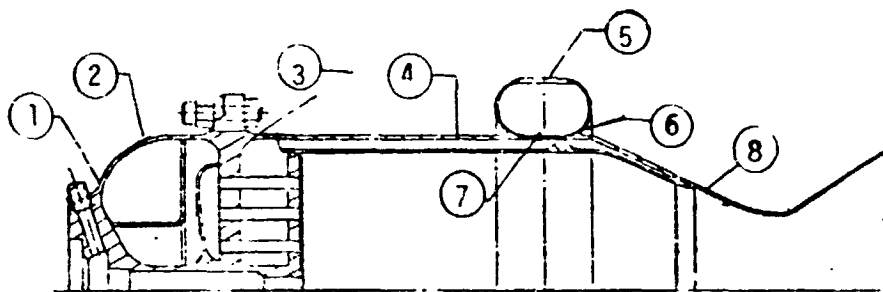
LOCATION	CONDITION	TEMP	MATERIAL	YIELD ALLOWABLE	EFFECTIVE STRESS	FACTOR OF SAFETY
1	Proof Pressure 603 N/cm^2	27°C (80°F)	304 SS	20,685 N/cm^2 (30,000 psi)	12,452 N/cm^2 (18,060 psi)	1.66
2	Proof, 603 N/cm^2 (875 psia)	27° (80°)	304 SS	20,685 (30,000)	11,177 (16,210)	1.85
3	Proof, 603 N/cm^2 (874 psi)	27° (80°)	304 SS	20,685 (30,000)	16,514 (23,950)	1.25
4	Steady-State @ 207 N/cm^2 (300 psi) & Temp.	54° (130°)	12-13-5 Stainless	44,818 (65,000)	28,359 (41,130)	1.57
5	Steady-State Proof @ 603 N/cm^2 (875)	-134° (-210°) 27° 80°	22-13-5 Stainless	51,712 (75,000) 44,818 (65,000)	11,485 (16,510) 33,164 (48,100)	4.54 1.35
6	Steady-State Proof @ 603 N/cm^2 (875)	-92° (-136°) 27° (80°)	22-13-5 Stainless	44,818 (65,000) 44,818 (65,000)	39,302 (57,000) 17,430 (25,280)	1.14 2.57
7	Steady-State	-53° (-63°)	22-13-5 Stainless	48,818 (65,000)	32,406 (47,000)	1.38
8	Steady-State	51° (123°)	Haynes 188	44,818 (65,000)	35,544 (51,550)	1.26

TABLE XVI

SUMMARY OF FATIGUE AND LIFE ANALYSIS
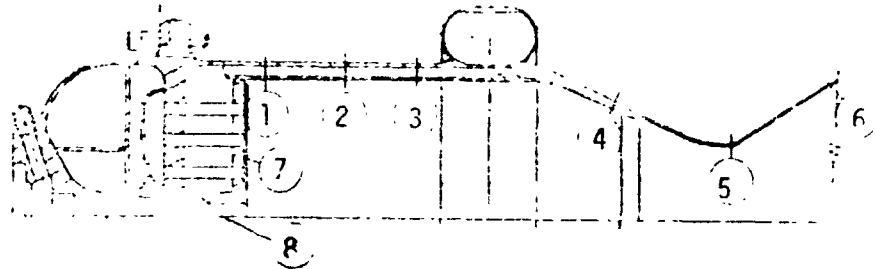
CONDITIONS: 207 N/cm^2 (300 psia), MR = 4, Fuel Temp = 139°K (250°R), 21% Film Cooling
248 N/cm^2 (360 psia) Channel Pressure, 80 Regen Slots, 160 ff$_c$, Slots
Zirc. Copper Liner, .102 cm (.040 in.) thick Stainless Shell

Location	Time	T_{WG}	T	t	Thermal Cycles (N_f)	Comments
1	S.S	160°C (320°F)	69°C (156°)	.24%	120,000	Nominal value based on all ZrCu test data.
2	S.S	138 (280°)	66 (150°)	.23%	140,000	Computer run made here.
3	S.S	72 (162°)	72 (162°)	.25%	100,000	Computer run made here.
4	.18 sec	193 (380°)	93 (200°)	.32%	50,000	Nominal value based on all ZrCu (Air data).
4	S.S	249 (480°)	72 (162°)	.26%	90,000	Nominal value based on all ZrCu.
5	Transient	249 (480°)	182 (360°)	.21%	1×10^5	Universal slope equation Lower Bound $N_f^1 = \dfrac{N_f}{10}$
6	S.S	982 (1800°)	0 (-18)	Creep = 483 N/cm^2 (700 psi)	1000 hrs	Could go to 2100° without structural problems
7	S.S	121 (250°)	66 (150°)	.18%	10^6	Higher propellant temperatures, Pressures and MR reduce life
8	Nominal Conditions		99 (210°)	.123%	60,000	$N_f^1 - \dfrac{N_f}{10}$ (Lower Bound)
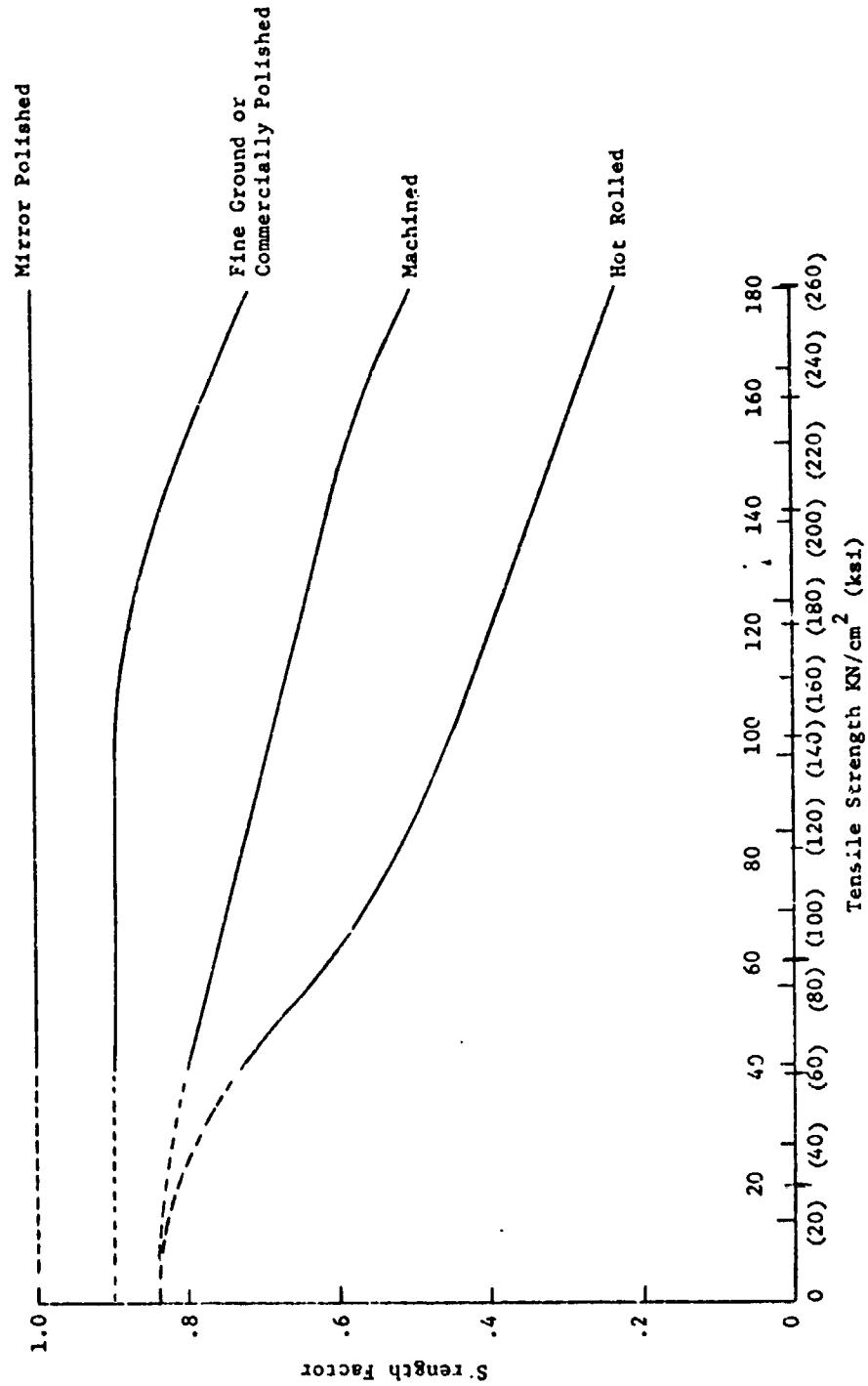
Figure 17. Reduction of Endurance Strength due to
Surface Finish

4.1, Integrated Thruster Design (cont.)

Process	Surface Roughness microns	(μ in.)
Mirror polished	.0254	(1)
Fine ground or commercially polished	.2	(8)
Machined	1.63	(64)
Hot rolled	12.7	(500)

Surface roughness values were assumed for the test specimens used to generate the S-N data. It was decided to use a range of surface roughness, namely .0254 mu (1 μ in.) to .203 mu (8 μ in.), since this range is achievable by honing and buffing, production and hand lapping, and superfinishing. Surface finish and residual surface stresses resulting from the method of machining probably vary from specimen to specimen and with the investigator and, therefore, probably contribute to the scatter in S-N data. The S-N curves for ZrCu and Haynes 188 (Section 4.1.4.4) were then reduced by the ratio of: the surface factor corresponding to various surface roughness values, to the surface factor corresponding to the surface roughness of the original test specimen. Surface factor is a stress ratio while the S-N curves relate cycle life to percent strain. This assumes that the reduction in stress produces a 1:1 reduction in allowable strain. The results are shown in Figure 18 for two values assumed for the surface texture of the test specimen with which the S-N data were obtained.

In order to determine what surface roughness can be achieved by conventional fabrication processes, surface roughness measurements were made on workhorse hardware residual from Contract 3-14354. The lowest surface roughness measured on the copper liner was .89 mu (35 μ in.) and on the nozzle was .51 (20). On the basis of 21 areas of the chamber, it was concluded that a .81 (32) finish was state-of-the-art for conventional machining of the ZrCu liner and Haynes 188 nozzle and extension. No manufacturer took exception to the .81 (32) surface finish requirement and the components were hand polished and vapor honed during fabrication to significantly better finishes.

The following conclusions were drawn from this numerical, but qualitative study:
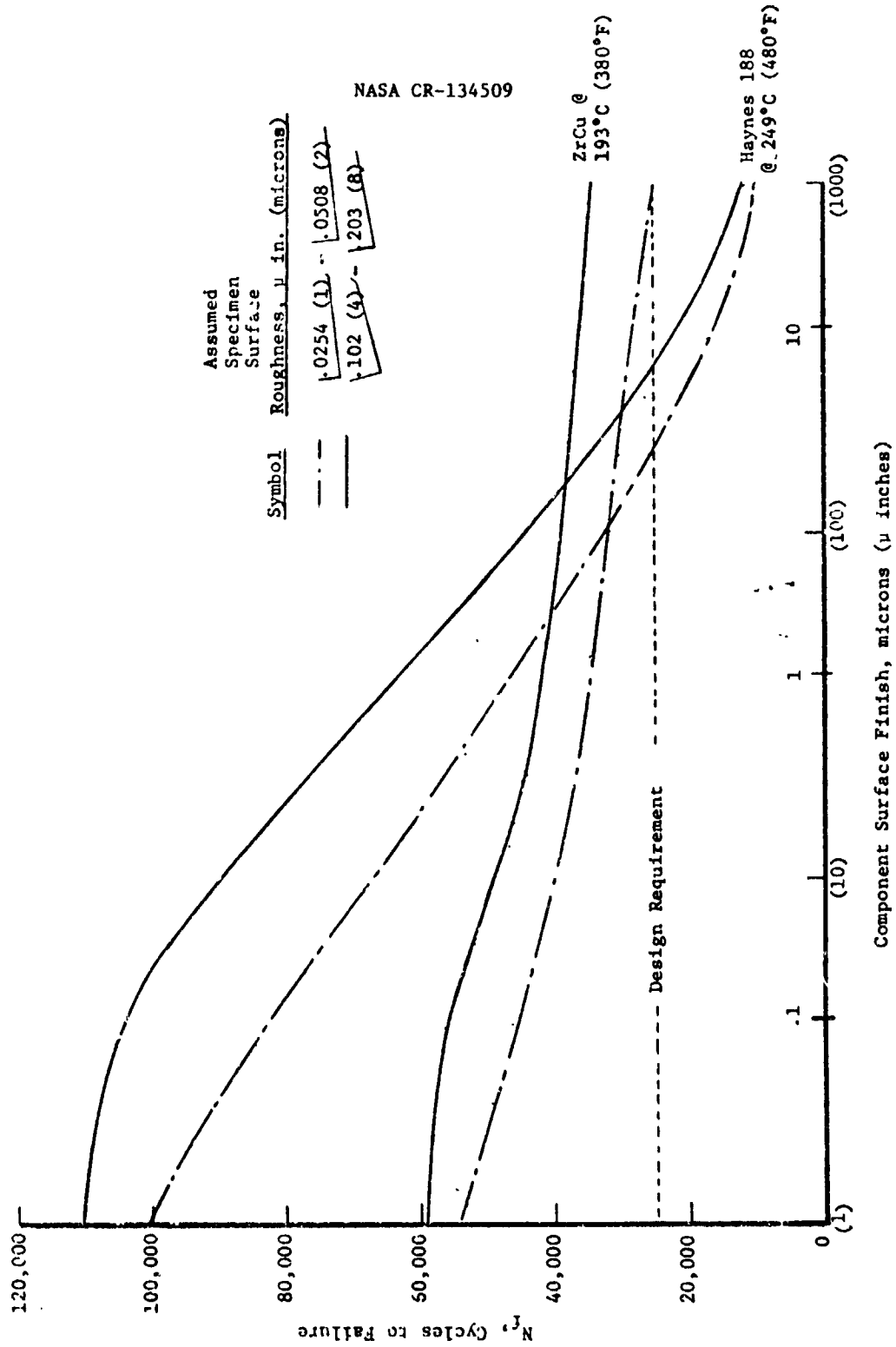
Figure 18. Effect of Surface Finish on Cycle Life

4.1, Integrated Thruster Design (cont.)

(a)   The cycle life of the ZrCu liner is not affected as much as that of the Haynes 188 nozzle because of the lower tensile strength of the ZrCu.

(b)   Both th.. ZrCu liner and the Haynes 188 nozzle would meet the 25,000 thermal cycle requirement with a 3.18 (125) surface roughness.

(c)   A surface finish of .81 (32) represents a reasonable fabrication requirement and will provide at least a factor of 2 margin (50,000 cycles) for the Hayness 188.

(d)   There is considerable margin in the design: the life cycle requirements have a safety factor of 5 built into them; the Hayness 188 and nickel S-N curves have been reduced by a factor of 10 to allow for the effect of unknowns such as hold time; the design value of cycle life including surface finish effects is in excess of the required value.

4.1.2   Igniter

The ITA capactive discharge, air gage, torch igniter consists of:

(1)   An integral exciter/spark plug

(2)   The igniter housing or body (miniature thrust chamber assembly*)

(3)   A support bracket

---

* $F = 111N$ (25 lb_f)

4.1, Integrated Thruster Design (cont.)

The following factors were considered in the design of the igniter: getting the spark in the right place (spark rate, breakdown potential, spark gap, and spark plug geometry); igniter (pressure, mixture ratio, wall temperature, spark energy, and propellant mixing); operating characteristics (structural life/cooling, electrode life, hydraulics). The design criteria are summarized in Table XVII.

4.1.2.1   Integral Exciter/Spark Plug

A spark rate of 500 sparks per second was selected as were the flow parameters in Table XVII based on the test experience obtained under Contract NAS 3-14354 (Hydrogen-Oxygen Auxiliary Propulsion for the Space Shuttle), and ALRC in-house work.

The voltage required to achieve sparking was predicted on the basis of Paschen's Law. Paschen's law defines the relationship between the voltage potential required to cause a spark to jump a given gap as a function of pressure. Figure 19 is a plot of Paschen's law (voltage - f (pressure * distance)) for air* and hydrogen. As voltage is increased on a spark plug, discharge will occur at the geometric location that satisfies Paschen's law at the lowest potential. Once the breakdown occurs, the spark discharge is maintained by a much lower potential because of the ionization created by the initial discharge.

The minimum in the Paschen's law curve (Figure 19) corresponds to a physical phenomenon that must be considered in igniter design. For pressure-distance products (P * d) greater than .00876 N/cm^2 * cm (0.005 psi * in.) (to the right of the minimum in Figure 19), the spark will always jump at the minimum gap. This simply states that, as long as the lowest pressure times the smallest gap is greater than .00875 N/cm^2 * cm (0.005 psia * in.) a larger

---

* Paschen's law plot for oxygen not available - assumed to be the same as air.

TABLE XVII

IGNITER DESIGN CRITERIA

Oxygen inlet pressure, N/cm^2 (psia)		276	(400*)
Oxygen inlet temperature, °K (°R)		208	(375)
Hydrogen inlet pressure, N/cm^2 (psia)		276	(400*)
Hydrogen temperature, °K (°R)		139	(250)
Oxygen flow rate, g/sec (lb/sec)		32.66	(0.072)

Fuel flow rate, g/sec (lb/sec)

Core	.726	(0.0016)	
Coolant	4.26	(0.0094)	
Total		4.99	(0.011)

Mixture ratio (O/F)

Core	45
Overall	6.5

Spark gap, cm (in.)	.0762	(0.030)
Spark rate, sps	500	
Spark energy, millijoules/spark	10	
Minimum ignition pressure, N/cm^2 (psia)	4.8	(7)
Maximum ignition pressure, N/cm^2 (psia)	103	(150)
Cold flow pressure, N/cm^2 (psia)	69	(100)
Igniter chamber diameter, cm (in.)	.762	(0.3)

---

* Assumes igniter valves used

PASCHEN'S LAW CURVE FOR AIR

$V_B = f(PRESSURE * DISTANCE)$
REF., INSULATION, MAR 1956
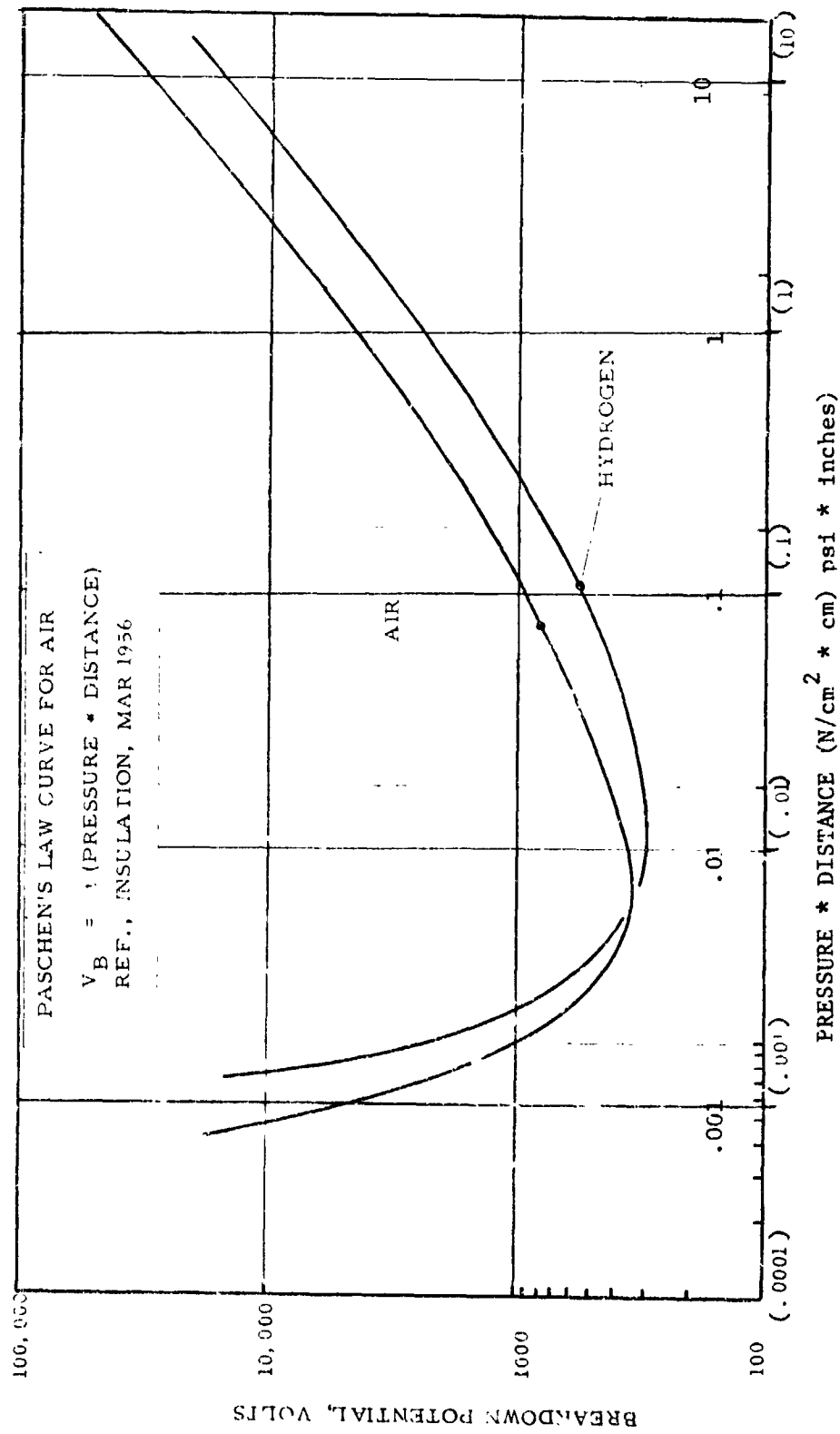
Figure 19. Paschen's Law Curves

4.1, Integrated Thruster Design (cont.)

gap will require a higher potential to cause the spark to jump. For P * d values less than .00525 (0.003) (to the left of the minimum in Figure 19), the spark will not necessarily jump at the minimum gap - it will jump at the location having the P * d closest to .00525 (0.003). At very low pressures, a long gap - not a short one - is required to satisfy Paschen's law. For example, if the pressure is .0069 N/cm^2 (0.01 psia), a .254 cm (0.1 in.) gap has a P * d = .00175 (0.001) and requires 3000 volts (Figure 19) to induce the spark to jump; a 1.02 cm (0.4 in.) gap at the same pressure has P * d = .007 (0.005) and requires only 350 volts to induce breakdown. In this example, the spark would jump at the 1.02 cm (0.4 in.) gap and not at the smaller .254 cm (0.1 in.) gap as an increasing voltage is imposed on the system.

The minimum in the Paschen's law curve for air occurs for P * d in the range of .00525 (0.003) to .00875 (0.005). The lowest pressure that will be obtained during vacuum testing will be .06895 N/cm^2 (0.1 psia). Thus, the gap must be .0762 cm (0.03) to .127 cm (0.05 in.) to obtain a minimum P * d of .00525 (0.003) to .00875 (0.005).

The gap size is also affected by exciter design. Based on the experience of Contracts NAS 3-14348 and NAS 3-14354, mentioned earlier, the exciter potential was selected at 25.000 volts, nominal (20,000 volts minimum) giving a maximum P * d of 7.88 (4.5), Figure 19). For a P * d of 7.88 (4.5), a .076 cm (0.030 in.) gap gives a maximum pressure at which breakdown will occur with 25,000 volts of 103 N/cm^2 (150 psia). A gap size of .076 cm (0.03 in.) was selected versus .127 cm (0.050 in.) as giving an equally low breakdown potential at low pressure .069 N/cm^2 (0.1 psia) and giving the greatest margin at high pressure.

In designing the spark plug, it is desired to keep the gap at the electrode small compared to other conductor-to-wall gaps and to keep the "creep distance" along the insulator long. (Deposition of conductive material on

4.1, Integrated Thruster Design (cont.)

the insulator surface with operation can result in discharge along the insulator surface.) There are no hard and fast rules for the ratio of electrode gap to the separation distance of other parts and for creep distance length. The minimum clearance, metal-to-metal, is .254 cm (0.1 in.), which is 3.3 times the electrode gap .076 cm (0.03 in.). The creep length along the electrode surface is 2.54 cm (1.0 in.).

In shaping the insulator, sharp corners were avoided. In previous programs, it was found that ceramic insulators crack at surface discontinuities.

Ignition depends on the ability to raise a small kernel of gas above the ignition temperature. Only a small portion of the electrical energy heats the gas, the remainder heats the electrode and walls. The larger the gap, the larger the kernel of gas that is heated, and thus the lower the energy requirements. Obviously, there is a conflict as a wider gap requires higher spark voltage but lower energy. The relationship between energy and spark gap is defined as:

$$Q_s D_s = K (T_{ign} - T_w)$$

where: Q_s = minimum spark discharge energy

K = constant which is dependent on O/F and the heat transfer coefficient

T_{ign} = ignition temperature

T_w = wall temperature

D_s = spark gap

Figure 20 shows the results of experimental evaluation of the above relationship. Data were obtained on an ALRC in-house program. The minimum spark energy required for the .076 cm (0.030 in.) gap is 2 millijoules. The exciter is designed to deliver 10 millijoules (Table XVII).
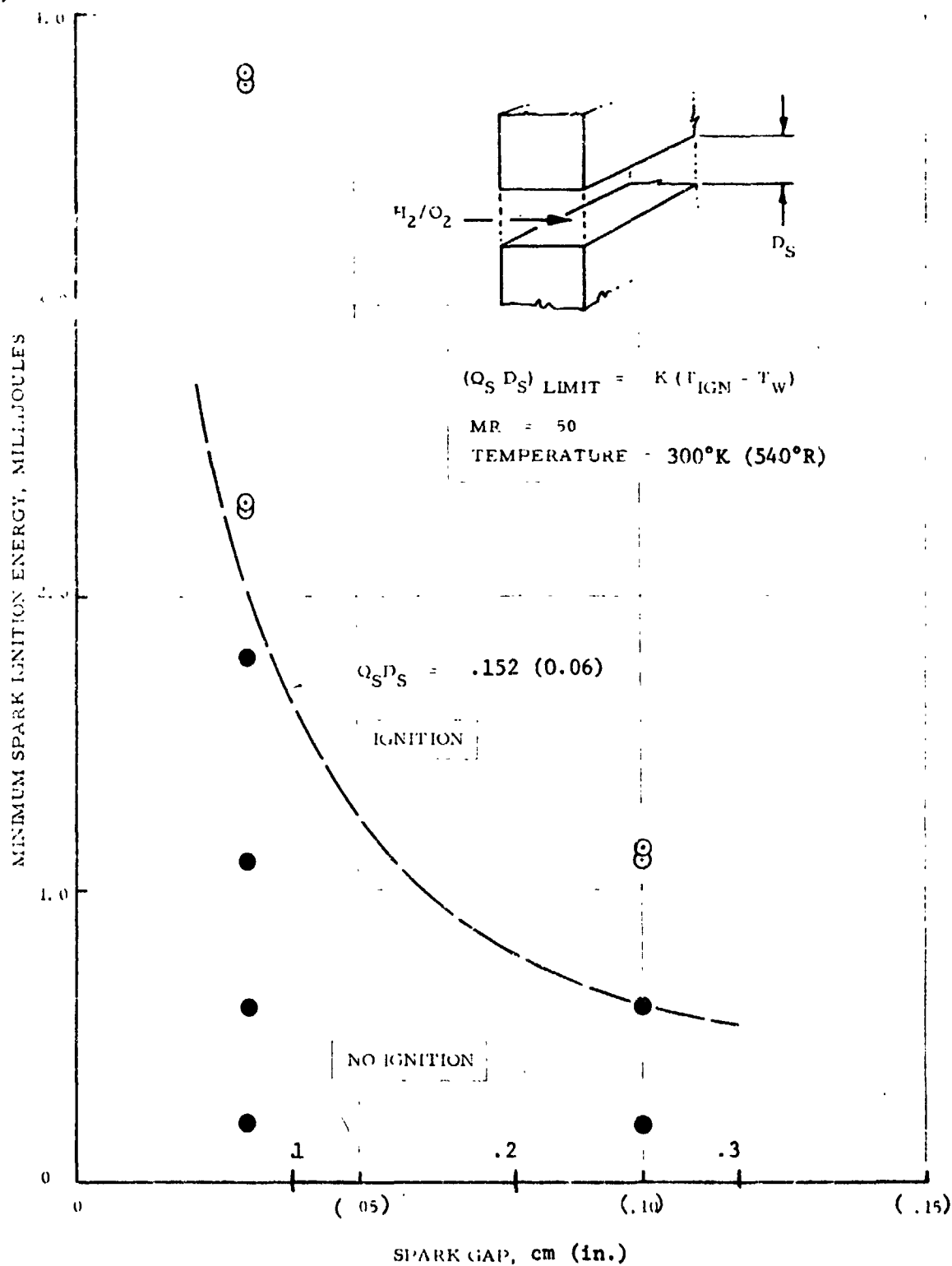
Figure 20. Effect of Spark Gap Spacing on Minimum Ignition Energy

4.1, Integrated Thruster Design (cont.)

The temperature at which ignition occurs (T_{ign}) is approximately 556° (1000°R) above the wall temperature 3000°K (540°R) at which the data were obtained. A lower wall temperature of 139°K (250°R) (approximate lower limit in GO_2 temperature) increases ($T_{ign} - T_w$) to 722°K (1300°R). The increase in $Q_s D_s$ ($\frac{1300}{1000}$) results in an energy requirement of 2.6 millijoules which is well within the 10 millijoule design value.

There is a low pressure/chamber size limit that is a consequence of flame quenching. Just as ignition cannot occur if the energy input to the kernel of gas is not sufficient to heat the gas above the ignition temperature, it cannot occur if the combination of gas density (pressure) and wall surface area are such that the heat loss exceeds the heat input, and the gas is not maintained above the ignition temperatures long enough to react.

The flame quenching parameter was defined on the FY 69 IR&D Oxygen-Hydrogen Igniter Development Program as a pressure-chamber diameter product ($P * D_c$) similar to the Paschen's law pressure-gap distance parameter. The following relationship was derived:

$$(P * D_c) = RT_o \left[\frac{4 h (T_F - T_w)}{K \Delta H_r \text{ Exp } (-E/RT_F)} \right]$$

where   P   = pressure

   D_c = chamber diameter

   R   = gas constant

   T_o = propellant temperature

   h   = heat transfer coefficient

   K   = reaction rate constant

   ΔH_r = heat of reaction

   E   = activation energy

   T_F = flame temperature

   T_w = wall temperature

The expression contains several parameters that cannot be evaluated analytically. Therefore, the quenching parameter was evaluated experimentally. Figure 21 summarizes the results.
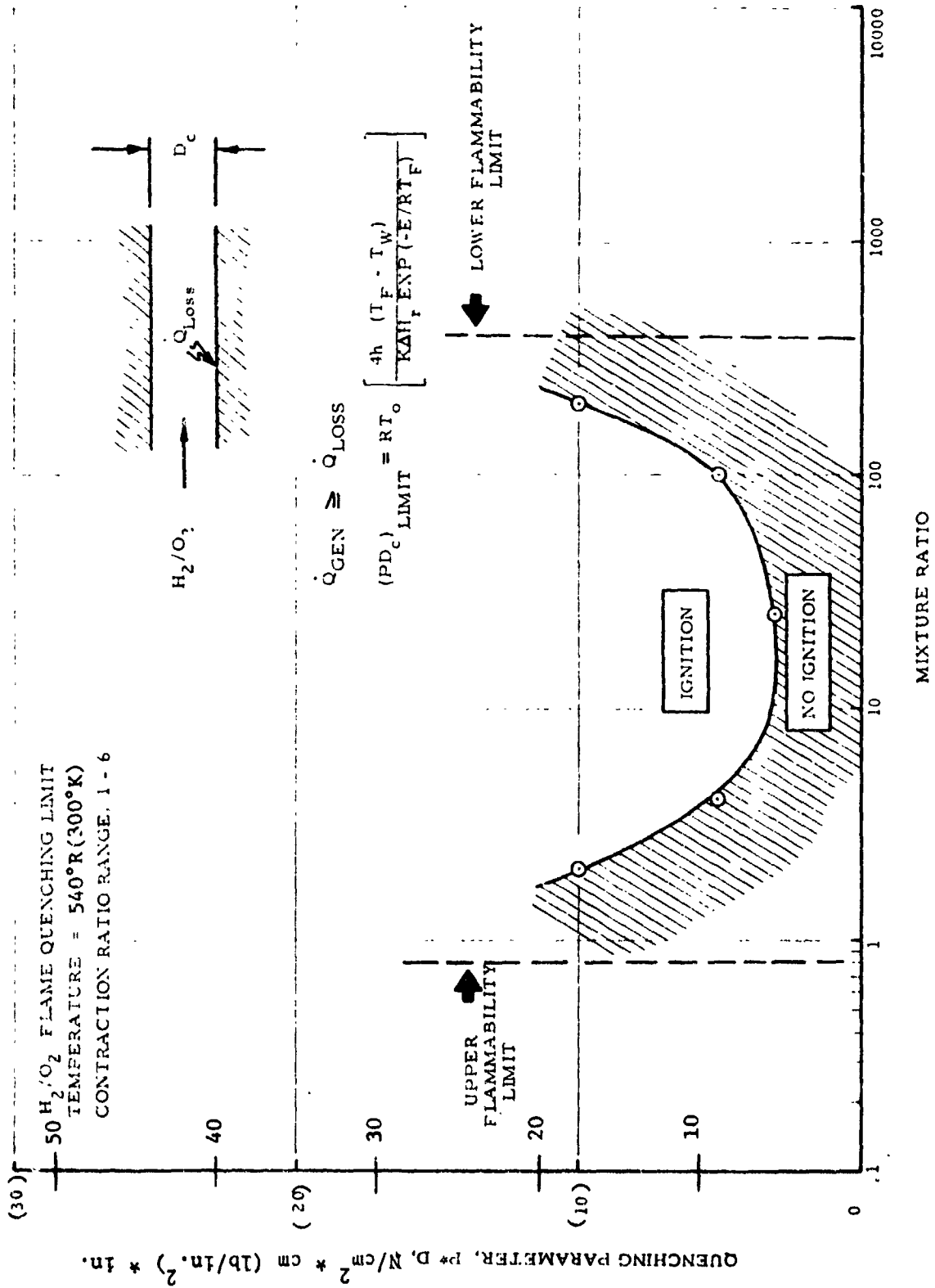
Figure 21. Effect of Mixture Ratio on Flame Quenching Parameter

4.1, Integrated Thruster Design (cont.)

The quenching parameter relationship implies that it is a direct function of propellant temperature. This has not proved to be the case experimentally as other parameters are temperatu e dependent and not only mitigate, but reverse the propellant temperature effect. The minimum value of the quenching parameter from Figure 21 is approximately 5.25 (3). Based on test results combined with computer prediction of ignition limits, a value of 8.76 (5) is generally used for cold propellants. Using the ratio (5/3) for cold propellants, Figure 21 and the relationship

$$\dot{w} \ \alpha \ \frac{P}{\sqrt{T}}$$

Table XVIII was constructed. The results indicate that the igniter will achieve a pressure above the lower flame quenching pressure limit for all conditions of propellant pressures and temperatures.

The selection of a nominal core mixture ratio of 45 results in a design which will ignite over a wide range of operating conditions and the resulting mixture ratios as shown in Table XVIII. The selection of the MR as 45 was also influenced by the effect of core mixture ratio on combustion temperature which in turn affects the wall temperatures. In this respect, the higher the MR, the cooler the walls (for the same fuel flow rate) and, therefore, the longer the igniter life (thermal cycling) over a wide range of operating conditions.

The igniter designs tested on in-house programs introduced the hydrogen through an annular gap normal to the wall. The igniter developed under Contract NAS 3-14348 and used in Contract NAS 3-14354 utilized six fuel orifices canted 45° to impinge approximately .381 cm (0 15 in.) downstream of the electrode. This design kept the flame front away from the electrode (improved electrode life) and kept the mixture ratio at the wall high (low wall temperatures). To maintain the long electrode life and long chamber life (low wall temperature) the six oxidizer orifice design was used for the ITA igniter.

TABLE XVIII

LOW PRESSURE IGNITION LIMITS

GO_2 Pressure N/cm^2 (psia)		GO_2 Temperature °K (°R)		GH_2 Pressure N/cm^2 (psia)		GH_2 Temperature °K (°R)		O/F	Low Pressure Limit N/cm^2 (psia)		Igniter Cold Flow Chamber Pressure N/cm^2 (psia)	
276	(400)	208	(375)	276	(400)	139	(250)	45	13	(19)	69	(100)
276	(400)	294	(530)	276	(400)	111	(200)	34	7.6	(11)	58	(84)
276	(400)	139	(250)	276	(400)	294	(530)	80	17	(25)	84	(122)
138	(200)	208	(375)	414	(600)	139	(250)	15	12	(17)	34	(50)
414	(600)	208	(375)	138	(200)	139	(250)	133	23	(33)	103	(150)
414	(600)	139	(250)	138	(200)	294	(530)	240	46	(67)	126	(183)
138	(200)	294	(530)	414	(600)	111	(200)	11	6.9	(10)	29	(42)

4.1, Integrated Thruster Design (cont.)

Electrode durability tests were conducted to determine the suitability of electrode materials for the spark plug electrode for extended duty cycles at igniter operating conditions as part of Contract NAS 3-14348. One million discharge pulses were run on each of the three candidate electrode materials, i.e., Inconel, Ni 200, and 347 SS. All tests were conducted with an oxygen flow of 4.54 g/sec (0.01 lb/sec) through the plug at a pressure of 69 N/cm^2 (100 psia). The discharge energy was 10 millijoules. The nominal pulse rate was 500 pulses per second on for 75 millisec and off for 275 millisec.

The Ni 200 sustained the lowest weight loss, 1.14%. The Inconel and stainless steel weight losses were slightly higher, 1.26 and 2.88%, respectively. Ni 200 appears to be the material of choice for the spark plug electrode. A complete description of the electrode durability tests is contained in Reference 1.

The factors affecting igniter design that were discussed above are summarized in Table XIX relative to the igniter design.

The design of the integral exciter/spark plug unit to the criteria given in Table XVII was subcontracted to General Laboratories Associates (GLA), a subsidiary of Simmonds Precision. GLA supplied the exciter/power supplier used for the in-house work and on Contracts NAS 3-14348 and NAS 3-14354.

4.1.2.2   Igniter Body (Housing)

4.1.2.2.1   Mechanical Design

The igniter housing is shown in Figure 22. This assembly is inserted in the center hole of the injector and secured against a crush gasket (seal) by six bolts. The igniter assembly is completed with another crush gasket and the spark plug/exciter assembly which is secured in the center of the igniter by an externally threaded slip nut.

TABLE XIX

SUMMARY OF FACTORS INFLUENCING IGNITER DESIGN

Factor	Design Value	Criterion
Spark Rate	500 sps	Used on Contract NAS 3-14354.
Potential	25,000 volts	(1) Provides ignition with .0762 cm (.030 in.) gap to pressure of 103 N/cm^2 (150 psia). (2) Recommended per in-house test experience.
Spark Gap	.0762 cm (0.030 in.)	(1) Recommended on basis of Contract NAS 3-14354 testing. (2) Provides 103 N/cm^2 (150 psia) upper limit pressure with 25,000 volts. (3) Results in lowest possible break down potential (350 volts) at electrode during vacuum p = .069 N/cm^2 (.1 psia) testing (P * d = .00525 (0.003)).
Spark Plug Geometry	Gap spacing: Min clearance = .254 cm (0.1 in.) Creep length = 2.54 cm (1.0 in.)	No hard-and-fast criteria. The smaller the gap relative to the next smallest anode to cathode gap the better. The longer the creep length the better.
Chamber Diameter	.762 cm (0.30 in.)	With this diameter the igniter cold flow pressure exceeds the low pressure limit required for ignition for all operating conditions (propellant temperature, pressure and MR).
Fuel Orifices	6 - .0368 cm (.0145 in.) dia. Canted 45°	(1) Control flow split between core and coolant. (2) Six canted 45° used on Contract NAS 3-14354. (3) Maintains momentum (avoid hot streak on chamber). (4) Impingement at center of chamber .381 cm (0.15 in.) below electrode (electrode life).

TABLE XIX (CONT.)

Factor	Design Value	Criterion
Electrode Material	Ni 200/201	Electrode life.
Mixture Ratio	45	(1) Chamber life improves with higher MR°.
		(2) MR near 20 results in low quenching parameter (Fig. 21).
		(3) Ignition over wide range of operating conditions (Table XVIII).
Energy	10 millijoules	(1) Minimum energy requirement is 2.6 millijoules.
		(2) 10 millijoules recommended on the basis of test experience on in-house programs and Contract NAS 3-14354.

Figure 22. Igniter Housing, Machined

4.1, Integrated Thruster Design (cont.)

The igniter is not a complete assembly by itself. The igniter cooling channels are formed by slots in the exterior of the igniter chamber (slots shown in Figure 23) and the I.D. of the injector outer hole. The fuel manifold is an annulus formed by the space between the igniter assembly and the injector center bore. The igniter fuel supply is introduced via a tube welded to the injector.

Details of the igniter housing assembly are shown in Figure 23. The igniter assembly is made from three components: flange, body and sleeve. The three components are joined by brazing.

The function of the sleeve is control of the hydrogen coolant flow. The sleeve blocks off the inlet to the coolant passages. Twelve orifices in the sleeve meter the flow to each coolant slot. The size of these orifices relative to the size of the orifices that meter the hydrogen to the igniter core determines the split of the fuel flow between the core (combustion) and coolant passages. On the basis of cold flow testing of the igniter, the 12 orifices in the sleeve were resized to .047 cm (.0185 in.) diameter and the six core orifices were resized to .037 cm (.0145 in.) diameter (see Section 4.3.2.1) from that shown in Figure 23.

4.1.2.2.2 Thermal Design

The igniter wall, made of Nickel-201, is cooled with gaseous hydrogen flowing through slotted channels. This section discusses the analyses conducted to determine the coolant channel design. The following igniter operating parameters were used for this study:
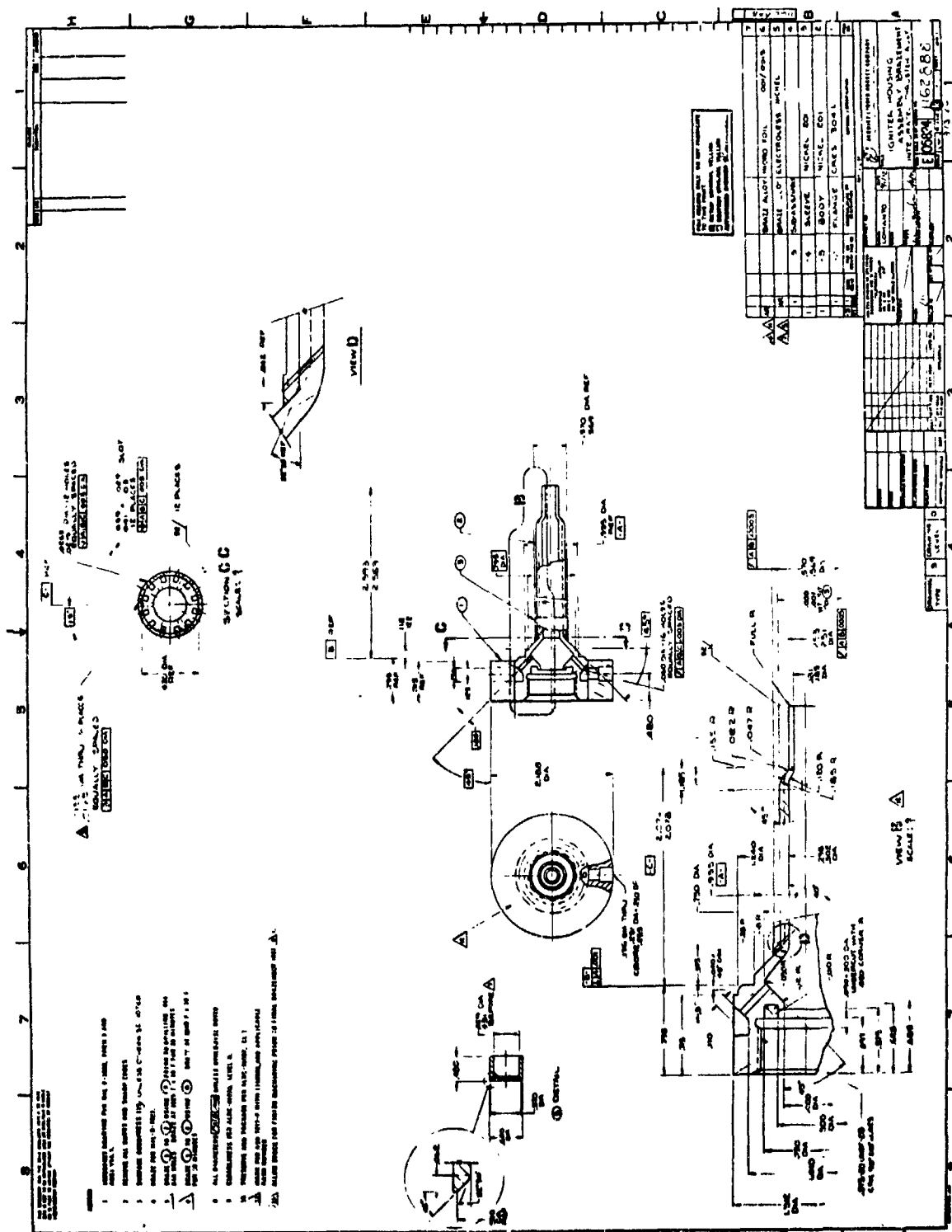
Figure 23. Igniter Housing Assembly – Brazement

4.1, Integrated Thruster Design (cont.)

Nominal Design

Thrust	111 N (25 lb)
Chamber Pressure	207 N/cm^2 (300 psia)
Mixture Ratio (core)	45.0
Mixture Ratio (overall)	6.5
Total Propellant Flow Rate	37.6 g/sec (0.083 lb/sec)
Coolant Flow Rate	4.26 g/sec (0.0094 lb/sec)
Fuel Inlet Temperature	139°K (250°F)
Fuel Inlet Pressure	276 N/cm^2 (400 psia)
Oxidizer Inlet Temperature	208°K (375°F)
Oxidizer Inlet Pressure	276 N/cm^2 (400 psia)

Igniter coolant channels were analyzed using the ALRC HEAT II computer program to determine the coolant channel design required to satisfy the nominal maximum wall temperature 538°C (1000°F) in the chamber. A two-dimensional heat transfer analysis was also conducted using the HT1U computer program (Reference 6) to obtain thermal gradients across the igniter wall. Primary emphasis of this study was concentrated in the chamber section because of the larger temperature gradients caused by the slotted channels; however, the throat temperatures were not ignored.

A cross-sectional temperature profile for the nominal conditions is shown in Figure 24 for the most limiting axial location. The temperatures vary from 466°C (870°F) on the hot-gas surface to a minimum backside temperature of 349°C (660°F); the temperature difference (ΔT) is 117°C (210°F). The analysis of the off-nominal condition predicts the gas-side wall temperature to be 544°C (1012°F) and the maximum ΔT to be 152°C (274°F) This increase in wall temperature and ΔT was primarily caused by the increase in combustion temperature from 2194°K (3950°R) to 2564°K (4615°R) as the core mixture ratio decreased from 45 to 33. The temperatures for the off-nominal case represent the most severe thermal conditions anticipated based upon the highest anticipated oxidizer inlet temperatures with the lowest fuel inlet temperatures.

NOTE:

1. P_c = 207 N/cm^2 (300 psia)

   MR (core) = 45

2. Fuel: T_{in} = 139°K (250°R)

3. Coolant Channel:

   Width: .102 cm (0.040 in.)
   Height: .076 cm (0.035 in.)

4. Gas-Side Wall: .089 cm (0.035 in.)

Model

Igniter Cross Section

Coolant
(0.7°F)
-17°C

(660)
349

(680)
360

(700)
371

(720)
382

(730)
388

(740)
393

(750)
399

(775)
413

(80g)
427

(850)
454

(870)
46

Hot Gas
1790°C (3255°F)

Not to Scale
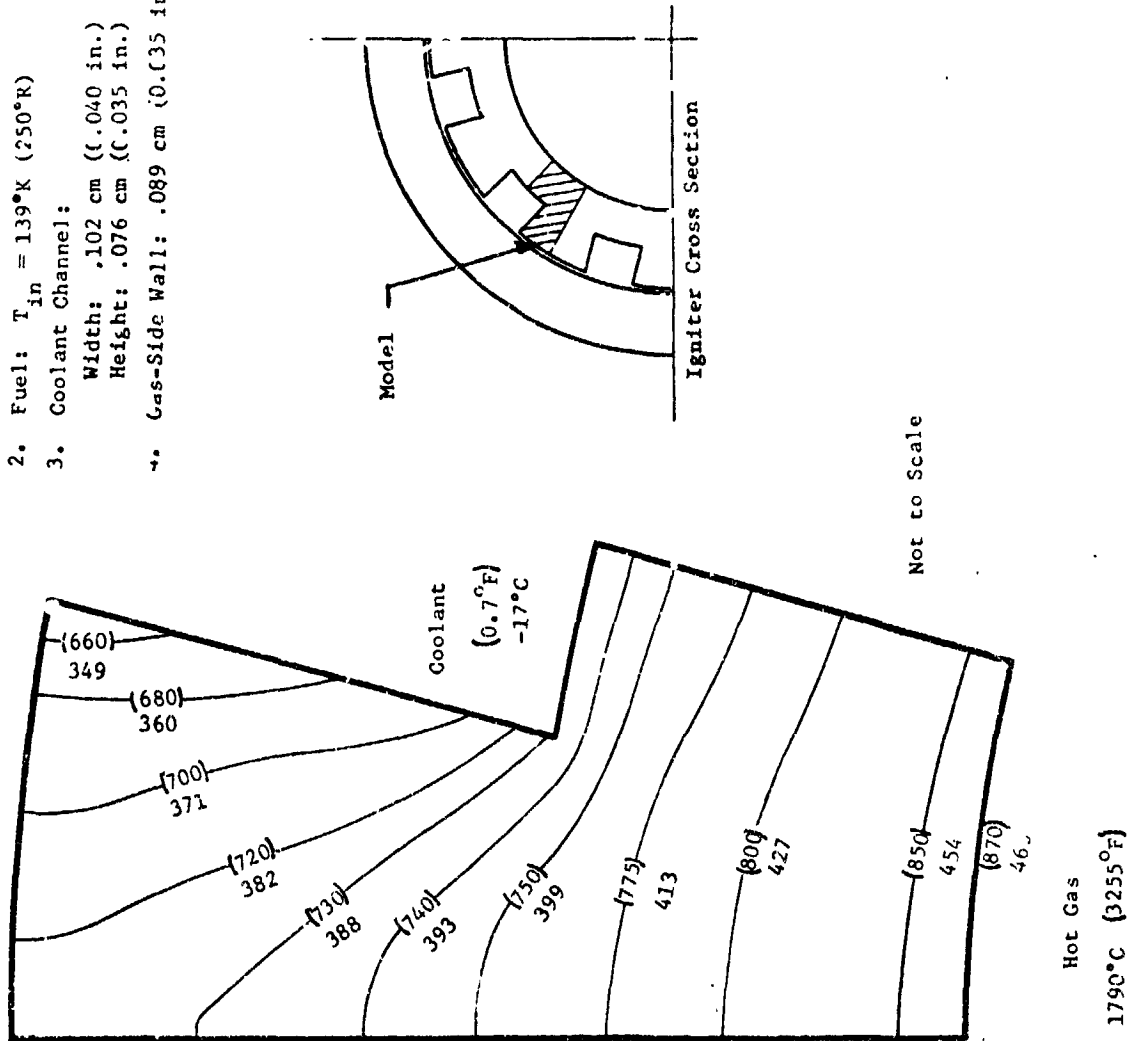
Figure 24. ITA Igniter Coolant Channel Thermal Model Nominal Design

4.1, Integrated Thruster Design (cont.)

The Nickel 201 igniter wall is cooled with gaseous hydrogen flowing through 12 slotted channels in the chamber section; the throat section has annular coolant passages. The following channel dimensions with the corresponding heat transfer results summarizes the results of this study.

Nominal Design
Chamber Section

Number of Channels	12
Channel Height	.076 cm (0.030 in.)
Channel Width	.102 cm (0.040 in.)
Gas-Side Wall Thickness	.089 cm (0.035 in.)
Coolant	GH_2
Gas-Side Wall Temperature (chamber)	466°C (870°F)
Coolant-Side Wall Temperature (chamber)	349°C (660°F)
Wall ΔT	117°C (210°F)
Coolant Temperature Rise	161°C (321°F)
Coolant Pressure Drop	17 N/cm^2 (25 psia)

4.1.2.2.3 Structural Fatigue Life Analysis

The temperature gradients shown in Figure 25 were used for this study. The cycles to failure characteristics for Nickel-201 at 538°C (1000°F) were calculated and plotted versus percent strain as shown in Figure 25. A lower bound curve which approximately represents the inclusion of duration hold time, is also shown and was selected by reducing the upper curve by a factor of ten.

Strain on the slotted wall was calculated using the following equation:

NOTE:

1. Mat'l Ref.: Huntington Nickel Alloys Catalogue

2. $\Delta G_t = \dfrac{3.5\sigma_u}{E} N_f^{-0.12} + D^{0.6} N_f^{-0.6}$

   Ref. S.S. Manson, Exp. Mechs. 1965
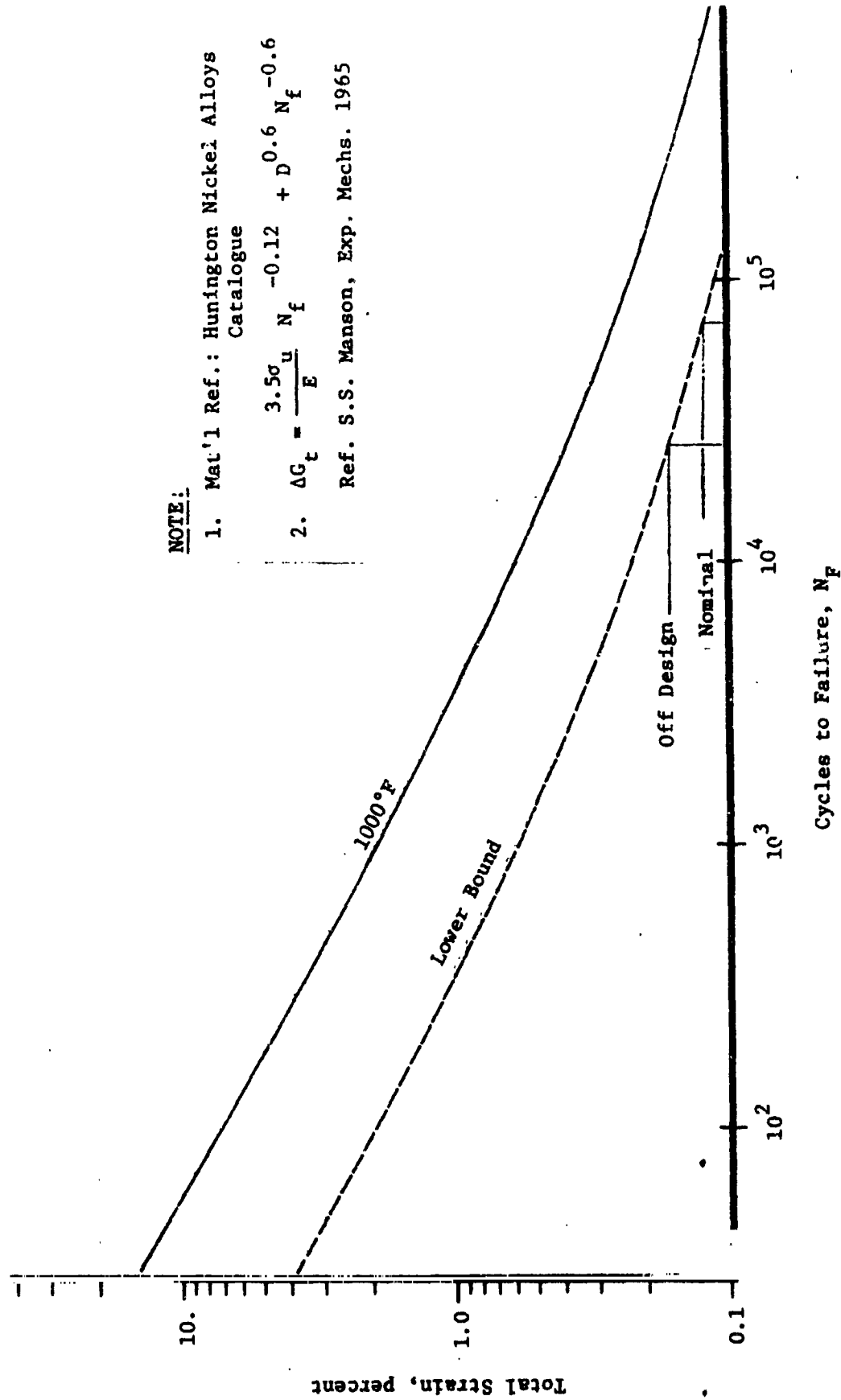
Figure 25. Fatigue Life of Nickel 201 at 1000°F (538°C)

4.1, Integrated Thruster Design (cont.)

$$S = \frac{1/2 \quad \alpha \quad T}{(1 - \nu)}$$

where:
                                                    Nickel-201

    α = Coefficient of thermal expansion 15.1×10^{-6} cm/cm-°C (8.4×10^{-6} in/in-°F)

    ν = Poisson Ratio   0.281

A tabulation of the calculated strain in percent and the corresponding predicted structural fatigue life is shown below.

	ΔT, °C (°F)		Strain, %	Fatigue Life Cycle Lower Bound
Nominal Design	117	(210)	0.123	60,000
Off-Design	152	(274)	0.16	26,000

The fatigue life cycle tabulated above are conservative because test data from Contract NAS 3-14354 (Reference 3) indicated that the actual test data were lower than the predicted wall temperature.

The following conclusions were drawn from this study:

(1)   The Nickel-201 slotted chamber wall maximum temperatures at the nominal design conditions is 466°C (870°F).

(2)   The minimum predicted structural fatigue life cycle for the nominal and off-design conditions are conservatively 60,000 and 26,000 cycles, respectively.

(3)   These temperature gradients and fatigue life cycle values are conservative and all thermal and structural requirements are satisfied.

4.1, Integrated Thruster Design (cont.)

4.1.2.2.4   Hydraulic Analysis

The hydraulic analyses were conducted to determine system pressure drops, to determine cold flow characteristics and to evaluate the effect of varying backpressure on igniter flow rates and mixture ratio; the back-pressure at the main engine injector face varies from 0 to 207 N/cm^2 (0 to 300 psia).

Two different basic methods of analysis were used depending upon the existence or nonexistence of backpressure. In the case of zero backpressure, a normal sonic compressible flow equation was used to calculate flow rates. Appropriate Rayleigh and Fanno line relations were employed where pressure losses were significantly influenced by heat additional and frictional losses. For the case of back subsonic compressible flow relationships were used.

Igniter flow distributions and pressure schedules were calculated for steady-state modes of operation of: flow without ignition (cold flow); igniter lit but mainstage not operating (zero backpressure); both igniter and mainstage operating. The results are summarized schematically in Figure 26. The "Mainstage" P_c is the backpressure to the igniter and to the coolant circuit. The mixture ratio (O/F) listed in Figure 26 under the mainstage heading is the overall igniter (core plus coolant) mixture ratio as it discharges to the mainstage, not the mainstage mixture ratio.

4.1.3   Injector

4.1.3.1   Mechanical Design

The injector assembly is shown in Figure 27 and consists of: a cover, body flange, two distribution plates, (called baffles in Figure 27),
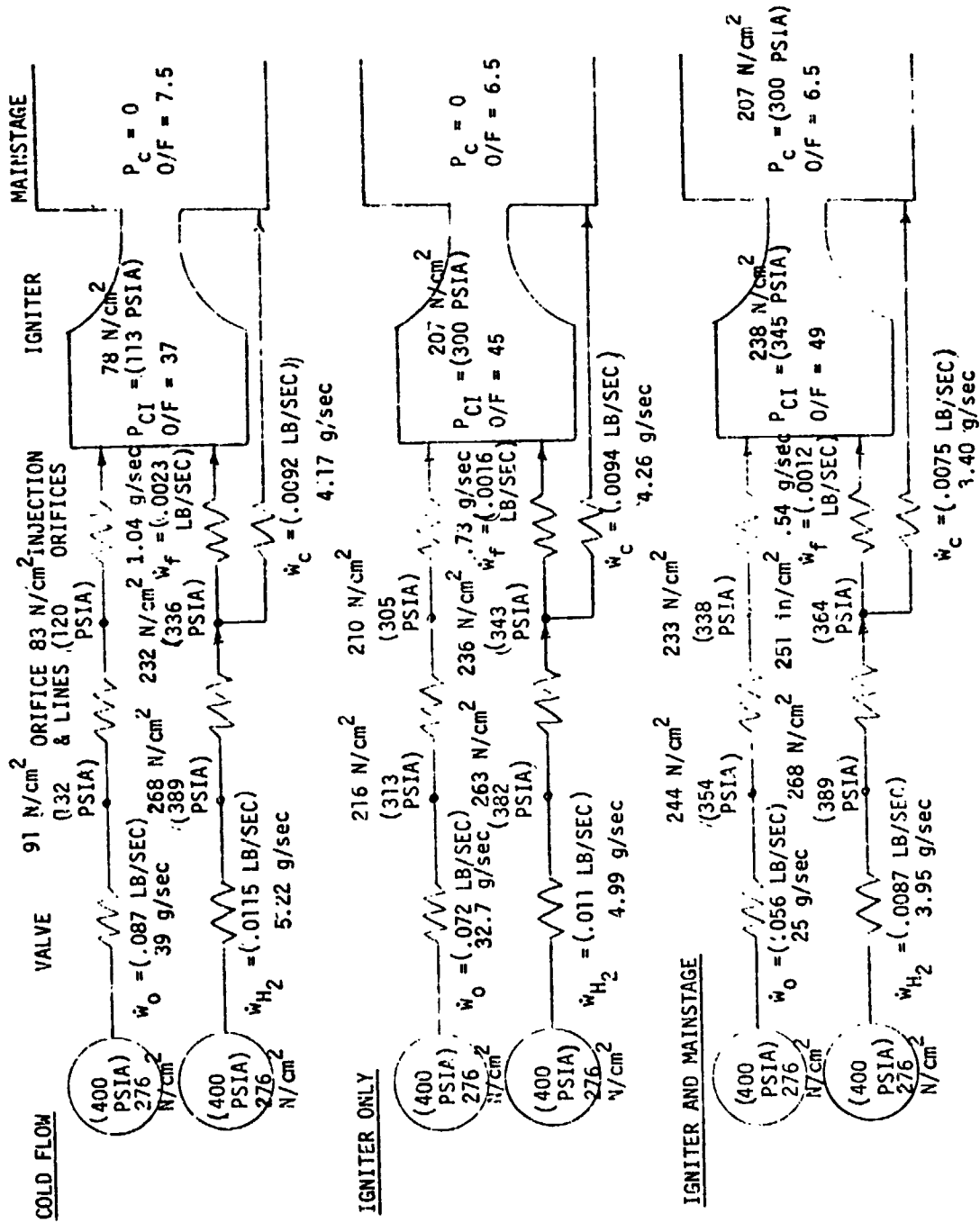
Figure 26. Igniter Hydraulics

Figure 27. Injector Assembly – Integrated Thruster Assembly

4.1, Integrated Thruster Design (cont.)

spacers, center spud (boss), oxidizer tube elements, face plate, and fuel platelet
assembly. The fuel platelet assembly is composed of platelet items 9 through 14
in Figure 27.

The cover forms the oxidizer manifold. The oxygen flows
from the inlet tube peripherally around the manifold and towards the center of the
injector. It then flows aft in the annular space between the center spud and the
center hole in the top distribution plate. The oxygen then flows radially outward
between the two distribution plates, makes a 180° turn at low velocity, and flows
radially inward to the 72 oxidizer elements between the distribution plate and
flange plate.

The oxidizer elements are tubes with a long ℓ/d orifice
located about midpoint. The oxygen velocity in the orifice is the highest in the
oxidizer flow circuit ($\sim$80 m/sec). The larger diameter inlet to each tube acts
as a flow straightener and the outlet section as a diffuser. These elements are
an important feature of the design. The tubes provide pressure drop, but low
injection velocity.

The next highest oxygen velocity in the oxidizer cir-
cuit, 40 m/sec, occurs at the inlet to the distribution plates. Because of the
radial flow outward, the flow is decelerated from the inlet. The velocity at the
turn and across the face is about 17 m/sec. The function of the diffuser plates
is to provide uniform radial flow to the elements.

The injector flange plate is shown in Figure 28. This
figure illustrates the one piece construction of the thrust takeout mounts (3 places)
and the attachment tabs for the two valves which are integral with the injector body.

The injector center stud (igniter housing), flange plate
(Figure 28), face plate and oxidizer tube elements are brazed together to form a
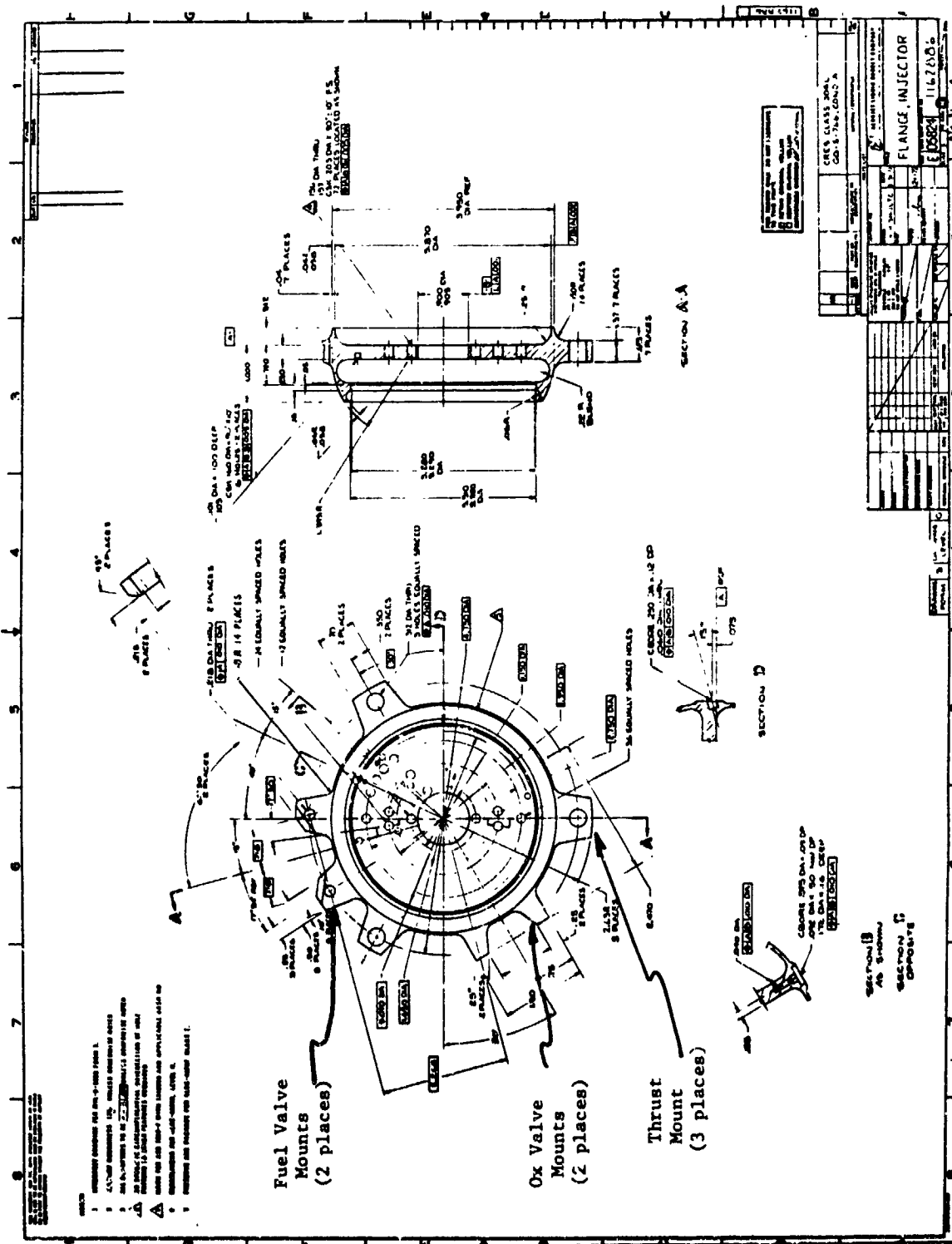
Figure 28. Flange, Injector

Fuel Valve
Mounts
(2 places)

Ox Valve
Mounts
(2 places)

Thrust
Mount
(3 places)

4.1, Integrated Thruster Design (cont.)

subassembly as shown in Figure 29. The fuel platelets are bonded to this sub-
assembly, the diffuser plates welded in place and the cover attached by welding.

The fuel platelet assembly contains the fuel injection
elements and face cooling passages, and forms a shallow mixing cup. The fuel mani-
fold is the area between the injector body flange and the face plate.

The oxidizer elements and fuel injection and face
coolant passages are very similar to the SN 006 and SN 007 designs tested on Con-
tract NAS 3-14354. The oxidizer flow distribution method is the same. The only
significant changes have been made to the dome, flanges and body to reduce weight
and improve cycle life. The volume of the oxidizer manifold was reduced to 268 cc
(16.3 in.^{3}) to obtain good performance at the Minimum Impulse Bit (MIB). Further
reduction of the oxidizer manifold volume would have increased the pressure drop,
and both increased and altered the velocity distribution which could adversely
offset flow uniformity. The current injector was designed to have the same pressure
drop and flow uniformity characteristics as its workhorse predecessor.

The distribution (or diffuser) plates in the workhorse
hardware (Contract NAS 3-14354) collapsed (Figure 30) following oxidizer over-
pressure spikes during pulsing operation that resulted in manifold pressure of
445 N/cm^2 (645 psia). The distribution plates in the current design are 8.5 times
stronger than the workhorse design and will withstand pressure differentials re-
sulting from pressure drops caused by flow rates that would result with oxidizer
manifold pressures as high as the proof pressure, 604 N/cm^2 (875 psia).

Ribs were added to the exterior of the injector dome
at the inlet to improve the structural integrity. The support provided by the ribs
results in the ribs, in effect, structurally replacing the material that was re-
moved for the inlet.

Figure 29. Body, Injector
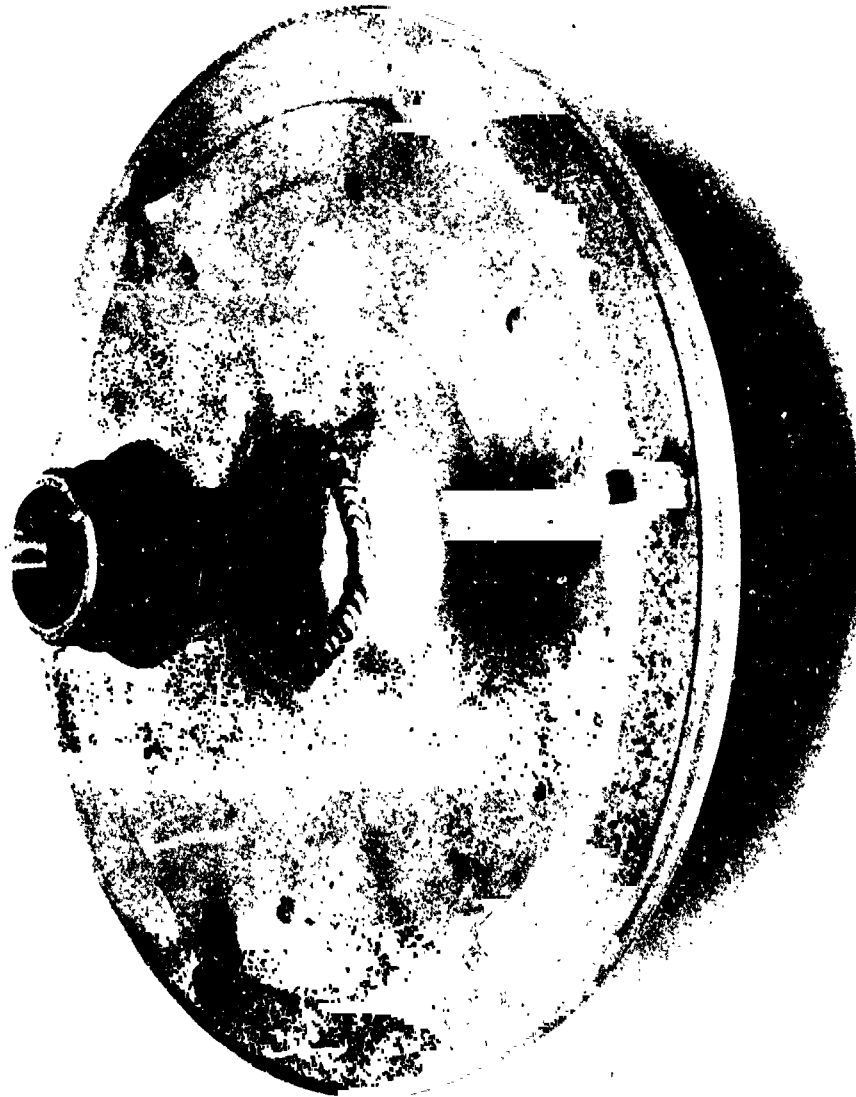
Figure 30. Collapsed Distribution Plate

4.1, Integrated Thruster Design (cont.)

There are three bosses in the injector flange to provide for measurement of the injector fuel and oxidizer manifold pressures and to provide an agress for the injector thermocouples.

4.1.3.2   Thermal Design

Measurements of the injector face temperatures were made on Contract NAS 3-14354 during test firings. Some of the measured steady-state temperatures are shown in Figure 31. The top figure shows the steady-state temperature versus core mixture ratio at nominal pressures and ambient propellant temperatures. The injector face temperature is nearly insensitive to mixture ratio. The two lower curves in Figure 31 show the influence of fuel supply temperature and chamber pressure on injector face temperatures. The dependency of injector face temperature on fuel inlet temperature is approximately one to one; i.e., a one-degree rise in fuel temperature results in a one-degree rise in face temperature. The effect of chamber pressure on injector face temperature is a second order effect with temperatures tending to drop as the chamber pressure is increased.

Review of the injector face steady state temperature data results in the following conclusions:

(1)   The data from Contract NAS 3-14354 are applicable to the injector to be used on this program because the design of the elements is identical.

(2)   The injector face temperature is not sensitive to MR variations.

(3)   The face cooling is not sensitive to P_c; the trend is toward lower temperatures at higher P_c.

(4)   Face temperatures are proportional to fuel supply temperatures.

MIXTURE RATIO EFFECTS

Core Mixture ratio

CHAMBER PRESSURE EFFECTS

Propellant Temperature

Ambient

Cold

Chamber Pressure, psia

PROPELLANT INLET TEMPERATURE EFFECTS

$P_c = 207 \ N/cm^2$ (300 psia)
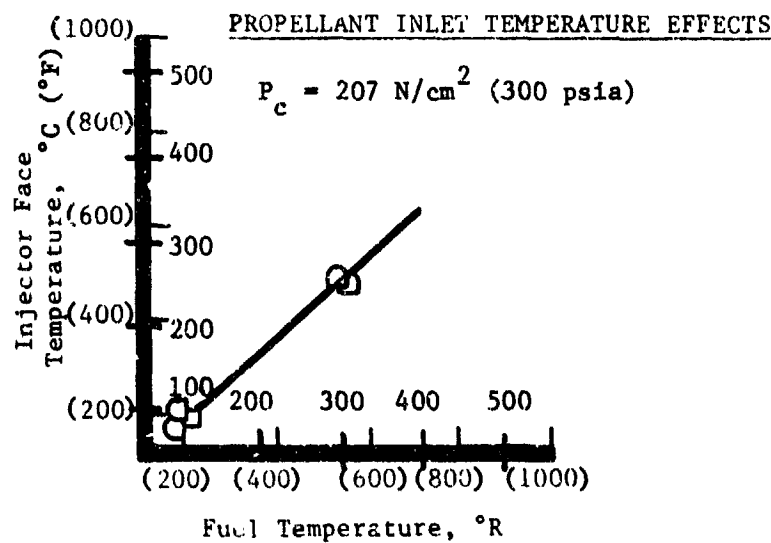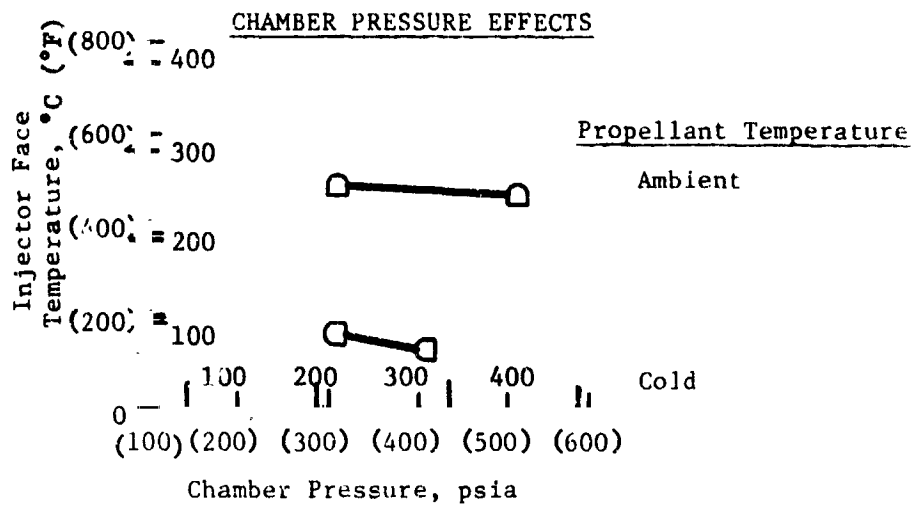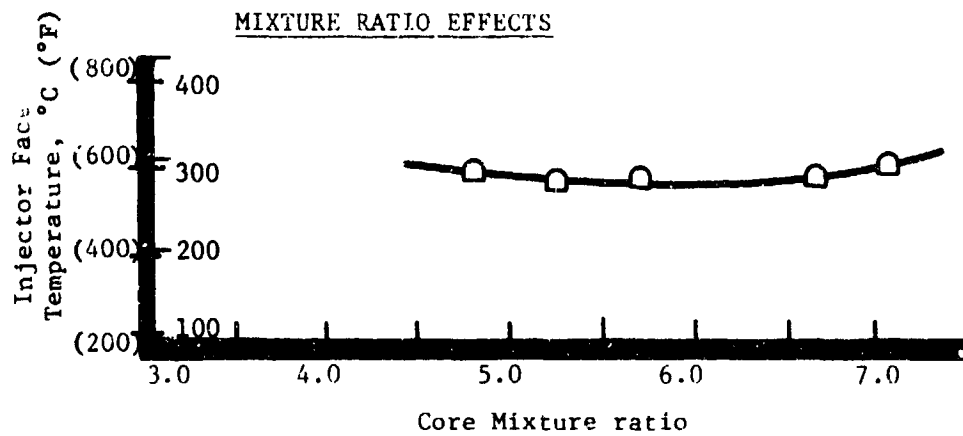
Fuel Temperature, °R

Figure 31. Predicted Steady State Injector Face Temperature

4.1, Integrated Thruster Design (cont.)

The injector thermal transient data are important in establishing injector cycle life. ITA predictions were based on Contract NAS 3-14354 pulse firing data. Typically, the premix injector face reaches 75% of its steady-state operating temperature in approximately 0.2 sec from the mainstage ignition. Short firings, therefore, do not constitute a full thermal cycle. Following shutdown, the injector face does not immediately return to its initial temperature. Face temperatures rise about 222°C (400°F) on the long firing and experience a 111°C (200°F) drop on shutdown. Actual pulse testing showed that in a subsequent firing, the face temperature increases by 111°C (200°F) to the steady-state value. Life is therefore duty-cycle sensitive. Another test variable identified by these data is the effect of valve sequencing and manifold venting at shutdown and its influence on injector face temperatures during this period. Several of the face temperature trances were noted to rise 28 (50) to 56°C (100°F) following the valve closure. Valve sequencing was found to influence the magnitude of the postfire thermal rise and, thus, eventually the life. These specific data are covered in detail in Reference (3).

4.1.3.3 Structural Life

The cycle life of the injector was predicted using measured face temperatures as input parameters to drive appropriate injector face thermal and structural models (see Figure 32). The thermally induced strain levels within the injector face were calculated and cycle life then predicted based on the appropriate material strain-cycle life properties. Details are presented in Reference (3) and are not repeated here. The design of the ITA face plate and of the nickel platelets bonded to the face plate is identical to that of the NAS 3-14354 SN 006 and SN 007 injectors.

The $S-N_f$ curve that was used in the life cycle analysis is shown in Figure 33. Also shown in Figure 33 is a plot of cycles to failure

Figure 32. Injector Face Temperature Profiles and Heat Flux
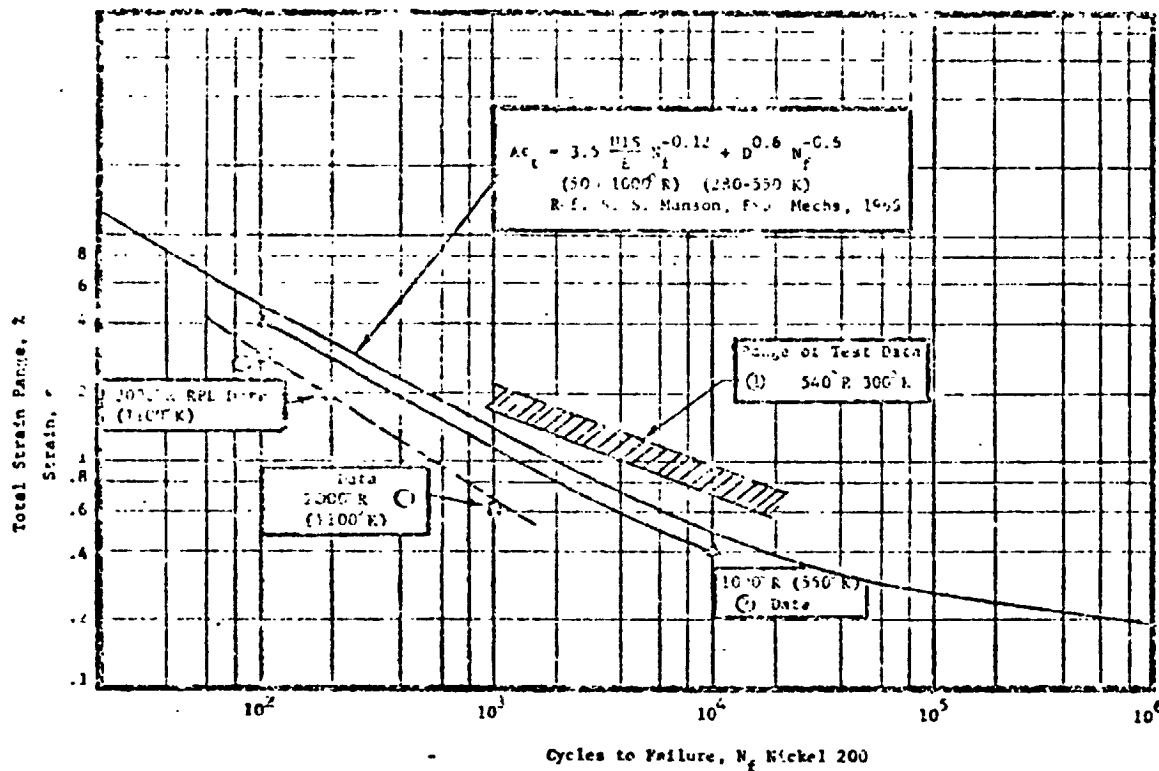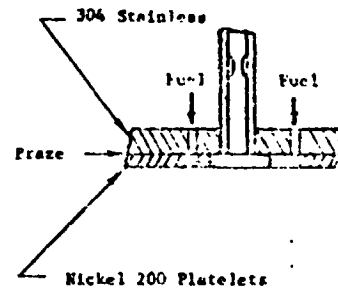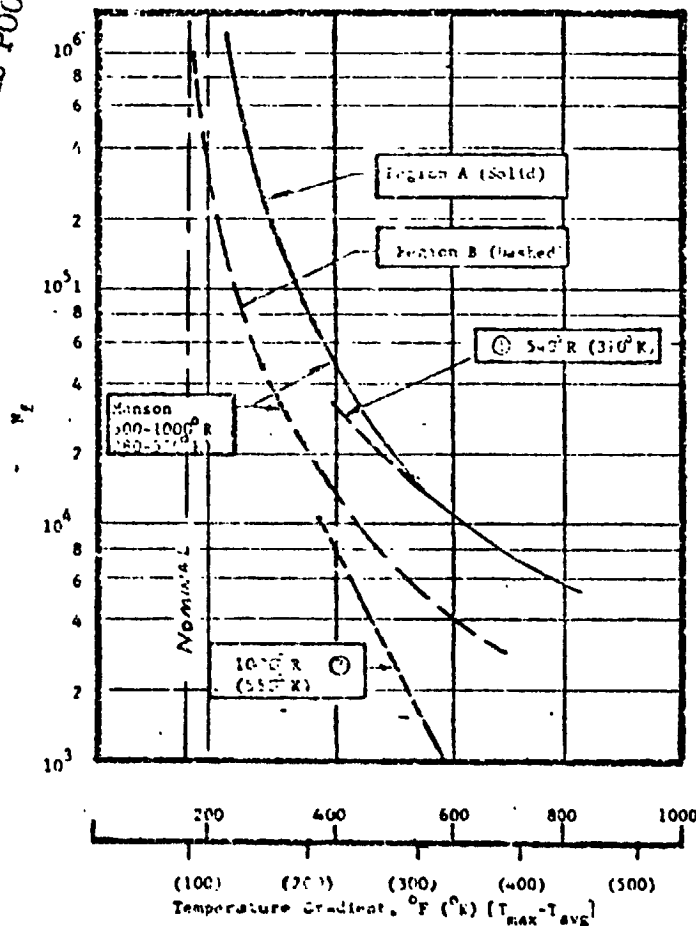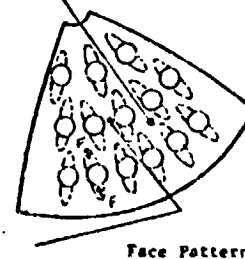
Figure 33. Premix Injector Thermal Strain vs Fatigue Life

4.1, Integrated Thruster Design (cont.)

versus temperature gradient for two locations on the injector face. The nominal ΔT results in a cycle life of 10^6 cycles at more limiting location.

Definition of the injector life under off-design and transient operation is provided in Figure 34, which is based on the temperature data obtained through extensive testing of the Contract NAS 3-14354 SN 7 unit. Several curves of life versus firing duration are indicated in the lower portion of this figure. The life for nominal pressures, mixture ratios, and optimum valve sequencing is greater than 10^6 thermal cycles for all anticipated propellant supply temperatures. The maximum gradient is influenced slightly by off-mixture ratio and higher pressure starts. This off-design sensitivity is shown by the scatter of steady-state data on the ΔT versus plot provided mid-page of Figure 34. The sensitivity of +31°C (55°F) to -25°C (-45°F) covers the deviation of data at all pressures, mixture ratios and surface locations from the average of the surface temperatures at a nominal mixture ratio of 4.0. It was mentioned in the previous section that the shutdown transient affected face temperature. This is shown as the top insert in Figure 34. The delay in fuel valve closing causes the fuel to react with the oxygen venting down from the oxidizer manifold. The oxidizer vents more slowly than the fuel. The low injection velocities moves the flame front closer to the face.

Based on these results, the design is predicted to be suitable for the following:

- More than 1,000,000 full thermal cycles at nominal conditions.

- 100,000 full thermal cycles at the most severe off-design conditions

- 1,000,000 pulses at the most severe off-nominal conditions for pulse widths up to 0.12 sec.
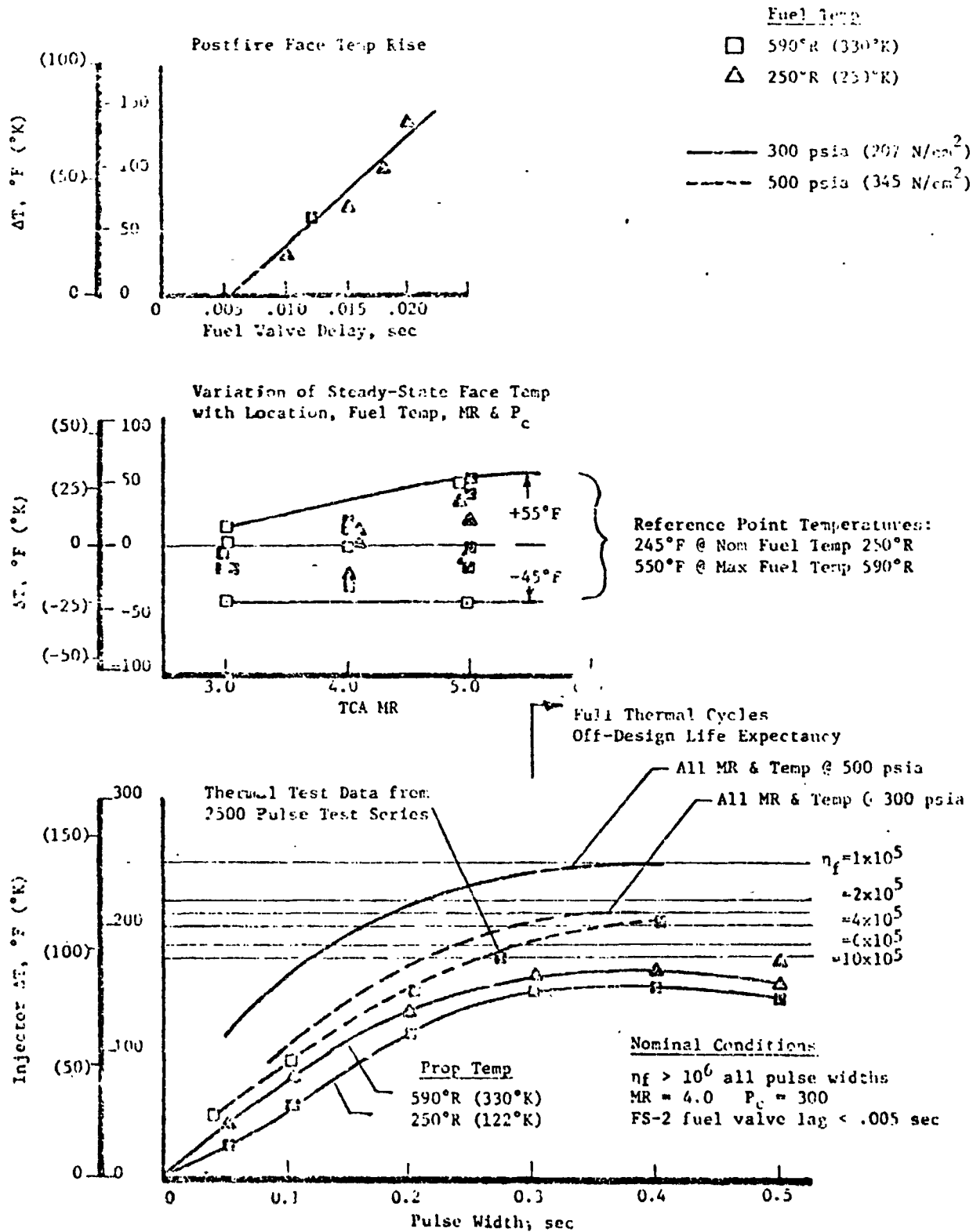
Figure 34. Predicted Life of Modified Premix "I" Injector

4.1, Integrated Thruster Design (cont.)

4.1.4   Thrust Chamber

The thrust chamber design is based on the regen-film cooled chamber tested on Contract NAS 3-14354. Performance, cooling and temperature design conditions are the same. Materials, weldment to the injector and fuel torus have been changed to reduce weight and improve structural life. The most significant design change, other than welding the injector to the chamber, is the use of a single fuel torus. The Contract NAS 3-14354 chamber controlled film coolant separately so that it could be investigated independently.

4.1.4.1   Mechanical Design

The chamber and nozzle assembly are shown in Figure 35, and is made from five components: nozzle, throat section, she l, liner and torus. The design is summarized in Table XX.

The zirconium copper liner is shown in Figure 36 after the coolant slots have been machined in the exterior. This figure provides details of the coolant passage geometry. View B (Figure 36) illustrates the geometrical configuration at the inception of the slots. The overlap of the film coolant slot into the land between regen slots avoids a rigid girdle of unmachined material under the torus.

Figure 37 shows the chamber after weldment of the throat section to the shell, brazing of the liner in place, machining of the liner and machining of the fuel orifices and inlets. One-half of the fuel torus is integral to the shell. The torus is completed by assembling the outer half of the torus (shown in Figure 38) to the shell-half and welding circumferentially fore and aft.
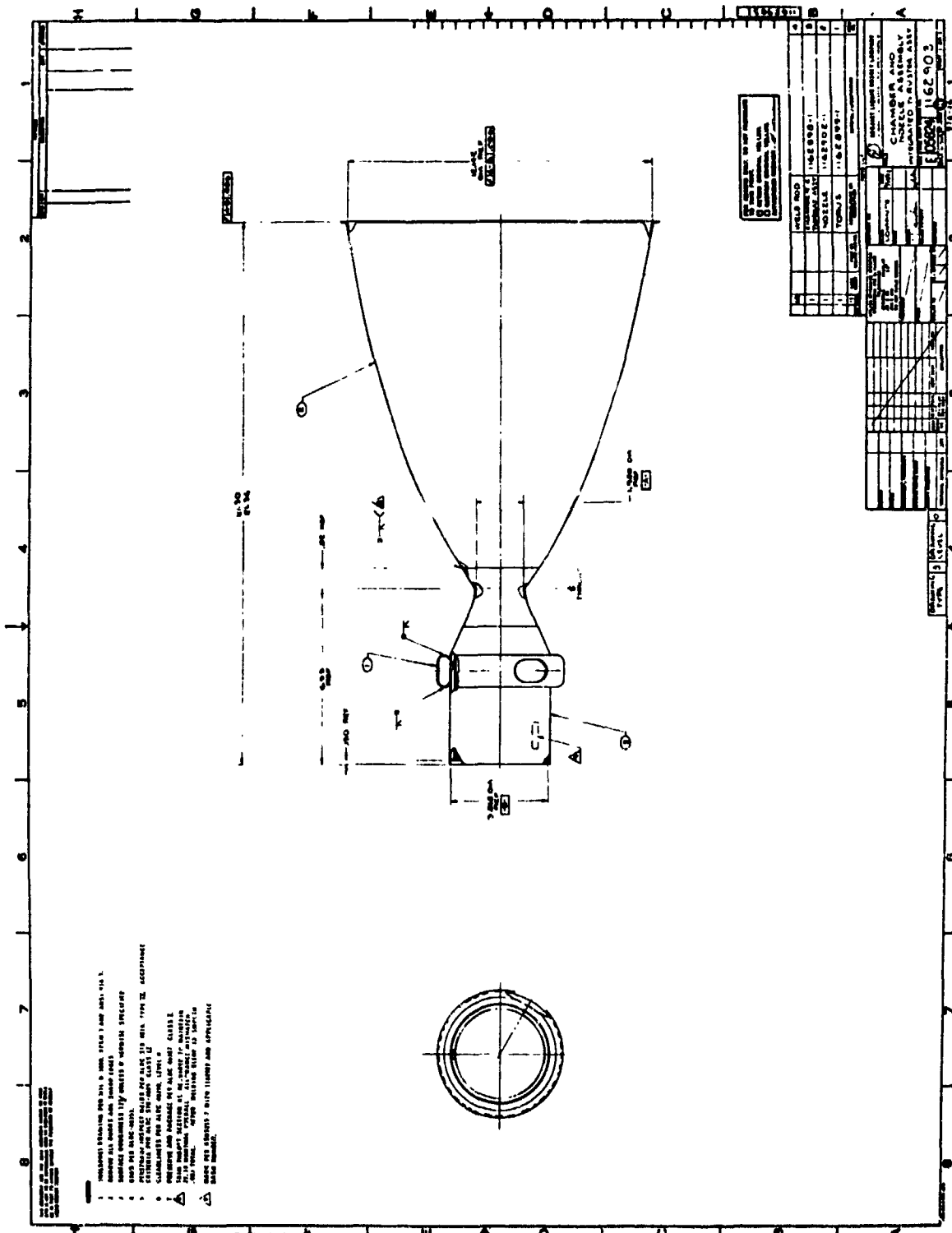
Figure 35. Chamber and Nozzle Assembly

TABLE XX

COMBINED REGENERATIVE-FILM COOLED THRUST CHAMBER DESIGN

Chamber Region

No. of channels	80
Material (liner)	ZrCu
Liner wall thickness	0.035
Jacket material	22-13-5
Jacket wall thickness	.102 Cm (0.040 in.)
Channel depth	.381 Cm (0.150 in.)
Channel width	.127 Cm (0.050 in.)

Coolant Injection Region

No. channels	160
Material (liner)	ZrCu
Liner wall thickness	.089 Cm (0.035 in.)
Jacket material	ARMCO 22-13-5
Jacket thickness	.102 Cm (0.040 in.)
Channel depth	Variable, tip .076 Cm (0.030 in.)
Channel width	.076 Cm (0.030 in.)

Throat

Material	Haynes 188
Thickness	.076 Cm (0.030 in.)

Skirt

Material	Haynes 188
Thickness	.076 Cm (0.030 in.)

Figure 36. Chamber Liner
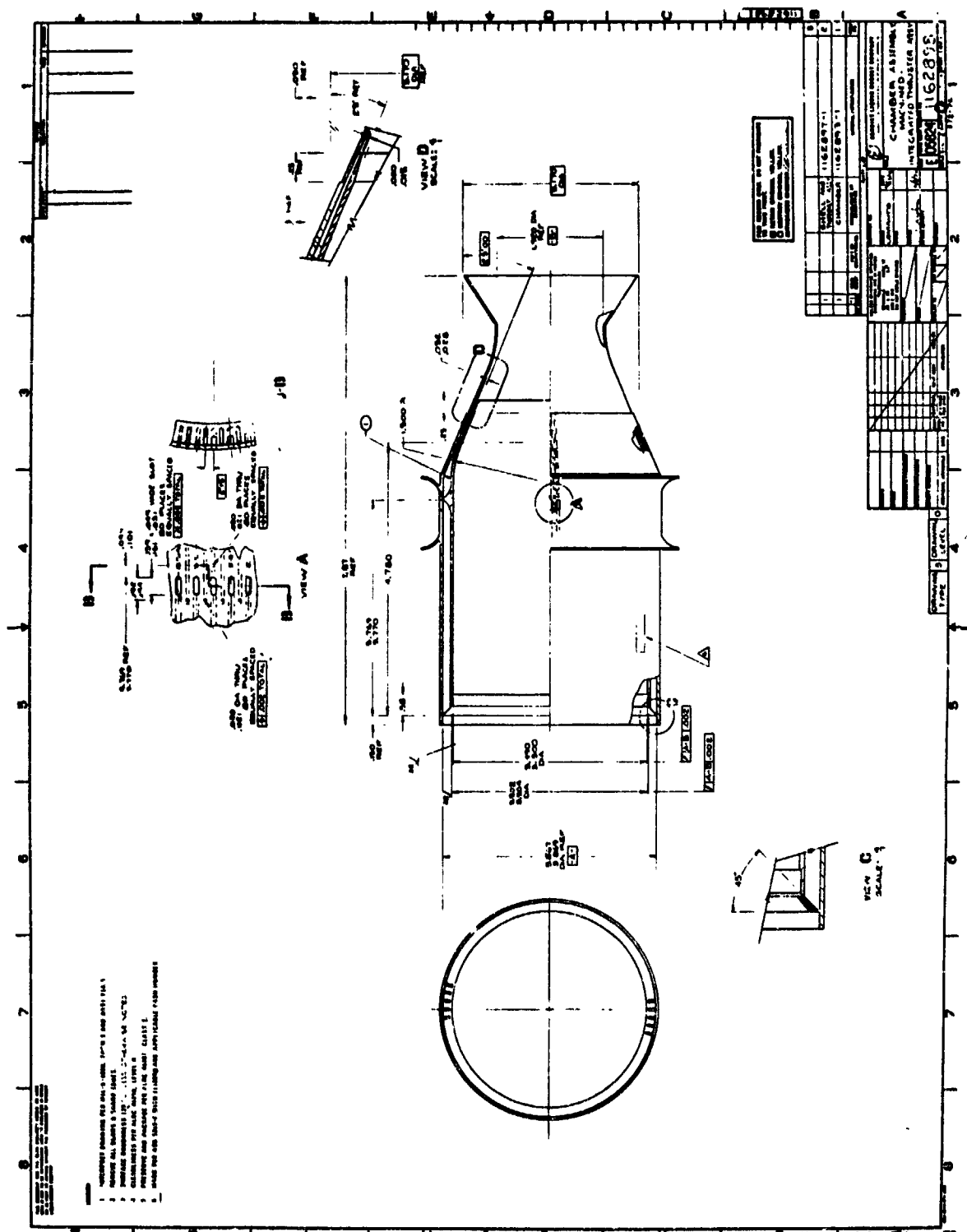
Figure 37. Machined Chamber Assembly
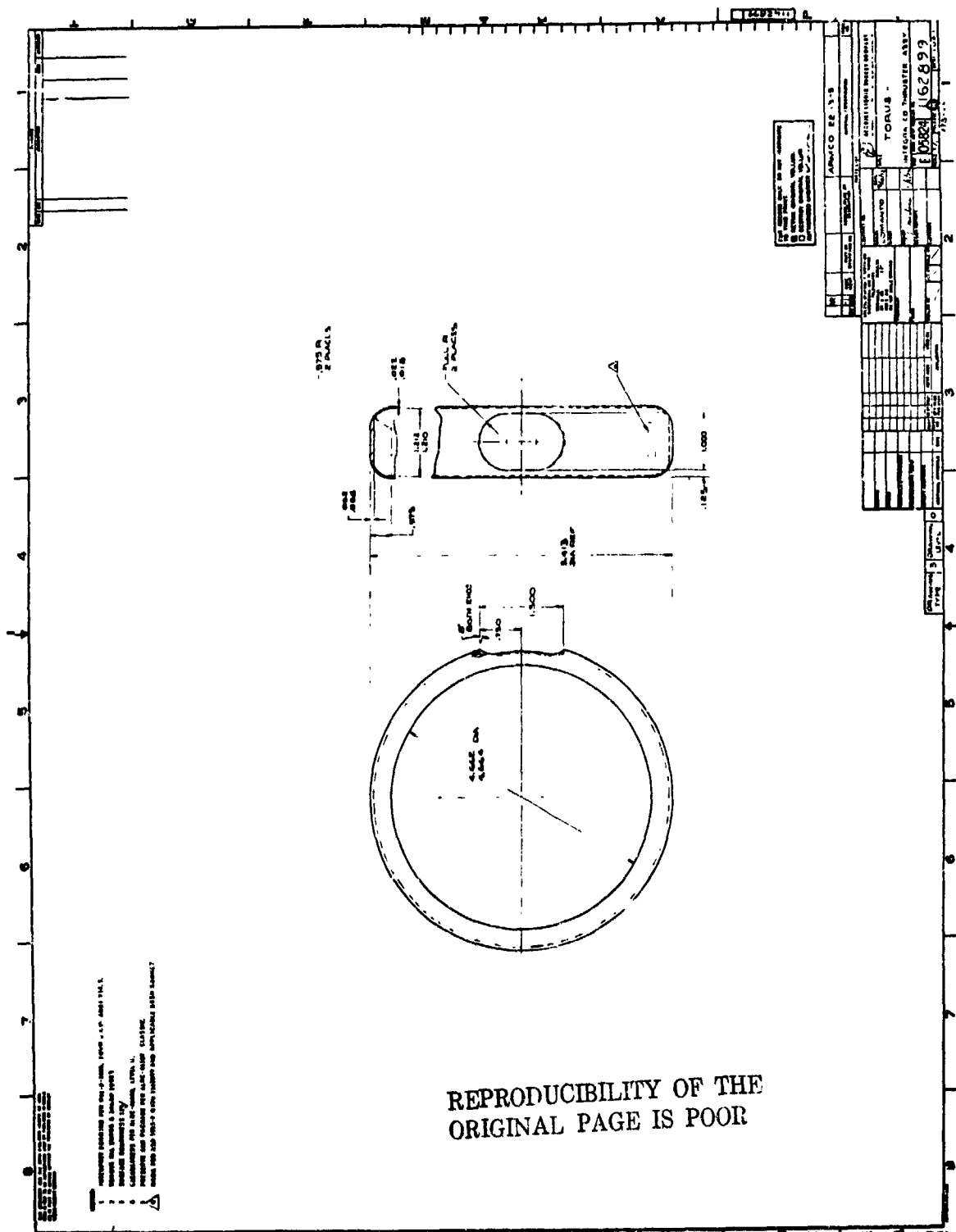
Figure 38. Torus

4.1, Integrated Thruster Design (cont.)

As discussed in Section 4.1.1.2, the orifices in the ffc
circuit were sized as .0562 cm (.0225 in.) on the basis of cold flow testing
with the channel model. A smaller size was specified for the orifices on the
drawing .0508 to .0533 cm (.020 to .021 in.), Figure 39, so that the first
chamber could be flowed, the orifice requirement verified, and then the orifices
drilled out to the required size. The experimental verification was accomplished
before he torus was welded in place and is described in Section 4.3.4.

The drawings for the throat section and the nozzle
extension are shown in Figures 39 and 40, respectively. These two components
are spun from Haynes 188 which was selected for high temperature strength and
oxidation resistance.

The fuel inlet line that is welded to the torus as part of
the thrust chamber assembly is shown in Figure 41. It is made from .020 CRES
304L.

The length of the fuel line shown in Figure 41 was selected
to avoid damage to the torus, line and valve mounts due to deflection resulting
from the expansion of the chamber relative to the valve, contraction of the line,
and radial expansion of the chamber. For example, heat transferred to the
chamber shell via the regen coolant causes the chamber to lengthen between the
valve mount and the torus relative to the valve and line; direct coupling of
the valve to the torus by a right angle elbo would result in a load of 14,234 N
(3200 lb$_f$) and a stress on the line in bendin, of 33,100 N/cm^2 (48,000 psi).
The analysis of the valve mounts, line and torus interface are given in
Reference (4).

4.1.4.2   Chamber Thermal Design

The thermal behavior of the workhorse regen-film cooled
thrust chamber was well characterized both in steady state and transient or
pulsing operation in Contract NAS 3-14354 (Ref. 3). These results are summarized
in this discussion in terms of operation at a nominal condition and the effects

Page 113

Figure 39. Throat Section

Figure 40. Nozzle Extension

Figure 41. Fuel Inlet Line
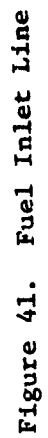
4.1, Integrated Thruster Design (cont.)

of variations in chamber pressure, propellant temperature, and mixture ratio on the operation. These data constitute the predicted thermal behavior of the ITA thrust chamber.

4.1.4.2.1 Steady State

Figure 42 is typical of the steady state temperature profiles throughout the Contract NAS 3-14354 thruster when operating at $207 \ N/cm^2$ (300 psia) with 294°K (530°R) propellants. Data are shown for three film cooling flow rates (20, 25 and 30%), and three mixture ratios (3, 4 and 5). The temperature data shown are for the gas-side and exterior of the regeneratively cooled cylindrical chamber section, the exterior behind the film cooling injection ring (dump section), and the exterior of the film-cooled, thin wall spun nozzle and skirt.

The data shown in the left half of Figure 42 were generated at constant thrust and mixture ratio with a varying split of fuel between the regenerative section and the dump film-cooled section. As coolant flow through the dump section is reduced from 30%, the nozzle temperatures rise, the chamber temperatures drop, and performance increases. At the same time, chamber temperatures drop because of the increased coolant flow through the regenerative section.

The right side of Figure 42 provides a parametric data presentation which identifies the relationship between mixture ratio and coolant flow. These curves are used to determine the influence of off-design operation on chamber life. The conclusions to be drawn from this figure are:

(1)   The chamber region is not influenced significantly by mixture ratio and only slightly by film coolant flow rates.

Figure 42. Measured Steady State Wall Temperatures

4.1, Integrated Thruster Design (cont.)

(2)   Maximum temperatures are attained midpoint in the skirt, 14 to 18 in. down from the injector face. Beyond this length, radiation cooling through the nozzle exit plane becomes significant and temperatures drop off.

(3)   The temperature gradient through the chamber wall, gas-side to exterior, in the regeneratively cooled region, is identified directly from test data.

The Contract NAS 3-14354 data show that chamber pressure is not a significant thermal parameter in the film-cooled nozzle and skirt region except at the very high area ratios where radiation cooling becomes important at the lower chamber pressures. This design does not depend on radiation cooling, and peak skirt temperatures change only slightly with chamber pressure. The regenerative portion of the chamber is only slightly influenced by chamber pressure except in the coolant inlet region. At the inlet, the additional cooling provided by peripheral flow in the inlet manifold aids in reducing the gas-side wall temperatures at lower pressures. The regenerative portion of the chamber is not influenced by MR changes while the throat and skirt are influenced significantly. The mechanism behind this change of temperature with MR is not related to the changing core gas propellant chemistry, but to the reduction of the fuel flow (coolant). If cross plotted, these data show that wall temperatures are dependent only on the coolant flow expressed as a fraction of total propellant flow and on propellant supply temperature (Ref. 3) over the normal range of operating conditions. It is anticipated that this experimentally determined relationship will begin to break down at high mixture ratios when the core mixture ratio approaches stoichiometric and reaction between the film coolant and core begins.

The influence which propellant supply temperature has upon chamber temperature depends on chamber location. The trends observed were independent of cooling percentage, mixture ratio, and chamber pressure. In the regenerative chamber region, a one-degree change in coolant temperature

Page 119

4.1, Integrated Thruster Design (cont.)

resulted in a one-degree change in wall temperature. When the above and other data are combined, the operating maps of Figure. 43 for the throat and skirt regions are obtained. These maps show the maximum throat and skirt temperatures as functions of the engine mixture ratio and film cooling flow rate for both nominal fuel temperature and fuel at ambient temperature. Using the design film coolant flow rate of 21%, the steady state operating conditions, summarized in Table XXI, are obtained. These experimentally based results indicate the thrust chamber to be capable of satisfactory operation over the entire required operating range.

TABLE XXI

CHAMBER OPERATING POINTS

	Nominal Design Point (MR = 4.0, T_F = 139°K (250°R)	Most Severe Operating Point (MR = 6.5, T_F = 333°K (600°R))
Max Skirt Temp	1760°C (1400°F)	1149°C (2100°F)
Max Throat Temp	454°C (850°F)	927°C (1700°F)
Max Chamber Temp	149°C (300°F)	482°C (900°F)
Cooling Ring Tip	177°C (350°F)	343°C (650°F)

4.1.4.2.2   Fuel Film Cooling (FFC)

The fuel film cooling flow rate influences both the thruster thermal operation and performance. As a result both were considered in establishing the design point coolant flow requirements.

The 1149°C (2100°F) worst case maximum nozzle temperature results in acceptable creep life (see Table XVI) and the thermal conditions at the nominal design point result in acceptable cycle life. Thus, 21% was selected as the film cooling requirement from a thermal view point. Figure 44
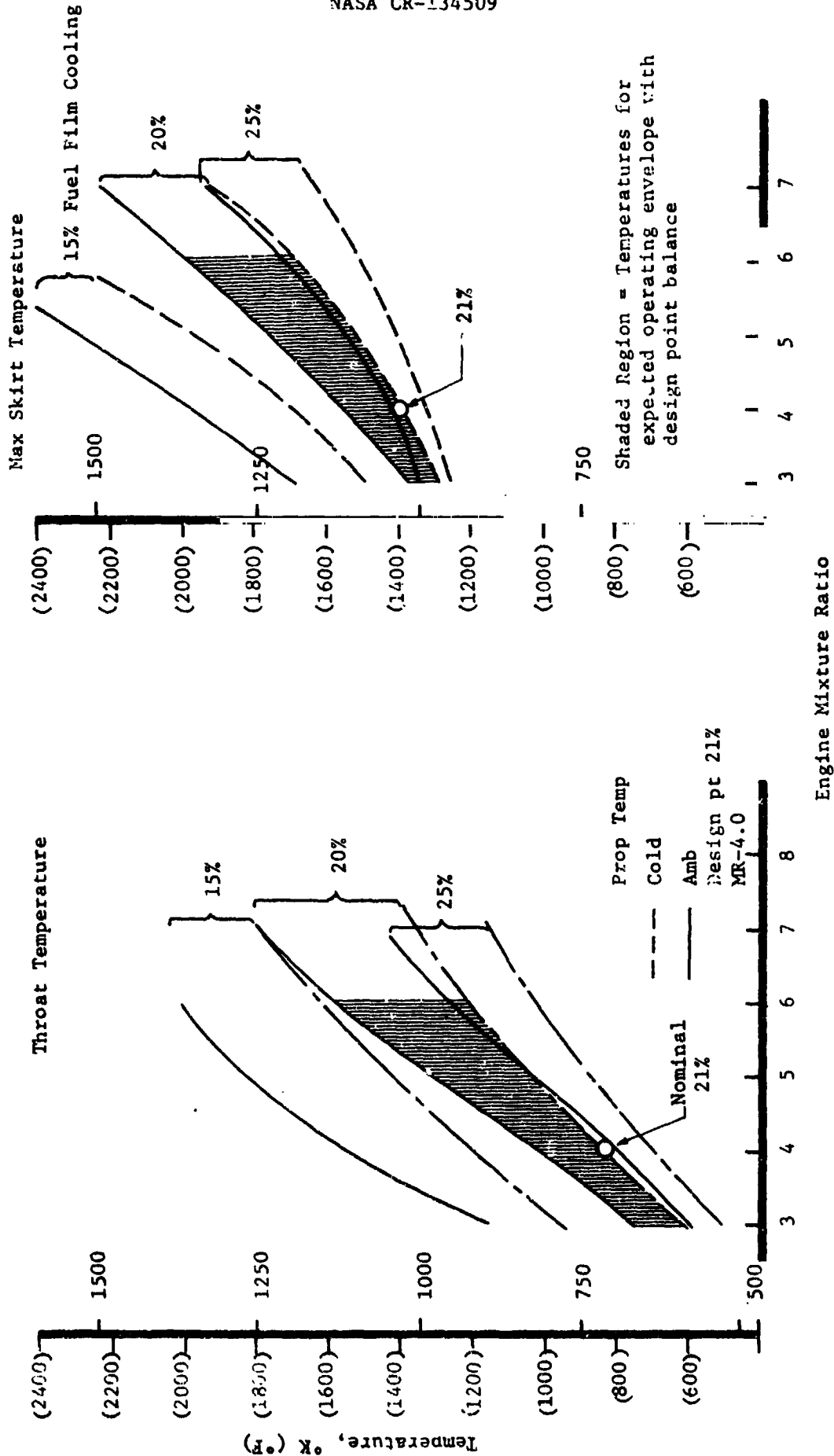
Figure 43. Steady State Throat and Skirt Temperatures vs Engine MR, % Film Cooling and Propellant Supply Temperature

INJECTOR PERFORMANCE

T_F = 139°K (250°R)

T_{OX} = 208°K (375°R)

MR = 3.8-4.2

SN 6 & 7, Contract NAS 3-14354
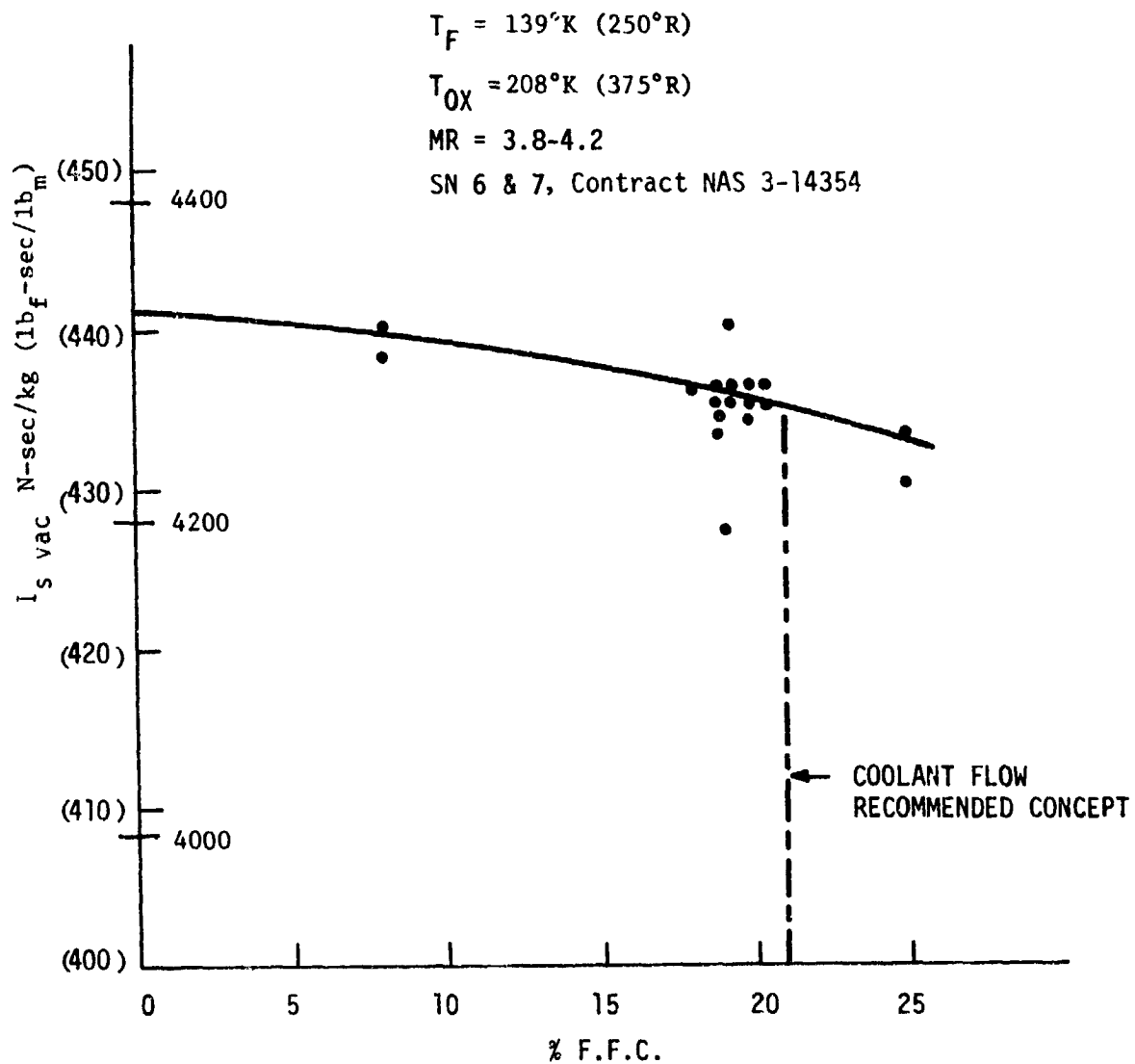
Figure 44. ITA Performance at Nominal Temperatures

4.1, Integrated Thruster Design (cont.)

shows the performance obtained with the NAS 3-14354 SN 007 injector as a function of percent ffc. A 21% ffc flow results in 4276 N-sec/kg (436 lb_f-sec/lb_m) specific impulse which meets the program design goal of 4266 N-sec/kg (435 lb_f-sec/lb_m). The design requirement was, therefore, set at 21% ffc. A greater percent ffc will compromise performance and less ffc will result in maximum nozzle temperatures in excess of the 1149°C (2100°F) limit.

4.1.4.2.3   Thermal Transients

The cyclic life of certain regions of the thrust chamber are determined by the thermal strains generated during rapid transient heating of the chamber wall. In addition, the peak temperatures established during pulse mode operation were evaluated to determine if the thruster can be thermally pumped to higher than steady state temperatures during pulsing operations.

Figure 45 summarizes the transient characteristics based on data from two Contract NAS 3-14354 tests with ambient temperature propellants at nominal chamber pressure and mixture ratio. The upper insert on this figure compares the measured gas-side and exterior temperature transients with a two-dimensional thermal model prediction. The predictions and data are in reasonable agreement demonstrating that, for this particular start condition, the maximum thermal gradient exists 0.35 sec after ignition and is more severe than the steady-state gradient. However, hot restarts or starts with cold propellants and ambient hardware are less severe in the transient than at steady state.

The center insert of Figure 45 provides the temperature vs. time history at six locations along the film-cooled nozzle. The insert at the bottom of Figure 45 identifies the maximum through-the-wall gradient for the
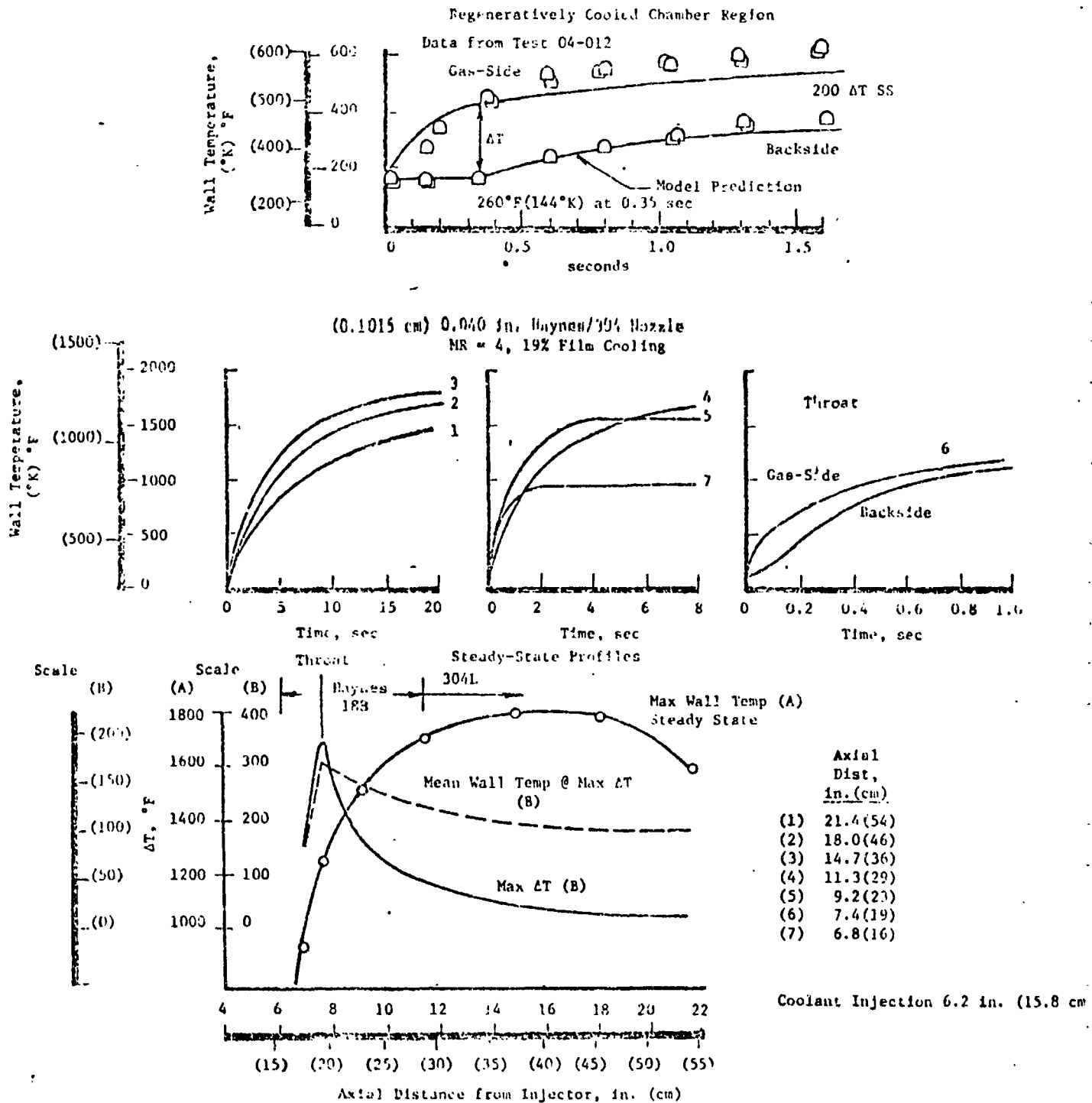
Figure 45. Transient Thermal Characteristics with Ambient Temperature Propellants

4.1, Integrated Thruster Design (cont.)

0.1 cm (0.040 in.) wall thickness design. The transient responses for this
wall thickness were obtained from the Contract NAS 3-14354 .127 cm (.050 in.)
wall data by computing the heat transfer coefficient and recovery temperature
from the transient and steady-state temperatures. These boundary conditions
were then used to compute the new profiles and heating rates with wall thickness
as a parameter. Steady-state temperatures are not influenced by changes in
wall thickness.

Stations 1, 2 and 3 at high exit area ratios heat
slowly and have low gas-side to exterior temperature differentials. Approxi-
mately 20 sec of firing and 300 sec of coast (cooldown) are required to achieve
a full thermal cycle of the skirt. Stations 4 and 5 are located downstream of
the throat; Station 7 is located upstream. The full thermal heating cycle times
for these stations are 10, 3 and 1 sec, respectively. Since the exterior and
the gas-side conditions are approximately the same, cnly the gas-side values
were shown. Maximum thermal gradients occur approximately 0.1 sec after ignition.
These were noted to be small compared to the throat values; Station 6. Both
gas-side and exterior temperatures are shown for the throat station since this
is the critical design region for pulse mode operation. In the throat, maximum
gradients with cold wall starts occur at approximately .10 sec; therefore, nearly
all single firings will represent a thermal strain cycle for this location. A
series of rapid pulses, however, will be less severe than a single, long burn
because hot starts do not constitute a thermal cycle.

The lower insert in Figure 45 provides the information
required for fatigue life and creep life analyses for 306°K (550°R) fuel inlet
temperature conditions. Identified therein are: (1) axial temperatuie
profile at steady-state (for creep analyses), and (2) maximum radial temperature
gradients and the mean wall temperatures at the time these gradi nts occur.
The chamber life analyses are covered in the next subsection.

4.1, Integrated Thruster Design (cont.)

Figure 46 is based on computer modeling of the Contract NAS 3-14354 thermal data and illustrates the thermal gradients and transients in the copper lined portion of the chamber. The upper insert series in Figure 46 shows the temperature response at five locations in the wall at 3 axial stations in the regen section. The spread between the curves is the thermal gradient which produces strain in the wall. The wider the spread, the greater the strain and the shorter the thermal fatigue life. The temperature responses shown in Figure 46 (top inserts) differ from that shown in Figure 45 (middle insert) because of the fuel temperature difference: Figure 45, ambient; Figure 46, 144°K (260°R). Figure 46 illustrates the point made earlier: with cold propellants the maximum Δ occurs in steady state. Other conclusions that can be drawn from these figures are: because the exterior temperature drops while the gas side rises the average temperature on shutdown is only slightly above ambient; in approximately .35 sec steady state is achieved.

The four inserts at the bottom of Figure 46 show the temperature transients for the dump cooled copper section. Unlike the regen section, the exterior temperature rises, even with cold propellants. The highest strain (ΔT) occurs at the coolant injection section (ffc tip) during transient. Although the steady state ΔT is only a little less than the maximum transient ΔT, it is important to recognize that the life is transient dependent. Pulse operation will not result in a full thermal cycle for the ffc tip for each pulse firing. The measure of the potential for thermal gradient is the difference between the final gas-side temperature and the initial wall temperature. The gas-side achieves the same steady state temperature irrespective of the initial wall temperature. A prior firing leaves the exterior of the wall at an elevated temperature and, consequently, the ΔT through the wall is not as large during succeeding transients.

The following conclusions were drawn relative to cycle life from the thermal characteristics of the NAS 3-14354 regen-film cooled chamber.

(1) With ambient propellant temperatures, the thermal gradient (strain) in the regen cooled wall (ZrCu liner) reaches the maximum value .35 sec after ignition and is more severe than occurs in steady state.

Figure 46. Copper Lined Region Thermal Transient
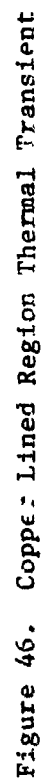
4.1, Integrated Thruster Design (cont.)

    (2) With nominal (cold) propellant temperatures, the maximum thermal gradient occurs in steady state.

    (3) The ZrCu regen section requires approximately .35 sec after ignition to achieve steady state.

    (4) The maximum thermal gradient in the ffc tip (ffc injection) occurs in the start up transient .18 sec after ignition.

    (5) The maximum thermal gradient in the nozzle occurs in the throat approximately .15 sec after ignition.

    (6) Cold hydrogen flowing in the regen passages of the chamber cools the exterior, while the gas-side heats up. On shutdown, the gradient equilibrates to a near ambient temperature. Thus, a repeat firing produces a thermal cycle, a full thermal cycle resulting for firings of .35 sec or longer.

    (7) The strain in the throat is caused by the temperature gradient that occurs as the gas-side heats up while the exterior is cold; thus, it occurs during the transient. The gas-side achieves the film coolant adiabatic wall temperature and, thus, its steady state or final level is unaffected by the initial wall temperature. Also the throat cools down slowly after shutdown. Consequently, repeat firings will produce less strain since the higher the initial wall temperature, the less the temperature differential that can exist between gas-side and exterior.

    (8) The strain in the ffc tip, being transient dependent, is not as great in succeeding pulses as in the case of complete cooldown between firings.

4.1, Integrated Thruster Design (cont.)

The temperature data obtained in pulse testing with ambient propellants are summarized below for various duty cycles. These data show the thruster is not thermally pumped during pulsing operation but rather runs cooler in pulsing.

		Maximum Pulsing Temperature as Fraction of Steady State Temperature On Time/Off Time Duty Cycle		
Location	Steady-State Temp., °C (°F)	0.2/0.3	0.1/0.15	0.054/0.046
Injector Face	288 (550)	0.81	0.82	0.76
Combustion Chamber Wall	316 (600)	0.87	0.87	0.79
Tip Film Cooling Ring	377 (710)	0.84	0.99	0.93
Throat	593 (1100)	0.78	0.83	0.80
Skirt (Max Temp)	882 (1620)	0.86	--	--

4.1.4.3   Structural Design

The thrust chamber analysis that was performed as part of Contract NAS 3-14354 and the proposal effort was reviewed. The existing stress computer program was changed to model the current design and was rerun to make comparative checks. All of the results for the chamber as reported in Reference (3) are valid. Additional analysis was performed to more fully evaluate the fuel torus inlet area. The inlet was modeled on a finite element shell program with the results showing the necessity for stiffening in the inlet area. It has been concluded that reinforcing ribs should be utilized to reduce bending stresses in the torus to acceptable levels. These high stresses arise from the pressure tension load exerted on the torus by the line over such a relatively large area. The details of these analyses are given in Appendix B of Reference 4.

4.1, Integrated Thruster Design (cont.)

Nominal pressures and temperatures were used in all calculations of fatigue life; then the required factors of safety were applied to verify strength adequacy. The nominal pressures used are itemized below, and the associated thrust loads were also applied to the structure.

Location	Pressure
Main chamber	207 N/cm^2 (300 psia)
Fuel inlet manifold 139°K (250°R)	269 N/cm^2 (390 psia)
Channel section	248 N/cm^2 (360 psia)
Throat region and skirt	Distributed two-dimensional pressure based on 207 N/cm^2 (300 psia) chamber
Injector pressure	235 N/cm^2 (340 psia)

A proof pressure for the entire structure was selected upon the basis of 345 N/cm^2 (500 psi) nominal chamber pressure with a 1.25 factor of safety to obtain design limit load as follows:

Nominal chamber pressure	= 345 N/cm^2 (500 psia)
Nominal injector pressure	= 414 N/cm^2 (600 psia)
Proof pressure, all components	= 483 N/cm^2 (700 psia)
Design limit pressure = 1.25 proof	= 603 N/cm^2 (875 psia)

Each major component of the thrust chamber assembly was analyzed with the aid of a finite element computer program. The nonlinear (plastic) plane-strain option was used to analyze the convectively cooled copper sections while the other regions were analyzed by use of elastic solutions with the appropriate secant moduli for copper material in the plastic range.

The approach used in design optimization and life prediction was to identify the location and time of the limiting stresses in each component. Consideration of the strains in transient heating are essential since the location of life limiting transient strains may be at a different location and greater in magnitude than those computed for steady-state thermal operation as discussed in the previous section. This process was an iterative

4.1, Integrated Thruster Design (cont.)

one involving the investigation of several geometries until satisfactory results
were attained.

The detailed computer analyses were conducted for the
nominal design point. Computer costs prohibited repeat runs for off-design
conditions. In order to provide the parametric results showing the influence
of MR, P_c, propellant temperature, film cooling flow, etc., for a given design,
simplified models were employed. The accuracy of the simplified approach was
established by comparing these results with the detailed computer prediction
available at the nominal design point. Where these results differed significantly,
empirical correction factors were added to the simplified equation at the design
point to make the simplified and computer solutions agree.

Transient thermal stresses in the single-layer shell
and skirt regions were calculated by use of the following expressions, derived
in Reference 7:

$$\sigma_1 = \frac{E \, \alpha \, \Delta T_f}{(1 - \nu) \, (1.5 + \frac{3.25k}{ht})}$$

$$\varepsilon_T = \frac{0.5 \, (\tau_1 + \tau_p)}{1 - \frac{0.5 \, (\tau_1 + \tau_p)}{UTS}}$$

where σ_1 = maximum surface stress level (thermal)

ε = total strain range

E = Young's modulus at point of maximum stress

α = coefficient of thermal expansion

ΔT_f = suddenly applied temperature (film) initial temperature

ν = Poisson's ratio

Page 131

4.1, Integrated Thrust Design (cont.)

k   = thermal conductivity

h   = heat transfer film coefficient

t   = material thickness

τ_p = stress from pressure loading

UTS = ultimate tensile strength

This expression allows a direct calculation of maximum thermal stress if either the flat plate Biot number $(\frac{ht}{k})$ or the film coefficient is known, without the intermediate heat transfer analysis to determine time of maximum thermal gradient. Stresses calculated by this technique agreed with computer solutions within 10% error.

The equation used for predicting thermal strains in the convectively cooled channel section is:

$$\epsilon_T = K \; \alpha \; \Delta T \pm \epsilon_p$$

where K = the empirical geometric constant determined for each components examined, either by means of analytical expressions or computer solution

ϵ_p = strain due to pressure loading

Δ_T = temperature difference between hot structure and colder restraining material

The values of "K" were found to vary from a minimum of 1.35 to a maximum of 2.0. The "K" values for the selected wall construction varied from 1.7 to 1.8, depending on the location.

Creep rupture life was determined by comparison of the steady-state stress levels to the Larsen-Miller plots of stress-rupture data at elevated temperatures.

4.1, Integrated Thrust Design (cont.)

Fatigue life was determined using the results of the stress-strain solution to plot stress-strain history of a full thermal cycle, cold start firing to steady state and subsequent cooldown. The peak strain obtained in this manner was used to obtain the number of cycles to failure.

The linear cumulative damage rule was used for predicting the remaining life available following the accumulation of short and long burns.

$$\text{Residual life} = 1 - \Sigma \frac{n}{N_f} + \Sigma \frac{t}{T_R}$$

where $\Sigma \frac{n}{N_f}$ is the summation of the number of pulses at a given pulse width divided by the allowable for that duration and $\Sigma \frac{t}{T_R}$ is the accumulated firing duration (hr) divided by the allowable creep life (hr) for the operating temperature and stress. The latter term is a negligible factor in thruster life.

The cycle life of the ZrCu liner was evaluated at four locations, three in the regen section of the chamber and one at the ffc injection tip. The results for all four cases are summarized in Table XVI (Section 4.1.1.3). The most limiting case is shown or the $S-N_f$ curve that was used for ZrCu (Figure 47). The most limiting location for the ZrCu liner is the ffc tip. The maximum strain, .32%, occurs .18 sec after ignition when the maximum gradient exists through the wall. Conduction to the exterior of the wall decreases the gradient for longer durations. As can be seen in Figure 47, a .32% strain results in a 50,000 cycle thermal fatigue life. The design requirements are 25,000 cycles. As discussion in section 4.1.1.4, surface finish may reduce the cycle life, but even with a .18 mu (32μ in.) surface roughness the design requirement is met.

In the application of the $S-N_f$ curve for ZrCu, no additional margin was applied to the curve because, as noted on Figure 47, the curve is based on test data. In addition, the test data were obtained at the
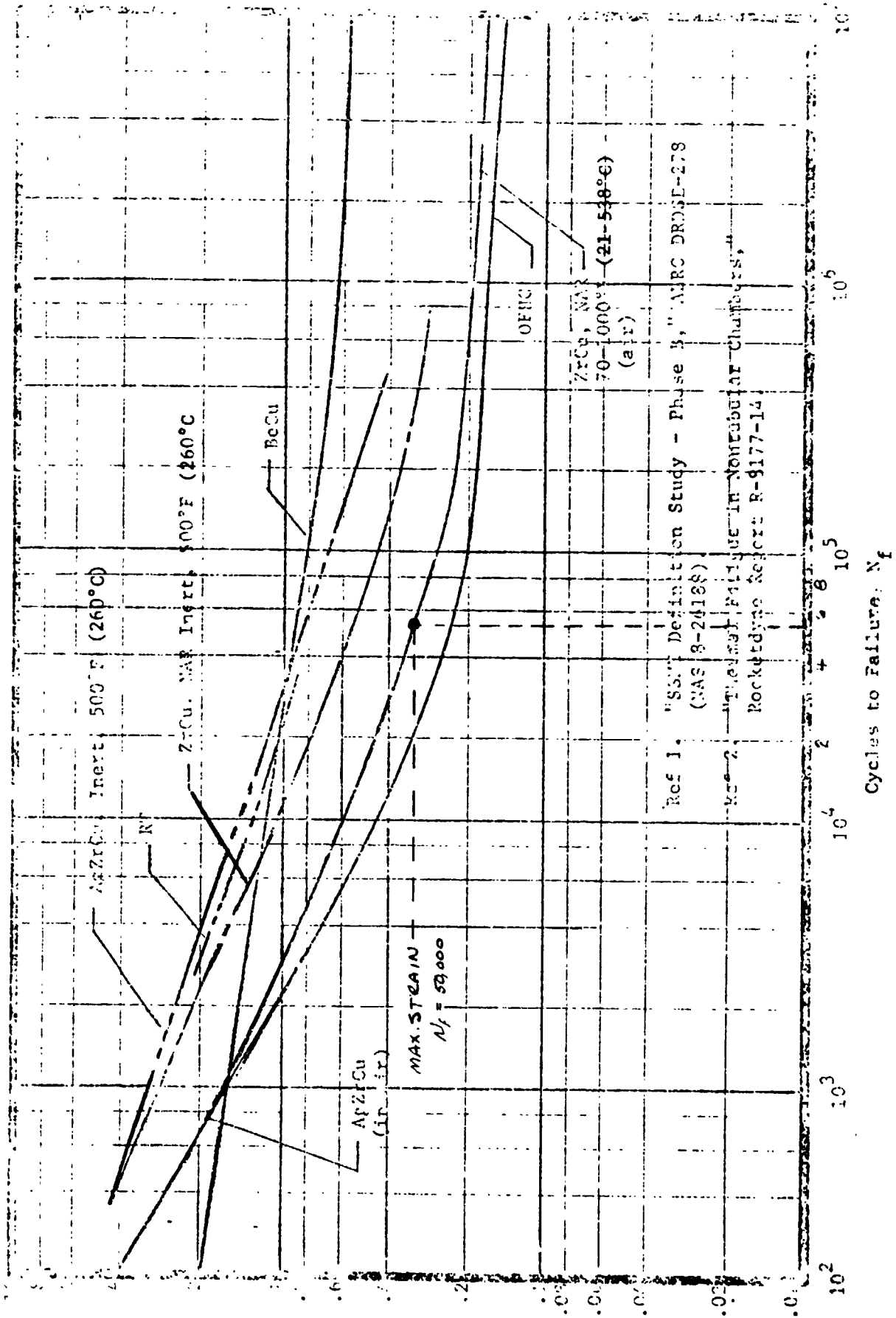
Figure 47. Total Strain vs. Fatigure Life (N_f), Copper and Copper Alloys

4.1, Integrated Thrust Design (cont.)

temperatures of interest in an air atmosphere, which makes the data somewhat conservative for the ITA application.

The ARMCO-22-13-5 components (chamber shell and torus) were checked for thermal fatigue. The most limiting location is the torus-shell interface. The maximum stress is produced in steady state and is the result of the contraction of the torus in contact with cold hydrogen and the expansion of the heated ZrCu liner. As can be seen from Figure 48, the 39,300 N/cm^2 (57,000 psi) stress that is produced results in a thermal fatigue life of approximately 700,000 cycles.

As can be seen from the lower insert in Figure 45, the Haynes 188 throat has by far the greatest ΔT and therefore the greatest thermally induced strain. The 200°C (360°F) ΔT produces .21% strain, which from the S-N$_f$ curve for Haynes 188 (Figure 49) is equivalent to a 1×10^5 thermal cycle life. There are no high cycle fatigue data for Haynes 188 so, as noted on Figure 49, the universal slope equation was used. Because there are no data and to allow for effects such as hold time, a lower bound was applied by reducing the cycles at each strain by a factor of ten (i.e., safety factor of ten).

Downstream of the throat the nozzle life is limited by high temperature creep. At the predicted maximum temperature for nominal operation, the creep life is in excess of 1000 hours. The required 10 year life capability (Table II) is 2500 minutes (41.7 hours). A temperature of 1149°C (2100°F) is considered to be the practical upper limit for the Haynes 188 material in this application.

The structural design studies focused on thermal fatigue as it is much more limiting than fatigue resulting from pressure induced strain. All components were evaluated for cycle life relative to pressurization with each firing and the 500,000 life cycle requirement. All components meet both the 500,000 pulse and 25,000 deep thermal cycle requirements.

ARMCO 22-13-5
Cycle Life

△ Low Cycle Fatigue Data
⊙ High Cycle Fatigue Data
▣ Extrapolated From
Low Cycle Fatigue Data

22-13-5 Components
$N_f > 5 \times 10^5$
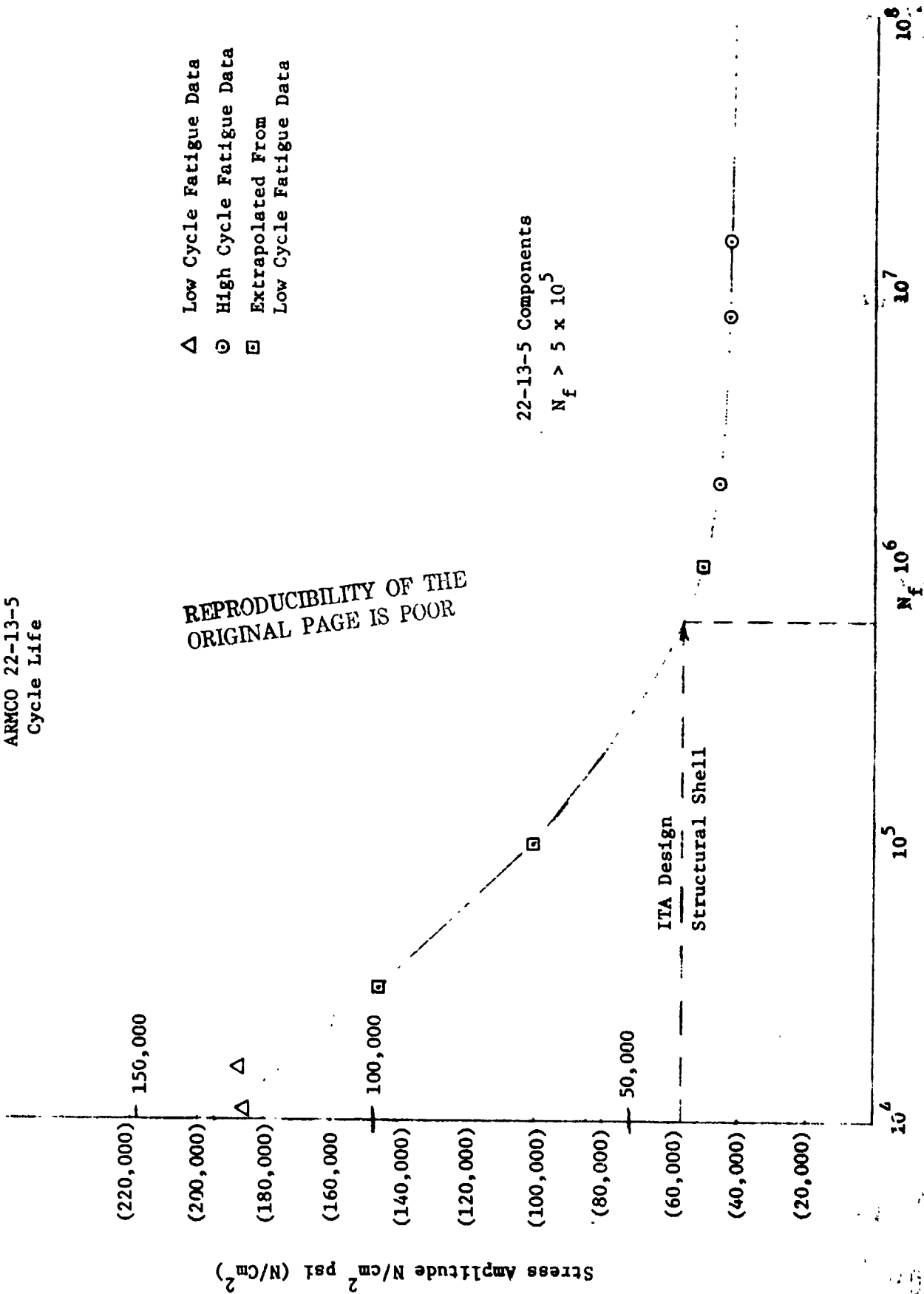
ITA Design
Structural Shell

10^5

10^6

10^7

10^8

N_f

Stress Amplitude N/cm² psi (N/Cm²)

150,000 (220,000)
(200,000)
(180,000)
(160,000)
100,000 (140,000)
(120,000)
(100,000)
(80,000)
50,000 (60,000)
(40,000)
(20,000)
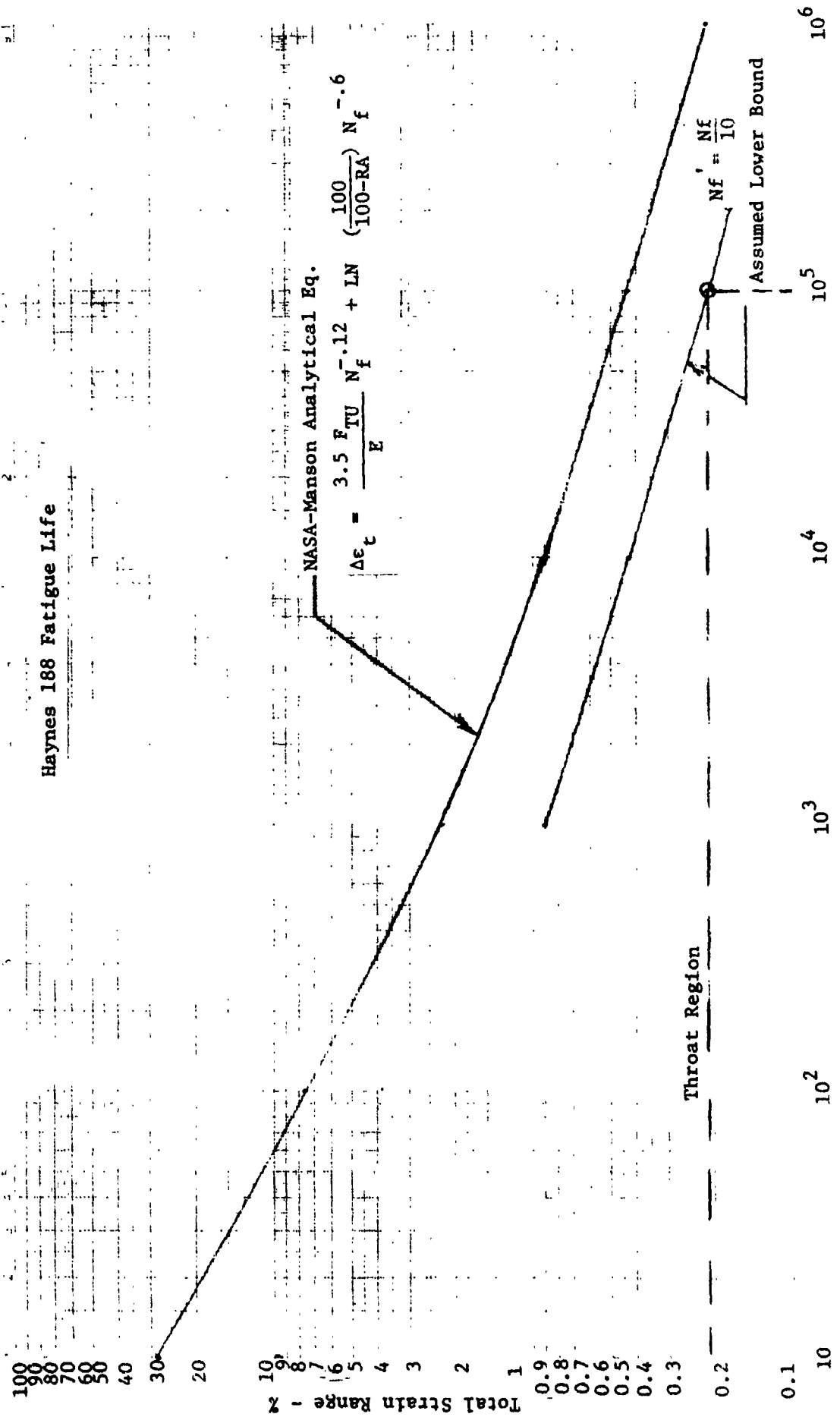
Figure 49. Haynes 188 Fatigue Life

Page 137

4.1, Integrated Thrust Design (cont.)

4.1.5 Valves

Two sets of valves were selected for the ITA, the main propellant valves and the igniter valves. The desire to control propellant sequencing to both the injector and igniter ruled out the use of bipropellant valves. The valves had to be applicable to cryogenic conditions and meet the cycle life requirments.

4.1.5.1 Igniter Valves

The specifications for the igniter valves are given in Table XXII. It appeared that a .635 cm (1/4 in.) valve would meet the flow $-\Delta P$ requirement of the igniter oxidizer schedule if the C_v was approximately .28. A valve with a lower C_v would not have the required flow capacity. A larger valve, besides being unattractive from a weight and size view point, had a cost disadvantage.

4.1.5.2 Main Propellant Valves

Main propellant valves applicable to ITA were being developed by Marquardt and Rocketdyne for NASA during the design phase of the program. The main propellant valve specifications (Table XXIII) were based on the Marquardt valve since two designs had been successfully tested; Rocketdyne was starting to test one design. Except for a .003 sec variation in closing time, the Marquardt valve met the ITA requirements. A response time improvement could be achieved by an orifice change.

Testing of a valve that was functionally identical to the ITA main propellant valve was performed by the Marquardt Co. during the design phase of this program. A leak developed in the bellows at 70,000/80,000

TABLE XXII

IGNITER VALVE CRITERIA

Parameter	Requirement
Fluids	Hydrogen, oxygen
Inlet pressure, N/cm^2 (psia)	431 (625) nominal 655 (950) maximum
Proof pressure, N/cm^2 (psia)	983 (1425)
Burst pressure, N/cm^2 (psia)	1517 (2200) minimum
Flow capacity	C_v of 0.28 minimum
Leakage	
Internal, scc/hr GHe	50 maximum
External, scc/sec GHe	1×10^{-6} maximum
Response time	
Open, sec	0.020 maximum @ 431 N/cm^2 (625 psia) and 28 VDC
Close, sec	0.020 maximum @ 431 N/cm^2 (625 psia) and 28 VDC
Voltage, VDC	28 ± 4
Duty cycle	Continuous
Life cycles	50,000
Temperature	
Fluid, °K (°R)	25 (45) minimum 333 (600) maximum
Environment, °K (°R)	222 (400) to 278 (500)

TABLE XXIII

MAIN PROPELLANT VALVE OPERATING REQUIREMENTS

Parameter	Requirements
Envelope	As defined by Marquardt Co. Drawing X28960.
Mechanical Interface	Bolted flange joints as defined by Marquardt Co. Drawing X28960.
Valve Mounting	The valve shall be capable of being mounted using either the outlet flange or the valve body joint flange. Two extended screws shall be provided in the body joint to accommodate mounting.
Weight	Weight goal shall be 3630 g (8.0 lb) including the pilot valve.
Service Fluid	Hydrogen vaporized from LH_2 per MIL-P-27201 Oxygen vaporized from LO_2 per MIL-P-22508A
Inlet Pressure, N/cm^2 (psia)	276 (400) nominal 172 (250) minimum – 448 (650) maximum
Proof Pressure, N/cm^2 (psia)	465 (675) bellows; 690 (1000) body assembly
Burst Pressure, N/cm^2 (psia)	827 (1200) minimum
Flow Rate, g/sec (lb/sec)	Hydrogen 313 (0.69) at 139°K (250°R) nominal. Oxygen 1500 (2.76) at 208°K (375°R) nominal.
Pressure Drop, N/cm^2 (psid)	14 (20) maximum at rated flow, nominal pressure, and ambient temperature.
Internal Leakage, scc/hr GHe	100 maximum
External Leakge, scc/hr GHe	1×10^{-6} Pilot valve: 690 (1000) maximum at acceptance with 310 N/cm^2 (450 psia) pressure.
Response Time, sec, open and close	0.040 signal to full travel, maximum 0.015 travel time, maximum
Response Time Repeatability, sec	Run to run: ±0.001 at nominal pressure, nominal voltage and ambient temperature. Unit to unit: ±0.003 at nominal pressure, nominal voltage and ambient temperature.
Temperature, °K (°R) Operating Fluid	 111 (200) to 333 (600) 111 (200) to 333 (600)

TABLE XXII (CONT.)

Parameter	Requirements
Voltage, VDC	18 to 32 operation 24 to 32 to meet response time
Current, amps	3 maximum
Duty Cycle	Continuous duty capability; minimum on time of 0.030 sec every 0.150 sec; maximum on time of 1000 sec
Life Functional, cycles Functional, hours Time, years	 60,000 minimum 50 10
Failure Mode	Fail closed with loss of power or pressure

4.1, Integrated Thrust Design (cont.)

with no malfunction and the ITA program requirements are 50,000 cycles, the increased bellows thickness change was approved as providing adequate margin. The stroke change was not made since it would increase pressure drop.

4.0, Technical Discussion (cont.)

4.2 FABRICATION

4.2.1 Integrated Thruster Assembly (ITA)

The ITA consists of the thrust chamber assembly, igniter assembly, two main propellant valves, and two igniter valves. These components and subassemblies are shown in the frontispiece.

The thrust chamber assembly consists of injector, chamber, torus, throat section, nozzle extension, fuel inlet line and flange. These components and subassemblies are shown in Figure 2 except for the fuel inlet line flange which is similar to that on the injector in Figure 2. The injector assembly shown in Figure 2 includes the inlet line and flange.

The igniter assembly consists of the igniter housing, integral exciter/spark plug, and the support bracket. These components are shown in Figure 4 with one of the igniter valves.

Four thrust chamber assemblies (TCA) (including igniter assemblies, but excluding valves) were fabricated. Five main propellant valves, six igniter valves and three spare exciter/spark plug units were fabricated. Three of the thrust chamber assemblies were instrumented.

The ITA was fabricated in the following sequence:

(1) A .010 x .1 in. (.025 x .254 cm) strip was spot welded to the ID of the chamber at the injector-chamber interface. One half the width of the strip protruded past the interface; the injector lip fitted over this half of the strip. Thus, the strip registered the chamber to the injector and served as a beam stopper.

4.2, Fabrication (cent.)

(2) Six to eight .020 dia x 1 in. (.051 d . x 2.54 cm)
wires were inserted in the ffc slots, equally spaced, at the aft end of the
chamber. These wires were spot welded to the ID of the ~1/4 inch (.635 cm)
of shell that extended beyond the ZrCu ffc tip (film coolant injection); the
wire protruded aft of the shell-throat section interface. These wires served
to register the throat section to the shell by aligning the ID of the two parts.

(3) The injector-chamber-throat section were held together
by a threaded rod that protruded through the igniter port in the injector and a
tapered plug in the divergent core of the throat section. The piston ring was
installed on the injector before the injector was mated to the chamber.

(4) The injector-chamber joint and then the chamber-throat
section joint were EB welded.

(5) The ID of the chamber was machined smooth at the chamber-
throat section point.

(6) Using an alignment fixture, the torus, fuel line and
inlet flange were fitted together, the inlet hole cut in the torus shell, and
the inlet flange TIG welded to the line.

(7) Two .010 x .040 in. (.025 x .051 cm) strips of CRES 349
was spot welded to the two lips on the chamber that formed part of the torus.
The strips were attached to the mating interface, flush on the torus ID, with
1/2 the strip protruding past the outer surface. This strip was consumed
during welding.

(8) The torus was installed with the CRES 349 strip
between the chamber-torus joint and protruding to the outside. The torus was
fixtured to constrain it during welding.

4.2, Fabrication (cont.)

(9) The torus was TIG welded on the aft side and then on the forward side.

(10) Using a dummy valve to hold and align the fuel line, the line-torus weldment was made using TIG.

(11) The inlet line flanges were machined, if required, for parallism, and flatness and surface finish (O-ring sealing surface).

(12) The nozzle extension was fitted to the throat section with an aluminum tapered plug providing backup at the joint. The plug was relieved under the joint to accomodate a Haynes 188 backup strip.

(13) The throat section-nozzle extension joint was EB welded.

(14) The weld penetration at the weld joint on the ID of the nozzle was removed by grinding, and the joint was polished and grained to have the same finish as the rest of the nozzle.

(15) The reinforcement ribs were machined to fit and welded to the injector (2 places) and to the torus (6 places).

(16) Thrusters SN 001, 002 and 003 were cleaned and thermal (thermocouples) instrumentation installed. Thruster SN 002 is shown in Figure 50. All openings were covered with nylon, then plastic and sealed with tape to preserve the cleanliness (oxygen service). A close up showing the thermocouple installation details is shown in Figure 51. Thruster SN 002 and SN 004 are shown in Figure 3.
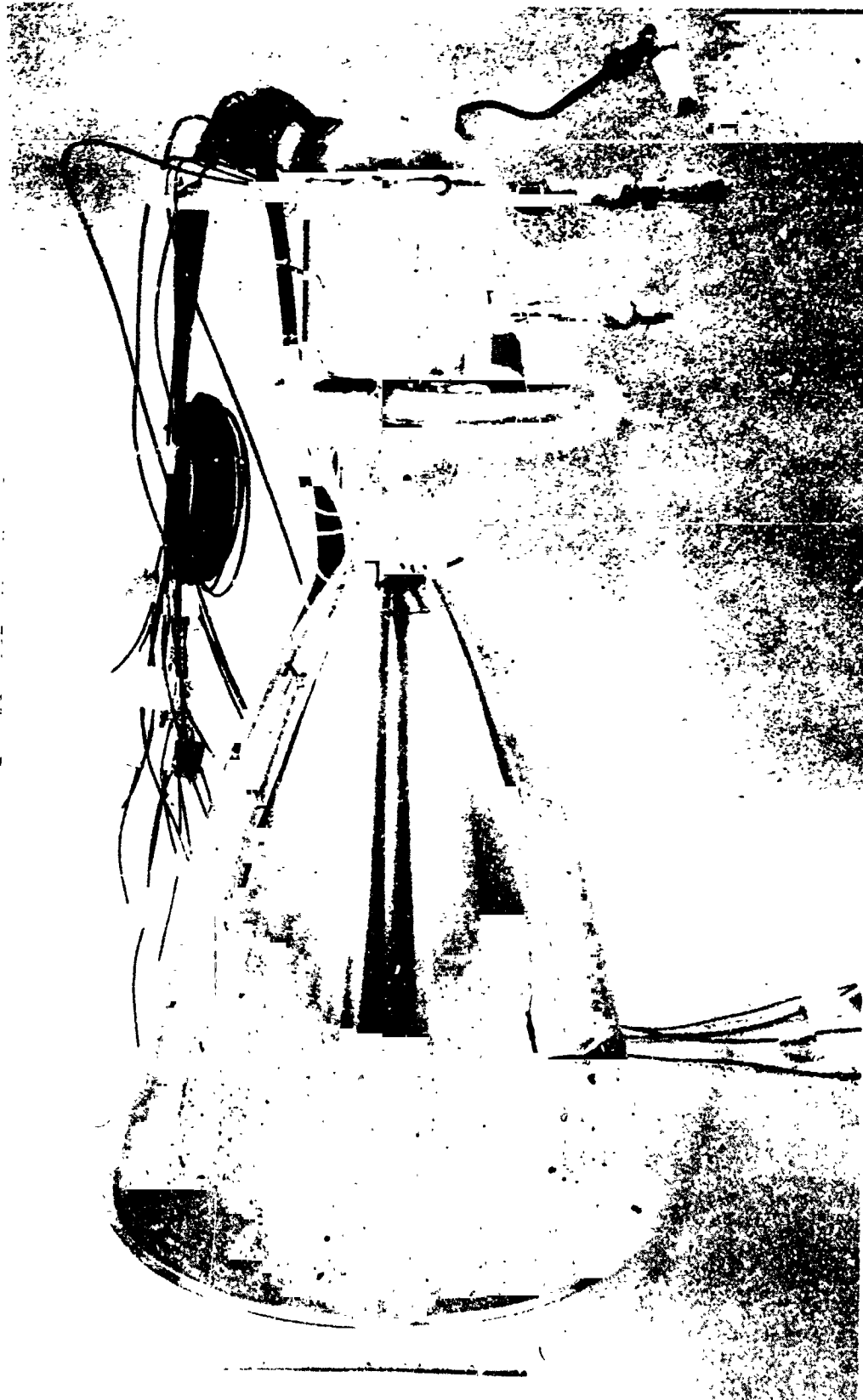
Figure 50.   ITA SN 002
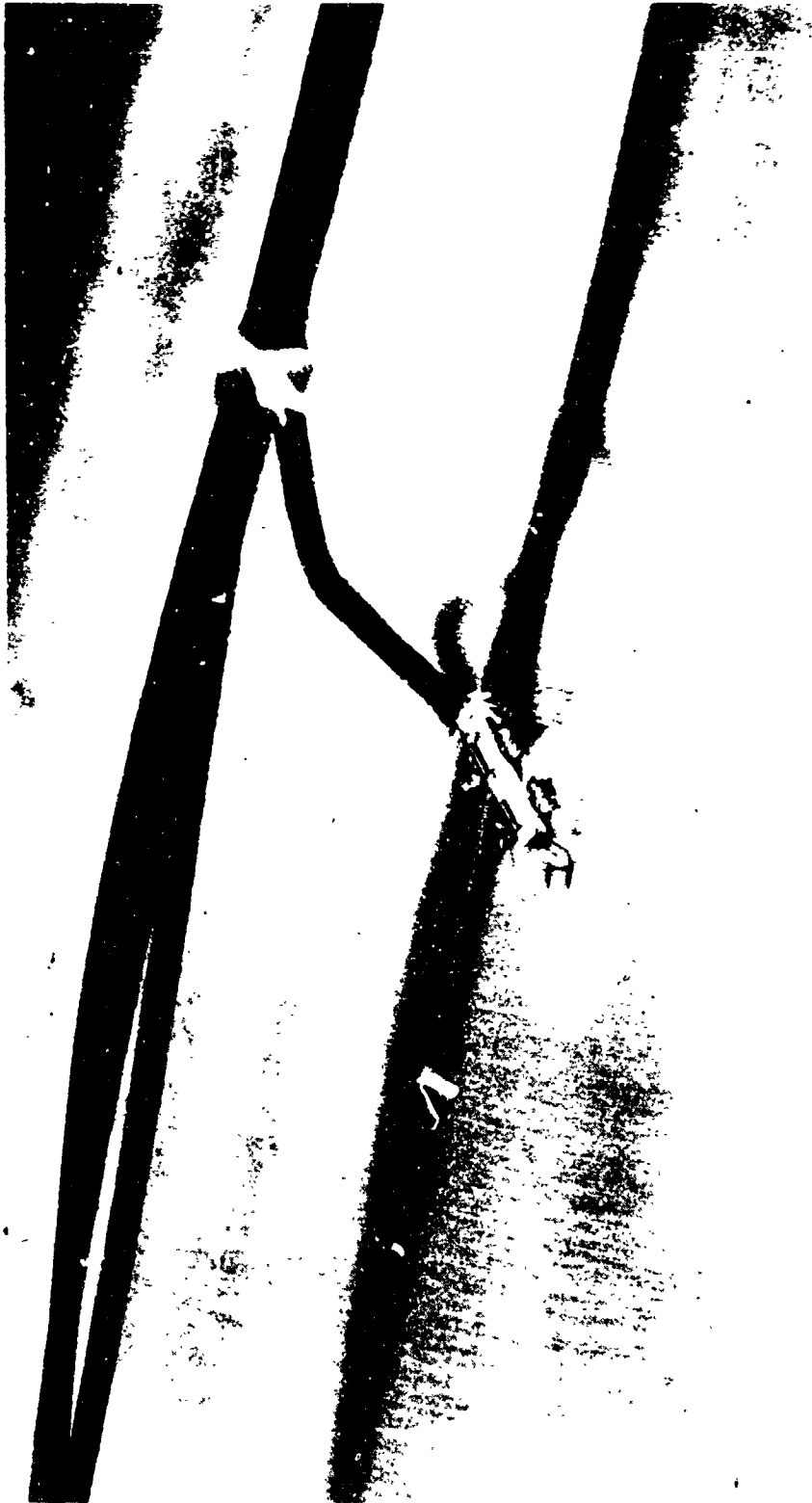
Figure 51.   TC Installation Detail

4.2, Fabrication (cont.)

(17) Thruster SN 003 was delivered to NASA. Thruster SN 001 was used for steady state and pulsing mode evaluation testing. Thruster SN 002 was used for life cycle testing. Thruster SN 003 was delivered unassembled. Thrusters SN 001 and SN 002 were assembled on the test stand since the main propellant valves were already installed from prior testing.

Three problems were encountered in fabrication of the thrusters involving the nozzle extension to throat section weld and the torus weld and alignment.

The nozzle extension to throat section weld is an EB welded butt joint with no filler added.   In machining the nozzle extension to match the throat section, the spinning vendor rolled the edge on two of the nozzle extensions to a knife edge. The two thrusters, SN 001 and SN 003, which had a full .076 cm (.030 in.) material thickness for both parts at the butt joint were welded with no difficulty. The two thrusters, SN 002 and SN 004, that were made with nozzle extensions that did not have the full .076 cm (.030 in.) thickness at the interface had weld joints of questionable quality. Thruster SN 004 was the spare so no rework was attempted. Rework of the weld on thruster SN 002 resulted in a burn through. The nozzle extension was machined off, a Haynes 188 insert made, and the insert EB welded to the throat section and nozzle. The throat sections of thrusters SN 002 and SN 004 are shown in Figure 52. An area of thin material can be seen for SN 004 and the insert and double weld on thruster SN 002. Additionally, Figure 52 shows details of the thermocouple instrumentation in the throat area of thruster SN 002.

The second problem in fabrication was securing the torus during weldment. There was a slight misalignment between the two halves of the torus on thruster SN 003 and a more severe misalignment on thruster SN 004.
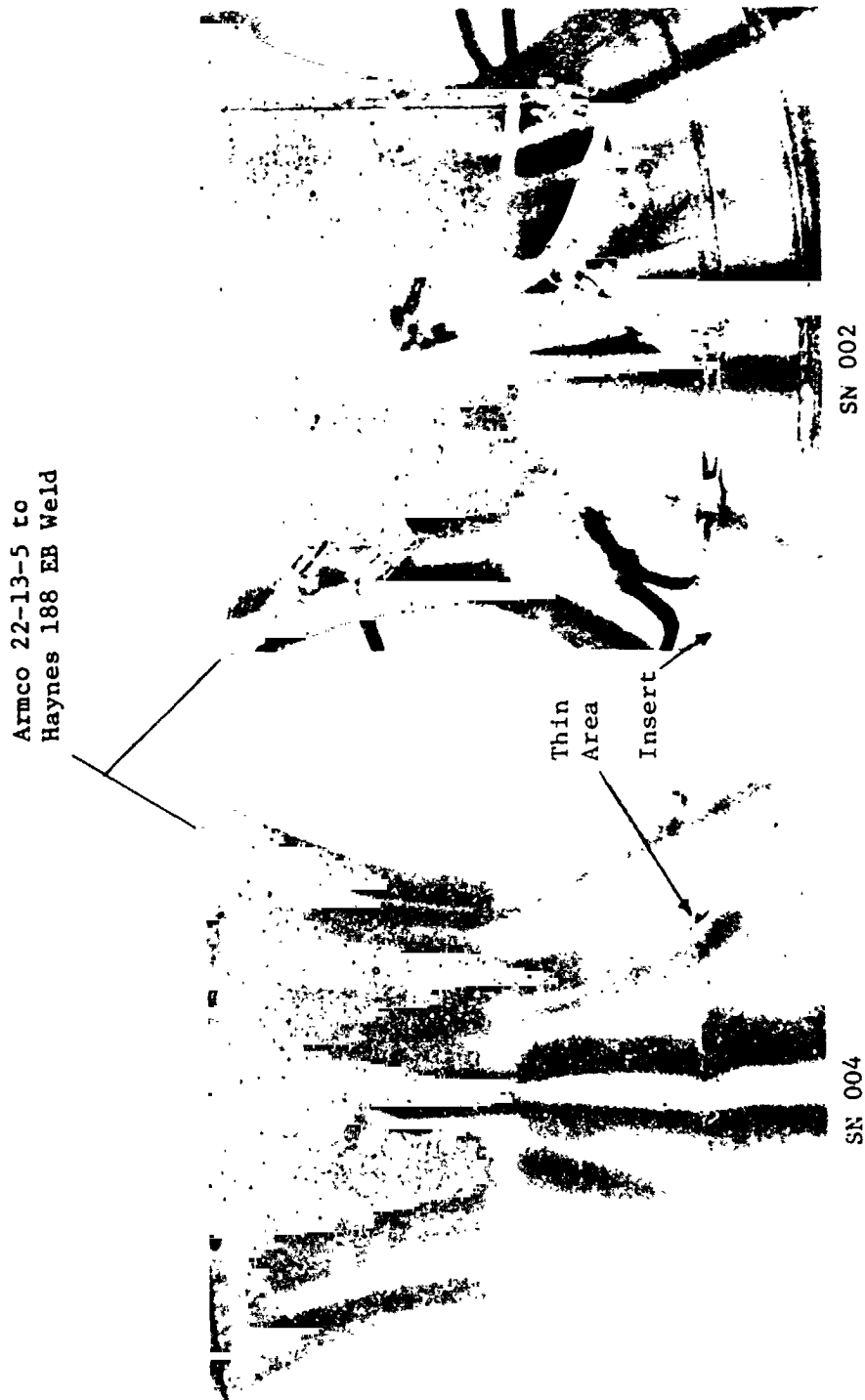
Figure 52. Throat Weldment

4.2, Fabrication (cont.)

The problem is illustrated in Figure 53. Additionally, there were four leaks found on the torus of thruster SN 004 which were repaired by welding; one of these repairs can be seen in Figure 53. Primarily because of the torus weld problem, but also because of the thin material in the throat section to nozzle extension weld area, thruster SN 004 was designated the spare. As can be seen in Figure 52, the quality of the EB weldment was good – especially the weld of the Haynes 188 throat section to the ARMCO 22-13-5 shell.

The third problem was one of alignment. The weldment of the fuel line to the torus was done with a dummy valve to align the fuel inlet line-torus shell assembly to the valve mounts during the torus welding operation. However, upon completion, the flange on the fuel inlet line of thruster SN 002 was out of alignment circumferentially with respect to the valve mount by about 4° of arc. This problem was not discovered until installation on the test stand. The test stand lines were hard mounted at the inlet to the valves to preclude transmission of deflection or loads to the ITA by reason of contraction of the feed lines as they chilled down. The position of these lines was established by plumbing up ITA SN 001. In order to fit SN 002 to this interface, the holes in the injector thrust mounts and in the fuel valve mounts had to be elongated by approximately .127 cm (.050 in.) to permit the thruster to be rotated into alignment.

ITS SN 001 differed from the other thrusters in three respects: instrumentation, annealing, and ffc inlet orificing.

ITA SN 001 had instrumentation that was not utilized on other thrusters. It had four .025 cm (.010 in.) dia thermocouples in the injector face in addition to the two .051 cm (.020 in.) dia ones which were installed in all injectors. ITA SN 001 has six gas-side thermocouples in the copper liner region of the chamber and a through-the-wall P_c tap.

SN 002
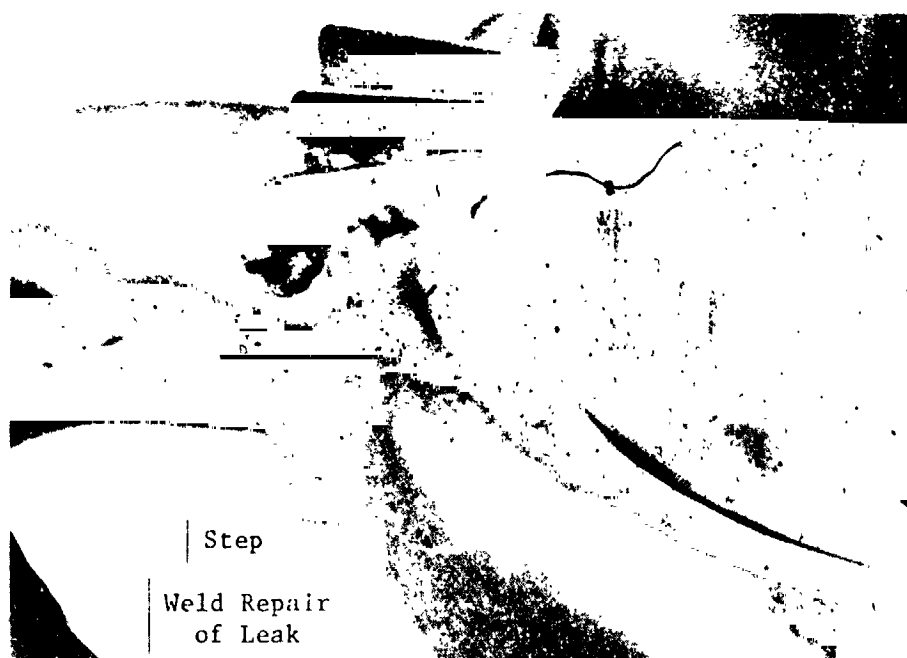
SN 004

Figure 53. Torus Weldment

4.2, Fabrication (cont.)

The gas-side thermocouples were installed after the torus and fuel line had been welded to the SN 001 unit. The thermocouples were bonded by furnace brazing. This constituted an anneal cycle for the torus and fuel line welds. None of the other units had the welds annealed.

The other unique feature of ITA SN 001 was the ffc inlet orifice fabrication. Undersized holes .051 to .053 cm dia (.020 to .021 in. dia) were machined by Electric Discharge Machining (EDM) into the shell at the inlet to each film coolant channel. EDM was used because it leaves no burr. The chamber was flow tested prior to welding the torus in place and the orifice sizes drilled out to get the required ffc flow rate. This may have left a slight burr on the downstream side of the orifice. EDM was used exclusively to provide the ffc inlet orificing for thrusters SN 002, 003 and 004.

Thrusters SN 001 and SN 003 were not photographed after fabrication. Figure 6 is a postfire photograph of thruster SN 001.

Table XXIV is a summary of ITA component, subassembly and assembly weights. Both calculated and actual weights are given. The itemization is in the form of an indentured part list with each subassembly and/or part. Neither the insulation nor the thruster with insulation was weighed. The final thruster weight includes the calculated weight for the insulation. The ITA weight, 6895 g (15.2 lb), is within 1.3% of the program goal, 6804 g (15 lb), and within 2% of the calculated weight, 6785 g (14.89 lb).

4.2.2 Igniter Fabrication

Four igniter housing assemblies and brackets, and seven integral exciter/spark plug units were fabricated. The additional exciter/spark plug units were spare in case of damage to the porcelain insulating material.

TABLE XXIV

ITA WEIGHT SUMMARY

Item	Weight gm (lb) Calculated	Actual
ITA (PN 1162900)	6758 (4.898)	6895 (15.20*)
Injector & Chamber Assembly (PN 1162904)	5559 (12.256)	5638 (12.43)
Injector Assembly	1888 (4.163)	1878 (4.14)
Injector (PN 1162889)	1663 (3.677)	-
Face Plate (PN 1161303)	233 (.514)	160 (.352)
Tube, Metering (PN 1161318)	91 (.201)	-
Baffle (PN 1162890)	129 (.285)	103 (.228)
Baffle (PN 1162891)	114 (.251)	89 (.197)
Platelets (PN 1157958-60 & 1161390)	41 (.090)	-
Flange (PN 1162886)	503 (1.110)	653 (1.44)
Cover (PN 1162892)	483 (.959)	412 (.909)
Boss (PN 1162887-1)	121 (.267)	116 (.256)
Lines and Flanges	220 (.486)	-
Flange (PN 1162901-1)	177 (.391)	-
Line (PN 1162885)	43 (.095)	-
Chamber Assembly	3671 (8.093)	-
Chamber (PN 1162898)	1562 (3.444)	1556 (-.43)
Liner, Final Machined (PN 1162893)	1107 (2.441)	-
Shell (PN 1162895)	377 (.832)	1470 (3.24)
Throat Section (PN 1162896)	76 (.171)	86 (.19)
Other Components	2109 (4.649)	-
Flange (PN 1162901-2)	162 (.358)	-
Line (PN 1162906)	134 (.295)	141 (.31)
Torus (PN 1162899)	185 (.407)	159 (.35)
Nozzle Extension (PN 1162902)	1628 (3.589)	1615 (3.61)
Igniter Assembly	935 (2.062)	995 (2.193)
Igniter Housing Assembly)PN 1162888	350 (.771)	308 (.678)
Bracket	85 (.188)	91 (.200)
Exciter/Spark Plug (GLA PN 47170)	500 (1.103)	596 (1.315)
Thermal Insulation	263 (.580)	*

*Calculated insulation weight used in total ITA actual weight of 6895 g (15.20 lb)

4.2, Fabrication (cont.)

The main igniter housing components (sleeve, body and flange) are shown in the top insert in Figure 54. The sleeve, body, flange, and oxidizer inlet line were assembled and furnace brazed together. The sleeve and flange were final machined. The fuel orifices to the igniter chamber were then machined by EDM through the sleeve and body and the coolant orifices were machined through the sleeve. There were no problems encountered in the fabrication of the igniter housing assemblies.

The titanium igniter support bracket and exciter/spark plug unit are shown in Figure 55. The fabrication of the support bracket and the design and fabrication of the exciter/spark plug were subcontracted. The initial exciter/spark plug units failed acceptance test. All units were reworked to an improved configuration and successfully passed acceptance test.

4.2.3 Injector Fabrication

The injector components (less platelets, ox line, ox inlet line flange, ox tubes, support pins and pressure fittings) are shown in Figure 56, These components are made by conventional machining.

The method of assembling the injector body is illustrated in Figure 57. The insert in the upper left corner shows the injector flange plate assembled with the center spud and face plate. The oxidizer element tubes are brazed to this subassembly at this point. In the upper right insert on Figure 57 the lower diffuser plate is shown in place. This plate is welded to the center spud on the ID. The OD of the diffuser plate is supported by six pins that are brazed to the injector flange plate and are welded to the diffuser plate. Six more pins that are brazed to the flange plate protrude through the six holes (located between the outer holes and the center hole) in this plate to support the upper distribution plate. In the lower left insert, the upper distribution plate

Ox Injection
Orifices

Sleeve

Body

Flange

Housing Components

Ox Inlet
Tube

Fuel Injection &
Coolant Orifices
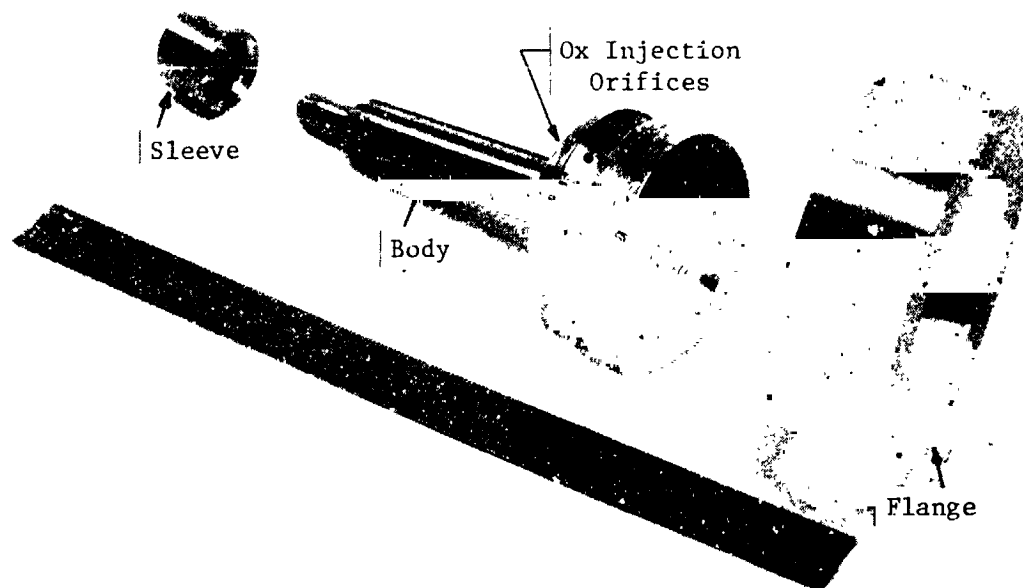
Coolant Slots
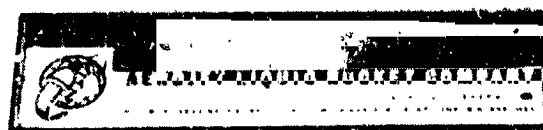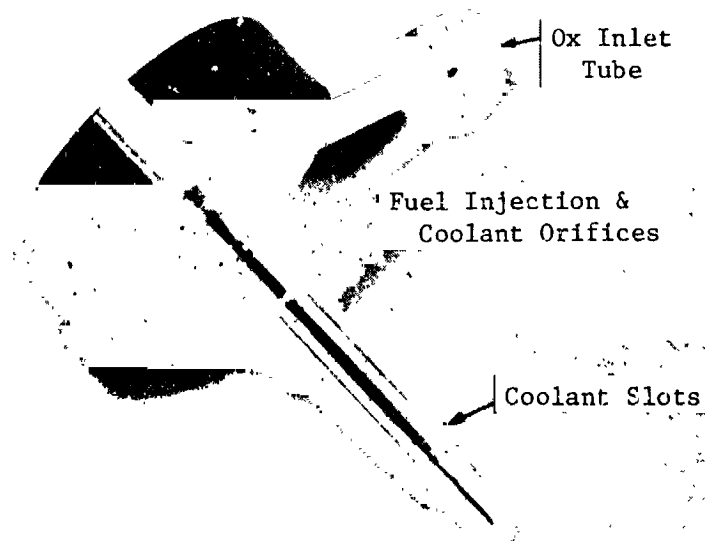
Igniter Housing, Final Machines

Figure 54. Igniter Housing Assembly

Figure 55. Integral Exciter/Spark Plug and Support Bracket
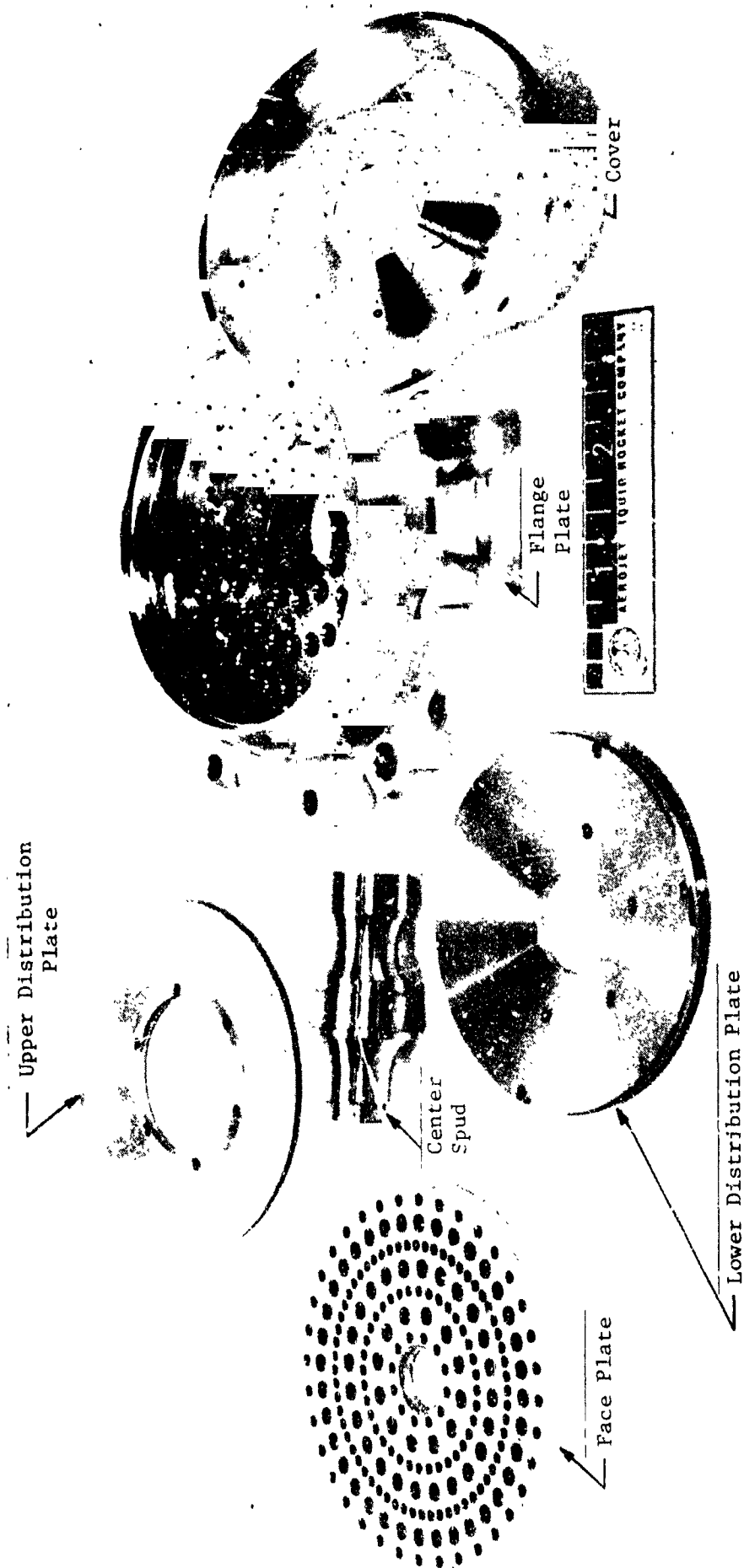
Figure 56. Injector Components
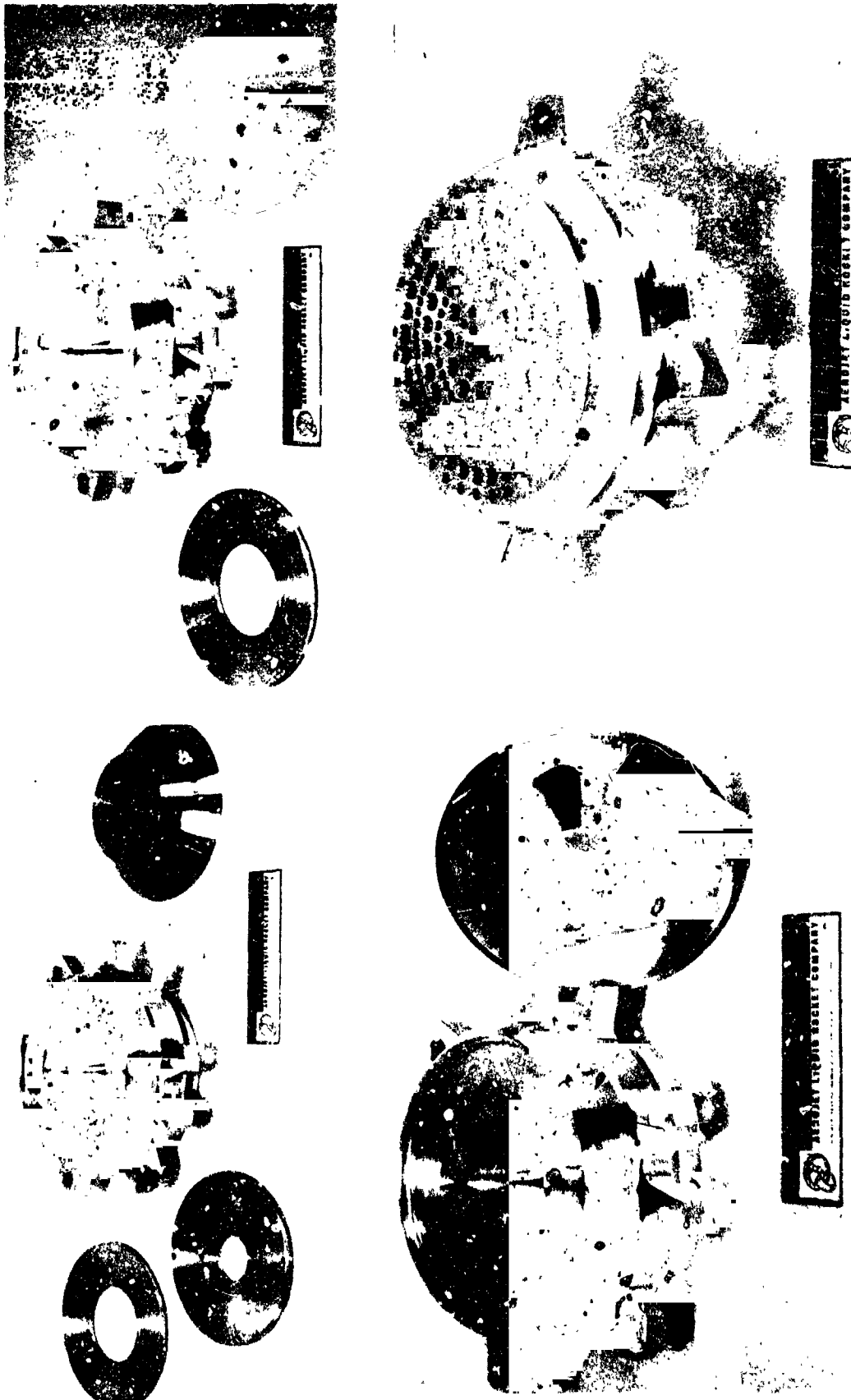
Figure 57. Injector Assembly

4.2, Fabrication (cont.)

is shown in place. It was welded to the flange plate on the OD and to the six pins that mate to the six holes at the ID. In the insert on the lower right of Figure 57, the oxidizer dome is in place and the injector body has been turned over to show the face plate.

Figure 58 shows an injector during the initial stage of assembly. The face plate, center spud, flange plate, 72-ox tube elements, and pressure and thermocouple fittings have been installed and furnace brazed. The brazement of the tubes to the face plate and flange plate are inspected at this point. If required, a second braze run with a lower melting alloy is used to correct any deficient joints. The ox tube elements are positioned by a specially machined braze fixture and are installed from the flange plate side via a tool that will fit only into the inlet end of the tube, thus insuring proper orientation of the tube inlet to the ox manifold.

The ox tubes are machined flush with the flange plate and the distribution plates and pins installed and welded. The lower insert of Figure 59 shows the injector body after weldment of the distribution plates. The top insert of Figure 59 shows that the oxidizer tubes protrude from the face plate at this stage of fabrication. This was done to facilitate leak check and tube-by-tube flow collection to check for flow uniformity prior to weldment of the cover to close out the ox manifold. If there was a flow problem due to distribution plate being improperly spaced or a plugged tube, the injector body could be reworked.

The final steps in the fabrication of the injector were machining the face plate flat, welding the manifold cover in place, machining the inlet in the cover, machining the igniter port in the center spud, machining the piston ring groove in the face plate, bonding the nickel platelets to the face plate, and welding the ox inlet line and flange in place. The igniter fuel inlet line is installed and brazed in place at the same time as the platelets. The platelets are shown in Figure 60 and the finished injector in Figure 61 (except for removal of the tabs from the platelets).
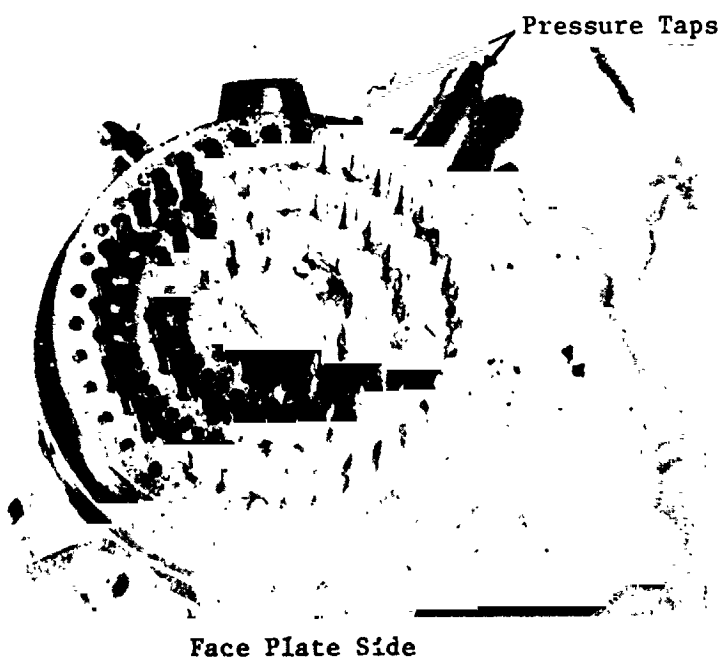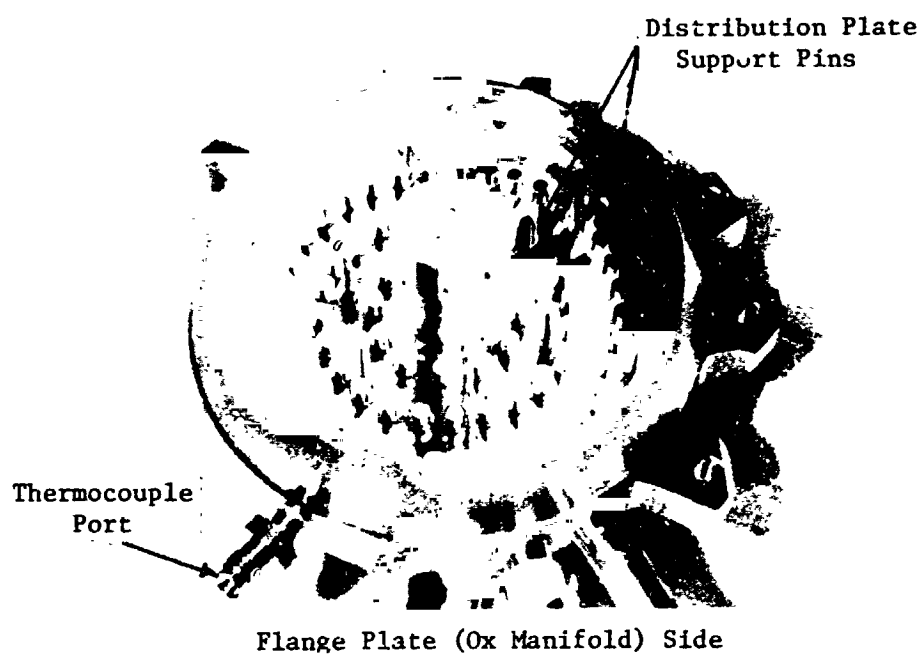
Figure 58. Injector Brazement
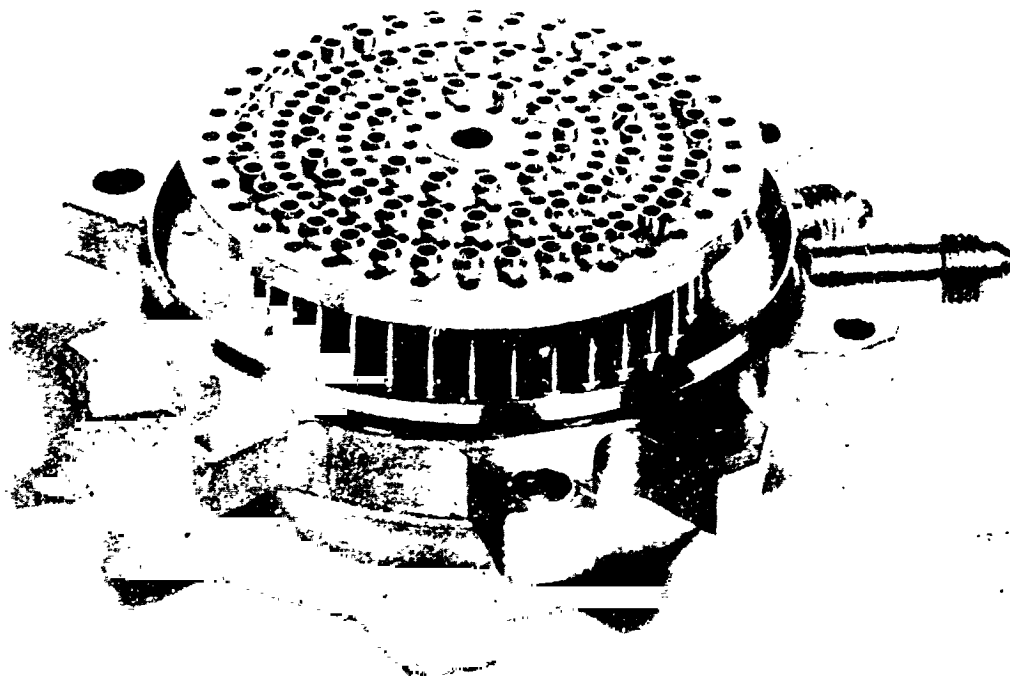
Figure 59.   Injector Body

Fuel

Fuel

Coolant Inlet

Fuel

Face

Cooling
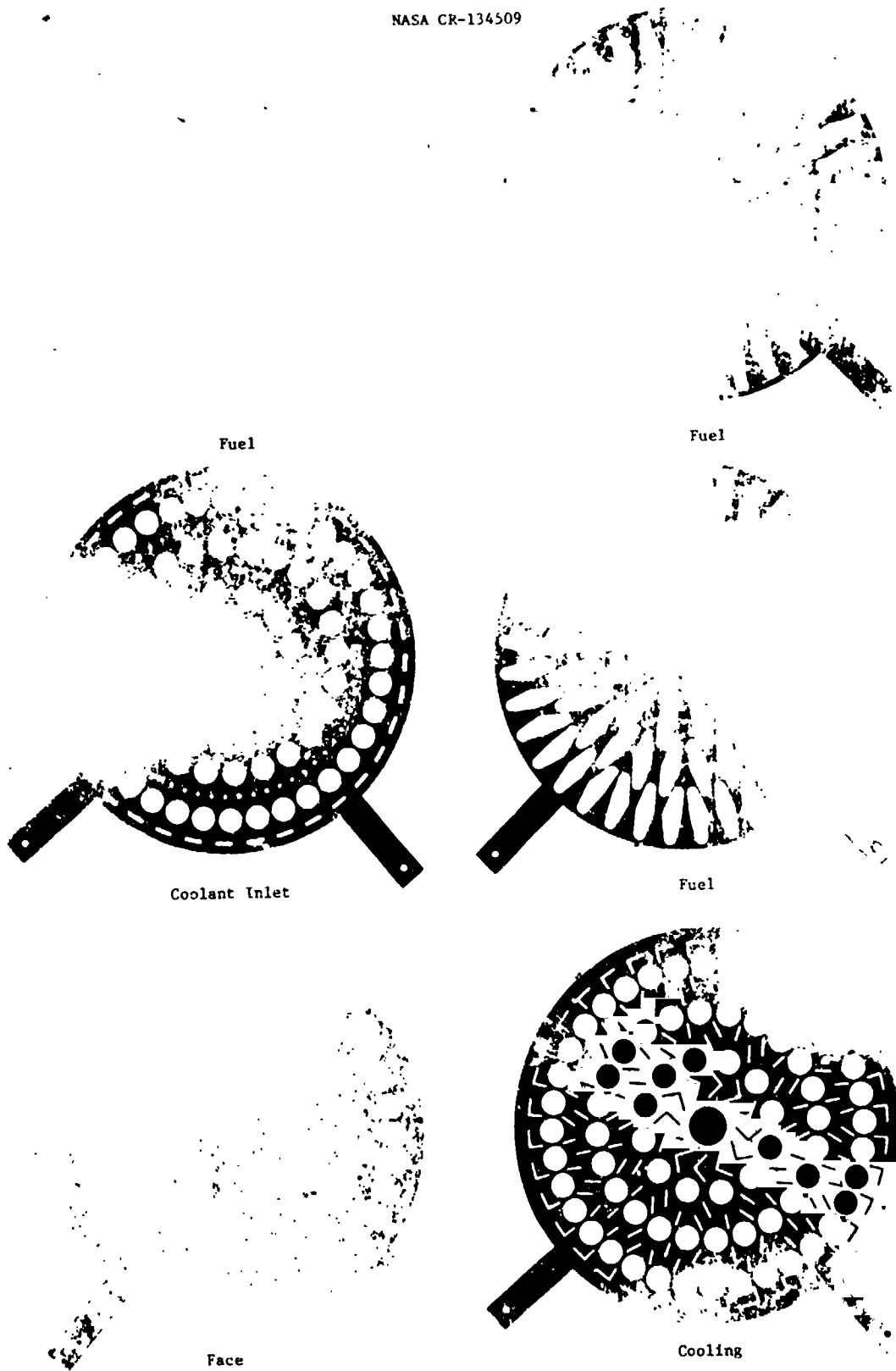
Figure 60.   Injector Platelets
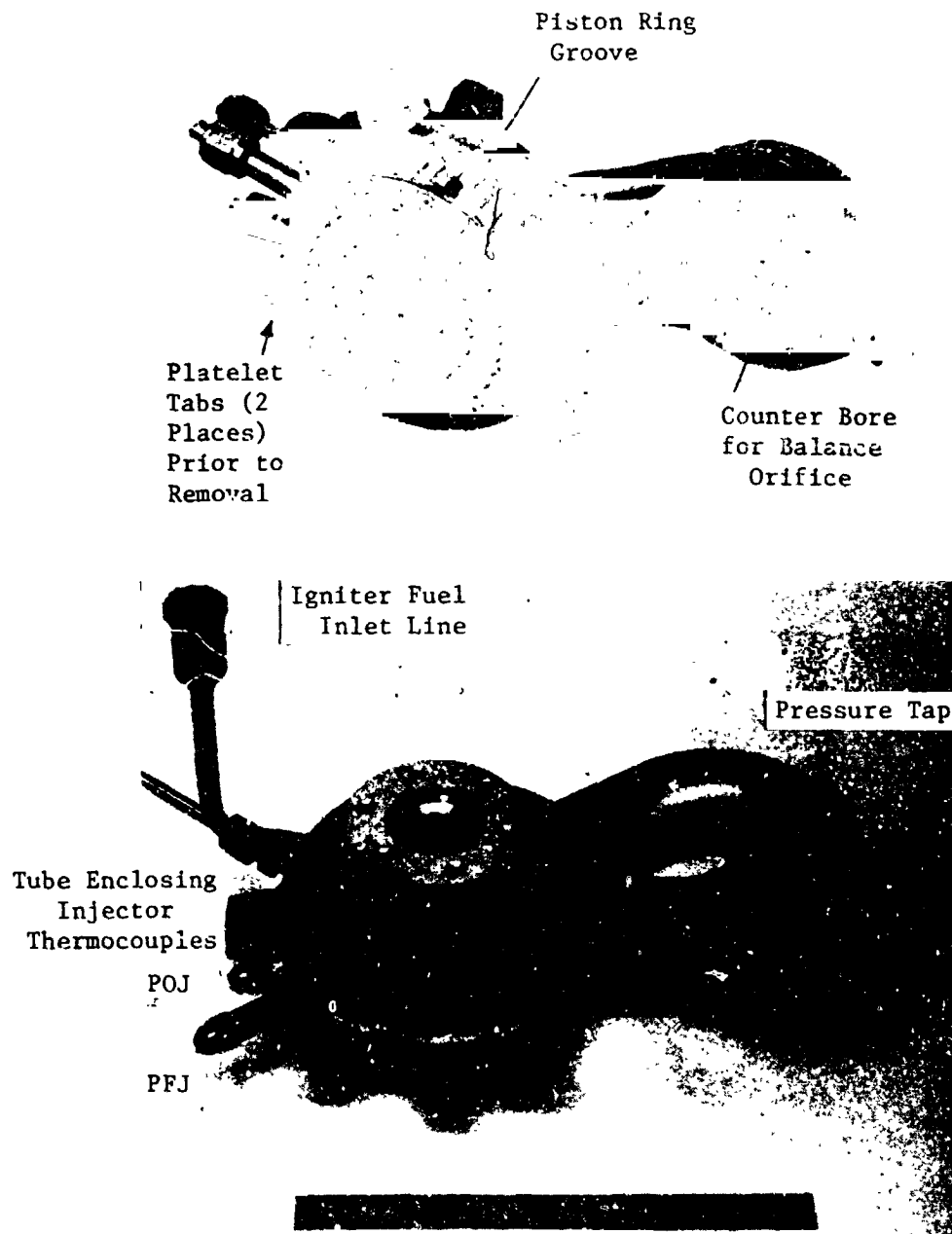
Figure 61. ITA Irjector

4.2, Fabrication (cont.)

There were no problems encountered in the fabrication of the injectors.

4.2.4 Thrust Chamber Fabrication

The thrust chamber consists of the liner, shell, throat, nozzle, torus, fuel inlet line, and inlet line flange. However, as described in Section 4.2.1, the injector was welded to the chamber liner-shell assembly before the throat was welded in place. Thrust chambers were not fabricated as a subassembly.

The fabrication of the chamber is illustrated in Figure 62. Figure (a) shows two ZrCu forgings. Both have been contour machined on the OD and slots have been milled in one. Figure 62 (b) shows the details of the slots primarily in the convergent or ffc section. Every other ffc slot is machined into the land between the regen slots rather than being terminated at the start of the regen slot to avoid the solid land that would encircle the chamber between the ffc and regen slots. The orifices in the shell that feed the ffc slots are staggered to match the slots.

Figure 62 (c) shows a ZrCu liner and ARMCO 22-13-5 shell prior to brazing the two together. The contour on the ID of the shell was match machined to the OD contour of the ZrCu liner. The shell has been machined on the OD to form the torus. After brazing the shell to the liner, the exterior was rough machined. Slots were machined in the torus area of the shell at the inlet to each regen channel and the orifices were machined at the inlet to each ffc channel. The inlet passages through the shell were machined by the EDM process.

Using flow fixtures, the chamber was then flowed for regen channel and ffc channel hydraulic resistance and uniformity (Section 4.3.4). This component checkout test verified the acceptability of the part relative to

(b) Detail of Slots in Liner

(d) Chamber Final Machined

(a) Unmachined and Machined ZrCu Liner

(c) Liner and Shell

Figure 62. Chamber Components

4.2, Fabrication (cont.)

flow distribution, ffc split, and pressure schedule. After the flow test, the chamber was finish machined on the ID and OD as is shown in Figure 62 (d). The ffc slots can be seen at the very top of the insert and the ffc orifices can be seen in the torus area on either side of the slots that open into the regen channels.

There were no problems encountered in the fabrication of the shell-liner subassemblies.

The torus shell that mates to the half of the torus that is part of the chamber was machined from an ARMCO 22-13-5 ring forging. It is approximately 13.7 cm (5.4 in.) in diameter. The flat OD section is .152 cm (.060 in.) thick. The curved flange like portions that mate to the chamber are .051 cm (.020 in.) thick.

Fabrication of the oxidizer and fuel inlet liner were sub-contracted to Arrowhead Products Division, Los Alamitos, Ca. Both were made from .051 cm (.020 in.) thick CRES 304L sheet stock. The ox line was fabricated by rolling and seam welding the sheet into a tube and then bending and forming to the final shape. The 120° arc of the fuel line was made in two halves by drop forging. The two halves were welded together. Twice the required number of parts were made; the right angle elbow was cut from half of these parts and welded to the inlet end of the remaining parts to form the finished line.

The spun Haynes 188 throat section and nozzle were sub-contracted to Monogram Industries, Culver City, Ca. The throat section is made by rolling and seam welding .076 cm (.030 in.) thick Haynes 188 sheet stock into a cylinder, grinding off excess weld material and spinning the cylinder into the required shape. Fabrication of the throat sections was completed with no problems.

4.2, Fabrication (cont.)

Some of the "sheet metal" components are shown in Figure 63. Figure 63 (a) shows the fuel line and torus. The inlet hole has been machined into the torus and the fuel line is shown fitted into the torus opening. A finished throat section is shown in Figure 63 (b).

The nozzle extension was made from Haynes 188 sheet stock .076 cm (.030 in.) thick. The sheet stock is rolled and seam welded into a truncated cone, the excess weld material ground off, and then spun into shape. The top insert in Figure 64 shows two throat sections, a partially spun nozzle and a sheet metal cone prior to spinning. The lower insert in Figure 64 shows the partially spun nozzle with a throat section on it to illustrate how the two parts mate.

Several problems were encountered in the fabrication of the nozzle extension which resulted in units being reworked. The problems are described below.

Annealing is very important in working Haynes 188. To restore ductile properties, the cool down must be accomplished rapidly (on the order of 15 minutes). The anneal must be done in an inert environment to avoid the formation of a tenacious oxide scale, which would have to be removed prior to subsequent spinning. Thus, the anneal furnace must have inert environment and forced cooling capabilities.

The initial skirt manufacturing problem was a tooling problem. A female die had been fabricated to the final configuration (with allowance for spring back). It was found that a second male spinning mandrel had to be made to accomplish the initial shaping of the skirt.

(a)   Torus and Fuel Inlet Line

(b)   Throat Section

Figure 63.   ITA Sheet Metal Components

Figure 64. Haynes 138 Throat and Nozzle Extension Fabrication

4.2, Fabrication (cont.)

A second problem occurred in the form of a brittle fracture in the forward end of all nozzle extensions. The problems was caused by grain growth during heat treat. The grain growth was exhibited only on the forward end; the aft end of the cones, which had been cold worked to a greater degree than the forward end, were ductile and workable after the heat treat. Apparently there is a cold work threshold for Haynes 188. Cold work less than the threshold value will result in grain growth during heat treat and loss of workability even though a rapid quench (less than 15 minutes) is used.

The first nozzle extension was completed by cutting off the forward end of the SN 001 unit, spinning a small cone to replace the removed section, welding the small cone to the unit, grinding down the weld, and final spinning. This nozzle extension was used on ITA SN 001. The welds could be seen because of lack of full penetration. The remaining nozzle extensions were made with excess weld material and the weld ground flush with the parent material.

The spinning procedure was changed so that the entire nozzle extension would be cold worked equally prior to each heat treat and four new nozzle extensions were started. After heat treat prior to the final spin longitudinal cracks appeared adjacent to the heat affected zone of the axial weld. The cracks were not repairable by welding. There was also a metal flow problem on the forward end. The problems are illustrated in Figure 65.

The original three remaining nozzle extensions were reworked in the same manner as the SN 001 unit. All welds were ground smooth and the surface of the finish parts polished and inspected for cracks using fluorescent dye.
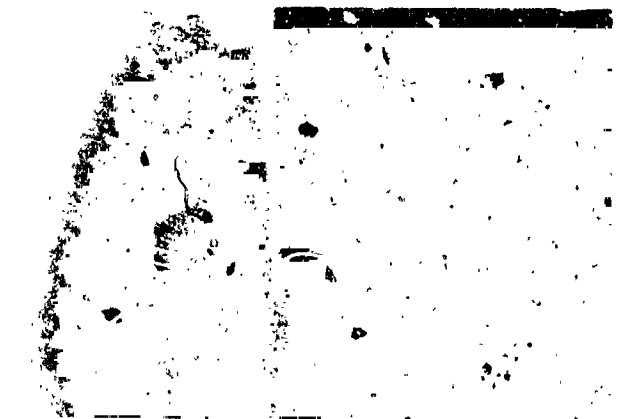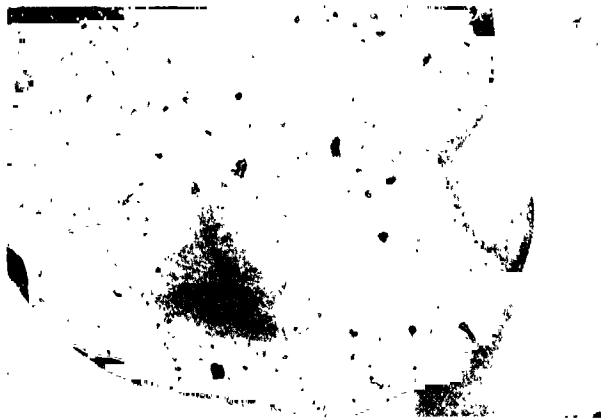
Figure 65.   Nozzle Extension Rejects

4.2, Fabr _ation (cont.)

4.2.5 Valve Fabrication

The igniter valve is a normally open, solenoid operated, two way, crogenic valve, PN V 27200-4871 made by the Valcor Engineering Corp. nhis ilve is a minor modification of a valve (Series 272-6) that has been manufactured in quantity. Valve SN 005 had a 250 scc/min (with 655 N/cm^2 (950 psia) inlet pressure) leakage rate. It was returned to the vendor and reworked to an acceptable quality. Six valves were purchased. Each valve weighs 526/531 g (1.16/1.17 lb).

Five main propellant valves were fabricated by Marquardt. The pilot valves are Wright Valves. Two spare bellows were fabricated so that this long lead item was available if a valve refurbishment was required. The opening response of the valves was .043 sec which exceeds the .040 sec specification. The leakage rate for the pilot valve on Valve SN 012 was 1620 scc/hr which exceeded the specified limit (1000 scc/hr). The valves were accepted with rework. The main propellant valve weight is 3379 g (7.45 lb).

4.3 COMPONENT CHECKOUT TESTING

The purpose of the component checkout testing was demonstration of
the acceptability of the ITA components by means of cold flow and functional
tests. The following components were tested: ITA, igniter assembly, igniter
housing, integral exciter/spark plug, injector body, injector assembly, chamber,
and valve.

4.3.1 ITA Checkout Testing

The purpose of the ITA cold flow testing was final evaluation
of the "as built" hydraulic characteristics and determination of the balance
orifice requirements.

The ITA cold flow testing was performed at ALRC in the
Aerophysics Laboratory. The test fluid was GN_2 at ambient temperature. The
operating conditions that the testing simulated and the test conditions are shown
in Table XXV. All testing was designed to provide Mach number simulation of the
flow.

The GN_2 was supplied to the fuel inlet and the oxidizer in-
let via a critical flow orifice that measured and controlled the flow rate. The
GN_2 test fluid was discharged to atmosphere. The test setup is shown schematically
in Figure 66.

The GN_2 flow rate was controlled by regulating the pressure
at the inlet to the flow control venturi. The pressures at the inlet and in the
manifolds were read on mercury or water manometers. Barometric pressure was read
before and after testing. The GN_2 flow rate to each circuit was varied in steps
by adjusting the pressure upstream of the critical nozzle. For each step, the
following were recorded: GN_2 supply pressure and temperature, inlet pressure and
manifold pressure. GN_2 flow rate was determined from the nozzle calibration curves
adjusted for temperature. The flow steps are summarized below.
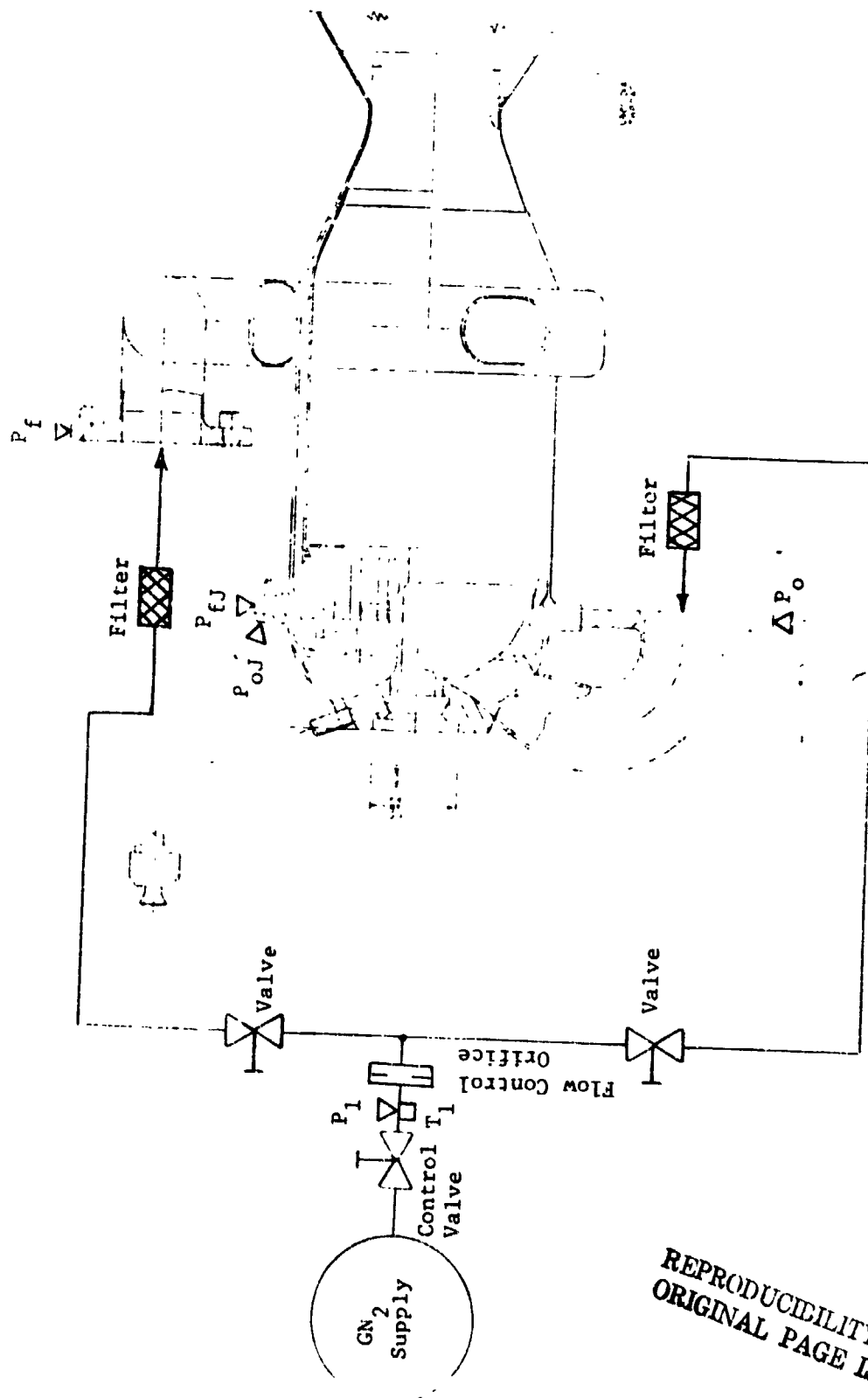
Figure 66. ITA Cold Flow Schematic

TABLE XXV

ITA OPERATING AND FLOW SIMULATION TEST CONDITIONS

	Fuel			Oxidizer		
	Actual	Pressure Ratio	Test Simulation	Actual	Pressure Ratio	Test Simulation
Inlet Pressure, N/cm^2 (psia)	276 (400)	.750	13.514 (9.6)	276 (400)	.750	13.514 (19.6)
Orifice Inlet Pressure, N/cm^2 (psia)	271 (393)	.763	13.278 (19275)	263 (382)	.785	12.906 (18.718)
Line Inlet Pressure, N/cm^2 (psia)	267 (387)	.775	13.075 (18.963)	241 (350)	.857	11.825 (17.150)
Pressure in Torus, N/cm^2 (psia)	259 (375)	.800	12.670 (18.375)	-	-	-
Injector Manifold Pressure, N/cm^2 (psia)	232 (337)	.890	11.386 (16.513)	234 (340)	.882	11.487 (16.660)
Chamber Pressure, N/cm^2 (psia)	207 (300)	1.0	10.136 (14.7)	207 (300)	1.0	10.136 (14.7)
Injector Flow Rate, g/sec (lb/sec)	247 (.545)	-	35.2 (.0777)	1252 (.252)	-	45.8 (.101)
ffc Flow Rate, g/sec (lb/sec)	66 (.145)	-	7.4 (.0163)	-	-	-
	313 (.69)		42.6 (.094)			

4.3, Component Checkout Testing (cont.)

GN_2 Flow Rate g/sec (lb/sec)

Step	Oxidizer	Circuit	Fuel	Circuit
1	45.8	(.101)	42.2	(.093)
2	18.1	(.04)	20.4	(.045)
3	27.2	(.06)	27.2	(.060)
4	36.3	(.08)	30.0	(.075)
5	45.8	(.101)	42.2	(.093)
6	61.2	(.135)	54.4	(.12)
7	77.1	(.170)	68.0	(.15)
8	90.7	(.20)	81.6	(.18)
9	45.8	(.101)	42.2	(.093)

The balance orifice requirements were determined by flowing each circuit at a fixed GN_2 flow rate with the balance orifice installed in the ITA inlet line flange. The orifice was drilled out and the inlet edge rounded until the required pressure was read upstream of the orifice. From Table XXV show that fo Mach number scaling, the GN_2 flow rate for the oxidizer circuit was 45.8 g/sec (.101 lb/sec) and the required pressure at the inlet was 12.906 N/cm^2 (18.718 psia); the GN_2 flow rate for the fuel circuit was 42.6 g/sec (.094 lb/sec) and the required pressure at the inlet was 13.278 N/cm^2 (19.257 psia).

4.3.2   Igniter Checkout Testing

The igniter testing consisted of cold flow testing of the housing, exciter/spark plug testing and igniter assembly functional testing.

4.3.2.1   Igniter Cold Flow Testing

The objective of the cold flow testing of the igniter housing was to determine the integrity of the assembly (leak check), evaluate hydraulic characteristics and determine balance orifice requirements.

4.3, Component Checkout Testing (cont.)

The igniter contains three hydraulic circuits: oxidizer, fuel coolant and fuel core. The sleeve on the igniter housing forms the seal between the fuel manifold and the coolant circuit, and contains the orificing that determines the fuel hydraulic resistance and the split of fuel flow between the core and the coolant circuit.

In order to complete the fuel manifolding, close out the coolant passages and provide a fuel inlet, t igniter housing was installed in the test fixture shown in Figure 67. The test fixture simulates the geometry of the injector at the injector/igniter interface. The larger flange on the forward end of the fixture contains a cooling passage that permits LN_2 to be used to chill in the hardware. The aft flange mates to the vacuum duct for igniter test firing. These features permitted the test fixture, after cold flow testing was completed, to be used for the checkout test firings at vacuum conditions.

A schematic of the igniter cold flow test setup is shown in Figure 68. With valve V_5 closed and the throat plug and aft closure plate in place, all flow passages are sealed and leak checks can be performed. With valve V_5 open and/or the throat plug removed, the oxidizer circuit and the fuel core circuit can be flowed. With the throat plug in place and valve V_5 closed and the aft closure plate removed, the coolant circuit can be flowed. The fuel and oxidizer valves are shown in phantom in Figure 68 as they were installed only for the balance flow testing.

The following cold flow tests were run:

(1) Leak check.
(2) Flow Characterization - SN 001

    Fuel Core Circuit
    Fuel Coolant Circuit
    Oxidizer Circuit
    Internal Leakage

(3) Acceptance test - all four units
(4) Balance tests
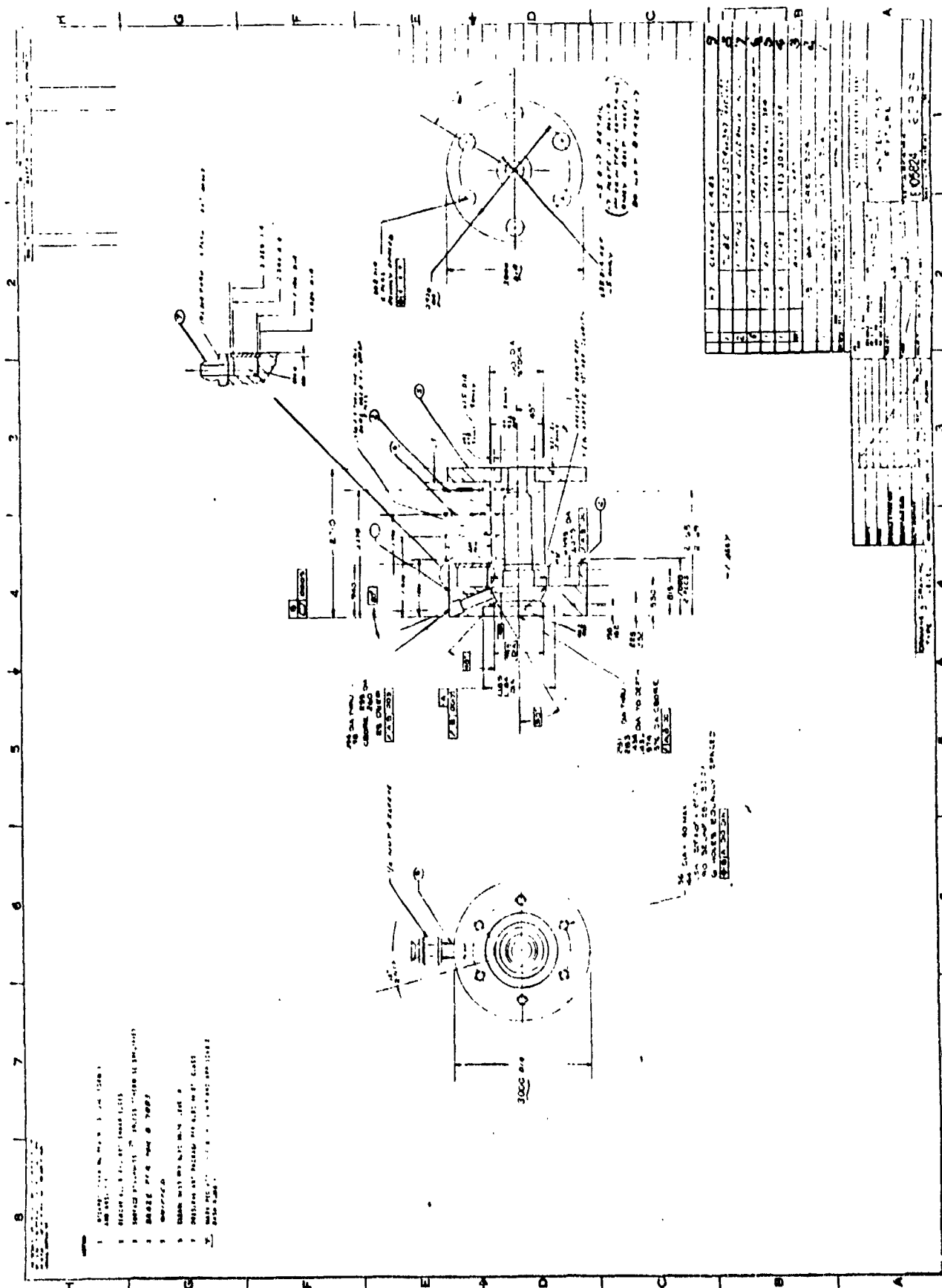
Figure 67. Igniter Test Fixture
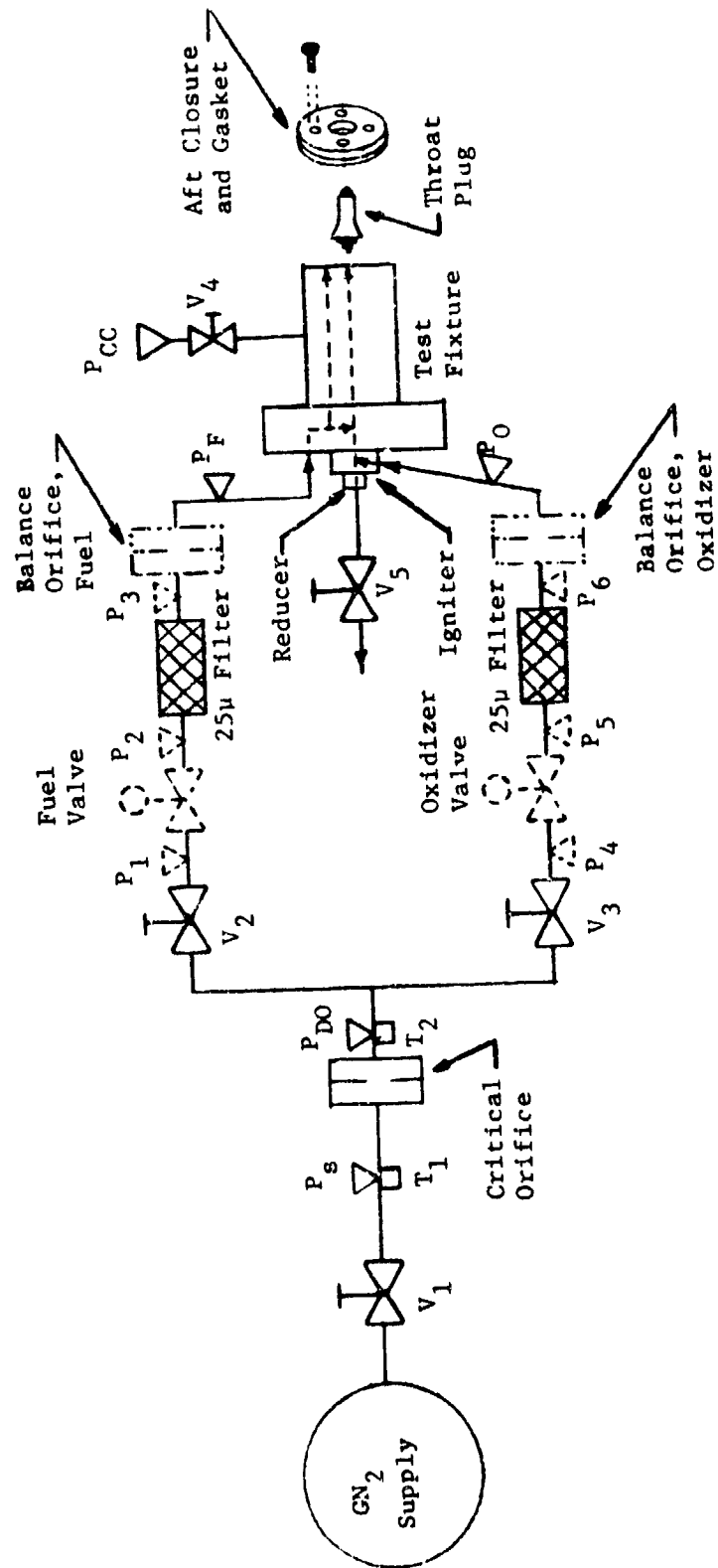
Figure 68. Igniter Cold Flow Test Schematic

4.3, Component Checkout Testing (cont.)

The igniter operating conditions and the flow test simulation test conditions are summarized in Table XXVI. The GN_2 flow rates were measured and controlled by setting the pressure upstream of the calibrated venturi's flowing critically. Igniter housing SN 001 was used for the cold flow testing.

4.3.2.1.1 Leak Check

The throat plug and aft closure were installed and valve V_5 (Figure 68) was closed isolating all flow circuits. The igniter was pressurized to 34.5 N/cm^2 (50 psia) and an external leak check was performed.

4.3.2.1.2 Flow Characterization

Igniter SN 001 was flow tested to determine first article hydraulic characteristics. Of primary interest was the pressure drop in the fuel circuit and the split in hydrogen flow between the core and the coolant circuits.

Each circuit (coolant, fuel core and oxidizer) were flowed individually. GN_2 was flowed through each circuit in steps by varying the inlet pressure to the critical venturis. For each step, the following were recorded: GN_2 supply pressure and temperature, inlet (manifold) pressure and temperature, coolant channel pressure and back pressure. The coolant circuit discharged to atmosphere. For the hydrogen core circuit and the oxidizer circuit chamber pressure is the back pressure. Chamber pressure was maintained at 20.7 N/cm^2 (30 psia) via valve V_5 (Figure 68) when flowing the oxidizer and fuel core circuits.

TABLE XXVI

IGNITER OPERATING AND FLOW SIMULATION TEST CONDITIONS

	Fuel		Oxidizer		Balance Test	
	Actual	Test Simulation	Actual	Test Simulation	Fuel	Ox
Valve Inlet Pressure, N/cm² (psia)	276 (400)	-	276 (400)	-	92 (133.3)	92 (133.3)
Manifold Pressure, N/cm² (psia)	236 (343)	23.6/70.9 (34.3/103*)	210 (305)	21 (30.5)	79 (114)	70 (102)
Chamber Pressure, N/cm² (psia)	207 (300)	20.7 (30.0)	207 (300)	20.7 (30.0)	69 (100)	69 (100)
Coolant Circuit Back N/cm² (psia)	-	10 (15)	-	-	10 (15)	-
Coolant Flow Rate, g/sec (lb/sec)	.726 (.0016)	3.28 (.00724)	-	-	3.28 (.00724)	-
Chamber (Core) Flow Rate, g/sec (lb/sec)	4.26 (.0094) 4.99 (.0110)	.187 (.000412)	.33 (.072)	2.54 (.0056)	.56 (.00123) 3.84 (.00847)	7.62 (.0168)

*Flow in coolant circuit is sonic because it normally discharges to vacuum prior to mainstage ignition. Because cold flow is done with atmospheric back pressure, manifold pressure must be greater than 32.8 N/cm² (47.5 psia) for flow to be sonic. Therefore, coolant circuit made with 30% simulation of pressure rather than 10%.

4.3, Component Checkout Testing (cont.)

The flow steps that were used are:

	Coolant		GN_2 H_2 Core		Flow Rate, g/sec (lb/sec) Oxidizer	
1	2.40	(.0053)	.408	(.0009)	11.3	(.025)
2	2.72	(.006)	.363	(.0008)	9.1	(.020
3	3.18	(.007)	.318	(.0007)	6.8	(.015)
4	3.63	(.008)	.272	(.0006)	4.5	(.010)
5	4.08	(.009)	.227	(.0005)	3.4	(.0075)
6	4.54	(.010	.181	(.0004)	2.3	(.005)
7			.136	(.0003)		
8			.019	(.0002)		
9			.059*	(.0013)		

*Approximate minimum

4.3.2.1.3 Internal Leakage Test

The sleeve on the igniter housing that contains the fuel orifices acts as a seal between the fuel manifold and the coolant circuit. One test was conducted with the SN 001 igniter housing to determine the leakage past this seal. A .00254 cm (.001 in.) thick stainless shim stock strip was wrapped around the sleeve and spot welded to the O.D. of the sleeve, effectively increasing its diameter by .0051 cm (.002 in.). The igniter housing was shrunk fit into the test fixture and the coolant circuit flow characterization test was repeated.

4.3.2.1.4 Acceptance Testing

On the basis of the cold flow data obtained with igniter SN 001, the fuel core and cooling orifices were resized to adjust the fuel circuit pressure drop and the split between core and coolant flow to the desired values.

4.3, Component Checkout Testing (cont.)

The sleeves were machined off of the two completed housings (SN 001 and SN 002) . new sleeves brazed in place and orifices machined in all four units using EDM. All four units were cold flow tested. The fuel core circuit, fuel coolant circuits and oxidizer circuit of each unit was flowed as described above for the SN 001 unit.

4.3.2.1.5 Balance Testing

Igniter housing SN 003 was instrumented with thermocouples. One land was machined at several axial locations by removing enough material to accommodate the thermocouple junction. The housing was installed in the test fixture and the thermocouples were fed out through the wall of the test fixture via thermocouple ports. The igniter valves were installed. Balance orifices were installed in both circuits in the form of dishpan orifices at the inlets to the igniter (outlet of the igniter valves). The aft closure plate was removed from the test fixture. Pressure in the chamber was maintained at 69 N/cm^2 (100 psia) via valve V_5 (Figure 68) with the inlet pressure held at 89.6 N/cm^2 (130 psia). Both the oxidizer circuit and the fuel circuit were flowed and the GN$_2$ flow rates determined from the venturi inlet pressures. The diameters of the balance orifices were changed until a GN$_2$ flow rate of 3.48 g/sec (.00846 lb/sec) was achieved in the fuel circuit and 7.6 g/sec (.0168 lb/sec) in the oxidizer circuit. No orifice was required in the oxidizer circuit. The exciter/spark plug and support bracket were installed after the cold flow balance test and the test fixture-igniter-valve and line assembly used for the igniter test firings (Section 4.3.2.2. and .3)

4.3.2.2   Integral Exciter/Spark Plug Testing

The following tests were conducted on the integral exciter/ spark plug units:

4.3, Component Checkout Testing (cont.)

> Acceptance test (GLA)
> Component checkout (ALRC)
> EMI (GLA)
> Temperature, life and operation (GLA)

In addition to verification of electrical characteristics, each exciter unit was acceptance tested at conditions simulating operation. Each exciter/spark plug was installed in a test fixture that was pressurized using one of the igniter valves. The exciter was turned on and the valve opened permitting pressure around the electrode to rise rapidly until the spark discharge was supressed. Each unit was operated this way 100 times before sealing and 200 times after sealing. This test duplicated the ALRC component checkout testing (described below) which had failed the original integral exciter/spark plug design.

In addition to the acceptance test on each unit, GLA ran temperature, life, operation, calibration and EMI tests on an engineering unit that duplicated the deliverable units except for potting. The engineering unit was operating .05 sec on and .05 sec off until steady state temperatures were reached at ambient room temperature and at $-79^{\circ}C$ ($-110^{\circ}F$). This provided energy input/temperature data required to determine if overheating could occur with extended operation at vacuum conditions or if heat loss by conduction to a cold injector would adversely affect operation.

In the life testing, the unit was operated .05 sec on and .05 sec off for 35 minutes. At the end of the test, the unit was operating within design specifications. Assuming that 50,000 pulses represents a ten year life service and that the exciter would be on approximately .04 sec each pulse, the required life would be approximately 33 min.

4.3, Component Checkout Testing (cont.)

As part of the operation and calibration tests current
and spark rate were measured as a function of temperature and input voltage.
Output voltage, peak voltage, current and power, and output voltage, current and
power history were determined.

Preliminary EMI evaluation of the exciter in the prototype
stage by GLA has shown that the requirements of MIL-STD-461A, Notice 3 for Class
A2 equipment will be met in formal bench testing, and that, when combined with
the ITA, compatibility for both steady state and transient conditions will be
ensured. Conducted EMI was measured (20 to 50 M Hz) on the positive and negative
input leads and on the monitor lead. Radiated EMI was measured over the frequency
range of 14 KHz to 1 GHz. Conducted susceptibility testing was performed in
accordance with the procedure of Method CS01 (30 Hz to 50 Hz). Additional
susceptibility (conducted per Methods CS02 and CS06, and radiated per Methods
RS02 and RS03) tests were not performed.

Component checkout testing of the integral exciter unit
at ALRC was performed by firing the igniter at simulated altitude conditions.
After cold flow of the instrumented SN 003 igniter housing, described above,
the igniter housing and fixture with valves and fuel balance orifice were installed
on the vacuum chamber test stand in the ALRC Research Physics Laboratory as
shown in Figure 69. A schematic of the test setup is shown in Figure 70. All
tests were conducted using ambient temperature propellants. The planned pressure
at the fuel valve was 286 N/cm^2 (415 psia), and was 338 N/cm^2 (490 psia) at the
oxidizer valve. The duty cycle was .1 sec firing followed by a .2 sec coast
repeated 100 times. Testing was terminated prior to 100 pulses in the event
of several successive no ignitions. All of the igniter test firings are summarized
in Table XXVII including the functional test series described in the next subsection.
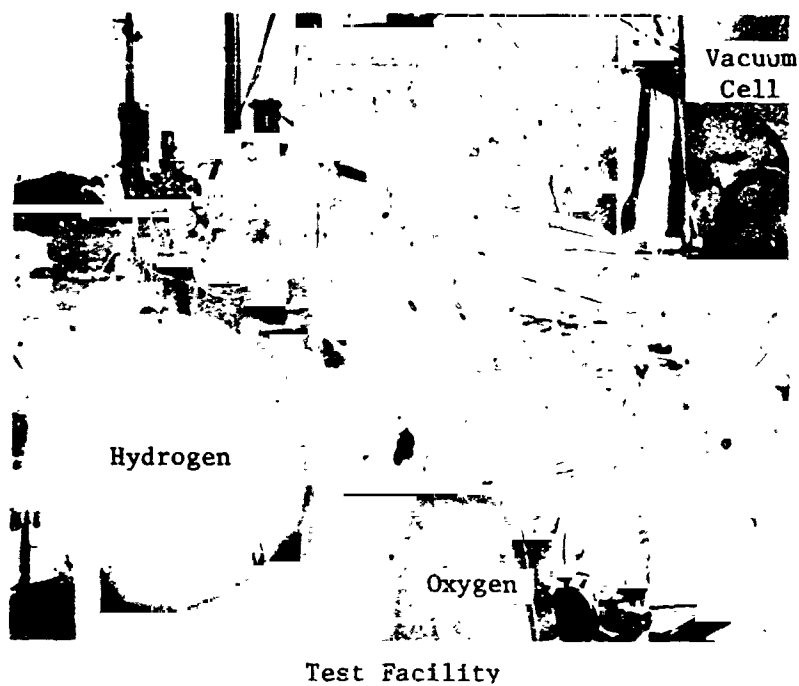
Test Facility

Figure 69.   Igniter Test Setup
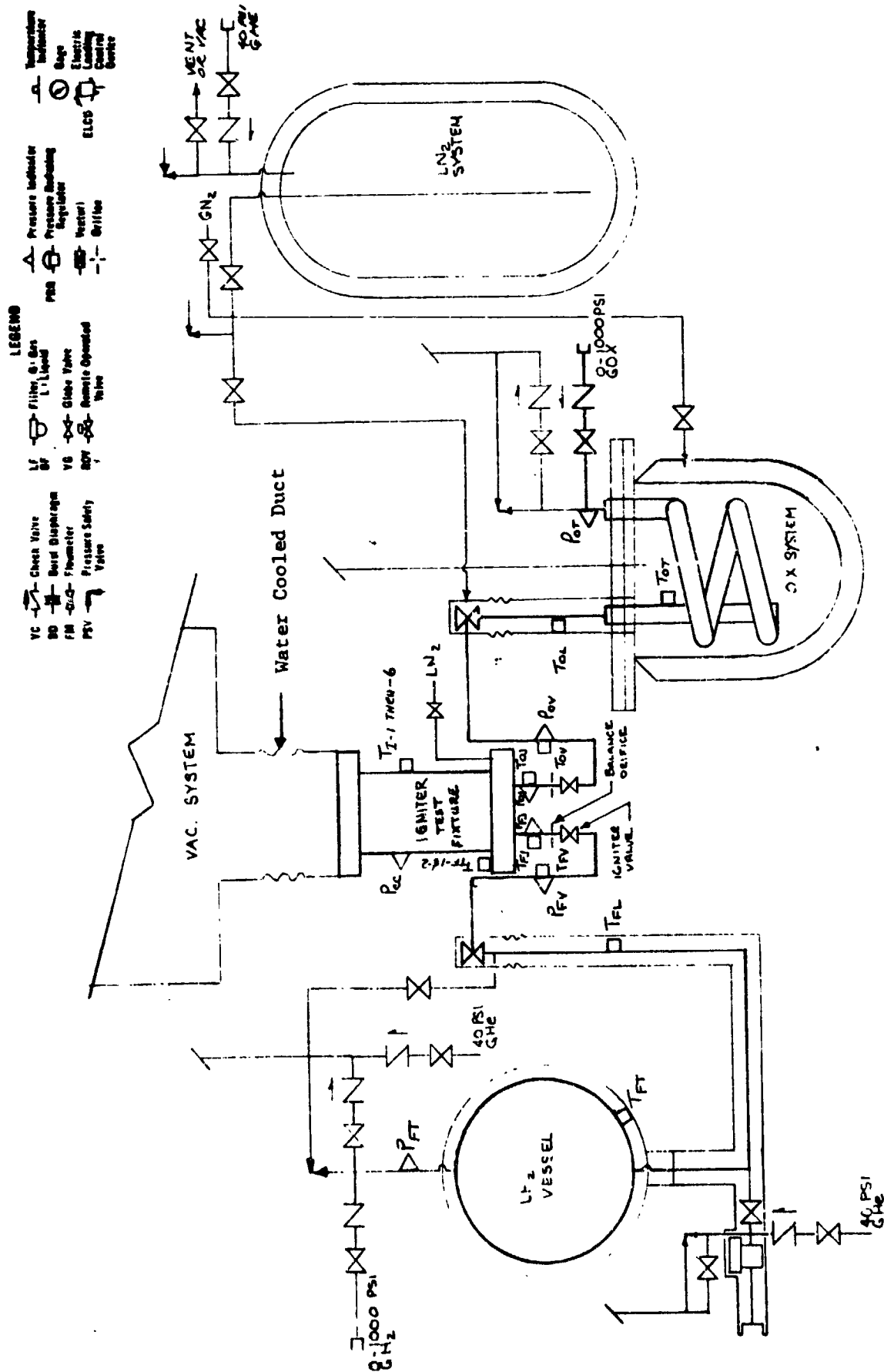
Figure 70. Igniter Facility Flow Schematic

TABLE XXVII

SUMMARY OF IGNITER TESTING

DATE	TEST	EXCITER SN	TEST SERIES IGNITER FUNCTIONAL	EXCITER CHECKOUT	BENCH TEST	COMMENTS
3-8-73	-101	005	x			Cold flow with GH_2 & GO_2 on test stand.
	-101A	005	x			Electrical checkout
	-102	005	x			Electrical checkout
	-103	005	x			One pulse checkout firing
	-104	005	x			Ambient test per plan -100 pulses
	-105	005	x			Ambient test per plan -100 pulses
	-106	005	x			100 puses - cooled duct to vacuum chamber overheated
3-22-73	-107	005	x			Repeat test- view duct - exciter SN005 fails
	-108A	005		x		Moved electrode - no ignitio
	-108B	005		x	x	Checkout of spark discharge
	-108C	005/003		x	x	Spark discharge - Compared SN 005 & SN 003
3-23-73	-109A	003		x		Test firing - SN003 fails
	-109B	003		x	x	Changed method of spark monitor
	-109C	003		x	x	Spark discharge test
3-26-73	-110A	007		x		Test firing - SN007 fails
	-110B	007		x	x	Spark discharge test
	-110C	004		x	x	500 pulses in air
	-110D	004		x	x	500 pulses at vacuum
	-111A	004		x		Test firing - SN004 intermittent operation
4-15-73	-110	sparkplug	x			Resumed functional testing with sparkplug & remote excite r
	-111/-118	sparkplug	x			Completed functional testing
4-24-73	-119A	004A		x	x	100 pulses in air
	-119B	004A		x	x	100 pulses - test setup- no vacuum
	-119C	004A		x	x	100 pulses - test setup - vacuum

TABLE XXVII (cont.)

DATE	TEST	EXCITER SN	TEST SERIES			COMMENTS
			IGNITER FUNCTIONAL	EXCITER CHECKOUT	BENCH TEST	
	-119D	004A		x	x	40 pulses – valve acutation – no propellants
	-119E	004A		x		Test firing – failure
	-119F	004A		x	x	Spark discharge
5-7-73	-120A	003A		x		Test firing 100 pulses
	-120B	003A		x		Test firing – 12 N/cm^2 higher pressure – 100 pulses
	-120C	003A		x		Test firing – $9N/cm^2$ higher pressure – 100 pulses
	-120D	003A		x		Test firing – higher pressure –failed on 87th pulse
5-8-73	121	008		x		Test firing – failed on 18th pulse
	122A	001A		x		Checkout test firing
	122B	001A		x		Test firing – 100 pulses – some no ignitions
	122C	001A		x		Test firing – 100 pulses – some no ignitions
	122D	001A		x		Test firing – 100 pulses – some no ignitions
	123	001A		x		Test firing – $241N/cm^2$– Oka,
	124	001A		x		Test firing – $276N/cm^2$ – one no ignition
	125	001A		x		Test firing – $283N/cm^2$ – few no ignitions
	126	001A		x		Test firing – $310N/cm^2$ – more no ignitions
	127	001A		x		Test firing – $328N/cm^2$ – many no ignitions
5-16 & 5-17-73	Test No's not Recorded	Breadboard		x		GLA testing with breadboard configuration – bench tests- test firings – gas flow tests over 1000 firings made in one configuration alone.

Page 189

4.3, Component Checkout Testing (cont.)

Seven integral exciter units were tested at ALRC, six to failure, in addition to a breadboard unit. The failure mode was duplicated by a rapid rise rate in pressure during the spark electrical discharge cycle using GN_2. This discovery permitted testing to be conducted at GLA on a bench scale under conditions which permitted better measurements to be made (less electrical interference).

4.3.2.3 Igniter Functional Test Firing

The objective of the igniter test firings was design verification and characterization. The test results were used to define sequencing requirements, verify repeatibility and most important of all to demonstrate that there was nothing in the design or construction of the igniter hardware that would preclude ignition under all conditions of ITA operation. This type of testing led to identification and replacement of an undersized component in the exciter. The test firings described in this section required the igniter components to operate over a range of propellant inlet temperature and pressure, with fuel lead and lag and with spark delays.

The igniter, test fixture, valves, fuel balance orifice, and set up that were used for the exciter checkout testing were used for the igniter functional testing.

The hydrogen was temperature conditioned using LN_2 and/or GN_2 in the jackets on the tank and line. Cold and warm GN_2 were bled into the jackets in the proportions required to obtain the desired temperature.

The GO_2 propellant was temperature conditioned by the bath around the oxygen heat exchanger coil, and maintained by the jackets on the line and tank. GO_2 temperatures were maintained in excess of 167°K (300°R) to avoid condensation to LO_2 in the system.

4.3, Component Checkout Testing (cont.)

The operating conditions at which the igniter tests were conducted and the significance of each test are summarized in Table XXVIII. The duty cycle consisted of repetitive firing for .1 sec followed by a .2 sec coast. The first three ox lead/lag conditions of Test 116 were investigated with a 10 pulse train. The remaining lead/lag conditions of Test 116 and all the Test 118 conditions were investigated with a 5 pulse train. Thus, each condition of propellant or spark lead or lag was repeated at least five times. All the remaining tests were made with 100 pulses each. A total of 1075 firings were made.

4.3.3   Injector Checkout Testing

Injector cold flow testing was done in two stages. A flow test was made on the injector body for uniformity of oxidizer flow distribution. This test was made prior to welding the injector dome in place so that the injector body could be reworked in the event of a flow maldistribution.

The second flow test was made on the completed injector assemblies. Both the oxidizer and fuel circuits were tested. The objective of the testing was hydraulic characterization and verification of uniformity of injection.

All four injector assemblies were subjected to cold flow testing during fabrication (injector body ox circuit and as completed assemblies).

The injector body testing was performed on PN 1162817 which is shown in Figure 59 (see Figure 29 for drawing). The test fixture shown in Figure 71 was used to complete the oxidizer circuit. The tubing bend and the geometry of the fixture are designed to duplicate the flow path at the inlet

TABLE XXVIII

IGNITER TEST CONDITIONS

Test	Propellant Temperature, °K (°R) Ox Valve	Fuel Valve	Pressure N/cm² (psia) Ox Valve	Fuel Valve	Comments
116	220 (396)	(100 (180))	259 (375)	279 (405)	Ox lead/lag (10*, 5, 0, -5, -10)
118	206 (370)	86 (155)	274 (397)	276 (400)	Spark lead/lag (25, 20, 5, 0, -3, -7, -12)
104	289 (520)	289 (520)	268 (398)	448 (650)	High and low MR with ambient propellant temperature.
106	289 (520)	289 (520)	309 (448)	286 (415)	
111	226 (406)	160 (288)	236 (343)	320 (464)	High and low MR with cold propellant temperature.
112	219 (394)	168 (303)	259 (375)	248 (360)	
113	213 (383)	176 (317)	431 (625)	396 (575)	High and low pressure with high MR and cold propellants.
115	237 (427)	122 (220)	167 (242)	159 (230)	
117	216 (389)	254 (457)	286 (415)	241 (350)	Pressure at valves = 276 ± 34 N/cm² (400 ± 50 psia).
110	283 (509)	155 (279)	221 (320)	338 (491)	
114	220 (396)	142 (256)	290 (420)	300 (435)	Propellant temperatures ranging between cold and ambient.
105	289 (520)	289 (520)	220 (319)	241 (350)	

*Time in msec.
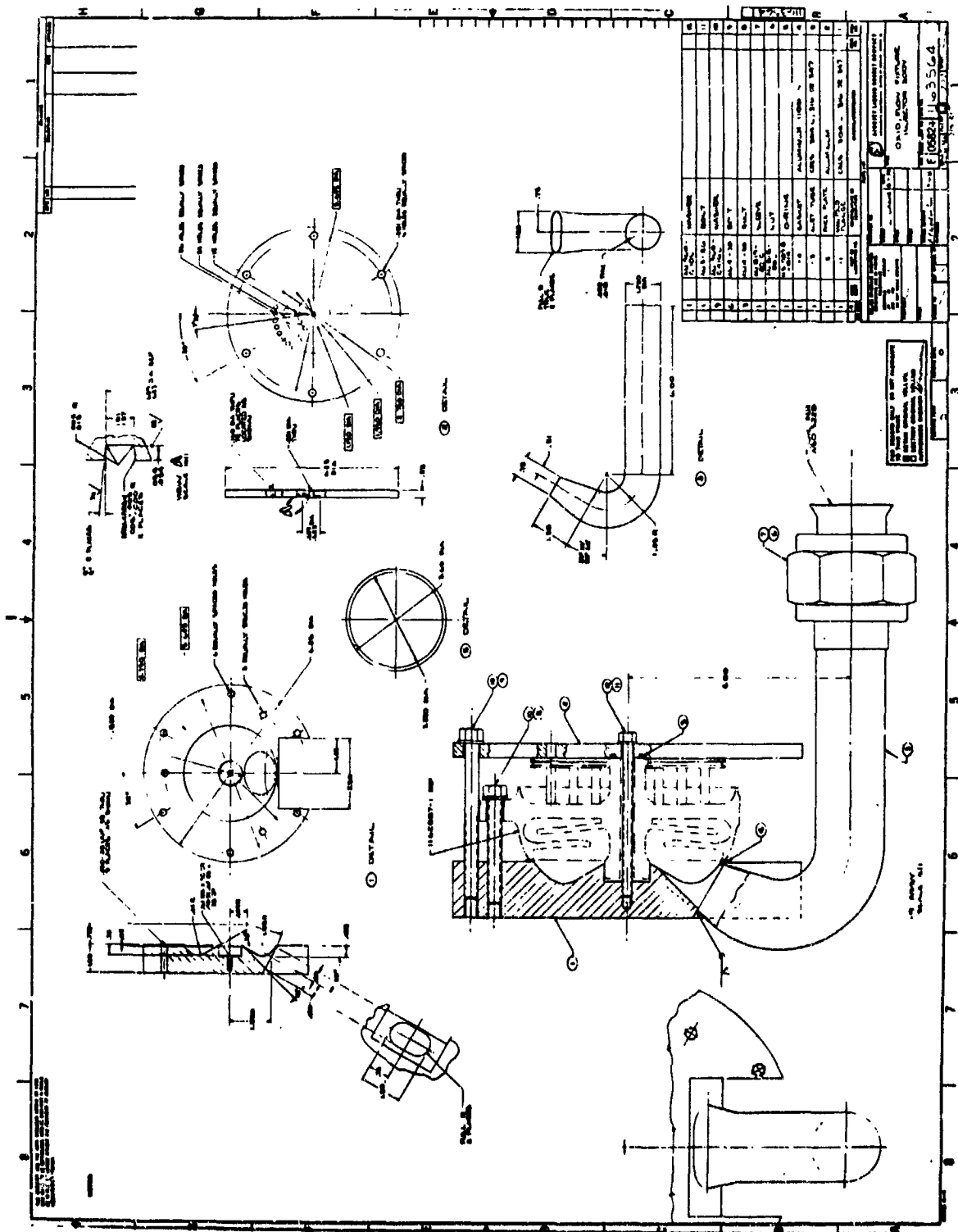
Figure 71. Injector Body Test Fixture

4.3, Component Checkout Testing (cont.)

to the injector and of the manifold. After flowing the SN 001 injector body,
the face plate (Item 2 in Figure 71) was not used. The tubes were not machined
flush as was done in SN 001, but were left as shown in Figure 59. The flow
collection probe was reworked to fit over the end of the oxidizer tubes. This
was found to be less restrictive than having the probe fit into the face plate
holes and eliminated the problems associated with gasket alignment.

The injector fuel circuit is fed from the regen section of
the chamber. Flow testing of the injector fuel circuit, therefore, required use
of the fixture shown in Figure 72 to introduce the GN_2 in the fuel plenum and
to complete the fuel manifold. The GN_2 test fluid is introduced into the fuel
manifold through 80 equally spaced orifices that duplicate the distribution
and pressure drop of the 80 chamber regen channels. The seal between the test
fixture and injector was accomplished by means of an O-ring in the piston ring
groove (Item 20 in Figure 72) and a gasket (Item 8 in Figure 72) between the
injector lip and the face of the fixture.

Testing was performed at ALRC in the Aerophysics
Laboratory. The test fluid was GN_2 at ambient temperature. GN_2 flow rates were
measured and controlled by setting the pressure at the inlet to a critical nozzle
(sonic flow in nozzle). The flow collected from each element was measured using
a rotameter. Manifold and inlet pressures were measured using mercury and water
manometers. A diagram of the test set up is shown in Figure 73. Testing for
flow uniformity of an injector body and an injector is shown in Figure 74.

The flow uniformity tests were made by setting the flow
rate to the injector and collecting the flow from each of the 72 elements.
Rotameter readings were recorded for each element. GN_2 supply pressure and
temperature, manifold pressure and atmospheric pressure were recorded at the
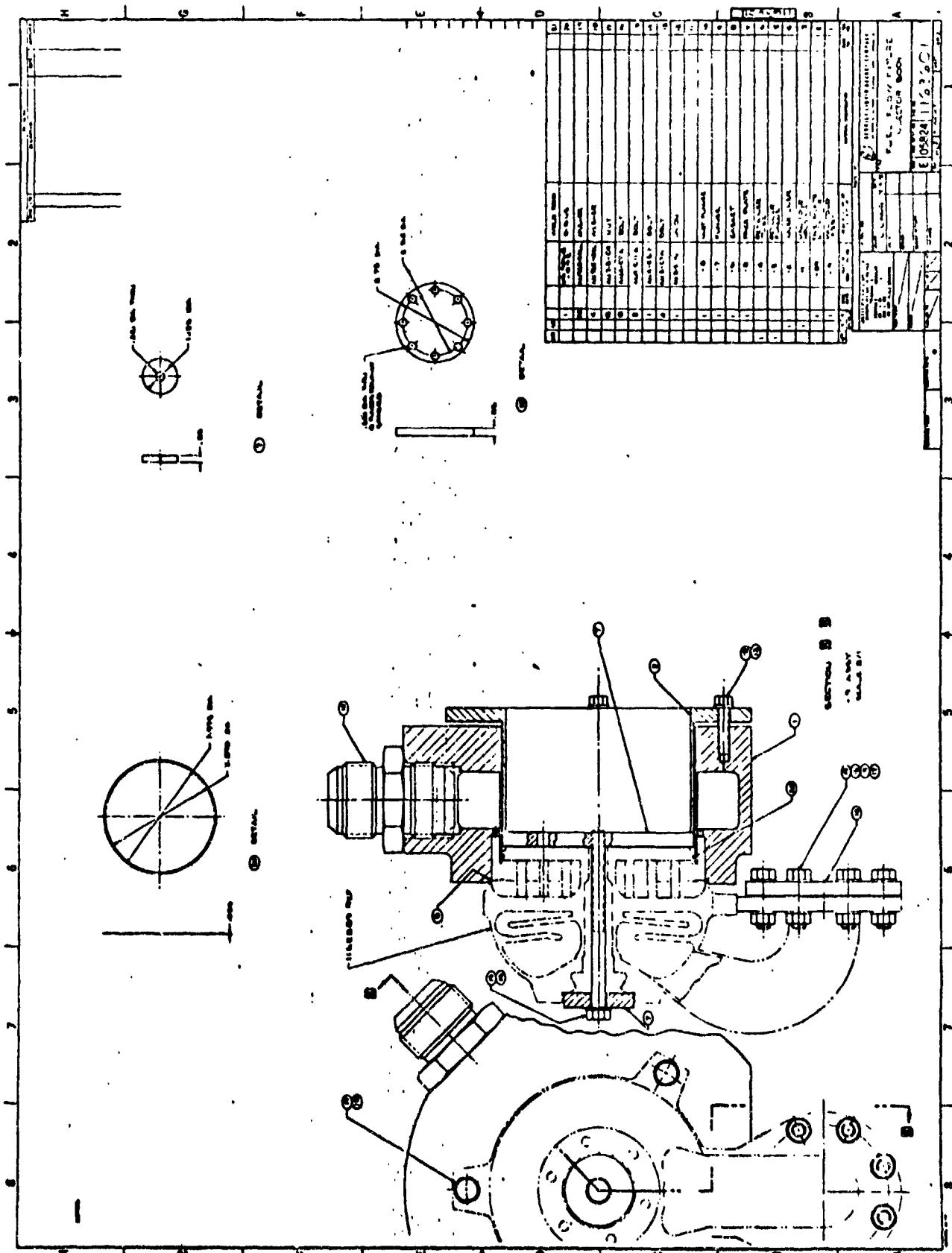
Figure 72. Fuel Flow Fixture Injector Body
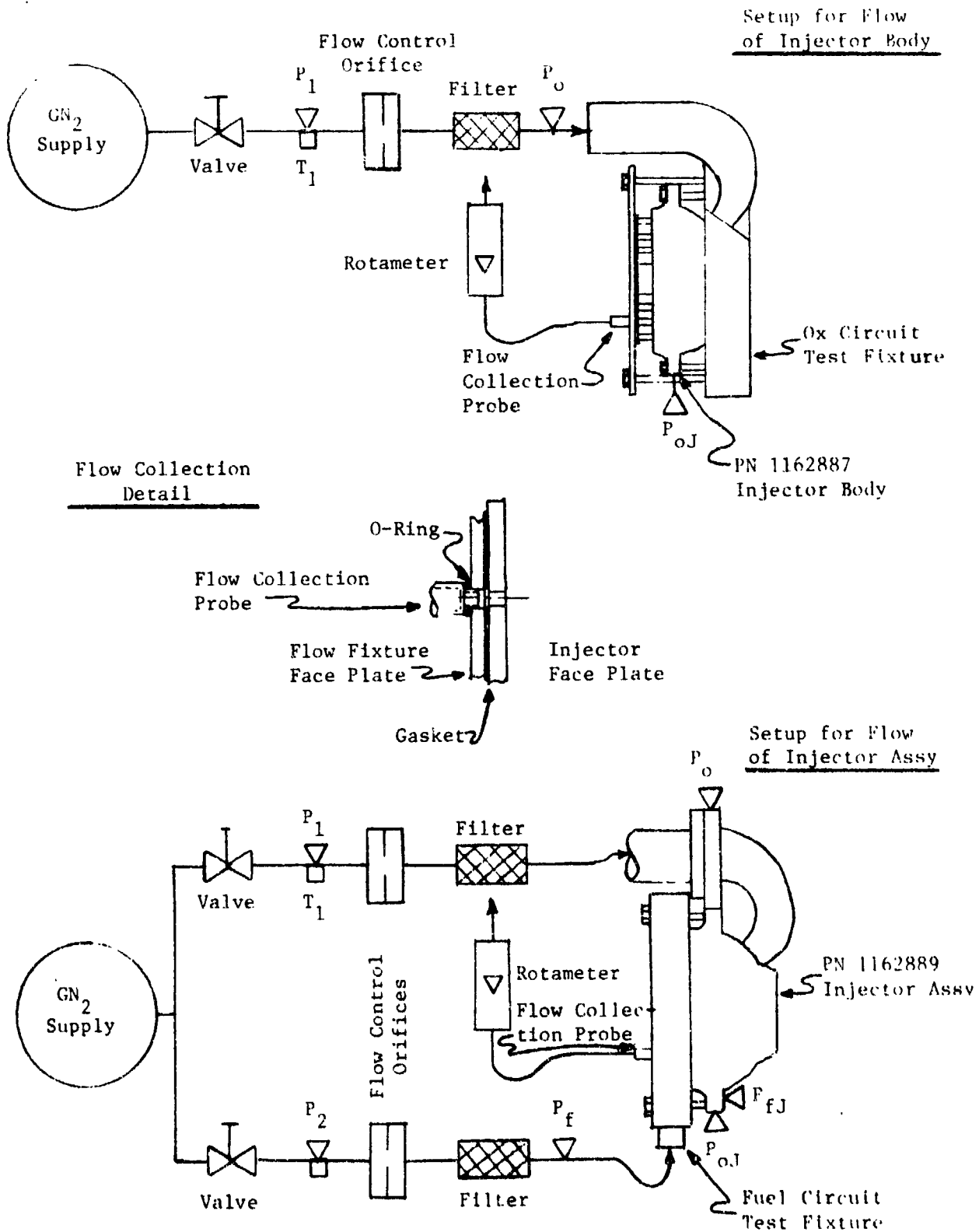
Figure 73. Injector Cold Flow Schematics
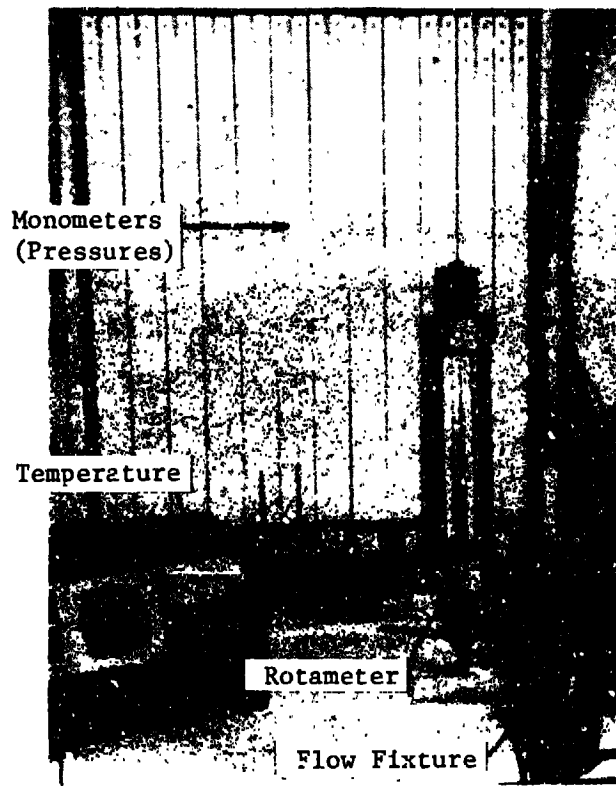
(a) Cold Flow Test Setup
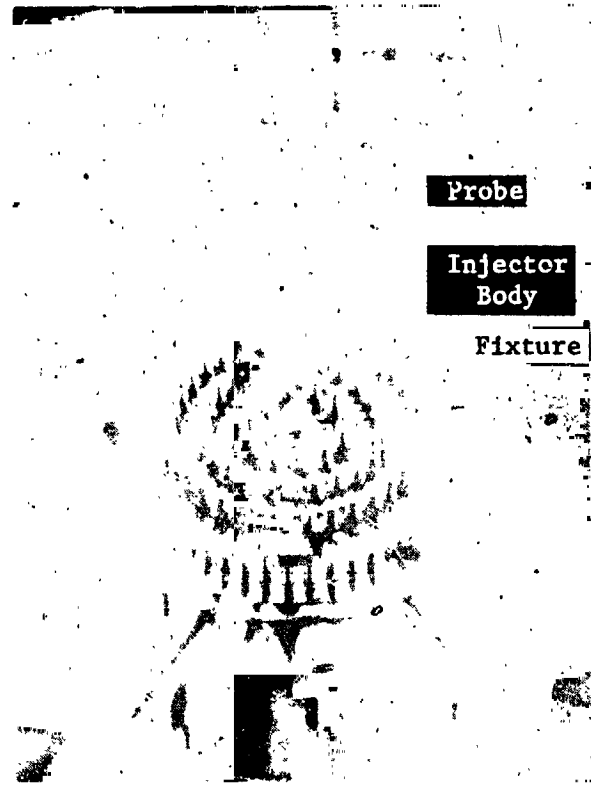
(b) Injector Body Testing
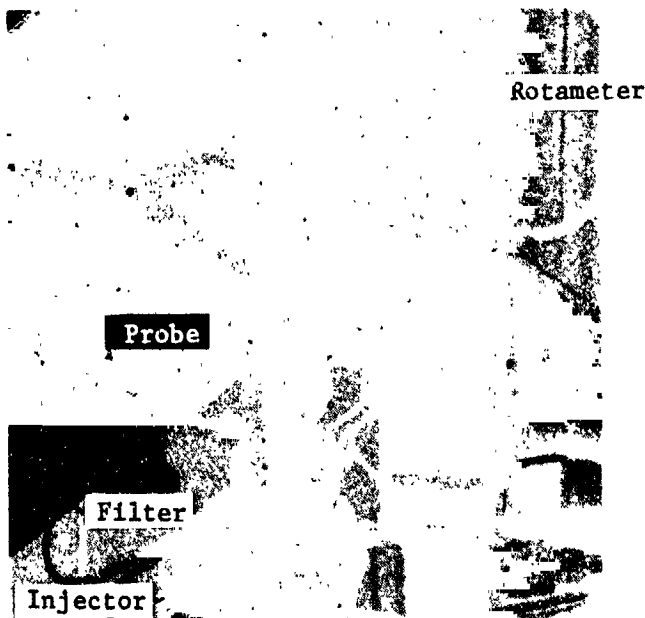
(c) Injector Testing

(d) ffc Circuit Water Flow

Figure 74. Cold Flow Testing

.4.3, Component Checkout Te-ting (cont.)

beginning and end of the t-st. The GN_2 supply pressure was monitored and adjusted to maintain a constant flow rate. The probes were designed to be nonrestrictive and the pressure drop in the collection circuit was periodically measured to insure that the resistance of the flow collection circuit was not affecting the measurements. The GN_2 flow rates in the oxidizer and fuel circuit were set to provide pressure ratio simulation of injector operating conditions as summarized in Table XXIX.

TABLE XXIX

INJECTOR OPERATING AND COLD FLOW TEST CONDITIONS

| | Oxidizer Circuit | | Fuel Circuit | |
	Actual	Test	Actual	Test
Manifold Pressure, N/cm^2 (psia)	234 (340)	11.5 (16.7)	232 (336)	11.2 (16.3)
Chamber Pressure, N/cm^2 (psia)	207 (300)	10.1 (14.7)	207 (300)	10.1 (14.7)
Flow Rate, g/sec (lb/sec)	1252 (2.76)	45.8 (.101)	242 (.545)	35.2 (.0777)

The injector flow characterization testing was performed by varying the GN_2 flow rate in steps via setting the pressure upstream of the critical flow nozzle. For each step the following was recorded: supply pressure and temperature, inlet pressure and manifold pressure. Barometric pressure was recorded at the start and conclusion of the testing. The flow steps that were used are listed below.

4.3. Component Checkout Testing (cont.)

	GN$_2$ Flow Rate, g/sec (lb/sec)	
Step	Oxidizer Circuit	Fuel Circuit
1*	45.8 (.101)	35.24 (.0777)
2	18.1 (.04)	1°.9 (.035)
3	27.2 (.06)	2ú.7 (.050)
4	36.3 (.08)	29.5 (.065)
5	45.8 (.101)	35.24 (.0777)
6	59.0 (.135)	49.9 (.11)
7	77.1 (.17)	68.0 (.15)
8	90.7 (.20)	81.6 (.18)
9	45.8 (.101)	35.24 (.0777)

---

*Step 1 not always used.

4.3.4   Chamber Checkout Testing

Chamber flow testing was performed prior to the final weldment of the torus. Cold flow testing was done prior to completion of the chamber so that the fuel flow split between the regen and the ffc section could be altered, if required, and the inlet could be modified in the event of a flow maldistribution. The SN 001 chamber was intentionally made with undersized orifices so that after the chamber was flow tested the orifices could be resized on the basis of the flow test data, and the chamber reflowed. The orifice sizes in subsequent chambers were based on the SN 001 data and none required modification. The purpose of the chamber cold flow testing, in addition to the design verification using chamber SN 001, was characterization of the film and regen coolant hydraulics and verification of flow uniformity.

As described in Section 4.2.4, the exterior of the chamber shell, after brazing the liner to the shell, was rough machined. The area of the chamber, comprised of the chamber half of the torus and the regen channel inlet

4.3, Component Checkout Testing (cont.)

slots and the ffc inlet orifices, were final machined. A flow fixture was made to simulate the torus close out and attached to the shell.

The flow fixture is shown in Figure 75. One of the spare thrust chamber fuel lines was used as the inlet line on the flow fixture, and, therefore, reproduced the flow geometry at the inlet to the torus. The removable cover flange (Item 3, Figure 75) was used to block the regen circuit so that the film coolant circuit could be flowed independently. As can be seen in Figure 75, the cover flange and the test fixture were sealed by O-rings that fitted into grooves machined into the chamber. The O-ring grooves were shallow enough and located so that they were removed in final machining.

The chamber cold flow testing was performed at the ALRC Aerophysics Laboratory. The test fluid was GN_2 at ambinet conditions. The GN_2 flow rate was controlled and measured by setting the pressure to a critical flow nozzle. Flow rates were established to produce Mach number similarity. The operating and test conditions are summarized in Table XXX. The chamber cold flow test schematic is shown in Figure 76.

TABLE XXX

CHAMBER OPERATING AND COLD FLOW TEST CONDITIONS

| | | Test Condition | |
	Actual	Regen Section	ffc Section
Inlet Pressure, N/cm^2 (psia)	267 (387)	11.65 (16.90)	14.27 (20.69)
Pressure in Torus, N/cm^2 (psia)	259 (375)	11.29 (16.38)	13.82 (20.04)
Injector Manifold Pressure, N/cm^2 (psia)	332.1 (336.6)	10.14 (14.7)	—
Chamber Pressure, N/cm^2 (psia)	207 (300)	—	—
FFC Back Pressure, N/cm^2 (psia)	190 (.545)	10.14 (14.7)	10.14 (14.7)
Regen Section Flow Rate, g/sec (lb/sec)	247 (.545)	29.9 (0.66)	—
FFC Section Flow Rate, g/sec (lb/sec)	65.8 (.145)	4.94 (.0109)	9.03 (.0199)
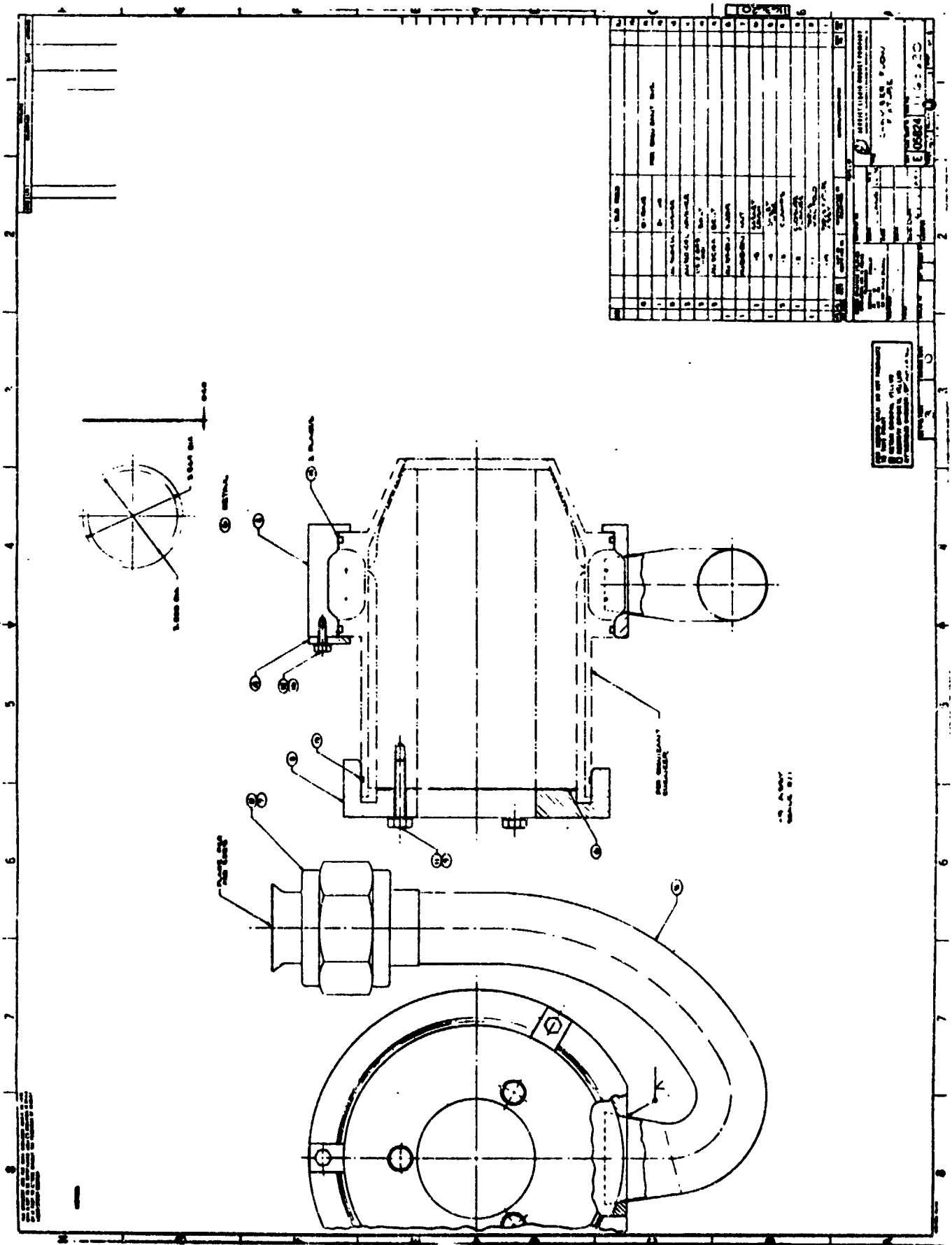
Figure 75. Chamber Flow Fixture
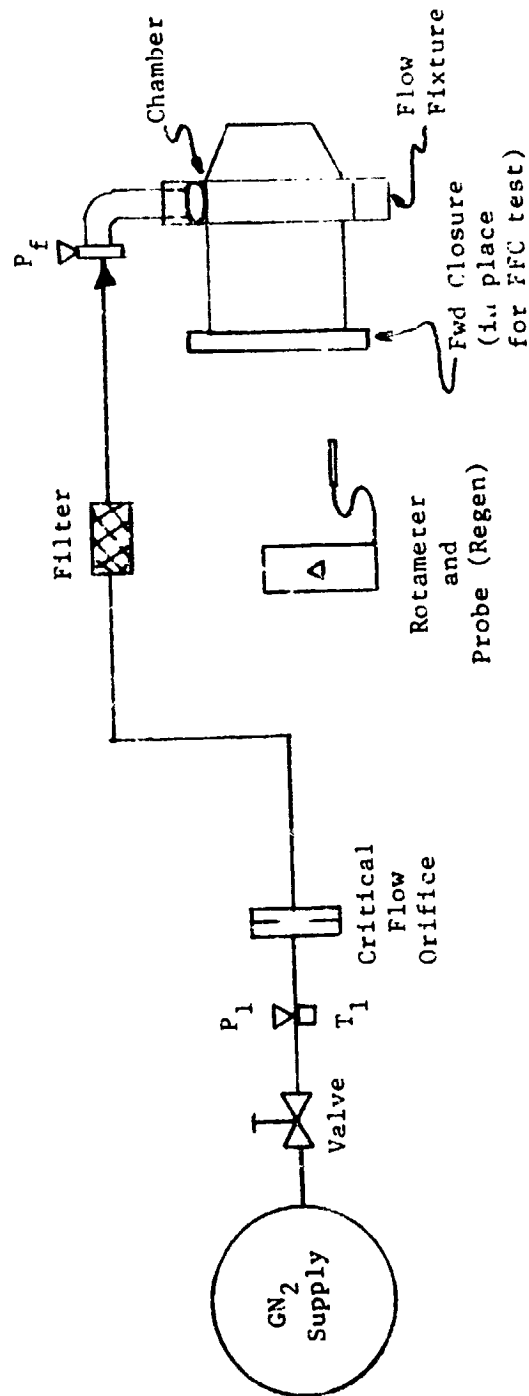
Figure 76. Chamber Cold Flow Schematic

4.3, Component Checkout Testing (cont.)

Three tests were performed on each chamber: ffc hydraulic characterization; regen channel hydraulic characterization; and regen channel flow uniformity.

In performing the hydraulic characterization tests, the GN_2 flow rate was varied in steps by adjusting the pressure of the GN_2 supply to the critical nozzle. For each step, the following were recorded: GN_2 supply pressure and temperature, and inlet pressure. Barometric pressure was read before and after the test. The ffc section was flowed independently (regen section capped off) and then both sections were flowed together. This permitted precise determination of the ffc flow rate and evaluation of the larger regen channel flow rate by subtracting out the smaller ffc flow rate from the total flow measured with both circuits flowing. The flow steps are summarized below:

GN_2 Flow Rate, g/sec (lb/sec)

Step	ffc Circuit	Regen and ffc Circuit
1	9.07 (.020)	34.9 (.077)
2	4.54 (.010)	17.2 (.038)
3	5.90 (.013)	23.1 (.051)
4	7.26 (.016)	29.0 (.064)
5	9.07 (.020)	34.9 (.077)
6	12.2 (.027)	46.7 (.103)
7	15.0 (.033)	58.5 (.129)
8	18.1 (.040)	69.9 (.154)
9	9.07 (.020)	34.9 (.077)

Flow uniformity testing was performed while holding the GN_2 flow rate at 34.88 g/sec (.0769 lb/sec). The flow from each of the 80 regen channels was collected by means of a nonrestrictive probe machined to the geometry of the regen channel outlets. The channel flow measurement was made using a rotameter with the rotameter reading being recorded for each channel. The GN_2 supply pressure and temperature, and barometric pressure were recorded at the beginning and end of each test.

4.3. Component Checkout Testing (cont.)

In order to verify that the ffc section was flowing uniformly the ffc section of chamber SN 001 was flowed after the liner had been machined on the I.D. Water was used as the test fluid and visual inspection was made to verify uniformity. The flow pattern is shown in Figure 75d. Visual flow checks of ffc uniformity were also made by flowing GN_2 through the ffc circuit with the aft end of the chamber oriented up. Freon was flowed down the ID of the chamber. Gravitational forces caused the freon to flow toward the ffc injection tip and the momentum of the GN_2 exiting from the ffc channels prevented the fluid from reaching the ffc tip. The gas flow uniformity was verified by observing the distance the fluid film was maintained from the ffc tip.

4.3.5   Main Propellant Valve Checkout Testing

Each main propellant valve was acceptance tested by Marquardt at their facility. The purpose of the testing was to determine if the valve met design specifications (Table XXIII). The following tests were run: coil resistance, proof pressure (bellows and valve body), external leakage, internal leakage, pull-in current, opening response, closing response, pressure drop and internal leakage. The flow testing was performed using GN_2 as the test fluid. Response times were measured using GN_2 as the pressurant and valve actuation fluid.

Two of the main propellant valves were tested at ALRC to evaluate the valve operating characteristics at cryogenic and ambient conditions using the actual propellants (GH_2 and GO_2). Testing was performed at vacuum conditions using the J-3 cell and steam system of the ALRC altitude facility. Valves SN 011 (GO_2) and SN 013 (GH_2) were mounted on the J-3 test stand using a dummy injector to allow flow testing with the inlet line configuration that was used for subsequent engine test firings. Orifices were located downstream of the main propellant valves in the dump lines so as to simulate the ITA volumes and pressure drop. The flow schematic for engine testing (Section 4.4.1) describes the set up. Leak checks at ambient conditions were performed before and after the cold flow tests. Flow measurement and control was accomplished by using venturis in the propellant lines upstream of the test stand valves.

4.3, Component Checkout Testing (cont.)

The following measurements were made for each valve:
propellant pressure and temperature at the main propellant valve inlet, pressure
and temperature at the valve outlet, poppet travel, pilot valve current and
voltage, and valve body external temperatures. The test conditions are summarized
in Table XXXI.

<u>TABLE XXXI</u>

MAIN PROPELLANT, VALVE TEST CONDITIONS

TEST NO.	FLUID	VENTURI INLET PRESSURE, N/cm^2 (psia)	VALVE INLET TEMPERATURE, °K (°R)	VALVE INLET PRESSURE, N/cm^2 (psia)	FLOW RATE, g/sec (lb/sec)
1972-001-CB					
-001	GO_2	180 (261)	301 (541)	132 (191)	518 (1.14)
-002		316 (458)	301 (541)	228 (330)	899 (1.98)
-003		441 (639)	300 (540)	314 (456)	1216 (2.68)
-005		181 (262)	175 (315)	132 (192)	659 (1.45)
-006		317 (460)	161 (289)	234 (340)	1170 (2.58)
-007		436 (633)	121 (218)	321 (465)	1716 (3.78)
-010	GH_2	320 (464)	294 (530)	152 (221)	352 (.777)
-011		419 (607)	294 (529)	199 (289)	459 (1.013)
-012		188 (272)	291 (523)	91.7 (133)	210 (.462)
-013		401 (582)	135 (243)	183 (266)	377 (.831)
-014		322 (467)	149 (269)	147 (213)	293 (.646)
-015		174 (253)	129 (233)	80.0 (116)	170 (.374)

4.4 INTEGRATED THRUSTER ASSEMBLY TESTING

4.4.1 Objective

The objectives of the ITA test firing task were experimental characterization of the flightweight thruster and demonstration of cycle life. The experimental characterization was an evaluation of thermal behavior and during both steady state and pulsing operation, over a wide range of operating conditions.

Although they were not necessarily run in separate test blocks, the tests were grouped into six series: checkout, steady state operation, valve sequencing, pulsing operation, chamber pressure and MR limits, and life limit. The checkout, steady state operation, and chamber pressure and MR limits tests were run concurrently. The sequence in which tests were run was dictated by propellant temperature conditioning requirements.

The checkout series had as its objective design verification. These tests provided checkout of the hardware, test stand, data acquisition system and feed system balancing, and provided design verification data in the areas of performance, hydraulics and heat transfer. The checkout tests were conducted with the propellants at their nominal temperatures.

The objective of the steady state operation test series was the evaluation of steady state thruster operation for the conditions defined in Table I. Operation was demonstrated with pressures at the values of 276 ± 34 N/cm^2 (400 ± 500 psia) and propellant temperatures ranging from $111°C$ ($200°F$) to ambient from the fuel and saturated vapor to ambient for the oxygen.

The chamber pressure and MR limits series were conducted to define the conditions that limit thruster operation. Two limits were imposed by the hardware: throat temperatures were not to exceed ~$900°C$ ($1650°F$) and the pressure at the inlet to the valves in the open position was not to exceed 465 N/cm^2 (675 psia).

4.4, Integrated Thruster Assembly Testing (cont.)

The valve sequencing tests included both main valve sequencing tests and ignition delay tests. The ITA was operated with both fuel and oxidizer lead on startup, and with the igniter operation leading and lagging flow of propellants to the main stage. These tests demonstrated that the thruster can tolerate minor shifts in valve and igniter timing and demonstrated ignition delays such as might be encountered when operating without the igniter valves. In addition, these tests provided data on valve timing required for the pulse mode of operation.

Pulsing tests were made to evaluate the mode of operation. Minimum impulse bit, performance and response were investigated. Four duty cycles were demonstrated. There are no duty cycle effects that limit operation due to thermal effects (soak or "pump up"). However, cycle life is affected by the duty cycle.

The life cycle testing had as its objective the evaluation of the fatigue life of the ITA and its components. The duty cycle used in pulsing the thruster provided one full thermal cycle every ten pulses. Thruster SN 001 had been used in all testing up to this point. Life cycle testing was performed on thruster SN 002 so that life evaluation was made on new hardware.

The objectives of each test series relative to the program goals are summarized in Table V (Section 2.4).

4.4.2 Test Methodology

4.4.2.1 Test Article

The article that was tested was the P/N 1162900 flightweight ITA. The thruster assembly consists of the P/N 1162904-1 chamber-injector

4.4., Integrated Thruster Assembly Testing (cont.)

assembly, the PN 1162883-1 igniter housing, PN X28960 (Marquardt) main
propellant valves (2), the PN GLA 47170 exciter/spark plug, and the PN V
27200-4871 (Valcore) igniter valves (2). The checkout, steady state operation,
chamber pressure and MR limits pulsing mode of operation and valve sequencing
test series were conducted using ITA SN 001. The life cycle tests were
conducted on ITA SN 002. The components that were used for each ITA are:

Component	Component Serial Number	
	ITA SN 001	ITA SN 002
Chamber injector assembly	001	002
Igniter housing	001	002
GLA exciter/spark plug	007	003
Igniter fuel valve	002	002/004
Igniter ox valve	006	006/003
Main propellant fuel valve	013	013*
Main propellant oxidizer valve	012	012/011*

4.4.2.2 Test Setup

All test firings were performed at simulated altitude in
the ALRC Test Area Zone J. The facilities are described in Appendix A. Test
Stand J-3 was used.

ITA SN 001 was tested using both the J-3 and J-4 steam
system. The J-3 system is a three stage steam ejector system utilizing two
barometric condensors and can pump 1590 g/sec (3.5 lb/sec) of rocket engine
exhaust. At nominal conditions, the altitude was maintained at 20.12 km
(66,000 ft). However, due to the low density of hydrogen, the J-3 system cannot
maintain altitude at low mixture ratio, except at low chamber pressure, and

*At the conclusion of testing, the fuel valve consisted of main body SN 013 and
pilot SN 011. The oxidizer valve consisted of main body SN 001 and pilot SN 012.

4.4, Integrated Thruster Assembly Testing (cont.)

cannot be utilized for high chamber pressure testing. For low MR testing and high chamber testing, the J-3 cell was linked to the J-4 steam system by means of the 1.22 m (4 ft) crossover duct. Ejector No. 7 of the J-4 system was used and can pump 4536 g/sec (10 lb/sec) of rocket engine exhaust. The J-3 system can operate with all three ejectors for approximately 2000 seconds. The J-4 system can operate for approximately 500 sec with Ejector No. 7.

The life cycle testing was performed using two steam ejectors of the J-3 system. This permitted altitude conditions to be held for more than six hours. With only two ejectors turned on, ample duct water spray was essential for maintaining altitude for operation with pulse widths in excess of .2 sec.

The test setup is shown schematically in Figure 77. Both propellant feed systems were similar. The propellants were temperature conditioned by LN_2 heat exchangers. The pressures in the accumulators, located outside the test cell, were monitored and controlled by flow control valves. The combination of the volume of the accumulators and the response of the flow control valves permitted a constant pressure to be maintained at the thrust chamber valves irrespective of flow demand or line pressure. For some tests, the flow control valve was programmed to adjust the accumulator pressures to compensate for propellant temperature. This permitted a constant MR to be maintained during the initial part of tests when propellant temperatures were varying as the hardware and lines were chilled down by heat transfer to the propellants.

Each propellant line contained a vent that was used while thermally conditioning the lines. There were vents and burst discs on each accumulator.
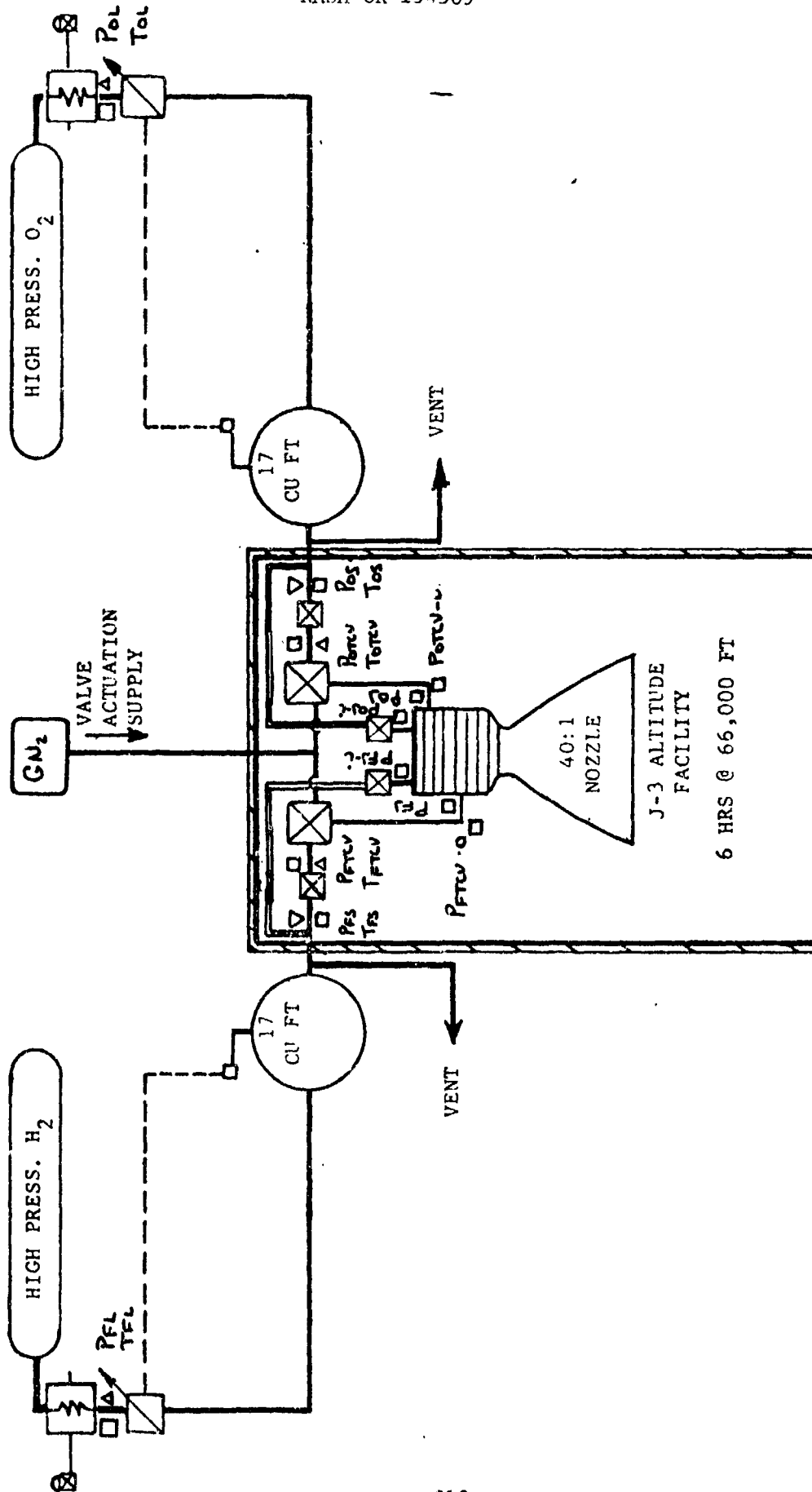
Figure 77. Flow Schematic for ITA Testing

4.4., Integrated Thruster Assembly Testing (cont.)

The main propellant valves were initially operated using the propellants themselves as the actuation medium. Subsequently, they were helium actuated and GN_2 actuated in an attempt to improve the closing time of the fuel valve. When self-actuated, the propellant was tapped off the inlet line upstream of the main propellant valve inlet. The igniter propellant supply was tapped off the inlet line downstream of the flow meter.

In order to obtain accurate thrust measurements, the standard thrust cell was remotely actuated so that thrust stand calibration could be performed at vacuum with the lines pressurized and chilled down.

Testing of ITA SN 001 was initiated with venturis in the propellant lines upstream of the test stand valves, and with hot wire anemometer flowmeters between the test stand valves and the thrust chamber valves. Calibration of the anemometers had been performed in part during the component check-out testing of the main propellant valves. The venturies were flowed sonically to provide flow measurement for in place calibration of the anemometers. The anemometers were not designed for the installation and were replaced after seven tests with Ramapo flowmeters. The venturis were removed at that time. The Ramapo flowmeter utilizes the flow stream drag forces acting on a body attached to a bending beam to measure flow. Once the Ramapo flowmeters were installed, no further changes were made to the system other than changing actuation of the main propellant valves from propellant to GN_2 or helium, replacement of the spark plug with an integral exciter/spark plug, and a change in the purge location.

ITA SN 001 prior to test and the test setup, are shown in Figure 78. The engine was fired horizontally into a water cooled diffuser. The test cell was isolated from the altitude system duct work by a bulkhead penetrated only by the diffuser. The diffuser not only resul_d in lower cell pressure when the engine was firing, but prevented recirculation of the hot combustion products around the engine.
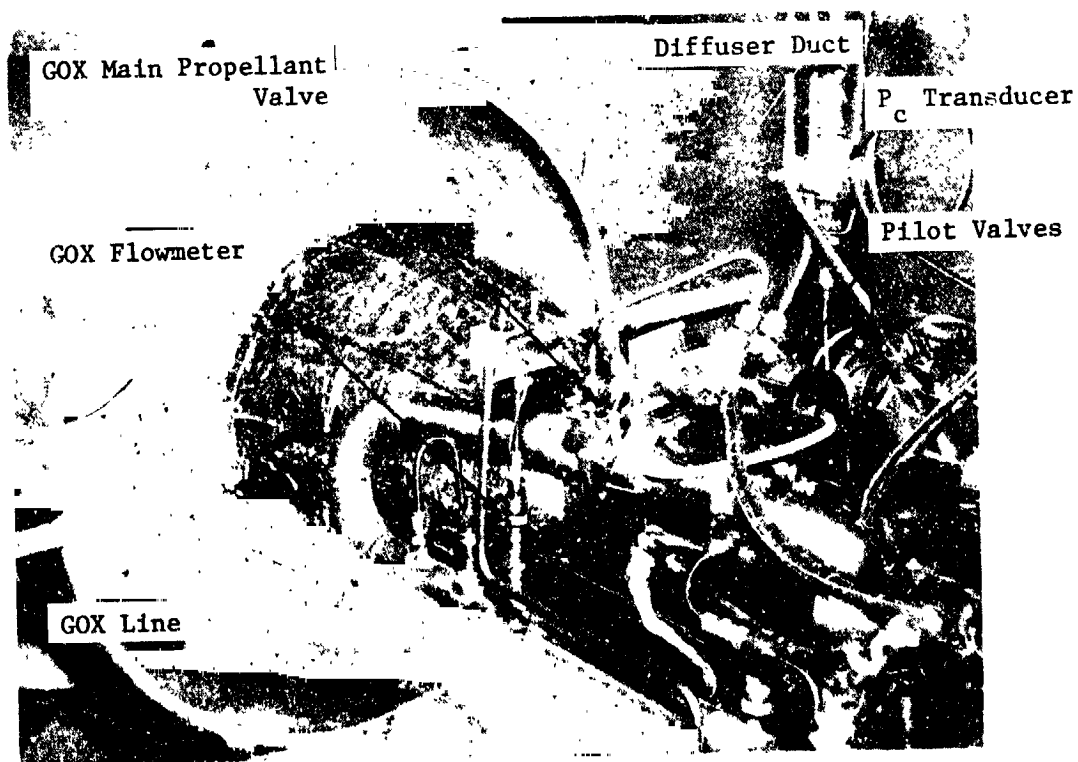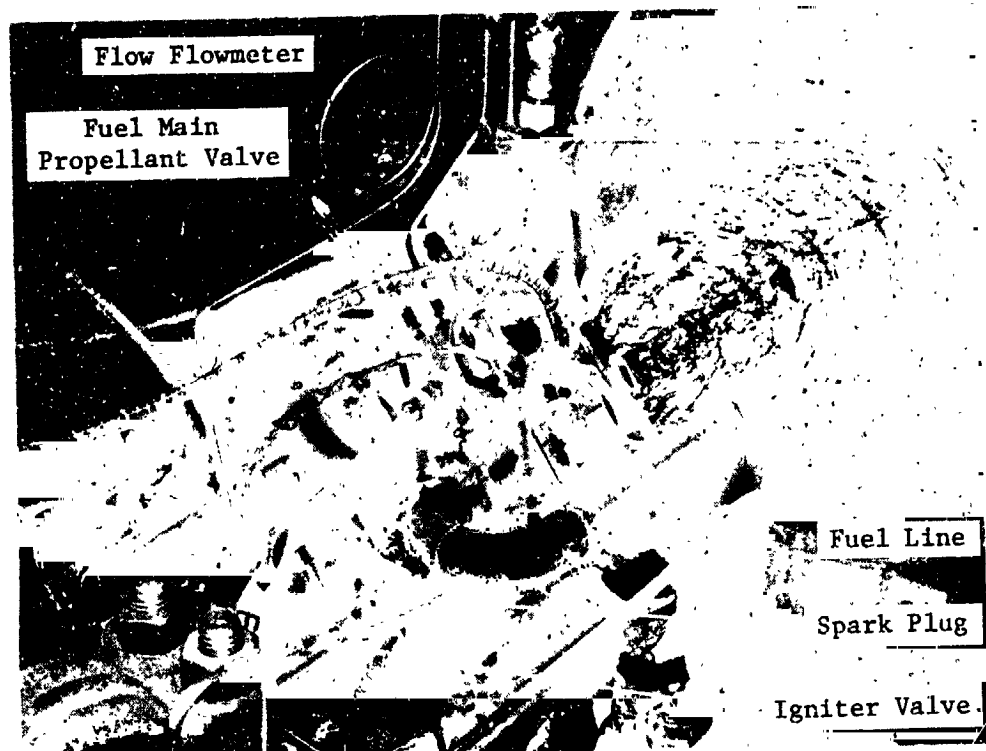
Page 211

Figure 78. ITA SN 001 Thruster Prior to Test

4.4., Integrated Thruster Assembly Testing (cont.)

however, there was also a disadvantage in operating with the diffuser. When the engine was shutdown, cell pressure was lower than the pressure in the duct downstream of the diffuser. Equalization of the pressure in the cell was accomplished by flow from the duct through the diffuser into the cell. This blowback apparently contained droplets of water entrained from the duct coolant spray as water was observed standing in the chamber after many tests, and on two occasions, ice was observed. This will be discussed later in more detail.

The propellant inlet lines were hard mounted at the inlet to the thrust chamber valves so that deflection resulting from feed system line temperature changes would not be transmitted to the ITA lines. Stresses resulting from deflection transmitted from the feed system would compromise life.

The thruster, feed lines and stand valves were mounted on the test flexure. The main propellant lines entered at right angles to the thrust vector.

4.4.2.3 Instrumentation

The thermocouple instrumentation that was used on chamber SN 001 and SN 002 is shown in Figures 79 and 80. The nomenclature is defined below. Thermocouples were numbered sequentially from forward to aft. Details of the TC installation are shown in Figures 50, 51 and 52.

Thermocouple Designation	Location
TFI	Injector fuel manifold (fuel temperature)
TJF	Injector face
TG	Chamber regen and dump cooled sections - gas side
TC	Chamber exterior - regen and dump cooled sections

Figure 79.   ITA Thermocouple Locations (Nominal) SN001

JF – INJECTOR FACE
FJ – FUEL, INJECTOR MANIFOLD
C   – CHAMBER
G   – GAS–SIDE
N   – NOZZLE
E   – EXTERIOR
P   – PAD

Figure 80. ITA Thermocouple Locations (Nominal) SN002

JF – INJECTOR FACE
FJ – FUEL, INJECTOR MANIFOLD
C – CHAMBER
N – NOZZLE EXT.
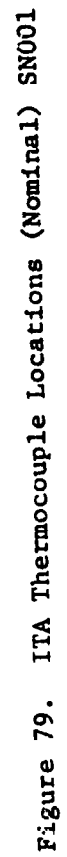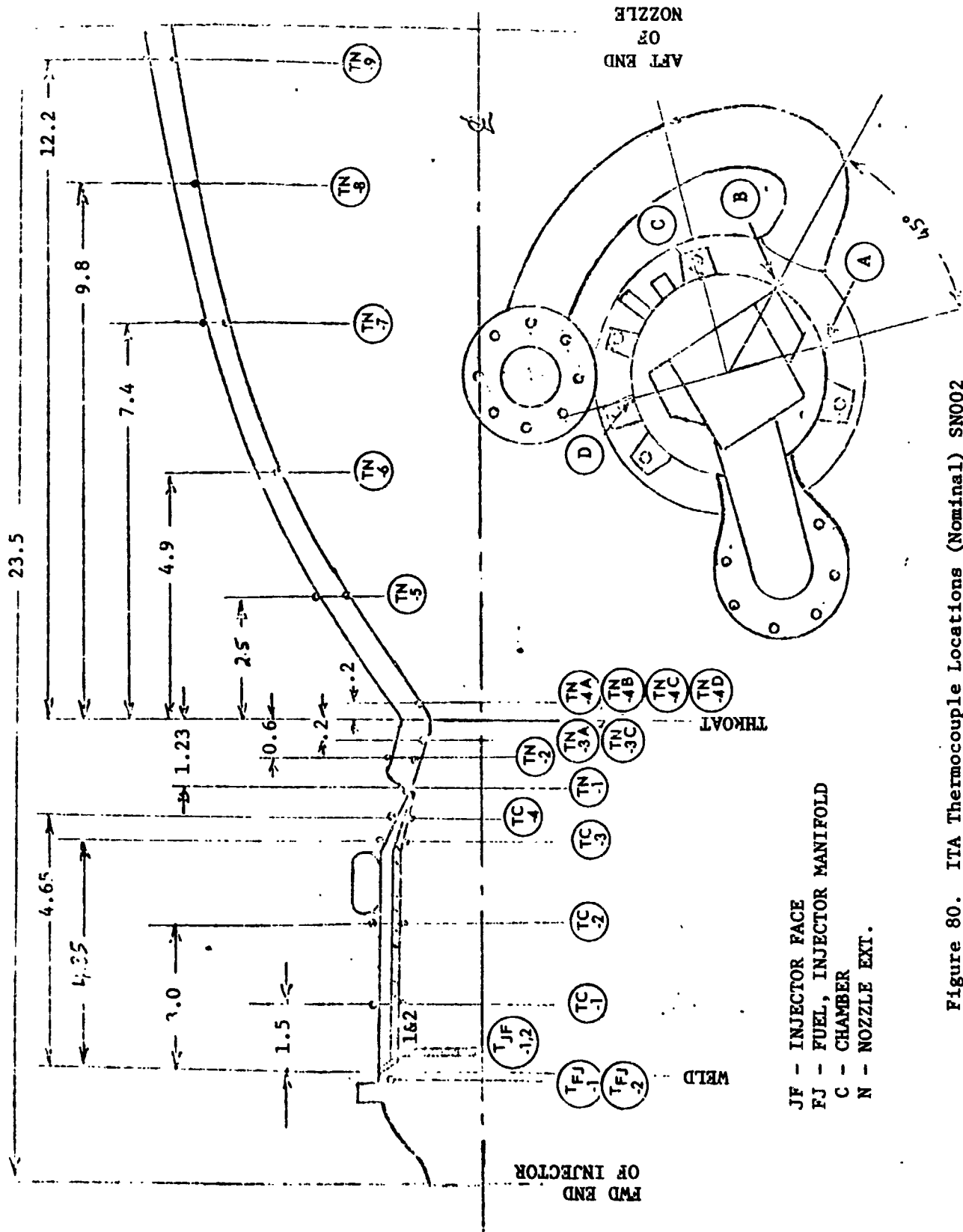
4.4., Integrated Thruster Assembly Testing (cont.)

Thermocouple Designation	Location
TN	Nozzle – film cooled (adiabatic) section including skirt
TE	Exterior – between insulation and cover
TP	TC on metal pad placed between insulation and skirt

ITA SN 001 had a through the wall P_c tap (P_c-1) located 3.8 cm (1.5 in.) aft of the injector chamber weld and opposite the fuel inlet to the torus. The diameter of the hole through the ZrCu land to the inside of the chamber was .115 cm (.045 in.).

The injector oxidizer manifold pressure (POJ) and the injector fuel manifold pressure (PFJ) were measured via .102 cm (.040 inch) ports drilled in the injector flange plate (PN 1162886). The details of the pressure tap installation and of the port through which the injector thermocouples are fed are shown in Figure 28. The pressure and temperature of the propellants entering the igniter (POJ-i, TOJ-i, PFJ-i and TFJ-i) were measured via fittings on the inlet lines. Propellant temperatures and pressures were measured at the inlet to the main propellant valves (POTCV, TOTCV, PFTCV, TFTCV), and pressures were measured at the outlet of the valves (POTCV-O, PFTCV-O).

The igniter oxidizer pressure (POJ-i) served as a P_c tap for measuring chamber pressure. After mainstage ignition, the igniter ox valve was closed; while the fuel valve was left open. Thus, the igniter served as a hydrogen cooled pressure tap. ITA SN 002, SN 003 and SN 004 had no other chamber pressure port. POJ-i was found to be a much more reliable measure of chamber pressure than the ITA SN 001 through-the-wall P_c tap which frequently froze up during testing. This P_c tap was plugged with a copper wire for pulse testing to avoid burning through the walls of the small diameter, low thermal capacitance tube as a result of heat transfer from the hot combustion gases as they were compressed and exhausted from the transducer and line with each pulse.

4.4, Integrated Thruster Assembly Testing (cont.)

The instrumentation that was used for ITA SN 001 testing and the range of each instrument are tabulated in Table XXXII. Also shown in the table is the method of data recording. The parameters that were recorded on strip charts were those that were used to run the tests. The data on the 0-graph were selected to permit evaluation of the time at which events occurred such as signal to valve, valve opening, flow initiation, ignition, etc.

Several parameters were monitored by the TR-48 analog computer and used to shudown the test in the event test conditions were such that damage to the hardware could occur. For ITA SN 001 these "kill" parameters were: low thrust, injector manifold (ox or fuel) overpressure, injector face temperatures in excess of $370^{c}C$ ($700°F$), throat temperatures in excess of $900°C$ ($1650°F$), skirt temperatures in excess of $1095°C$ ($2000°F$), and pressure at the inlet to the valves in excess of 448 N/cm^2 (650 psia).

For the life cycle testing with ITA SN 002, instrumentation was used somewhat differently than for the SN 001 testing. Only one sweep per pulse was made for digital data. This provided one line of data for each pulse, but held the record of the data to a manageable size. Sixteen parameters were recorded on the ADC for digital print out. To provide a continuous record in the event of a malfunction, 30 parameters were recorded on FM tape. The oscillo-graph was set up a₂ for SN 001 testing, but was only operated every 250 to 500 pulses to provide a check on operation and sequencing.

One change was made to the kill parameters for the ITA SN 002 life cycle testing. The low thrust shutdown, the valve overpressure, and the chamber temperature protective circuits were utilized as was done for SN 001 testing. The injector manifold pressures trips were set for detection of pro-pellant in the manifolds prior to each pulse rather than overpressure during the pulse. How the kill parameters and the 0-graph were used to protect the hardware and test facility is summarized in Table XXXIII.

Page 217

TABLE XXXII

INSTRUMENTATION FOR ITA SN 001 TESTING

Symbol	Parameter	Range		TR-S Shutdown	ADC Digital	Visual	Strip Chart	Oscillograph
PFT	Pressure, Fuel Tank	2086 N/cm^2	(3000 psig)			X		
PFTCV	Pressure, Fuel - Thrust Chamber Valve	690	(1000)	X	X		X	X
PFTCV-O	Pressure, Fuel - TC Valve Outlet	690	(1000)		X			
PFJ	Pressure, Fuel Manifold - Injector	690	(1000)	X	X			X
PFJ-i	Pressure, Igniter Fuel Inlet	690	(1000)		X			X
PC-1	Pressure, Chamber	690	(1000)	X	X		X	
PALT	Pressure, Cell (2)	10	(15 psia)		X			
PFL	Pressure, Fuel Line	2086	(3000 psig)		X			
PFS	Pressure, Fuel Supply	690	(1000)		X		X	
POT	Pressure, Ox Tank	2086	(3000)			X		
POTCV	Pressure, Ox Thrust Chamber Valve	690	(1000)	X	X		X	X
POTCV-O	Pressure, Ox Thrust Chamber Valve Outlet	690	(1000)		X			
POJ	Pressure, Ox Manifold - Injector	690	(1000)	X	X			X
POJ-i	Pressure, Igniter Ox Inlet	690	(1000)	X	X		X	X
POL	Pressure, Ox Line	2086	(3000)		X			
POS	Pressure, Ox Supply	690	(1000)		X		X	
FMFR	Flowrate, Fuel (Ramapo)	680 g/sec	(1.5 lb/sec)		X			X
FMOR	Flowrate, Ox (Ramapo)	2495	(5.5 lb/sec)		X			X
TFS	Temperature, Fuel Supply	333°K	(600°R)		X		X	
TFL	Temperature, Fuel Line	333	(600)		X			
TFTCV	Temperature, Fuel @ TC Valve	333	(600)		X		X	
TFJ	Temperature, Fuel in Manifold (2)	333	(600)		X			
	Temperature, Fuel @ Cascade	333	(600)		X			
TOS	Temperature, Ox @ Supply	333	(600)		X		X	
TOL	Temperature, Ox @ Line	333	(600)		X			
TOTCV	Temperature, Ox @ TC Valve	333	(600)		X		X	
F	Thrust (2 Bridges)	22,240 N	(5000 lbf)	X	X		X	X
FSC	Load, Standard Cell (2 Bridges)	22,240	(5000)		X			
TSC	Temperature, Standard Cell	333°K	(600°R)		X			
TFMVB	Temperature, Valve Main (TC Fuel)	1667	(3000)		X			
TFPVB	Temperature, Pilot Valve (TC Fuel)	1667	(3000)		X		X	
TFIVB	Temperature, Valve (Igniter Fuel)	1667	(3000)		X			
TOMVB	Temperature, Main Valve (TC Ox)	1667	(3000)		X			
TOPVB	Temperature, Pilot Valve (TC Ox)	1667	(3000)		X			
TFJ	Temperature, Injector Face (2-5)	1667	(3000)		X		X	
TC&TN	Temperature, Chamber (26)	1667	(3000)	X	X		X	X
EFV	Voltage, TC Fuel Valve	30 VDC						X
EOV	Voltage, TC Ox Valve	30						X
EIGN	Voltage, Exciter	30						X
EIGHV	Voltage, Spark Monitor	5						X
LFVDT	TC Fuel Valve Position Monitor							X
LOVDT	TC Ox Valve Position Monitor							X
IFV	Current, TC Fuel Valve	3						X
IOV	Current, TC Ox Valve	3						X
I-FIV	Current, Igniter Fuel Valve	2						X
I-OIV	Current, Igniter Ox Valve	2						X

TABLE XXXII

PROTECTIVE MODES FOR LIFE TESTING

	EVENT	RESULT	PROTECTION
1.	Main valve fails to open	Accumulation of propellant damage to hardware or cell on subsequent pulse	Low thrust shutdown
2.	Main valve delays	Damage to hardware due to ignition with fuel in ox dome or ox in torus	Low thrust shutdown
3.	Igniter fails to light	Propellants light in chamber or duct on next pulse	Low thrust shutdown
4.	Spark delays	Ignition with chamber or cell full of propellants	Low thrust shutdown
5.	Main valve fails to close or delays	Same as 1. above	Overpressure shutdown on PQJ or PFJ
6.	Hardware deterioration	Hardware damage	Low thrust or high temperature shutdown; monitor O-graph
7.	Sequencer malfunction	(a) Double pulse (b) Skipped pulse or (c) No shutdown	(a) Overpressure on PQJ and PFJ (b) Low thrust shutdown (c) Does not damage hardware or cell

4.4, Integrated Thruster Assembly Testing (cont.)

4.4.2.4 Method of Testing

Some of the tests had as their objective operation at a given MR and p_c; other tests required operation with a given pressure and propellant temperature at the inlet to the valves. In order to permit a common operating method, all test requirements were reduced to the conditions at the inlet to the valves. The tests were run by controlling the pressure in the accumulators and the propellant supply temperature.

The flow control valves were used in a feedback loop to maintain the pressure in the accumulators at a set value. The pressure was sensed at the inlet to the test stand valves (PFS and POS). The TR-48 analog computer compared the measured pressure to a reference value set on the control panel and programed the valves to maintain that pressure level. The pressure at either or both valves could be changed during the test by changing the value of the reference pressure.

Some tests were run with a temperature compensation circuit to program the pressure to the square root of the temperature. Temperature compensation was used when the objective of the test was operation at a given MR, and was used to maintain a constant MR as propellant temperature changed with chilldown of the lines. The temperature compensation was not used otherwise.

The accumulator pressure was sensed at the inlet to the test stand valves since it is the closest point to the thruster than cannot be isolated from the accumulator. Sensing the pressure at the accumulator was not done because of the pressure drop and change in propellant temperature that would occur between the accumulator and the thruster. It was not sensed downstream of any valve since closing the valve would isolate the sensor from the component being pressurized and would result in a pressure demand signal to the flow control valve that was not related to the pressure in the accumulator.

4.4, Integrated Thruster Assembly Testing (cont.)

The propellants were temperature conditioned by passing them through a heat exchanger containing LN_2. The temperature of the propellants was controlled by the level of LN_2 in the heat exchangers and by the pretest chill in of the accumulator and feed lines since they acted as a heat exchanger.

The fuel system was chilled in with LN_2 and the ox system was chilled in with LO_2. LN_2 was added to the heat exchangers during a test as required to main the propellant temperatures (read visually in the control room).

The fuel temperature could be varied from ambient to approximately 111°C (200°R). There was not enough capacity in the heat exchanger for lower fuel temperatures. The oxygen temperature could be varied from saturated vapor to ambient. Generally, oxygen temperatures were maintained with 167°K (300°R) as the lower limit. This provided margin above the critical temperature, 154°K (278°R), and thus generally avoided liquid oxygen in the system. Test -042, however, was shutdown by a high chamber temperature; an oxygen temperature of 122°K (220°R) (liquid) was measured at the outlet of the heat exchanger.

The checkout, steady state, and chamber pressure and MR limits tests had as their objectives obtaining thermal and performance data during the steady state mode of operation. These tests were run concurrently. Many data points, often from different test series, were obtained in a single long duration firing as propellant temperatures changed during the course of the testing and by changing the pressure of the propellants at the inlet to the valves.

Propellant temperatures were changed by not cooling the lines downstream of the accumulator. Cold propellant from the heat exchanger picked up heat from the lines. Thus, the propellant at the thrust chamber valves started out warm and decreased in temperature as the test progressed. Small increases in temperature were obtained on long tests by letting the system warm up as it ran (no addition of LN_2 to the heat exchanger).

4.4, Integrated Thruster Assembly Testing (cont.)

Figure 81 shows how several data points are obtained in a single test firing. During the initial part of the test oxidizer temperature decreased, illustrating how data was obtained as a function of propellant temperature. Approximately 35 seconds into the test the pressure at the fuel valve was increased, changing the MR from 3.3 to 2.5. Throat temperature responded immediately (decreased). Approximately 47 seconds into the test the pressure at both propellant valves was increased which increased chamber pressures. The change in pressure to the valves that was made at 69 seconds in the run resulted in a 5.8 MR data point and high throat temperatures. At 86 seconds a transition step was introduced to reduce the pressure to the ox valves. Generally, when both propellants were to be reduced in pressure, the oxidizer was reduced first. This avoided ox rich transients that could occur because the fuel system responded faster than the ox system. At 94 seconds into the run, the fuel pressure was reduced which resulted in a 6.0 MR data point at different pressures (P_c and at inlet to valves) than the prior 5.8 MR data point. Approximately 106 seconds into the run the pressure at the inlet to the fuel valve was increased to produce a data point at 2.5 MR and 207 N/cm^2 (300 psia) chamber pressure.

The valve sequencing tests were run just like the steady state tests except that they were only .1 to .2 sec in duration. Test -014 (64 sec duration) was run prior to the first valve sequencing test to temperature condition the system. Valve and igniter sequencing were changed between tests on the basis of data read from the O-graph. There was no change made to the method of testing for the pulse tests and cycle life except, of course, for the sequencing.
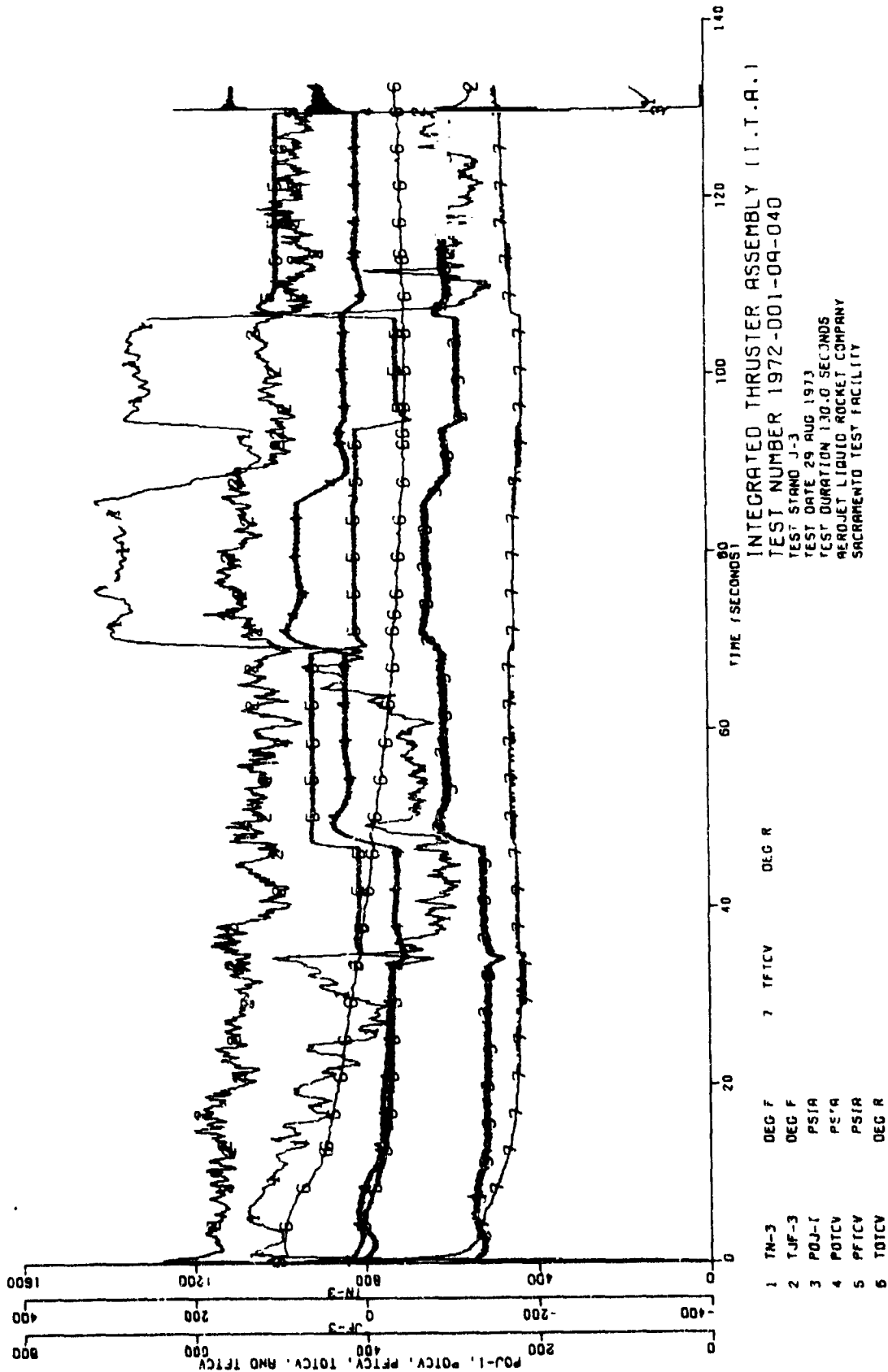
Figure 81. ITA Test Number 1972-001-0A-040

4.4, Integrated Thruster Assembly Testing (cont.)

4.4.3 Test Description (ITA SN 001)

4.4.3.1 Steady State Testing

The tests described in this section include the checkout, steady state operation, and the P_c and MR limits tests.

Testing was initiated with venturis in the fuel line and ox line upstream of the test stand valves. The pressure transducers POS and PFS and temperature sensors TOS and TFS were located at the inlet to the venturis. The integral exciter/spark plug units were not available when testing started; a variable energy remote power supply, with a spark plug and high voltage cables was used. The high voltage cable inside the cell was jacketed with a plastic tube and vented to atmosphere to keep it dry.

The first test was a propellant cold flow. Test -002 was a one second checkout test. Test -003 was a repeat for data acquisition. These tests were made with ambient propellants. The one second duration was long enough to establish that the balance orifices in the propellant lines were properly sized, and that throat temperatures were approximately as predicted.

Prior to each of the early tests, an "igniter only" test was made. The igniter was test fired for a short duration (~20 msec) as a checkout. Prior to Test -004, only one ignition was achieved in 12 attempts. Moisture was visible inside the plastic tube jacketing the high voltage line. The exciter system was taken apart component by component (including the spark plug), checked, cleaned and reinstalled. The cause of the electrical short was not isolated. However, it functioned properly for the next eleven tests until replaced by the integral exciter unit. This was the only time a no ignition occurred.

The tests starting with Test -003 are summarized in Table XXXIV.

TABLE XXXIV

SUMMARY OF CHECKOUT, STEADY STATE AND LIMIT TESTING

Date 1973	Test No. 1972 DO1-0A-	Total Duration, sec	Time, sec	Data Point	Pressure @ Valve Inlet, N/cm² (psia) P_OTCV	P_FTCV	Temperature @ Valve Inlet, °K (°R) T_OTCV	T_FTCV	P_c, N/cm² (psia)	MR	Comments
6-11	003	1.013		1	207 (300)	290 (420)	297 (535)	297 (535)	137 (198)	2.57	Venturis in propellant lines. J-3 steam system – spark plug & remote exciter – repeat of Test 002 for data.
6-13	004	.54		2	285 (413)	270 (39?)	205 (369)	193 (347)	194 (282)	4.24	Planned .5 sec eenkout. At end of test overpressurized system – blew burst discs.
6-14	005	.11		3	227 (330)	240 (348)	262 (472)	208 (375)	142 (206)	2.5	Sequencer inadvertently set for .1 sec.
6-14	006	37.50	15.3	4	214 (311)	245 (356)	222 (399)	146 (262)	141 (204)	2.45	Decreasing propellant temperatures.
			24.5	5	216 (314)	248 (360)	214 (386)	141 (253)	142 (206)	2.41	Decreasing propellant temperatures.
			31.7	6	225 (326)	253 (367)	209 (377)	140 (252)	147 (213)	2.52	Nominal propellant temperatures.
			35.5	7	227 (330)	192 (279)	208 (375)	135 (243)	168 (244)	4.0	Low altitude shutdown.
6-14	007	.61		8	310 (450)	215 (312)	238 (428)	231 (415)	62 (90)	–	Chamber temperature shutdown – eroded throat – icing problem.
7-2	008	26.63	17.0	9	200 (290)	181 (263)	232 (418)	141 (254)	135 (196)	4.0	Chamber repaired – Ramapo flow meters installed – data point – warm ox, cold fuel.
			22.0	10	200 (290)	176 (256)	231 (416)	134 (241)	134 (195)	4.2	Redundant for performance.
			25.5	11	199 (289)	175 (254)	230 (414)	132 (237)	134 (194)	4.2	Chamber temperature shutdown – trip set too close to operating condition.
7-3	009	8.35		12	292 (423)	273 (396)	208 (375)	139 (250)	200 (290)	3.6	Chamber temperature shutdown – temperature excursion 3 sec into run – icing.
7-5	010	76.73	4.0	13	191 (277)	283 (411)	315 (568)	310 (558)	127 (184)	2.1	Checkout of icing problem – ambient propellant temperatures to avoid icing.
			12.0	14	193 (280)	284 (412)	316 (568)	309 (557)	128 (185)	2.1	
			15.0	15	193 (280)	284 (412)	316 (568)	309 (557)	128 (185)	2.1	Redundant for performance.
			22.0	16	239 (347)	230 (334)	321 (577)	304 (548)	143 (208)	4.2	Changed MR.
			32.0	17	239 (347)	230 (334)	317 (571)	308 (555)	143 (208)	4.2	Fuel flow meter shorts out. (Electrical cable shorted – insulation melted).
			40	18	239 (347)	230 (334)	314 (565)	309 (556)	144 (209)	4.1	Redundant

TABLE XXIV (cont.)

Date 1973	Test No. 1972 D01-QA-	Total Duration, sec	Time, sec	Data Point	Pressure @ Valve Inlet, N/cm² (psia) P_OTCV	P_FTCV	Temperature @ Valve Inlet, °K (°R) T_OTCV	T_FTCV	P_c, N/cm² (psia)	MR	Comments
	010 (cont.)		61	20	216 (313)	257 (372)	310 (560)	309 (556)	145 (210)	-	Hold for altitude recovery.
			68	21	250 (362)	250 (363)	309 (557)	308 (555)	170 (247)	-	Transition step inserted to avoid large pressure changes.
			73	22	297 (431)	421 (611)	312 (564)	318 (572)	199 (289)	-	Short hold for performance.
			76	23	266 (386)	250 (363)	311 (559)	318 (572)	159 (230)	-	Low altitude shutdown - after test noted electrical insulation on flow meters melted.
7-5	011	36.02	6	24	230 (333)	267 (388)	316 (569)	312 (561)	147 (213)	2.8	
			16	25	229 (332)	267 (388)	316 (569)	309 (557)	146 (212)	2.8	Redundant.
			26	26	229 (332)	267 (388)	316 (569)	308 (555)	147 (213)	2.9	Redundant.
			36	27	229 (332)	267 (389)	316 (559)	308 (554)	147 (213)	2.9	Started propellant chilldown - increased H₂ flow resulted in low altitude shutdown.
7-5	012	120.47	6	28	231 (335)	230 (334)	310 (558)	279 (502)	147 (213)	3.2	
			15	29	229 (332)	230 (333)	307 (553)	228 (440)	145 (210)	3.3	Fuel temperature change provides new data point.
			24	30	227 (329)	219 (317)	301 (541)	204 (368)	144 (209)	3.4	Fuel chilldown underway.
			52	31	210 (304)	203 (294)	256 (460)	173 (312)	139 (202)	3.5	Both propellant temperatures changed.
			62	32	205 (296)	199 (289)	245 (441)	167 (301)	139 (201)	3.6	Ox chilldown underway.
			67	33	350 (508)	310 (450)	243 (438)	168 (302)	230 (333)	-	Transition - ox pressure increased to avoid low altitude shutdown due to fuel.
			89	34	444 (443)	218 (407)	219 (394)	157 (283)	207 (301)	4.3	MR and P_c changed.
			96	35	305 (443)	279 (405)	219 (395)	156 (281)	207 (300)	4.3	Near nominal operation.
			102	36	294 (426)	292 (423)	219 (395)	151 (272)	203 (295)	-	Pressures changed at inlet to valves.
			110	37	305 (443)	277 (407)	220 (396)	151 (274)	207 (300)	4.3	Redundant for performance.
			115	38	305 (443)	277 (402)	221 (397)	152 (273)	207 (300)	4.3	Redundant for performance.
			120	39	305 (443)	276 (400)	220 (396)	150 (271)	207 (300)	4.3	Hydrogen fire on test stand. Pin hole leak found in stand line.

TABLE XXXIV (cont.)

Date 1973	Test No. 1972 D01-0A-	Total Duration, sec	Time, sec	Data Point	Pressure @ Valve Inlet, N/cm² (psia)		Temperature @ Valve Inlet, °K (°R)		P_c, N/cm² (psia)	MR	Comments
					P_OTCV	P_FTCV	T_OTCV	T_FTCV			
7-6	013	247.60	12	40	227 (329)	230 (334)	306 (550)	229 (413)	145 (210)	3.4	Warm Propellants
			19	41	228 (331)	220 (319)	299 (539)	207 (373)	143 (207)	3.6	Fuel chilldown underway.
			75	42	209 (303)	198 (287)	250 (450)	164 (295)	138 (200)	3.9	Warm ox, cold fuel.
			100	43	206 (299)	196 (284)	242 (435)	162 (291)	137 (199)	3.9	Ox chilldown underway.
			125	44	204 (296)	195 (283)	237 (427)	518 (288)	136 (198)	3.9	Propellant temperatures steadying out.
			140	45	302 (438)	301 (437)	237 (426)	167 (300)	205 (297)	3 6	P_c - changed.
			147	46	309 (448)	303 (440)	231 (416)	167 (301)	209 (303)	3.8	Oxygen temperature changing.
			175	47	309 (446)	290 (420)	227 (408)	169 (305)	207 (301)	4.4	Oxygen temperature changing.
			190	48	307 (446)	290 (420)	225 (405)	169 (305)	207 (300)	4.4	Redundant for performance.
			217	49	305 (443)	282 (409)	219 (395)	163 (293)	205 (298)	4.6	Decreasing propellant temperatures.
			222	50	270 (392)	275 (399)	217 (391)	163 (294)	187 (272)	3.7	Transition.
			229	51	314 (455)	273 (396)	220 (396)	163 (294) T_FS*	206 (299)	5.2	High MR.
			233	52	301 (437)	267 (388)	219 (394)	164 (295)	199 (289)	5.1	Fuel pressure decrease.
			237	53	305 (443)	263 (382)	213 (394)	164 (295)	199 (289)	5.4	Fuel pressure decrease.
			241	54	305 (443)	259 (375)	218 (393)	164 (296)	197 (286)	5.6	Fuel pressure decrease.
			247	55	305 (442)	251 (364)	218 (393)	165 (297)	194 (282)	5.9	910°C (1670°F) temperature in throat - high MR limit.

*T_{FTCV} not working. Temperatures based on T_{FS}. For Test 013 $T_{FTCV} = T_{FS} + 2°C$ based on prior readings. For Test -014 $T_{FTCV} = T_{FS}$. Normally T_{FTCV} lags (reads higher) T_{FS} at start. Little difference in steady state.

TABLE XXXIV (Cont.)

Date 1973	Test No. 1972 DOi-0A-	Total Duration, sec	Time, sec	Data Point	Pressure @ Valve inlet, N/cm² (psi) P_OTCV	P_FTCV	Temperature @ Valve Inlet, °K (°R) T_OTCV	T_FS*	P_c', N/cm² (psia)	MR	Comments
7-10	014	54.06	8	56	215 (312)	204 (296)	266 (478)	172 (309)	141 (204)	3.7	GLA integral exciter/spark plug installed (SN 007). Conditioning for pulse tests.
			15	57	216 (313)	194 (281)	261 (469)	154 (278)	140 (203)	4.0	Propellant temperatures decreasing.
			20	58	210 (305)	189 (274)	249 (449)	147 (264)	138 (200)	4.0	Same.
			32	59	204 (296)	182 (264)	235 (423)	136 (245)	135 (196)	4.1	Same.
			45	60	197 (286)	178 (258)	220 (396)	129 (233)	133 (193)	4.1	Same.
			53	61	194 (281)	177 (257)	212 (382)	128 (231)	132 (192)	4.1	Near nominal.
			61	62	316 (459)	279 (404)	204 (360)	133 (239)	216 (314)	4.9	P_c and MR increased.
			63.5	63	295 (428)	271 (393)	200 (360)	132 (237)	205 (298)	4.5	Normal shutdown - igniter and valve sequence tests followed immediately.
8-28	039	.501		64	281 (407)	263 (381)	260 (468)	T_{FTCV} 158 (285)	183 (265)	-	J-4 steam system - checkout test.
8-29	040	129.434	2	65	270 (392)	283 (410)	274 (494)	157 (283)	181 (263)	3.1	Performance data point early in run.
			16	66	305 (442)	285 (374)	246 (442)	127 (228)	179 (259)	3.3	Propellant chilldown.
			26	67	257 (373)	254 (369)	235 (423)	123 (222)	178 (258)	3.3	Fuel temperature sta'le, ox decreasing.
			38	68	250 (362)	282 (409)	224 (404)	124 (223)	179 (260)	2.5	MR decreased.
			46	69	250 (363)	280 (406)	218 (392)	124 (224)	181 (262)	2.6	Ox temperature decreasing.
			59	70	290 (421)	316 (459)	209 (376)	128 (230)	211 (306)	3.0	Changed P_c and MR.
			56.5	71	290 (420)	316 (459)	202 (364)	128 (230)	212 (308)	3.1	Ox temperature decreasing.
			78	72	327 (474)	282 (409)	200 (360)	125 (225)	224 (325)	5.7	First point in high MR test.
			84	73	327 (474)	282 (409)	197 (355)	124 (224)	225 (326)	5.8	Second point in high MR test.
			93	74	293 (425)	280 (406)	195 (351)	120 (216)	210 (304)	4.4	Transition point - changed one valve inlet pressure at a time.

TABLE XXXIV (cont.)

Date 1973	Test No. 1972 D01-0A-	Total Duration, sec	Time, sec	Data Point	Pressure @ Valve Inlet, N/cm² (psia)		Temperature @ Valve Inlet, °K (°R)		P_c, N/cm² (psia)	MR	Comments
					P_{OTCV}	P_{FTCV}	T_{OTCV}	T_{FTCV}			
	040 (cont.)		105	75	289 (419)	247 (359)	194 (349)	119 (214)	199 (288)	6.0	High MR condition - cold propellants.
			123	76	279 (404)	342 (496)	197 (354)	130 (234)	208 (302)	2.5	Low MR condition - back-to-back with high MR.
			129	77	279 (404)	342 (496)	197 (354)	131 (236)	208 (302)	2.5	Planned shutdown.
	041	300.728	1	78	264 (383)	263 (381)	304 (548)	282 (508)	170 (246)	4.4	1st of series of data points obtained with warm ox and decreasing fuel temperature.
			2	79	263 (384)	267 (387)	367 (552)	271 (488)	171 (248)	4.1	2nd of series of data points obtained with warm ox and decreasing fuel temperature.
			5.5	80	274 (397)	270 (392)	308 (555)	235 (429)	177 (257)	4.2	3rd of series of data points obtained with warm ox and decreasing fuel temperature.
			21	81	274 (397)	271 (393)	301 (542)	173 (311)	182 (264)	3.7	4th of series of data points obtained with warm ox and decreasing fuel temperature.
			35	82	274 (397)	272 (394)	296 (533)	162 (292)	184 (267)	3.7	5th of series of data points obtained with warm ox and decreasing fuel temperature
			40	83	274 (398)	272 (394)	292 (525)	157 (282)	185 (269)	3.7	6th of series of data points obtained with warm ox and decreasing fuel temperature.
			62	84	274 (398)	272 (394)	283 (510)	151 (271)	187 (271)	3.7	Fuel temperature stable - final data point with warm ox and cold fuel.
			76	85	245 (356)	309 (448)	278 (500)	150 (270)	175 (254)	2.3	Low MR.
			90	86	245 (356)	309 (448)	277 (499)	150 (270)	175 (254)	2.3	Redundant for performance.
			92	87	246 (357)	309 (448)	277 (498)	150 (270)	175 (254)	2.4	Ox chilldown started.
			140	88	275 (399)	272 (395)	270 (486)	143 (258)	190 (275)	3.8	1st of a series of data points obtained with increasing fuel and decreasing ox temperature.
			160	89	275 (399)	272 (395)	269 (484)	143 (258)	190 (275)	3.8	2nd of a series of data points obtained with increasing fuel and decreasing ox temperature.
			190	90	275 (399)	272 (395)	250 (464)	149 (269)	191 (277)	4.0	3rd of a series of data points obtained with increasing fuel and decreasing ox temperature.
			230	91	276 (400)	272 (395)	245 (441)	156 (280)	192 (278)	4.2	4th of a series of data points obtained with increasing fuel and decreasing ox temperature.
			265	92	276 (400)	272 (395)	234 (422)	161 (290)	193 (280)	4.4	5th of a series of data points obtained with increasing fuel and decreasing ox temperature.
			282	93	276 (400)	272 (395)	229 (413)	165 (297)	194 (281)	4.5	6th of a series of data points obtained with increasing fuel and decreasing ox temperature.
			300	94	276 (400)	272 (395)	224 (403)	167 (301)	194 (282)	4.6	Final point - shutdown - trend established - ample data - temperature changes too slowly.

TABLE XXXIV (cont.)

Date 1973	Test No. 1972 D01-0A-	Total Duration, sec	Time, sec	Data Point	Pressure @ Valve Inlet, N/cm² (psia)		Temperature @ Valve Inlet, °K (°R)		P_c, N/cm² (psia)	MR	Comments
					P_{OTCV}	P_{FTCV}	T_{OTCV}	T_{FTCV}			
9-5	042	17.219	4	95	266 (386)	270 (391)	292 (526)	161 (290)	181 (262)	—	Pressure in ox line (POL) starts to drop. Temperature on ox line (TOL) cold TOL = 122°K (219°R) TOL = 1325 N/cm² (1921 psia)
			6	96	271 (393)	270 (392)	289 (520)	152 (273)	136 (270)	—	TOL = 183°K (330°R) POL = 867 N/cm² (1258 psia)
			9	97	300 (435)	272 (395)	299 (520)	151 (272)	204 (296)	—	Flow control valve comes open.
			17	98	284 (412)	271 (394)	212 (381)	128 (230)	196 (285)	—	TOL = 206°K (370°R) POL = 1425N/cm² (2066 psia)
9-6	043	350.081	1.6	99	281 (407)	312 (452)	227 (408)	130 (234)	202 (293)	2.8	Ox temperature at valve drops rapidly – chamber high temperautre shutdown. Warm ox – cold fuel.
			14	100	268 (389)	300 (435)	206 (370)	110 (196)	204 (296)	2.6	Coldest fuel temperature.
			22	101	267 (387)	309 (448)	201 (361)	117 (211)	199 (289)	2.6	Cold propellants – low MR.
			30	102	265 (384)	314 (455)	197 (355)	120 (216)	199 (288)	2.5	Redundant for performance.
			36	103	263 (382)	316 (459)	195 (351)	123 (222)	199 (288)	2.5	Ox temperature decreasing.
			64	104	260 (377)	323 (469)	188 (339)	128 (231)	198 (287)	2.5	Cold propellants – low MR.
			83	105	299 (434)	281 (407)	187 (337)	125 (225)	216 (314)	5.1	MR increased.
			85	106	301 (436)	278 (403)	185 (333)	124 (224)	217 (315)	5.3	High MR with cold propellant.
			103	107	282 (409)	275 (399)	181 (326)	121 (217)	208 (302)	4.6	1st of series of data points of increasing MR.
			105	108	285 (413)	218 (408)	180 (324)	120 (216)	212 (307)	4.5	2nd of series of data points of increasing MR.
			117	109	311 (451)	306 (444)	182 (328)	122 (220)	2-- (335)	4.6	3rd of series of data points of increasing MR.
			125	110	334 (484)	307 (445)	183 (329)	122 (220)	242 (351)	5.5	4th of series of data points of increasing MR.
			140	111	250 (363)	318 (462)	178 (321)	125 (225)	194 (281)	2.5	Transition to low P_c @ low MR – 1st of series.
			153	112	210 (304)	265 (385)	175 (317)	124 (224)	162 (235)	2.4	Transition to low P_c @ low MR – 2nd of series.
			156	113	207 (301)	25. (364)	177 (318)	126 (227)	159 (231)	2.7	Transition to low P_c @ low MR – 3rd of series.

TABLE XXXIV (cont.)

Date 1973	Test No. 1972 DO1-QA-	Total Duration, sec	Time, sec	Data Point	P_OTCV	P_FTCV	T_OTCV	T_FTCV	P_c, N/cm² (psia)	MR	Comments
	043 (cont.)		185	114	168 (244)	210 (305)	178 (320)	125 (225)	129 (187)	2.5	Transition to low P_c @ low MR - 4th of series.
			186	115	169 (245)	211 (306)	179 (322)	125 (225)	129 (187)	2.5	Start of series to high MR at low P_c.
			222	116	168 (244)	152 (220)	182 (328)	122 (220)	119 (172)	5.4	1st.
			255	117	182 (264)	150 (218)	184 (332)	120 (216)	123 (179)	6.7	2nd.
			263	118	184 (267)	151 (219)	185 (334)	121 (217)	124 (180)	6.8	3rd - 879°C (1614°F) throat temperature limit achieved.
			296	119	210 (304)	202 (293)	190 (342)	131 (235)	150 (218)	4.6	1st of data series increasing ox pressure to high MR limit @ nominal P_c.
			317	120	205 (297)	205 (297)	192 (346)	133 (240)	157 (228)	5.3	2nd of data series increasing ox pressure to high MR limit @ nominal P_c.
			325	121	229 (332)	253 (367)	193 (348)	141 (254)	170 (246)	3.4	3rd (transition - fuel pressure increased).
			342	122	288 (418)	259 (375)	200 (360)	145 (261)	200 (290)	5.6	4th.
			346	123	298 (432)	260 (377)	201 (362)	146 (262)	203 (295)	6.0	5th 915°C (1679°F) throat temperature - chamber limit demonstrated.
			350	124	294 (427)	260 (377)	201 (362)	140 (263)	202 (293)	5.9	Slight reduction in ox pressure prior to planned shutdown.
9-7	044	270.28	6	125	341 (494)	407 (591)	214 (385)	131 (235)	256 (372)	2.6	Start of a series of tests at high pressure - chilldown.
			20	126	384 (557)	431 (625)	188 (338)	132 (237)	296 (429)	3.5	Fuel valve at pressure limit - ox temperature decreasing.
			40	127	421 (611)	434 (630)	179 (323)	137 (246)	323 (469)	4.7	Transition - ox pressure increased.
			59	135	436 (632)	435 (631)	181 (325)	136 (245)	332 (482)	4.8	High P_c - cold propellants - valves at pressure limit.
			80	128	436 (634)	436 (632)	184 (332)	136 (245)	329 (477)	5.2	High P_c - both valves at pressure limit.
			125	129	432 (627)	406 (589)	195 (351)	137 (247)	314 (455)	5.8	Fuel pressure decreased to get high MR - transition.
			157	130	428 (621)	380 (551)	203 (365)	142 (255)	299 (434)	6.5	High P_c, high MR - ox valve at pressure limit - throat at temperature limit.
			175	131	312 (452)	372 (539)	196 (355)	152 (274)	166 (341)	3.3	Transition down in P_c.

Column headings: Pressure @ Valve Inlet, N/CM² (psia); Temperature @ Valve Inlet, °K (°R)

TABLE XXIV (cont.)

Date 1973	Test No. 1972 D01-0A-	Total Duration, sec	Time, sec	Data Point	Pressure @ Valve Inlet, N/cm² (psia) POTCV	PFTCV	Temperature @ Valve Inlet, °K (°R) TOTCV	TFTCV	Pc, N/cm² (psia)	MR	Comments
	044 (cont.)		263	132	265 (384)	282 (409)	199 (358)	155 (279)	195 (283)	4.2	Near nominal.
			239	133	263 (381)	241 (349)	200 (371)	155 (279)	183 (265)	5.8	High MR operation - near nominal propellant temperatures and Pc. Throat temperature = 896°C (1644°R).
			270	134	251 (364)	239 (347)	208 (375)	159 (285)	176 (250)	5.2	MR reduced prior to shutdown.
9-10	045	79.00	2	136	186 (270)	218 (316)	302 (544)	301 (541)	125 (181)	3.4	J-3 steam system - ambient temperature data.
			20	137	212 (307)	219 (318)	305 (549)	301 (542)	136 (198)	4.2	924°C (1695°F) throat temperature. MR limit with ambient propellants.
			40	138	209 (303)	219 (317)	300 (540)	301 (542)	135 (196)	4.4	917°C (1683°F) throat temperature.
			76	139	193 (280)	219 (317)	296 (532)	302 (544)	128 (186)	3.7	Reduced MR.
			79	140	226 (328)	234 (340)	299 (538)	303 (546)	147 (213)	4.4	Chamber high temperature shutdown, 942°C (1727°F) during switch to higher pressure.
9-10	046	229.08	2	141	214 (311)	257 (373)	301 (541)	301 (542)	141 (204)	3.1	Start up condition.
			20	142	229 (332)	259 (376)	300 (540)	303 (545)	148 (214)	3.5	Ox pressure increased.
			40	143	245 (356)	260 (377)	299 (538)	303 (546)	151 (226)	3.9	Ox pressure increased.
			60	144	251 (364)	276 (400)	297 (534)	305 (549)	161 (234)	3.7	Fuel pressure increased.
			100	145	284 (412)	296 (429)	298 (536)	304 (548)	181 (262)	4.0	Fuel and ox pressure increased. 1st of series to reach nominal Pc.
			120	146	287 (416)	296 (430)	296 (532)	304 (548)	181 (263)	4.1	2nd.
			140	147	290 (421)	303 (439)	294 (529)	304 (547)	185 (268)	4.1	3rd.
			160	148	301 (437)	316 (458)	293 (528)	304 (547)	129 (279)	4.1	4th.
			200	149	318 (461)	329 (477)	292 (525)	303 (546)	203 (294)	4.2	5th.
			220	150	324 (470)	336 (487)	292 (525)	303 (545)	207 (300)	4.2	6th.
			229	151	328 (476)	336 (487)	292 (526)	303 (545)	208 (302)	4.2	Throat temperature = 888°C (1630°F). MR limit with ambient propellants @ nominal Pc.

TABLE XXXIV (cont.)

Date 1973	Test No. 1972 D01-0A-	Total Duration, sec	Time, sec	Data Point	Pressure @ Valve Inlet, N/cm² (psia)		Temperature @ Valve Inlet, °K (°R)		P_c', N/cm² (psia)	MR	Comments
					P_{OTCV}	P_{FTCV}	T_{OTCV}	T_{FTCV}			
9-11	.047	512.64	1.5	152	283 (410)	314 (456)	232 (418)	216 (389)	206 (299)	3.9	Start up condition – 1st of series with ox and fuel chilldown.
			10	153	275 (399)	290 (420)	194 (350)	163 (293)	200 (290)	4.1	2nd.
			20	154	265 (385)	274 (39.)	194 (349)	148 (266)	200 (290)	4.4	3rd.
			46	155	259 (376)	266 (386)	184 (331)	139 (251)	197 (286)	4.5	4th.
			80	156	277 (402)	274 (398)	175 (323)	131 (236)	211 (306)	5.2	5th.
			135	157	282 (409)	280 (406)	185 (333)	128 (231)	214 (311)	5.2	6th.
			175	158	282 (409)	280 (406)	121 (344)	128 (231)	212 (308)	5.1	From this point on fuel temperature increases – 1st of series.
			190	159	281 (408)	280 (406)	194 (350)	130 (234)	211 (306)	5.0	2nd.
			250	160	281 (408)	280 (406)	192 (345)	138 (249)	210 (305)	5.1	3rd.
			280	161	281 (408)	280 (406)	187 (336)	145 (261)	210 (305)	5.3	4th.
			325	162	281 (408)	280 (406)	179 (322)	153 (275)	212 (308)	5.6	5th.
			336	163	282 (409)	280 (406)	174 (313)	157 (282)	213 (309)	5.7	6th.
			390	164	280 (406)	279 (405)	172 (310)	167 (300)	211 (306)	5.8	7th.
			430	165	265 (385)	272 (395)	173 (312)	177 (318)	201 (292)	5.9	Throat temperature = 887°C (1630°F). Limit with cold oxygen
			449	166	215 (312)	239 (346)	170 (306)	178 (320)	165 (240)	4.4	Pressure decreased to make duration.
			475	167	215 (312)	236 (343)	171 (308)	183 (330)	165 (240)	4.5	Redundant for performance.
			512	168	179 (259)	180 (261)	170 (306)	183 (330)	134 (194)	5.3	Ox Pressure decreased as fuel tank blows down.- 500 sec duration demonstration.

4.4, Integrated Thruster Assembly Testing (cont.)

Tests -004 through -007 were made with propellants con-
ditioned to approximately nominal temperatures. Following Test -004, an attempt
was made to reset pressure conditions so that a second test could be made
immediately. The flow control valves were inadvertently opened pressurizing both
propellant systems. The burst discs on both accumulators ruptured limiting the
pressure experienced by the main propellant valves (closed) to 580 N/cm^2
(840 psia). The bodies of main propellant valves were proofed to 690 N/cm^2
(1000 psia). Since they were self-actuated, there was no ΔP across the bellows
as a result of this incident.

During Test -006, operation at a 2.5 MR resulted in loss
of altitude. A switch to a 4.0 MR was made in an attempt to recover, but it was
too late. The engine exhaust flow detached from the diffuser and blowback into
the cell occurred. The blowback heated the thrust load cell. The load cell is
temperature compensating when uniformly heated, but has a negative bias when a
temperature gradient exists in the cell. There was a negative bias of approximately
100 lb$_f$ at the end of the test. Figure 82 shows some of the Test -006 transient
parameters. About 16 seconds into the test, cell pressure (P$_{alt}$-1A and 1B) can
be seen to start to ramp up. Load cell temperature (TSC) is measured on the
exterior of the cell and changes with cell pressure. During the first 16 seconds
of operation, thrust and P$_c$ are increasing. With the cell pressure increase and
load cell heating starting 16 seconds into the test, indicated thrust decreases
while P$_c$ increases.

Following Test -006, testing was terminated any time altitude
dropped below 60,000 ft and no further load cell heating problems occurred. The
load cell was subsequently (after Test -007) coated with RTV rubber to provide
thermal insulation.

After Test -006 and an inspection of the hardware, the engine
and feed system were chilled down and Test -007 attempted. Shutdown was made by
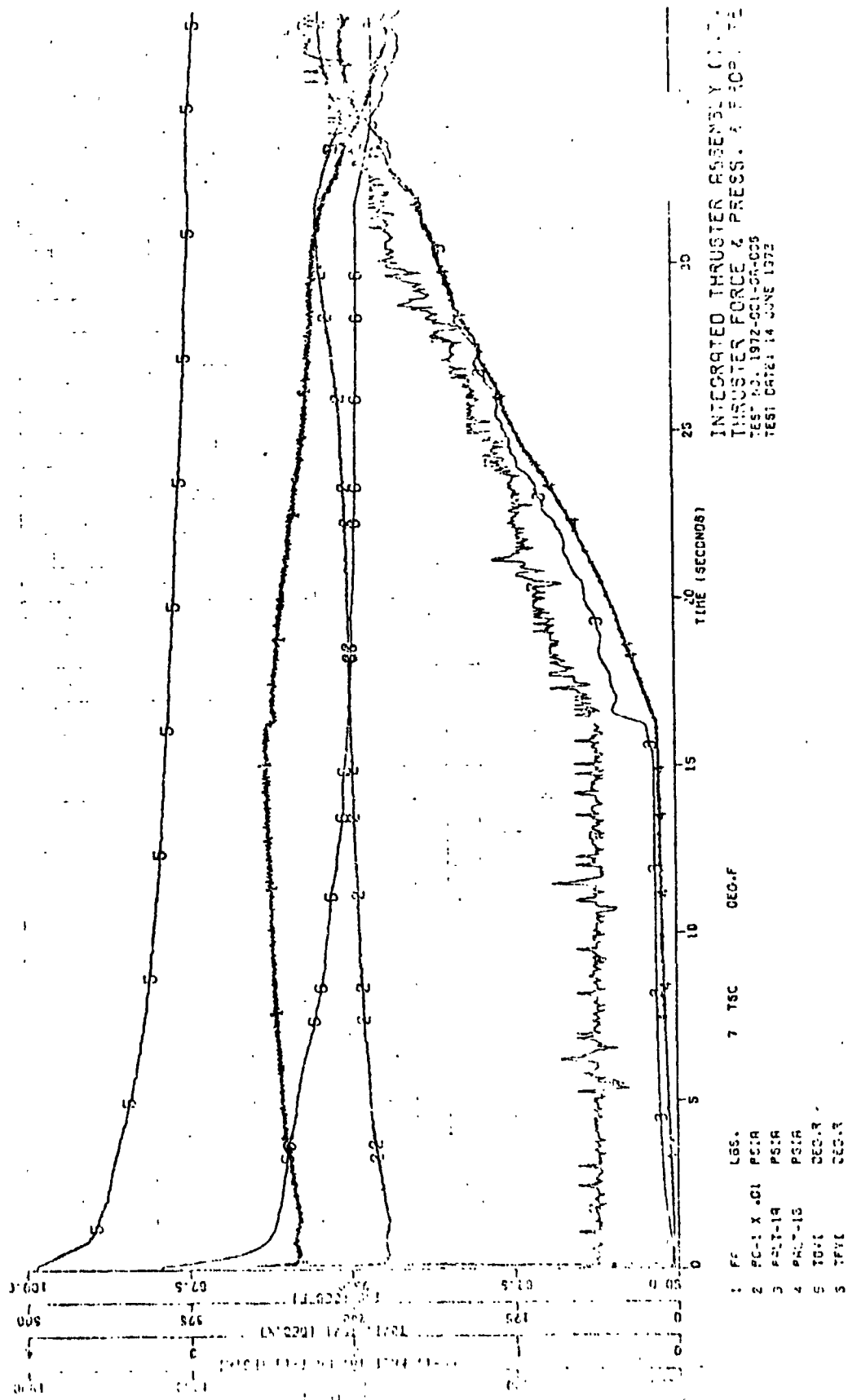
Figure 82. ITA Thruster Force and Pressure

4.4, Integrated Thruster Assembly Testing (cont.)

a high temperature trip circuit. Inspection of the hardware indicated that there was minor erosion on the surface of the throat in two locations and a small burn through in one location about 6 mm downstream of the ffc injection station.

The oscillograph data indicated low P_c and blockage in the fuel circuit. (Details of the hydraulics of this test are discussed in the next section.) The cell was secured, returned to altitude and the hardware chilled down. A flow test was made and gave no indication of blockage. The cell was rapidly repressurized and opened. The face of the injector was completely covered with ice, including the oxidizer orifices. The ice had formed during repressurization of the hardware which was at cryogenic temperatures as a result of the flow test.

It was concluded that the low fuel flow was caused by icing since ice formation was physically observed and since the blockage that occurred during Test -007 was not present after the engine had been allowed to reach ambient temperature.

The engine was removed from the test stand. The hole in the Haynes throat section was TIG welded closed. The area of the weld repair and the two areas where surface erosion occurred were ground smooth. Two additional thermocouples were added to the chamber on the exterior surface in the area of the weld repair and erosion. The chamber was reinstalled on the test stand.

Several changes were made to the test setup. The anemometers were replaced with Ramapo flowmeters in both circuits. The GN_2 purge locations were moved from downstream of the thrust chamber valves to the injector in order to increase the purge gas flow rate. The critical flow venturis were removed from both propellant circuits. The test operations computer was programed to control the pressure of the propellants at the inlet to the test stand valves. A temperature compensation circuit was introduced so that the pressure at the inlet

4.4, Integrated Thruster Assembly Testing (cont.)

to the valves would be proportioned to the square root of the actual propellant temperature. This was done to prevent an MR excursion from occurring if one of the propellants was at a temperature significantly different from that on which the pressure was based.

Testing was resumed with Test -008 terminated because the temperature shutdown circuit was set to trip at a temperature too close to the operating temperature. Test -009 started normally, but 3 seconds into the test the throat and nozzle thermocouples registered an excursion resulting in a high temperature shutdown. Ice in the chamber at the injector face was observed on visual inspection after the test. There were no abnormalities in the chamber hydraulics after the hardware warmed up, but an increase in fuel circuit pressure drop occurred during the last five seconds of the test.

A review of the test procedure suggested that during the chilldown process there were times when the purges were not operated which allow moisture to be condensed and frozen in the fuel passages. In Test -009, the purges were operated most of the time. Ice formation was minimal. The ice apparently broke loose during the test as the hardware contracted as it chilled down.

A hot (93°C) GN_2 purge was added to the set up. The heated GN_2 was introduced downstream of the thrust chamber fuel valve. The purges were maintained on at all times with their start and stop during a test controlled by the sequencer.

Test -010 was made with ambient temperature propellants. Test -011 was started with ambient propellants and the propellants chilled during the test. The fuel cooled faster than the oxidizer resulting in fuel rich operating conditions that precluded maintaining altitude. Test -012 and -013

4.4, Integrated Thruster Assembly Testing (cont.)

were initiated with ambient temperature propellants (lines chilled down to and including the accumulators). The system downstream of the accumulators chilled in as the tests progressed. The two tests at ambient conditions (-010 and -011) and the two starts with ambient propellants followed by a chilldown (-012 and -013) encountered no hydraulic anomalies. The fact that no problems occurred with warm hardware and better purging verified that the flow anomalies of Tests -007 and -009 were caused by icing.

Integral exciter/spark plug unit, SN 007, was installed on the ITA prior to Test -014. All subsequent ITA SN 001 tests were made with this unit. Test -014 was run to temperature condition the hardware prior to the valve sequence test series. Tests -015 through -038 were run with varying main fuel propellant valve lead/lag times and with varying igniter valve lead/lag times. No significant overpressures were observed during these tests. However, it should be noted that the transducers were not coupled to the hardware closely enough to provide the response necessary to detect combustion of the propellants in the manifolds. These tests are discussed subsequently.

H_2 fires on the test stand occurred during some of the tests. During Test -010, the Ramapo flowmeters shorted out. After the test, the insulation on the electrical cables from the meters were found to be melted. A pin-hole leak in the 180° bend in the feed system fuel line was found and repaired. Test -012 was shutdown because of a H_2 fire on the test stand. Two small H_2 leaks were found in AN fittings. Prior to Test -014, the feed system was chilled down and an igniter only test made. Temperatures on the nozzle extension started to rise indicating that there was a H_2 fire on the test stand. No leak could be found, however, several of the large H_2 fittings were tightened. There was no evidence of fire on the stand in the subsequent 25 valve sequencing tests.

The problem with the fire on the test stand is mentioned because it caused nozzle temperatures to read high and may have affected the thermocouple data from tests prior to -014.

4.4, Integrated Thruster Assembly (cont.)

Figure 83 shows the SN 001 thruster after Test -038. The
condition of the thermal insulation on the nozzle extension has been deteriorated
by the blowback that occurs on shutdown. The engine firing into the diffuser
pumped the cell down to a pressure that was lower than the pressure downstream in
the J-3 duct. As discussed earlier, engine exhaust flow detached from the diffuser
on shutdown, and pressure equalization caused blowback of the hot combustion
gases into the cell. The flow past the nozzle extension gradually blasted off
the low density, light weight insulation. This blowback with the resulting
deleterious effect on the insulation would not occur in actual operation in space.

The flowmeters seen in Figure 83 are Ramapo flowmeters. As
described above, the anemometers were replaced after Test -007.

The condition of the ITA SN 001 thruster after Test -038
is shown in Figure 84. The view is from the nozzle looking forward inside the
chamber.

Figure 84a shows the condition of the throat. The polish
marks seen on the throat were the result of the hand grinding operation that was
performed on the chamber to repair the minor erosion that occurred on Test -007.
As can be seen in the figure, no further degradation had occurred with the tests
following -007.

Figure 84b shows the injector face as seen through the
throat. There were no heat marks on the injector face except at the location of
the face thermocouples (braze alloy chemical reaction). The mirror like finish
of the ZrCu chamber liner was evidenced in Figure 84b by the reflection of the
injector elements on the chamber wall. As can be seen in Figure 84, the ITA
SN 001 thruster was in excellent condition after 620 seconds of operation and
38 tests.
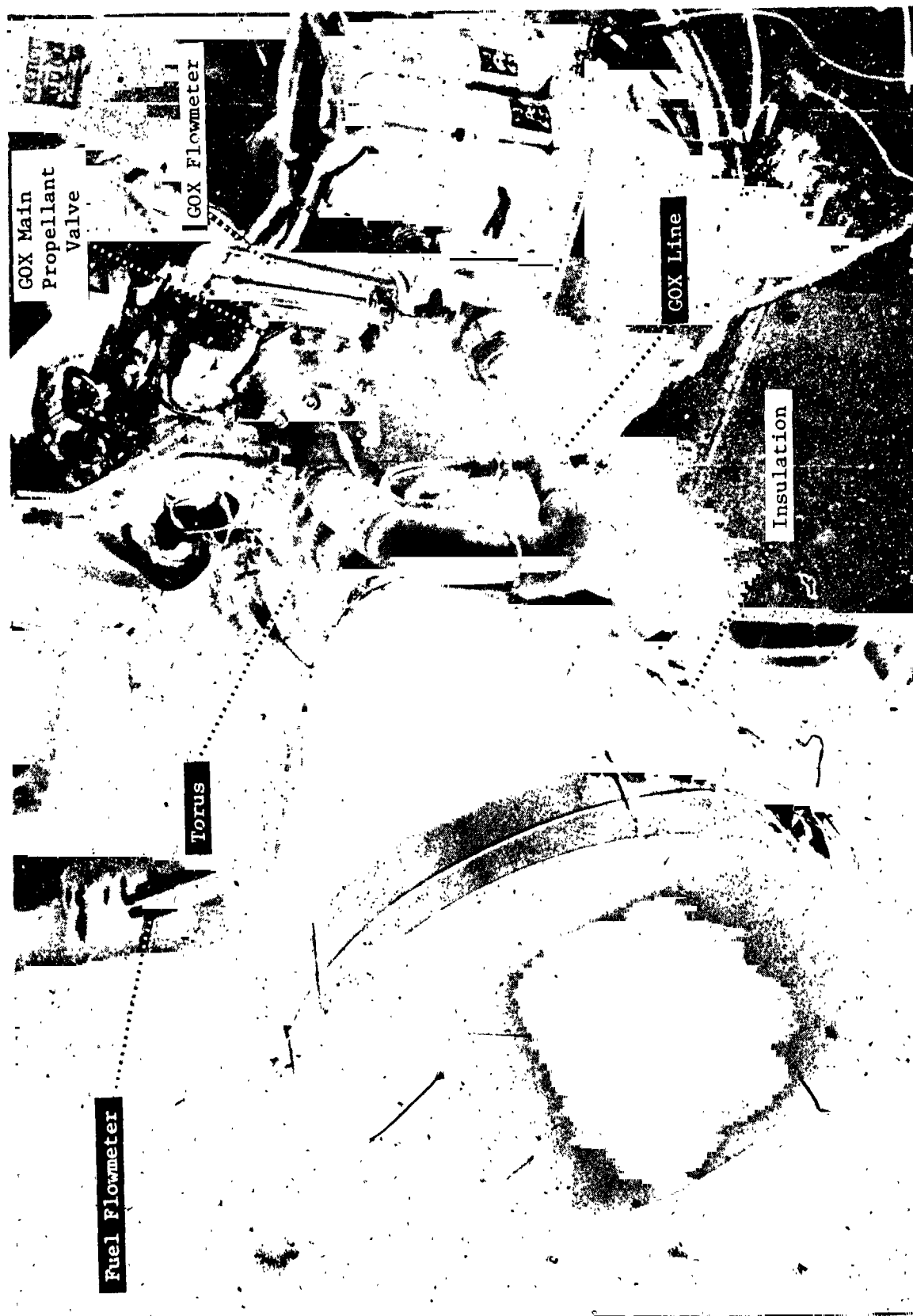
Figure 83. ITA SN 001 Thruster After Test -038
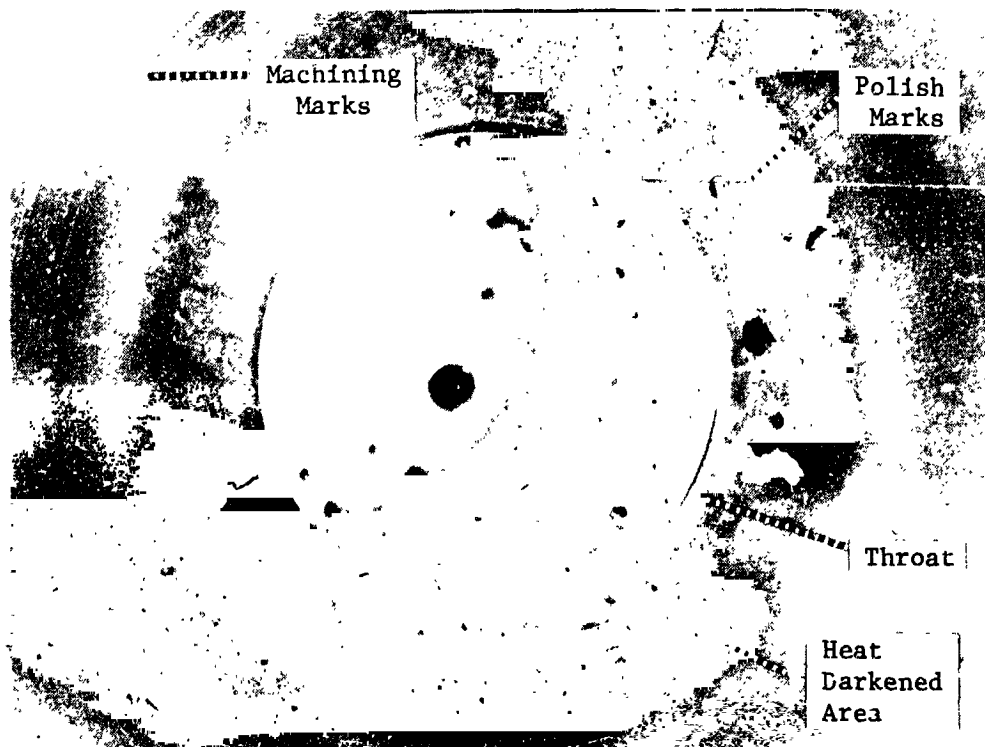
a. Post Fire View of Throat Area
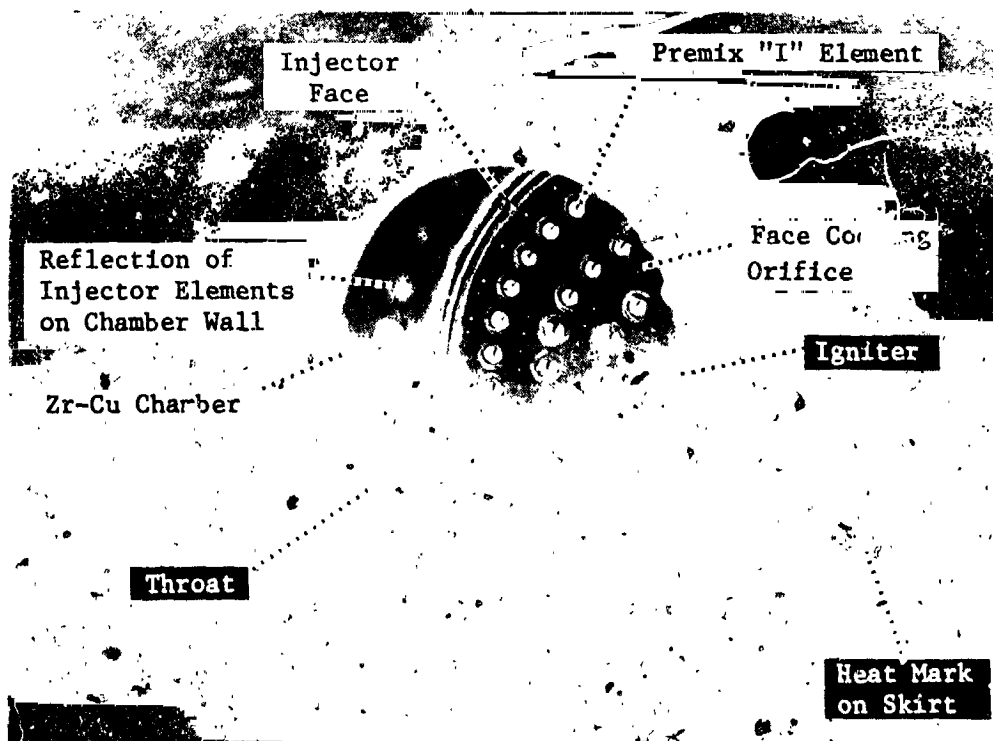
b. Post Fire of Injector thru Throat

Figure 84. Interior of ITA SN 001 Thruster After Test -038

4.4, Integrated Thruster Assembly (cont.)

Seven thermocouples were added to the SN 001 thruster after Test -038. Thermocouple TN 3B (Figure 79) was added 5 mm upstream of the throat and TN 4-B was added 5 mm downstream of the throat in line with the fuel inlet. Three thermocouples were spot welded to the throat, one (TN 3.5A) in line with the other thermocouples 45° from the fuel inlet, one (TN 3.5B) in line with the fuel inlet, and one (TN 3.5C) 180° from the fuel inlet. Two thermocouples (TN 5B and 5C) were added 63.5 mm downstream of the throat which is generally the location of the highest temperatures on the nozzle.

Test -039 was the first of six tests run using the J-4 steam system, and was a .5 sec checkout test. As mentioned earlier, the high capacity J-4 steam system was utilized for low MR and high P_c tests that exceeded the volumetric exhaust removal rate capabilities of the J-3 steam system. Test -045 through -047 were run using the J-3 steam system.

In running Tests -039 through -047, there were two unscheduled shutdowns, both by the high temperature trip circuit. Approximately 4 seconds into Test -042, the pressure in the oxidizer lines (POL) decreased from 1425 N/cm^2 (2066 psia) to 1325 N/cm^2 (1921 psia). The temperature of the oxidizer leaving the heat exchanger (TOL) was 122°K (219°R), indicating the presence of liquid oxygen. Two seconds later, 6 seconds into the test, POL read 867 N/cm^2 (1258 psia), which can only mean there was still considerable liquid oxygen coming out of the heat exchange (gox supply pressure at the heat exchanger inlet is in excess of 1425 N/cm^2). The temperature of the oxygen at the inlet to the thruster at this time was ambient. At shutdown (17 sec test duration) the thermal sensor at the ox thrust chamber valve inlets was indicating a sharply decreasing oxygen temperature. However, chamber temperatures increased to levels observed only in high MR tests resulting in a shutdown by the chamber temperature trip circuit. Apparently, the liquid oxygen from the heat exchanger reached the chamber – although there was almost no change in thrust, chamber pressure or measured ox flow rates. The ITA was carefully inspected and leak checked after this test and was found to be undamaged.

4.4, Integrated Thruster Assembly (cont.)

Test -045 was shutdown by the chamber high temperature trip circuit during an attempt to increase P_c from 135 N/cm^2 (200 psia) to 207 N/cm^2 (300 psia) at high mixture ratio conditions. The thruster was restarted with no inspection and Test -046 was made with no problems. Inspection of the thruster after Test -046 revealed the hardware to be in excellent condition.

In order to operate the thruster at the highest P_c without being shutdown by the 448 N/cm^2 (650 psia) valve protection circuit, and at the highest MR without being shutdown by the chamber 900°C (1650°F) temperature trip circuit, the thruster was operated manually. In reaching the highest P_c, for example, in Test -044 the main propellant valve pressure limit was redlined on the strip chart recorder. Instead of using preset valve pressures selected by switches, the control of the pressure was switched to two potentiometers set near the limit; the test engineer then fine tuned the pressures to within about 14 N/cm^2 (9.6 psia) of the limit, reading the pressures on the recorder. A similar approach was used in obtaining the high MR limit data, except temperatures were used instead of the pressure at the valve inlet.

Near the end of Test -013, the hydrogen supply was nearly exhausted. The high MR test condition that concluded that test was achieved by letting the fuel pressure decay (flow control valve wide open), with shutdown being accomplished when the chamber temperature limit was reached.

In Test -047, the throat temperature limit was reached by operating for a long time and letting the fuel warm up. When 887°C (1630°F) was reached (430 sec), the oxidizer pressure was decreased to reduce the throat temperature and the test continued for a total duration of 512.6 sec.

As can be seen in Table XXXIV, most of the tests were started with an MR of approximately 3, and low chamber pressure. Pressures and mixture ratios were then changed. This was found to be a safe way to start up both for hardware protection and for maintaining altitude.

4.4, Integrated Thruster Assembly Testing (cont.)

4.4.3.2 Valve Sequencing Tests

The valve and igniter sequence tests are summarized
in Table XXXV. Except for the last two tests, all tests were run twice (the even
numbered tests are a repeat of the odd numbered ones). The tests were to have
been run at nominal propellant temperature conditions, but sensible heat trans-
ferred to the propellants from the lines between tests resulted in propellant
temperatures 15 to 20% in excess of nominal. To compensate for the higher
propellant temperatures, the pressures at the inlet to the valves was increased,
maintaining chamber pressure slightly in excess of nominal.

As shown in Table XXXV, the main propellant oxidizer valve
lead time was reduced in five steps until Tests -025 and -026 were made with a
10 msec fuel lead. Sequencing was reset to the times that were used on Test
-020 and had resulted in simultaneous valve opening. However, slight changes in
valve response or the sequencing resulted in a 2 to 6 msec fuel lead for the rest
of the tests. Starting with Test -027 the igniter lead was cautiously reduced
until Tests -037 and -038 were made with the igniter not lighted until 2 to 6
msec after propellant flow to the mainstage.

The main oxidizer propellant valve lead times shown in
Table XXXV were based on propellant flow rates. Valve lead times and propellant
lead times were almost identical. Since initiation of propellant flows is of
primary interest and more accurately determined from the O-graph than valve
motions, the time lapse between ox and fuel flow as measured by the flowmeters
is reported in Table XXXV under the heading "Main Valve Ox Lead". Igniter lead
times were determined from the igniter pressure rise on ignition relating to the
flow of the lagging propellant.

There was no visible damage to the hardware as a result
of these tests. Subsequent testing evidenced no change in operation. No pressure

SUMMARY OF VALVE AND IGNITER SEQUENCING TESTS

Test No. 1972-D01-OA-	Dur. Total (sec)	P_c, N/cm² (psia)	Pressures, N/cm² (psia) Ox. Valve P_{OJCV}	Fuel Valve P_{CTCV}	Temperatures, N/cm² (psia) Oxygen Supply T_{OS}	Valve T_{OTCV}	Fuel Supply T_{FS}	Valve T_{FTCV}	Main Valve Ox Lead (msec)	Igniter Lead (msec)	Comments
015	.203	217 (315)	321 (465)	313 (454)	250 (450)	256 (460)	156 (280)	291 (524)	14	16	Fuel valve not closing properly.
016	.107	216 (314)	325 (471)	314 (455)	257 (462)	257 (463)	168 (302)	288 (518)	13	17	Repeat.
017	.288	231 (335)	358 (520)	307 (446)	250 (450)	247 (445)	170 (306)	289 (520)	8	13	Reduced ox lead.
018	.214	211 (306)	312 (452)	309 (448)	244 (440)	241 (433)	164 (295)	257 (516)	9	16	Repeat.
019	.214	214 (310)	324 (470)	310 (450)	246 (443)	246 (442)	171 (308)	287 (516)	1	17	Reduced ox lead.
020	.214	216 (314)	316 (459)	307 (445)	236 (425)	239 (430)	163 (293)	287 (517)	0	19	Repeat.
021	.219	229 (332)	350 (507)	311 (451)	233 (419)	234 (422)	169 (304)	287 (517)	(5)*	16	Fuel lead.
022	.235	214 (311)	210 (449)	307 (446)	232 (417)	220 (407)	162 (291)	287 (517)	(4)	16	Repeat.
023	.214	215 (312)	316 (459)	307 (445)	228 (411)	228 (410)	163 (293)	287 (516)	(5)	11	Increased fuel lead on timer. No change.
024	.214	212 (307)	312 (453)	307 (44?)	8 (-10)	230 (414)	160 (288)	287 (517)	(5)	10	Repeat.
025	.213	214 (311)	318 (462)	305 (442)	236 (425)	240 (432)	162 (292)	288 (509)	(10)	13	Attempted -15 msec fuel lead.
026	.214	214 (311)	315 (457)	303 (440)	233 (420)	238 (428)	151 (272)	283 (509)	(10)	14	Repeat.
027	.192	212 (308)	315 (457)	303 (440)	242 (435)	241 (434)	159 (287)	285 (513)	(4)	12	Attempted 0-5 msec ox lead. 5-10 msec ign. lead.

*Parenthesis indicate negative value, i.e., lag instead of lead.

TABLE XXXV (cont.)

Test No. 1972 D01-OA-	Dur. Total (sec)	P_c: N/cm² (psia)	Pressures, N/cm² (psia) Ox. Valve P_{OJCV}	Fuel Valve P_{CICV}	Temperatures, N/cm² (psia) Oxygen Supply T_{OS}	Valve T_{OTCV}	Fuel Supply T_{FS}	Valve T_{FTCV}	Main Valve Ox Lead (msec)	Igniter Lead (msec)	Comments
028	.203	213 (309)	314 (456)	302 (438)	240 (432)	241 (434)	153 (276)	284 (511)	(3)	10	Repeat
029	.203	214 (311)	299 (433)	301 (437)	217 (391)	223 (401)	159 (286)	235 (513)	(3)	7	Reduced ign. lead by 5 msec.
030	.203	212 (307)	303 (440)	299 (433)	217 (391)	223 (401)	153 (27.)	285 (513)	(2)	5	Repeat.
031	.203	211 (306)	299 (434)	302 (438)	217 (391)	220 (396)	158 (285)	283 (509)	(4)	4	Reduced ign. lead by 5 msec.
032	.203	210 (305)	303 (439)	299 (433)	217 (391)	220 (396)	154 (277)	283 (510)	(3)	5	Repeat.
033	.203	212 (307)	309 (448)	299 (433)	221 (398)	226 (407)	157 (283)	283 (513)	(6)	4	Reduced ign. lead by 2 msec.
034	.203	210 (305)	303 (440)	295 (428)	218 (393)	226 (407)	153 (275)	287 (516)	(2)	1	Repeat.
035	.203	210 (304)	296 (430)	302 (438)	212 (381)	219 (395)	157 (283)	289 (520)	(4)	1	Reduced ign. lead by 2 msec.
036	.203	210 (305)	296 (430)	300 (435)	213 (384)	219 (395)	151 (274)	289 (521)	(2)	0	Repeat
037	.203	212 (308)	296 (430)	303 (440)	220 (396)	226 (407)	159 (287)	285 (513)	(6)	(2)*	Reduced ign. lead by 2 msec.
038	.214	214 (310)	302 (438)	301 (437)	217 (391)	227 (409)	152 (273)	284 (512)	(3)	(6)	Reduced ign. lead by 2 msec.

*Parenthesis indicate negative value, i.e., lag instead of lead.

4.4, Integrated Thruster Assembly Testing (cont.)

spikes were seen on any of the manifold pressures – however, the transducers were
not close coupled and would not have responded to impulse type pressure transients.
The only transducer that was small enough and coupled by a small diameter line,
was the chamber P_c transducer. However, it froze up during these tests.
Apparently combustion products pulsing into the small hole (1.15 mm dia.)
through the cooled wall were frozen by the cryogenic wall temperatures. The
transducer read zero pressure during the latter tests. It continued to give a
zero reading as the cell was being pressurized after the test series, then
suddenly it read cell pressure.

4.4.3.3 Flow Tests and Hardware Repair

Tests -048 and -049 were flowmeter calibration tests. The
Ramapo flowmeters were flowed in place using cold and ambient propellants. The
data, however, are questionable. The presence of the chamber caused the back-
pressure in the fuel circuit to be about 90% of the pressure upstream of the
venturi. The venturi may not have flowed critically. The cold oxygen flow
tests resulted in conditions close to the saturation temperature. Much of the
cold oxygen flow data is suspect. The oxidizer flow rates as measured by the
flowmeter appears to be about 3.5% low. The data are discussed in the next
section (4.5).

A pressure check of the chamber revealed four leaks in the
throat section. There were two cracks in the Haynes that could be seen with the
naked eye. The other two leaks were very small; no crack could be seen; they
were in the Haynes to ARMCO 22-13-5 weld. The two visible cracks were in the
areas where erosion had occurred during Test -007 and are shown in Figure 85.
Figure 85 also shows the weld repair that was made to the throat section after
Test -007. Both the original burn through (Test -007) and the crack shown in
the right insert (Figure 85) were in areas that normally have low stress and
run cold because of their close proximity to the ffc injection.
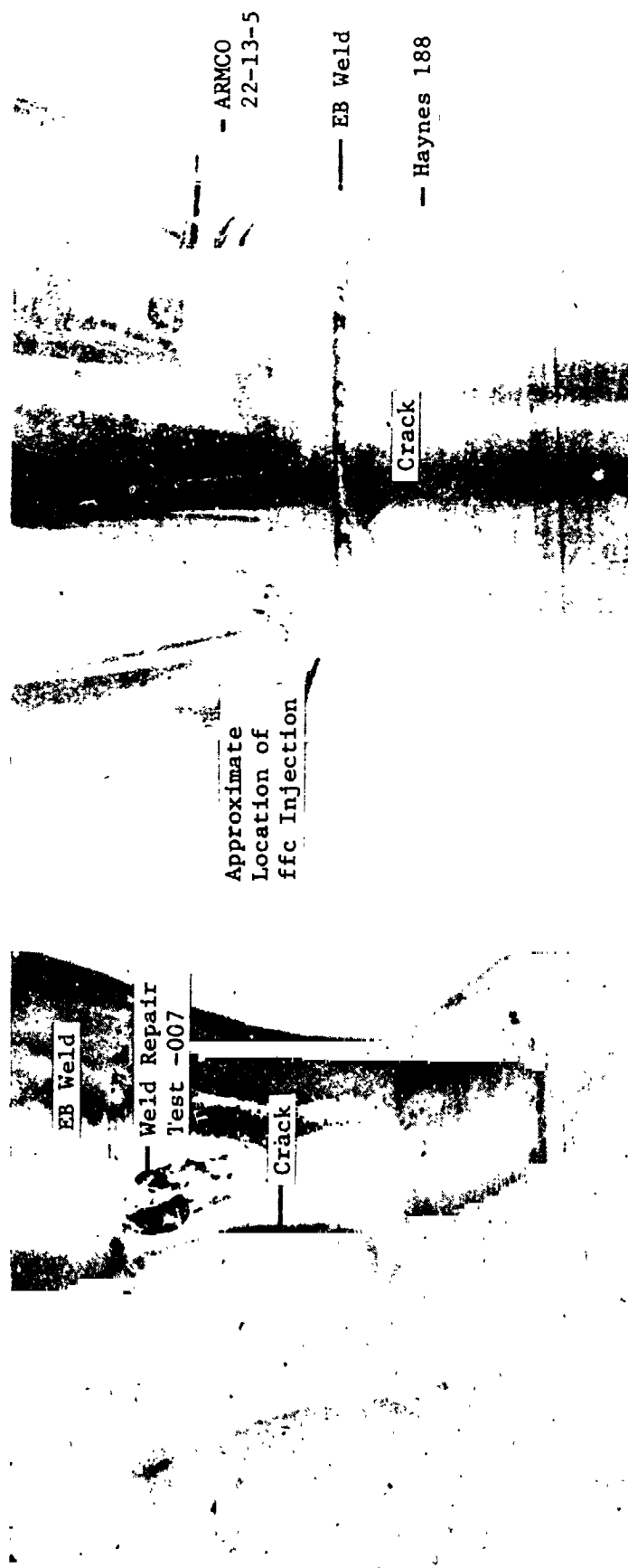
Figure 85. Cracks in Haynes Throat Section - Posttest -047

4.4, Integrated Thruster Assembly Testing (cont.)

The repair of the cracks by welding was done using a very cold weld. However, the shrinkage apparently resulted in more cracks as a post weld leak check indicated new leaks in the ARMCO-22-13-5 to Haynes 188 EB weld. The leaks were small; no hole or crack could be seen with the naked eye. These leaks were repaired by welding. Figure 86 shows the chamber after weld repair of the leaks. The weld penetration area on the ID of the chamber was ground smooth and polished.

When ITA SN 001 was removed from the test stand for weld repair of the cracks, both balance orifices were found to be loose. These orifices had been installed in a counterbore in the inlet line flanges and secured by spot welding a 1.14 mm dia (.045) wire ring to the orifice at its OD and to the I.D. of the recess in the flange. The fuel orifice was bent ($\approx 30°$). There were minor abrasions on the OD of the oxidizer orifice. The OD of the fuel orifice was more severely "chewed up" especially on the downstream side where it contacted the ledge in the flange. The orifices were straightened and reinstalled as before.

The main propellant valves were switched from self actuation to actuation using an inert gas. Helium was used for the fuel valve and GN_2 was used for the ox valve. The change was made in an attempt to improve fuel valve response on closing. The fuel valves lag on closing that had been occurring was unacceptable for pulse mode of operation.

4.4.3.4 Pulsing Tests

Two types of pulse tests were run: constant pulse width tests and duty cycle tests. The constant pulse width tests were run to evaluate the optimum valve sequence and to determine the minimum impulse bit (MIB). These

Figure 86. AN 001 Nozzle After Weldment to Repair Leaks

4.4, Integrated Thruster Assembly Testing (cont.)

tests were run using ten pulses of the same width. The testing is summarized in Table XXXVI. Data were obtained for combinations of oxidizer lead on startup with fuel valve lag on shutdown.

As summarized in Table XXXVI, Tests -050 through -058 were one pulse checkout tests. These tests addressed two problems: altitude/thrust stand ringing and fuel valve delay on closing.

When altitude was not maintained, thrust would oscillate. This oscillation did not occur when all three stages of the steam ejector system were used as shown by prior testing and confirmed by Test -053. Increasing the duct coolant spray reduced the oscillation problem, but did not eliminate it. The spray was adequate for the constant pulse width tests (.2 sec duration). Upon completion of the constant pulse width tests and prior to the duty cycle pulse tests, the duct spray system was overhauled. Plugged heads were replaced and more were installed. An aspirator was installed to prevent water accumulation. The improved duct coolant spray ended the thrust oscillation problems.

As can be seen in Table XXXVI, the main ox valve closing lead times went from 30 msec on Test -050 to .2 sec on Test -053. This was not a change in sequence. The fuel valve was hanging open. It was a pilot valve problem that seemed to get worse as the valve chilled down. The change to helium actuation for the fuel valve that was made prior to the start of this series was done to keep the valve warmer. Since the pilot valve leaked, it was though that teh temperature of the valve would remain higher if it leaked ambient temperature helium rather than cryogenic hydrogen. Prior to Test -057, nitrogen was used for the actuation fluid in place of helium since the higher molecular weight gas would leak less. Also, heaters were put on the exterior of the valve. The closing delay problem went away for the time being.

TABLE XXXVI

SUMMARY OF CHECKOUT AND CONSTANT PULSE WIDTH TESTS

Date 1973	Test No. 1972- D01-0A-	No. of Pulses	Pulse Width, sec	P_c, N/cm² (psia)	Pressure @ Valve N/cm² (psia)		Temperatures & Valve Inlet, °K (°R)		Main Ox Valve Lead		Comments
					P_{OTCV}	P_{FTCV}	T_{OTCV}	T_{FTCV}	Open	Close	
9-24	050	1	.2	199 (288)	295 (428)	285 (414)	239 (430)	193 (347)	25	30	Single pulse checkout.
9-25	051	1	.4	223 (324)	334 (484)	314 (455)	239 (430)	198 (357)	30	50	Thrust oscillation – slight delay in fuel valve closing.
	052	1	.4	205 (298)	296 (430)	315 (457)	244 (440)	198 (357)	20	120	Repeat – fuel valve delayed closing – thrust oscillation.
	053	1	.2	222 (322)	325 (472)	314 (456)	230 (414)	198 (357)	25	200	3 stages steam ejector – long delay in fuel valve closing – no thrust oscillation.
	054	1	.2	221 (320)	329 (477)	319 (463)	230 (424)	198 (356)	30	166	2 stages steam ejector – increased water spray – no thrust oscillation – delay in fuel valve closing.
	055	1	.4	219 (318)	328 (476)	308 (445)	242 (435)	181 (325)	30	115	Repeat – pulsed fuel valve prior to test – still delays – thrust oscillation.
	056	1	.2	220 (319)	331 (480)	300 (447)	241 (433)	187 (336)	30	130	Repeat computer shutdown – fuel valve delayed closing.
9-26	057	1	.2	207 (300)	302 (438)	304 (441)	236 (424)	184 (332)	10	40	Checkout – GN_2 actuation of fuel valve.
	058	1	.4	213 (309)	314 (456)	312 (452)	241 (433)	197 (355)	22	33	Checkout – thrust oscillation.
	059	10	.2	196 (284)	302 (438)	278 (403)	253 (455)	155 (279)	30	50	st of series in which main propellant valve lead/lag varied.
	060	10	.2	192 (278)	289 (419)	383 (411)	247 (444)	164 (296)	15	20	Shortened ox valve lead on opening.

TABLE XXXVI (cont.)

Date 1973	Test No. 1972 DOI-OA-	No. of Pulses	Pulse Width, sec	P_c, N/cm² (psia)	Pressure @ Valve N/cm² (psia)		Temperatures & Valve Inlet, °K (°R)		Main Ox Valve Lead		Comments
					P_{OTCV}	P_{FTCV}	T_{OTCV}	T_{FTCV}	Open	Close	
	061	10	.2	197 (286)	301 (436)	278 (403)	248 (448)	159 (287)	10	20	Shortened ox valve lead on opening.
	062	10	.2	191 (277)	288 (418)	280 (406)	247 (445)	159 (287)	5	20	Shortened ox valve lead on opening.
	063	10	.2	192 (278)	286 (415)	273 (396)	242 (435)	157 (283)	30	0	Simultaneous valve closing times.
	064	10	.2	190 (276)	286 (415)	277 (402)	241 (433)	158 (284)	15	0	Shortened ox valve lead on opening.
	065	10	.2	202 (293)	302 (438)	272 (394)	238 (428)	157 (283)	8	0	Shortened ox valve lead on opening.
	066	10	.2	194 (281)	288 (418)	281 (407)	243 (437)	152 (273)	0	0	Simultaneous opening and closing.
	067	1	.1	216 (314)	326 (473)	299 (433)	223 (401)	173 (311)	–	–	Low thrust shutdown – shortened thrust shutdown monitor time.
	068	8	.1	192 (278)	277 (402)	285 (413)	233 (419)	173 (312)	(5)	10	Shortened pulse width.
	069	10	.075	203 (295)	327 (474)	293 (425)	234 (422)	173 (311)	5	0	Shortened pulse width.
	070	10	.050	–	–	–	–	–	–	–	No fire – valves did not open.
	071	10	.065	202 (293)	308 (445)	301 (437)	222 (400)	178 (320)	(3)	7	Valves signaled closed as poppets start travel.

4.4, Integrated Thruster Assembly Testing (cont.)

As can be seen in Table XXXVI, Tests -060 through -062 and -063 through -066 were run with 20 msec and 0 msec main ox valve lead on closing, and varying main ox valve lead on opening. In Tests -068, -069 and -017 the pulse widths were shortened. The pulse widtns in Table XXXVI are electrical.

Test -067 was shutdown by the low thrust monitor. The monitor "window" extended beyond the shutdown. The problem was solved by shortening the monitor time so that the entire low thrust window occurred within the pulse firing time.

Test -070 resulted in no firings. The pulse width was too short and the main propellant valves never opened. In Test -071, the valves were being signalled closed approximately .005 sec before they opened, but they opened because of a .015 sec delay in pilot valve response. Pulse width could have been reduced another .005 sec, but no more than .010 sec at the very most. In Test -071, a minimum impulse bit of 267 N-sec (60 lb_f-sec) was achieved. Because of problems that had been occurring with the fuel valve delay in closing, and because the valve response time exceeded .050 sec, especially with GN_2 actuation, there was no way that the 222 N-sec (50 lb_f-sec) goal could be achieved, so no further reductions in pulse widths were attempted.

Table XXXVII is a summary of the duty cycle tests that were run. These tests served to debug the operation for the life cycle testing, provided data on pulse mode of operation with ambient and cryogenic temperature propellants, and demonstrated that the pulsing duty cycle imposed no limits. The B and C duty cycles (Table XXXVII) were the same except for coast time; the D duty cycle was used for cycle life testing.

TABLE XXXVII

SUMMARY OF DUTY CYCLE PULSE TESTING

Date 1973	Test No. 1972 DC1-0A-	No. of Pulses	Duty Cycle	P_c, N/cm² (psia)	Pressures @ Valve Inlet, N/cm² (psia)		Temperatures @ Valve Inlet, °K (°R)		Comments
					P_{OTCV}	P_{FTCV}	T_{OTCV}	T_{FTCV}	
10-1	072	1	A	152 (220)	227 (330)	227 (330)	296 (533)	295 (537)	Checkout - 12 msec ox lead on startup - 10 sec ox lag on shutdown.
	073	5	B	152 (221)	231 (335)	224 (326)	296 (533)	297 (536)	Shutdown by chamber high temperature. Set trip point higher.
	074	57	B	153 (222)	227 (330)	236 (343)	299 (538)	299 (538)	Computer shutdown - set low pressure to valves (276 - 34 = 242 N/cm² (350 psia).
	075	7	B	172 (250)	254 (368)	267 (387)	299 (539)	299 (539)	Computer shutdown - low thrust trip.
	076	60	B	172 (249)	258 (374)	268 (389)	301 (541)	299 (539)	Wanted nominal valve inlet pressure. Pressures a little low.
	077	60	C	152 (220)	239 (347)	227 (330)	300 (540)	298 (537)	Optimized valve timing. Same as Test -074 - new duty cycle.
	078	23	C	173 (251)	255 (370)	267 (387)	301 (542)	306 (540)	Computer shutdown prior to 6th pulse of 4th series - lo. thrust.
	079	60	B	197 (286)	272 (394)	254 (269)	206 (371)	137 (247)	Cold propellants optimized main propellant valves lead/lag.
	080	60	C	186 (270)	279 (405)	258 (374)	214 (387)	143 (263)	Same as Test -079 except for duty cycle.
	081	10	D	205 (297)	281 (407)	270 (392)	214 (386)	157 (282)	Computer shutdown because fuel valve does not close.
	082	15	D	199 (289)	283 (411)	276 (401)	214 (385)	213 (285)	Double pulse (no coast time between 2 pulses).
	083	31	D	204 (296)	286 (415)	277 (402)	232 (418)	158 (285)	.5 sec coating pulse at end. Sequence triggered by water valve

TABLE XXXVII (cont.)

Date 1973	Test No. 1972 D21-0A-	No. of Pulses	Duty Cycle	P_c, N/cm² (psia)	Pressure @ Valve Inlet, N/cm² (psia)		Temperatures @ Valve Inlet, °K (°R)		Comments
					P_{OICV}	P_{FTCV}	T_{OICV}	T_{FTCV}	
	084	50	D	200 (290)	284 (412)	3 (3/4)	230 (416)	137 (247)	1.0 sec cooling pulse at end. Sequence triggered by water valve.
	085	60	D	199 (288)	279 (405)	256 (372)	231 (416)	1?? (241)	1.5 sec cooling pulse at end.

DUTY CYCLES

Duty Cycle	Pulse	1	2	3	4	5	6	7	8	9	10	11
A	On (sec)	1.385	(single pulse)									
	Off (sec)											
B	On (sec)	.5	.3	.2	.15	.1	.08					
	Off (sec)	1.0	.5	.29	.24	.19	.18					
C	On (sec)	.5	.3	.2	.15	.1	.08					
	Off (sec)	2.0	1.0	.53	.43	.33	.33					
D	On (sec)	.15	.15	.15	.15	.4	.08	.09	.09	.09	.09	.3*
	Off (sec)	.3	.3	.3	.3	.6	.18	.18	.18	.18	2.0	15/20

*Fuel valve only.

4.4, Integrated Thruster Assembly Testing (cont.)

The problems that were debugged concerned setting the kill monitor times such that they didn't shut the sequence down with minor changes in valve timing, and elimination of electrical cross talk that resulted in the sequence being triggered by the opening of a valve such as the LN_2 valves to the heat exchanger. The final selection of the minimum pulse width as approximately .080 sec for the D duty cycle solved much of the shutdown monitor problems. With a valve response time on the order of .060 sec an .030 sec electrical pulse width means the thrust monitor must be less than .020 sec or must extend past the shutdown signal.

The last pulse of the D duty cycle is made with only the fuel valve opened to cool the hardware down. This mode of operation was basic to the cycle life testing in order to accomplish one full thermal cycle every ten pulses. The length of time the fuel valve was open was increased on each of the last two tests (084 and 085) to provide data on cooldown versus valve open time.

4.4.3.5   ITA SN001 Post Test

At the conclusion of the pulse tests (-085), there were three very small external leaks in the weld of the Haynes 188 throat section to ARMCO-2-13-5 chamber shell. They were so small that only one of three could be found with a dye penetrant check. Since the weld in which the cracks occurred is only 6 mm downstream of the fuel film coolant injection station, the cracks leak cold hydrogen film coolant and therefore do not render the ITA inoperable. Whether they would have deteriorated with continued testing can only be speculated. The cracks probably resulted from stresses introduced by prior weld repairs of the throat section. The ARMCO shell is relatively rigid and the throat section adjacent to the Haynes to ARMCO EB weld had shrunk because of the welding.

4.4, Integrated Thruster Assembly Testing (cont.)

ITA SN001 after testing is shown in Figure 87. The three inserts in the figure are views taken 120° apart to show the entire exterior. As can be seen in the pictures there were no problems other than the weld repair of the throat section.

The interior of the SN001 chamber is shown in Figure 88. The skirt (Fig. 88a) was fairly uniformly a dull green in color and a little darker in the throat. There were no heat streaks.

As can be seen Figure 88b the discoloration of the Haynes was different for the throat secti which is darker than the nozzle extension to which it was welded (dark area stops at the weld). Despite the early erosion, polishing, etc., the throat of the chamber was in excellent condition.

The center of the injector face is shown in Figure 88c. It showed some evidence of being fired, but apparently ran quite cool. There was no over heating, erosion, delamination, bulging of face cooling channels or any other physical appearance that would suggest and damage from high MR tests, pulsing, valve sequencing tests, ignition delays, etc. The injector chamber interface photograph shown in Figure 88d displays some of the outer row of injector elements that cannot be seen in Figure 88c, and illustrates the excellent condition of the injector after 2513 sec of testing.

Two additional view of the injector-chamber interface are shown in Figure 89 to illustrate the condition of the ZrCu liner. The liner on one side of the chamber, although darkened, still had a mirror like finish as evidenced by the reflection of the injector elements on the sall (insert on right of Figure 89). The other side of the chamber was much darker (insert on left in Figure 89); the surface on that side was also very smooth. The walls of the
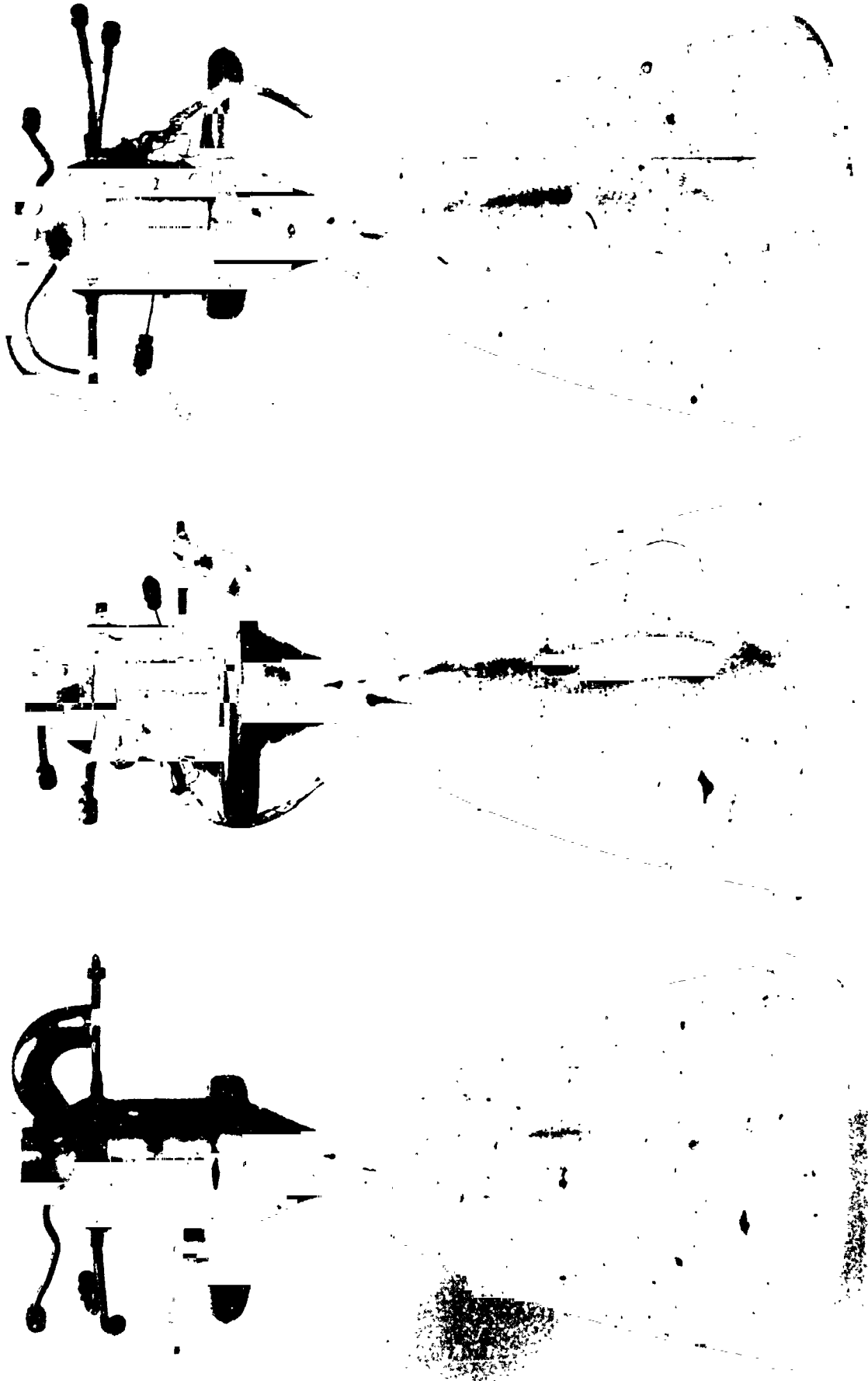
Figure 87. SN 001 After Test Firing (3 Views Rotated 120°)

(a) Skirt
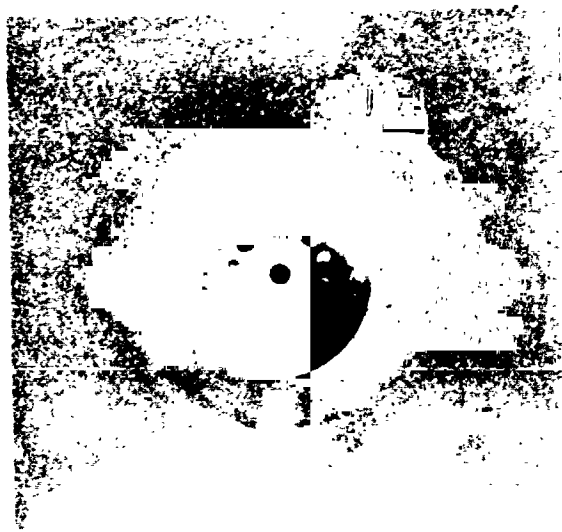
(b) Throat
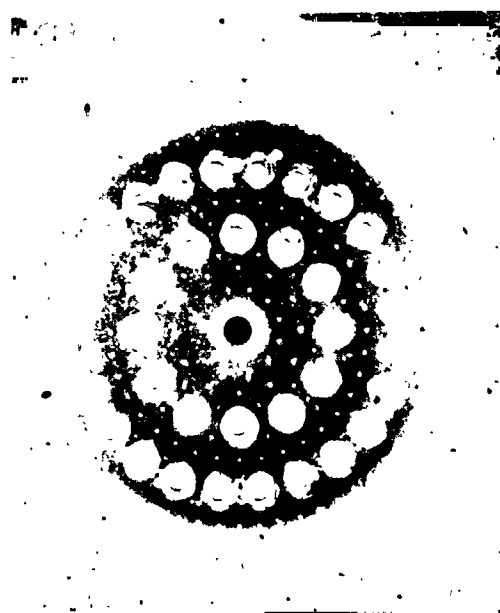
(c) Injector
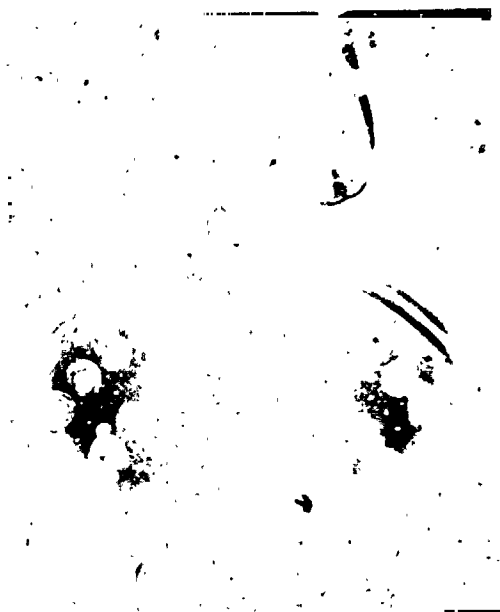
(d) Injector-Chamber Innerface

Figure 88. Interior of ITA SN 001 After Testing
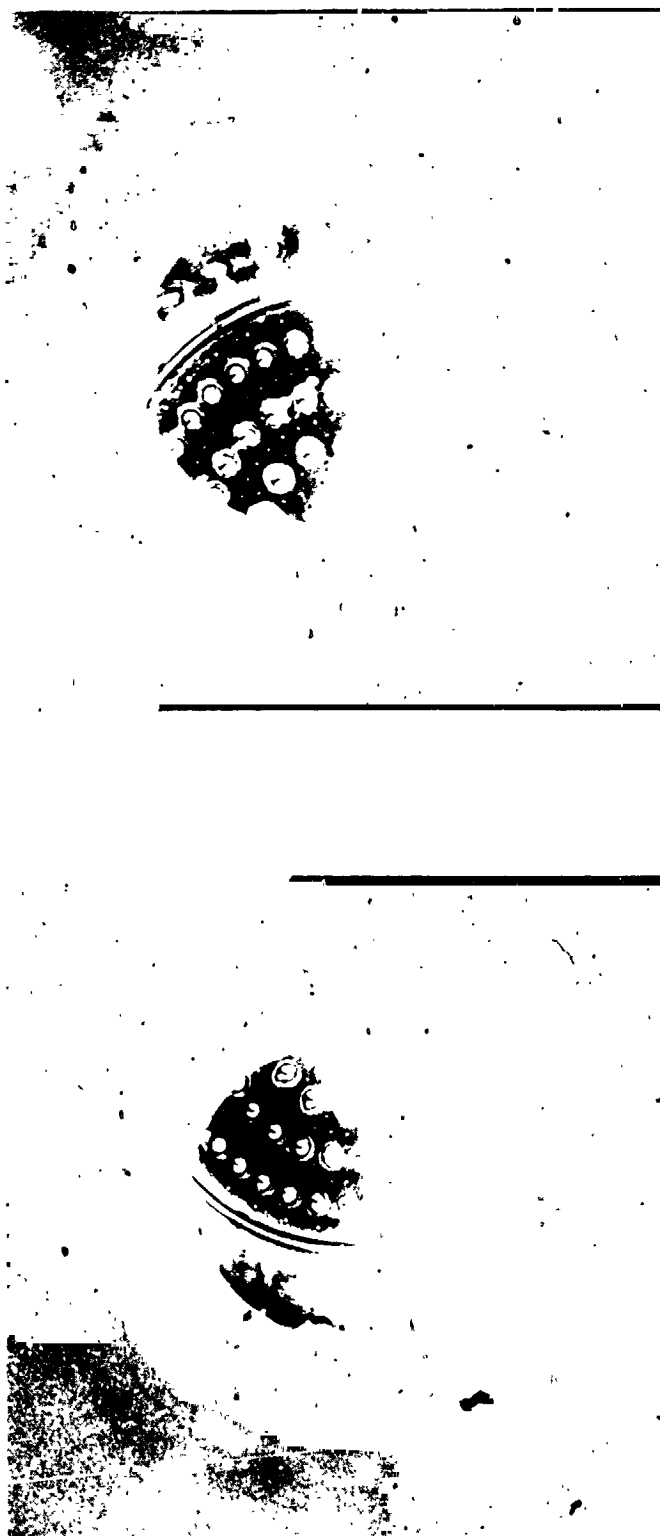
Figure 89. ITA SN 001 Injector-Chamber Interface after Testing

4.4, Integrated Thruster Assembly Testing (cont.)

injector face were very dark after the high MR and high P_c testing. They became lighter with continued test ..g as a result of the hydrogen anneal that occurred with fuel lag on shutdown and warm chamber walls. The sharp edge of the P_c tap was rounded. In general, the ZrCu liner appeared to be in excellent condition.

4.4.4   ITA SN 002 Testing (Cycle Life)

The duty cycle that was initially used for the life cycle testing is shown in Table XXXVII as Duty Cycle D. The rationale for selection of this duty cycle is discussed in the next section. The life cycle pulse train consisted of the eleven pulse series repeated approximately every 30 seconds. The pulse train was like a closed loop with pulse #1 following 20 seconds after pulse #11. Only the fuel valve was opened on the eleventh pulse to cool down the hardware and thus provide a full thermal cycle for every ten firings.

The ITA life cycle tests are summarized in Table XXXVIII. A total of 42,266 pulses were fired in eleven days of testing.

There were many shutdowns by the protective circuits on the first day of cycle life testing. Most of the shutdowns were caused by the main fuel valve. Delays in opening resulted in low thrust shutdowns, and delays in closings caused PFJ overpressure shutdowns duri the off times. The low thrust shutdown was delayed until it was inoperative for the five short pulses of the duty cycle. The time between pulses was increased to permit the PFJ over-pressure monitor to be delayed. Shutdown was also caused by the PFJ line freezing up, which slowed its response. The fuel pressure monitor was switched to PFTCV-O, the valve outlet. The final problem was a long delay in the fuel valve opening on the first pulse of the 11 pulse sequence. Since it did not occur on subsequent pulses, the eleventh pulse - the pulse in which only the hydrogen valve was opened - was changed. Instead of running it two seconds after the tenth pulse followed by the 20 second coast, it was run 20 seconds after the tenth pulse and

TABLE XXXVIII

SUMMARY OF LIFE CYCLE TESTS

Date	Test Number	Pulses	Comments
10-15-73	1972-001-0A-		
	086	1	.1 sec checkout test
	087	1	Data acquisition checkout
	088	1	.5 sec checkout
	089	1	Low thrust shutdown - changed setting
	090	1	1.5 sec checkout
		10	Low thrust shutdown on 11th pulse (H_2 bleed)
	091	28	Fuel lead on startup - changed sequence
	092	1	Temperature shutdown - thermocouple malfunction
	093	1	1.8 sec test - computer not reset
	094	1	Low thrust shutdown - changed setting
	095	1	Low thrust shutdown - fuel valve delay
	096	21	Low thrust shutdown - delayed shutdown
	097	21	PFS shutdown - fuel valve delay on closing
	098	1	Inadvertently changed POS monitor time
	099	33	PFS shutdown - fuel valve delay on closing
	100	35	PFS shutdown - transducer freezing up
	101	11	PFS shutdown - transducer freezing up
	102	34	PFS shutdown - transducer freezing up
	103	50	PFS shutdown - transducer freezing up - changed to PFTCV-0 monitor
	104	140	Fuel valve delay on opening
	105	1	Fuel valve delay on opening - low thrust shutdown
	106	1	Fuel valve delay on opening - low thrust shutdown
	107	81	PFTCV-0 shutdown - fuel valve delay in closing
	108	365	Low thrust shutdown - fuel valves
	109	710	Shutdown caused by fuel valve delay
	110	1	Shutdown caused by fuel valve delay - operated fuel valve several times
	111	1861	POS transducer fails - POS shutdown - 514 N/cm^2 (730 psia) oxidizer valve pressure in open position (3413 pulses total)
10-17-73	112	471	Low thrust shutdown
	113	91	Low thrust shutdown
	114	101	Low thrust shutdown
	115	111	Low thrust shutdown
	116	81	Low thrust shutdown
	117	170	Sequencer malfunction - last pulse 7 sec firing
	118	1183	PFTC-0 transducer froze up (5621)
10-19-73	119	1	.5 sec checkout
	120	1	2 sec checkout
	121	3090	Normal shutdown
10-22-73	122	2730	Normal shutdown (11,443)
10-24-73	123	2910	Normal shutdown (14,353)

TABLE XXXVII (cont.)

Date	Test Number	Pulses	Comments
10-25-73	1972-001-0A-		
	124	6371	Normal shutdown - gross bellows leak on oxidizer main valve - fuel pilot valve does not close - cannibolized SN 001 (20,724)
10-30-73	125	1	.5 sec duration checkout
	126	1	2 sec checkout
	127	1	Sequencer malfunction
	128	112	PFTCV-O shutdown
	129	2290	PFTCV-O failure
	130	37	Sequencer malfunction
	131	320	Oxidizer valve timing delay
	132	90	Oxidizer valve timing delay
	133	130	Oxidizer valve timing delay - GN_2 valve actuation pressure low
	134	300	Sequencer malfunction
	135	2062	Normal shutdown (26,068)
10-31-73	136	1540	Sequencer malfunction
	137	1651	Fuel igniter valve not closing
	138	790	Replaced igniter valves - crack in torus (30,049)
11-1-73	139	4335	POS shutdown - checked oxygen system
	140	210	Line bleed valve leaking - torus crack (34,594)
11-2-73	141	4920	Fire in cell. Hole in fuel line (39,514)
11-6-73	142	1	.5 sec checkout - fuel valve bellows leak getting worse
	143	1	Repeat - replaced fuel valve pilot - self actuated
	144	2332	Fuel valve delay very severe
	145	418	Fuel valve hardly closing. Fire on stand. Chamber damaged (42,266 pulses total)

4.4, Integrated Thruster Assembly Testing (cont.)

followed by a 6 second coast. Operation of the fuel valve, 6 seconds before
the first pulse instead of 20 seconds, solved the problem. The valve delay
occurred on the cooling pulse where there were no shutdown monitors. The
throat thermocouples were monitored and showed that the delay in the valve
opening did not compromise the cooldown. One further change was made in the
duty cycles. The 20 second coat time after the tenth pulse was shortened to
15 seconds.

The duty cycle as finally used was:

Pulse	1	2	3	4	5	6	7	8	9	10	11*
On (sec)	.175	.175	.175	.175	.425	.09	.09	.09	.09	.09	.3
Off (sec)	.3	.3	.3	.3	.6	.25	.25	.25	.25	15	6

The times in this duty cycle are electrical widths. They
are comparable to those shown in the D Duty Cycle, Table XXXVII. Because of
difference in sequencing and because the fuel valve was delaying longer on
opening, both duty cycles resulted in approximately the same firing times.

The hardware was carefully inspected after 3413 pulses.
A GN_2 ring had been installed around the throat to aid in the cooldown. It had
been smashed into the convergent section by blowback. An additional brace was
added to the structure, and no further movement occurred.

In repairing the GN_2 coolant ring around the throat, the
chamber was damaged. There was a dent in the divergent section of the nozzle
at the location of the throat section to skirt insert weld. There was a sharp
bend in the weld. No attempt was made to remove the dent for fear of cracking
the weld.

4.4, Integrated Thruster Assembly Testing (cont.)

After a cumulative total of 5621 pulses, a leak check indicated three leaks in the torus area, and a dye penetrant check showed that the weld was cracked in the dent in the Haynes nozzle.

The crack in the Haynes weld is shown in Figure 90. The dent was about the size of ellipse drawn in the developer around the dye (Figure 90b). The crack was repaired by welding. The ID of the nozzle was ground and polished to remove the excess weld material. There were no further difficulties with this repair.

The small crack in the inlet line to torus weld and under one of the reinforcement ribs could best be seen using dye penetrant as shown in Figure 91. Figure 91(a) shows the dye pen in the area of the crack where a reinforcement was welded to the inlet line. At the location of the crack, the weld is a fillet weld of a rib to the line and not a seal weld.

Figure 91(b) shows the cracks in this inlet line to torus weld. The welds appeared to have been put on cold (the inlet line is only 1/2 mm thick) and lacked penetration. The dye pen spot above the crack in Figure 91(b) did not leak; there was enough of a discontinuity between the weld and parent material to trap some of the dye. The location to which the arrow in the developer is pointing on the bottom of Figure 91(b) is the one shown in Figure 91(a).

The torus leak location is shown in Figure 92. The defect appeared to be a pin hole in the weld. The dye pen inspection showed other little hole-like irregularities in the weld as indicated by the question marks (?) in Figure 92(b) that were scribed in the developer; these did not leak.

The leaks in the torus welds were not without parallel. As discussed in Section 4.2.1, chamber SN 004 had four leaks that were found during the component checkout leak check. They were repaired by welding as shown earlier in Figure 53.

(b) Dye Pen
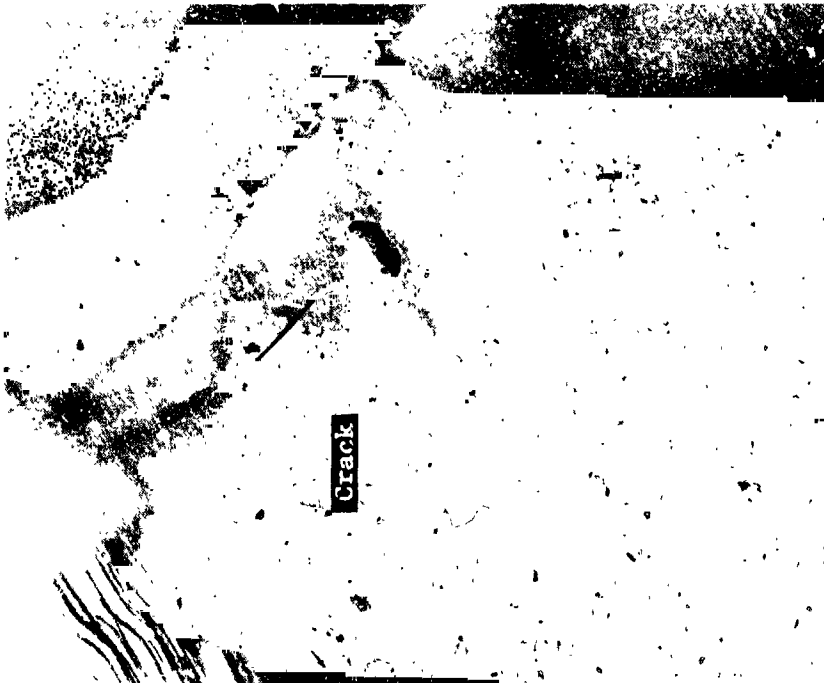
(a) Dye Pen Removed

Figure 90. Crack in TTA SN 002 Haynes Weld

(a) Top

(b) Bottom

Figure 91. Dye Penetrant Inspection of Line-Torus Weldment
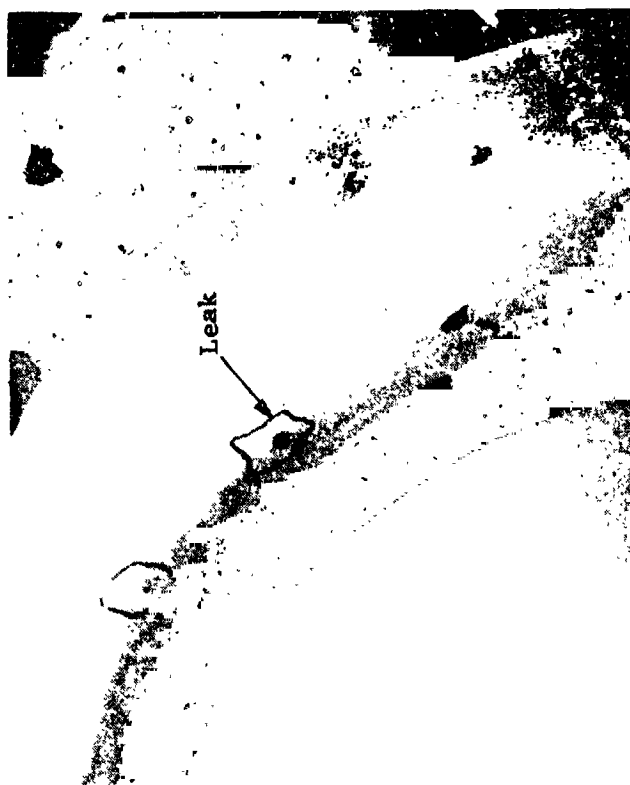
(b) Dye Pen

(a) Dye Pen Removed

Figure 92. Pin Hole Leak in Torus

4.4, Integrated Thruster Assembly Testing (cont.)

Based on the chamber SN 004 experience, the appearance
of the welds on ITA SN 002, their location, etc., it was concluded that the
leaks were not the result of fatigue or even high stress, but were flaws in
the weldment. The chambers were not dye pen inspected after welding and leak
checks we run at a low pressure, 13.8 N/cm^2 (20 psia), using nitrogen (not
helium).

The leaks were repaired by TIG welding, and leak checked
using helium at 34.5 N/cm^2 (50 psia). There were no further difficulties with
the repairs

The injector face is shown in Figure 93 as it appeared
after 5,621 and 11,44 pulses. There was some discoloration between some of
the elements and in the cups. The face showed some light brown coloration.
The color was a little darker over some of the face cooling passages and around
the dump cooling orifices in the face. The appearance of the face did not
change appreciably with continued testing.

In Figure 94, ITA SN 002 is shown on the test stand after
11,443 pulses. This photograph shows the condition of the chamber as well as
the test setup. The Haynes weld repair appears as a dark area aft of the
throat at about a 10:00 o'clock position. Upstream of the throat, the injector-
chamber interface can be seen with some of the injector elements visible and
also appearing as a reflection on the chamber wall. The system propellant lines
had been insulated to help maintain propellant temperature conditioning. The
two main propellant lines that were described earlier as being mounted
horizontally at right angles to the thrust vector can be seen at the top of
Figure 94 on the right (oxygen) and left (fuel).

During Test 111, the POS transducer failed. This pressure
was the feedback source for the flow control valve to maintain accumulator

(a)   5621 Pulses

(b)   11,443 Pulses

Figure 93.   ITA SN 002 Injector Face During Testing
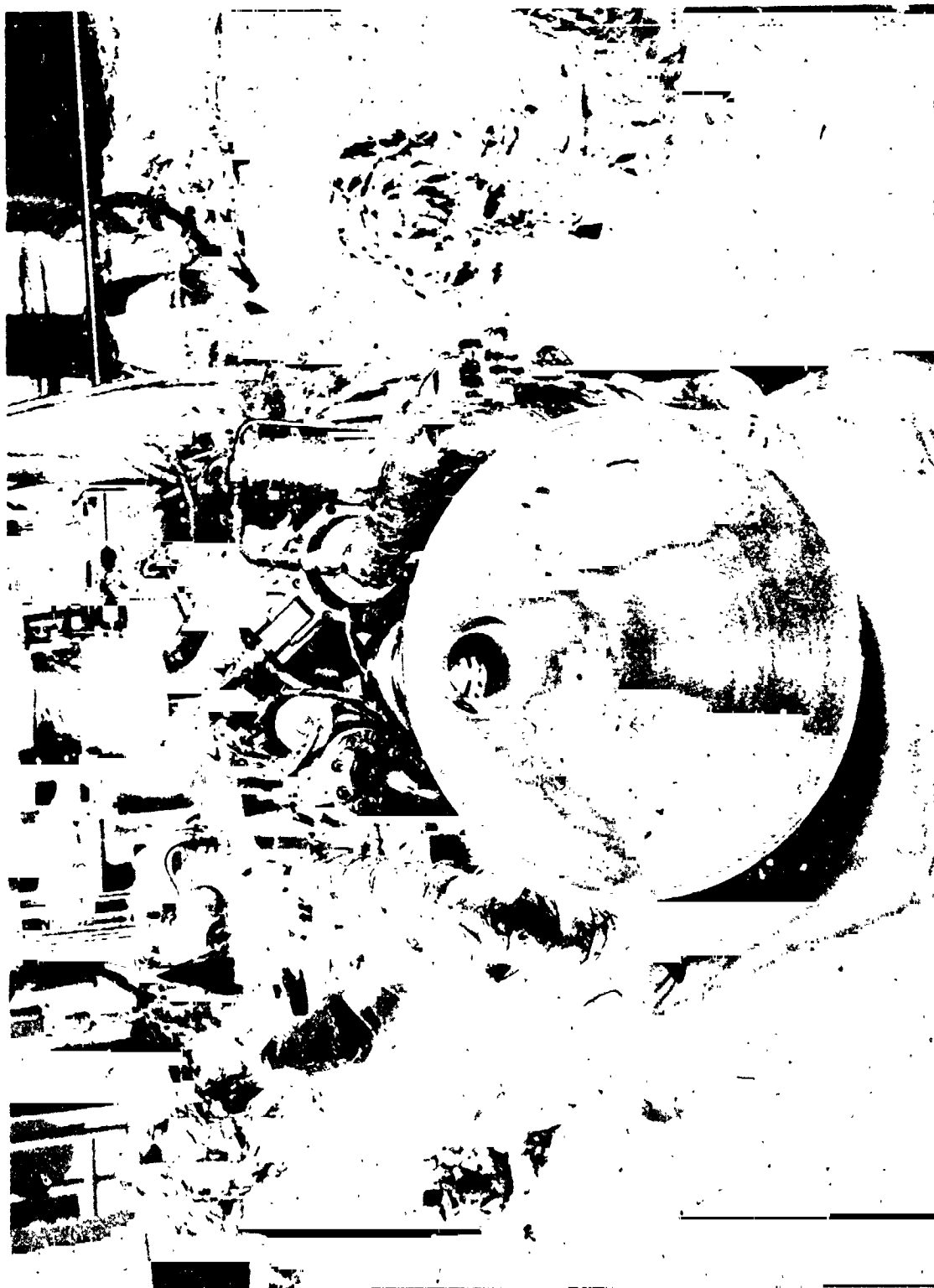
Figure 94. ITA SN 002 on Test Stand After 11,443 Pulses

4.4, Integrated Thruster Assembly Testing (cont.)

pressure. The main propellant valve protect ve circuit was also based on the pressures indicated by the POS transducer. With the failure of the transducer the flow control valve opened in response to the zero pressure signal. The valve protection circuit did not shut the test down because it too was being signaled a zero pressure by the failed transducer. The burst disc in the accumulator ruptured at 503 N/cm^2 (730 psia) exposing the main oxygen valve, in the open position, to a pressure 38 N/cm^2 (55 psia) in excess of the bellows proof pressure, 465 N/cm^2 (675 psia). After this test, the valve protective circuits were changed to shutdown on an overpressure at either the valve inlet (POTCV and PFTCV) or the stand supply (POS and PFS).

During Test -124, fluctuations were noted in the GN_2 valve actuation pressure. At the conclusion of testing, a leak check revealed that the GN_2 pressurant to the oxygen pilot valve was leaking to the main valve upstream of the seat. The leak rate was quite high as the regulator on the GN_2 hand loader could maintain less than 69 N/cm^2 (100 psia) pressure at the inlet to the pilot valve when set for 345 N/cm^2 (500 psia). The spare main propellant valve (SN 011) was used to replace the main oxidizer valve (SN 012); however, the pilot valve was not replaced. Main propellant valve SN 012 was disassembled as shown in Figure 95. The pilot valve port was pressurized with helium at less than .7 N/cm^2 (1 psia) pressure and the bellows leak found. It was a crack about 2 cm long on the OD of the fourth convolute from the seat as shown in Figure 95.

A leak check was run on the main fuel valve. Its bellows assembly was also leaking as indicated by a rise rate in pressure measured upstream of the valve with the test stand valve closed and the pilot valve pressurized and deenergized. Closing the test stand valve locked up a small volume between the two valves that could be monitored using the valve inlet pressure port (PFTCV). The leakage rate was measured as 14 cc/min at ambient temperature with 286 N/cm^2 (415 psia) GN_2 pressure at the pilot valve inlet.
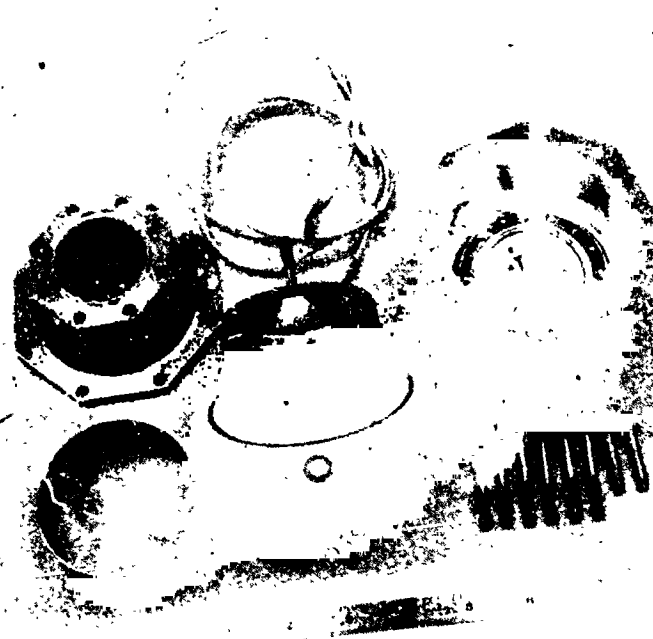
Dissassembled

Seat

Crack

Bellows

Figure 95. Marquardt Main Propellant Valve SN 012

4.4, Integrated Thruster Assembly Testing (cont.)

During the functional tests run prior to Test -125, the fuel main propellant valve (SN 013) did not operate. The three way pilot valve was stuck in an intermediate position. The GN_2 supply pressure to the pilot valve was being short circuited to the vent port. The fuel pilot valve was replaced with the pilot valve from the spare (SN 011). Subsequently, pilot valve SN 013 was disassembled and the ball was found to be wedged in its cage in the position half way between the two seats.

After replacement of the main oxygen valve and the fuel pilot valve, the main propellant valve response times were significantly improved. There were no delays during the next few tests on opening or closing. The only problem encountered was low GN_2 actuation pressure to the oxidizer valve. (Separate supplies were used for the two valves.) The low actuation pressure caused the oxidizer valve closing to delay and resulted in shutdowns on Test -131 through -133 due to the POTCV-O monitor that senses pressure (valve open) during the coast times.

During Test -137, the fuel igniter valve began to operate intermittently. It would fail to close on some pulses. During Test -138 it remained open sometimes for 30 to 40 pulses in a row. Both igniter valves were replaced after Test -138 (30,049 pulses). Igniter valve SN 002 in the fuel circuit was replaced with SN 004 and igniter valve SN 006 in the oxidizer circuit was replaced with SN 003.

There were cracks in the torus after 30,049 and 34,594 pulses. The weld repair of these two cracks can be seen in the top insert of Figure 96. The crack that occurred after 30,049 pulses is shown in the bottom insert of Figure 96. Both cracks were in the heat affected zone adjacent to the weld. As shown in Figure 96 (bottom insert), there was an area of mechanical damage on the torus in close proximity to the first crack (30,049 pulses). The mechanical damage was a series of abrasions about 23 mm long and 5 mm across at
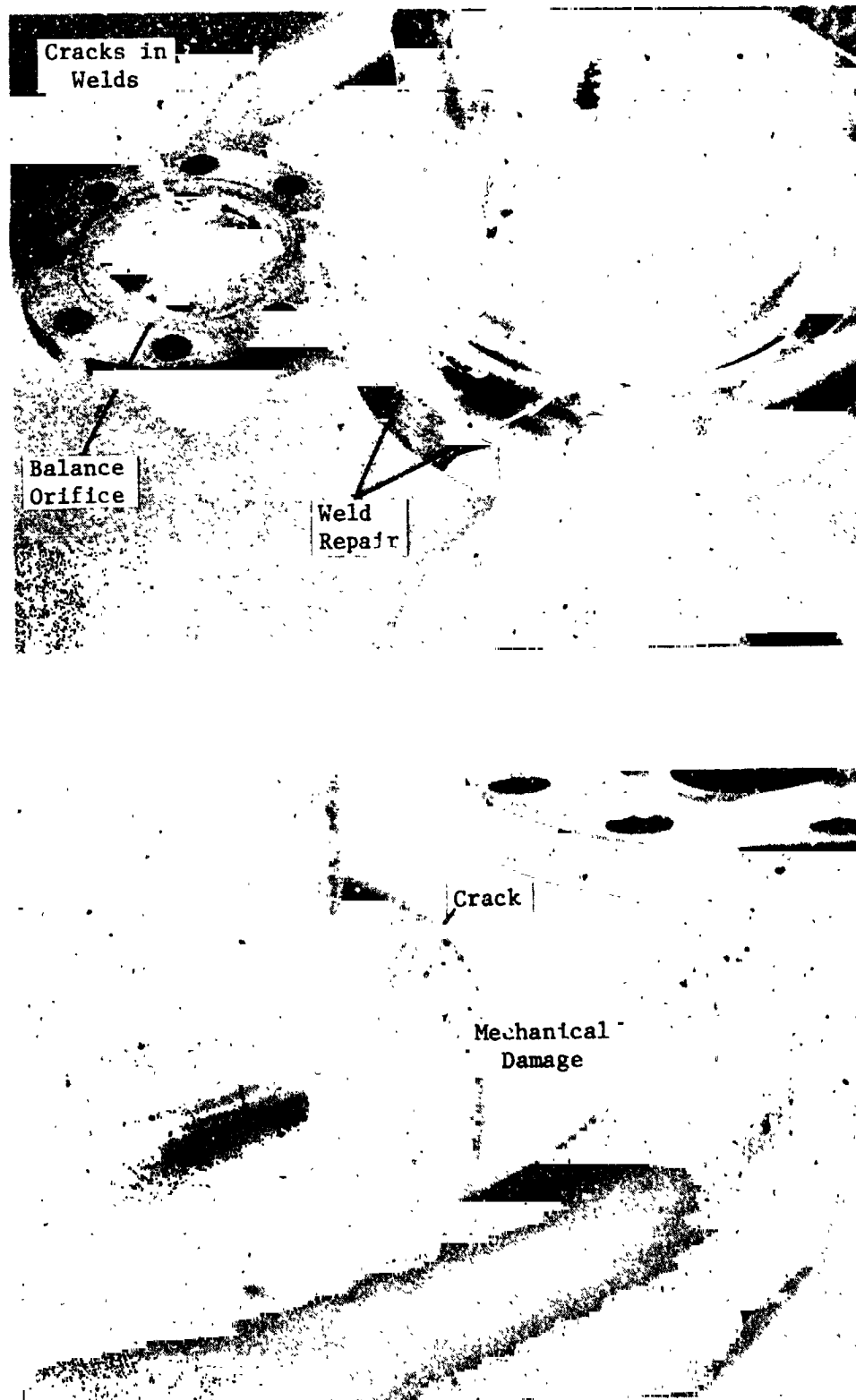
Figure 96. Torus Crack and Weld Repair

4.4, Integrated Thruster Assembly Testing (cont.)

the widest point. The damaged surface had the appearance of a file, and was probably caused by the knurling on the handle of the socket extension that was used to remove the nut on one of the bolts that mounts the fuel valve to the chamber valve mounts. When the chamber was removed from the test stand for repair, the valves were left in place. This meant the bolts holding the valves to the chamber had to be removed. In order to remove one of the nuts, a socket wrench was used and it had to be inserted between the fuel line and torus at the location that was damaged. The damage was initially noted when the chamber was removed from the stand after 5621 pulses.

The fuel balance orifice is shown in Figure 96. As can be seen in the figure, the orifice was welded in place by four TIG welds and these welds were cracked at the time the picture was taken. The orifice had the shape of a bellville washer with the ID protruding toward the upstream direction. The orifice was rewelded and the next time the chamber was removed the welds were again cracked. The welds on the oxidizer orifice were not cracked.

The cracking of the welds and distortion of the fuel orifice in ITA SN 002 coupled with the face that the fuel orifice in ITA SN 001 was found to be bent and loose indicates that the orifices were being subjected to considerable force. It would take more than $137S$ N/cm^2 (2000 psid) pressure difference across the orifice to produce the distortion observed in the SN 002 fuel orifice. No pressure spike was ever observed on any transducer; despite the transducers not being close coupled, it is difficult to imagine no response to pressures of that magnitude. Moreover, the lines, the torus, and especially the flat OD of the torus show no distortion from overpressurization.

At the beginning of a test, the orifice and flange were warm due to the hot purge. On startup, cryogenic hydrogen would flow through them. The thin orifice would cooldown much more rapidly than the flanges and its thermal contraction would pull it away from the walls of the flange thus cracking the welds.

4.4, Integrated Thruster Assembly Testing (cont.)

Test 141 was shutdown when evidence of fire was seen on the TV monitor. There was a large rupture in the fuel inlet line as shown in Figure 97. The failure appeared to start at the apex of the chevron shaped opening next to the weld and to tear back from there. The edges did not appear to have failed in tension, but shear. The tear was repaired by welding as shown in Figure 97. There were 39,514 pulses on the thruster.

The line rupture did not result in a low thrust shutdown. This is a little hard to understand considering all the low thrust shutdowns that occurred previously. Shutdown was done manually on the basis of visual detection of fire exterior to the engine. On the last pulse series, chamber pressure and thrust were low by about 15% and fuel flow rate was high about 20% (long pulse) to 35% (short pulse). The high level of performance means one of two things: (1) there was a crack in the line and the tear did not occur until the last pulse or until shutdown (induced by deflection resulting from thermal changes), or (2) the combination of cross velocity and sonic flow out the hole kept the hydrogen loss low enough that the chamber could operate.

There are four factors that favor the latter explanation. (1) The hydrogen flow is only 25% of the total so relatively high thrust and P_c would be maintained even with a significant reduction in fuel flow rate. (2) Because constant pressure was maintained upstream of the valves the fuel flow rate increased which would practically offset the loss. (3) The ITA can probably operate at very high mixture ratios with short pulses – especially with the hardware cooldown that occurs with fuel valve lag on closing. (4) The rupture occurred on the inside of the bend in the tube; momentum forces result in the bulk of the gas flow being on the outside of the bend.

The fuel line rupture occurred with 34,594 pulses on the thruster. The inside of the chamber, the injector and the nozzle did not look any different that earlier in testing as will be seen in subsequent photographs.

Fuel Inlet Line Rupture

Weld Repair

Figure 97. Inlet Line Failure and Repair

4.4, Integrated Thruster Assembly Testing (cont.)

The FM tape of the Test -141 was played back and an oscillograph record made from it. There were no anomolies, such as pressure spikes in the data.

At the end of Test -141, the leak in the fuel valve bellows was so large that the next test could not be started with GN_2 actuation. The GN_2 pressure was set by hand prior to testing and had to be done before the line could be pressured or the fuel valve would open. When the GN_2 was turned on, the fuel system upstream of the valve filled with GN_2. To preclude this problem, the valves were switched to self actuation. Main valve cold flow tests were run and the fuel valve would not close.

The pilot valve that had been removed from the fuel valve earlier was disassembled. It was at this time that the ball was found to be stuck in its cage half way between the two seats. The ball was freed and the cage wiped clean with a soft tissue and solvent. The ball then moved freely in the cage.

The reassembled pilot valve was reinstalled on the fuel valve (main valve SN C13 was restored to its original configuration). The valve operated perfectly in a cold flow checkout and on the first two .5 second check-out test firings (Tests -142 and -143). However, during Test -144 when pulsing was performed, it behaved very erratically. It did not delay on closing on pulse #5 which is of .45 second duration; there was a lag on the order of 50 msec on closing after the .15 second pulses and a 100 to 200 msec lag on closing after the short pulses. Figure 98 illustrates the problems. At times, the delay would almost disappear; at other times, the valve would operated as shown in Figure 99. The delay in closing got worse on the short pulses as the test progressed so that the duration of pulse #8 was changed to 390 msec in an attempt to break up the five short pulses where the worst delay was occurring.
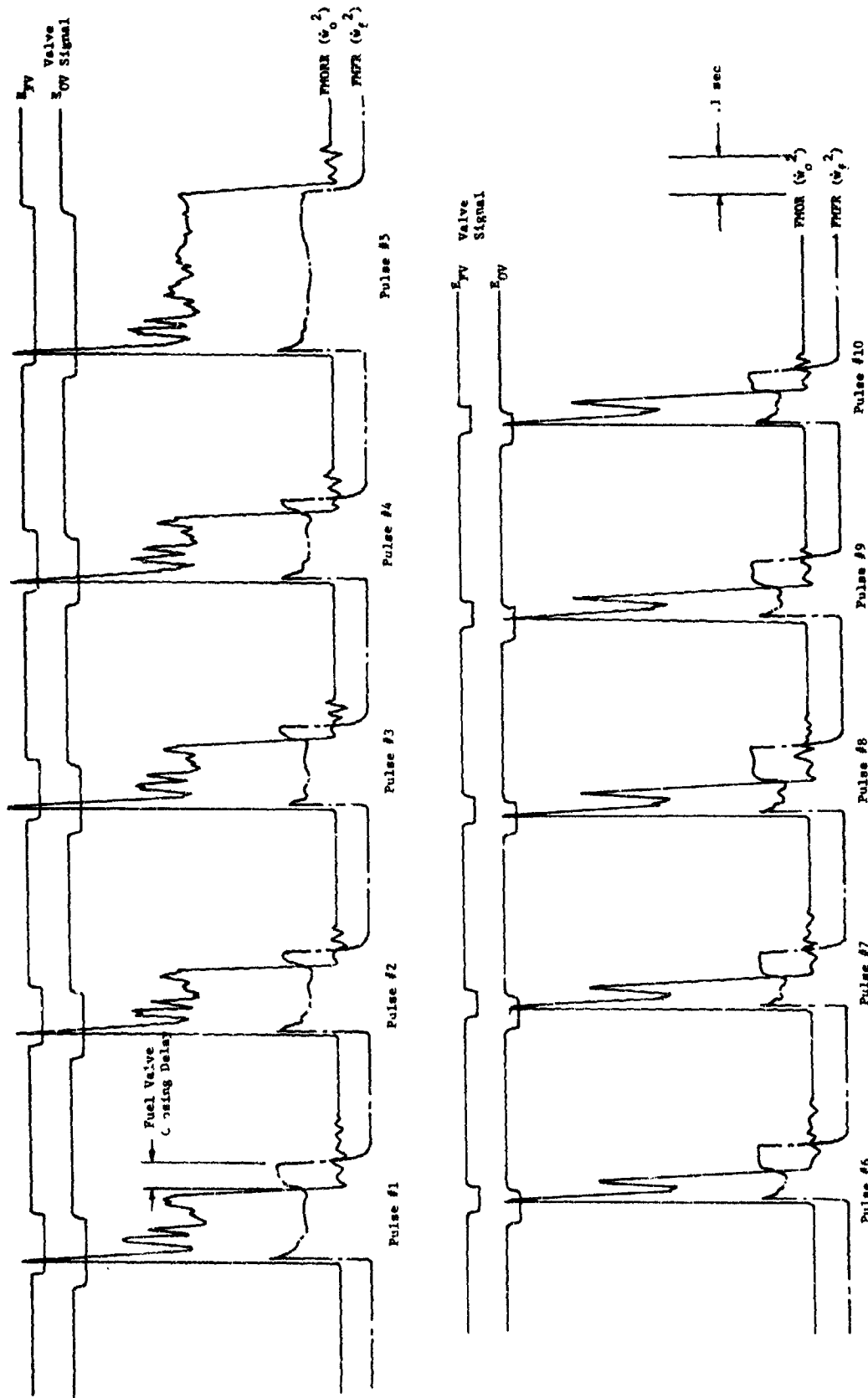
Figure 98. Test ~144 Pulse Transients
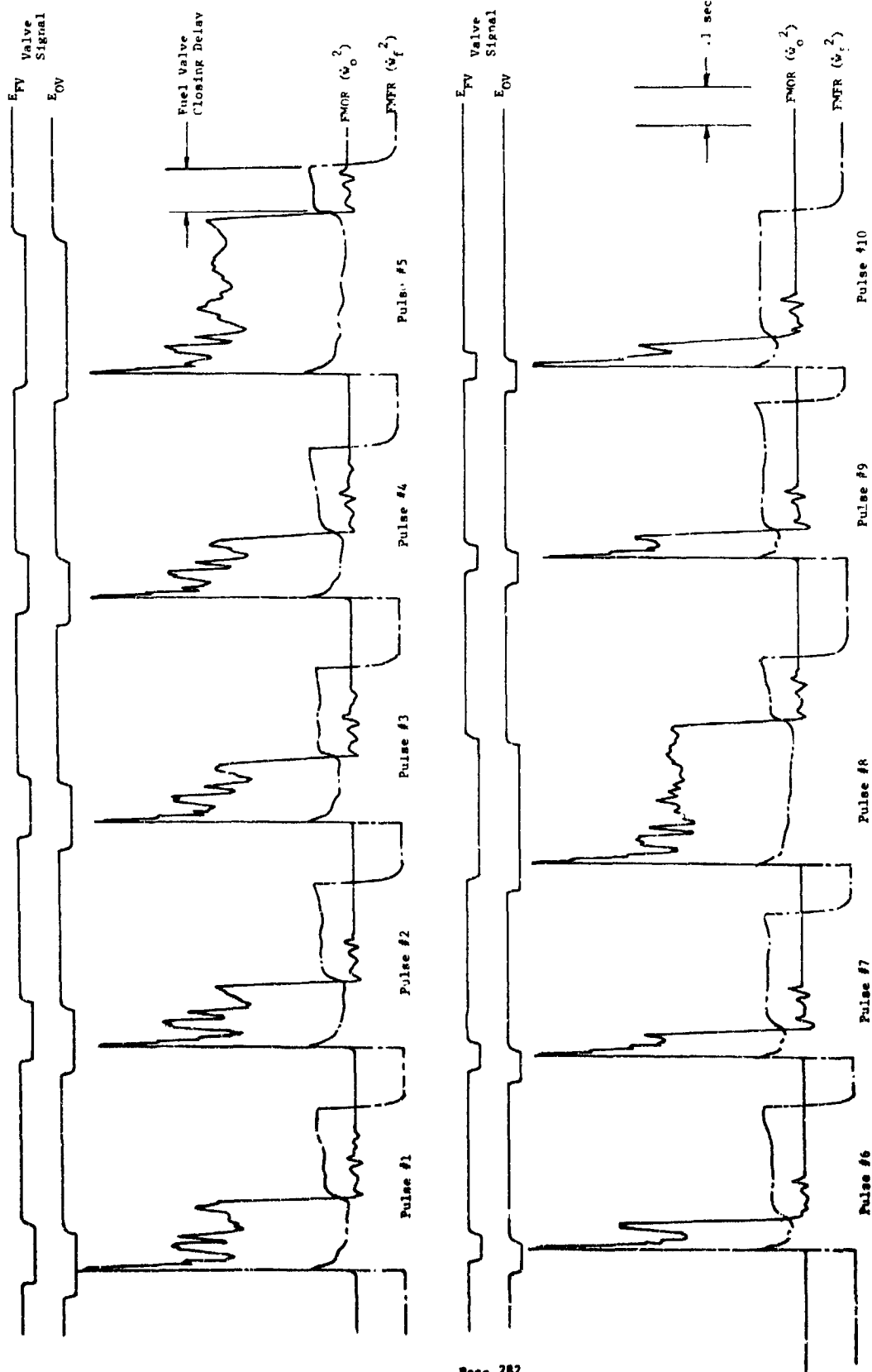
Figure 39. Test -145 Pulse Transients

4.4, Integrated Thruster Assembly Testing (cont.)

Test -144 was shut down by a computer malfunction.
Test -145 was started immediately as had been done many times. Test -145 was
shut down after 418 pulses when flashes were seen on the TV monitor. There were
two heat streaks in the nozzle and burn through the chamber in one of the streaks.

ITA SN 002 after Tes -145, is shown in Figure 100.
Judging by the amount of material removed, the failure probably occurred at
about the throat section to skirt weld (lower weld in insert on left of Figure
100). The burn through worked aft from there because of disruption of the film
coolant and flow through the rupture in the pressure boundary. It worked forward
because of thermally induced cracks such as seen in Figure 100.

The condition of the chamber would suggest that the crack
did not occur first. There was a heat streak forward of the crack - the crack
cannot explain it. Secondly, if the crack had occurred first, it is in a high
pressure region of the chamber and surely would have eroded more because of
hot gas flow through, especially since the heat streak shows that the ffc has
been interrupted. The burn through of ITA SN 001 occurred in this area.

A close-up of the entire burn through area is shown in
Figure 101. The start of the heat streak can also be seen more clearly in this
photograph. There were two heat streaks in the nozzle of chamber SN 002 after
Test -145 that were not there before.

The ITA SN 002 throat and nozzle are shown in Figure 102.
The photographs, with the exception of the one of the hardware before test were
aligned to have approximately the same orientation in each picture as the chamber
had on the test stand - the alignment was done on the basis of the weld repair to
the Haynes which is in the 10:00 o'clock position in each photograph, and on the
basis of a white marking that occurred in the 1:00 to 2:00 o'clock position. The
heat streak that can be seen in the 3:00 o'clock position and the heat streak/
burn-through that can be seen in the 5:00 o'clock position after 42,266 pulses,
do not appear in any of the other photographs.
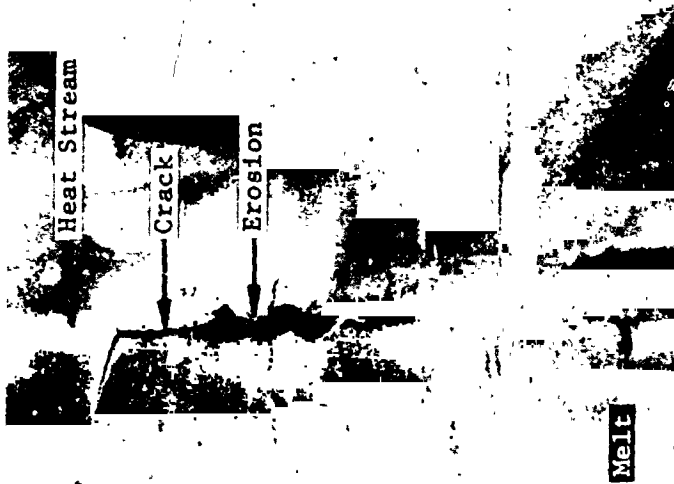
Close Up of Erosion

ITA SN 002

Figure 100. ITA SN 002 After Test -145

Figure 101. Erosion of ITA SN 002
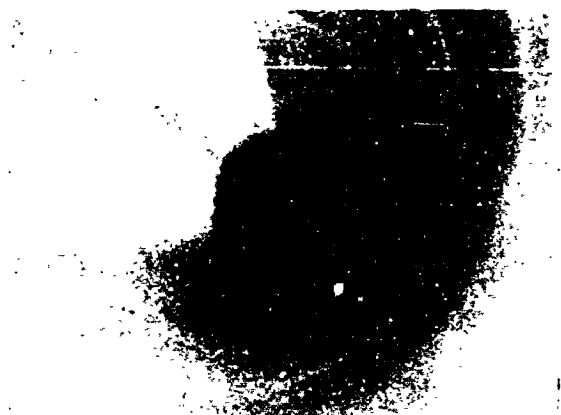
Unfired

5621 Pulses

11,443 Pulses

30,049 Pulses

39,514 Pulses
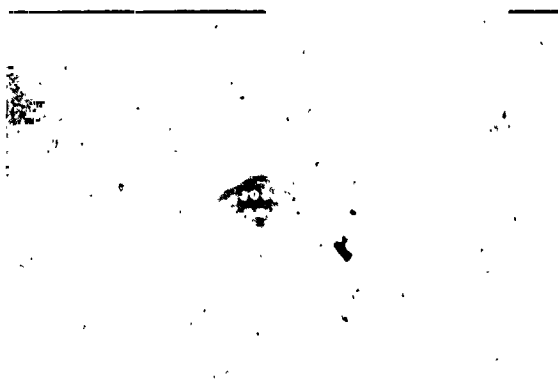
42,266 Pulses

Figure 102.   ITA SN 002 Throat and Nozzle

4.4. Integrated Thruster Assembly Testing (cont.)

When the chambers were cold flow tested as part of the component checkout testing, the flow 45° from the hydrogen inlet (clockwise looking from forward to aft) was consistently lower than the average (see Section 4.5). The thermocouples were placed in this location because of the slightly lower flow and were generally found to run hotter than others located circumferentially. The small burn through that occurred on ITA SN 001 (Test -007) was at the location of the thermocouples and about 5 mm aft of the ffc injection tip. The heat streak that contains the burn through on ITA SN 002 start about 5 mm aft of the ffc injection tip at the location of the thermocouples. The burn through of ITA SN 001 and ITA SN 002 occurred at the same location.

Because of the heat streaks which were not seen earlier, the similarity to icing problems that occured on Test -007 and -009, the chilldown caused by the fuel valve delay on closing, and the blowback of water into the chamber that occurs with shutdown, the burn through probably was caused by over-heating resulting from ice blockage of the ffc passages.

After Test -009 with ITA SN 001, ice was seen in the chamber; it had a slush-like appearance, and was in spaghetti-like shapes. It appeared to have been extruded from the injector orifices. After many tests, water was observed standing in the chamber to the level of the outer row of injector elements. The orientation of the chamber was such that the fuel inlet line was the low point in the system. Water standing in the chamber could run into the lower fuel elements, down into the fuel plenum of the injector, down into the regenerative passages, down into the torus, and down into the inlet line where it would collect.

Normally, the chamber was warm enough after a firing that the water did not freeze or perhaps was vaporized - 40,000 pulses had been made

4.4, Integrated Thruster Assembly Testing (cont.)

with no problem and no streaking. As Test 145 progressed, the fuel valve delay increased until it was almost not closing on every pulse - see Figure 99. The chamber got cold enough as the fuel valve delay got longer to freeze the water in the inlet line. Ice or slush blocked the ffc passages causing the heat streaks and burn through. The ice would impinge on the ffc orifices as the point of lowest flow on the basis of the flow pattern from the inlet line to the torus.

Figure 103, showing some of the chamber temperatures during pulse testing, has been included for two reasons. The first is to demonstrate that one full thermal cycle is produced every ten pulses. The second is to show that chamber temperatures are low enough for icing to occur during the cycle life testing, circumstances which are different from Test -007 and -009.

Figure 103 shows two temperature plots from the strip charts. They were recorded early in the testing as flowback stripped all thermocouples off the chamber after a few pulses. From the response of TN-3A and 3C, it can be seen that the GN_2 and H_2 produced a complete cooldown. Uneven GN_2 flow distribution and differences in thermocouple installation probably caused the GN_2 to affect the two thermocouples differently. As can be seen from the injector face thermocouple even components tnat are heated and normally return to their initial temperature, such as the injector and regenerator section, are chilled well below freezing by the hydrogen flow and stay cold.

Components such as the torus and fuel inlet line would get quite cold since there is very little heat conduction to them. The problem may well have been ice formation in the cold fuel line that was broken loose by blowback rapping the fuel inlet line.

Three views of the chamber, taken 120° apart to show the complete chamber exterior are shown in Figure 104. The nozzle extension is shown in Figure 105. As can be seen from the photographs of the exterior and skirt,
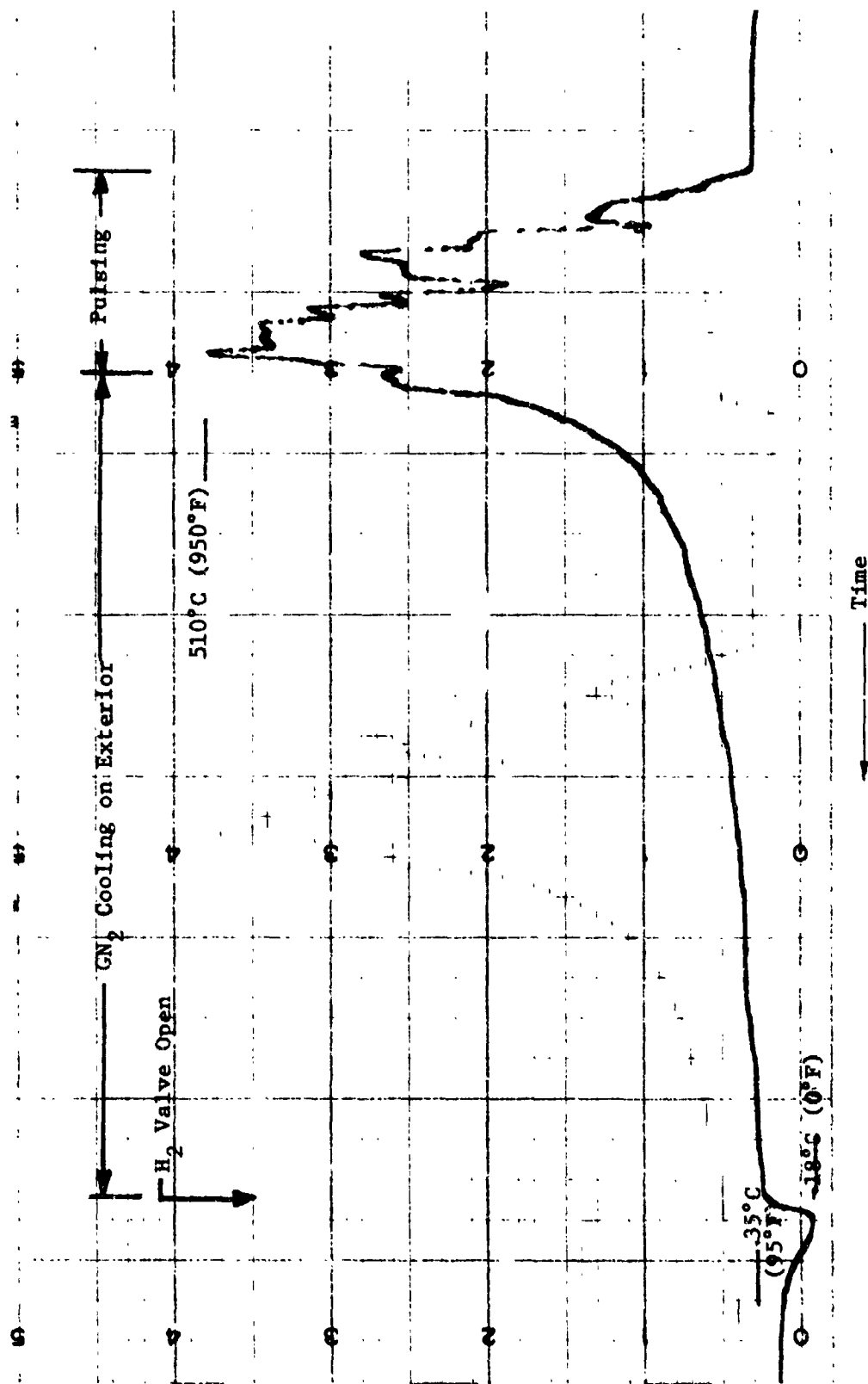
Figure 103. Cooldown with H_2 Flow

(a) TN-3A
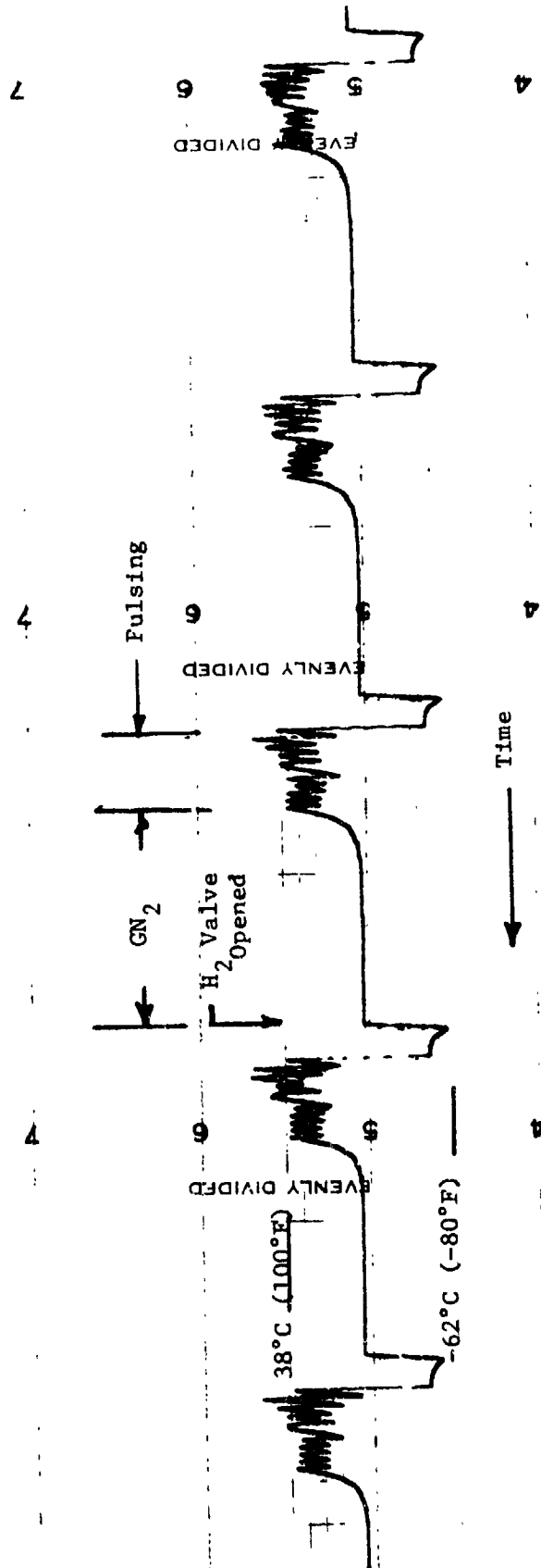
Figure 103. Cooldown with H_2 Flow (cont.)
(b) Injector Face Temperature
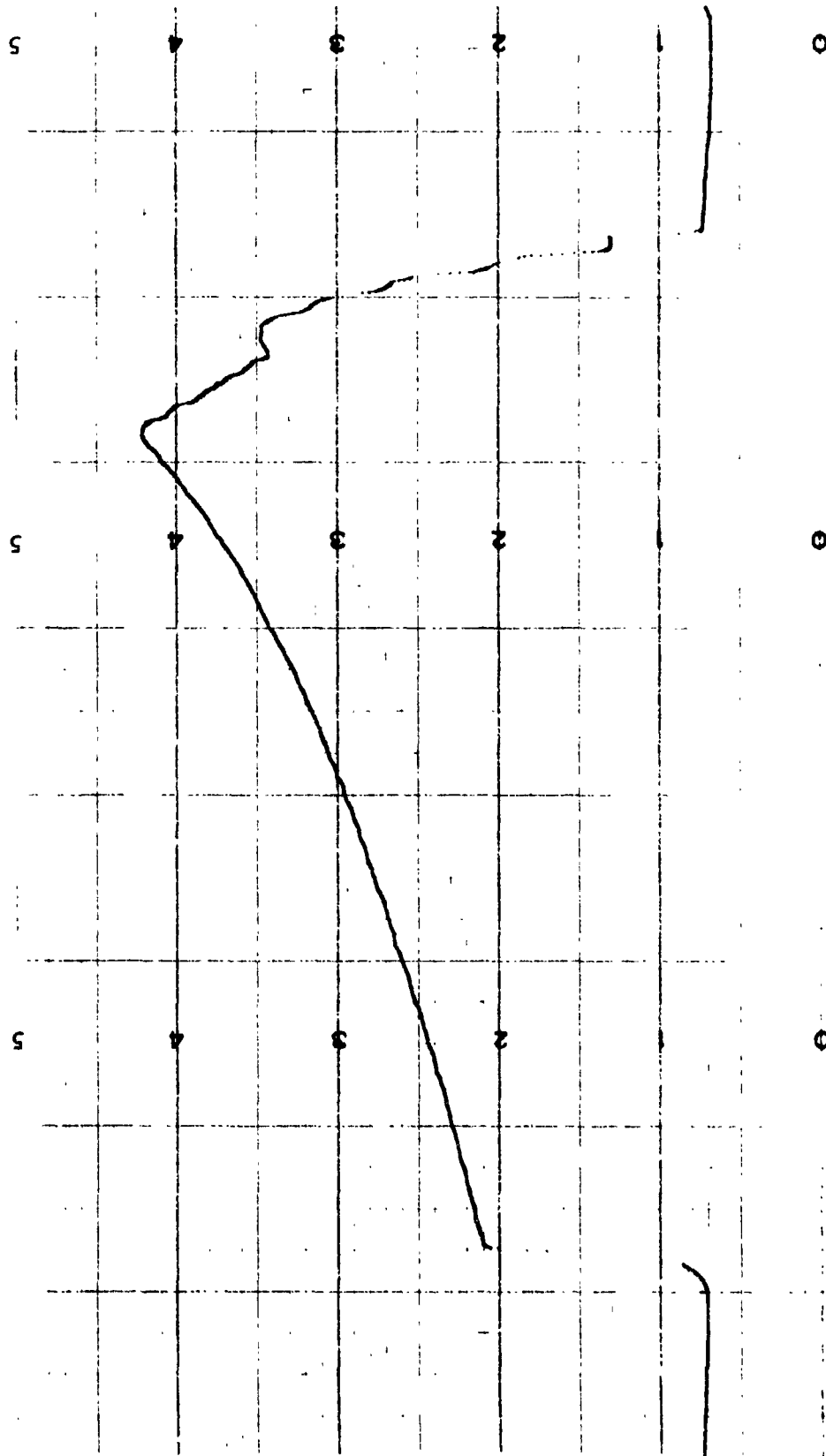
Figure 103. Cooldown with H_2 Flow (cont.)

(c) TN 3c)

Figure 103. Cooldown with H_2 Flow (cont.)

(d) TN 3a)
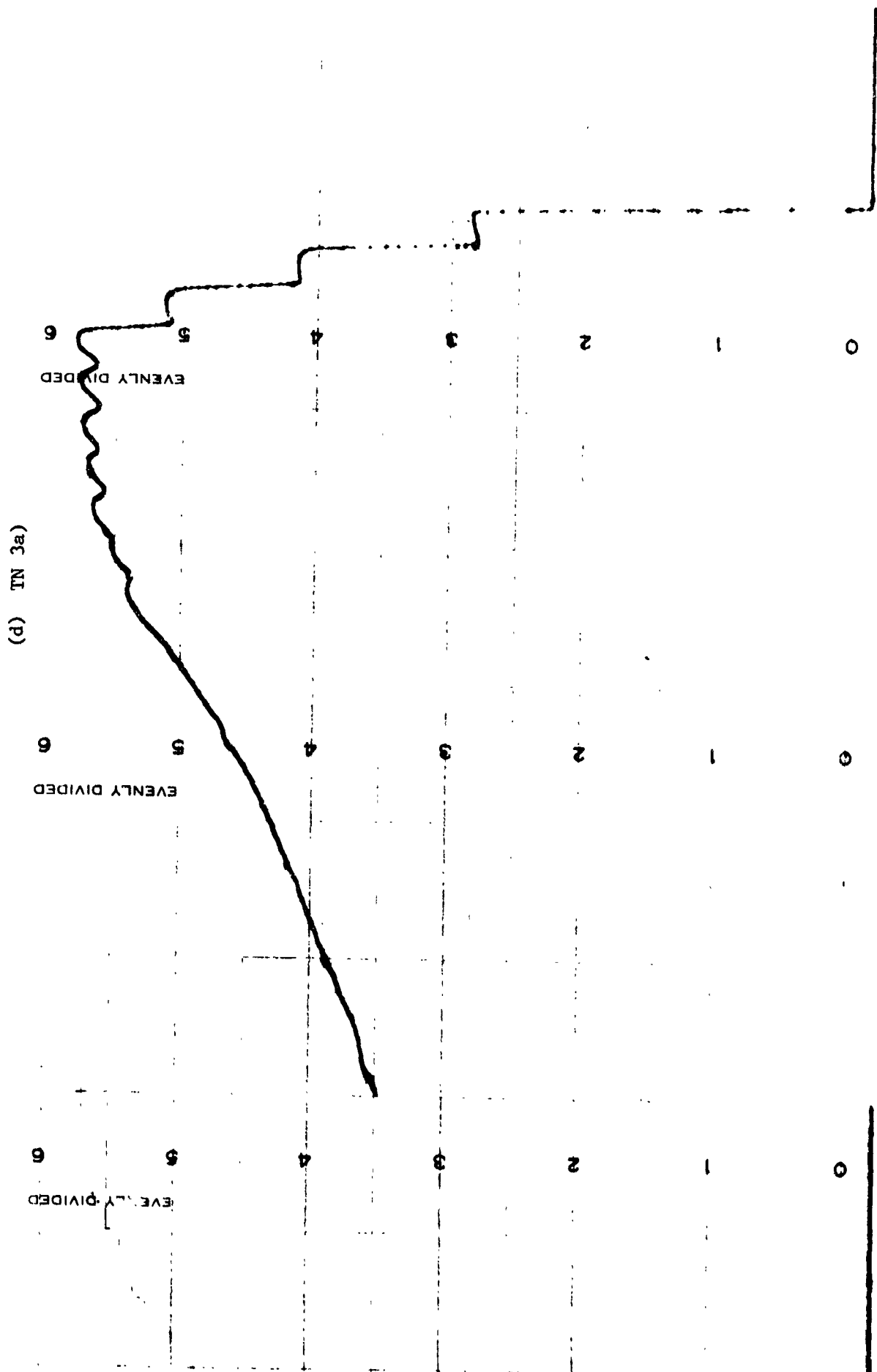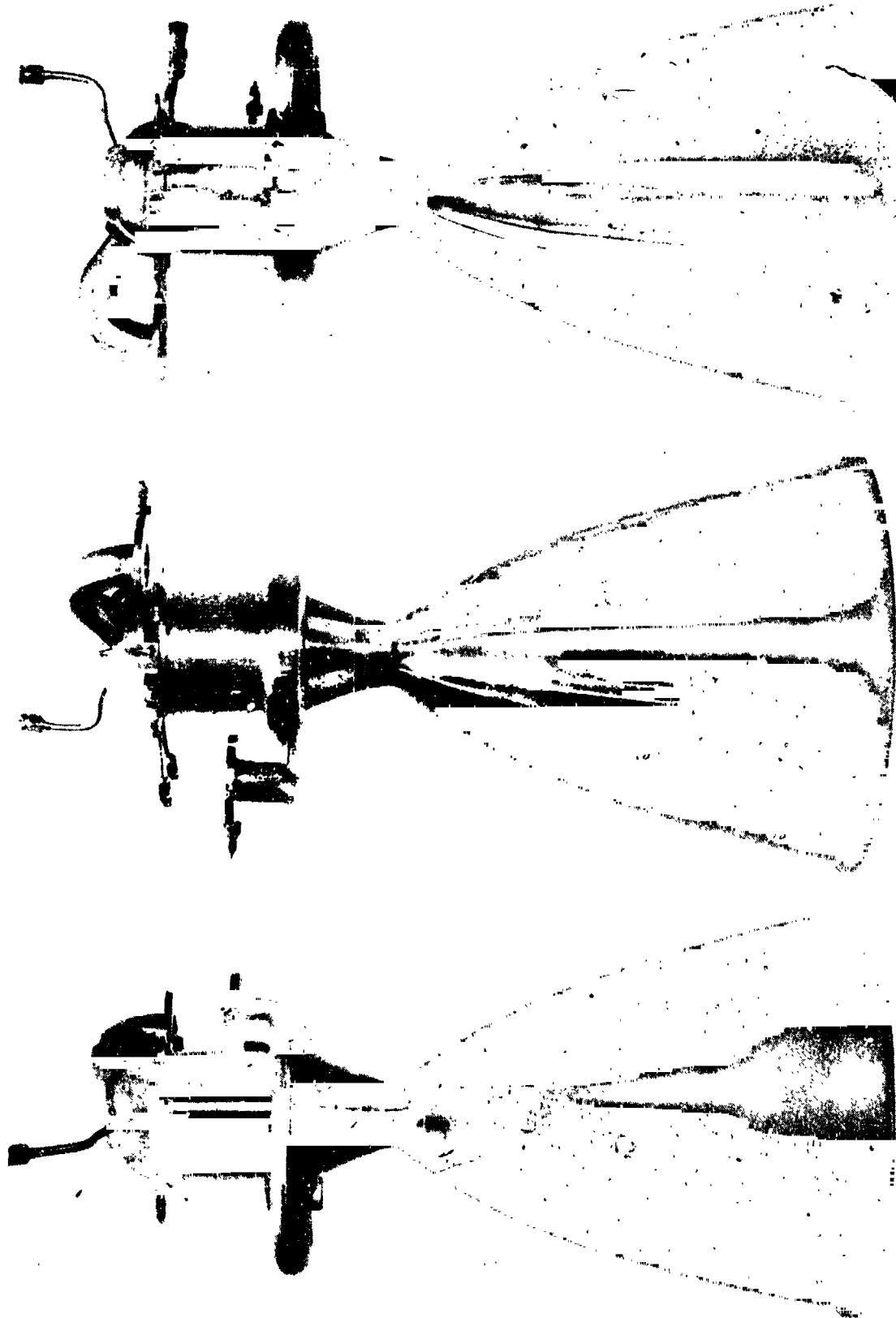
Figure 104. ITA SN 002 After Testing (3 Views Rotated 120° Apart)

White Deposit

Erosion
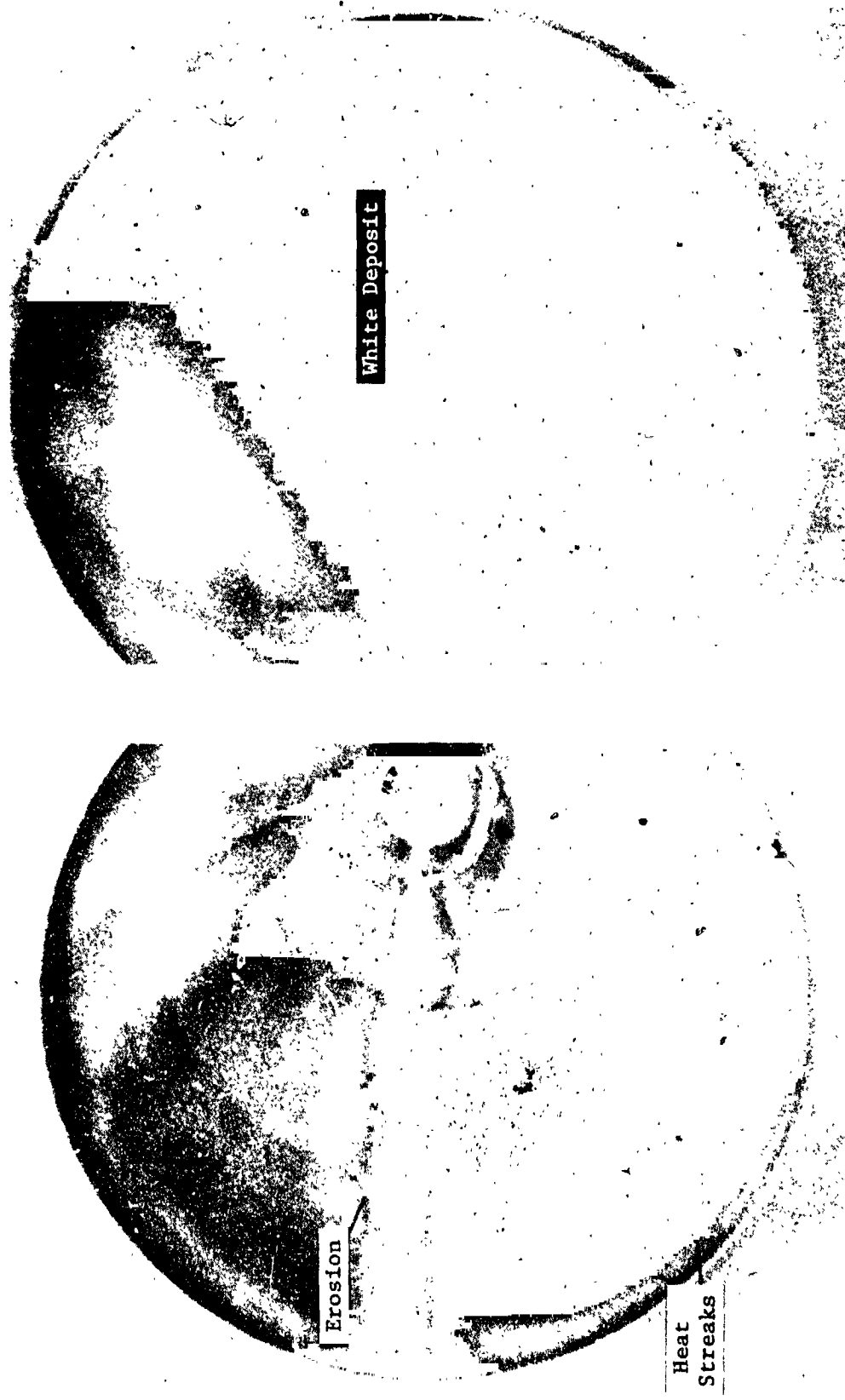
Heat Streaks

Figure 105. ITA SN 002 Skirt After Testing

4.4, Integrated Thruster Assembly Testing (cont.)

the thruster looked normal except of course for the heat streaks and erosion. The Haynes throat and skirt did not have the green color oi ITA SN 001 indicating it had not reached as.high temperatures. The only place where the green color occurred on ITA SN 002 was the heat streak area on either side of the burn-through.

The throat is shown in Figure 106. It did not look like ITA SN 001 or even like it did in earlier tests. First, of course, there were the heat streaks. Secondly there were areas that were a bright silver color; they did not have the grained appearance of the original finish or the oxidized/ fired appearance of the rest of the chamber. The silver spots had an appearance similar to parts freshly removed from a hydrogen furnace - which suggests that they got quite warm and then were exposed to hydrogen. There were two other places where a bright silver surface could be seen - they were two slender fingers extending from the ffc injection point on the·convergent section of the chamber, one to the throat at the location of the heat streak, and one to the crack in the eroded heat streak.

The ffc tip of chambers SN 001 and SN 002 are shown in Figure 107. There was no pitting, melting or cracking that could be seen in either chamber. The convergent section of the ZrCu felt grainey indicating that some metal was being removed. The ffc tip of chamber SN 002 upstream of the two heat streaks was not damaged.

The SN 002 injector chamber interface is shown in Figure 108 at various stages of the cycle life testing. There was very little change in appearance after the first few thousand pulses. The chamber wall got rougher and darker, but after 42,226 pulses was still smooth enough over 2/3 of its circumference to reflect the injector elements.
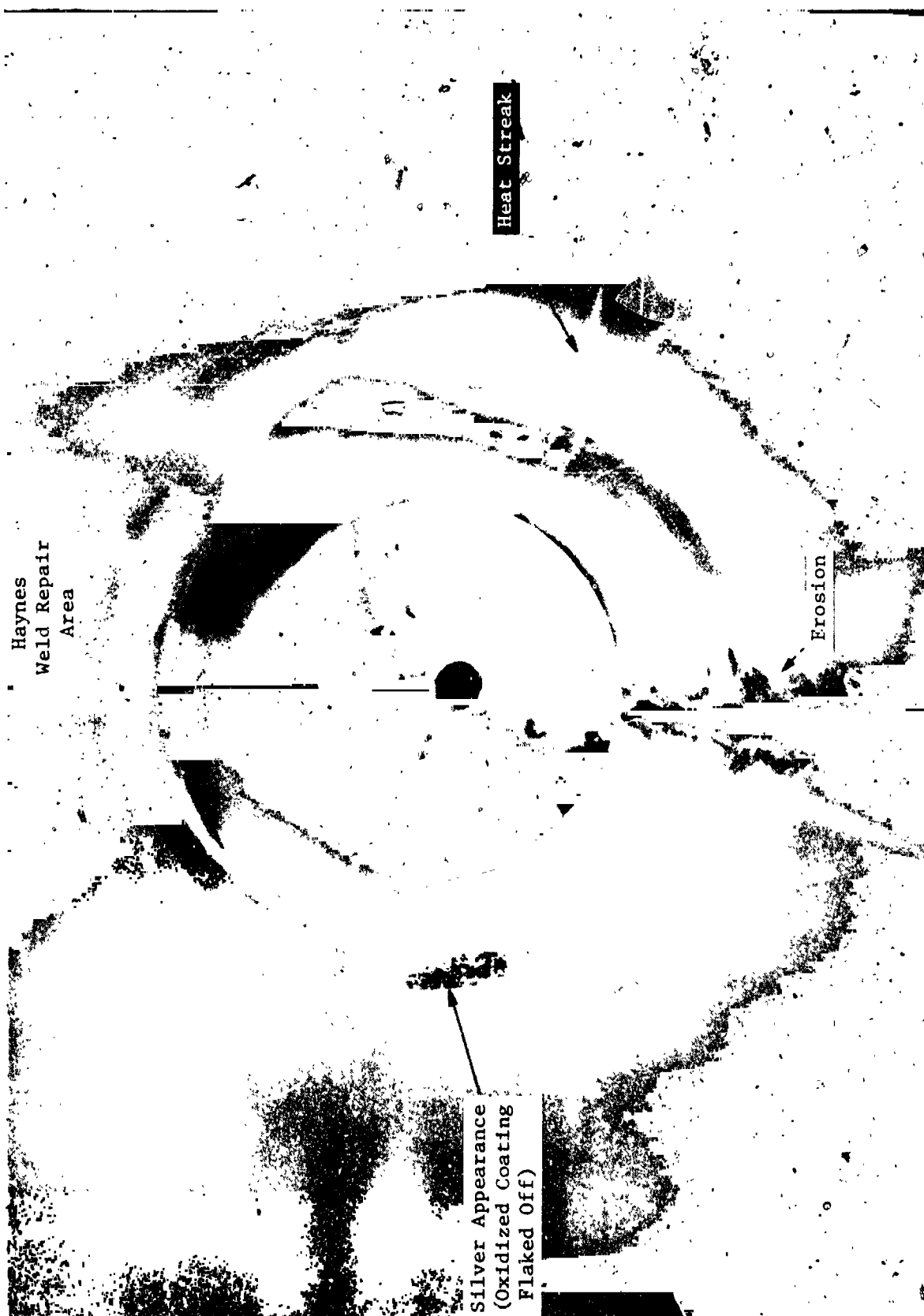
Figure 106. Throat of ITA SN 002 After Testing

ITA SN 002
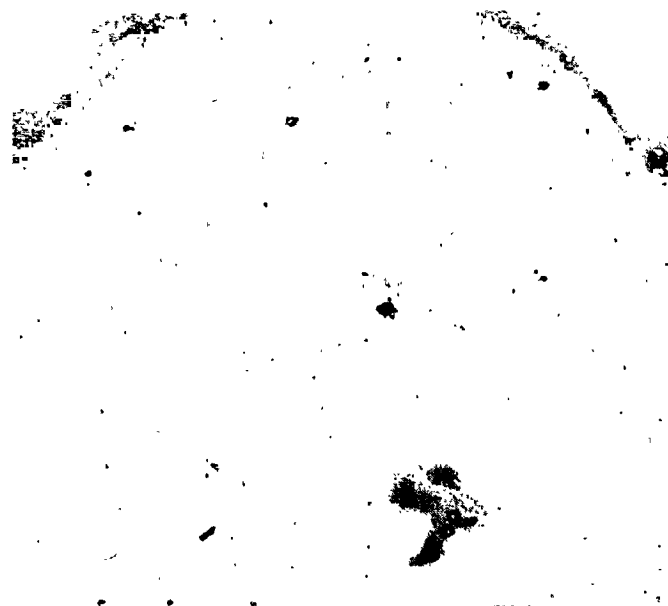
ITA SN 001

Figure 107. ffc Injection Tip After Test

Unfired (Left)
5615 Pulses (Right)

11,440 Pulses

30,049 Pulses

39,514 Pulses
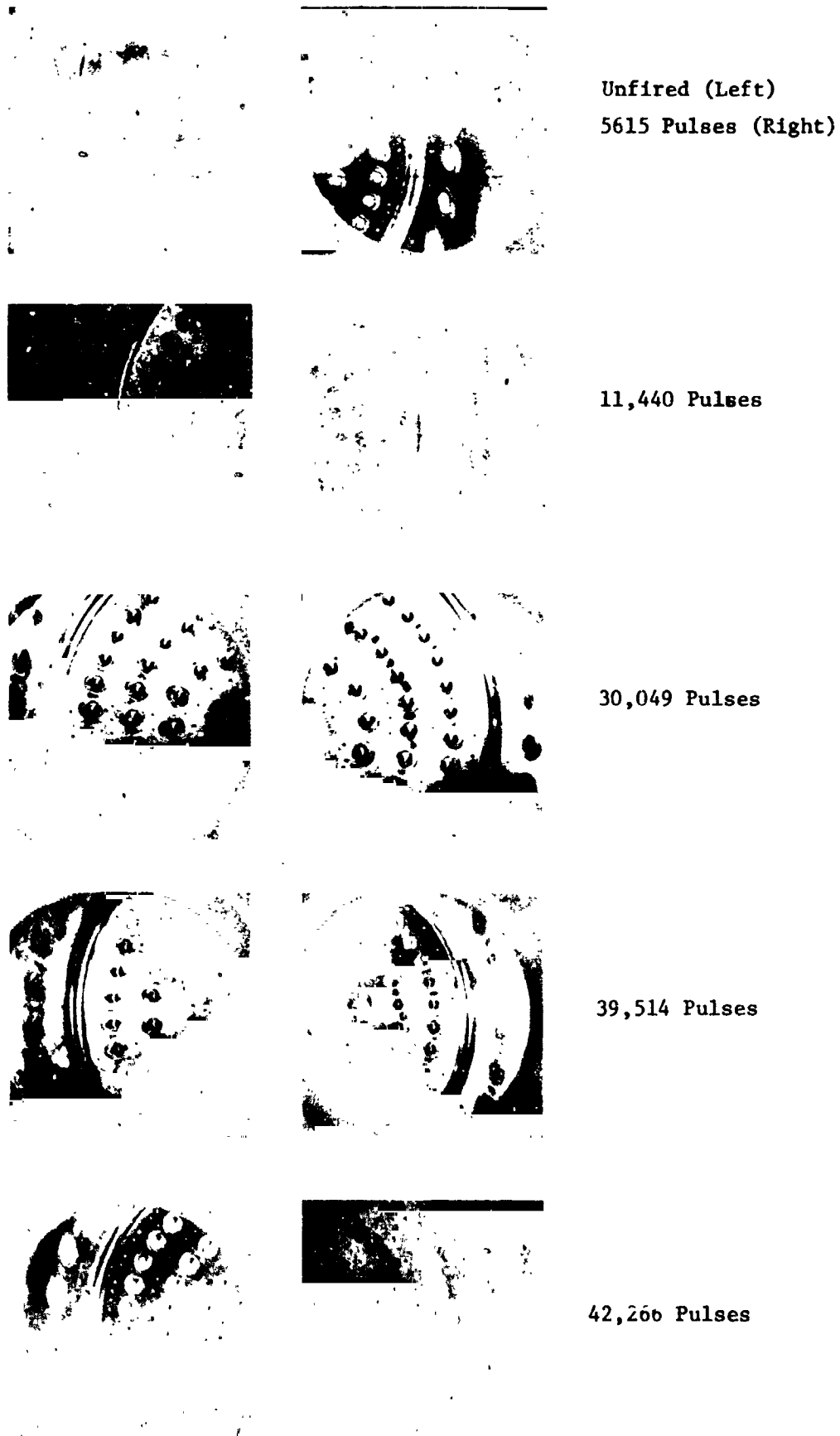
42,266 Pulses

Figure 108. ITA SN 002 Injector – Chamber Interface

4.4, Integrated Thruster Assembly Testing (cont.)

Three views of the body of igniter SN 002 that was used for the 42,266 pulses is shown in Figure 109. Except for a little dark area on the very tip where the hole made by the face platelets was larger than the hole in the face plate, the unit hardly looked fired. The inside was similar in appearance.

The igniter assemblies that were used with ITA SN 001 and 002 are shown in Figure 110. In both cases, the porcelain on the spark plug broke back a little, but in neither case did it interfere with their operation. The two units shown in Figure 110 produced ignition every single time. The SN 001 unit was fired over a wide range of MR, pressure and temperature conditions and the SN 002 unit was fired 42,266 times.

ITA SN 002 after 42,266 pulses, is shown in Figure 111. The Haynes weld repair can be seen and obviously held up quite well. After 42,266 pulses, the chamber shows no signs of fatigue damage.

Table XXXIX is a summary to the chamber repair and component failure history of ITA SN 002.
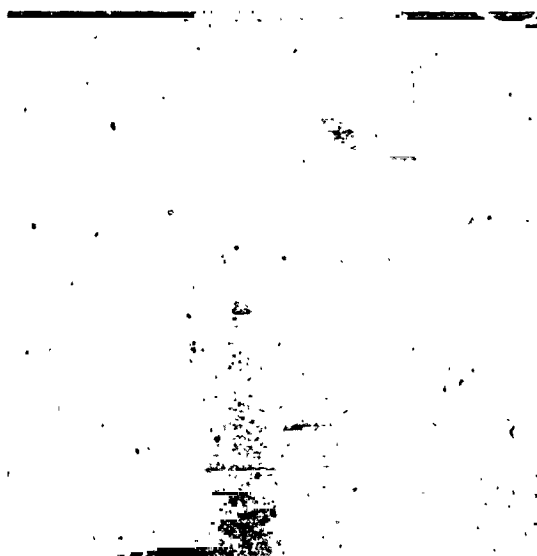
Close up of Tip

0°

120°
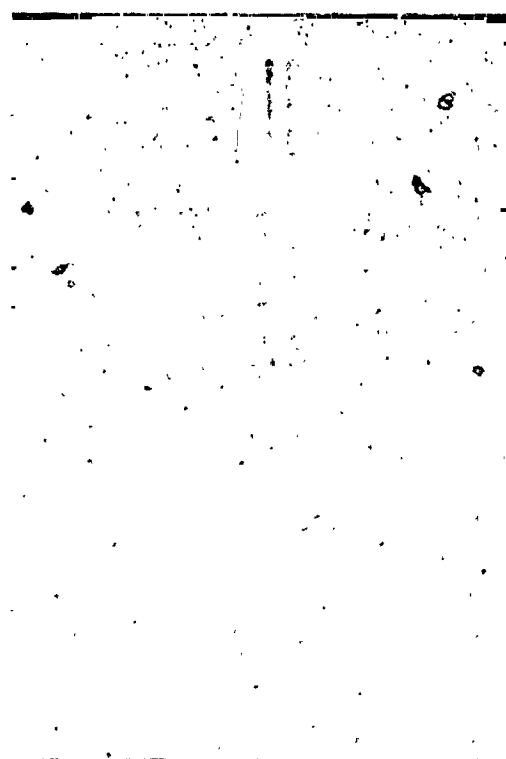
240°

Figure 109. ITA SN 002 Igniter Body After 42,266 Pulses

Figure 110. Igniter Assemblies After Testing

Figure 111. ITA SN 002 After Testing

TABLE XXXIX

SUMMARY OF COMPONENT FAILURES

Pulse	Event	Probable Cause
5621	a. Leak in torus weld.	a. Pin hole in weld.
	b. Leaks in fuel line to torus weld.	b. Flaws in welds.
	c. Crack in Haynes weld.	c. Mechanical damage.
20,724	a. Bellows leaks – both main propellant valves. (Main ox valve, SN 012, replaced.)	a. Overpressurization of ox valve due to transducer failure. Crack in bellows.
	b. Fuel pilot valve inoperative.	b. Critical tolerances disrupted by deposit from nickel plating.
30,049	a. Fuel igniter valve closure intermittent (igniter valves replaced).	a. Valve was not disassembled – cause unknown.
	b. Crack in torus.	b. High stresses induced by mechanical damages.
34,594	Crack in torus	Residual stresses from prior weld repair.
39,514	a. Fuel inlet line rupture.	a. Fatigue at high stress level resulting from installation.
	b. Bellows leak in main fuel valve severe.	b. Propogation of crack in bellows.
	c. Fuel pilot valve inoperative self actuated.	c. Critical tolerances disrupted by deposit from nickel plating.
42,266	Chamber burn through	Ice formation in cooling passages due to test cell water blowback and chilldown by fuel valve closing delay.

4.5   DATA ANALYSIS

4.5.1 Igniter Tests

4.5.1.1   Exciter

4.5.1.1.1 EMI

Procedure conducted EMI was measured on each of the two isolated power input leads to exciter PN 47170 SN 001 over the 20 KHz to 50 MHz frequency range. No evidence was found to indicate the presence of narrowband EMI as defined by the tests of MIL-STD-462. All measurements were made using the slideback substitution method. Peak detector function was used for all tests. Each tuning range was slowly scanned during the 1 sec on time of a 1 sec ON, 3.5 sec off duty cycle. At least three frequencies per octave, indicative of the highest noise levels, were selected for measurement. Where no EMI was detected, the instrument background EMI level was recorded at the three frequencies per octave distribution.

Figure 112 shows the results of the steady state tests. Steady state ON conducted EMI was on the order of 30 dB below the limit at low frequencies and the margin increased as frequency increased. At .8 MHz for the positive lead and 1.8 MHz conducted EMI was not detected above instrument background levels. The data for the spark monitor circuit are not shown as conducted EMI was not significantly above the instrument background levels in the 20 to 150 KHz range, and 12 dB above instrument background levels at 900 KHz for frequencies greater than 150 KHz.

Transient conducted EMI was 122 DBUI/MHz at 20KHz (spec limit is 134) and 102 to 104 at 28 KHz (spec limit is 127.5). At frequencies above 35 KHz the transient was not detected.
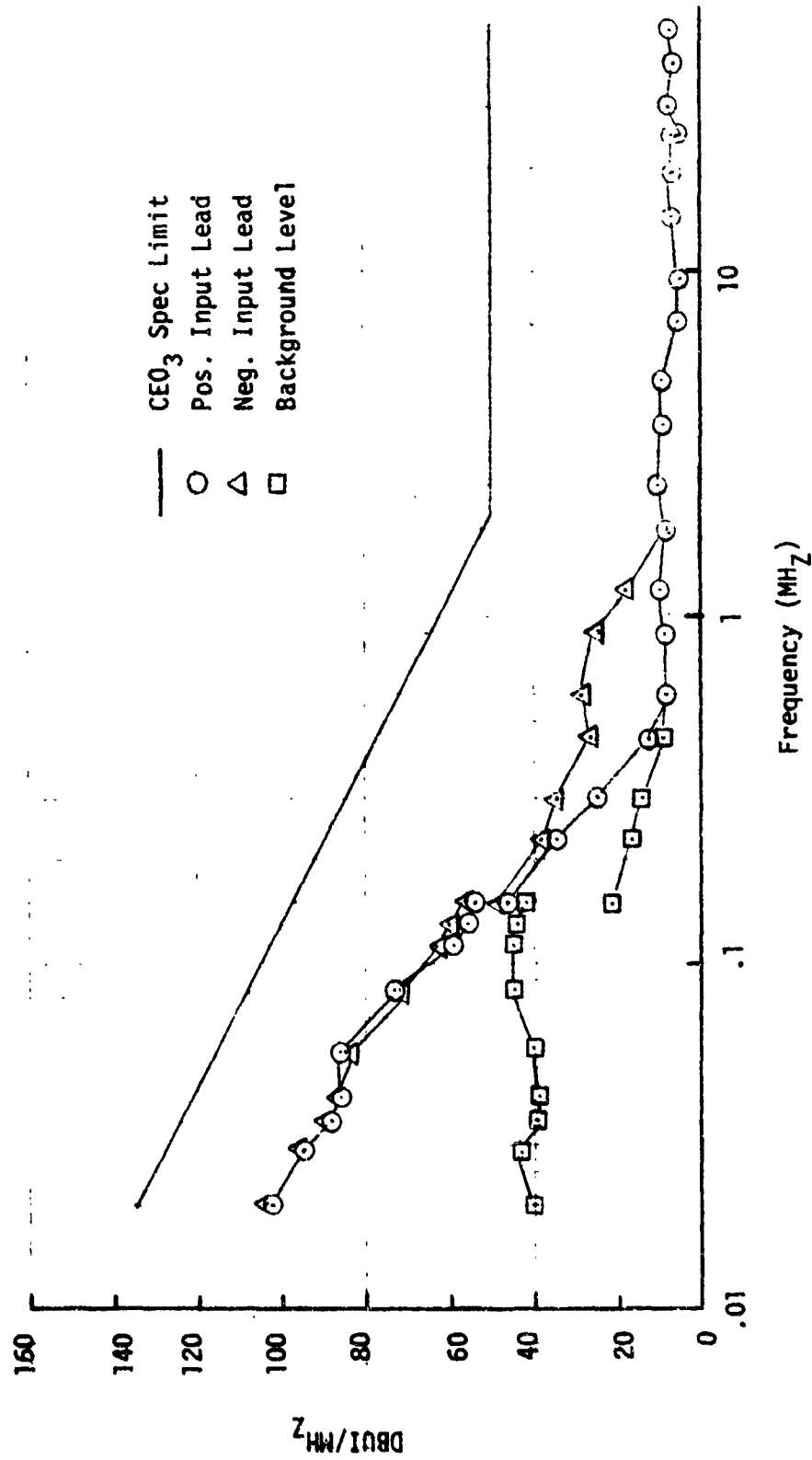
Figure 112. Conducted EMI CEO^3 K$_{HZ}$ to 50 MH$_Z$

4.5, Data Analysis (cont.)

The same methods of measurement and frequency selection employed for the conducted EMI testing were used to measure radiated EMI to Method REO2 over the 14 KHz to 1 GHz range. With the spark monitor lead shielded, no radiated EMI was detected above the instrument background levels.

Procedure-Susceptibility signals corresponding to the levels of MIL-STD-461A, Notice 3, Figure 17, were injected in series with the positive input lead to exciter SN 001.

The spark rate of the exciter is dependent both on voltage and component temperature. Consequently, the spark rate at frequencies below 500 Hz was observed to increase and decrease in accordance with the peaks and valleys of the sum of the AC and DC inputs, and variation in rate was detected depending upon whether the susceptibility ON or OFF condition was measured first since some heating occurred. With 38 VDC input, the maximum variation in spark vs. susceptibility signal frequency was only 2.5%. An acceptable spark rate could be maintained over a given period of time when the exciter is subjected to the conducted susceptibility signals of MIL-STD-461A, Notice 3, Method LS01.

4.5.1.1.2 Temperature, Energy and Life Tests

The engineering exciter unit, SN 001, (vermiculite filled), was subjected to temperature and life tests.

The unit was operated with a 50% duty cycle (50 msec ON and 50 msec OFF) for 85 minutes in 29°C air and also in -79°C air. The case was unsulated from heat loss by conduction. The temperature of the case and eight components were measured. The exciter case temperature transients are shown in Figure 113. The operation and calibration results are shown in Table XL.
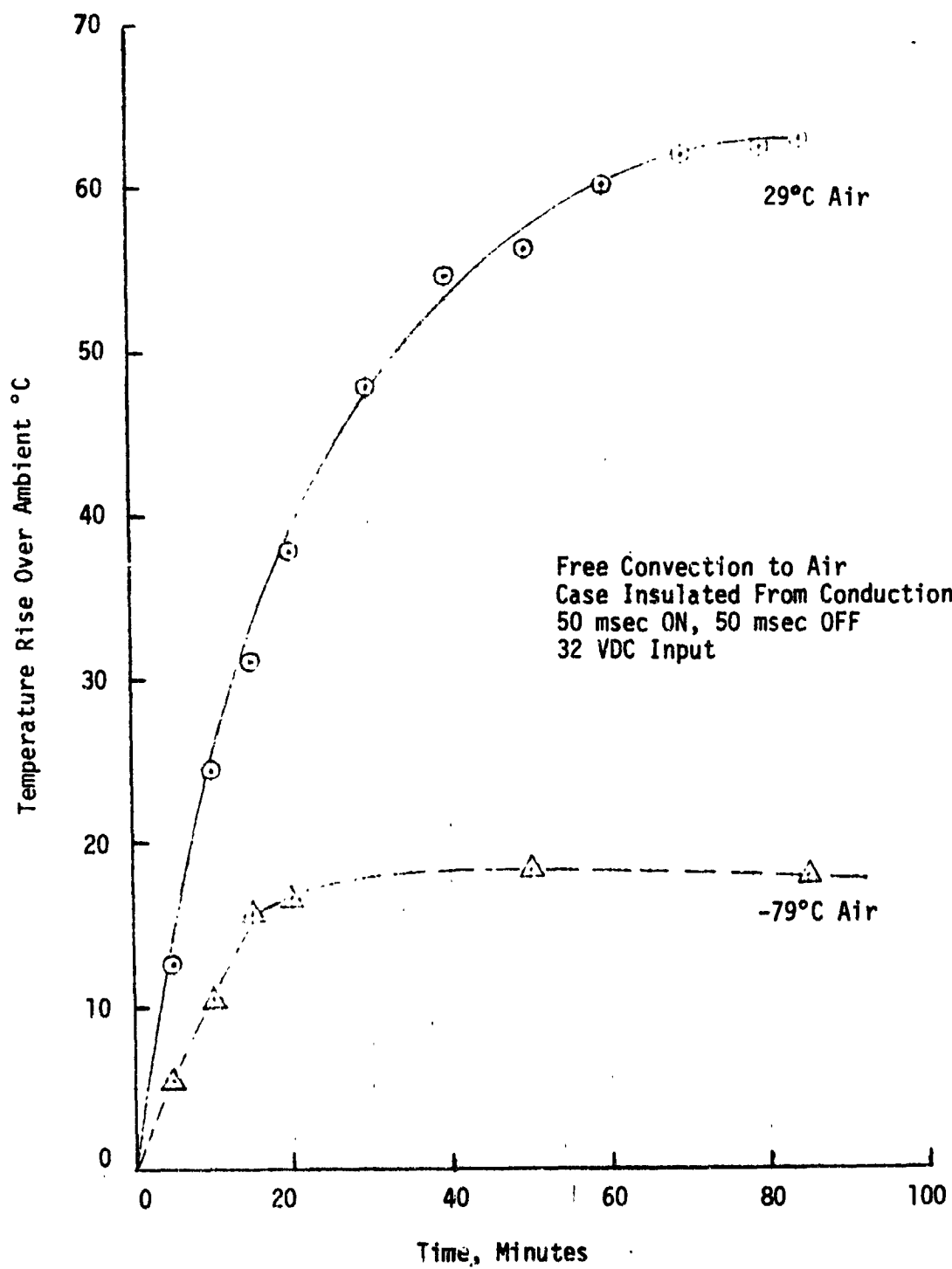
Figure 113. Exciter Case Temperatures

4.5, Data Analysis (cont.)

TABLE XL

EXCITER OPERATION AND CALIBRATION

Room Temp. °C	Input Voltage VDC	Input Current Amps	Spark Rate SPS	Monitor Output Voltage	Comments
24	24	.85	480	3	Room temperature calibration
	28	.86	590	2.9	
	32	.88	710	2.9	
-79	24	.5	182	2.8	Operation before low temperature
	28	.6	278	2.8	test.
	32	.65	358	2.8	
-79	24	.69	400	2.7	Operation after low temperature
	28	.74	500	2.7	test.
	32	.76	606	2.7	
24	24	.83	445	2.8	Posttest room temperature
	28	.85	552	2.8	calibration.
	32	.87	625	2.8	

The temperature data indicate that the exciter does not require special temperature conditioning to operate satisfactorily. With an emissivity coating, the igniter could be operated extensively in the vacuum conditions of space with temperatures no higher than those measured in the ambient temperature test. The chilldown of the oxidizer dome to which the igniter and support bracket are mounted will not cause the exciter to malfunction because of low component temperatures resulting from heat loss to the injector. The low temperature tests demonstrated operation at a temperature (194°K) below the oxidizer nominal temperature (208°K).

The lifetime demonstrated in the tests (equivalent to 85 minutes continuous operation) is probably in excess of any 10 year space shuttle requirement. An ON time of .040 to .050 sec per firing for 50,000 firings, for example, constitutes 33 to 42 minutes of cumulative operation.

4.5, Data Analysis (cont.)

The output voltage measured for the SN 001
engineering unit was 15 Kv by oscilloscope and 16.5 Kv by ball-gap.

Additional data on the spark energy were obtained
with the SN 004 exciter. The stored energy was 17.5 mjoules and the total spark
energy was 8.3 mjoules for a spark efficiency of 47%. The first spark duration
was 28.5 μsec; the peak power was 1320 watts.

4.5.1.2 Igniter Functional Test Firing

The igniter was test fired over a wide range of
operating conditions. Pressures at the inlet to the valves varied from 159 N/cm^2
(230 psia) to 448 N/cm^2 (650 psia). The hydrogen temperatures varied from ambient
to 166°K (298°R). Igniter chamber pressures were 114 (167) to 295 N/cm^2
(428 psia) and the core mixture ratio 14 to 77. The test conditions are summarized
in Table XLI.

Test 116 was a valve sequencing test. Ignition
was accomplished with oxidizer valve lead times of 10, 5, 0, -5 and -10 (lag)
msec. Test 118 was an ignition delay test. Spark lead time was varied in six
steps from being on 25 msec before opening the valves to 12 msec after opening
the valves. A total of 1075 firings were made. The igniter operated with 100%
reliability.

The components that were used for the igniter
functional test firings are shown in Figure 114. Figure 114a shows the exciter,
support bracket and test fixture. The "crosses" at the inlets were utilized for
propellant pressure and temperature measurements. Igniter housing SN 003 which
was used for all the functional testing summarized in Table XLI and for all the
exciter checkout test firings is shown in Figure 114b; as can be seen in the
picture, there are no heat marks on the igniter body. The highest temperature

TABLE XLI

IGNITER TEST DATA

| Test | Tank Pressures, N/cm² (psia) | | Valve Pressure N/cm² (psia) | | Manifold Pressure N/cm² (psia) | | Propellant Temperatures, °K (°R) | | | | Igniter Chamber Pressure N/cm² (psia) | Propellant Flow Rates, g/sec (lb/sec) | | | | MR | |
| | | | | | | | @ Valves | | @ Manifolds | | | | | | | | |
	GO₂ POT	GH₂ PFT	GO₂ POV	GH₂ PFV	GO₂ POJ	GH₂ PFJ	GO₂ TOV	GH₂ TFV	GO₂ TOJ	GH₂ TFJ		Coolant $(\dot{w}H_2)c$	GH₂ Core $(\dot{w}H_2)I$	Total $\dot{w}H_2$	GO₂ Core $\dot{w}O_2$	Core	Overall
116	283 (410)	274 (405)	259 (375)	279 (405)	186 (270)	220 (319)	220 (396)	100 (180)	268 (483)	173 (312)	177 (257)	4.99 (.0110)	1.13 (.0025)	6.12 (.0135)	16.9 (.0417)	16.7	3.1
118	299 (434)	276 (400)	274 (397)	276 (400)	193 (280)	217 (315)	206 (370)	86 (155)	269 (485)	183 (330)	183 (266)	2.70 (.00564)	.52 (.00114)	3.22 (.0071)	16.05 (.0354)	31.1	5.0
104	292 (424)	448 (650)	268 (388)	448 (650)	196 (285)	350 (508)	289 (520)	289 (520)	286 (514)	289 (520)	187 (271)	3.19 (.00704)	.48 (.00106)	3.67 (.0081)	23.2 (.0512)	48.3	6.3
106	338 (490)	286 (415)	309 (448)	286 (415)	207 (300)	223 (324)	289 (520)	289 (520)	286 (514)	289 (520)	197 (285)	4.72 (.0104)	1.10 (.00243)	5.82 (.0128)	15.8 (.0348)	14.3	2.7
111	259 (375)	320 (464)	236 (343)	320 (464)	169 (245)	250 (363)	226 (406)	160 (288)	269 (484)	185 (329)	161 (233)	4.46 (.00984)	.98 (.00216)	5.44 (.0120)	19.4 (.0427)	19.8	3.6
112	283 (410)	248 (350)	259 (375)	248 (360)	186 (270)	194 (281)	219 (394)	168 (303)	265 (477)	185 (333)	177 (257)	3.46 (.00762)	.45 (.00099)	3.91 (.00861)	21.4 (.0471)	47.6	5.5
113	471 (683)	396 (575)	431 (625)	396 (575)	310 (450)	312 (453)	213 (383)	176 (317)	266 (479)	188 (339)	295 (428)	5.49 (.0121)	.59 (.00130)	6.08 (.0134)	36.1 (.0796)	61.2	5.9
115	182 (264)	159 (230)	167 (242)	159 (230)	121 (175)	124 (180)	237 (427)	122 (220)	268 (483)	166 (298)	115 (167)	4.24 (.00935)	.73 (.00160)	4.97 (.0109)	24.0 (.0529)	33.1	4.8
117	312 (453)	241 (350)	286 (415)	241 (350)	186 (270)	189 (274)	216 (389)	245 (457)	267 (480)	246 (442)	177 (257)	2.32 (.00512)	.28 (.00062)	2.60 (.00574)	13.1 (.0289)	46.6	5.0
110	241 (350)	338 (491)	221 (320)	338 (491)	162 (235)	265 (384)	283 (509)	155 (279)	277 (498)	167 (300)	154 (224)	4.02 (.00887)	.75 (.00165)	4.77 (.0105)	21.2 (.0469)	28.4	4.5
114	316 (459)	300 (435)	290 (420)	300 (435)	207 (300)	234 (340)	220 (396)	142 (256)	267 (481)	178 (320)	197 (285)	2.92 (.00644)	.33 (.00072)	3.25 (.00716)	25.3 (.0557)	77.4	7.8
105	241 (350)	241 (350)	220 (319)	241 (350)	155 (225)	189 (274)	289 (520)	289 (520)	286 (514)	283 (520)	148 (214)	3.86 (.00852)	.57 (.00147)	4.53 (.0100)	23.7 (.0522)	25.5	5.2
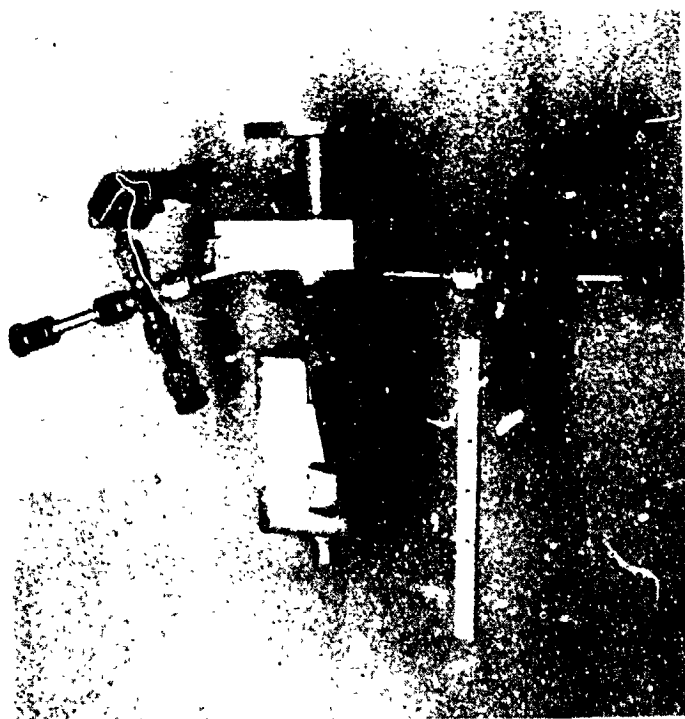
b. Igniter Housing

a. Test Fixture, Bracket and Exciter

Figure 114. Igniter Test Components

4.5, Data Analysis (cont.)

recorded on the body was 273°C (524°F) which indicates that the igniter is operating at lower temperatures than assumed in the design analysis.

4.5.2   Hydraulics

4.5.2.1 Cold Flow Results

4.5.2.1.1   ITA

The data from the cold flow testing of the four ITA units are summarized in Table XLII for the ox circuit and in Table XLIII for the fuel circuit. The data consists of the GN_2 flow rates, pressures at the inlet to each circuit, the manifold pressures (PO_J and PF_J) and the discharge coefficient * area products (C_DA) that correlates the data. The GN_2 flow rate was varied over the range of 1/2 to 2X the value that was calculated to give Mach number simultation at nominal conditions. The C_DA was calculated from the expression

$$\dot{w} = C_D A \ P \sqrt{\frac{2g}{R} \frac{M}{T} \left(\frac{\gamma}{\gamma-1}\right) \left[\left(\frac{Pd}{P}\right)^{\frac{2}{\gamma}} - \left(\frac{Pd}{P}\right)^{\frac{\gamma+1}{\gamma}}\right]}$$

where:

A   = Area

C_D = Discharge coefficient

g   = Gravitational constant

M   = Molecular weight

P   = Inlet pressure

Pd = Discharge pressure

R   = Gas constant

T   = Temperature

γ = Ratio of specific heats

$\dot{w}$ = Flow rate

TABLE XLII

ITA COLD FLOW DATA -- OX CIRCUIT

Step	Flow Rate g/sec (lb/sec)	Inlet Pressure, N/cm² (psia) SN 001	SN 002	SN 003	SN 004	Manifold Pressure, N/cm² (psia) SN 001	SN 002	SN 003	SN 004	C_D A cm² (in.²) SN 001	SN 002	SN 003	SN 004
1	45.8 (.101)	11.839 (17.171)	11.639 (16.880)	11.704 (17.157)	11.704 (15.975)	11.238 (16.299)	11.173 (16.204)	11.273 (16.349)	11.215 (16.265)	2.31 (.358)	2.45 (.380)	2.33 (.361)	2.38 (.369)
2	18.1 (.04)	10.391 (15.070)	10.356 (15.019)	10.383 (15.059)	10.337 (14.992)	10.286 (14.918)	10.271 (14.896)	10.310 (14.953)	10.252 (14.869)	2.51 (.358)	2.45 (.380)	2.31 (.358)	2.37 (.368)
3	27.2 (.06)	10.7 (15.565)	10.666 (15.469)	10.742 (15.580)	10.658 (15.457)	10.502 (15.232)	10.484 (15.205)	10.529 (15.271)	10.472 (15.188)	2.30 (.356)	2.42 (.375)	2.31 (.356)	2.37 (.367)
4	36.3 (.08)	11.201 (16.245)	11.071 (16.057)	11.188 (16.226)	11.097 (16.094)	10.799 (15.662)	10.761 (15.607)	10.825 (15.700)	10.776 (15.628)	2.30 (.357)	2.45 (.380)	2.34 (.362)	2.38 (.369)
5	45.8 (.101)	11.846 (17.181)	11.632 (16.870)	11.816 (17.137)	11.704 (16.975)	11.238 (16.299)	11.168 (16.194)	11.255 (16.324)	11.218 (16.270)	2.31 (.358)	2.46 (.381)	2.34 (.362)	2.38 (.369)
6	61.2 (.135)	13.204 (19.150)	12.787 (18.545)	13.113 (19.018)	12.971 (18.812)	12.184 (17.671)	12.095 (17.541)	12.201 (17.696)	12.177 (17.661)	2.32 (.360)	2.48 (.385)	2.35 (.365)	2.39 (.371)
7	77.1 (.17)	15.088 (21.883)	14.357 (20.823)	14.903 (21.614)	14.693 (21.310)	13.619 (19.752)	13.462 (19.525)	13.586 (19.704)	13.579 (19.694)	2.31 (.358)	2.50 (.387)	2.35 (.365)	2.40 (.372)
8	90.7 (.20)	17.148 (24.870)	16.198 (23.492)	16.895 (24.503)	16.669 (24.175)	15.341 (22.250)	15.134 (21.949)	15.274 (22.153)	15.334 (22.240)	2.30 (.357)	2.46 (.382)	2.34 (.363)	2.36 (.369)
9	45.8 (.101)	11.813 (17.132)	11.612 (16.841)	11.796 (17.108)	11.677 (16.936)	11.218 (16.270)	11.166 (16.194)	11.239 (16.300)	11.190 (16.241)	2.33 (.361)	2.48 (.384)	2.35 (.364)	2.40 (.372)
									Avg. =	2.31 (.358)	2.46 (.382)	2.34 (.362)	2.39 (.370)
									σ (%) =	.39	.88	.89	.48

TABLE XLIII

ITA COLD FLOW DATA - FUEL CIRCUIT

Step	Flow Rate g/sec (lb/sec)	Inlet Pressure, N/cm² (psia)				Manifold Pressure, N/cm² (psia)				C_DA cm² (in.²)			
		SN 001	SN 002	SN 003	SN 004	SN 001	SN 002	SN 003	SN 004	SN 001	SN 002	SN 003	SN 004
1	42.2 (.093)	12.535 (18.180)	12.415 (18.006)	12.403 (17.989)	12.252 (17.769)	10.799 (15.662)	10.795 (15.656)	10.817 (15.688)	10.709 (15.531)	1.497 (.232)	1.529 (.237)	1.542 (.239)	1.581 (.245)
2	20.4 (.045)	10.766 (15.614)	10.727 (15.558)	10.749 (15.590)	10.658 (15.457)	10.336 (14.918)	10.271 (14.896)	10.310 (14.953)	10.225 (14.830)	1.393 (.216)	1.406 (.218)	1.413 (.219)	1.458 (.226)
3	27.2 (.060)	11.204 (16.250)	11.166 (16.194)	11.154 (16.177)	11.063 (16.045)	10.411 (15.099)	10.406 (15.092)	10.428 (15.124)	10.350 (15.011)	1.445 (.224)	1.452 (.225)	1.477 (.229)	1.510 (.234)
4	34.0 (.075)	11.779 (17.083)	11.694 (16.968)	11.695 (16.961)	11.576 (16.789)	10.580 (15.344)	10.564 (15.322)	10.597 (15.369)	10.496 (15.222)	1.458 (.226)	1.451 (.229)	1.497 (.232)	1.529 (.237)
5	42.2 (.093)	12.521 (18.160)	12.432 (18.031)	12.387 (17.965)	12.262 (17.784)	10.799 (15.662)	10.795 (15.656)	10.817 (15.688)	10.709 (15.531)	1.503 (.233)	1.523 (.236)	1.548 (.240)	1.445 (.244)
6	54.4 (.12)	13.923 (20.139)	13.767 (19.966)	13.653 (19.801)	13.535 (19.630)	11.238 (16.299)	11.233 (16.292)	11.255 (16.324)	11.131 (16.143)	1.542 (.239)	1.568 (.243)	1.600 (.248)	1.620 (.251)
7	68.0 (.15)	15.747 (22.838)	15.454 (22.414)	15.32 (22.226)	15.200 (22.045)	11.846 (17.181)	11.841 (17.174)	11.830 (17.157)	11.688 (16.951)	1.600 (.248)	1.632 (.253)	1.665 (.258)	1.677 (.260)
8	81.6 (.18)	17.756 (25.752)	17.380 (25.206)	17.165 (24.895)	17.040 (24.714)	12.535 (18.180)	12.550 (18.202)	12.522 (18.161)	12.346 (17.906)	1.665 (.258)	1.703 (.264)	1.729 (.268)	1.742 (.270)
9	42.2 (.093)	12.488 (18.111)	12.399 (17.982)	12.387 (17.965)	12.218 (17.720)	10.793 (15.653)	10.795 (15.656)	10.810 (15.678)	10.691 (15.506)	1.516 (.235)	1.535 (.238)	1.548 (.240)	1.600 (.248)
						Avg. =				1.510 (.234)	1.535 (.238)	1.561 (.242)	1.587 (.246)
						σ (%) =				5.42	5.85	6.17	5.46

4.5, Data Analysis (cont.)

As shown earlier in Table XXV, the ox circuit simulation flow rate of 45.8 g/sec (.101 lb/sec) should correspond to an 11.825 N/cm^2 (17.150 psia) inlet pressure and 11.487 N/cm^2 (16.660 psia) manifold pressure. The average of the 12 measurements (3 measurements on each of the four units) is 11.742 N/cm^2 (17.030 psia) for the inlet pressure and 11.216 N/cm^2 (16.267 psia) for the manifold pressure. These measurements scale to 240 N/cm^2 (348 psia) vs 241 N/cm^2 (350 psia) for the inlet line pressure and 229 N/cm^2 (332 psia) vs 234 N/cm^2 (340 psia) for the manifold pressure. The agreement of the measured hydraulics with the design hydraulics is well within the experimental accuracy.

The C_D A values were included primarily to show consistency from unit to unit, with prior measurements, and over the range of flows. The spread in the C_D A values for all the units is 6.7% indicating that the fabrication process is repeatable. The average C_D A value for the four units agrees with the average of the prior measurements for the four units as injector assemblies within .55%. Finally, the standard deviation of the average C_D A values from the values calculated for each flow step is less than 1% for all four units and indicates that the subsonic flow expression provides good correlation of the data.

The ITA fuel circuit cold flow data (Table XLIII) do not provide as much information as the oxidizer circuit data. The reason is the complexity of the fuel flow system. The fuel circuit contains two parallel flow paths (the regen and the ff$_c$ circuit) each with a different back pressure. There is heat addition to the regen circuit, the fuel in the injector is heated and therefore at a temperature different from the rest of the circuit, and finally the inlet line and torus flow is the sum of the regen and ff$_c$ circuit flows.

In calculating the GN$_2$ flow rate that provides Mach number simulation of the ITA fuel circuit, the regen circuit was simulated and the flow in the ffc circuit that resulted was calculated and added to the

4.5, Data Analysis (cont.)

regen flow to get a total flow rate. There is no constant temperature GN_2 flow rate that will simulate the actual H_2 flow conditions with heat addition and different temperatures in different parts of the circuit. The overall conditions were simulated; the pressure at each station cannot be simulated.

By comparing the inlet pressure and manifold pressure data of Table XLIII at the simulation flow rate, 42.6 g/sec (.093/.090 lb/sec), with the predicted test simulation pressures summarized in Table XXV it can be seen that the measured pressures are less than the predicted pressures. At the inlet the pressure ratios to a 253 N/cm^2 (367 psia) from the data versus a 267 N/cm^2 (387 psia) design pressure. The lower pressure was considered of no consequence since the final balance was achieved by means of an orifice in the inlet line.

The C_D A values for the ITA fuel circuit show two things. The variation of the average values from unit to unit results in a spread of 5.1% indicating good manufacturing repeatability. Secondly, the simple subsonic flow expression does not describe the complex fuel system as indicated by the systematic variation in C_D A with flow rate, and further demonstrated by the 5 to 6% standard deviation of the average C_D A from the values calculated for each measurement.

The balance orifices were sized to give the required pressure ratio at the GN_2 flow rate that provides Mach number simulation as summarized in Table XXV. The requirements and results are summarized in Table XLIV. The required inlet pressures were achieved within .6%.

4.5, Data Analysis (cont.)

TABLE XLIV

ITA BALANCE DATA

ITA SN	INLET PRESSURES, N/cm^2 (PSIA)	
	OXIDIZER	FUEL
001	12.39 (18.70)	13.28 (19.26)
002	12.92 (18.74)	13.29 (19.28)
003	12.89 (18.70)	13.28 (19.26)
004	12.89 (18.69)	13.21 (19.16)
Design (Table XXV)	12.91 (18.72)	13.29 (19.28)

4.5.2.1.2 Igniter

As described in Section 4.3.2.1, igniter housing SN001 was flow tested and on the basis of the data the orifices that determine the split in H_2 flow between the core and the coolant circuit were resized. An internal leakage check was also made using this unit as described in 4.3.2.1.3. The C_D A reduced from the data obtained for SN001 without the seal around the sleeve (internal leakage) was .0382 cm^2 (.00592 in.^{2}). The C_D A obtained with a seal around the sleeve (no internal leakage) was .0336 cm^2 (.00521 in.^{2}). From the two C_D A values the coolant flows not going through the orifices were approximately 13.5%. When the igniter was cold this internal leakage would occur. When the igniter was operating and warm the leakage would be reduced. The average temperature of the igniter sleeve would have to be approximately 280°C (536°F) for thermal expansion of the sleeve to be sufficient to eliminate the .00508 cm (.002 in.) dimetrical clearance between the sleeve and the counterbore in the injector.

4.5, Data Analysis (cont.)

The igniter cold flow data for the fuel circuit
are given in Table XLV. Flow rates, inlet pressures and a C_D A calculated using
the subsonic flow equation are given at each flow value for each of the four igniter
units. The data for the first two flow steps in Table XLV are suspect. These low
flow values were obtained with back pressures at a nominal 20.7 N/cm^2 (30.0 psia).
For the two lowest flow conditions the inlet pressure and the back pressure are
so close to the same value that the sum of the accuracies of the two transducers
used to measure the pressures was about the same order of magnitude as the pressure
difference. It is virtually impossible at these low flow rates to accurately de-
termine the pressure ratio (back pressure divided by inlet pressure).

The spread in the average C_D A values obtained for
the four units in 6.5% indicating consistency in fabrication. The average C_D A for
the four units is .00504 cm^2 (.0007815 in.^{2}) which is within .6% of the design value,
.00501 cm^2 (.000777 in.^{2}).

The igniter cold flow data for the coolant circuit
are given in Table XLVI. The C_D A values were calculated using the sonic flow
equation

$$\dot{w} = C_D \ A \ P \ \sqrt{g\left(\frac{M\gamma}{TR}\right)\left(\frac{2}{\gamma+1}\right)^{\frac{\gamma+1}{\gamma-1}}}$$

where: A = area

C$_D$ = discharge coefficient

g = gravitational constant

M = molecular weight

P = pressure

R = gas constant

T = temperature

$\dot{w}$ = flow rate

γ = ratio of specific heats

TABLE XLV

IGNITER COLD FLOW DATA - FUEL CORE CIRCUIT

Step	Flow Rate, g/sec (lb/sec)				Inlet Pressure, N/cm² (psia)				$C_D A$ cm² (in.²)			
	SN 001	SN 002	SN 003	SN 004	SN 001	SN 002	SN 003	SN 004	SN 001	SN 002	SN 003	SN 004
1	.0880 (.000194)	.0857 (.00189)	.1270 (.000280)	.0771 (.000170)	20.8 (30.2)	22.1 (32.1)	22.1 (32.1)	21.0 (30.5)	.00690 (.0001107)	.00362 (.000561)	.00496 (.000769)	.00513 (.000795)
2	.1238 (.000273)	.1279 (.000282)	.1715 (.000378)	.1238 (.000273)	21.2 (30.7)	22.9 (33.2)	22.9 (33.2)	21.4 (31.0)	.00658 (.0001102)	.00452 (.000700)	.00499 (.000774)	.00532 (.000825)
3	.1719 (.000379)	.1719 (.000379)	.3191 (.000483)	.1715 (.000378)	22.8 (33.1)	23.2 (33.7)	25.2 (36.6)	23.1 (33.5)	.00441 (.000829)	.00481 (.000745)	.00362 (.000754)	.00509 (.000789)
4	.2191 (.000483)	.2164 (.000477)	.2536 (.000559)	.2532 (.000492)	24.0 (34.8)	25.1 (36.4)	26.5 (38.5)	24.5 (35.6)	.00506 (.000784)	.00488 (.000757)	.00481 (.000745)	.00502 (.000778)
5	.2545 (.000561)	.2463 (.000543)	.2558 (.000564)	.2558 (.000564)	25.6 (37.1)	25.9 (37.6)	26.9 (39.0)	25.8 (37.4)	.00523 (.000744)	.00499 (.000773)	.00464 (.000750)	.00508 (.000787)
6	.3062 (.000675)	.2985 (.000658)	.3021 (.000666)	.3044 (.000671)	28.3 (41.0)	27.7 (40.2)	29.6 (42.9)	28.1 (40.8)	.00512 (.000794)	.00519 (.000805)	.00475 (.000736)	.00515 (.000799)
7	.3430 (.000756)	.3375 (.000744)	.3484 (.000768)	.3429 (.000756)	30.1 (43.7)	29.6 (42.9)	32.2 (46.7)	30.0 (43.4)	.00517 (.000801)	.00525 (.000814)	.00481 (.000746)	.00519 (.000804)
8	.3887 (.000857)	.3883 (.000856)	.3964 (.000874)	.3942 (.000869)	32.8 (47.6)	31.9 (46.3)	35.3 (51.2)	33.0 (47.9)	.00520 (.000806)	.00538 (.000835)	.00487 (.000755)	.00526 (.000810)
Avg. =									.00517 (.000801)*	.00401* (.000776)**	.00485 (.000752)	.00515 (.000798)
σ (%) =									1.96*	5.95**	1.72	1.85

* Excluding Steps 1 and 2
** Excluding Step 1

TABLE XLVI

IGNITER COLD FLOW DATA - COOLANT CIRCUIT

Step	Flow Rate, g/sec (lb/sec)				Inlet Pressure, N/cm² (psia)				C_DA, cm (in.²)			
	SN 001	SN 002	SN 003	SN 004	SN 001	SN 002	SN 003	SN 004	SN 001	SN 002	SN 003	SN 004
1	2.282 (.00503)	2.313 (.00510)	2.286 (.00504)	2.295 (.00306)	42.9 (62.2)	44.6 (64.7)	42.3 (61.4)	49.3 (71.5)	.0230 (.00356)	.0223 (.00346)	.0236 (.00362)	.0201 (.00311)
2	2.540 (.00560)	2.572 (.00567)	2.590 (.00571)	2.594 (.00572)	48.3 (70.0)	49.2 (71.3)	47.4 (68.7)	55.3 (80.2)	.0227 (.00352)	.0225 (.00349)	.0236 (.00366)	.0202 (.00313)
3	3.048 (.00672)	2.944 (.00649)	3.034 (.00669)	3.066 (.00676)	57.2 (82.9)	55.7 (80.8)	54.9 (79.7)	64.6 (93.7)	.0230 (.00357)	.0228 (.00353)	.0238 (.00369)	.0204 (.00317)
4	3.493 (.00770)	3.474 (.00766)	3.456 (.00762)	3.561 (.00785)	65.4 (94.9)	65.2 (94.6)	62.2 (0.2)	74.9 (108.6)	.0230 (.00357)	.0233 (.00361)	.0239 (.00371)	.0205 (.00318)
5	3.905 (.00861)	3.937 (.00868)	3.896 (.00859)	3.937 (.00868)	73.4 (105.7)	73.3 (106.3)	69.8 (101.2)	82.6 (119.3)	.0230 (.00358)	.0232 (.00359)	.0241 (.00373)	.0206 (.00320)
6	4.363 (.00962)	4.336 (.00956)	4.341 (.00957)	4.341 (.00957)	81.1 (117.7)	80.1 (116.2)	77.4 (112.2)	90.2 (130.8)	.0232 (.00359)	.0233 (.00361)	.0242 (.00375)	.0208 (.00322)
Avg. =									.0230 (.00356)	.0228 (.00354)	.0238 (.00369)	.0204 (.00317)
σ (%) =									.72	1.62	1.29	1.26

4.5, Data Analysis (cont.)

There is about a 4% spread in the average C_D A values for igniter SN001, SN002 and SN003. Igniter SN004 has an average C_D A value that is 13.5% lower than the .0232 cm^2 (.00360 in.^{2}) value averaged from the C_D A values for units SN001, SN002 and SN003. This suggests plugging of one or more of the coolant orifices, or no internal leakage. If this unit has been used for testing the orifices would have been inspected and/or probed to insure no plugging.

The average C_D A value for units SN001, SN002 and SN003, .0232 cm^2 (.00360 in.^{2}), compares to a design value of .0201 cm^2 (.00312 in.^{2}). In effect, when the igniter was cold the coolant flow including internal leakage was 15.4% above the design value; when the igniter warmed up and there was no internal leakage the igniter coolant circuit flowed 1.9% more than the design value.

The cold flow data for the oxidizer circuit are summarized in Table XLVI. The C_D A values were derived from the data using the subsonic flow equation described earlier. As was the case for the H_2 core circuit the C_D A at the two lowest flow rates are suspect. The inlet pressure and chamber pressure were so close to the same value at the low flow rate that the accuracy of the transducers relative to each other could introduce significant error in the ratio of the two pressures which was required to calculate the C_D A values. The C_D A value for the four units averaged from the three highest flow rates have a 3.7% spread, indicating part to part consistency. There was no design pressure drop requirement for the oxidizer system. The design concept utilized low pressure drop in the igniter since the resistance of the value limited the oxidizer flow to the design value.

The resistance of the valve in the oxidizer circuit was such that the igniter ox system flowed 69% of the design flow rate. The balance orifice was selected for the fuel system such that it flowed at approximately the same percentage (71%) of design flow. Thus, the actual overall MR (6.2) was maintained relatively close to the design value (6.5).

4.5, Data Analysis (cont.)

4.5.2.1.3 Injector

As discussed in Section 4.3.3 the injector cold
flow was done in two stages. The injector body was flowed with a fixture to close
out the manifold as shown in Figure 71 to check the oxidizer circuit hydraulics
prior to completion of fabrication. Both the oxidizer circuit and the fuel circuit
of the completed injectors were cold flow tested. The tests consisted of flow
uniformity measurement and hydraulic characterization.

The hydraulic characterization results for the
four injector bodies (ox circuit) are given in Table XLVII. The C_D A values for
each injector body and flow rate were calculated using the subsonic flow equation
discussed earlier. The C_D A values vary approximately 10% with flow rate (or
pressure ratio) indicating that the flow characteristics cannot be described by
a simple correlation over a range of flow that varies by a factor of 5 from minimum
to maximum. The variation in C_D A with flow as shown in Table XLVIII is consistent
from unit to unit and the average C_D A values calculated for each injector body
have a spread that is less than 5% indicating consistency in fabrication.

The flow from each oxidizer element was measured.
The results are shown in Figure 115. The rotameter readings for each injector
(72 values) were averaged and the flow for each element was expressed as percent
of the average value for that injector. The injector elements were configured
in concentric rings around the igniter port. There were 12 elements in the inside
ring, 24 elements in the second or middle ring and 36 elements in the outside ring.
A different symbol was used for each ring in Figure 115. In general, significant
deviation from the average flow occurs only for elements in the center of the
injector (inside ring). The outside ring, which was closest to the chamber wall,
showed the least variation.

TABLE XLVII

IGNITER COLD FLOW DATA – OXIDIZER CIRCUIT

Step	Flow Rate, g/sec (lb/sec)				Inlet Pressure, N/cm² (psia)				$C_D A$, cm² (in.²)			
	SN 001	SN 001*	SN 003	SN 004	SN 001	SN 001	SN 002	SN 004	SN 001	SN 001	SN 002	SN 004
1	2.21 (.00487)	2.19 (.00482)	2.23 (.004492)	2.15 (.004474)	20.5 (29.7)	22.1 (32.0)	21.7 (31.4)	21.4 (31.0)	.149 (.0231)	.084 (.0130)	.093 (.0144)	.105 (.0163)
2	3.22 (.00711)	3.24 (.00715)	3.29 (.00725)	3.30 (.00728)	21.9 (31.7)	23.2 (33.7)	22.5 (32.7)	22.7 (32.9)	.112 (.0173)	.093 (.0144)	.099 (.0153)	.102 (.0158)
3	4.36 (.00961)	4.20 (.00926)	4.19 (.00923)	4.28 (.00943)	23.9 (34.7)	24.6 (35.4)	23.9 (34.7)	24.2 (35.1)	.107 (.0166)	.99 (.0154)	.101 (.0156)	.102 (.0158)
4	6.49 (.0143)	6.40 (.0141)	6.33 (.01395)	6.40 (.0141)	28.7 (41.7)	28.8 (41.8)	28.5 (41.4)	29.0 (42.0)	.107 (.0166)	.104 (.0161)	.103 (.0159)	.103 (.0160)
5	8.66 (.0191)	8.62 (.0190)	8.62 (.0190)	8.57 (.0189)	34.7 (49.7)	84.7 (50.4)	34.7 (50.4)	34.9 (50.7)	.110 (.0170)	.108 (.0167)	.108 (.0167)	.106 (.0165)
6	10.89 (.0240)	10.977 (.0242)	10.93 (.0241)	10.89 (.0240)	41.4 (60.1)	42.2 (61.2)	41.8 (60.7)	42.2 (61.2)	Sonic	Sonic	Sonic	Sonic
							Avg. =		.109 (.0169)**	.107 (.0156)**	.103 (.0159)**	.104 .0161
							σ (%) =		1.99**	6.5**	3.71**	2.01

* SN 001 ox circuit flowed twice – SN 003 not flowed.
**Excluding Step 1

TABLE XLVII

INJECTOR BODY COLD FLOW DATA (OX CIRCUIT)

Step	Flow Rate g/sec (lb/sec)	Manifold Pressure, N/cm² (psia)				C_DA, cm² (in.²)			
		SN 001	SN 002	SN 003	SN 004	SN 001	SN 002	SN 003	SN 004
1	18.1 (.04)	10.222 (14.826)	10.333 (14.987)	10.33 (14.98)	10.34 (14.99)	2.88 (.447)	2.90 (.449)	2.92 (.454)	2.30 (.449)
2	27.2 (.06)	10.462 (15.174)	10.553 (15.305)	10.55 (15.30)	10.553 (15.305)	2.80 (.434)	2.87 (.444)	2.88 (.446)	2.86 (.444)
3	36.3 (.08)	10.776 (15.629)	10.853 (15.741)	10.85 (15.73)	10.857 (15.746)	2.81 (.436)	2.87 (.445)	2.88 (.447)	2.86 (.444)
4	45.8 (.101)	11.232 (16.290)	11.279 (16.358)	11.28 (16.36)	11.286 (16.368)	2.79 (.432)	2.86 (.443)	2.85 (.442)	2.84 (.441)
5	61.2 (.135)	12.218 (17.720)	12.191 (17.681)	12.19 (17.68)	12.225 (17.730)	2.76 (.428)	2.84 (.440)	2.84 (.440)	2.81 (.436)
6	77.1 (.17)	13.698 (19.866)	13.545 (19.645)	13.54 (19.64)	13.616 (19.747)	2.70 (.418)	2.78 (.431)	2.78 (.431)	2.75 (.427)
7	90.7 (.20)	15.437 (22.388)	15.230 (22.089)	15.20 (22.04)	15.291 (22.177)	2.63 (.407)	2.68 (.416)	2.70 (.418)	2.67 (.414)
8	45.8 (.101)	11.215 (16.266)	11.279 (16.358)	11.26 (16.33)	11.279 (16.358)	2.81 (.436)	2.86 (.443)	2.88 (.446)	2.86 (.443)
					Avg. =	2.77 (.430)	2.83 (.439)	2.84 (.440)	2.82 (.437)
					σ (%) =	2.89	2.38	2.50	2.64

Figure 115a. Injector Body Ox Flow Distribution SN 001
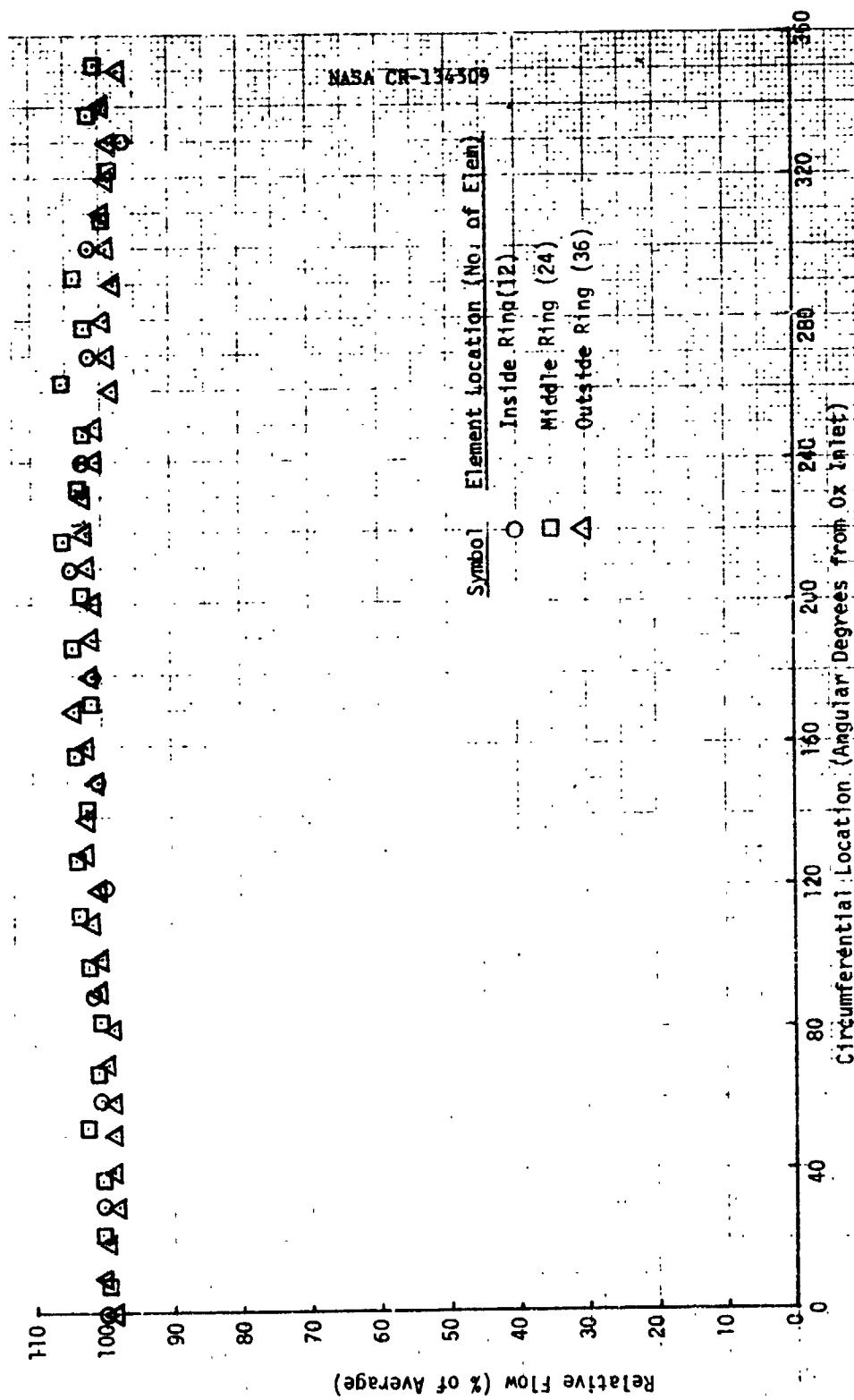
Figure 115b. Injector Body Ox Flow Distribution SN 002
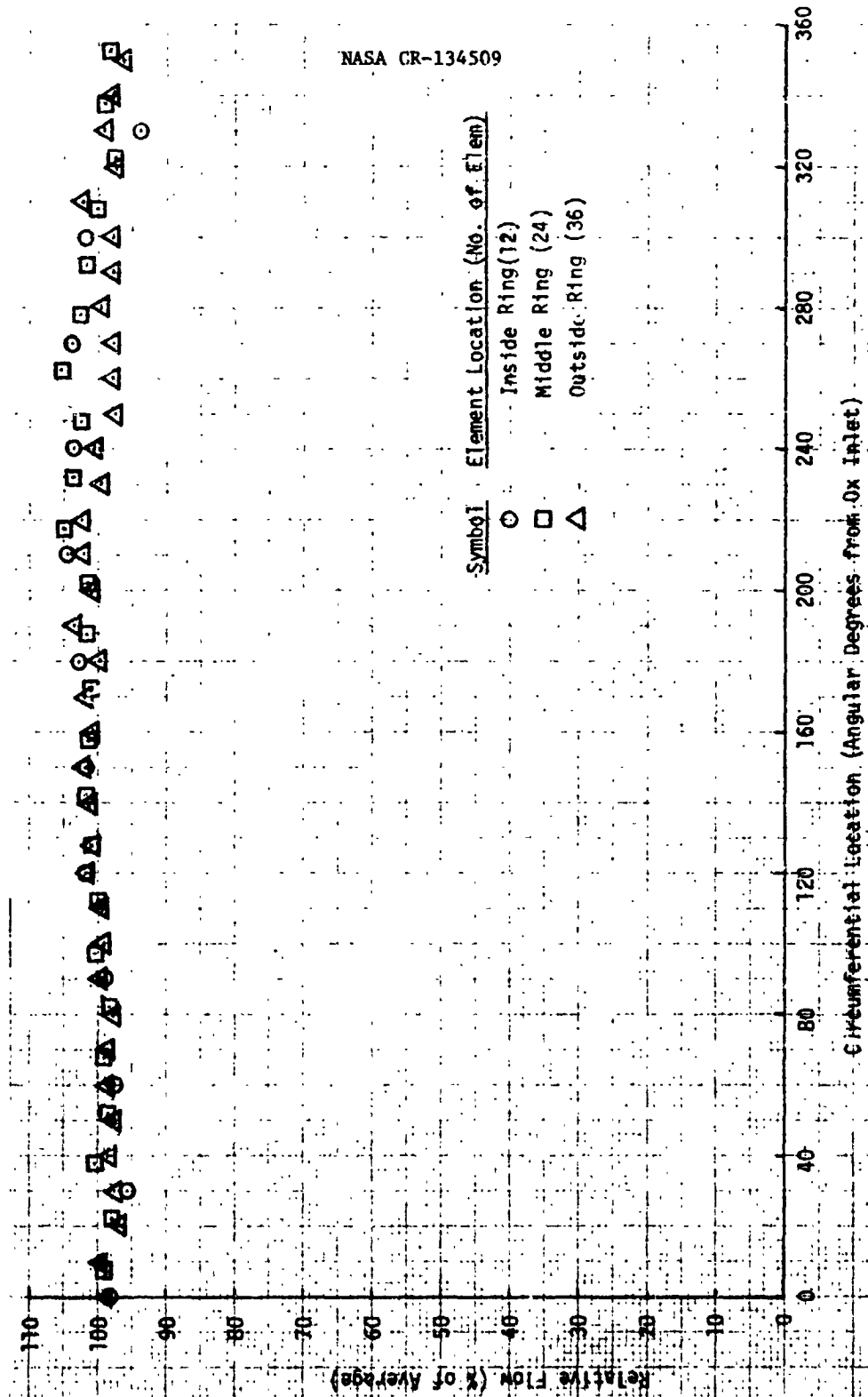
Figure 115c. Injector Body Ox Flow Distribution SN 002
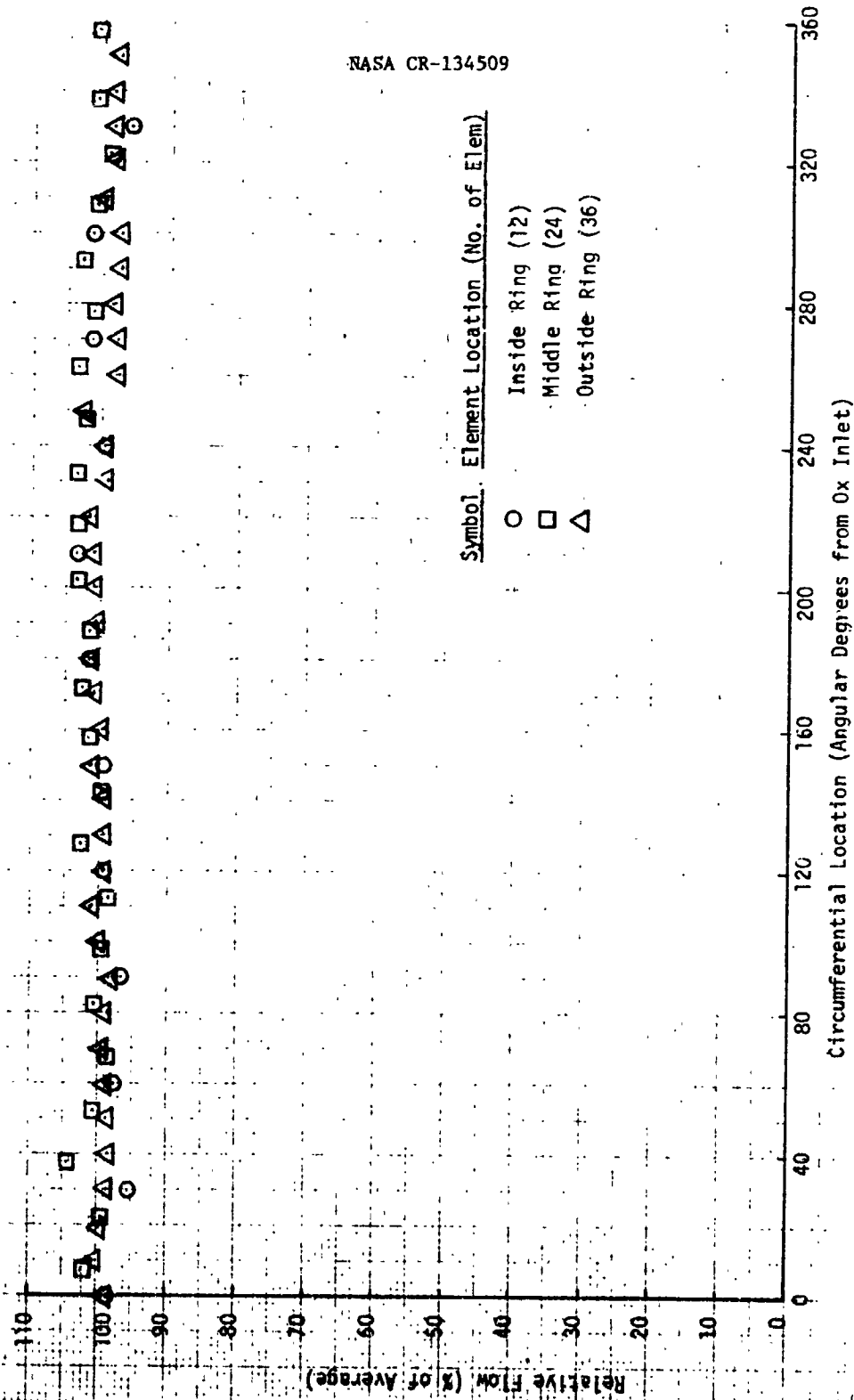
Figure 115d. Injector Body Ox Flow Distribution SN 004

4.5, Data Analysis (cont.)

Figure 115 depicts the flow uniformity pictorially. To provide numerical assessment the standard deviation from the average value was calculated for each injector and for each ring of elements. The results are presented in Table XLIX.

TABLE XLIX

STANDARD DEVIATIONS (%) - INJECTOR BODY COLD FLOW

ELEMENTS COMPARED	SN001	SN002	SN003	SN004
Inside Ring (12 elements)	3.9	2.3	3.4	2.6
Middle Ring (24 elements)	1.9	3.0	2.3	2.2
Outside Ring (36 elements)	1.2	1.6	2.0	1.5
All Elements (72 elements)	2.1	2.2	2.3	2.0

The injector assembly cold flow data are presented in Table L for the oxidizer circuit and in Table LI for the fuel circuit.

The oxidizer circuit C_D A values obtained for the completed injector (Table L) are 15 to 18% lower than the C_D A values obtained for the injector body. A lower C_D A means more resistance. There are two other differences in the oxidizer data -- body versus assembly. The average C_D A for injector SN001 is 5% lower than the average values of units SN002, 003 and 004. The differences in the SN001 injector body data from those obtained with the other three units was 2%. Finally, there is no systematic variation in the injector C_D A values with flow rate as there was with the C_D A values obtained for the injector body.

The greater restriction (lower C_D A values) apparent in the injector data versus the injector body data and in the SN001 injector data versus data for the other three injectors is probably due to the inlet

TABLE 1

INJECTOR COLD FLOW DATA - OX CIRCUIT

Step	Flow Rate g/sec (lb/sec)	Inlet Pressure N/cm² (psia)				Manifold Pressure N/cm² (psia)				$C_D A$, cm² (in.²)			
		SN 001	SN 002	SN 003	SN 004	SN 001	SN 002	SN 003	SN 004	SN 001	SN 002	SN 003	SN 004
1	18.1 (.04)	10.347 (15.007)	10.341 (15.071)	10.39 (15.07)	10.36 (15.026)	10.239 (14.856)	10.300 (14.938)	10.31 (14.95)	10.276 (14.904)	2.30 (.356)	2.41 (.374)	2.40 (.372)	2.37 (.368)
2	27.2 (.06)	10.719 (15.546)	10.722 (15.551)	10.71 (15.54)	10.698 (15.501)	10.465 (15.178)	10.520 (15.178)	10.54 (15.28)	10.513 (15.247)	2.24 (.348)	2.36 (.366)	2.37 (.367)	2.35 (.365)
3	36.3 (.08)	11.198 (16.241)	11.161 (16.187)	11.15 (16.17)	11.120 (16.128)	10.766 (15.614)	10.813 (15.683)	10.84 (15.72)	10.817 (15.688)	2.26 (.351)	2.37 (.368)	2.39 (.370)	2.38 (.369)
4	45.8 (.101)	11.877 (17.225)	11.762 (17.059)	11.75 (17.04)	11.719 (16.995)	11.208 (16.256)	11.228 (16.285)	11.29 (16.37)	11.262 (16.334)	2.26 (.351)	2.38 (.369)	2.39 (.370)	2.39 (.370)
5	61.2 (.135)	13.268 (19.243)	12.995 (18.847)	12.99 (18.84)	12.950 (16.783)	12.164 (17.642)	12.147 (17.617)	12.24 (17.75)	12.224 (17.729)	2.28 (.354)	2.41 (.373)	2.41 (.373)	2.41 (.374)
6	77.1 (.17)	15.227 (22.084)	14.724 (21.354)	14.72 (21.35)	14.666 (21.271)	13.606 (19.733)	13.542 (19.640)	13.67 (19.82)	13.653 (19.802)	2.28 (.353)	2.40 (.372)	2.40 (.372)	2.41 (.374)
7	90.7 (.20)	18.350 (26.614)	16.632 (24.122)	16.64 (24.14)	16.571 (24.033)	15.311 (22.206)	15.197 (22.040)	15.345 (22.255)	15.341 (22.250)	2.13 (.331)	2.39 (.370)	2.34 (.370)	2.39 (.371)
8	45.8 (.101)	11.850 (17.186)	11.735 (17.020)	11.728 (17.01)	11.695 (16.961)	11.184 (16.221)	11.219 (16.271)	11.27 (16.34)	11.246 (16.310)	2.28 (.353)	2.40 (.372)	2.40 (.372)	2.40 (.372)
									Avg. =	2.27 (.352)	2.39 (.370)	2.39 (.371)	2.39 (.370)
									σ (%) =	.80	.76	.51	.86

TABLE LI

INJECTOR COLD FLOW DATA – FUEL CIRCUIT

Step	Flow Rate, g/sec (lb/sec)	Inlet Pressure, N/cm² (psia)				Manifold Pressure, N/cm² (psia)				$C_D A$, cm² (in.²)			
		SN 001	SN 002	SN 003	SN 004	SN 001	SN 002	SN 003	SN 004	SN 001	SN 002	SN 003	SN 004
1	15.87 (.035)	10.34 (14.997)	10.4 (15.11)	10.4 (15.08)	10.38 (15.051)	10.21 (14.804)	10.27 (14.889)	10.2 (14.85)	10.22 (14.816)	2.04 (.316)	2.01 (.311)	2.01 (.311)	2.01 (.312)
2	22.68 (.050)	10.65 (15.443)	10.72 (15.551)	10.7 (15.50)	10.66 (15.467)	10.35 (15.018)	10.41 (15.100)	10.4 (15.06)	10.36 (15.026)	1.98 (.307)	1.97 (.305)	1.99 (.309)	2.00 (.310)
3	29.48 (.065)	11.06 (16.035)	11.13 (16.138)	11.1 (16.08)	11.08 (16.070)	10.54 (15.286)	10.59 (15.360)	10.6 (15.305)	10.54 (15.296)	1.97 (.305)	1.96 (.304)	1.96 (.307)	1.97 (.306)
4	35.24 (.0777)	11.49 (16.662)	11.54 (16.741)	11.5 (16.68)	11.49 (16.667)	10.73 (15.561)	10.78 (15.639)	10.7 (15.57)	10.73 (15.560)	1.94 (.301)	1.95 (.302)	1.99 (.308)	1.96 (.304)
5	49.9 (.11)	12.88 (13.680)	12.93 (18.759)	12.9 (18.70)	12.88 (18.680)	11.33 (16.427)	11.38 (16.506)	11.3 (16.43)	11.32 (16.422)	1.98 (.307)	1.98 (.307)	1.99 (.308)	1.99 (.308)
6	68.0 (.15)	15.30 (22.182)	15.36 (22.285)	15.3 (22.23)	15.31 (22.201)	12.30 (17.847)	12.36 (17.926)	12.3 (17.82)	12.27 (17.794)	1.99 (.309)	1.99 (.308)	1.99 (.309)	1.99 (.309)
7	81.6 (.18)	17.43 (25.292)	17.48 (25.356)	17.5 (25.34)	17.47 (25.336)	13.19 (19.131)	13.24 (19.199)	13.1 (19.07)	13.15 (19.067)	2.03 (.315)	2.03 (.314)	2.03 (.314)	2.03 (.314)
8	34.93 (.077)	11.47 (16.633)	11.52 (16.702)	– –	11.47 (16.643)	10.71 (15.541)	10.77 (15.624)	– –	10.71 (15.541)	1.96 (.304)	1.97 (.305)	– –	1.97 (.306)
									Avg. =	1.97 (.306)	1.98 (.307)	1.99 (.308)	1.99 (.309)
									σ (%) =	.88	1.26	.89	1.10

4.5, Data Analysis (cont.)

line/dome interface configuration. The injector body data were obtained with a
single inlet configuration, namely that of the flow fixture (Figure 71). The
inlet line to fixture joint was accessible from the "inside" after welding; there-
fore, the geometry of the inlet line discharge area could be cleaned up. After
the weld of the inlet line to the dome of the injector was made the internal
geometry could not be cleaned up. Moreover, injector SN001 was the first article
and the machining of the opening in the dome, the fit of the inlet line to the
opening and the weldment were not as clean as was the case for the subsequent
assemblies which benefited from the techniques learned with SN001.

The C_D A values for the oxidizer circuit are
tabulated in Table LII as they were obtained for the cold flow of the injector
body, injector assembly, and complete ITA. The ITA flow test of the oxidizer
circuit was basically a repeat of the injector flow test. There were no changes
in the oxidizer flow circuit. The circuit was flowed as a thruster to verify that
subsequent fabrication processes had not introduced foreign material, etc., that
would alter the hydraulics or disrupt the uniform flow distribution.

TABLE LII

OXIDIZER CIRCUIT CHARACTERISTICS

CONFIGURATION	C_D A, cm^2 (in.^{2})				
	SN001	SN002	SN003	SN004	AVG.
Injector Body	2.77 (.430)	2.83 (.439)	2.84 (.440)	2.82 (.437)	2.82 (.436)
Injector Assembly	2.27 (.352)	2.39 (.370)	2.39 (.371)	2.39 (.370)	2.36 (.366)
ITA	2.31 (.358)	2.46 (.382)	2.34 (.362)	2.39 (.370)	2.38 (.368)

Page 332

4.5, Data Analysis (cont.)

The fuel circuit hydraulic characteristics, as summarized in Table LI, were very consistent. The C_D A values have a spread of approximately 5% over a flow rate range that was varied by a factor of 5. The spread in the average C_D A values for the four injectors is 1%.

Like the oxidizer injector body data the injector assembly fuel circuit data were obtained using a test fixture. The fixture shown in Figure 71 was used to simulate the regen channels and to close out the fuel manifold. On the other hand, the measurements made for the ITA (Table XLIII) were made on the complete fuel circuit (inlet line, torus, regen channels, manifold and injector) and with the ffc circuit flowing (additional pressure drop in the inlet line). The hydraulic characteristics as determined for the injector fuel circuit and for the ITA fuel circuit are compared in Table LIII. The ITA circuit had 28% more resistance than the injector plus fixture circuit. The spread in the average C_D A values for the four ITA units was 5%.

TABLE LIII

FUEL CIRCUIT CHARACTERISTICS

| CONFIGURATION | C_D A, cm^2 ($in.^2$) | | | | |
	SN001	SN002	SN003	SN004	AVG.
Injector	1.97	1.98	1.99	1.99	1.98
	(.306)	(.307)	(.308)	(.309)	(.3075)
ITA	1.51	1.54	1.56	1.59	1.55
	(.234)	(.238)	(.242)	(.246)	(.240)

4.5, Data Analysis (cont.)

The C_D A values for the injector circuits (Tables XLVIII, L, LI, LII and LIII) were calculated using the pressure ratio of the chamber (atmospheric pressure) to inlet pressure. These data, while suitable for the purpose of the cold flow testing, namely checkout (fabrication/design), are not exactly applicable to the operating conditions. There are two factors that preclude and exact correlation of the C_D A values to test firing conditions: (1) in cold flow testing the inlet pressure was measured in a fitting upstream of the inlet line flanges; a balance orifice was subsequently installed in the inlet flange; (2) the flow of the propellants in the premix cup during a firing results in a pressure drop that is a function of the flow of both propellants. Thus, the cold flow data are based on atmospheric back pressure in the chamber with negligible cup pressure loss while in actual operation the circuit back pressure depends not only on chamber pressure, but the flow rate of the other propellants.

The cold flow testing was based on Mach number simulation. A GN_2 flow rate was calculated to give the same pressure ratio (chamber to inlet, for example) as would be achieved with the propellants at nominal conditions. The scaled down test conditions for the injector were presented in Table XXIX. In Table LIV the test conditions are compared to the predicted test manifold pressures, and operating manifold pressures are projected from the test data for comparison to the design values. The manifold pressures that are projected for nominal operation from the test data are 4.8 N/cm^2 (7 psia) lower than design for the oxidizer and 12.4 N/cm^2 (18 psia) lower than design for the fuel. The lower pressures are at least in part due to the premix cup pressure drop that was not reproduced in the cold flow testing.

4.5, Data Analysis (cont.)

<div align="center">TABLE LIV</div>

<div align="center">INJECTOR MANIFOLD PRESSURES PROJECTED FROM COLD FLOW DATA</div>

	OXIDIZER				FUEL			
		TEST		PREDICTED			TEST		PREDICTED
	DESIGN	DESIGN		(DATA	DESIGN	DESIGN			(DATA
	VALUE	SIMULATION	DATA	SCALED UP)	VALUE	SIMULATION	DATA	SCALED UP)
Flow Rate,	1252	45.8	45.8	1252	242	25.2	35.2	242
g/sec (lb/sec)	(2.76)	(.101)	(.101)	(2.76)	(.545)	(.0777)	(.077)	(.545)
Manifold Pressure,	234	11.5	11.237	229	232	11.2	10.749	219
N/cm^2 (psia)	(340)	(16.7)	(16.298)	(333)	(336)	(16.3)	(15.577)	(318)
Chamber Pressure,	207	10.1	10.1	207	207	10.1	10.1	207
N/cm^2 (psia)	(300)	(14.7)	(14.7)	(300)	(300)	(14.7)	(14.7)	(300)

     The injector flow uniformity data are summarized
in Figure 116 for the oxidizer circuit and in Figure 117 for the fuel circuit. In
comparing the flow uniformity data for the ox circuit obtained for the injector
body (Figure 115) to that obtained for the injector assembly (Figure 116) it can be
seen that there is slightly more scatter in the injector assembly data, especially
for unit SN001. The standard deviation of the flows measured for each oxidizer
element from the average for each injector is summarized in Table LV. By comparison
to corresponding standard deviations in the data obtained with the injector body
it can be seen that while there is more scatter in the injector data than the in-
jector body data. The injector flow distribution is quite uniform with 95% (2 σ)
of the data falling within ± 5% of the average flow rate.

     In Figure 116a one data point (60°) is shown at 84%
of the average flow rate. The point was included to show that the flow measurement
technique was sensitive to flow variation (probe pressure drop was low). Probing
the element increased the flow to about the average value indicating the presence
of a foreign object or burr at the inlet to the tube.
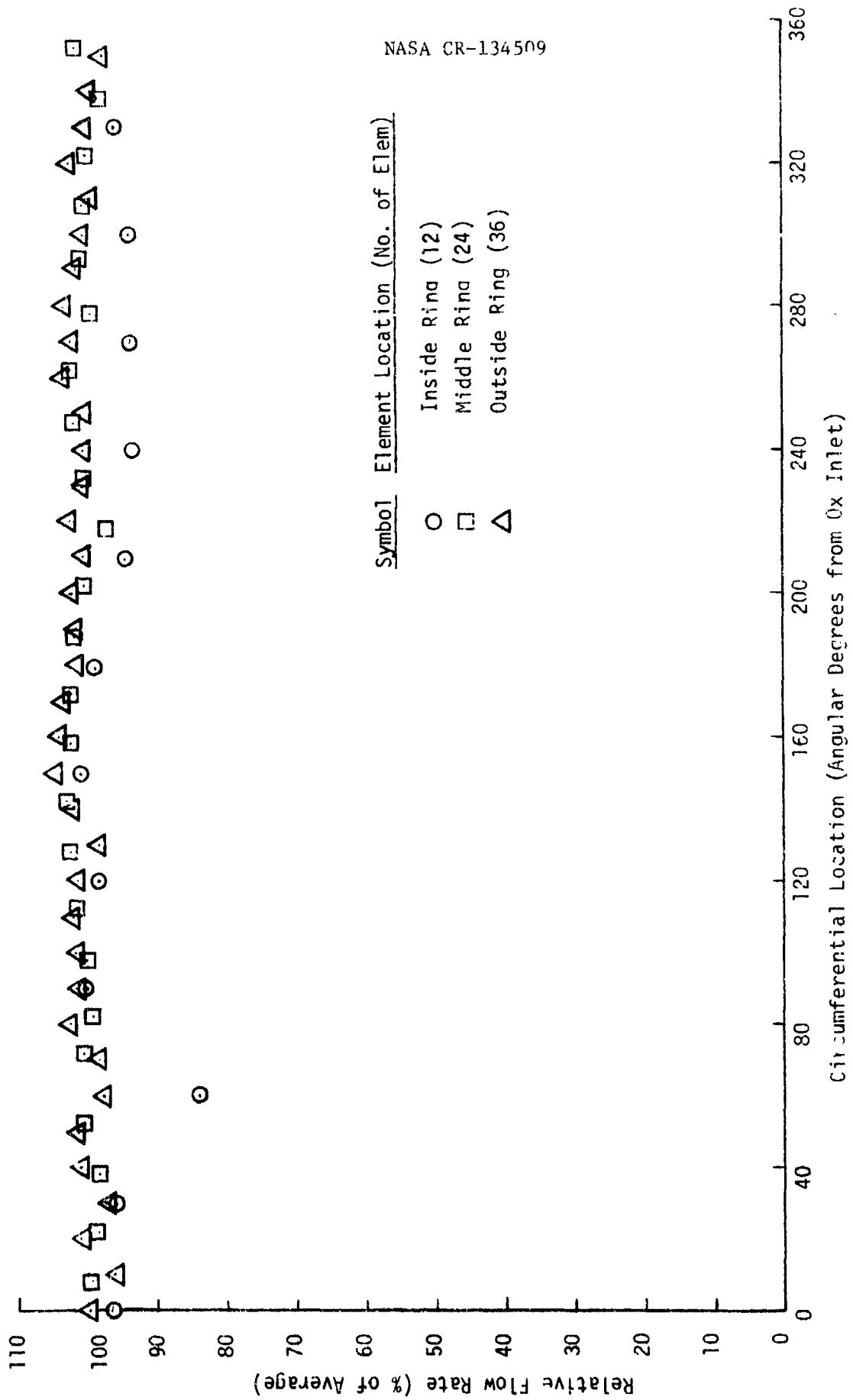
Figure 116a. Injector Assembly Ox Distribution - SN 001

NASA CR-134509
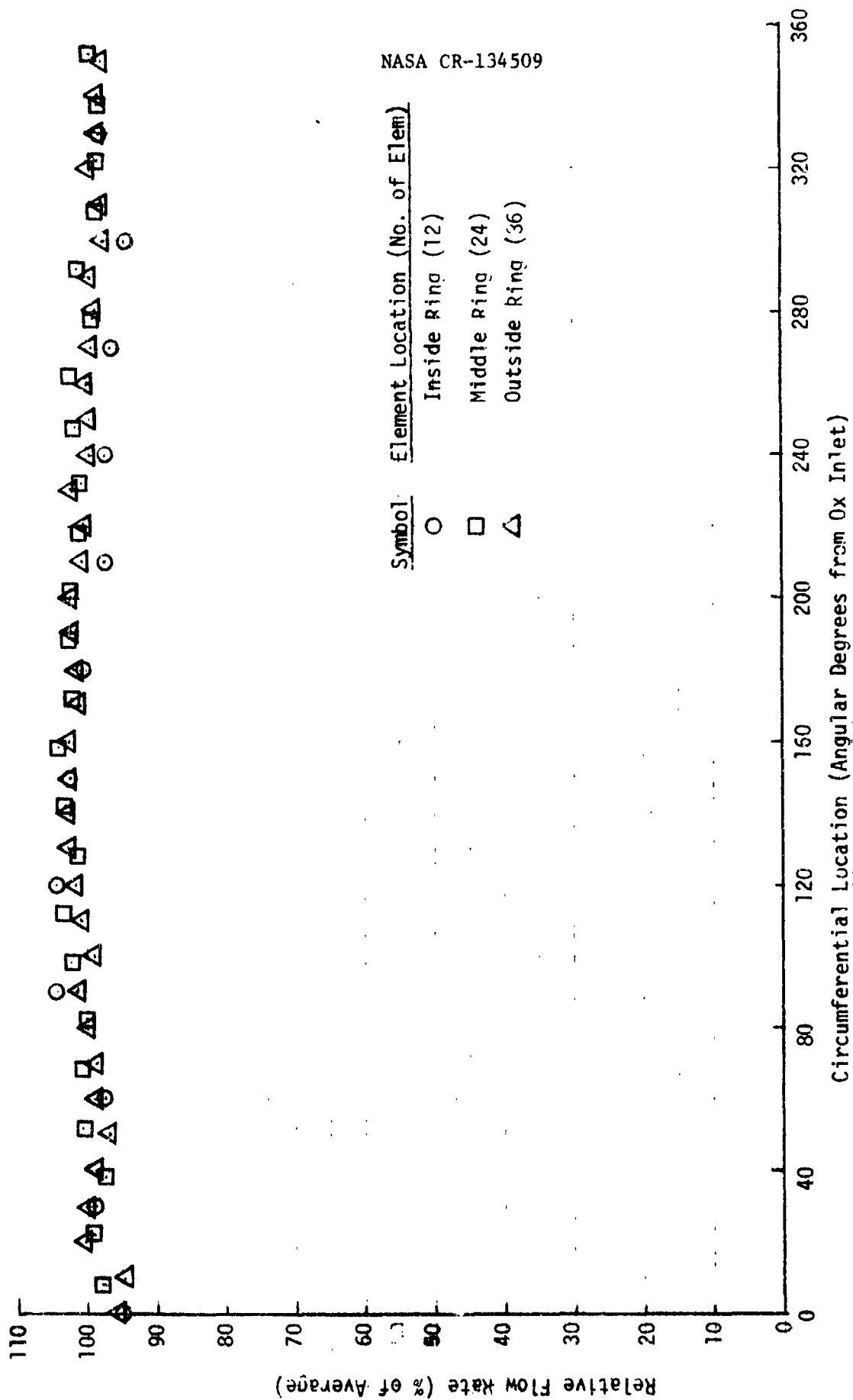
Figure 116b. Injector Assembly Ox Distribution -- SN 002
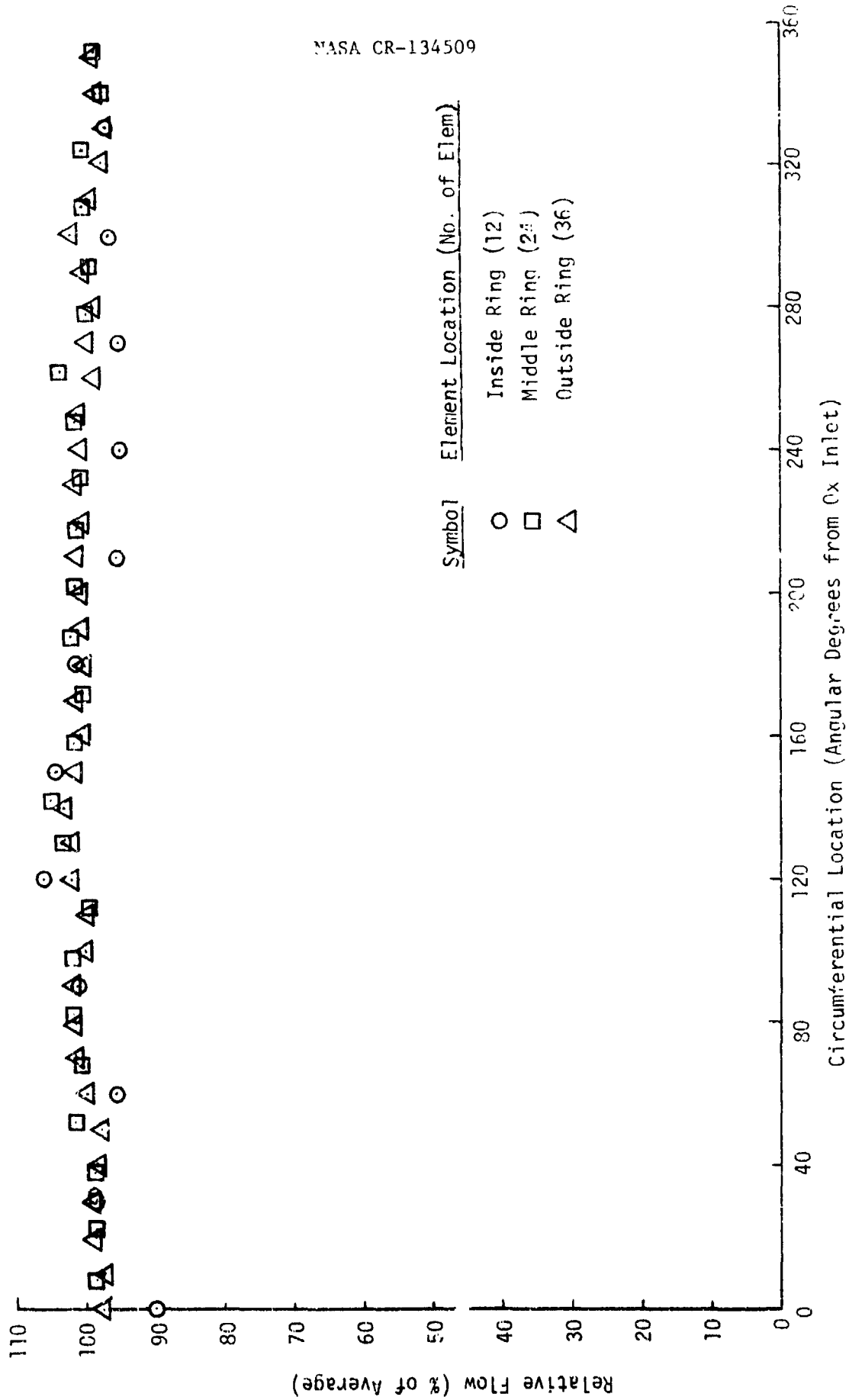
Figure 116c. Injector Assembly Ox Distribution – SN 003
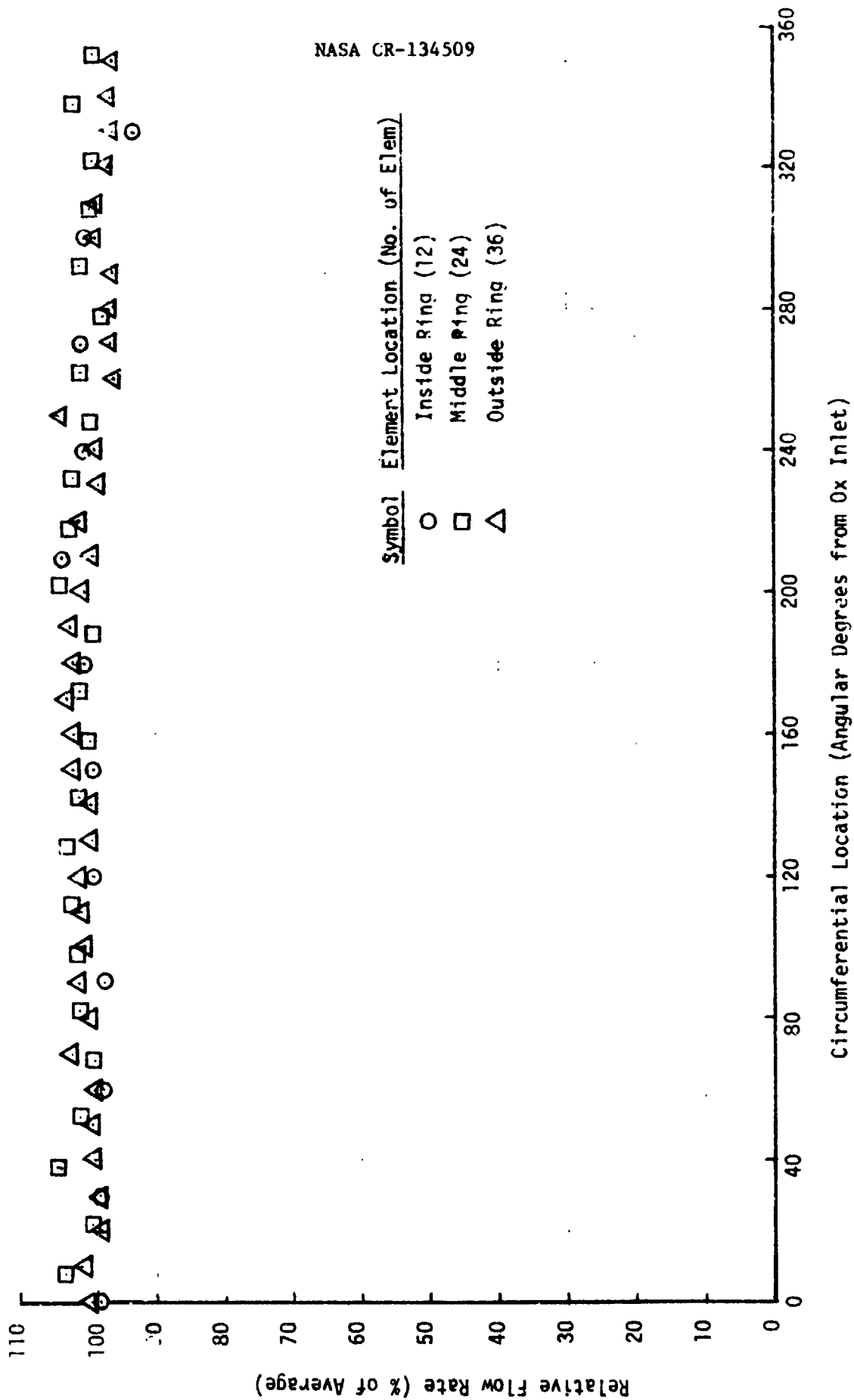
Figure 116d. Injector Assembly Ox Distribution - SN 004
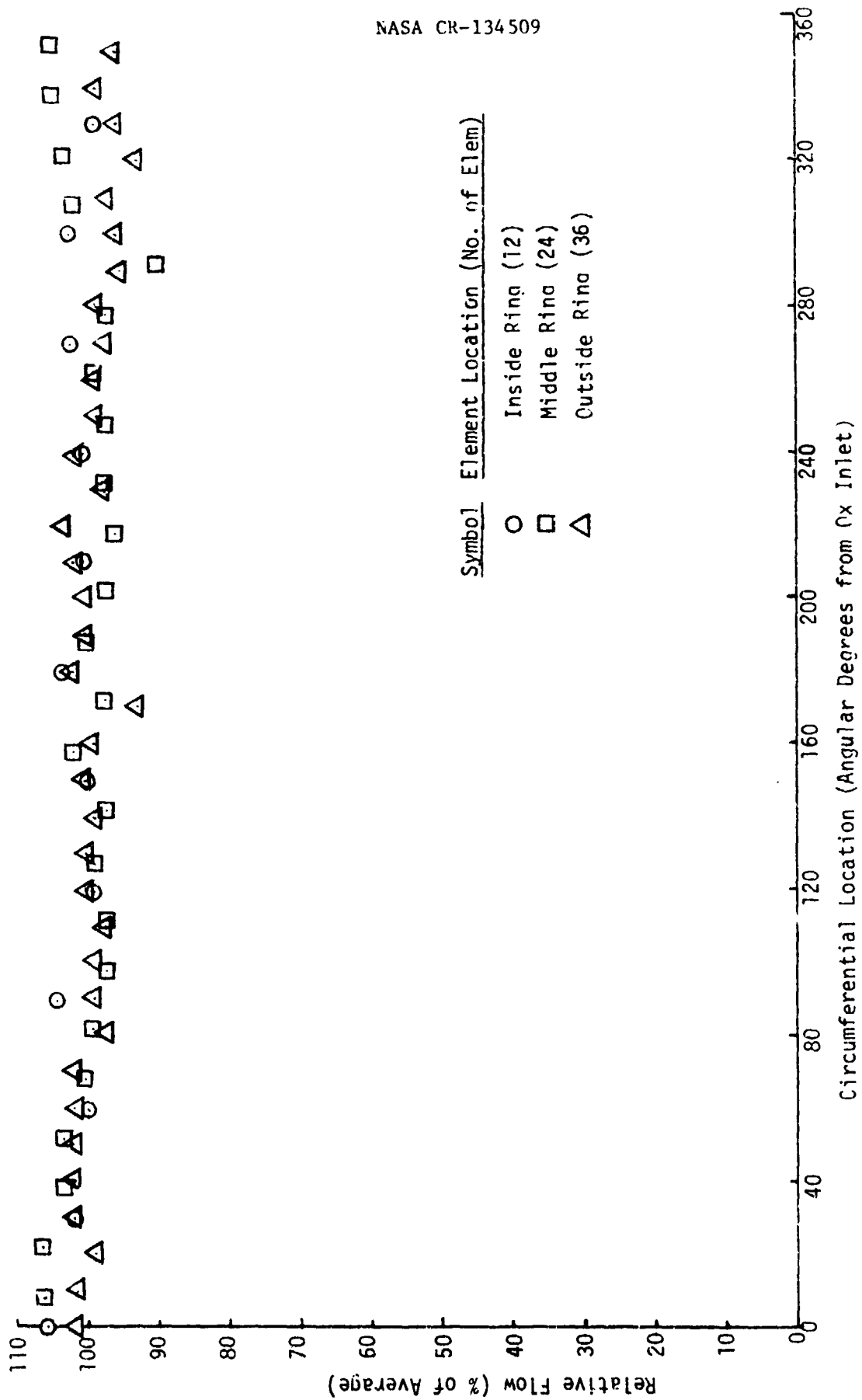
Figure 11/a. Injector Fuel Ox Distribution - SN 001
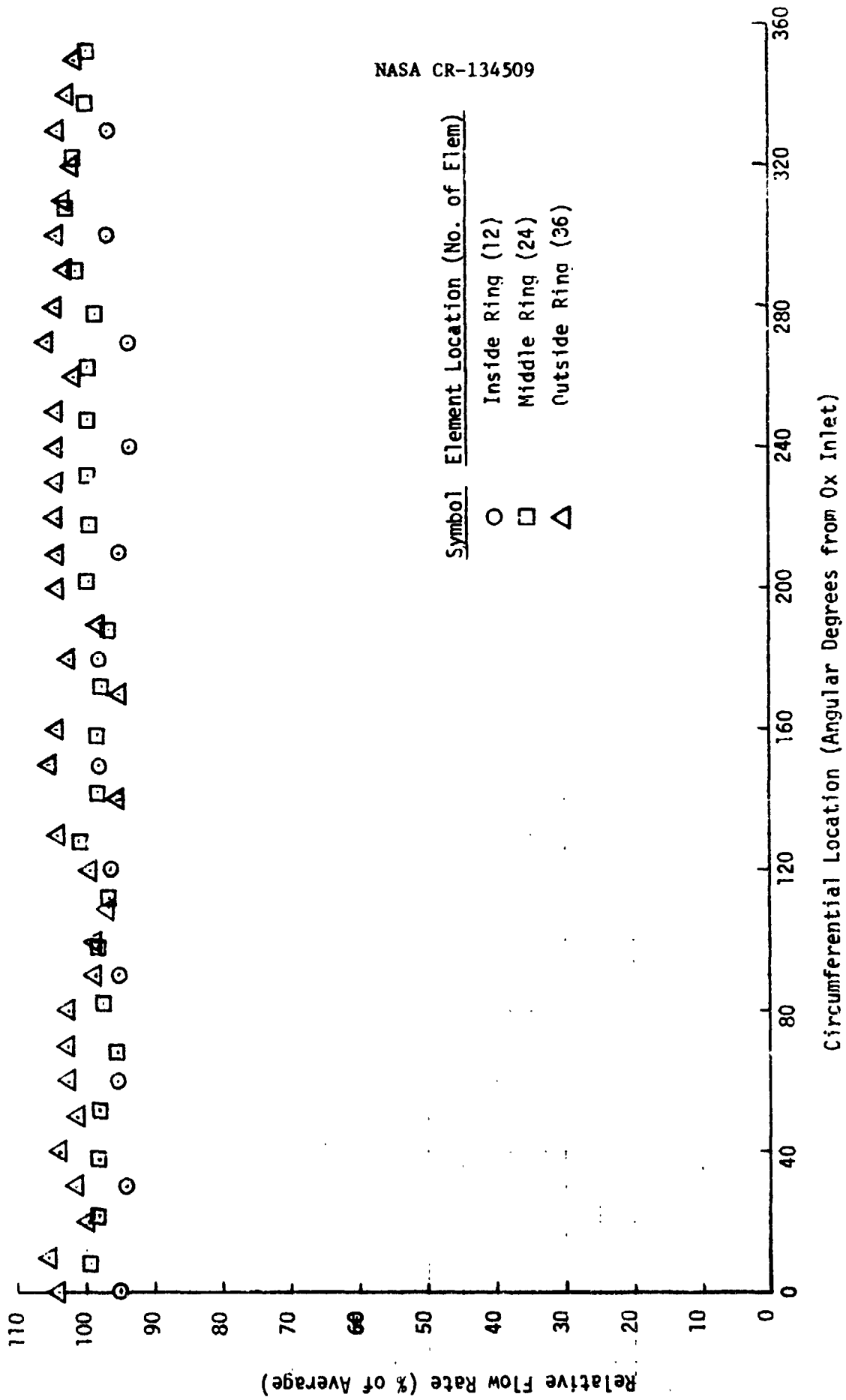
Figure 117b. Injector Fuel Ox Distribution – SN 002
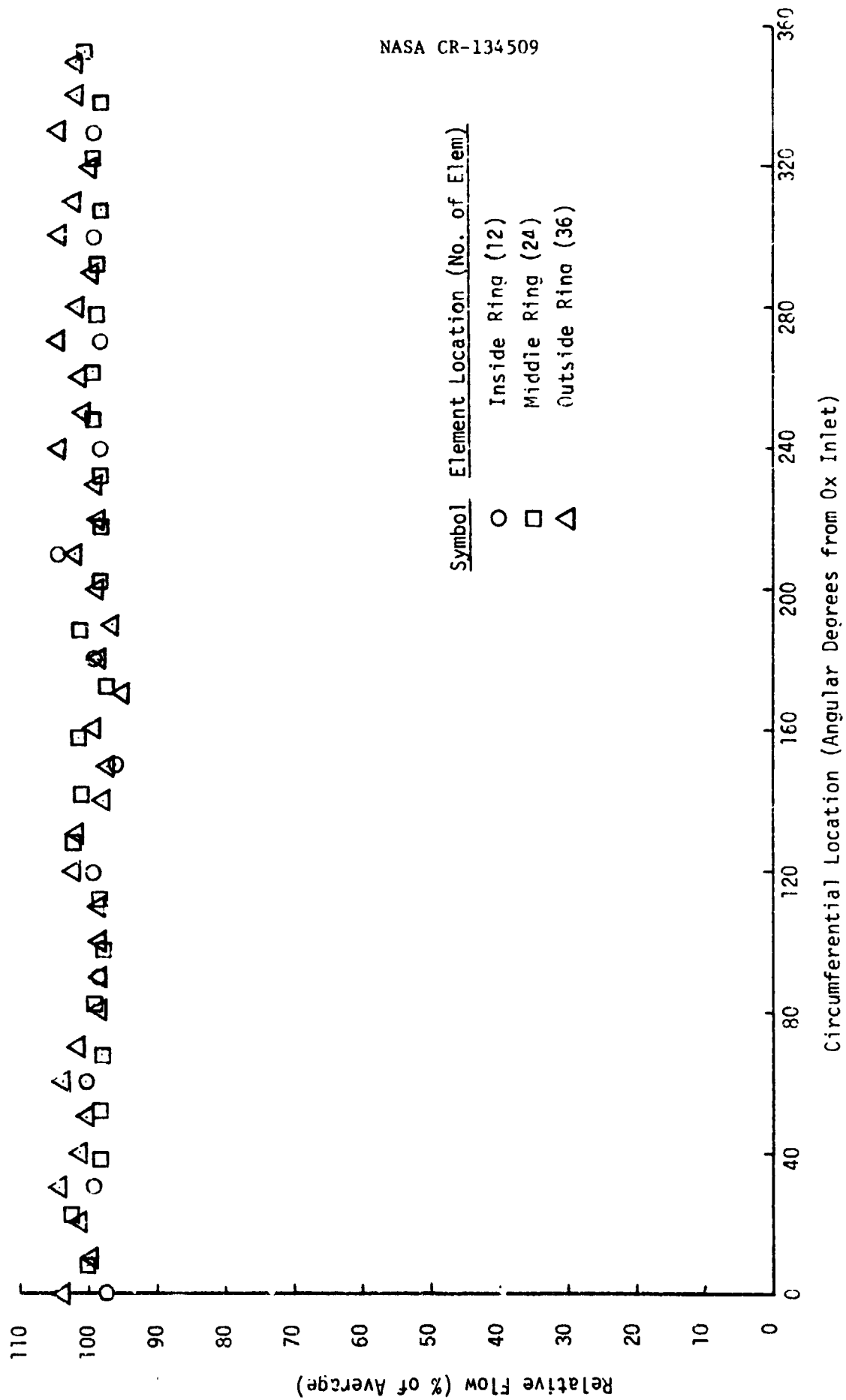
Figure 117c. Injector Fuel Ox Distribution - SN 003
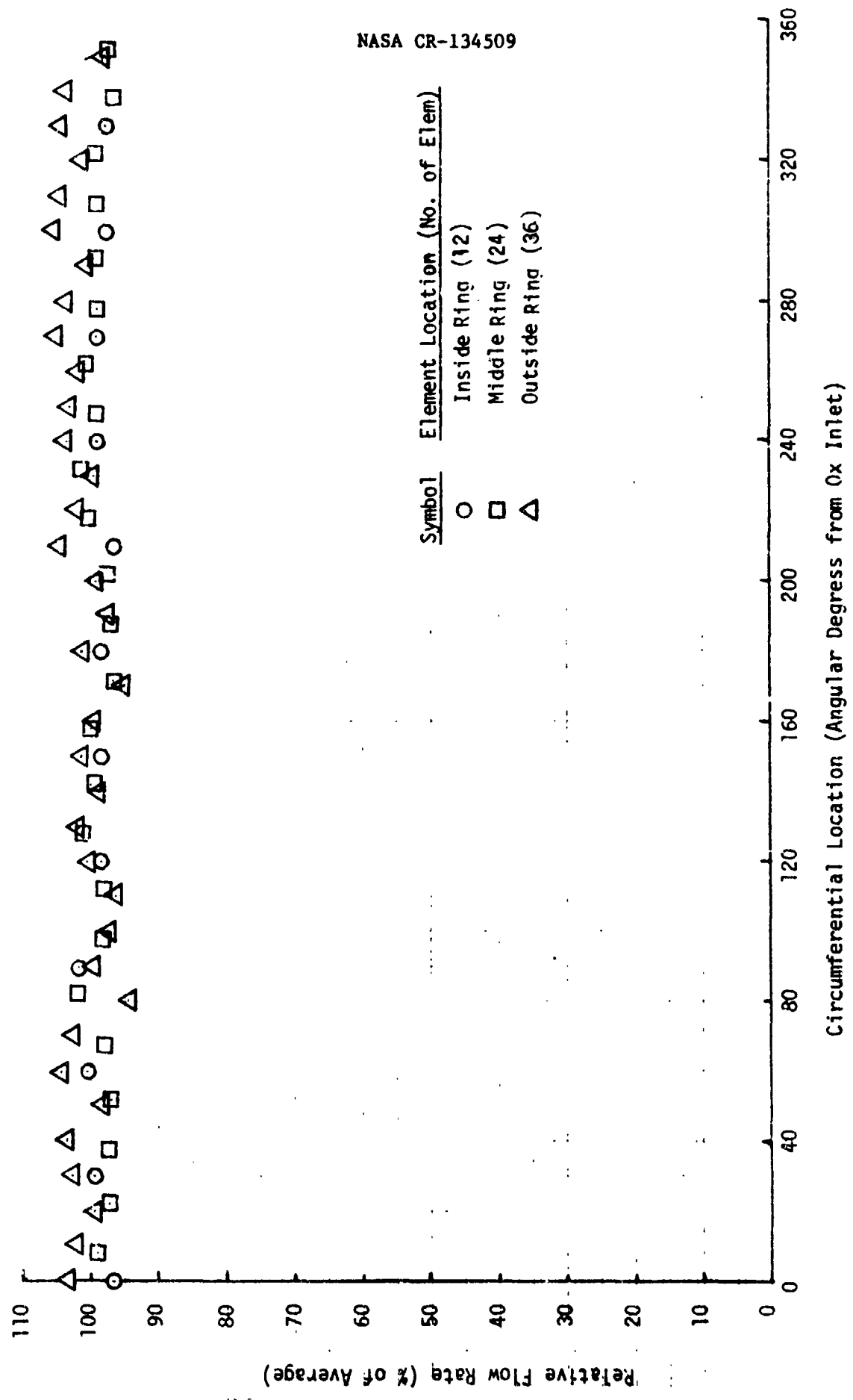
Figure 117d. Injector Fuel Ox Distribution – SN 004

4.5, Data Analysis (cont.)

TABLE LV

STANDARD DEVIATION (%) - INJECTOR ASSEMBLY OXIDIZER CIRCUIT

ELEMENTS COMPARED	SN001	SN002	SN003	SN004
Inside Ring (12 elements)	6.43	3.48	4.98	2.72
Middle Ring (24 elements)	1.65	2.04	1.95	2.01
Outside Ring (36 elements)	2.10	1.87	1.63	2.27
All Elements (72 elements)	3.08	2.22	2.54	2.23

There is slightly more scatter in the fuel flow uniformity data than in the ox data as shown in Figure 117 and summarized as standard deviation in Table LVI. In general, the distribution across the injector face is uniform, with 95% (2σ) of the fuel elements flowing within $\pm$ 5.8% of the average value.

TABLE LVI

STANDARD DEVIATION (%) - INJECTOR ASSEMBLY FUEL CIRCUIT

ELEMENTS COMPARED	SN001	SN002	SN003	SN004
Inside Ring (12 elements)	2.82	4.56	2.2	1.78
Middle Ring (24 elements)	4.93	2.01	1.56	2.01
Outside Ring (36 elements)	2.71	3.53	2.59	3.04
All Elements (72 elements)	3.56	3.27	2.20	2.52

4.5, Data Analysis (cont.)

4.5.2.1.4 Chamber Cold Flow

The chamber cold flow testing consisted of flow of the ff_c circuit with the regen circuit blocked off and flow of the regen and ffc circuits. The fixtures shown in Figure 75 were used to complete the torus and simulate the inlet line, and to block off the regen passages for flowing the ff_c passages.

The ff_c cold flow data are summarized in Table LVII. The C_D A values are based on the inlet pressure to the flow fixture and atmospheric back pressure. The C_D A value increases with increasing flow rate. There is a systematic 3% variation in the C_D A value with a 400% change in flow rate ($\pm$ 25% variation in pressure ratio). The conditions marked sonic in Table LVII correspond to pressure ratio in which:

$$P_d/P \leqslant (\frac{2}{\gamma+1})^{\frac{\gamma}{\gamma-1}}$$

where:

P = inlet pressure

P_d = discharge pressure

γ = ratio of specific heats

The average C_D A of chamber SN001 differs by approximately 5% from the other three chambers. The ffc inlet orifices were drilled to size as part of the cold flow testing to size the orifices. The orifices in the other three chambers were made by EDM*. There were probably small burrs on the discharge end of the SN001 ffc orifice. EDM leaves no burr

---

* Electric Discharge Machining

Page 345

TABLE LVII

CHAMBER COLD FLOW DATA - ffc CIRCUIT

Step	Flow Rate, g/sec (lb/sec)	Inlet Pressure, N/cm² (psia)				$C_D A$, cm² (in.²)			
		SN 001	SN 002	SN 003	SN 004	SN 001	SN 002	SN 003	SN 004
1	9.07 (.020)	13.90 (20.166)	13.52 (19.611)	13.5 (19.66)	13.54 (19.640)	.0311 (.0482)	.0326 (.0505)	.0324 (.0502)	.0325 (.0504)
2	4.54 (.010)	11.24 (16.297)	11.02 (15.986)	11.06 (16.035)	11.03 (16.001)	.0287 (.0445)	.0308 (.0478)	.0306 (.0469)	.0310 (.0481)
3	5.90 (.013)	11.86 (17.203)	11.60 (16.829)	11.6 (16.85)	11.62 (16.848)	.C298 (.0462)	.0316 (.0490)	.0314 (.0487)	.0317 (.0491)
4	7.26 (.016)	12.65 (18.354)	12.37 (17.945)	12.37 (17.945)	12.34 (17.891)	.0304 (.0471)	.0318 (.0493)	.0318 (.0493)	.0319 (.0499)
5	9.07 (.020)	13.97 (20.264)	13.55 (19.660)	13.5 (19.66)	13.54 (19.640)	.0308 (.0478)	.0324 (.0502)	.0323 (.0501)	.0325 (.0~4)
6	12.25 (.027)	16.67 (24.183)	16.13 (23.392)	16.1 (23.43)	16.05 (23.274)	.0321 (.0498)	.0324 (.0518)	.0333 (.0517)	.0337 (.0522)
7	14.97 (.033)	19.43 (28.174)	18.72 (27.153)	18.79 (27.25)	18.67 (27.084)	(Sonic)	.0344 (.0534)	.0343 (.0532)	.0346 (.0536)
8	18.14 (.040)	(Sonic)	(Sonic)	(Sonic)	(Sonic)	(Sonic)	(Sonic)	(Sonic)	(Sonic)
9	9.07 (.020)	13.99 (20.289)	13.56 (19.670)	13.62 (19.76)	13.55 (19.650)	.0308 (.04771)	.0324 (.0502)	.0321 (.0497)	.0325 (.0504)
					Avg. =	.031 (.0477)	.032 (.0503)	.032 (.0500)	.0326 (.0505)
					σ (%) =	3.53	3.49	3.79	3.72

4.5, Data Analysis (cont.)

as cutting is accomplished by a spark. The excellent agreement of the ffc C_D A average values for chambers SN002, 003 and 004 indicate that the fabrication process was highly repeatable.

The cold flow data for the chambers' regen sections are shown in Table LVIII. There is a 22% variation in the C_D A values with a 400% change in the flow rate (pressure ratio +8%, -16%), which indicates that the simple subsonic flow expression does not provide an exact description of the distributed pressure drop -- regen system over a wide range of conditions.

The flow rates shown in Table LVIII are total (regen plus ffc) measured flow rates. The C_D A values were based on the regen flow rate which was determined by subtracting out the ffc flow rate. The ffc flow rates were calculated from the ratio of atmospheric pressure (back pressure) to inlet pressure using the expression:

$$\dot{W}_{ffc} = b - ar$$

where:

a = correlating constant

b = correlating constant

r = ratio of back pressure to inlet pressure

$\dot{W}_{ffc}$ = film coolant flow rate

The correlation of the ffc flow data by a linear expression in terms of pressure ratio is shown in Figure 118. The correlation coefficients are presented in Table LVIX as well as the standard deviation of the ffc cold flow data from the flow calculated using the correlation. The standard deviations expressed as % of nominal flow, 9.07 g/sec (.02 lb/sec), are 1.85, 1.52, 1.49 and 1.38% for chambers SN001, 002, 003 and 004, respectively.

Page 347

TABLE LVIII

CHAMBER COLD FLOW DATA - REGEN CIRCUIT

Step	Flow Rate, g/sec (lb/sec)	Inlet Pressure, N/cm² (psia)				$C_D A$, cm² (in.²)			
		SN 001	SN 002	SN 003	SN 004	SN 001	SN 002	SN 003	SN 004
1	34.9 (.077)	11.27 (16.346)	11.17 (16.197)	11.17 (16.20)	11.19 (16.236)	1.90 (.294)	1.90 (.295)	1.91 (.296)	1.90 (.294)
2	17.2 (.038)	10.46 (15.171)	10.36 (15.031)	10.38 (15.06)	10.40 (15.080)	1.73 (.269)	1.76 (.273)	1.72 (.266)	1.73 (.268)
3	23.1 (.051)	10.67 (15.474)	10.58 (15.340)	10.58 (15.35)	10.61 (15.384)	1.83 (.284)	1.83 (.284)	1.83 (.283)	1.82 (.282)
4	29.0 (.064)	10.93 (15.856)	10.84 (15.717)	10.85 (15.74)	10.87 (15.771)	1.88 (.292)	1.89 (.293)	1.87 (.290)	1.87 (.290)
5	34.9 (.077)	11.26 (16.339)	11.16 (16.182)	11.17 (16.20)	11.20 (16.246)	1.90 (.295)	1.92 (.297)	1.91 (.296)	1.89 (.293)
6	46.7 (.103)	11.98 (17.375)	11.87 (17.221)	11.89 (17.25)	11.93 (L7.304)	1.99 (.309)	1.99 (.310)	1.99 (.308)	1.97 (.306)
7	58.5 (.129)	12.84 (18.624)	12.74 (18.474)	12.75 (18.49)	12.82 (18.592)	2.06 (.319)	2.06 (.319)	2.06 (.319)	2.03 (.315)
8	69.8 (.154)	13.80 (20.020)	13.74 (19.929)	13.22 (19.17)	13.81 (20.026)	2.12 (.328)	2.12 (.328)	2.30 (.356)	2.08 (.323)
9	34.9 (.077)	11.23 (16.287)	11.15 (16.172)	11.17 (16.20)	11.17 (16.197)	1.94 (.300)	1.94 (.298)	1.91 (.296)	1.93 (.299)
					Avg =	1.93 (.299)	1.94 (.300)	1.94 (.301)	1.92 (.297)
					σ (%) =	6.0	5.7	8.5	5.6
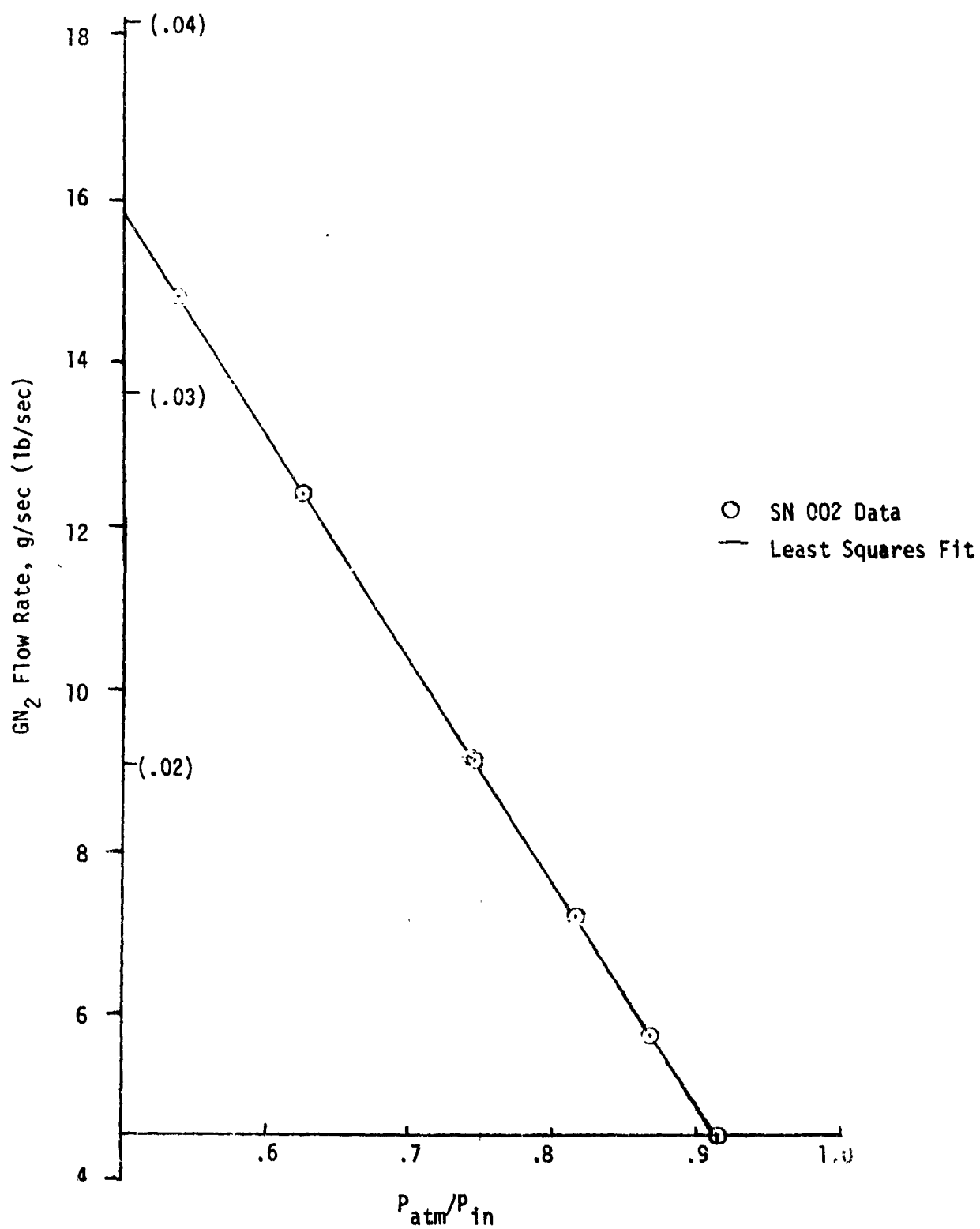
Figure 118. Correlation of GN_2 Cold Flow of ffc Circuit

Page 349

4.5, Data Analysis (cont.)

TABLE LVIX

FFC CORRELATION PARAMETERS

	SN001	SN002	SN003	SN004
b, g/sec (lb/sec)	28.73	29.44	29.42	29.61
	(.96334)	(.06491)	(.064857)	(.065285)
a, dimensionless	.05916	.06012	.060197	.060412
σ, g/sec (lb/sec)	.168	.138	.135	.125
	(.000371)	(.000305)	(.000298)	(.000276)
	1.85%	1.52%	1.49%	1.38%

$$\dot{W}_{ff_c} = b - a\left(\frac{Patm}{Pin}\right) \pm \sigma \text{ (standard deviation)}$$

The results of the regen channel flow uniformity measurements are shown in Figure 119. The channel location relative to the inlet was measured clockwise from the discharge end of the passage (forward end). For all four chambers the highest flow occurred approximately 5° clockwise from the inlet and the lowest flow occurred approximately 45° clockwise from the inlet. The reason for this flow pattern can be visualized with the aid the thruster top view (Figure σ, p. 42, Sheet 1 of 2). Momentum forces would cause the gaseous H_2 to flow to the outside of the curvature in the fuel inlet line. Thus, the H_2 entered the torus from the side of the inlet line located clockwise from the tube center line and this resulted in the slightly higher flow rates approximately 5° from the inlet center line. The momentum of the GH_2 which produced the clockwise bias in the flow pattern would also result in the bulk of the GH_2 flowing in a clockwise direction. This would produce a high cross velocity at the inlet to the channels located approximately 45° from the inlet and would account for the low flow rate at that location. Although most pronounced for chamber SN001 all the data show a higher than average flow approximately 270° from the inlet. This suggests no cross velocity and was probably the location of the null point. The location of the null point at 270° from the inlet instead of 180° is consistent with the hypothesis that the bulk of the hydrogen flowed in a clockwise direction in the torus.
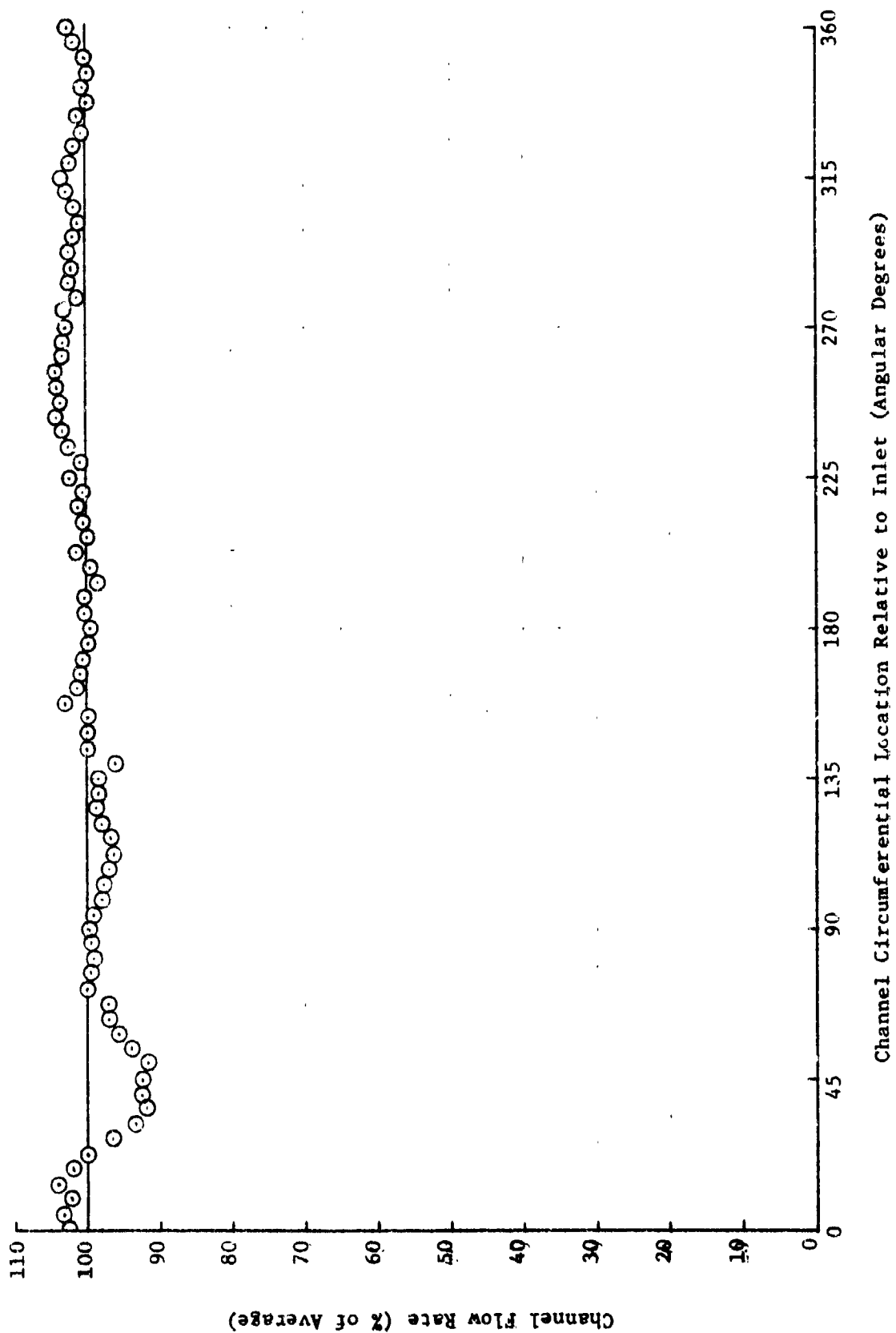
Figure 119a. Regen Channel Flow Distribution - Channel SN 001
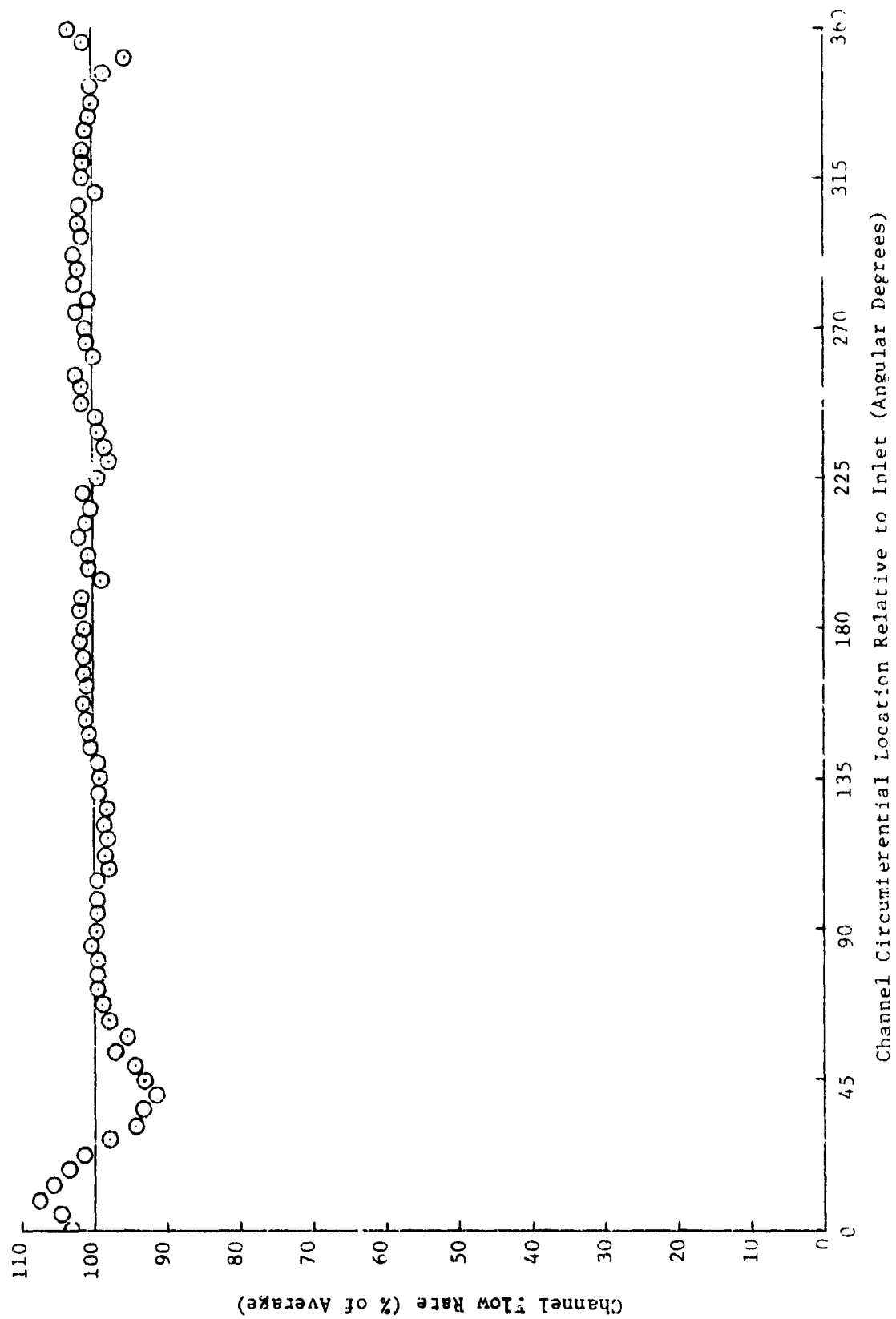
Figure 119b. Regen Channel Flow Distribution - Channel SN 002.
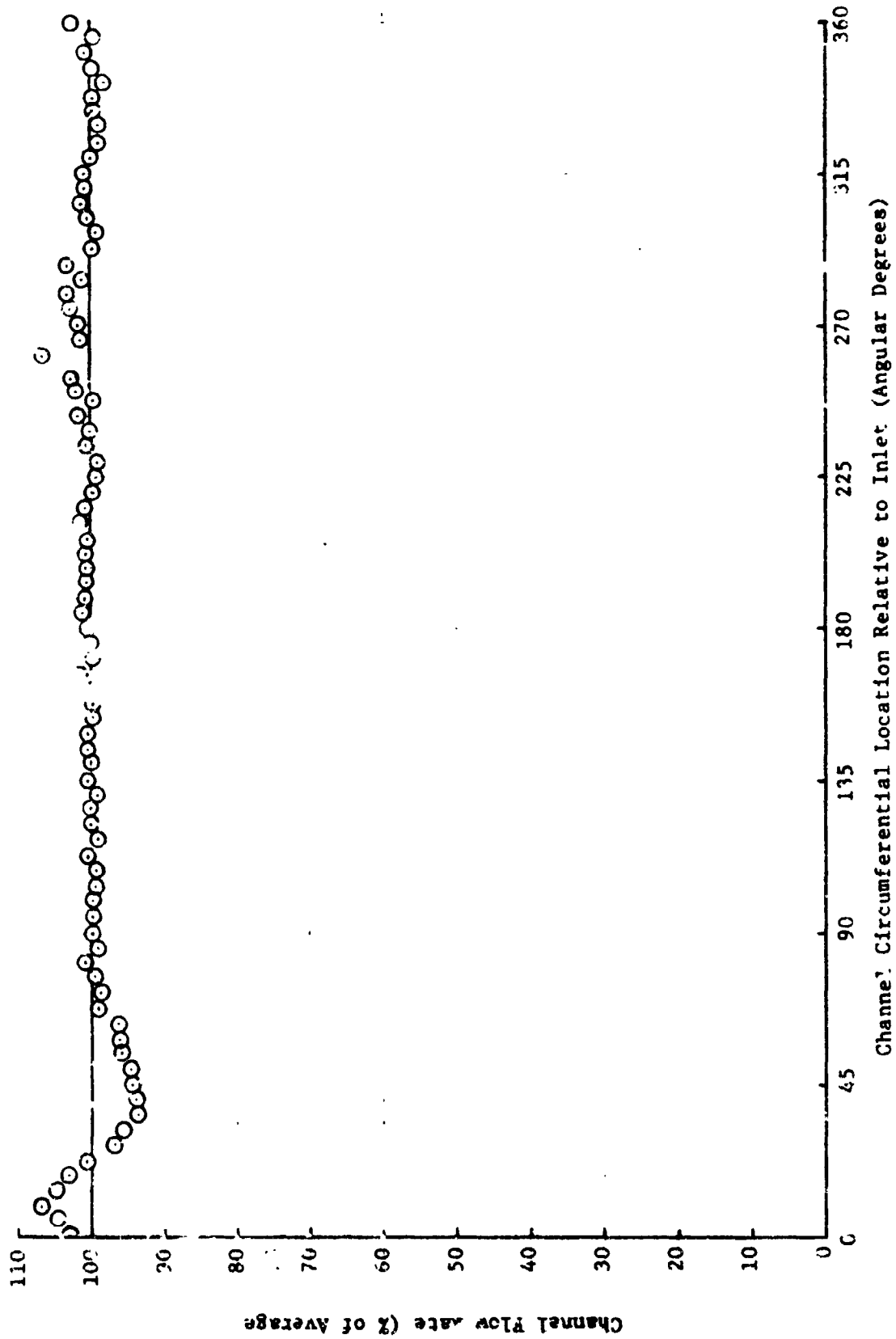
Figure 119c. Regen Channel Flow Distribution - Channel SN 003
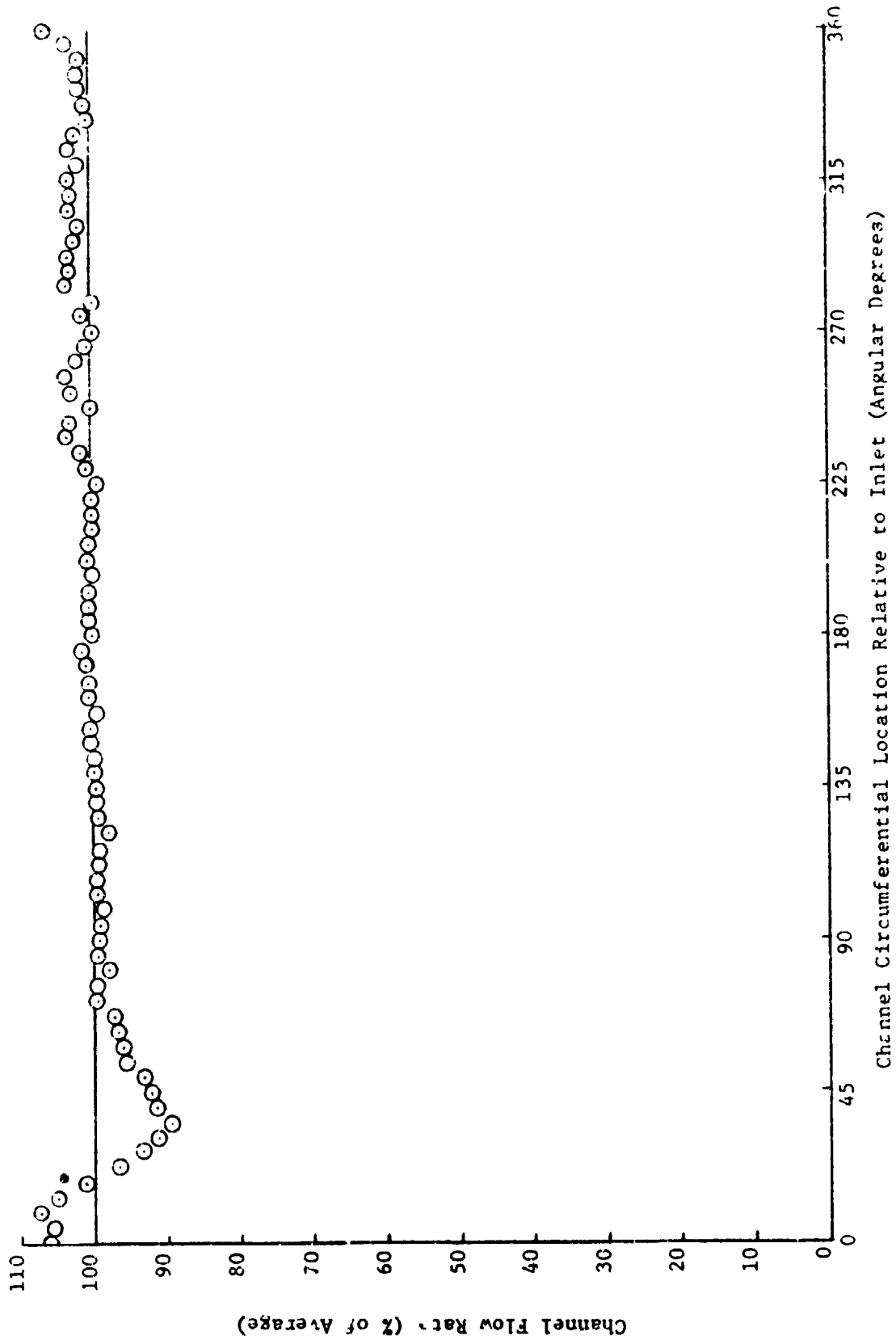
Figure 119d. Regen Channel Flow Distribution - Channel SN 004

4.5, Data Analysis (cont.)

The effect of the low flow rate on the life of the ff_c tip was evaluated because it was the most limiting component. Although slightly higher temperatures resulted they were not enough to significantly alter the strain (temperature gradient) or to adversely affect the cycle life correlation. No evaluation was made on the effect on throat temperatures (film cooled). Because of the slightly lower flows 45° from the fuel inlet this location was selected for the axial array of thermocouples (see Figures 79 and 80). The thermocouples at this location in the throat generally read higher and responded much more rapidly than those located circumferentially. The erosion of both thrusters SN001 (test -007) and SN002 (test -145) occurred at this location.

The regen channel flow distribution was considered satisfactory. The ~10% lower flow rate at one location was evaluated as having no adverse effect on cycle life of the ff_c tip and a modest, acceptable increase in throat temperatures were projected since the lower flow would correspond to 19% ff_c locally instead of the nominal 21%.

4.5.2.1.5 Film Cooling

The design film cooling flow rate was 21% of the total fuel flow. It is estimated that the actual ff_c flow percentage was 20.6%

The determination of the ff_c flow rate was not simple because the pressure drop in the inlet line was a function of total flow rate, because the cold flow testing does not simulate heat addition and because, when both regen and ff_c circuits were flowed, atmospheric backpressure could not be used to simulate both the 207 N/cm^2 (300 psia) chamber pressure that was backpressure to the regen/injector circuit and the 190 N/cm^2 (275 psia) back-pressure at the ff_c discharge.

4.5, Data Analysis (cont.)

       The orifices that controlled the flow of coolant to the film cooled section were sized for the nominal operating conditions. On the basis of the subsonic flow equation, 21% of the total fuel as film coolant, a 259 N/cm^2 (375 psia) torus pressure (Table XXX), a 190 N/cm^2 (275 psia) local chamber pressure at the ffc discharge, and nominal fuel inlet temperature the C_D A of the ffc circuit was .314 cm^2 (.0487 in.^{2}). The C_D A values calculated for the ffc circuit of the four chambers are summarized in Table LX.

TABLE LX

FFC CIRCUIT HYDRAULIC CHARACTERISTICS

Chamber SN	C_D A, cm^2 (in.^{2})		$\dfrac{C_D \ A}{(C_D \ A)_{design}}$ percent	$\left[\dfrac{C_D \ A}{(C_D \ A)_{design}}\right]$ 21%
001	.3078	(.04771)	98.0	20.6
002	.3240	(.05022)	103.1	21.7
003	.3226	(.0500)	102.7	21.6
004	.3251	(.05039)	103.5	21.7
Avg.	.3199	(.^.9^)	101.8	21.4

       The actual ffc circuit hydraulics were considered acceptable relative to the design requirements on the bases of the data shown in Table LX. However, the data shown in the last column in Table LX, while providing a measure of the acceptability of the chamber relative to "as built" ffc hydraulics, are not a true measure of the regen-ffc fuel split; since the split was also dependent on the regen-injector "as built" hydraulics.

       Table LXI is a summary of the ITA cold flow data in which the amount of GN_2 flowing in the ffc circuit has been expressed as a percentage of the total GN_2 flow rate. The percent ffc was less than 21% because the resistance of the regen/injector circuit was less than nominal.

4.5, Data Analysis (cont.)

TABLE LXI

FLOW SPLIT FROM ITA COLD FLOW DATA

ITA SN	ffc Split (% of Total GN_2)
001	20.2
002	20.0
003	20.6
004	20.1
Avg.	20.2

The actual split of fuel flow betwwen the ffc section and the regen section was influenced by three factors. (1) The ffc flow rates were derived from a correlation (Table LVIX) that was made with only the ffc circuit flowing. Because of the low flow rates, there was very little pressure drop between torus and the inlet line where pressure measurements were made. With both circuits flowing, the pressure drop between the line and the torus was appreciable. Thus, the correlation of ffc flow rate on the basis of inlet line pressure would be high. At simulated nominal conditions, the effect of the lower torus pressure was estimated as a 3% reduction in ffc flow rate. (2) In cold flow of the ITA units, both the regen-injector circuit and the ffc circuit saw the same back pressure (atmospheric). In practice, the back pressure at the ffc injection station would be lower. The effect of the lower back pressure was calculated to increase the ffc flow rate by 10.4%. (3) The regen-injector circuit has less resistance than predicted. It was estimated that this would result in a regen circuit flow 5% higher than nominal. In practice, these three factors would result in the actual torus pressure being less than the predicted value. The adjustment of the ffc and regen flow rates to the lower torus pressure would result in a fuel split slightly different than the 20.2%

4.5, Data Analysis (cont.)

average shown in Table LXI for the ITA cold flow. The pressure schedule was not recalculated, but the % ffc was estimated to be 20.6% from the 20.2% ITA cold flow average value, the 3% reduction in ffc flow due to lower torus pressure, 10.4% increase in ffc flow due to lower chamber pressure, the 5% higher regen flow rate due to lower resistance, and allowing that the total flow rate would be held at the nominal value by reason of the balance orifice in the inlet line compensating for the deviations in actual resistance from nominal elsewhere.

4.5.2.2 Flow Meter Calibration

The Ramapo flow meters were calibrated using water as the test fluid before and after the ITA test firings. Calibration pre- and post-test was done in a straight pipe configuration. The post firing recalibration was also performed with the Ramapo meters in the test stand lines so that "in place" configuration effects would be measured. Additionally, Tests -048 and -049 were flow meter calibration tests that were made on the test stand using venturis for flow standards and oxygen and hydrogen gases at ambient and cryogenic temperatures as the test fluids.

To provide momentum simulation of the ITA flow rates, the Ramapo flow meters were flowed at 3.6 kg/sec (8 lb/sec) and 5.9 kg/sec (13 lb/sec) in the water calibrations. At the two flow rates, the fuel Ramapo in the straight line configuration read .4 and 1.6% higher than it did pre-test. In the actual configuration, it read 1.7 and 2.0% higher than in the post-test straight line configuration. At the two flow rates, the ox Ramapo read 1.3% higher and .35% lower than it did pre-test. In the actual configuration, it read .35 and 0% higher than in the post-test straight line configuration.

Tests -048 and -049 were run with ITA SN 001 in place by installing venturis in the system upstream of the test stand valves. Test -048 was made with ambient temperature propellants and Test -049 with cold propellants. There were problems with both the oxidizer and the fuel data.

4.5, Data Analysis (cont.)

The high back pressure c .sed by the distributed resistance of the 1TA fuel circuit resulted in the fuel venturi not flowing sonically and, therefore, the venturi fuel flow rates could not be determined. None of the 39 fuel flow data points could be used.

The Ramapo calibration data that were obtained with oxygen are characterized by gas temperatures at the meter that are less than the temperature of the gas as it leaves the heat exchanger due to the expansion of the gas, and results in anomalies in both the cold and ambient data. Adiabatic expansion of the oxygen at the conditions of the first data point would have resulted in two phase flow. The expansion of the cold gas from the high supply pressures to pressure less than the normal meter inlet pressure, cooled the oxygen to the point that six of the 19 data points were obtained with measured temperatures that were less than $10°K$ ($18°R$) above the saturation temperature. Of the 19 data points obtained with cryogenic oxygen, 15 are characterized by negative values for the venturi Johnson Critical Flow Factor indicating extrapolation into a region of unknown accuracy.

The data obtained with ambient oxygen are not without difficulties. Initially, the lines, accumulator and system were all at ambient temperature. Gas temperatures calculated assuming isentropic expansion, were $35°K$ ($63°R$) less than ambient. By the end of the test, the temperature measured at the venturi inlet was the isentropic expansion temperature for the pressure measured there and the temperature at the valve was within $.3°K$ ($.5°R$) of the isentropic expansion temperature for oxygen expanding from the supply pressure and temperature to the pressure measured at the valve. The anomaly in the data is that the temperature of the oxygen measured at the venturi and at the engine valve (the Ramapo was located between them) differed by as much as $20°K$ ($36°R$) for identical conditions depending on whether the point had been reached by

4.5, Data Analysis (cont.)

increasing flow or decreasing flow. The difference in the Ramapo indicated
flow rate from that calculated for the venturi at its inlet conditions was
proportional to the difference between the measured temperature and the gas
temperature calculated assuming isentropic expansion. The two phenomena
suggest varying degrees of heat transfer between the gas and the Ramapo and
that while the Ramapo meter is a temperature compensated device, it was
affected by temperature graidents, as has been the experience with temperature
compensated load cells. Seven of the 20 data points obtained with the ambient
temperature oxygen were not used.

On the basis of the oxygen flow data shown in Figure
120, it was concluded that the Ramapo flow meter was reading low by 3.66%.
There is a considerable scatter in the data; a $\pm$ 1.6% band includes all but
one data point. The flow correction factor in Figure 120 was determined as:

$$(1 - \frac{\dot{w}_{Ramapo}}{\dot{w}_{Venturi}}) \times 100$$

The oxidizer flow rate that was used in making the performance calculations
(Section 4.5.4) was the Ramapo indicated flow rate divided by .9634 (1 - .0366).

Several methods of verifying the fuel flow rate were
attempted. An unsuccessful attempt was made to correlate the hydrogen flow data
by calculating the subsonic flow rate through the venturi. Correlation of the
flows by the C_D A values that would be obtained from the injector and/or chamber
GN_2 cold flow data did not appear possible since the GN_2 data were subsonic
and the hydrogen data were sonic.
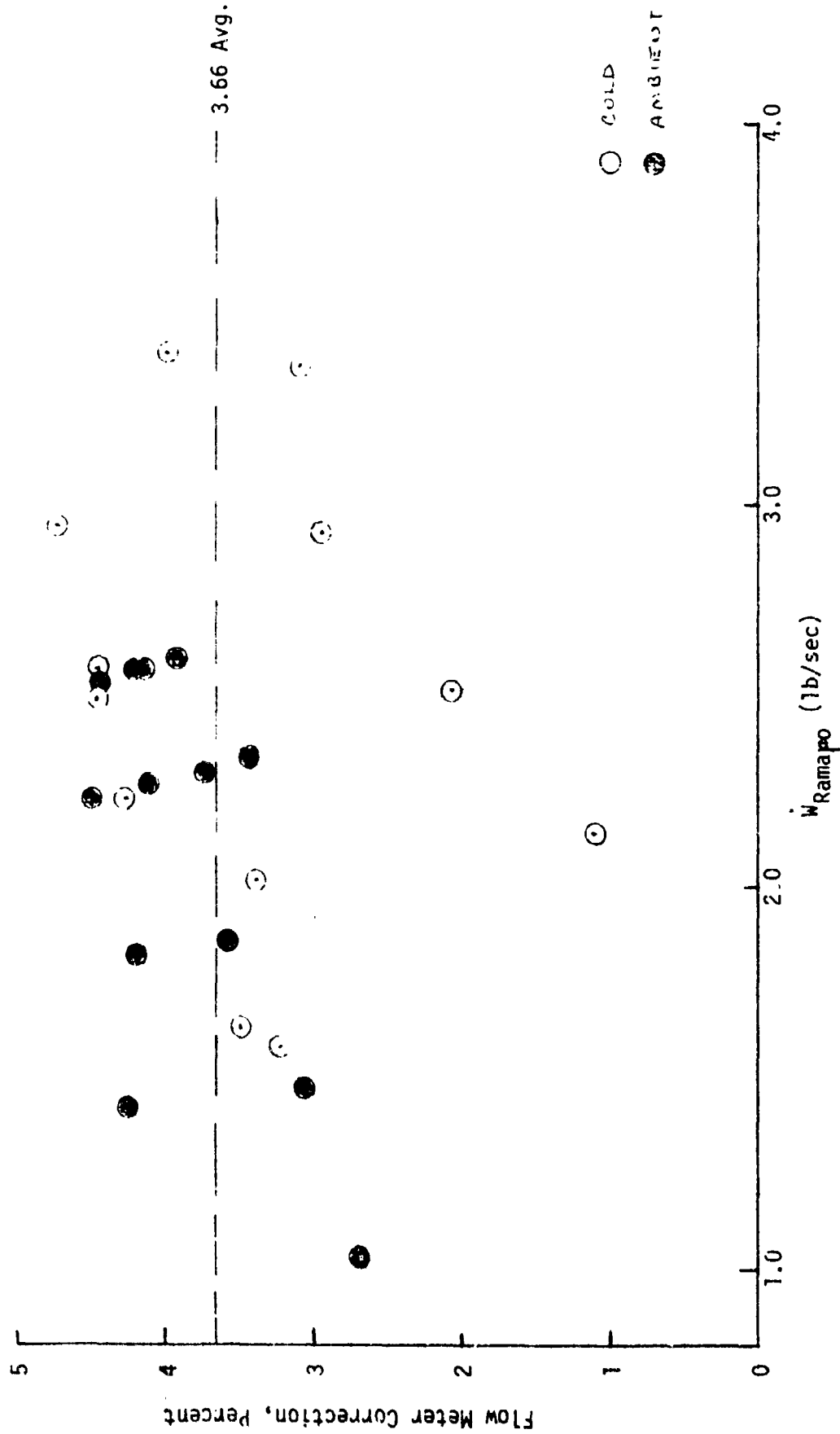
Figure 120. Correction to Oxygen Flow Rate

4.5, Data Analysis (cont.)

An attempt was made to provide a measure of the hydrogen flow rate by correlating C_D A values from the test firing data for comparison to those obtained from the component checkout testing with GN_2. C_D A values were calculated for the fuel flow seven ways for the six combinations of (1) valve inlet pressure, (2) valve outlet pressure, (3) injector fuel manifold pressure, and (4) chamber pressure. All combination involving the chamber pressure, i.e., (1-4), (2-4) and (3-4) did not work because, as discussed earlier, the pressure drop in the premix cup was influenced by the oxygen flow rate and thus there is an unknown pressure drop between chamber pressure and the fuel circuit discharge. The remaining three combinations - (1 - 2), (1 - 3) and (2 - 3) - did not work either because the balance orifice, as discussed earlier, was found to be loose.

The first seven test firings were made with the flow controlled and measured by venturis. Unfortunately, the Ramapo flow meters were not installed until after the venturis were removed. A C_D A value was calculated for 9 data points from Tests -003, -004 and -006 for the pressure ratio from the injector manifold (P_{FJ}) to the fuel valve inlet (P_{FTCV}). The ratio of specific heats was based on the pressure and temperature at the inlet to the valve. C_D A value was also calculated for four data points from Tests -008 and -009 under the assumption that the orifice was in place at this time. (The chamber was removed from the test stand after Test -007 and repaired as discussed earlier, therefore, the orifice was known to be in place for Test -008). The C_D A values calculated using the venturi flow data (Tests -003, -004 and -006), using the Ramapo data (-008 and -009), and the design value are summarized in Table LXII. On the basis of the good agreement of these C_D A values, it was assumed that the fuel Ramapo meter did not require a correction.

TABLE LXII

FUEL FLOW CORRELATION

Test	Time	Pressures Inlet to Valve P_{FTCV}, N/cm² (psia)	Injector Manifold P_{FJ}, N/cm² (psia)	Fuel Temp. @ Valve T_{FTCV}, °K (°R)	Fuel Flow Rate $\dot{w}_f$, g/sec (lb/sec)	$\dfrac{P_{FJ}}{P_{FTCV}}$ R	C_D A, cm² (in.²)	Comments
-003	.48	288 (418)	180 (261)	308 (554)	.288 (.636)	.624	1.66 (.258)	Venturi flow data.
	.98	288 (418)	179 (259)	297 (534)	.288 (.636)	.619	1.66 (.258)	
-004	.38	271 (393)	223 (323)	198 (356)	.290 (.640)	.822	1.81 (.281)	Same
	.58	270 (391)	223 (323)	193 (347)	.290 (.639)	.825	1.81 (.280)	
-006	2	232 (337)	170 (246)	190 (344)	.268 (.590)	.729	1.66 (.258)	Same
	15.3	245 (356)	184 (267)	146 (262)	.316 (.696)	.750	1.66 (.258)	
	24.5	248 (360)	186 (270)	141 (253)	.324 (.714)	.752	1.66 (.258)	
	31.7	252 (365)	191 (277)	140 (252)	.327 (.720)	.758	1.66 (.257)	
	35.5	192 (279)	159 (230)	136 (244)	.230 (.508)	.825	1.69 (.262)	
						Avg =	1.70 (.263)	
						σ =	3.74%	Standard Deviation

TABLE LXII (cont.)

Test	Time	Pressures Inlet to Valve P_{FTCV}, N/cm² (psia)	Injector Manifold P_{FJ}, N/cm² (psia)	Fuel Temp. @ Valve T_{FTCV}, °K (°R)	Fuel Flow Rate $\dot{w}_f$, g/sec (lb/sec)	$\dfrac{P_{FJ}}{P_{FTCV}}$ R	C_D A, cm² (in.²)	Comments
-003	17	181 (263)	152 (221)	141 (254)	.206 (.455)	.840	1.70 (.263)	Ramapo flow data.
	22	177 (256)	150 (218)	134 (241)	.201 (.444)	.852	1.71 (.265)	
	24.5	175 (254)	15? (2?7)	132 (237)	.199 (.439)	.855	1.70 (.264)	
-009	3.0	285 (413)	230 (333)	153 (275)	.323 (.713)	.805	1.63 (.253)	Same
						Avg =	1.68 (.261)	
						σ =	2.13%	Standard Deviation
-		276 (400)	232 (336.6)	139 (250)	313 (.69)	.8415	1.68 (.261)	Design

4.5, Data Analysis (cont.)

4.5.2.3   Valve Characteristics

4.5.2.3.1   Igniter Valves

Table LXIII is a summary of the acceptance test data for the Valcore PN V27200-4871E, normally closed, solenoid operated, 2 way valve.

TABLE LXIII

IGNITER VALVE ACCEPTANCE TEST DATA

	SN	002	003	004	006
Water flow rate 6.9 N/cm^2 (10 psi) pressure drop, kg/min (lb/min)		2.81 (6.2)	2.86 (6.3)	2.81 (6.2)	2.76 (6.1)
Minimum pull in with 666 N/cm^2 (950 psig) at inlet, amps		.6	1.0	.9	1.0
Maximum drop out with 217 N/cm^2 (300 psig) at inlet, VDC.		2.5	2.5	2.0	2.5
Opening response at room with 30 VDC and 442 N/cm^2 (625 psig) inlet pressure, msec.		20	22	21	20
Closing response at room temperature with 217 N/cm^2 (300 psig) at inlet, msec.		10	10	10	10

Valve SN 002 was used in the igniter fuel circuit and valve SN 006 was used in the igniter ox circuit. $C_D A$ values were derived for each from the igniter cold flow data. For 89.7 N/cm^2 (130 psia) inlet pressure, 267°K (481°R) inlet temperature, 3.81 g/sec (.00839 lb/sec) GN$_2$ flow rate and a pressure ratio of .893 across valve SN 002. The $C_D A$ was calculated to be .0274 cm^2 (.00425 in.^{2}). For 105.5 N/cm^2 (153 psia) inlet pressure, 272°K (490°R) inlet temperature, 7.63 g/sec (.0169 lb/sec) GN$_2$ flow rate and a pressure ratio of .653 across valve SN 006, the $C_D A$ was calculated to be

4.5, Data Analysis (cont.)

.C $_2$ cm^2 (.00483 in.^{2}). The approximately 13.5% difference in C_D A values for the two valves is probably the result of difference in line configurations and pressure tap locations.

Because of the importance to sequencing for pulse tests, the igniter valve opening times have been documented. Figure 121 shows the valve opening response time as a function of the pressure at the inlet to the valve. Response time was defined as time from electrical signal to initiation of poppet travel and was determined from oscillograph records by the infliction in the current trace with poppet motion and from pressure rise rates at the igniter inlets. The poppet travel time, that is the time from initiation of poppet travel to full open, was approximately 4 msec. The valve closing times were 10 to 15 msec.

The data from this program shown in Figure 121 were from Tests -003 through -020. The data from the ETR program (Ref. 8) that were obtained with valves SN 001 and -005 were included in Figure 121 to show the valve response characteristics at high pressures.

As can be seen in Figure 121, the igniter valve response times that were obtained with cold hydrogen are shorter than the response time with oxygen or warm propellants. This point is further illustrated by the valve response time presented in Table LXIV, which was included primarily to provide information on repeatibility since the tests were made with very little change in propellant pressures and temperatures. From the data in Table LXIV, the average response time of the fuel valve was 16.8 ± 1.0 msec at 335 ± 5.7 N/cm^2 (486 ± 8.2 psia) and 177.8 ± 5.9°K ($320.1 \_ 10.7$°R); that of the ox valve was 21.5 ± 1.1 msec at 336.8 ± 5.9 N/cm^2 (488.5 ± 8.5 psia) and 227.5 ± 7.9°K (409.5 ± 14.2°R).
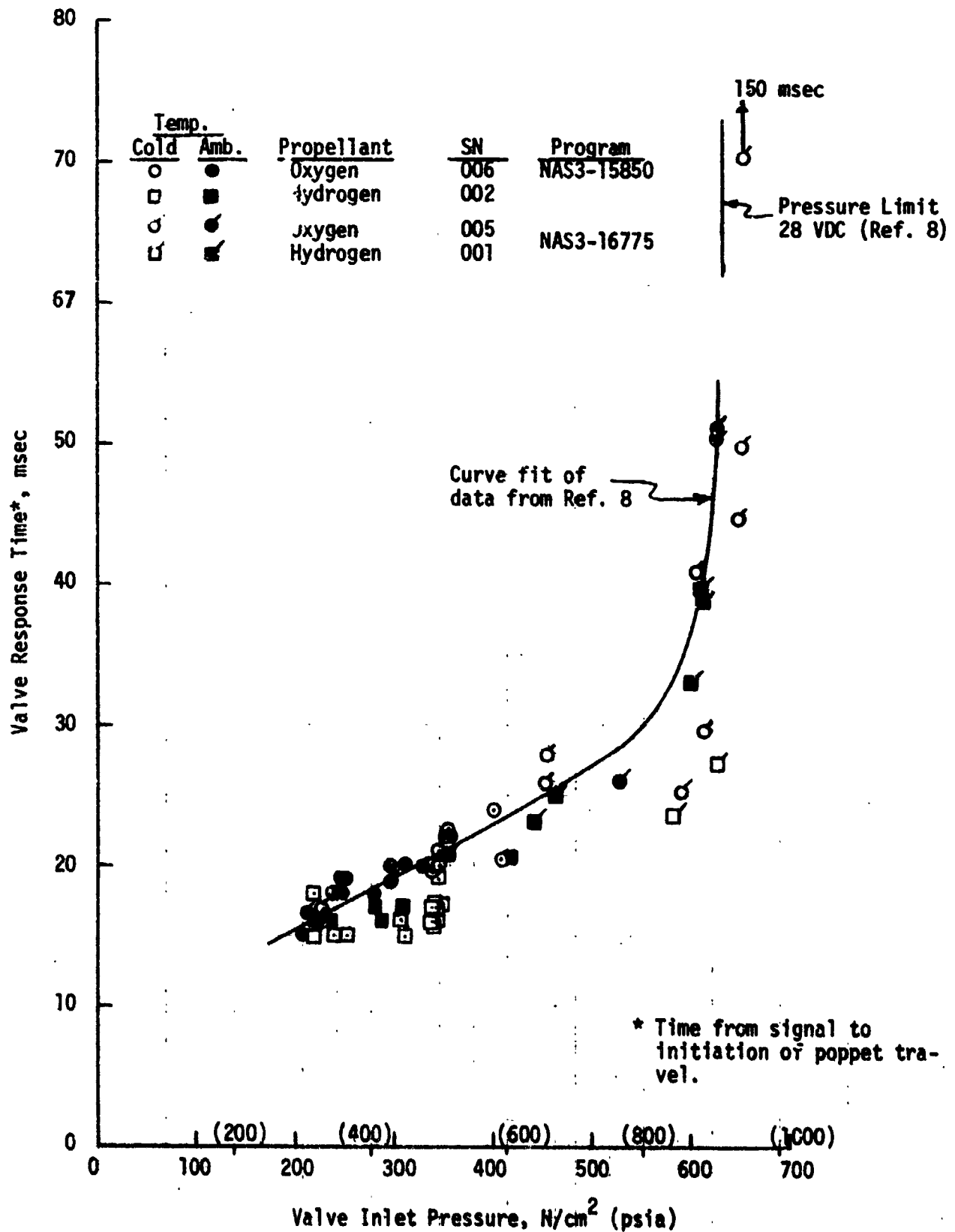
Figure 121. Igniter Valve Opening Response Time

TABLE LXIV

IGNITER VALVE OPENING RESPONSE REPEATIBILITY

Test No.	Ox Temp., °K (°R)	Ox Press., N/cm² (psia)	Fuel Temp., °K (°R)	Fuel Press., N/cm² (psia)	T_{ox}* msec	T_{fuel} msec
-021	234 (421)	383 (555)	186 (335)	341 (495)	22	17
-022	226 (407)	341 (495)	183 (330)	341 (495)	23	16
-023	228 (410)	343 (498)	183 (330)	338 (491)	23	17
-024	229 (413)	341 (494)	180 (325)	336 (488)	24	17
-025	239 (430)	345 (500)	179 (323)	336 (487)	22	16
-026	239 (430)	341 (494)	175 (315)	334 (484)	21	15
-027	241 (434)	345 (500)	176 (317)	334 (484)	21	17
-028	242 (435)	345 (500)	172 (310)	331 (480)	22	17
-029	222 (400)	338 (490)	174 (314)	332 (482)	20	17
-030	222 (400)	332 (481)	172 (309)	330 (478)	21	15
-031	220 (396)	334 (484)	174 (314)	331 (480)		
-032	219 (395)	329 (477)	170 (306)	329 (477)	22	17
-033	226 (407)	336 (487)	173 (312)	328 (475)	20	15
-034	226 (407)	334 (485)	171 (307)	324 (470)	21	17
-035	219 (395)	332 (482)	173 (311)	332 (481)	21	19
-036	221 (398)	327 (474)	171 (308)	331 (480)	20	17
-037	226 (407)	331 (480)	177 (319)	334 (485)	22	19
-038	221 (398)	344 (485)	171 (308)	331 (480)	21	.17

*Time from electrical signal to initiation of poppet travel.

4.5, Data Analysis (cont.)

4.5.2.3.2 Main Propellant Valves

The Marquardt PN 38961, normally closed, pneumatically actuated, co-axial poppet, two way valve acceptance test results are shown in Table LXV for the three valves delivered to ALRC. The opening response of all three valves (43 msec) was out of spec (40 msec). Valve SN 013 had a closing time that was 8 to 9 msec faster than the other two valves. The C_D A values for the valves was calculated using the subsonic flow equation and the GN_2 flow rate and valve inlet and outlet pressures.

Two of the main propellant valves were tested at ALRC at altitude using ambient and cryogenic hydrogen and oxygen as the test fluids. The valves were self actuated, that is, the actuation fluid was the propellants themselves tapped off the upstream inlet lines. There was an orifice downstream of each valve installed in a length of vent line so that the volume and resistance downstream of the valves simulated the ITA thruster. The inlet line configuration was the setup that was used for the ITA test firings.

The hydraulic data are summarized in Table LXVI. C_D A values were calculatd for each test condition using the subsonic flow equation, the venturi measured flow rates, propellant temperatures and the valve inlet and outlet pressures. The C_D A for the ox valve (SN 011) averaged from the six data points was 3.59 cm^2 (.557 in.^{2}). The average C_D A for the fuel valve (SN 013) was 3.74 cm^2 (.579 in.^{2}). The data obtained with the fuel valve are more reliable because the pressure differences are larger than the ox valve pressure differences. The standard deviation of the fuel valve C_D A values from the average was 1.5%.

Based on the C_D A values, valve SN 013 had about 10% less resistance with GN_2 (Table LXV) in the acceptance test than with hydrogen (Table LXVI). The same was true of valve SN 011. The difference is probably due to differences in the line configuration and pressure tap location.

TABLE LXV

MAIN PROPELLANT VALVE ACCEPTANCE TEST DATA

	SN 011	SN 012	SN 013
Pull in current at ambient temperature and 441 N/cm^2 (640 psia), amps	1.5	1.5	1.75
Opening response at ambient temperature, 28 VDC and 286 N/cm^2 (415 psia) GN_2 pressure			
Signal to full open, msec	43	43	43
Poppet travel time, msec	7	7	7
Closing response at ambient temperature, 28 VDC and 286 N/cm^2 (415 psia) GN_2 pressure			
Signal to fully closed, msec	36	37	28
Poppet travel time, msec	9	10	8
Hydraulic characteristics at ambient temperature and GN_2 inlet pressure of 269 N/cm^2 (390 psia)			
Pressure drop, N/cm^2 (psid)	12.4 (18)	12.4 (18)	11.7 (17)
GN_2 flow rate, g/sec (lb/sec)	1080 (2.38)	1080 (2.38)	1080 (2.38)
C_D A, cm^2 ($in.^2$)	4.0 (.621)	4.0 (.621)	4.12 (.638)

TABLE LXVI

MAIN PROPELLANT VALVE HYDRAULIC CHARACTERISTICS

Test No. 1972-D01-OB	Condition	Pressure, N/cm² (psia) Inlet	Pressure, N/cm² (psia) Outlet	Inlet Temp., °K (°R)	Pressure Drop N/cm² (psia)	Flow Rate g/sec (lb/sec)	$C_D A$ cm² (in.²)
-001	Oxidizer SN 011 Ambient	135 (196)	128 (186)	301 (541)	6.90 (10)	418.5 (1.143)	3.45 (.535)
-002		228 (331)	218 (316)	301 (541)	10.3 (15)	899.5 (1.983)	3.75 (.581)
-003		313 (454)	300 (435)	300 (540)	13.1 (19)	122. (2.68)	3.84 (.595)
-005	Cold	135 (196)	129 (187)	172 (310)*	6.21 (9)	658.6 (1.452)	3.48 (.540)
-006		239 (346)	228 (331)	158 (284)*	10.3 (15)	1169. (2.579)	3.45 (.534)
-007		323 (469)	312 (452)	120 (216)*	11.7 (17)	1716. 2 Phase flow	
-010	Fuel SN 013 Ambient	152 (221)	910 (132)	294 (530)	61.4 (89)	352. (.777)	3.79 (.587)
-011		199 (289)	120 (174)	294 (529)	79.3 (115)	459.5 (1.013)	3.78 (.586)
-012		917 (133)	538 (78)	291 (523)	37.9 (55)	210. (.463)	3.72 (.576)
-013		183 (266)	166 (241)	135 (243)	17.2 (25)	377. (.831)	3.75 (.581)
-014		147 (213)	132 (192)	149 (269)	14.5 (21)	293. (.646)	3.75 (.581)
-015		800 (116)	717 (104)	129 (233)	8.2 (12)	170. (.374)	3.63 (.563)

*Outlet temperature. Inlet temperature invalid.

4.5, Data Analysis (cont.)

The main propellant valves were intially operated as self actuated. For Tests -050 through -056, the fuel valve was helium actuated and the oxygen valve was GN$_2$ actuated; for Test -057 and subsequent tests, both valves were GN$_2$ actuated. The response times were a function of the temperature and of the pressure of the actuation fluid. The pilot valve vented the main valve body to open and pressurized it to close the valve. A 40 msec response time was specified for the valves so that the 50 msec contract goal (signal to 90% thrust) could be met with allowance for fill times.

The main propellant valve response times from the checkout testing are shown in Table LXVII. The opening time for the ox valve (SN 011) (signal to full open) went from 50 msec at ambient conditions to 72/80 msec at cryogenic conditions. The closing time increased with increasing pressure; improved with cryogenic temperatures at the lower pressures, but was very slow at cryogenic temperatures and the highest pressure, 448 N/cm^2 (645 psia). For these latter conditions, the valve closing time was on the order of .5 second and in one instance, did not close in .6 second at which time it was signaled open for the next pulse. The fuel valve (SN 013), on the other hand, did not exhibit either the erratic opening or closing behavior (Table LXVII) that was exhibited by the ox valve.

Additional response data are provided for the main propellant valve operating self actuated in Tables LXVIII and LXIX. Oxidizer valve SN 011 that had been used for the checkout testing had been replaced with SN 012. The fuel valve was still SN 013. The opening times of the two valves varied by 16 to 19 msec. The closing times were even more erratic (Table LXIX).

In an attempt to improve the closing time of the valves, they were switched to external actuation prior to Test -050. Helium was used as the actuation fluid for the fuel valve and GN$_2$ for the ox valve. The ox valve improved, but on Tests -050 through -056 the fuel valve closing time

TABLE LXVII

MAIN PROPELLANT VALVE RESPONSE TIMES, SELF ACTUATED (CHECKOUT TEST DATA)

Test No. 1972-D01-0B-	Valve SN	Propellant	Temperature, °K (°R)	Inlet Pressure N/cm² (psia)	Pilot Valve Voltage Suppression Circuit	Opening Times, msec — Signal to Pilot Travel	Pilot to Main Valve Initiation	Main Valve Travel	Signal to Fully Open	Closing Times, msec — Signal to Main Valve Initiation	Main Valve Travel	Signal to Fully Closed	Cycle
001	011	Ox	Amb.	179 (259)	Yes	8	35	6	49	63	10	73	2
						8	35	6	49	61	10	71	5
						9	35	6	50	61	10	70	8
002				314 (456)		11	31	5	47	57	10	67	2
						11	32	5	48	56	10	66	5
						12	31	5	48	56	10	66	8
003				434 (630)		15	31	4	50	77	11	88	2
						15	31	5	51	93	10	103	3
						15	31	5	51	115	10	125	4
						15	29	4	48	91	10	101	5
						16	30	5	51	86	11	97	6
						15	30	5	50	93	10	103	7
						15	30	5	50	89	10	99	8
						–	–	5	51	90	10	100	9
						16	31	5	52	92	10	102	10
005			184 (331)	190 (274)	No	9	48	7	64	34	13	47	2
						8	49	6	63	34	13	47	5
						9	49	6	64	33	13	46	8
006			179 (322)	529 (477)		12	49	6	67	38	13	51	2
						11	48	6	65	37	14	51	5
						11	48	5	64	36	13	49	8
007			160 (288)	445 (645)		15	70	5	90	Did not close in .6 sec			1
						Open from first cycle				71	15	86	2
						15	60	5	80	533	16	549	3
						15	58	5	78	535	15	550	4

TABLE LVII (Cont.)

Test No. 1972-D01-0R-	Valve SN	Propellant	Temperature, °K (°R)	Inlet Pressure N/cm² (psia)	Pilot Valve Voltage Suppression Circuit	Opening Times, msec				Closing Times, msec			Cycle
						Signal to Pilot Travel	Pilot to Main Valve Initiation	Main Valve Travel	Signal to Fully Open	Signal to Main Valve Initiation	Main Valve Travel	Signal to Fully Closed	
007 (cont.)	011	Ox	160 (288)	445 (645)	No	15	57	5	77	531	15	546	5
						15	58	5	78	497	14	511	6
						15	52	6	73	412	14	426	7
						15	59	6	80	430	15	445	8
						15	61	5	81	489	15	504	9
						15	52	5	72	494	15	509	10
012	013	H₂	Amb.	176 (255)		12	4	8	24	16	7	23	2
						13	4	7	24	15	7	22	5
						13	4	7	24	16	7	23	8
010				312 (453)		16	4	4	24	19	6	25	2
						16	4	4	24	20	5	25	5
						16	4	5	25	21	6	27	8
011				415 (602)		20	4	5	29	26	6	28	2
						20	4	4	28	21	5	26	5
						18	3	4	25	22	5	27	8
015			144 (259)	150 (217)		12	12	5	29	18	6	24	2
						11	12	5	28	17	6	23	5
						12	12	4	28	18	6	24	8
014			138 (249)	330 (479)		16	9	4	29	21	5	26	2
						15	10	4	29	20	4	24	5
						15	10	5	30	19	5	24	8
013			129 (233)	427 (620)		20	9	4	33	27	6	33	2
						21	7	5	33	27	5	32	5
						20	9	4	33	27	5	32	8

TABLE LXVIII

MAIN PROPELLANT VALVE OPENING RESPONSE, SELF ACTUATED

| Test 1972-D01-0A | Inlet Conditions | | | | | | | | Response Times, msec | | | | | |
| | Oxidizer Temperature Pressure | | | | Fuel Temperature Pressure | | | | Oxidizer | | | Fuel | | |
	°K	(°R)	N/cm²	(psia)	°K	(°R)	N/cm²	(psia)	Delay (Signal to Main Valve Initiation)	Travel	Total	Delay (Signal to Main Valve Initiation)	Travel	Total
-003	297	(535)	310	(450)	297	(535)	419	(606)	46	14.5	60.5	30.5	12.5	43
-004	202	(365)	407	(590)	197	(355)	345	(500)	54	11.5	65.5	26	14	40
-005	261	(470)	296	(430)	215	(387)	310	(450)	45	14	59	25	14	39
-006	259	(467)	280	(406)	227	(408)	307	(446)	48	11	59	22	12	34
-007	237	(428)	338	(490)	253	(455)	217	(315)	43	11	54	22	13	35
-008	226	(480)	238	(345)	242	(435)	238	(345)	50	12	62	25	20	45
-009	238	(430)	338	(490)	200	(360)	341	(495)	50	13	63	28	12	40
-010	311	(560)	207	(300)	307	(552)	307	(445)	43	15	58	22	20	42
-011	311	(560)	248	(360)	311	(560)	286	(415)	45	17	62	21	20	41
-012	308	(556)	252	(365)	302	(545)	234	(340)	42	14	56	20	21	41
-013	302	(545)	348	(360)	297	(535)	279	(405)	48	17	65	24	18	42
-014	270	(486)	326	(473)	247	(446)	252	(365)	54	14	68	24	20	44
-015	255	(460)	353	(513)	180	(325)	343	(498)	53	15	68	27	18	45
-016	255	(460)	351	(509)	180	(326)	340	(493)	53	14	67	26	19	45
-017	247	(446)	399	(580)	187	(337)	339	(492)	53	11	64	25	18	43
-018	240	(433)	343	(497)	184	(332)	341	(495)	53	20	73	26	19	45
-019	245	(441)	352	(510)	190	(342)	346	(502)	53	12	65	26	19	45
-020	238	(430)	345	(500)	182	(328)	341	(495)	52	8	60	27	18	45
-021	233	(421)	383	(555)	186	(335)	341	(495)	52	12	64	26	22	48
-022	226	(407)	341	(495)	184	(330)	341	(495)	51	13	64	28	20	48
-023	227	(410)	343	(498)	184	(330)	338	(491)	47	15	62	27	23	50

TABLE LXVIII (cont.)

Test 1972-D01-0A	Inlet Conditions								Response Times, msec					
	Oxidizer				Fuel				Oxidizer			Fuel		
	Temperature		Pressure		Temperature		Pressure		Delay (Signal to Main Valve Initiation)	Travel	Total	Delay (Signal to Main Valve Initiation)	Travel	Total
	°K	(°R)	N/cm²	(psia)	°K	(°R)	N/cm²	(psia)						
-024	229	(413)	341	(494)	180	(325)	336	(488)	47	15	62	26	23	49
-025	238	(430)	345	(500)	179	(323)	336	(487)	47	14	61	28	22	50
-026	238	(430)	341	(494)	175	(315)	334	(484)	48	15	63	28	20	48
-027	241	(434)	345	(500)	176	(317)	334	(484)	56	11	67	27	19	46
-028	242	(435)	345	(500)	172	(310)	331	(480)	55	11	66	27	19	46
-029	222	(400)	338	(490)	174	(314)	332	(482)	56	8	54	27	17	44
-030	222	(400)	332	(481)	172	(309)	330	(478)	54	8	62	28	18	46
-031	220	(396)	334	(484)	174	(314)	331	(480)	57	11	68	28	20	48
-032	219	(395)	329	(477)	170	(306)	329	(477)	56	12	68	27	18	45
-033	226	(407)	336	(487)	174	(312)	327	(475)	57	12	69	25	20	45
-034	226	(407)	334	(465)	170	(307)	324	(470)	56	12	68	28	17	45
-035	219	(395)	332	(482)	173	(311)	332	(481)	56	10	66	28	17	45
-036	221	(398)	327	(474)	171	(308)	331	(480)	55	12	67	28	19	47
-037	226	(407)	331	(480)	177	(319)	334	(485)	57	13	70	25	22	47
-038	221	(398)	334	(485)	171	(308)	331	(480)	54	7	61	25	19	44

TABLE LXIX

MAIN PROPELLANT VALVE CLOSING RESPONSE, SELF ACTUATED

| Test 1972-D01-OA | Inlet Conditions | | | | | | | | Response Times, msec | | | | | |
| | Oxidizer Temperature Pressure | | | | Fuel Temperature Pressure | | | | Oxidizer | | | Fuel | | |
	°K	(°R)	N/cm²	(psia)	°K	(°R)	N/cm²	(psia)	Delay (Signal to Main Valve Initiation)	Travel	Total	Delay (Signal to Main Valve Initiation)	Travel	Total
-003	298	(536)	207	(300)	161	(536)	290	(420)	285	14	299	25	14	39
-004	203	(365)	269	(390)	186	(335)	193	(280)	56	16.5	72.5	26	14	40
-005	264	(475)	227	(330)	208	(375)	241	(350)	34	17	51	48	15	63
-006	206	(370)	233	(338)	133	(210)	199	(288)	38	17	55	17	15	32
-007	223	(401)	310	(450)	236	(425)	216	(313)	37	17	54	22	15	37
-009	209	(376)	298	(425)	139	(250)	276	(400)	35	23	58	25	20	45
-014	198	(357)	290	(420)	132	(238)	272	(394)	32	26	58	22	22	44
-015	251	(452)	321	(465)	150	(270)	303	(439)	48	20	68	77	17	94
-016	255	(460)	325	(472)	168	(302)	294	(426)	39	18	57	120	19	139
-017	248	(446)	363	(527)	167	(300)	283	(410)	116	17	133	58	21	79
-018	261	(433)	312	(453)	158	(285)	277	(402)	49	19	68	125	19	144
-019	245	(441)	325	(472)	171	(308)	312	(453)	48	19	67	40	21	61
-020	239	(430)	317	(460)	163	(293)	305	(443)	78	17	95	36	21	57
-021	234	(421)	350	(507)	169	(304)	311	(451)	70	21	91	39	22	61
-022	226	(407)	308	(447)	163	(294)	307	(445)	98	19	117	77	20	97
-023	238	(410)	317	(460)	163	(293)	287	(416)	55	15		95	17	112
-024	229	(413)	314	(456)	158	(285)	285	(413)	52	14	66	71	20	91
-025	239	(430)	317	(460)	161	(290)	283	(410)	54	15	69	106	20	126
-026	239	(430)	316	(458)	150	(270)	283	(410)	53	17	70	105	21	126
-027	241	(434)	315	(457)	157	(282)	285	(413)	52	16	68	102	20	122
-028	242	(435)	314	(455)	150	(270)	283	(410)	52	14	65	98	18	116
-029	222	(400)	300	(435)	158	(284)	301	(437)	59	17	76	57	21	78
-030	222	(400)	303	(440)	152	(275)	299	(433)	57	14	71	52	19	71

TABLE LXIX (cont.)

| Test 1972-D01-0A | Inlet Conditions | | | | | | | | Response Times, msec | | | | | |
| | Oxidizer Temperature Pressure | | | | Fuel Temperature Pressure | | | | Oxidizer | | | Fuel | | |
	°K	(°R)	N/cm²	(psia)	°K	(°R)	N/cm²	(psia)	Delay (Signal to Main Valve Initiation)	Travel	Total	Delay (Signal to Main Valve Initiation)	Travel	Total
-031	220	(396)	298	(433)	157	(283)	302	(438)	54	15	69	49	20	69
-032	219	(395)	303	(440)	154	(277)	297	(431)	52	16	68	43	21	64
-033	226	(407)	309	(448)	156	(280)	299	(433)	55	18	73	41	22	63
-034	226	(407)	303	(440)	151	(271)	295	(428)	52	18	70	42	20	62
-035	219	(395)	296	(430)	155	(279)	300	(435)	53	18	71	45	21	66
-036	217	(390)	296	(430)	151	(272)	301	(436)	52	17	69	41	18	59
-037	226	(407)	303	(440)	158	(285)	302	(438)	53	15	68	48	19	67
-038	221	(398)	303	(440)	149	(268)	301	(436)	62	17	79	56	20	76

4.5, Data Analysis (cont.)

ranged from .060 to .237 seconds, the fuel value was switched to GN_2 actuation prior to Test -057. Although still quite erratic, the response times of the fuel valve on closing was improved by going to GN_2 actuation. There was in general, a trend of longer delays with colder propellant temperatures.

The response times of the main propellant valves with the fuel valve actuated using helium and GN_2, and the oxidizer valve actuated using GN_2, were measured at ambient and cryogenic conditions. The response data for helium actuation of the fuel valve and GN_2 actuation of the ox valve at ambient conditions are given in Table LXX; the actuation pressure was 286 N/cm^2 (415 psia) and the GN_2 pressure at the valve inlets, 252 to 286 N/cm^2 (365 to 415 psia). The response times with He (fuel valve) and GN_2 (ox valve) actuation at cryogenic conditions, are given in Table LXXI; the pressure and temperature of the propellants are given in Table XXXVI for these tests. The response times for both valves GN_2 actuated and at ambient temperature are given in Table LXXII; the actuation pressure was 355 N/cm^2 (515 psia) and the inlets to the valves were pressurized to 286 N/cm^2 (415 psia) using GN_2. The valve response times, GN_2 actuated at cryogenic and ambient conditions, are given in Table LXXIII.

In general, the response time of the valves, both opening and closing, was faster the lower the molecular weight of the actuation fluid, and response time was slower the colder the valve. The higher the actuation pressure over the pressure at the inlet to the valve, the slower the valve opened and the faster it closed (ox valve Table LXX vs. Table LXXII). The problem of the long delay on closing only occurred at low temperatures (ox valve Table LXVII and fuel valve Table LXX vs. Table LXXI), and was improved by increasing the molecular weight of the actuation gas (Table LXXI vs. LXXIII, fuel valve).

TABLE LXX

MAIN PROPELLANT VALVE RESPONSE TIMES WITH He ACTUATION
OF FUEL VALVE AND N_2 ACTUATION OF OXIDIZER VALVE AT AMBIENT TEMPERATURE

Cycle	Opening Delay Time, sec (Signal to Inception of Travel)		Closing Time, msec (Signal to Fully Closed)	
	Oxidizer	Fuel	Oxidizer	Fuel
1	41	27	42	37
2	40	23	43	35
3	40	22	40	40
4	39	23	40	38
5	39	23	39	37
6	40	24	39	36
7	40	25	39	38
8	42	25	38	38
9	42	24	38	36
10	43	24	37	36

TABLE LXXI

MAIN PROPELLANT VALVE RESPONSE TIME WITH He ACTUATION
OF FUEL VALVE AND N_2 ACTUATION OF OXIDIZER VALVE AT CROGEYNIC CONDITIONS

Test No. 1972-D01-OA	Opening Delay Time, sec (Signal to Inception of Travel)		Closing Time, msec (Signal to Fully Closed)	
	Oxidizer	Fuel	Oxidizer	Fuel
-050	52	30	51	60
-051	45	30	65	⁻90
-052	54	30	55	⁻145
-053	50	29	60	237
-054	49	30	59	197
-055	49	30	56	146
-056	46	31	58	164

TABLE LXXII

MAIN PROPELLANT VALVE RESPONSE TIMES WITH
GN_2 ACTUATION AT AMBIENT CONDITIONS

Cycle	Opening Delay Time, sec (Signal to Inception of Travel)		Closing Time, (Signal to Fully Closed)	
	Oxidizer	Fuel	Oxidizer	Fuel
1	56	55	34	43
2	53	55	33	44
3	54	55	33	42
4	55	55	37	41

TABLE LXXIII

MAIN PROPELLANT VALVE RESPONSE TIMES,
WITH GN$_2$ ACTUATION AT CRYOGENIC CONDITIONS

Test No. 1972-D01-0A	Opening Delay Time, msec- Signal to Inception of Travel Ox	Fuel	Closing Time, msec - Signal to Fully Closed Ox	Fuel	Pulse	Ox Valve Inlet Conditions Temp. °K (°R)	Pressure N/cm² (psia)	Fuel Valve Inlet Conditions Temp. °K (°R)	Pressure N/cm² (psia)
-057	55	63	53	75	1	246 (422)	327 (474)	194 (350)	339 (491)
-058	50	57	55	62	1	239 (430)	341 (495)	203 (365)	348 (505)
-059	49	65	50	74	1	253 (456)	346 (505)	178 (320)	341 (495)
	49	63	51	73	2	253 (456)	348 (500)	167 (300)	322 (467)
-060	49	61	50	63	1	240 (433)	341 (494)	204 (368)	349 (506)
	50	62	50	69	2	244 (440)	336 (488)	182 (328)	333 (483)
-074	50	50	33	37	7	299 (538)	259 (375)	299 (538)	256 (372)
	57	52	33	39	8	↓	↓	↓	↓
	55	55	33	41	9				
	55	54	33	43	10				
	55	54	31	43	11				
	51	51	31	40	12				
	48	50	33	39	49				
	57	55	35	35	50				
	54	53	34	38	51				
	54	33	31	37	53				
	50	52	31	34	54				
-076	44	42	36	40	49	300 (540)	239 (425)	300 (540)	293 (425)
	50	50	37	42	50	↓	↓	↓	↓
	50	49	35	42	51				
	47	47	37	42	52				
	49	47	35	39	53				
	44	46	36	38	54				
-080	56	65	44	54	55	211 (380)	303 (440)	144 (260)	283 (410)
	60	76	48	68	56	↓	↓	↓	↓
	60	74	40	45	57				
	59	71	41	50	58				
	57	68	42	46	59				
	57	67	34	38	60				

Page 381

4.5, Data Analysis (cont.)

One of the contract goals was a 50 msec response time (electrical signal to 90% thrust). Since the ITA was operated with fuel leads that were positive, zero and negative, simultaneous valve opening was not only possible, but was demonstrated. Thus, since there were no valve lead/lag requirements imposed by the hardware, other than avoiding too long of a lead by either propellant, the optimum response time was simply the response of the slowest valve plus the hardware fill time (time from flow initiation to 90% of thrust).

The response time of 40 msec was specified for the main propellant valve assuming 10 msec would be required to go from initiation of flow to 90% of thrust. The actual time required from initiation of flow to reach 90% of thrust was on the order of 6 msec. However, at cryogenic conditions, self actuated or with external actuation, one valve or another had a delay time (signal to initiation of travel) in excess of 50 msec as can be seen from Tables LXVII (ox valve), LXVIII (ox valve), LXXI (ox valve), and LXXIII (fuel and ox valves). The data in Table LXXIV illustrate the point. The response time in Table LXXIV was time from signal to the fuel valve to 90% thrust and for the 24 pulses shown, averaged 62 msec. The fuel valve delay times (signal to initiation of main valve poppet travel) are also shown in Table XXIV. The difference between the response time and the fuel valve delay averaged 6.1 msec for the 24 pulses shown in Table XXIV: this difference was the time required to go from initiation of flow to 90% thrust.

From Table LXXIV, the response time for the six pulses from Test -076 averaged 53 msec which was close to the 50 msec contract goal and on one pulse, a 50 msec response was achieved. However, Test -076 was made at ambient temperature conditions. Operating self actuated the slower main propellant valve, the ox valve, had a delay time (electrical signal to initiation of flow) of 53 msec (average of 36 data points shown in Table LXVIII). Thus, a response time of 59 msec (53 msec valve delay time plus 6 msec from initiation of flow to 90% thrust) was considered to represent the average ITA response time (signal to 90% thrust) with simultaneous valve openings, and the valves self actuated.

TABLE LXXIV

RESPONSE TIMES

Test	Response* Time, msec	Fuel** Valve Opening Delay Time, msec		Test	Response* Time, msec	Fuel** Valve Opening Delay Time, msec
-074	55	50		-076	50	42
	58	52			56	50
	63	55			55	49
	61	54			53	47
	61	54			54	47
	59	51			52	46
	57	50				
	61	55		-080	69	65
	60	53			81	76
	59	53			79	74
	60	53			76	71
	58	52			72	68
					71	67

* Time from electrical signal to 90% thrust.

** Time from electrical signal to initiation of poppet travel (also initiation of flow)

4.5, Data Analysis (cont.)

4.5.2.4 Icing

As discussed earlier, erosion of ITA SN 001 occurred on Test -007, the problem was attributed to ice formation in the fuel manifold on the basis of v.sual observation of ice present in the thruster after testing and on the basis of the pressure data. The pressure histories from Test -106 and -107 are shown in Figure 122 to illustrate how blockage is evidenced in the data.

In the Test -006 data, it can be seen that the normal flow of the fuel resulted in about 48 N/cm^2 (70 psid) pressure drop through the venturi, about 34 N/cm^2 (50 psid) pressure drop across the valve, (28 N/cm^2) (40 psid) line and regen-section pressure loss (valve outlet - P_{fj}) and an injector pressure drop ($P_{fj}-P_c$) of 45 N/cm^2 (65 psid). It should also be noted that the valve outlet transient pressure on startup did not overshoot, but asymptotically approached the steady state value.

By contrast, the following observations can be made for the Test -107 data:

1. There is very little difference in the pressures measured at the venturi inlet (PFV-I), the venturi outlet (PFV-O), the fuel thrust chamber valve inlet (PFTCV) and the fuel thrust chamber valve outlet (PFTCV-O). The smaller the pressure drop the smaller the flow. Therefore, there was very little fuel flow.

2. The approximately 14 N/cm^2 (20 psid) pressure drop through the injector ($P_{fj} - P_c$) indicates that there was some fuel flow and that the blockage was not in the injector.

3. P_c for Test -007 was approximately 1/2 that of Test -006. This indicates low flow.
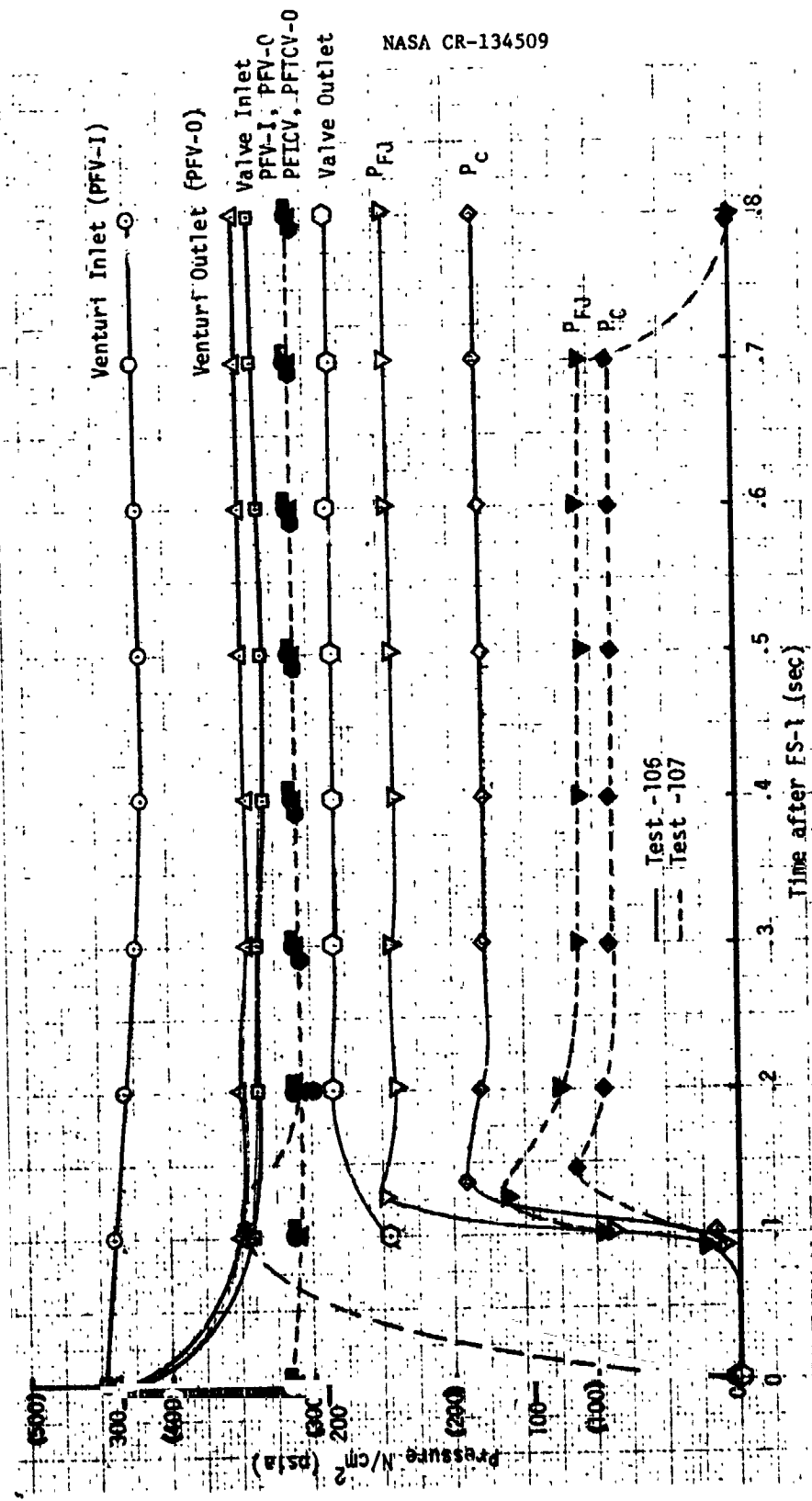
Figure 122. Tests -106 and -107 Pressure Histories

4.5, Data Analysis (cont.)

4. The very high pressure drop between the valve outlet and the injector $[(P_{FTCV-0} - P_{fj} = 28)_{Test -006}$ vs. $(P_{FTCV-0} - P_{fj} = 138)_{test -007}]$ accompanied by a low fuel rate means there was blockage between the valve and the injector.

5. The fact that the valve outlet pressure rises more rapidly in Test -007 than it did in Test -006 and the fact that it overshoots the steady state pressure indicates that either there was less capacitance in the system (smaller volume) or more rapid accumulation (due to reduced outflow). Either of these would be caused by blockage.

The point of blockage indicated in the data would correspond physically to the fuel line downstream of the valve, the torus and the regen section of the chamber. The regen-passages were .127 x .361 cm (.050 x .150 in.) and therefore susceptable to blockage by ice formation. The ice could be formed by cryopumping during the hardware chilldown. Chamber temperatures were on the order of 12°C (-10°F) at the start of the test.

The blockage could have occurred in the fuel line. Following Test -006, there was considerable water standing in the chamber. If there was enough water standing in the chamber it would flow through the injector, down the regen-passages of the horizontally mounted chamber, into the torus and from there into the fuel line. The inlet to the torus was underneath the chamber. The bend in the fuel line that ducts the flow from the 120° circumferential segment of the fuel line to the radial inflow segment was the lowest point in the ITA. Water would collect there and could be frozen by the 139°K (250°R) hydrogen that was used to chill in the hardware.

Test -009 was shut down by the high temperature trip circuit as a result of a temperature excursion registered by thermocouple TN 3.5A (see Figure 79 for thermocouple locations). The temperature transient is shown in Figure 123, where it can be seen that the throat temperature leveled

NASA CR-134509
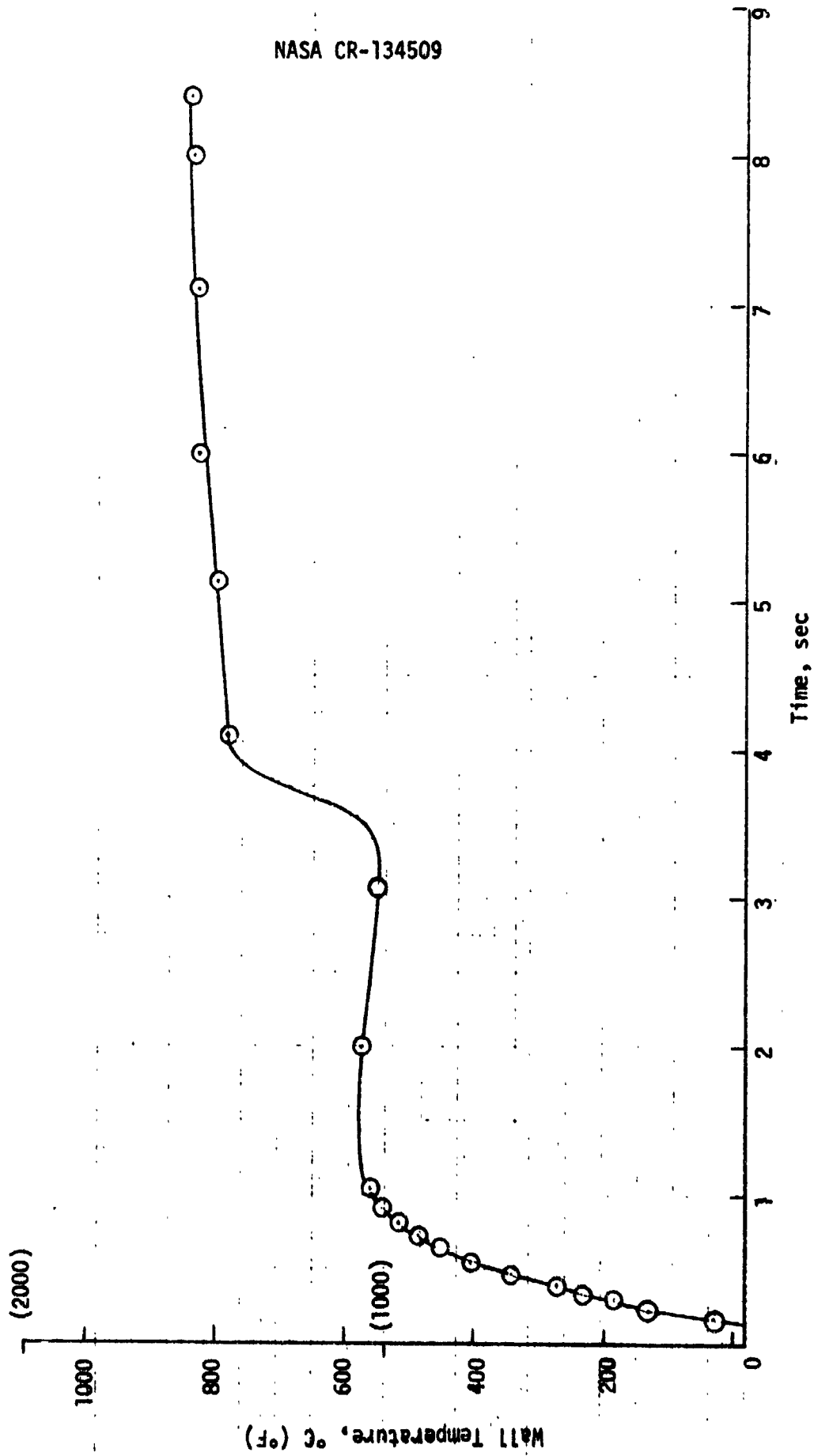
Figure 123. Test -009 Throat Temperature Transient

4.5, Data Analysis (cont.)

out at the normal value and then after 3 sec of elapsed time rose sharply to
a significantly higher value. The excursion was attributed to partial block-
age of the ffc circuit by ice that had formed by cryopumping after the cold flow
that preceeded the test, was broken loose by the vibrations during firing and
was carried to the ffc orifices by the flow. As in the case of Test -007, there
were no abnormalities in the pressure readings taken during a cold flow after
the test indicating that whatever blocked the flow was not present after the
test.

The hydraulic data for Test -009 are shown in Figure 124.
The pressures at the valves are controlled relative to the propellant temperatures.
For this reason, and because of the volume of the accumulators in the system, they
did not reflect the problem, but were included to show pressure drop. Two
items are significant in Figure 124. First, the chamber pressure dropped at
the time the temperature excursion occurred indicating reduced propellant flow.
Secondly, there was a sharp fall off in fuel flow at the time of the excursion
accompanied by an increase in pressure drop $(P_{fj} - P_c)$ indicating blockage.

4.5.3   Thermal

4.5.3 1   Igniter

Igniter SN 003 that was used for the igniter component
checkout test firings was instrumented with six thermocouples as shown in
Figure 125. Four of the six thermocouples were damaged during installation of
the igniter housing into the test fixture and were inoperative (the igniter
test components are shown in Figure 114). The igniter thermal data obtained
with the two remaining thermocouples are given in Table LXXV.
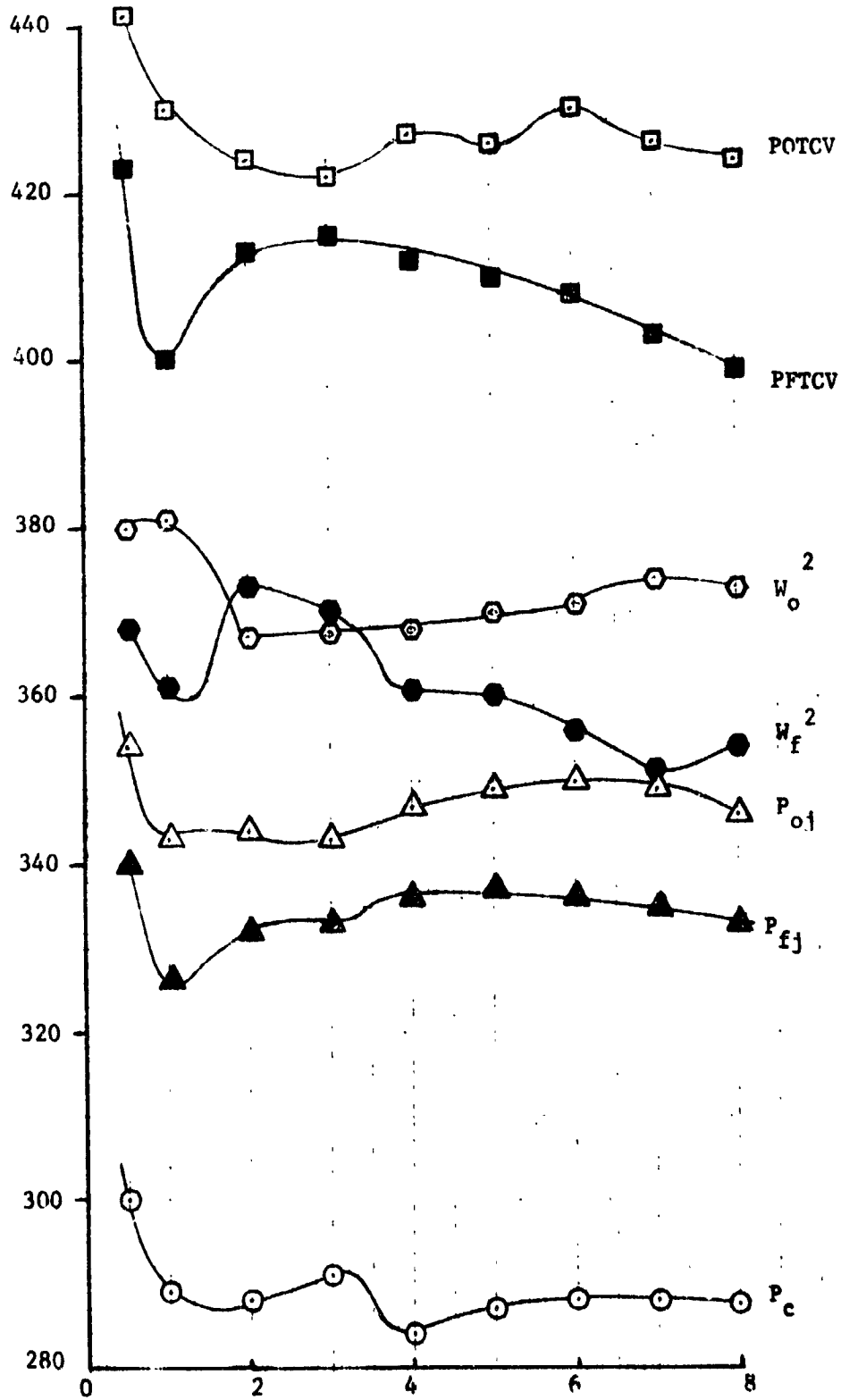
Figure 124. Test -009 Hydraulic Data
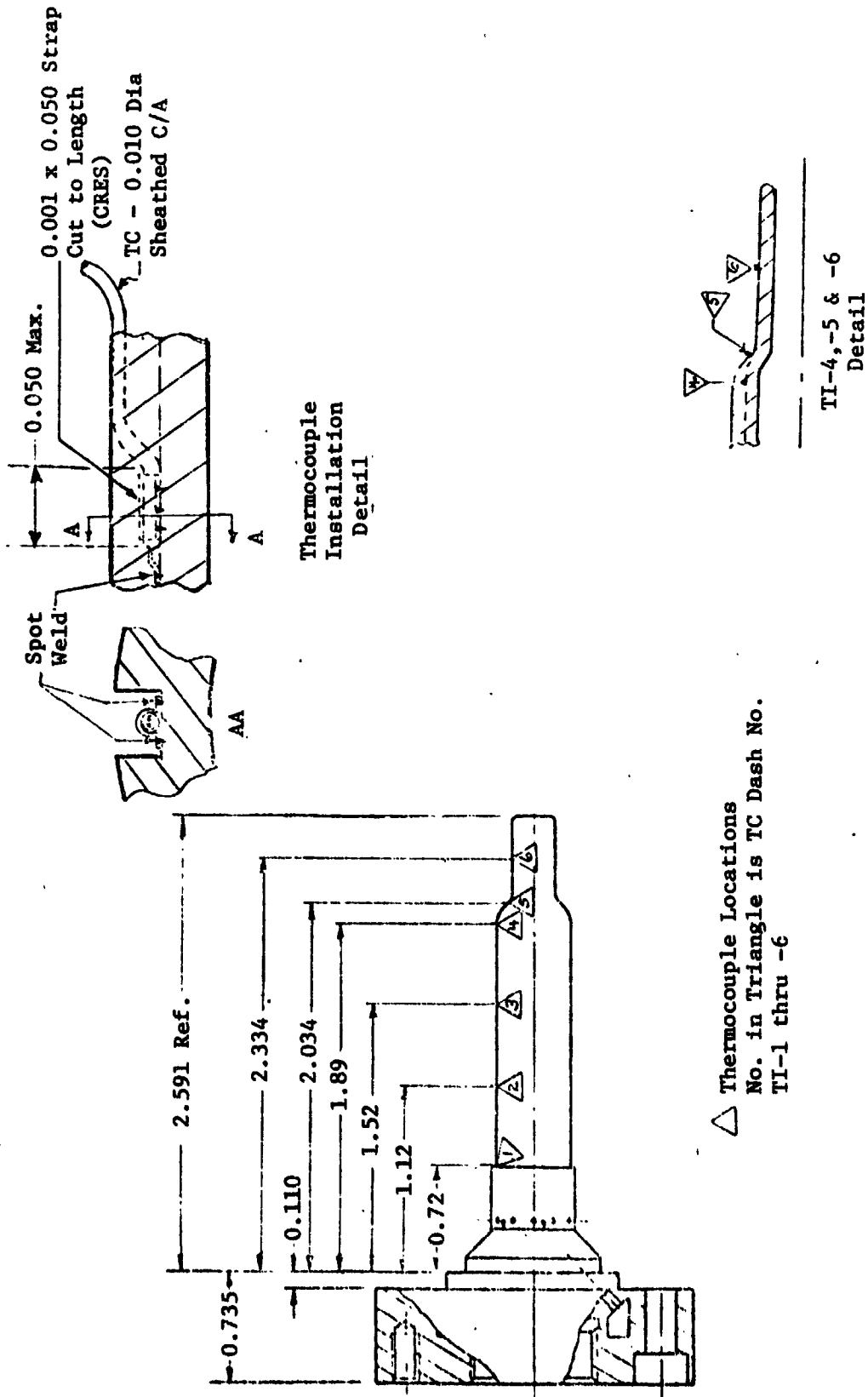
Figure 125. Igniter Thermocouple Locations

TABLE LXXV

IGNITER THERMOCOUPLE DATA

Test	Fuel Temp. °K (°R)	Overall MR	Chamber Pressure, N/cm² (psia)	Temperature, °C (°F)	
				T3	T5
116	173 (312)	3.1	177 (257)	49 (120)	61 (141)
118	183 (330)	5.0	183 (266)	31 (88)	59 (139)
104	289 (520)	6.3	187 (271)	27 (81)	170 (339)
106	289 (520)	2.7	197 (285)	18 (65)	253 (487)
111	183 (329)	3.6	161 (233)	49 (120)	84 (183)
112	185 (333)	5.5	177 (257)	61 (142)	84 (183)
113	188 (339)	5.9	295 (428)	49 (120)	84 (183)
115	166 (298)	4.8	115 (167)	61 (142)	84 (183)
117	246 (442)	5.0	177 (257)	61 (142)	111 (232)
110	167 (300)	4.5	154 (224)	42 (108)	78 (173)
114	178 (320)	7.8	197 (285)	31 (88)	54 (130)
105	289 (520)	5.2	148 (214)	48 (118)	273 (524)

4.5, Data Analysis (cont.)

In the design analysis, a 388°C (730°F) temperature was predicted for the rib location where the thermocouples were installed; the measured igniter temperatures were considerably lower. It is poss.ble that the cooling of the thermocouples by the hydrogen flow resulted in some reduction in the indicated temperature. However, there were factors that would mitigate such an effect; (1) a small cut was made in the rib of the igniter body so that the thermocouple was not installed in the channel itself. The thermocouples were in an area of eddy flow rather than direct flow. (2) The thermocouple would insulate the surface to which it was attached from the coolant flow. Temperatures under the thermocouple should have been higher than if no thermocouple were there.

From the discoloration of the SN 002 igniter housing (Figure 109) that was used for the life cycle testing, it was obvious that the hottest part of the igniter was the aft end. Only the aft -.5 mm was discolored. The heating was probably due to the larger diameter of the injector at that location which would have resulted in lower coolant velocities. The larger diameter resulted because the injector face platelets had a larger ID hole in them than did the ID of the hole in the injector body in which the igniter body was inserted.

The heating of the aft end of the igniter body was not considered to be a problem since: the igniter body was unrestrained; the wall was very thin; the body was made from nickel which has high thermal conductivity and ductility; igniter SN 002 was operated 42,266 times with no evidence of fatigue.

4.5, Data Analysis (cont.)

4.5.3.2 Injector

Injector face temperature data are shown in Figure 126 as
a function of the hydrogen inlet temperature at the thruster valve. The data
shown in Figure 126 are the average of three thermocouple readings and were
t.ken from tests in which the mixture ratio was $4.0 \pm .5$. The predicted face
temperature relationship shown in Figure 126 was based on NAS 3-14354 data
(Ref. 3) and was used in the life cycle design analysis. The predicted
injector face temperature curve in Figure 126 represents an approximate upper
limit for the data obtained on the program, and therefore the injector cycle
life predictions should be conservative.

4.5.3.3 Thrust Chamber

The steady state temperature data for the injector,
chamber (convergent section, throat and skirt) and fuel coolant are tabulated
for each list in Appendix B.

Some of the data for the cha ber are shown in Figure 127.
Only the gas-side data recorded on thermocouple TG-3B (see Figure 79 for thermo-
couple location) have been shown. Gas-side thermocouples, TG-2A, -2B, -3A
and -4A protruded into the gas stream and, as a result, read very high. The
temperatures recorded on these thermocouples, 427 to 538°C (800 to 1000°F) are
inconsistent with the temperatures measured on the exterior and with the physical
appearance of the surface of the copper. There is no way that a 538°C (1000°F)
gradient (gas-side temperature minus exterior) could have been maintained in
the copper liner at the heat flux incident on the chamber wall. Likewise, a
427 to 538°C temperature could not have occurred and the surface of the copper
remained bright as was observed.
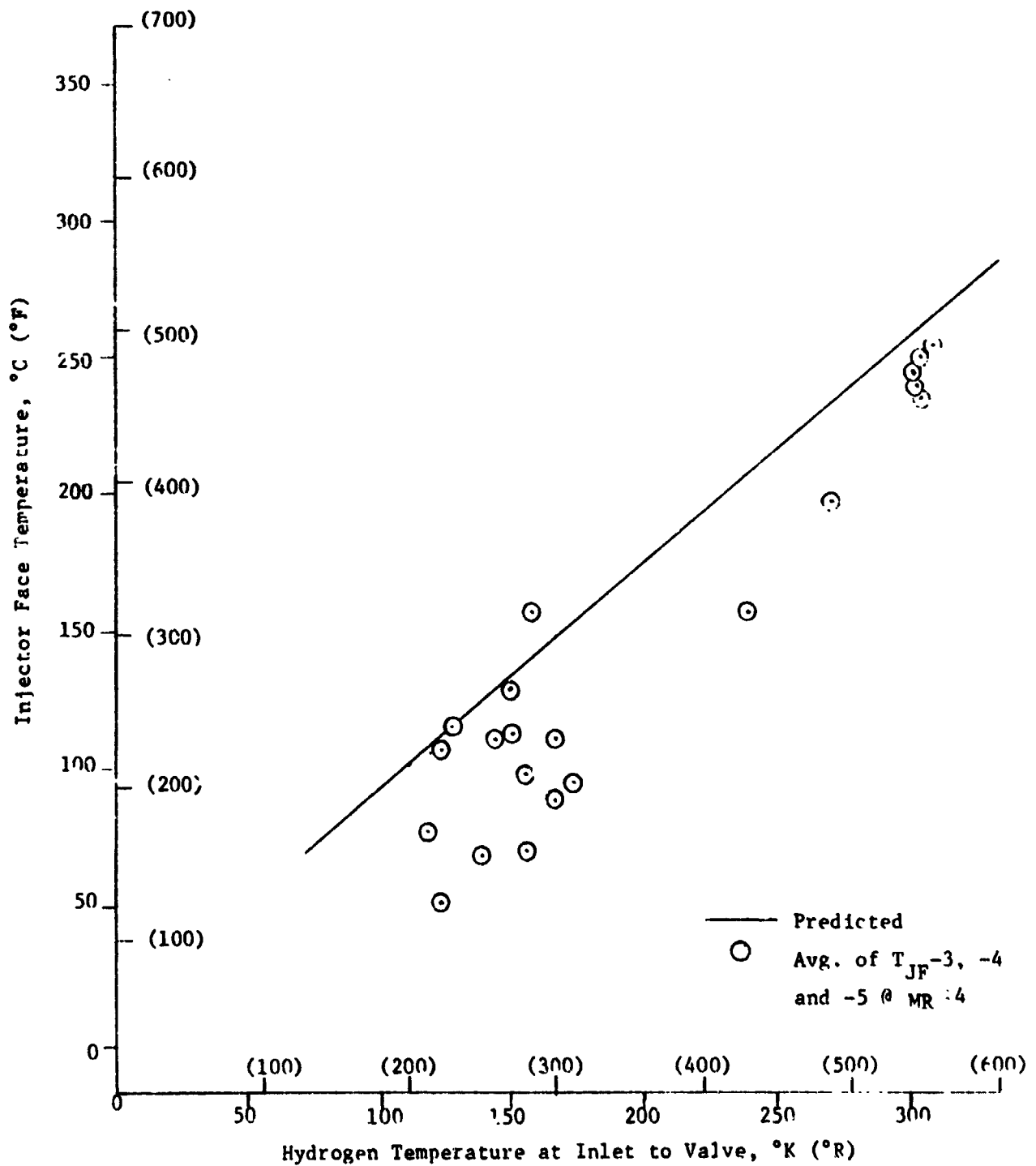
Figure 126. Injector Gas-Side Temperature as a Function of Hydrogen Temperature
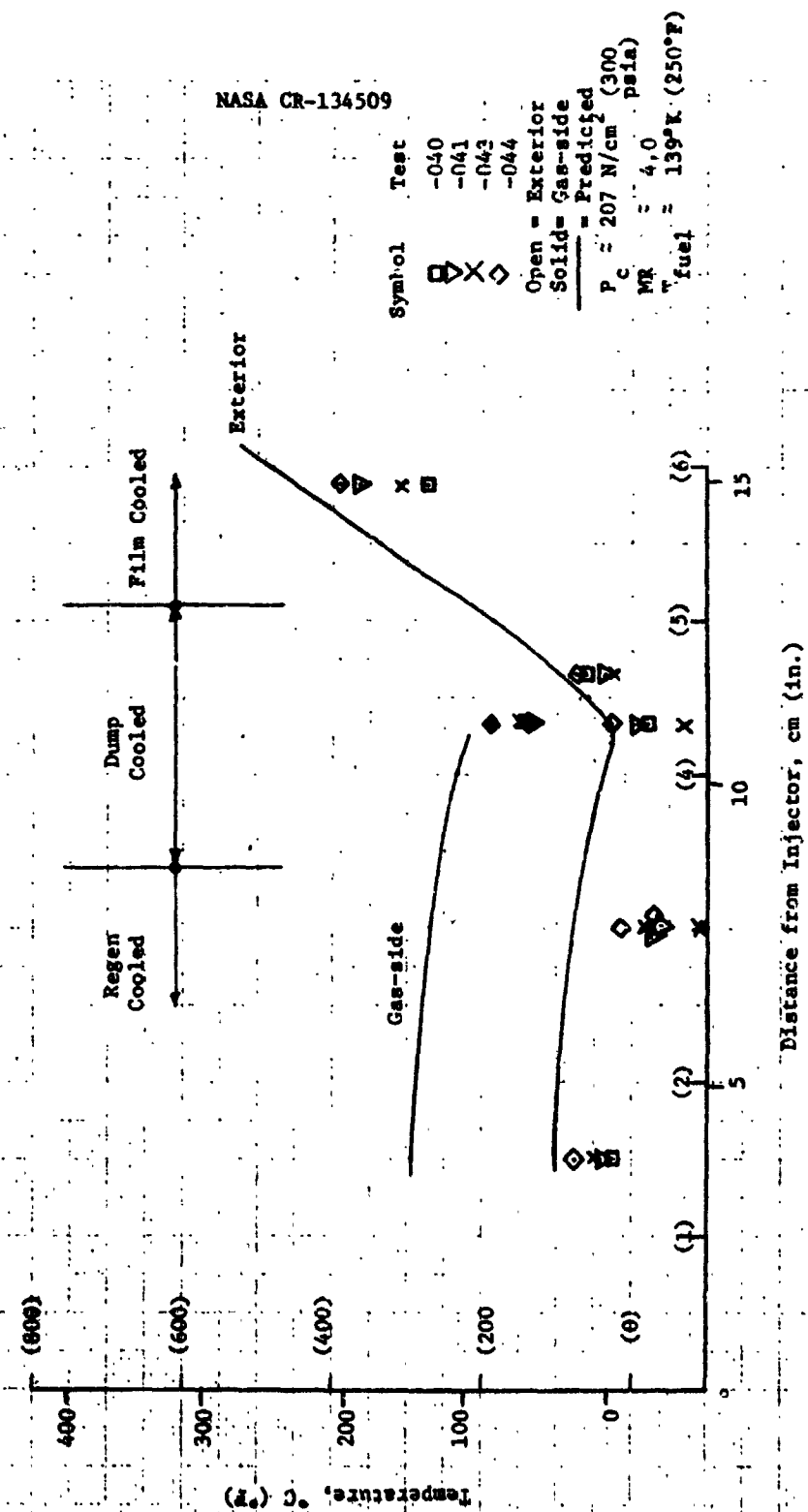
Figure 127. Chamber Steady State Temperature Data

4.5, Data Analysis (cont.)

The predicted temperatures shown in Figure 127 and subsequent figures in this section, were based on Contract NAS 3-14354 data (Ref. 3) and were used in the design analysis. Since the temperatures recorded for the regen section of the chamber were equal to or less than the predicted temperatures, the cycle life predictions for the regen section are considered to be conservative.

The steady state adiabatic wall temperature data for the film cooled portion of the thruster (throat and 40:1 nozzle extension), are shown in Figure 128. There are considerable scatter in the data as a result of the variations in fuel temperature and mixture ratio. The thermocouple data shown in Figure 128 were averaged for each axial station to provide a clearer picture of the axial profile and are shown in Figure 129. The measured temperatures were, in general, higher than predicted and the axial profile has a different shape than predicted. There were slight differences in the ffc injection geometry between the ITA and the NAS 3-14354 chamber on which the prediction was based. The ITA data being lower at the injection point was probably due to more shielding (slightly larger step). The ITA temperature data being higher than predicted from the throat on was probably due to a lower injection velocity. Shear between the core flow and the film coolant reduced the effectiveness of the coolant.

The steady state throat temperatures are shown as a function mixture ratio, hydrogen temperature and chamber pressure in Figures 130, 131 and 132, respectively.

From Figure 130, it can be seen that the throat temperature at a mixture ratio of 4 was 111°C (200°F) higher than predicted; the mixture
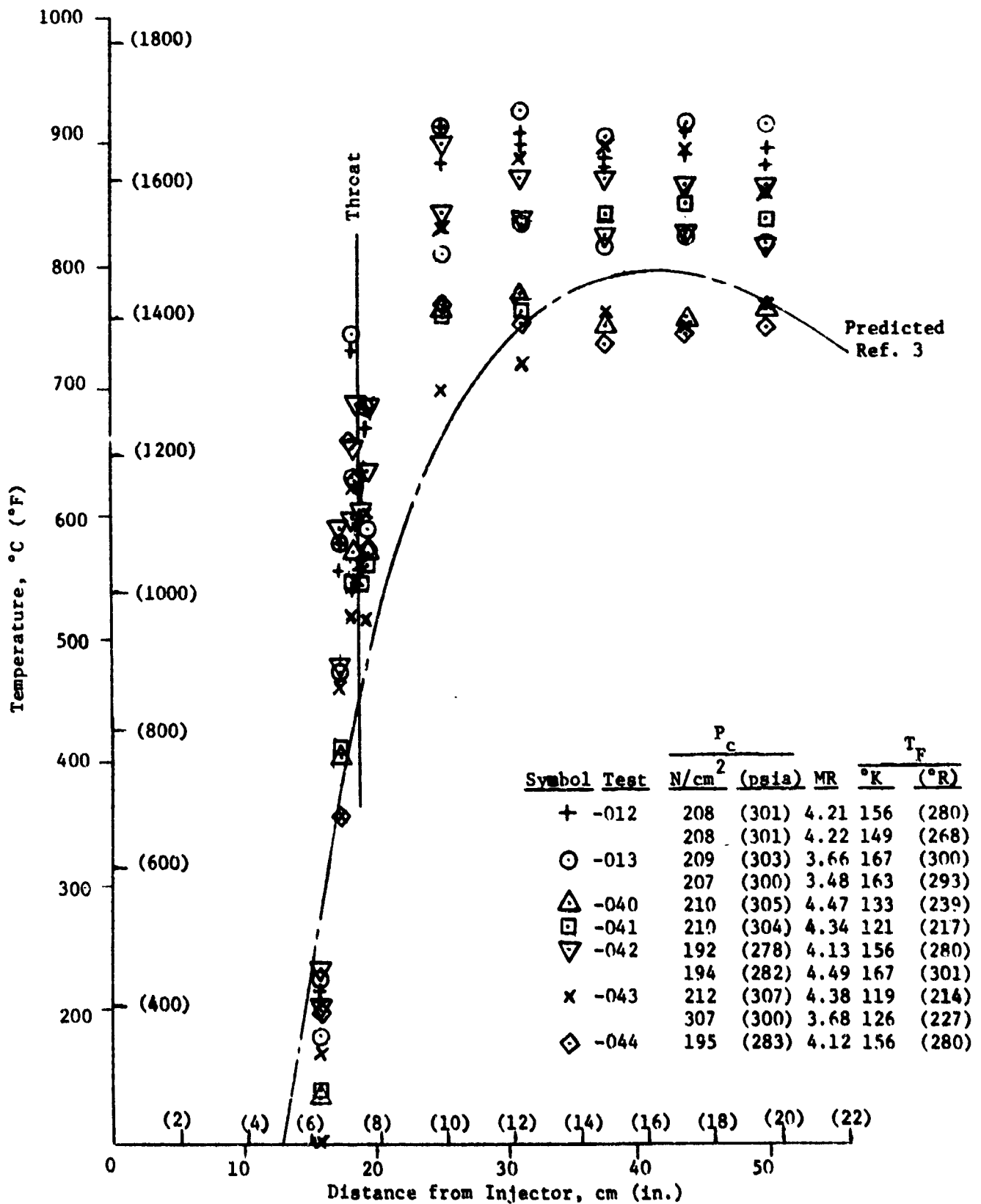
Figure 128. Adiabatic Wall Temperature Profile
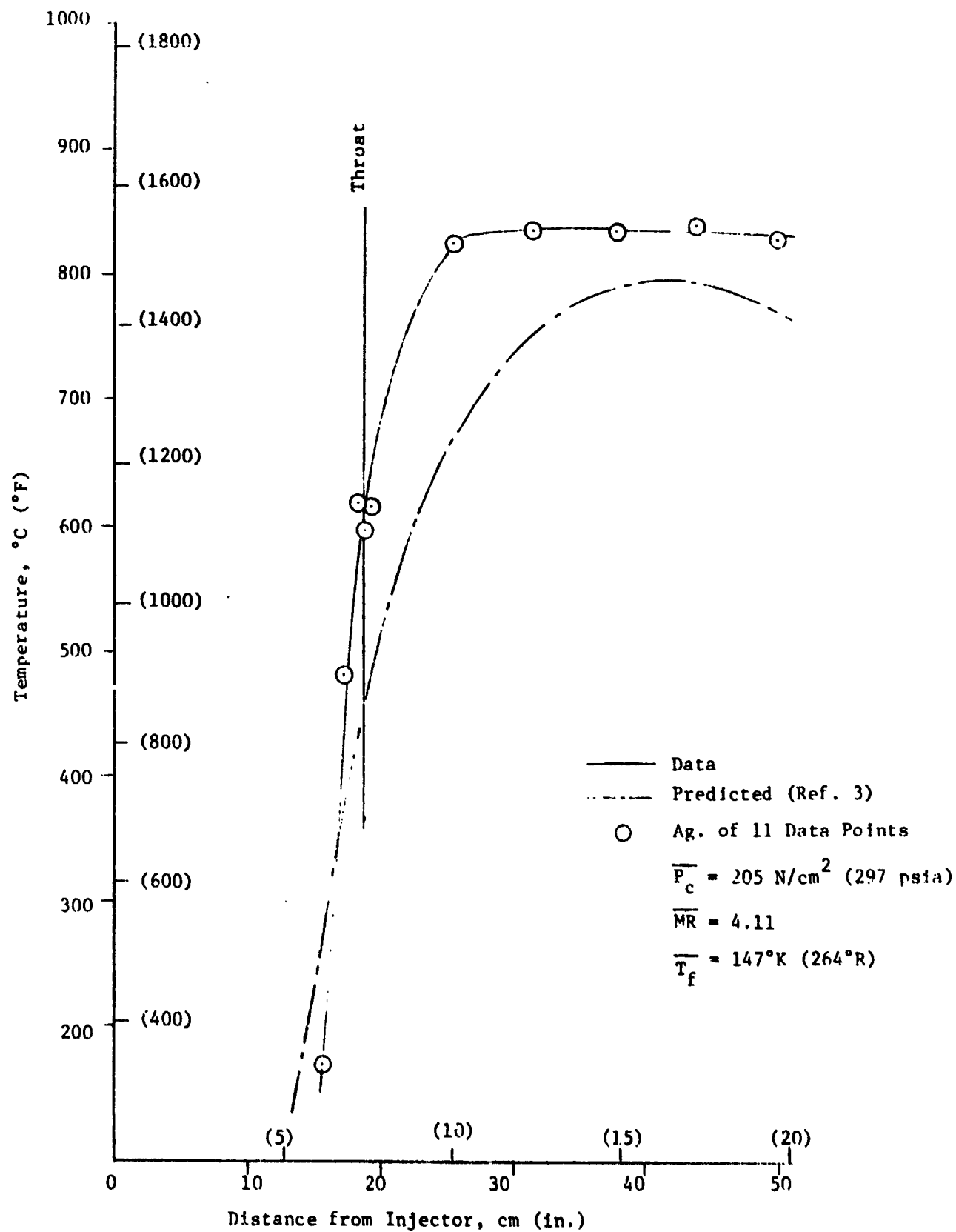
Figure 129.   Nozzle Axial Temperature Profile
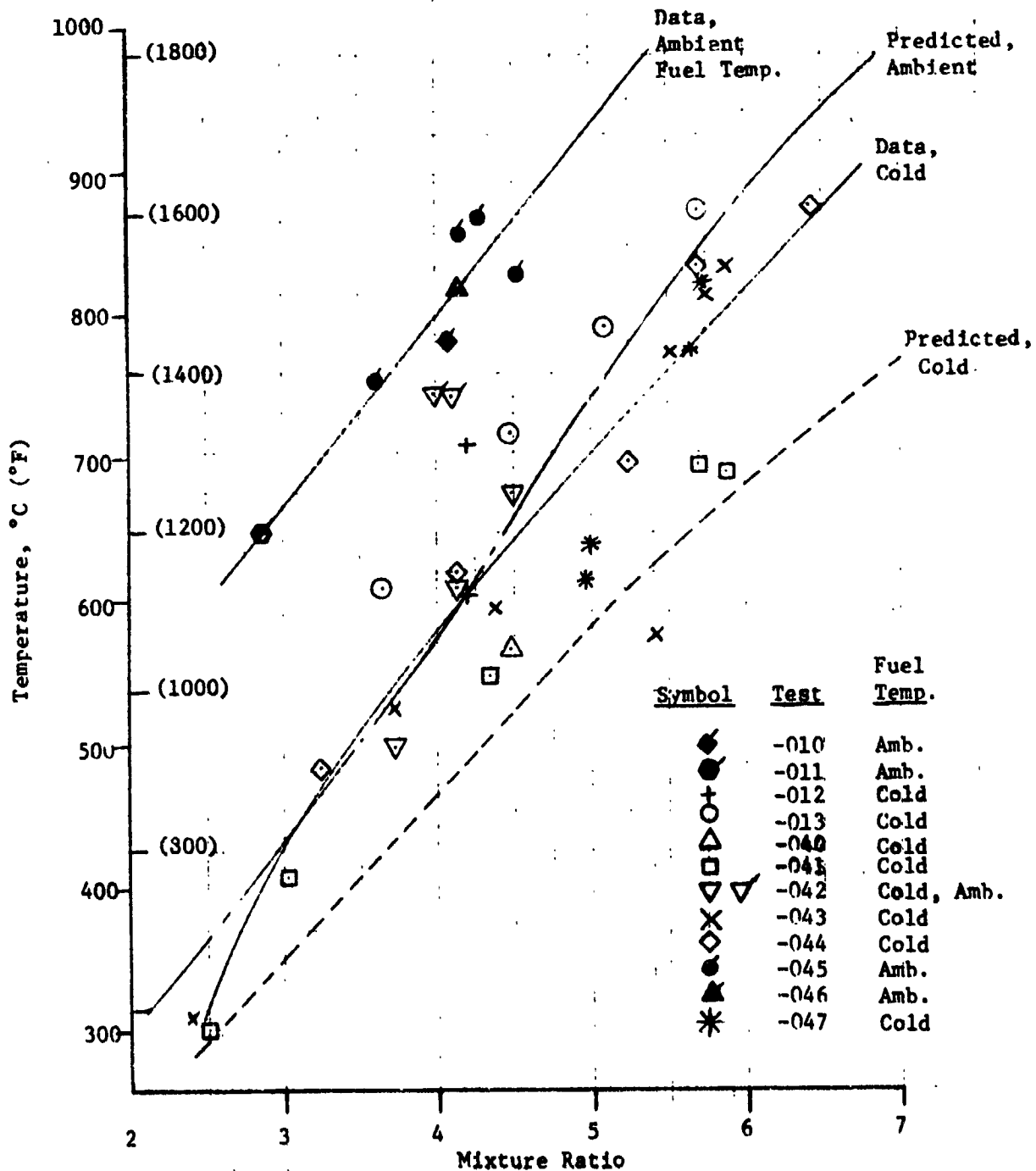
Figure 130. Steady State Throat Temperature vs. Mixture Ratio
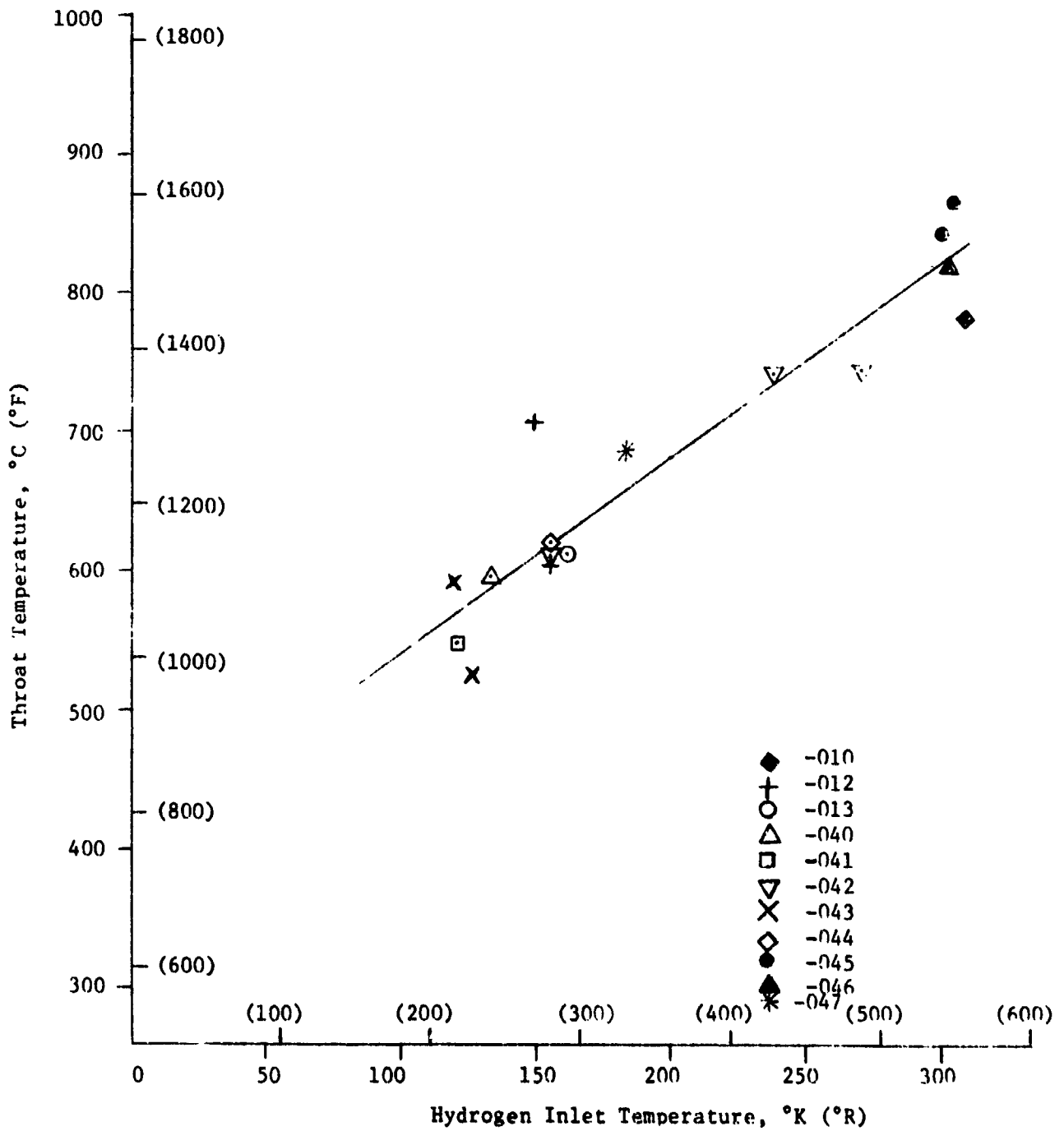
Figure 131. Steady State Throat Temperature as a Function of Hydrogen
Temperature at Inlet to Fuel Valve
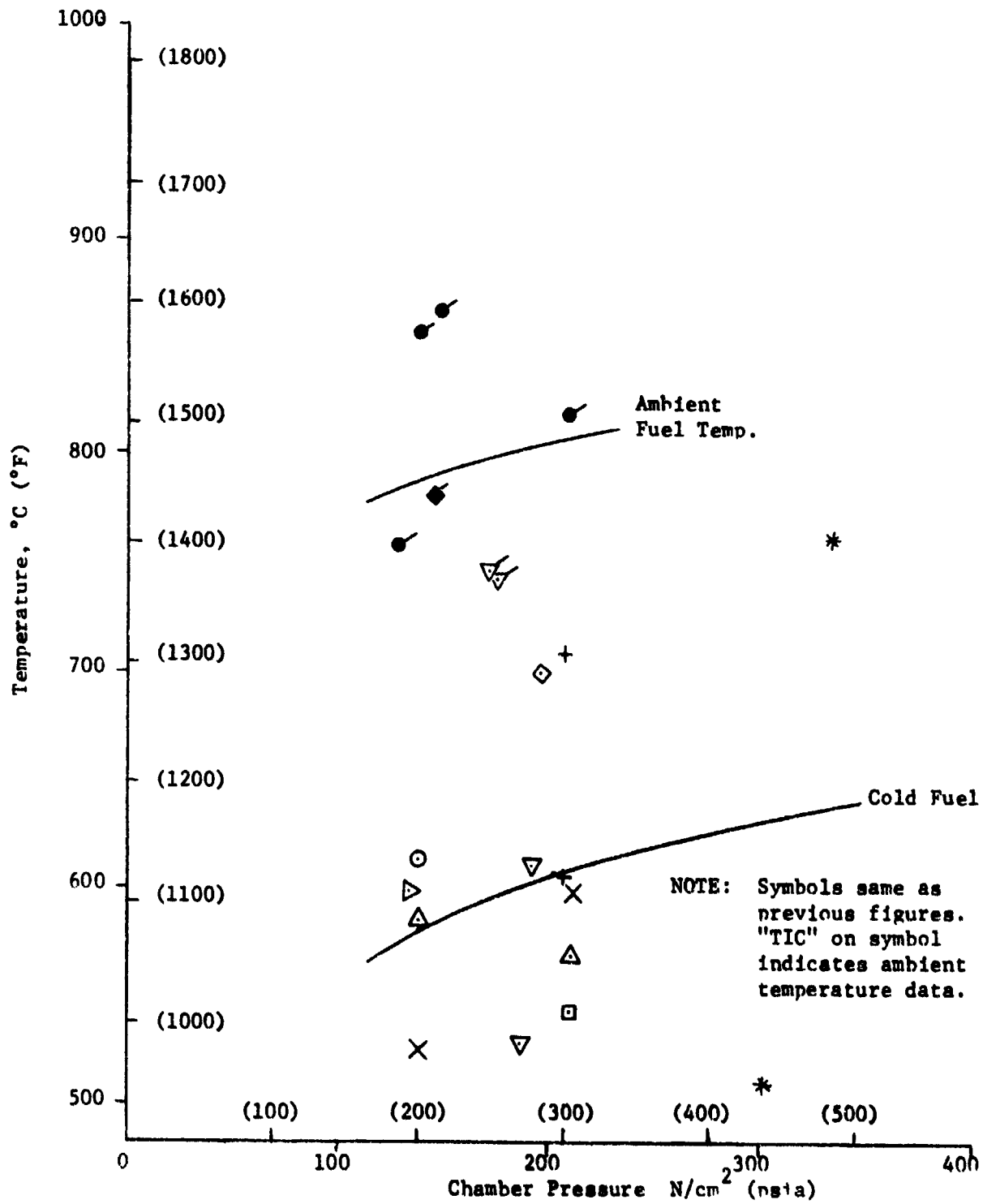
Figure 132. Effect of Pressure on Steady State Throat Temperature

4.5, Data Analysis (cont.)

ratio limit for cold propellants was 6.5 and for ambient propellants, 4.5, on the basis of a 871°C (1600°F) limit. The 871°C (1600°F) limit was selected because Haynes 188 has good yield strength to 871°C (1600°F). The yield strength of Haynes 188 decreases markedly as the temperature is increased above 871°C. The hoop stress in the throat based on adverse tolerances and 345 N/cm^2 (500 psia) chamber pressure would be 25% of yield at 871°C (1600°F), 41% of yield at 982°C (1800°F) and 82% of yield at 1093°C (2000°F).

Based on the data of Ref. 3, it was predicted that there would be a one degree change in throat temperature for each degree change in the fuel temperature. The slope of the line fitted to the data in Figure 131 corresponds to a 1.4 degree change in throat temperature for each degree change in fuel temperature. The difference in sensitivity to fuel inlet temperature probably results from the differences in the method of supplying the fuel film coolant. The Reference 3 data were obtained with a chamber that had a fuel film cooling manifold that was independent of the regen inlet manifold. The film coolant was controlled externally and separately from the regen coolant. The temperature of the fuel influenced only its effectiveness as a coolant not its flow rate. The ITA thruster utilized a common manifold for the regen and film coolant. The flow split was determined by the resistance of the regen section and injector versus the orifices at the inlet to the film coolant channels. The split of hydrogen between the regen section and the film cooled area was affected by the temperature and pressure of the coolant and the heat input to the regen section. Thus, the increased sensitivity to fuel inlet temperature seen in the data from this program was the result of a slight change in film coolant flow in addition to the change in the effectiveness of the coolant.

From Figure 132, it can be seen that there was possibly a slight effect of chamber pressure on throat temperature. However, the effect

4.5, Data Analysis (cont.)

would be difficult to determine precisely because of the scatter in the data
and because it was small (on the order of 50°C increase for a 100% increase
in pressure).

Allowing that chamber pressure has a negligible effect on
ITA throat temperature, affected primarily by mixture ratio and coolant inlet
temperature. An MR vs. P_c operating map based on an 871°C (1600°F) throat
temperature limit is shown in Figure 133. Performance and cycle life operating
limits are discussed in the next two sections.

The nozzle extension temperature data are shown in Figure
134 as a function of mixture ratio for cold and ambient temperature propellants.
Based on the upper limit of the data, the nozzle extension would always be
1093°C (2000°F) or less when the throat reached the 871°C (1600°F) limit. Because
of the low stresses in the nozzle extension and demonstrated capability of the
Haynes 188 at these temperatures, the nozzle extension was not limiting.
Temperatures in the nozzle extension up to 1204°C (2100°F) were considered
acceptable.

The duty cycle that was selected for the cycle life
testing of ITA SN 002 is discussed in Appendix D. In the thermal analysis that
was made to describe the transient temperature response of the throat for the
purpose of evaluating thermal strain, a simple one-dimensional conduction model
was used and heat transfer coefficients derived from Contract NAS 3-14354 data
(Ref. 3). In order to substantiate the analysis, the analytical results were
compared with temperature data obtained during the pulse mode of operation of
ITA SN 001. As shown in Figure 135, the analysis and the thermal data are in
substantial agreement.
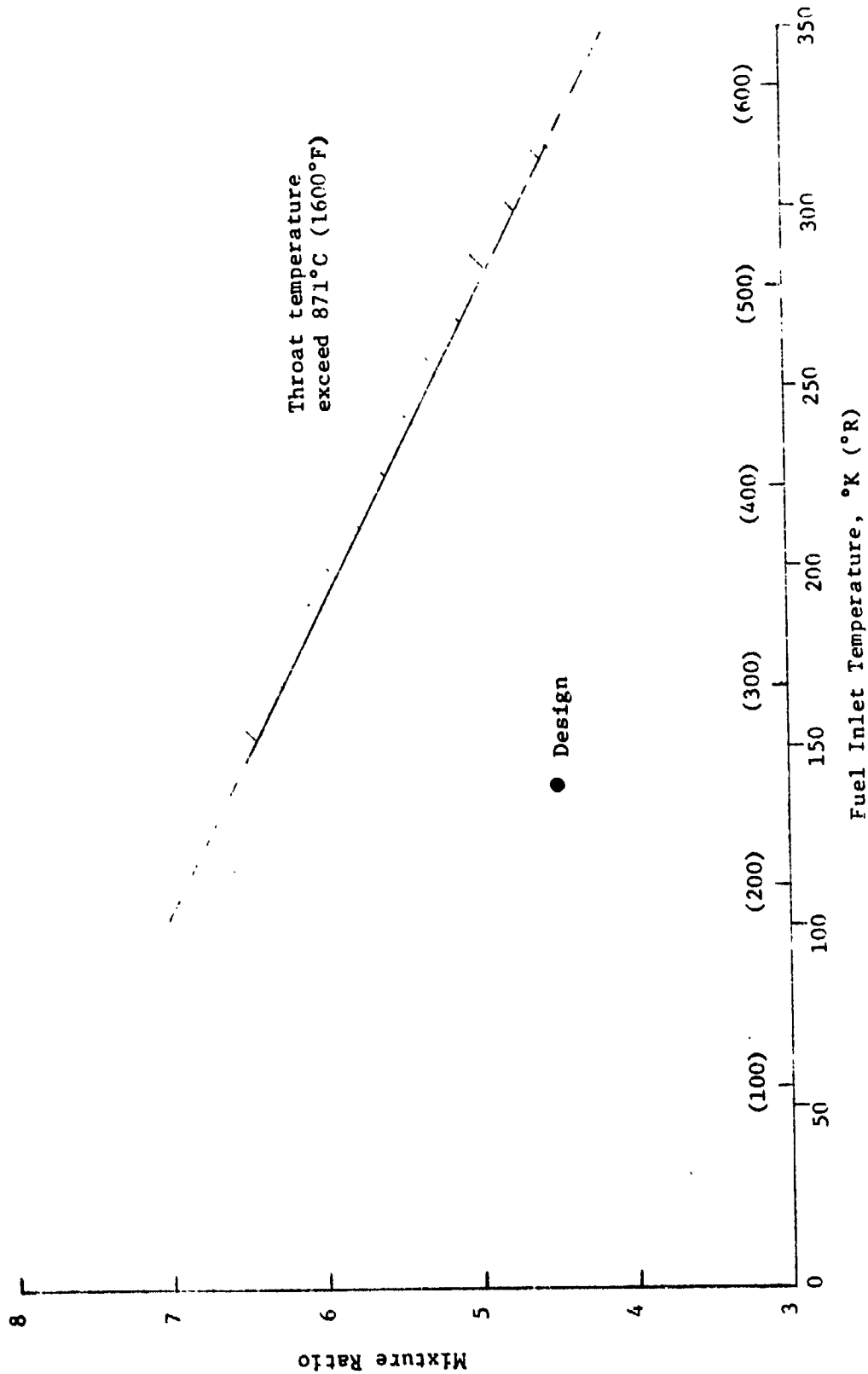
Figure 133. ITA Thermal Operating Limit
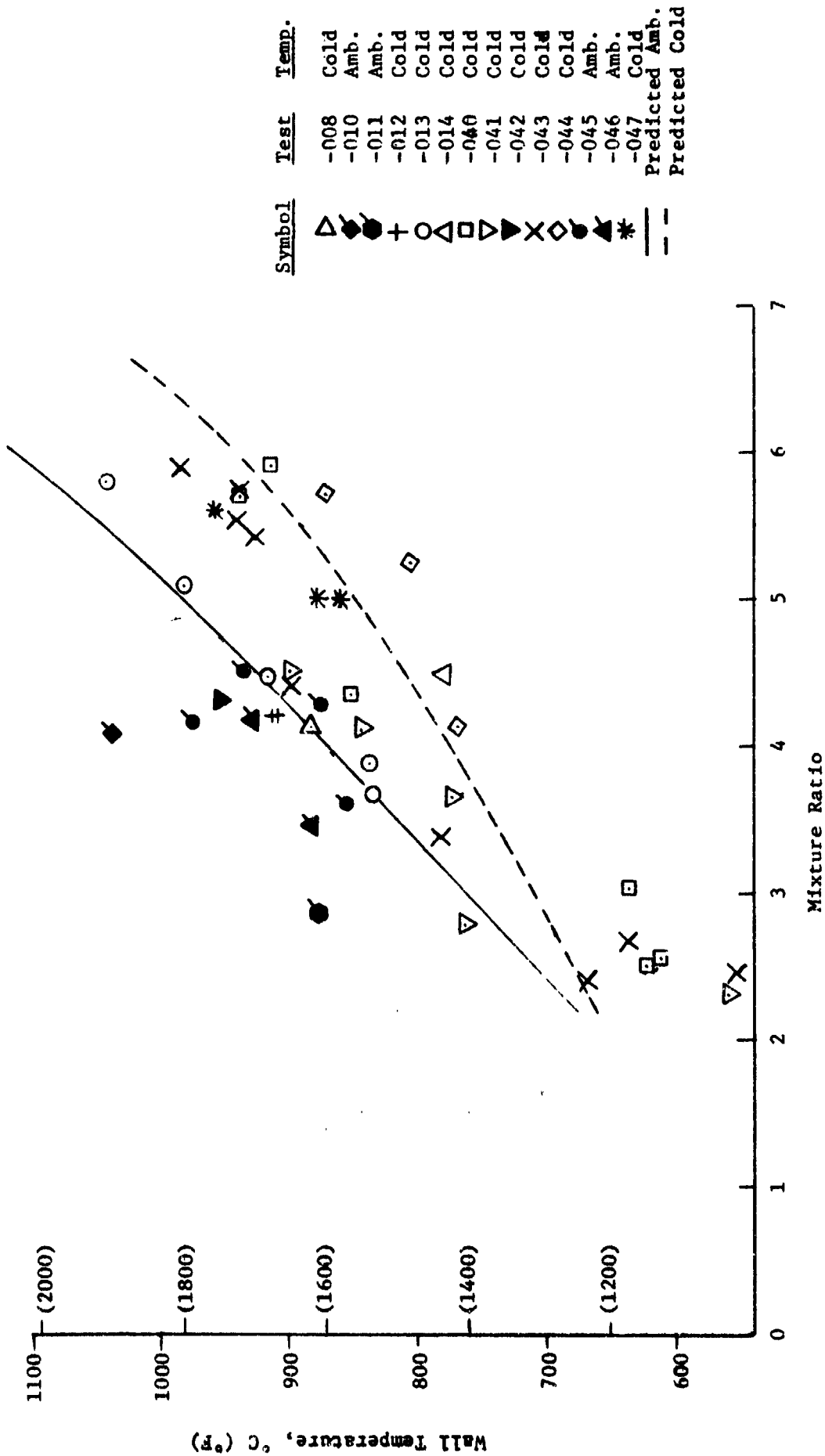
Figure 134. Maximum Skirt Temperature
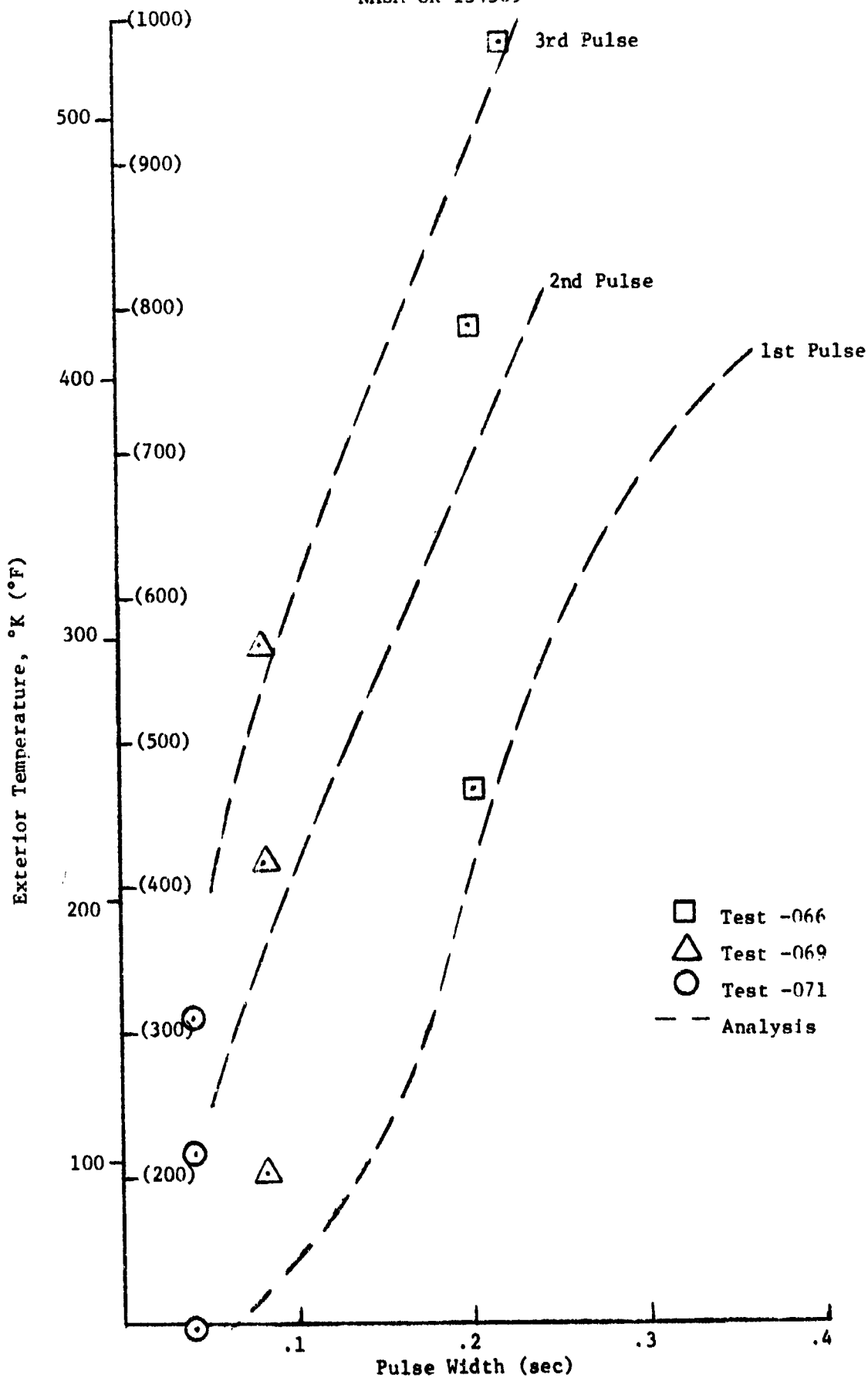
Figure 135.   Transient Throat Temperatures

4.5, Data Analysis (cont.)

Two observations were made from the thermal data obtained during the pulse mode of operation. First, it was not possible to "pump up" any component to a temperature greater than the steady state temperature. ITA SN 001 was pulsed with consecutive pulses of constant on and off times as described in Table XXXVI and with four duty cycles in which the on and off times were varied as described in Table XXXVII; component temperatures during pulsing operation did not exceed those measured during steady state operation at comparable operating conditions. There were no duty cycle limitations that were found relative to thermal operation.

Second, the regen cooled section and injector would rapidly equilibrate after a pulse on steady state firing with cold propellants to a temperature level approximately equal to ambient. Thus, no matter what the firing duration, these components returned to essentially their initial conditions.

These observations have led to two general rules relative to ITA operation and cycle life. Components such as the regen section and injector which exhibit a decrease in temperature on one face due to the cooling of the cryogenic hydrogen, while the other face was heated, reach their maximum ΔT, and therefore thermal strain, in steady state operation. Each pulse produced cumulative damage with the degree of damage approaching that of a full thermal cycle the longer the pulse. On the other hand, the dump cooled section and the film cooled throat were both characterized by increasing temperature for both the exterior and gas-side. The maximum ΔT, and therefore strain, occurred during the start up transient and was more severe the colder the inital temperature. Pulsing increased the initial temperature of these components to a value near steady state. After three or four pulses, very little ΔT and thermal strain were effected by continued pulsing.

4.5, Data Analysis (cont.)

The duty cycle that was selected for the cycle life testing of ITA SN 002 attempted to reconcile the conflicting requirements of components that achieve maximum strain in the start up transient versus those that achieve it in steady state in such a way as to produce one full thermal cycle for every ten pulses and to produce maximum cumulative damage in the throat. Details are given in Appendix D.

4.5.4   Performance

4.5.4.1   Performance Evaluation Methodology

The performance model recommended by the JANNAF Performance Standardization Working Group (Ref. 9) was used on this program to the extent that it is applicable to the designs being evaluated. For the gaseous hydrogen, gaseous oxygen thruster, the JANNAF methodology is incomplete in modeling the combustion process and the film coolant process. The following paragraphs will provide a discussion of the general methodology including the applicable portions of the JANNAF procedures.

The technique used for evaluation and prediction of performance considers the one-dimensional equilibrium (ODE) flow conditions to be the base case. As seen in the following equations, all performance losses are subtracted from the base case:

$$I_{sp_{(delivered)}} = I_{sp_{(ODE)}} - \Sigma I_{sp \; losses}$$

4.5, Data Analysis (cont.)

Theoretical thermochemical performance is evaluated using the NASA-LeRC One Dimensional Equilibrium computer program (Ref. 10). This documented program computes one-dimensional flow in chemical equilibrium and is the basis for all $\% I_{sp}$ and $\% c^*$ quotations.

Six primary specific impulse losses are considered in the specific impulse performance methodology: kinetic (expansion), nozzle divergence, boundary layer, mixture ratio distribution, energy release, and coolant performance loss. The first four losses are evaluated in a manner similar to the JANNAF methodology. These will be briefly described along with specification of the applicable computer program(s) and required input assumptions.

The kinetic performance loss accounts for the performance degradation because of chemical recombination lag during the gas expansion process. Kinetic effects are considered in the JANNAF Two Dimensional Kinetic Computer Program (Ref. 11) (TDK). The program calculates the kinetic rate limited performance for an axisymmetric nozzle on either a one or two dimensional basis. JANNAF recommended reaction rate constants (Ref. 12) were used in the analysis.

Nozzle divergence loss is a measure of the performance which is lost due to non-axially directed momentum at the nozzle exit. Nozzle divergence efficiency is calculated with the TDK computer program described in the previous paragraph.

The boundary layer loss accounts for the degradation in performance due to shear drag and nonrecoverable heat transfer at the thruster walls. The JANNAF Turbulent Boundary Layer Program (Ref. 12) (TBL) is used to evaluate this loss.

4.5, Data Analysis (cont.)

The coolant model described herein accounts for the
performanc penalty associated with the resultant nonuniform propellant mixture
ratio distribution and the thermal energy transport from the high temperature
core to the low temperature boundary flow. The basic assumptions are summarized
as:

1.   Film bulk temperature is obtained from empirically
     measured thermal data.

2.   Energy is assumed to be exchanged upstream of throat.

3.   Energy is extracted uniformly from core.

4. $\Delta h = \int_{T_{IN}}^{T_B} C_p \, (dt)$

5. $(\dot{w}\Delta h)_{core} = (\dot{w}\Delta h)_{coolant}$

where:

Δh = enthalpy

C_p = specific heat at constant pressure

T_B = bulk film coolant temperature

T_{IN} = inlet film coolant temperature

Computationally, the heat is removed from the core by reducing the propellant
enthalpy by an amount which corresponds to the total enthalpy gained in the
coolant stream tube when it is heated from its inlet temperature to the final
bulk coolant temperature. Both stream tubes -- the heated coolant and reduced
enthalpy core -- are then expanded to the nozzle exit conditions and the
coolant performance decrement is computed using the following relationship:

4.5. Data Analysis (cont.)

$$\Delta I_{sp,coolant} = I_{sp,O/F,overall} - \frac{\left[\dot{w}_{core} \, I_{sp,core \, O/F \atop -\Delta h} + \dot{w}_{coolant} \, I_{sp,O/F = 0 \atop +\Delta h}\right]}{\dot{w}_T}$$

        The model assumes no species transport between the core and coolant stream tubes. However, parametric evaluation of this model with variable species transport and variable coolant bulk temperature rise show the coolant performance loss to be insensitive to these influences. The percentage of hydrogen coolant is the primary determinant of the coolant performance loss.

        If a nonuniform propellant injection occurs across the injector face, a performance loss will result (MRDL). This loss is primarily caused by uneven manifold flow paths and igniter cooling. The igniter cooling loss is considered separately using a stream tube flow model. The loss due to mixture ratio maldistribution caused by manifolding related distribution is included in the injector (ERL) Energy Release Loss.

        Energy Release Loss (ERL) accounts for the performance caused by incomplete mixing of the injected gases and thus is a measure of the injector mixing efficiency. For the gaseous propellants, the energy release performance loss is attributed to an enthalpy reduction resulting from incomplete mixing and reaction. Since the chemical reaction rates of gaseous hydrogen – gaseous oxygen are sufficiently fast above 2760°K (4500°F) (3 < O/F < 30) reaction rate limitations are a second order effect. Deviations in local mixture ratio from the overall injection mixture ratio, however, result in nonuniform heat release, added thermal dissociation, and nonoptimum chemistry

4.5, Data Analysis (cont.)

so that the mass weighted sum of the enthalpies of all stream tubes is less than the enthalpy which would result from a homogeneous mixture. Thus, local micro-scale mixture ratio nonuniformity has a first-order effect on gaseous hydrogen – gaseous oxygen thruster energy release efficiently and is considered to be the rate controlling energy release mechanism.

Because of the complexity of the process, no analytical model is currently available which will reliably predict gas/gas energy release efficiency from design and operating conditions without empirical data. There-fore, the energy release efficiencies presented in this section are based on test data analysis results. This is expressed mathmatically by the following relationships:

$$ERL \text{ (sec)} = I_{sp_{(ODE)}} - I_{sp_{DEL}} - \left[\Delta I_{sp_{KL}} + \Delta I_{sp_{DL}} + \Delta I_{sp_{BL}} + \Delta I_{sp_{MRMD}} + \Delta I_{sp_{CL}}\right]$$

and

$$\% \ ERE = 1 - \frac{ERL}{I_{sp_{ODE}}} = \frac{I_{sp_{DEL}}}{I_{sp_{ODE}}} + \frac{1}{I_{sp_{ODE}}} \left[\Delta I_{sp_{KL}} + \Delta I_{sp_{DL}} + \Delta I_{sp_{BL}} + \Delta I_{sp_{MRMD}} + \Delta I_{sp_{CL}}\right]$$

where

$I_{sp_{ODE}}$ = One dimensional equilibrium specific impulse (theoretical), sec

$I_{sp_{DEL}}$ = Delivered specific impulse, corrected to vacuum, sec

$\Delta I_{sp_{KL}}$ = Specific impulse loss due to kinetic expansion

$\Delta I_{sp_{DL}}$ = Specific impulse loss due to nozzle divergence

4.5, Data Analysis (cont.)

Early in the data analysis task, both thrust and flow measurement problems were identified. It was noted that there was generally a negative thrust bias at the conclusion of the cold propellant tests. The bias was correlated as a function of run duration and a thrust correction in factor was developed based on the pretest zero.

Two types of flow measurements were used during the test program. Tests -003, -004 and -006 were made with the flow controlled and measured by venturis upstream of the test stand valves. Starting with Test -008 and for all subsequent tests, propellant flow rates were measured with Ramapo flow meters. In calculating performance, the measured fuel flow rate was increased by 2% on the basis of the post-test water flow calibration of the fuel Ramapo meter and the oxidizer flow was increased by 3.8% on the basis of the results from the propellant flow calibration tests, -048 and -049 (see Section 4.5.2.2). The data presented in Appendix C include the corrections to thrust and flow rate described above.

To determine the cause of the apparent high performance reported in Appendix C, the % ERE was plotted as a function of propellant temperature, time and propellant injection velocity ratio. The only anomaly that was apparent existed in the correlation relative to the oxidizer temperature. The plot of % ERE versus oxygen temperature at the inlet to the valves is shown in Figure 136. Of the approximately 100 data points with oxygen temperatures in excess of 211°K (380°R), only nine (four Test -010 data points are obscured by the list of symbols in Figure 136) have ERE values less than 100%. Of the 35 data points corresponding to oxygen temperatures between 189°K (340°R) and 211°K (380°R), 30 have ERE values less than 100%. There was a dramatic decrease in performance when operating with oxygen temperatures less than 211°R (380°R).
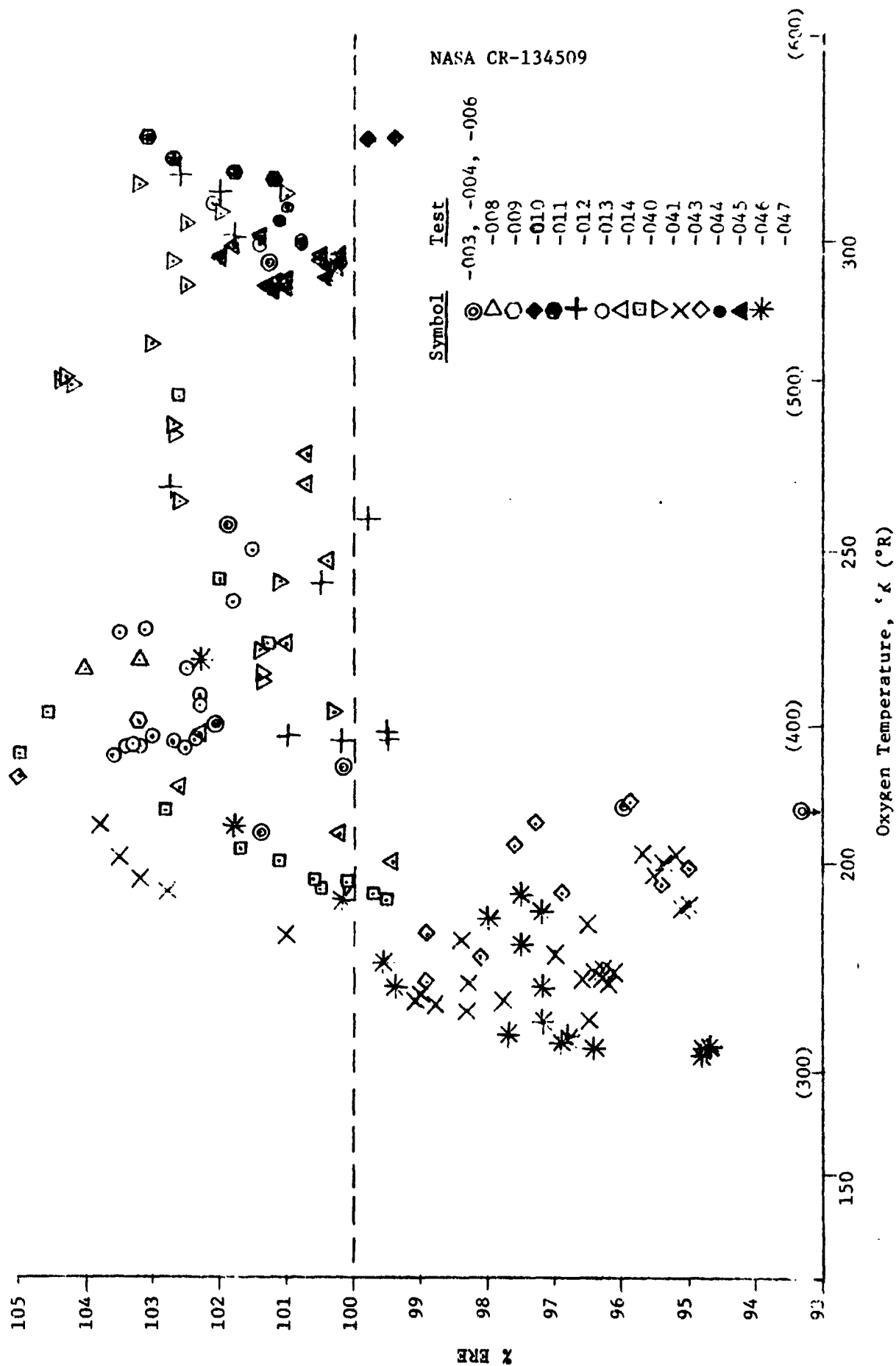
Figure 136. % ERE as a Function of Oxygen Inlet Temperature

4.5, Data Analysis (cont.)

The sharp decrease in performance at near-nominal oxygen temperatures does not necessarily suggest a thrust problem. A thrust problem that was temperature related would probably have to result from contraction of a line and therefore should have occurred uniformly over the entire temperature range. Moreover, the low ERE data points have low c* values. Although not as pronounced as the % ERE vs. oxygen temperature, a plot of % c* vs. oxygen temperature has the same general appearance. This relationship suggests a $\dot{w}$ flow measurement problem. The problem was not peculiar to the Ramapo flow meter, however, since data obtained with venturi flow measurements (Tests -003, -004 and -006 in Figure 136) show the same effect with oxygen temperature.

The problem may have resulted from liquid oxygen being present in the feed system. Prior to fire switch, the gaseous oxygen was pressurized in the system which includes a heat exchanger using liquid nitrogen to chill the oxygen. The oxygen in the heat exchanger coils in contact with liquid nitrogen, liquifies and is subsequently vaporized by the sensible heat from the heat exchanger coils not in contact with liquid nitrogen (only a small part of the heat exchanger was required to be filled with liquid nitrogen to accomplish the oxygen temperature conditioning) and the outlet line from the heat exchanger. With one exception (Test -042), the measured temperature of the oxygen leaving the heat exchanger was in excess of the saturation of critical temperature, however, the oxygen flow could have been a two phase mixture of warmer gas with entrained liquid.

4.5.4.2 Steady State Performance

The performance data are tabulated in Appendix C. As can be seen from the data, the % ERE is 100 or greater for 62% of the data points. In some instances, even the delivered performance efficiencies (% I_s and % c*) are greater than 100%.

4.5, Data Analysis (cont.)

All aspects of the testing from thrust stand calibration to flow meter calibration were reviewed relative to the two anomalies (ERE in excess of 100% and performance shift with oxidizer temperature). On the basis of Test -042, the flow meter calibration problem discussed in Section 4.5.2.2 and the fact that both % c^* and % I_s are affected by oxygen temperature, the shift in performance would appear to be a flow measurement problem possibly resulting from two phase flow. In Test -042, oxygen at liquid temperatures was detected leaving the heat exchanger; the chamber throat temperatures subsequently increased abnormally to levels characteristic of a high MR, but there was no change in chamber pressure, thrust or indicated flow rates. In Tests -048 and -049, the Ramapo flow meters were calibrated against the venturis using cold and ambient propellants. The results for the ox system varied from agreement between the two flow devices to as much as 10% difference depending on proximity to the saturation temperature and whether a given data point was being approached from a lower flow rate (pressure increased) or a higher flow rate (pressure decreased).

The two anomalies, high performance and performance change with oxygen temperature, apparently result from phenomena or interactions that are too subtle or complex to be discovered from data from this program. In order to circumvent the problem and obtain an evaluation of performance, the following approach was taken.

On Contract NAS 3-14354 (Ref. 3) and on an ALRC IR&D program, three thrust chamber assemblies utilizing a regen chamber, a regen/dump-film cooled chamber similar to the ITA and a film cooled chamber were tested using gaseous hydrogen-oxygen propellants. The injectors used for those thrust chamber assemblies were identical to the ITA in the essential design features. The ITA fuel circuit was composed of essentially the same design of platelets; the original platelet photoetch negatives (fabrication masters) had been retained and were used to make the ITA fuel platelets. The ITA oxidizer elements were made to the same drawing that was used to make all earlier elements.

4.5, Data Analysis (cont.)

It was therefore reasonable to expect that the injector would have the same ERE as the prior hardware. In Figure 137, the performance of the three earlier thrust chamber assemblies is shown as a function of % ffc. Also shown are lines corresponding to various values of ERE. At operating conditions corresponding to 21% ffc, all three designs have an 98.75% ERE. If it is assumed that the ERE of the ITA injector is 98.75%, then the ratio of 98.75% to the % ERE calculated for each data point from the measured conditions constitutes a correction factor.

Figure 138 summarizes the ITA performance data corrected to a 98.75% ERE as described above. The data shown in Figure 138 were taken from all tests whose operating conditions fall in the range specified in the figure and cover the entire range of oxygen temperatures. The smoothed data correlate excellently to hydrogen temperatures and chamber pressure. Using Figure 138 to describe performance, it can be seen that at nominal hydrogen inlet conditions, 207 N/cm^2 (300 psia) chamber pressure and a mixture ratio of 4 the performance was 4266 N-sec/kg (435 lb$_f$-sec/lbm).

The effect of fuel inlet temperature on performance was the same as correlated in Ref. 3. The smoothed specific impulse data are shown in Figure 138 as a function of the hydrogen temperature at the inlet to the fuel valve. No attempt was made to distinguish between 138 N/cm^2 (200 psia) and 207 N/cm^2 (300 psia) chamber pressure data because the variation due to pressure was approximately equal to that resulting from the MR range (3.8 to 4.2). The slope of the line in Figure 138 reflects identical sensitivity of performance to hydrogen temperature as stated in Ref. 3.
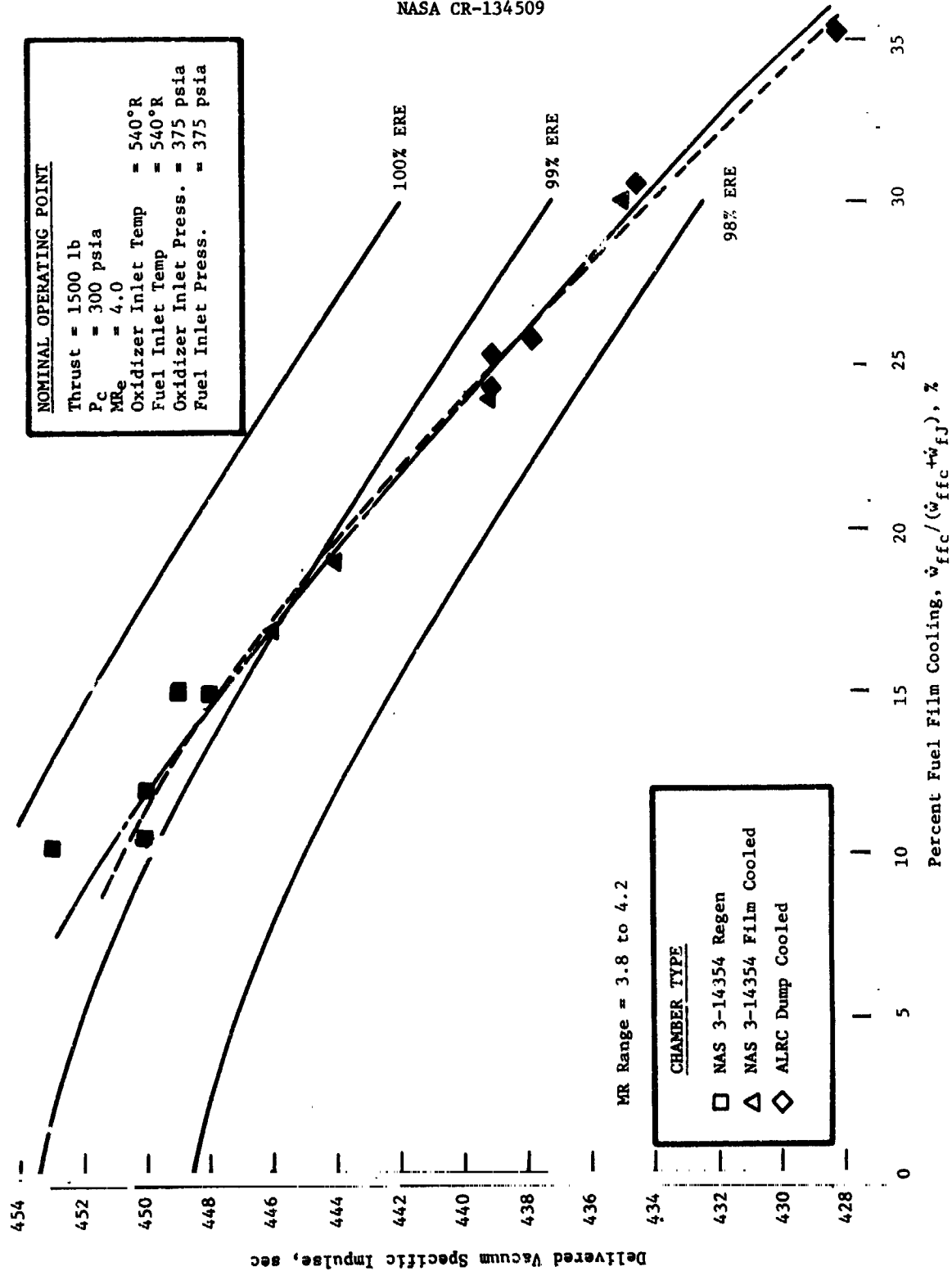
Figure 137. Effect of Chamber Type on "I" Premix Injector Performance
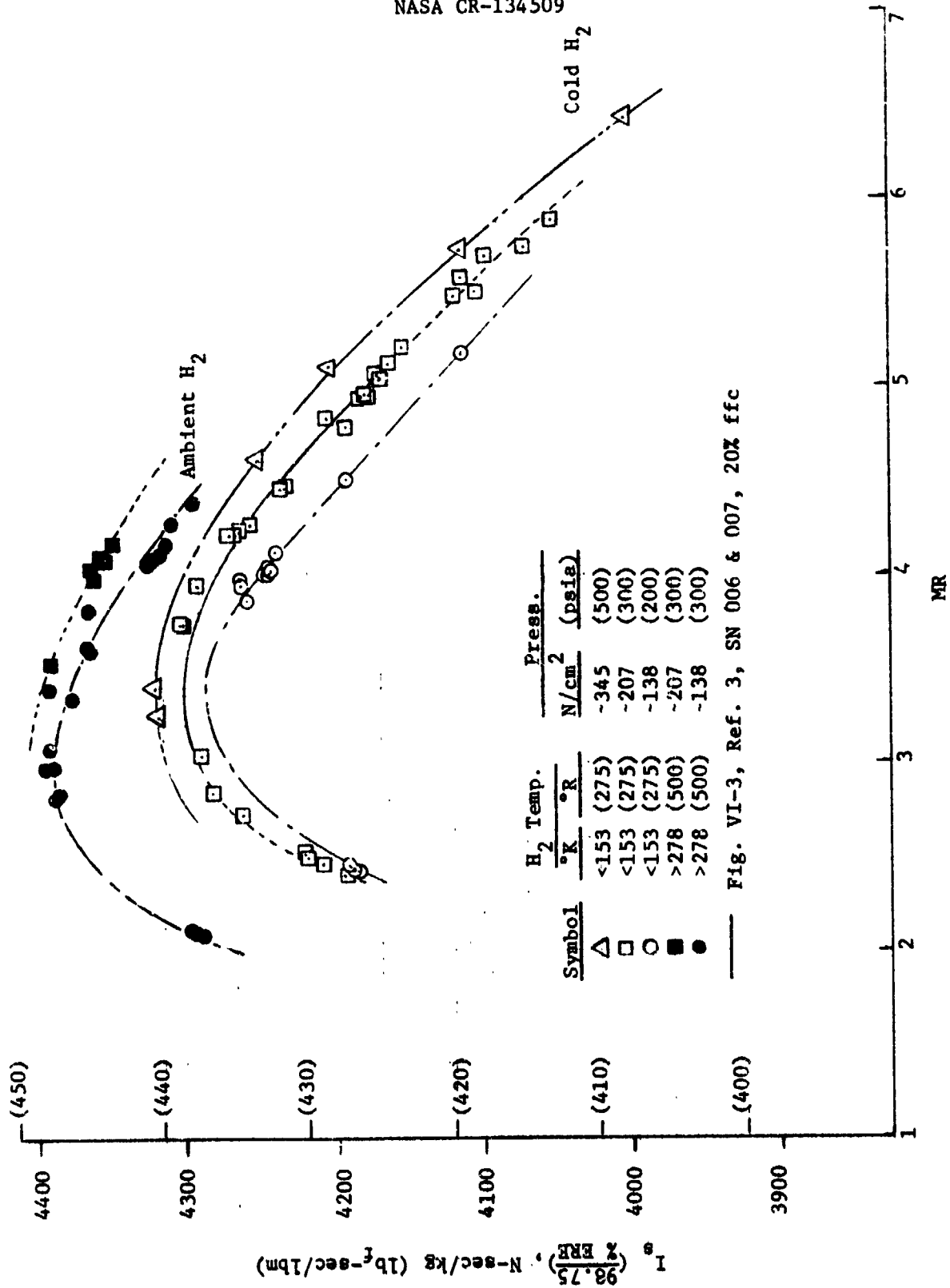
Figure 138. Performance as a Function of Mixture Ratio
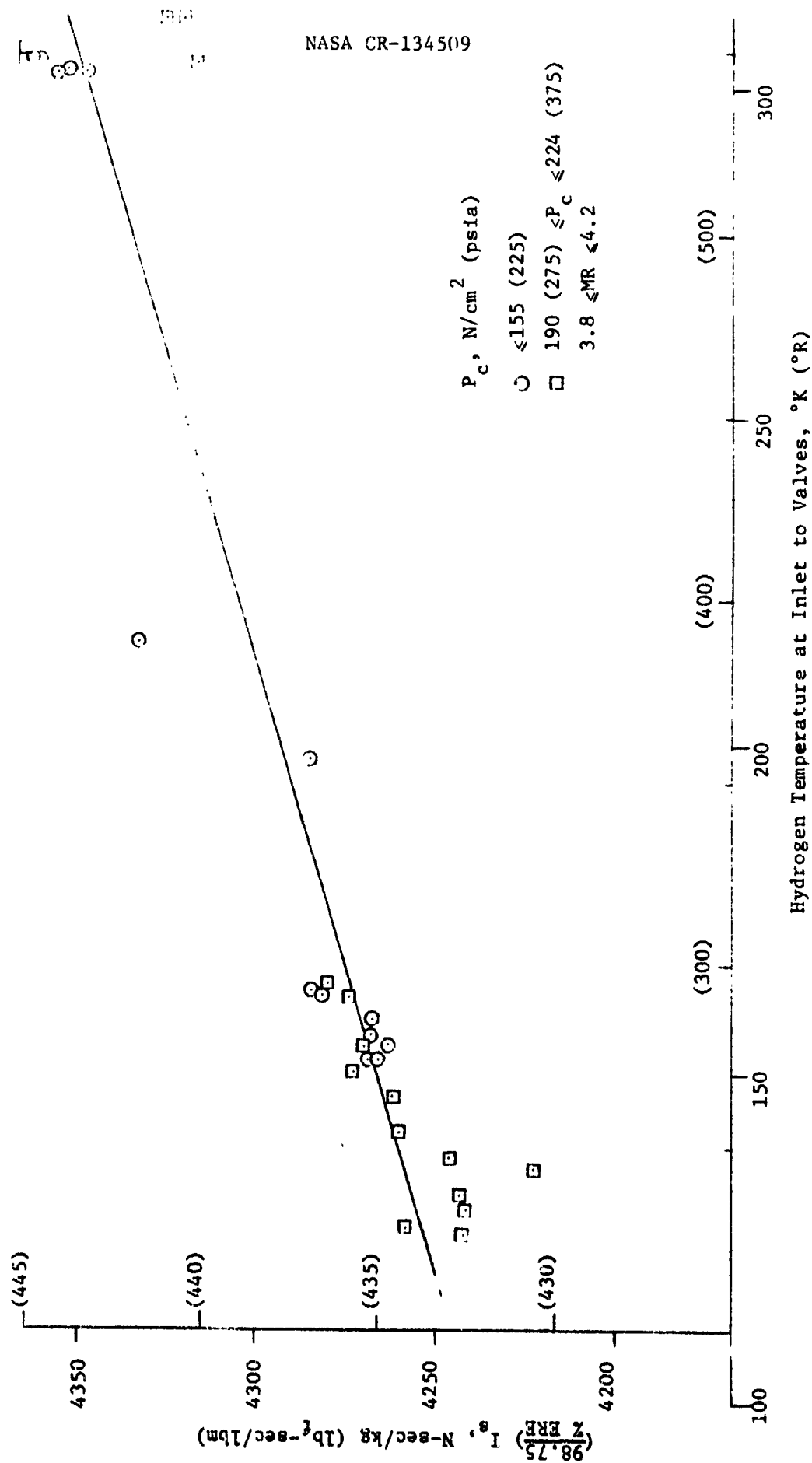
Figure 139. Effect of Fuel Temperature on Performance

4.5, Data Analysis (cont.)

4.5.4.3 Pulsing Operation

Figure 140 shows some of the key parameters that character-
ize the pulse mode of operation. The data were taken from Test -071. Figure 140
was traced from the oscillograph records and reflects the fact that voltages and
currents were reversed; thus, the voltage applied to the pilot valves, the
igniter valves' current and the spark monitor tracer appear as decreasing
functions during activation; the Ramapo flow meter signals are shown and are
proportional to flow rate squared. Chamber pressure was monitored via the igniter
oxidizer manifold (P_{oj-1}). The oxygen to the igniter was shut off during the
mainstage operation, but the hydrogen was left on; thus, the igniter served as a
cooled P_c tap.

Figure 140 illustrates the pulsing sequence. The response
characteristics of the main propellant valves dictated that the fuel valve be
signalled open first. In order to achieve a short impulse bit, both valves
were signalled closed before they had opened. There was a .005 sec fuel lead to
the igniter and igniter ignition preceeded mainstage ignition by .020 sec. As
a matter of fact, the igniter ox valve was closed and the igniter was shutting
down at the time of main stage ignition (P_{oj-1} trace). The main propellant valves
opened nearly simultaneously with perhaps a slight fuel lead. The fuel valve
closed before the oxidizer valve which hurt performance as will be seen subsequently.
Normally, the fuel valve was delayed to close approximately .010 sec after the
ox valve. The overshoot on the fuel valve trace and the round-off on the ox valve
trace were electrical and do not represent actual valve motion.

Longer duration pulses are shown in Figure 141 to illustrate
additional details of the pulse mode of operation. There was a .010 sec ox lead
on start up. The flow of the propellants started to decay with about a .005 sec
fuel delay on shutdown (fuel valve signal lagged ox valve signal by about .015 sec),
but the oxidizer flow decayed at a slower rate than the fuel. The igniter ox
manifold pressure trace (P_{oj-1}) reflected igniter start up, main stage ignition
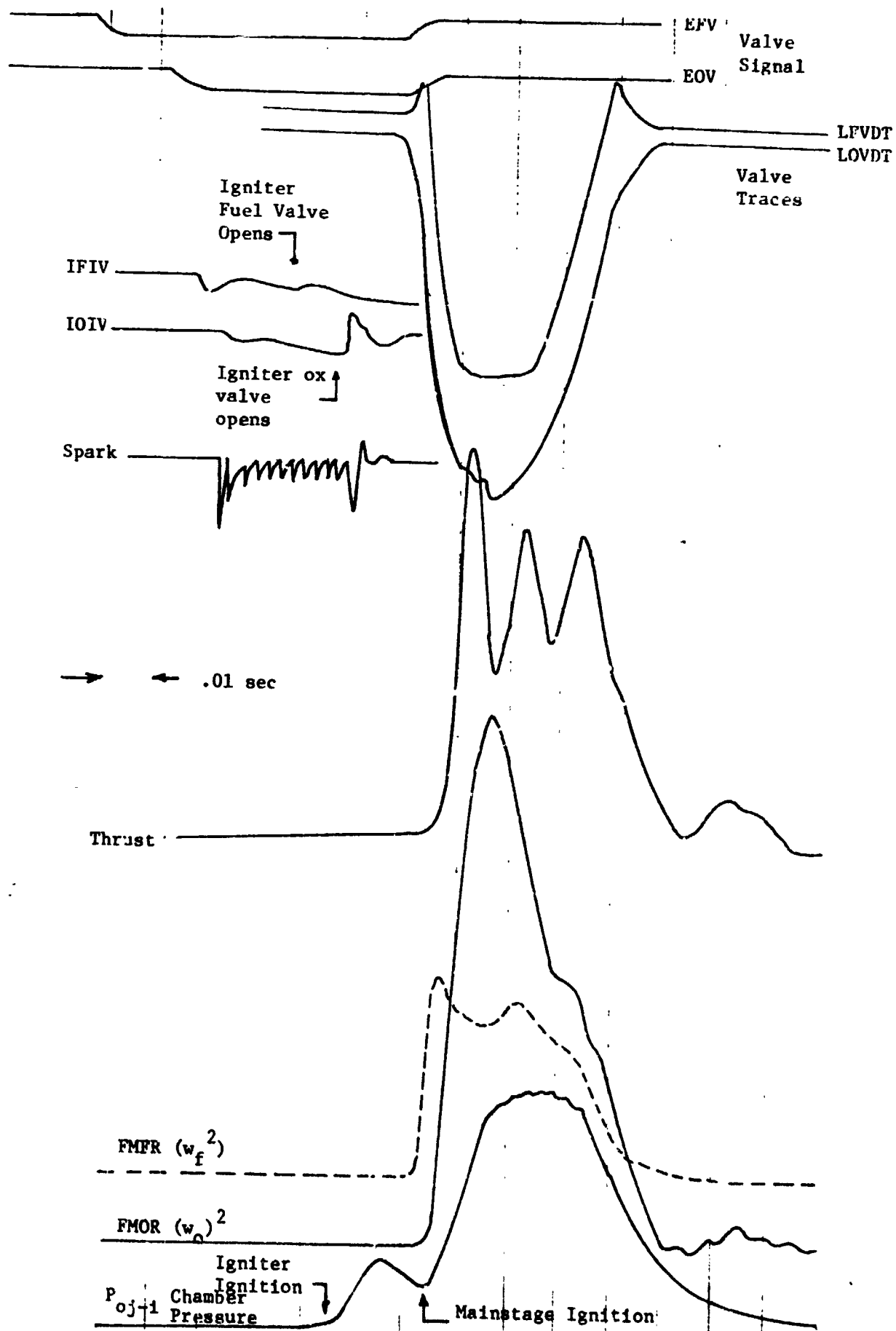
Figure 140. Test -071 Pulse Transients
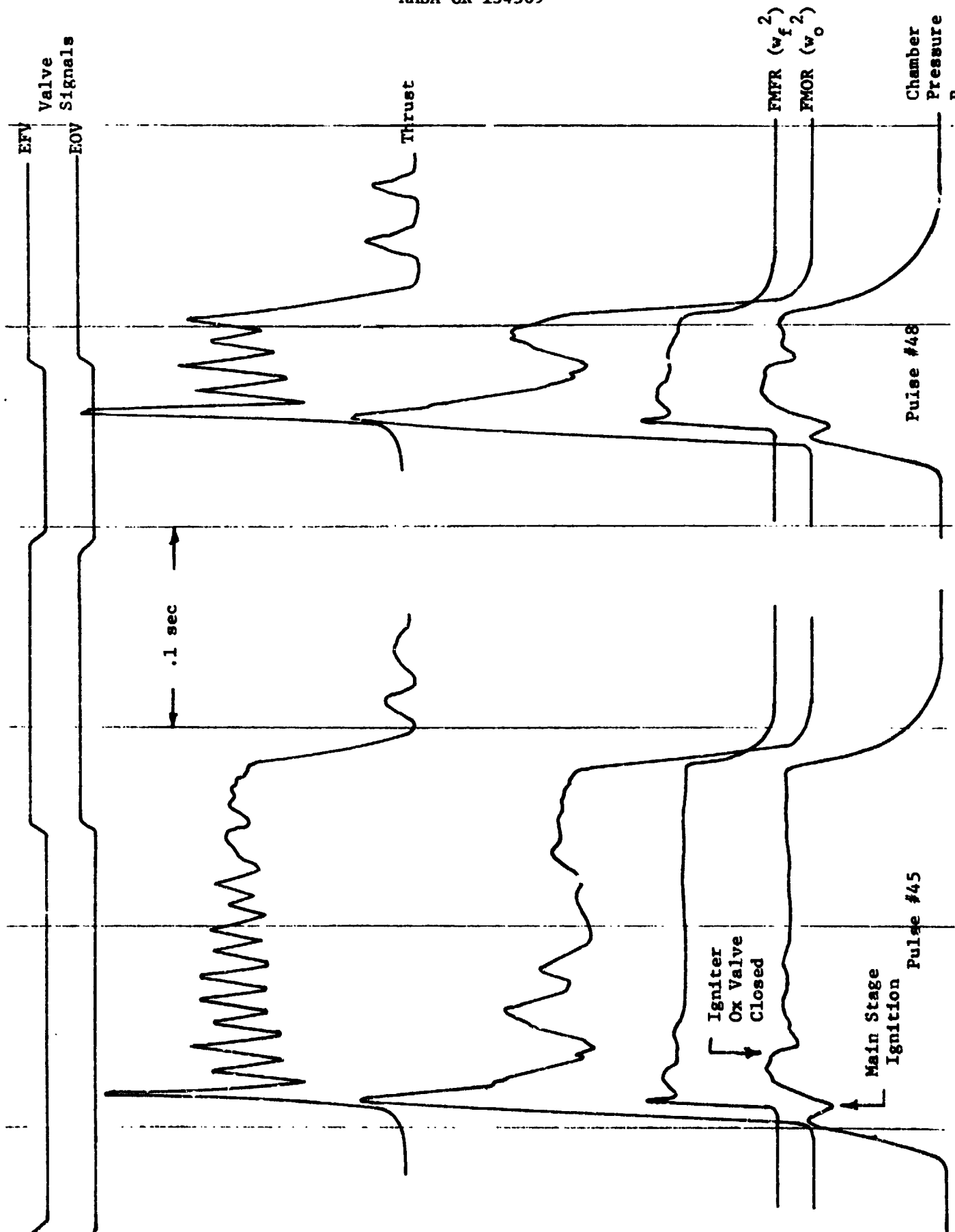
Figure 141. Test -077 Pulse Transients

4.5, Data Analysis (cont.)

and igniter shutdown (P_{oj-1} read chamber pressure from that point on). The thrust stand rung at its natural frequency on start up, but this ringing was dampened out after about .110 sec. There was some thrust stand ringing after shutdown. The start up and shutdown of the two pulses shown in Figure 141 was repeatable as was the transient for the 1st .050 sec (approximate duration of the shorter pulse).

Figure 142 shows the pulse to pulse variation in total impulse, specific impulse and mixture ratio for Test -068. The total impulse of the first pulse was generally lower than subsequent pulses because of the fuel valve delay on opening and/or or closing. After the first two pulses, the total impulse was repeatable within ± 1.5%.

The minimum impulse bit was demonstrated in Test -071. One of the pulses from that test was shown in Figure 140. The pulse to pulse performance is shown in Figure 143. As stated above, fuel valve delay causes the first pulse to be shorter than subsequent pulses (lower total impulse); after the first pulse, the next nine pulses have a total impulse that was repeatable within ± 5%. Both Test -068 and -071 consisted of pulse trains of constant on and off times.

Test-to-test repeatability was evaluated using data from the last four pulse tests that were made with ITA SN 001. These tests, -082 through -084, were made with the D duty cycle (see Table XXXVII). The pulses were nominally: four of .15 sec duration, a fifth pulse of .4 sec duration and five pulses of .090 sec duration. The data from these tests are shown in Figure 144. The total impulse data shows good test-to-test repeatability in addition to pulse-to-pulse repeatability for the first four and last five pulses of each test. The standard deviation of the total impulse for the last five pulses from test-to-test was 5 to 6%.

NASA CR-134509
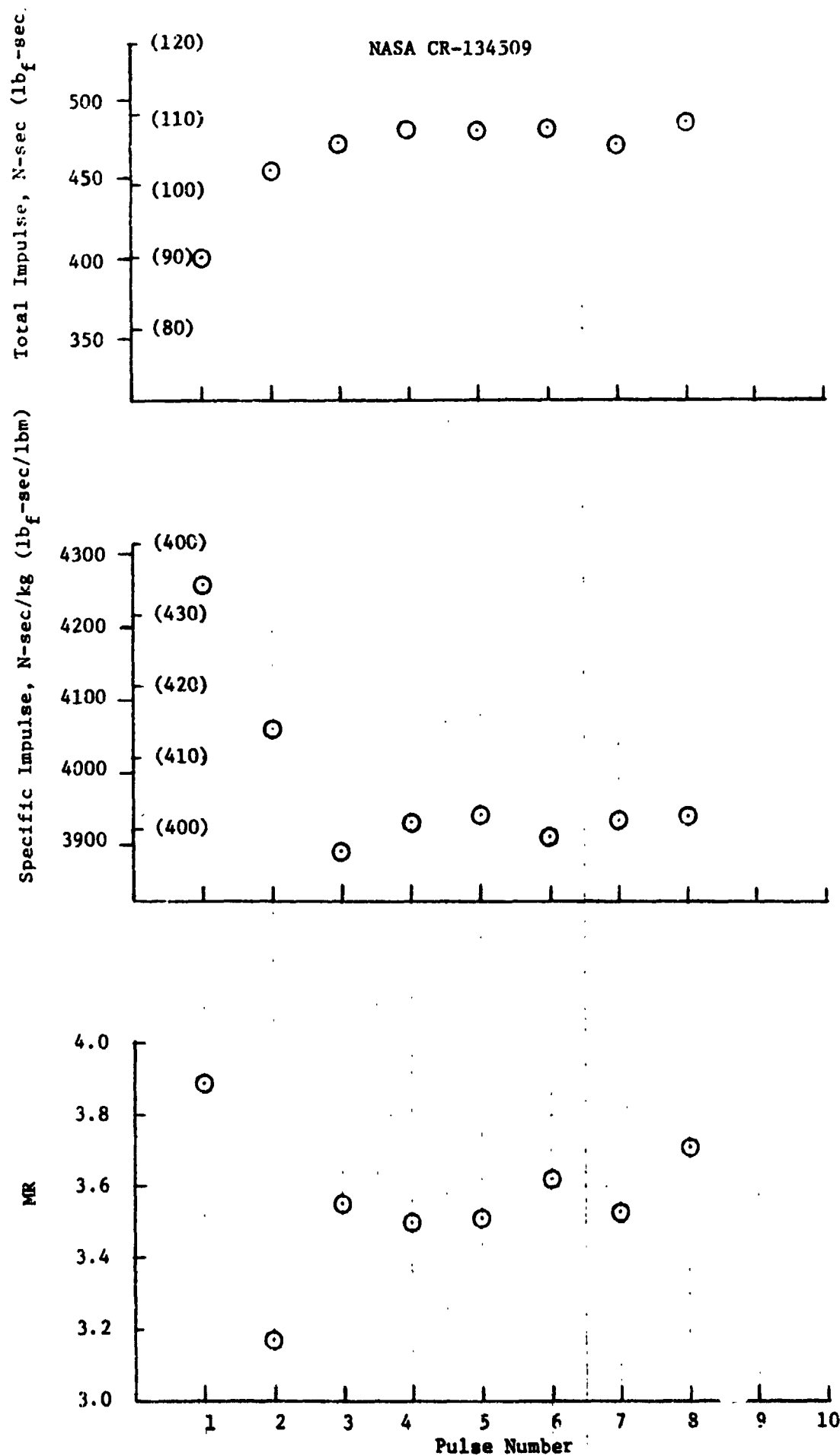
Figure 142. Repeatability of Test -068

Page 425
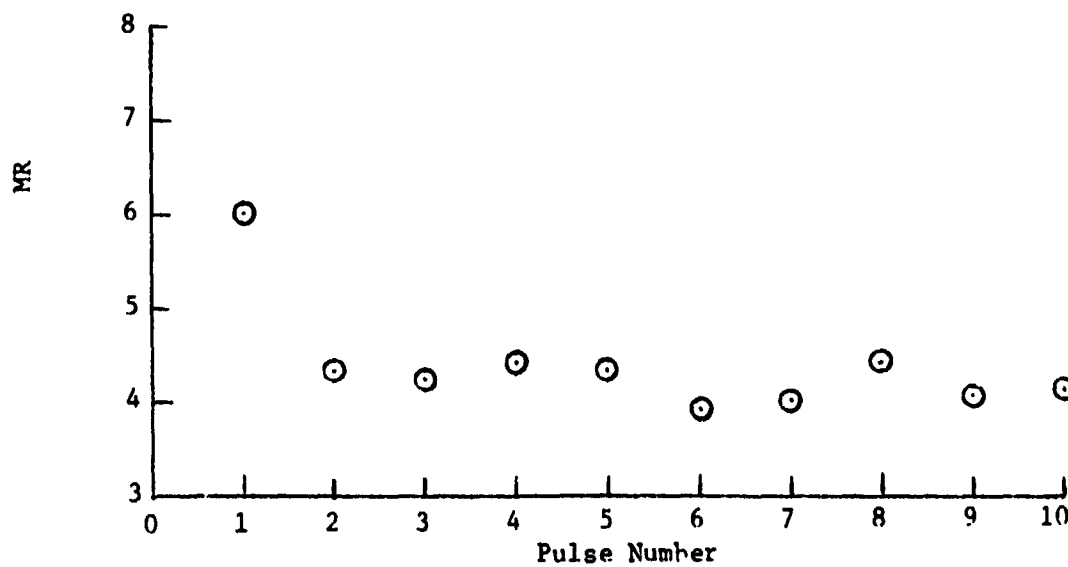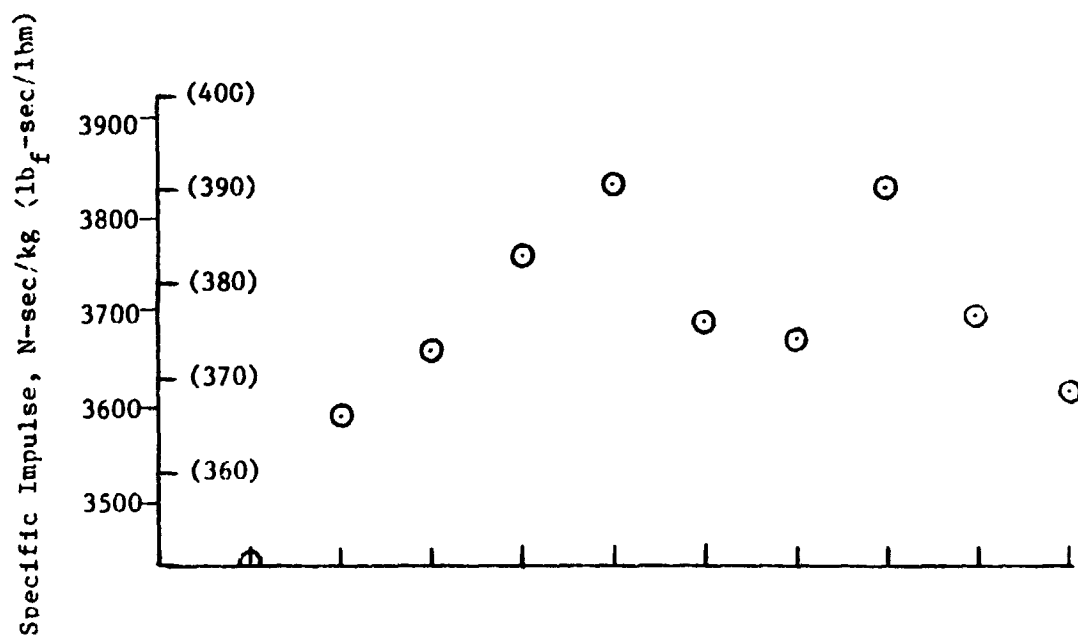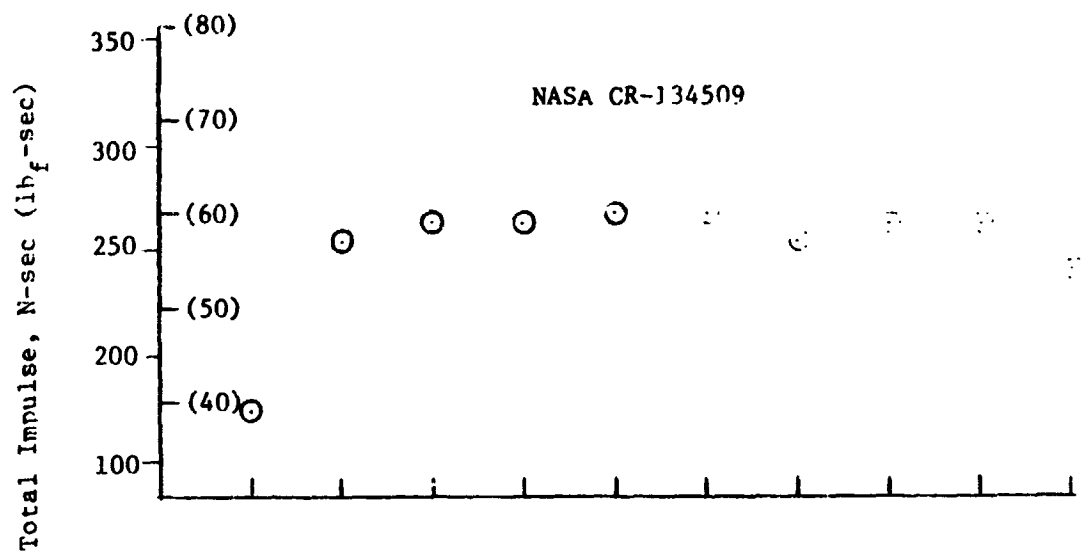
Figure 143. Repeatability of Test -071

Page 426
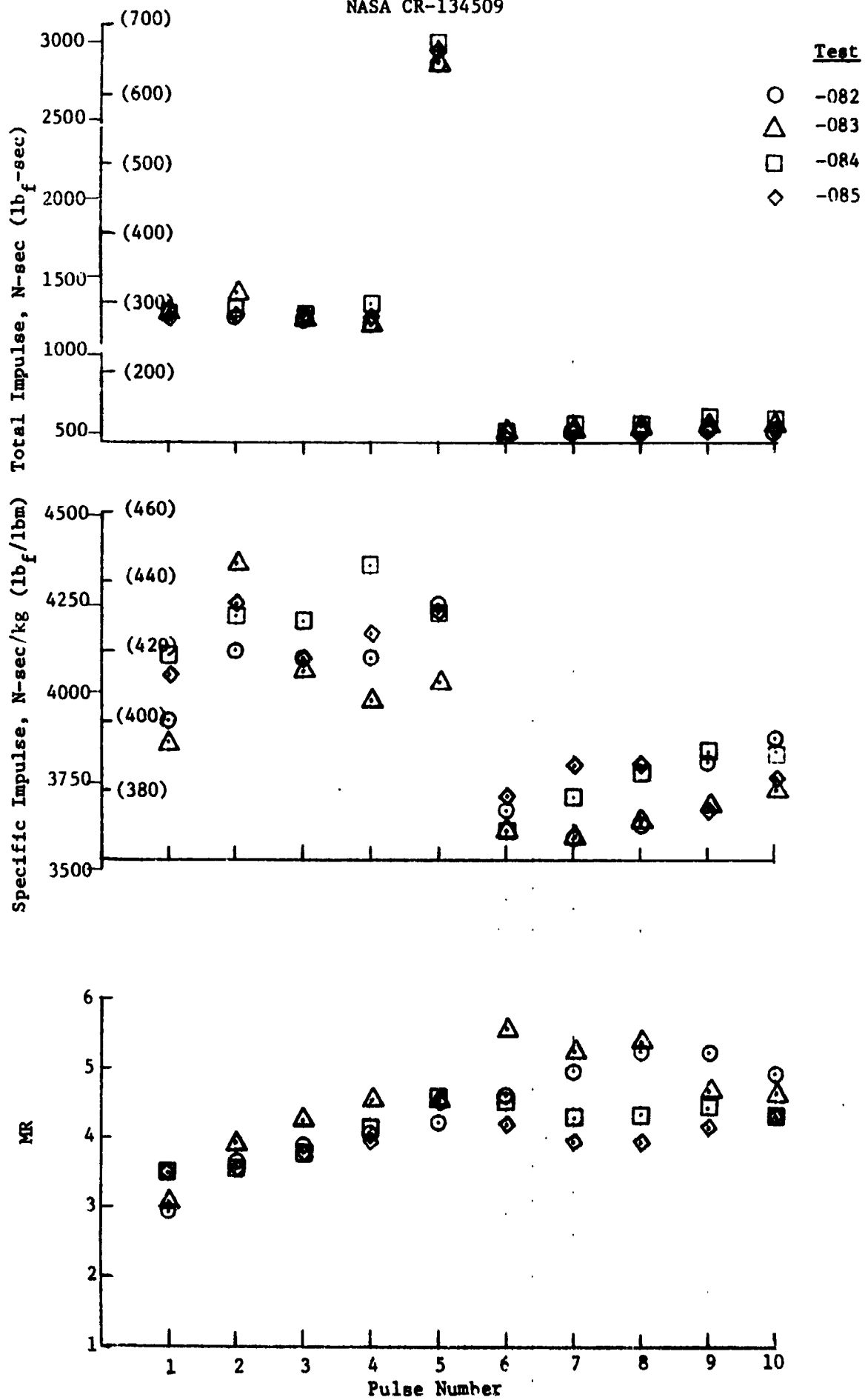
Figure 144. Test-to-Test Pulse Repeatability

4.5, Data Analysis (cont.)

The actual pulse width, as measured by the time from rise
of thrust to its return to a zero value, is shown in Figure 145 as a function
of the electrical pulse width (valves signaled open to valves signaled closed).

In Figure 146, the total impulse is shown as a function
of on time (electrical width) for cold and ambient propellants. The exact
propellant inlet conditions for the two tests whose data are shown in Figure 146
are given in Table XXXVII. The inlet pressure to the valves was approximately
the same for both tests and was on the order of 156 N/cm^2 (381 psia). This resulted
in more flow with the colder propellant, a higher chamber pressure, 172 N/cm^2
(249 psia) vs. 197 N/cm^2 (286 psia), and therefore a higher total impulse.

Tests -076, -077 and -079 were run with 8 to 16 msec ox
lead on start up and with a valve shutdown that varied from 14 msec fuel lag
to a 5 msec lead. As will be shown subsequently, this was not optimum for per-
formance. However, these tests each contain six different pulse durations and
two were made with ambient propellants (-076 and -077) while the third (-079)
was made with cold propellants. The data from these tests were used to show the
effect of propellant temperature on pulsing performance. The results are shown
in Figure 147 It must be noted that: this figure is intended to show the
relative effect of propellant temperature; performance was in general low for
these tests because of non-optimum valve sequencing; at the short pulse duration
end of the curve all of the decrease in performance was not due to pulse width
effects only, but included some effect due to fuel valve closing time changing
with time (temperature) that resulted in less fuel lag on shutdown.

The effect of propellant temperature on pulsing performance
shown in Figure 147 was twice the effect found in the steady state (Figure 139).
It is probable that some of the degradation in performance may be due to the
oxidizer temperature effect shown in Figure 136. The oxidizer temperature was

Page 428
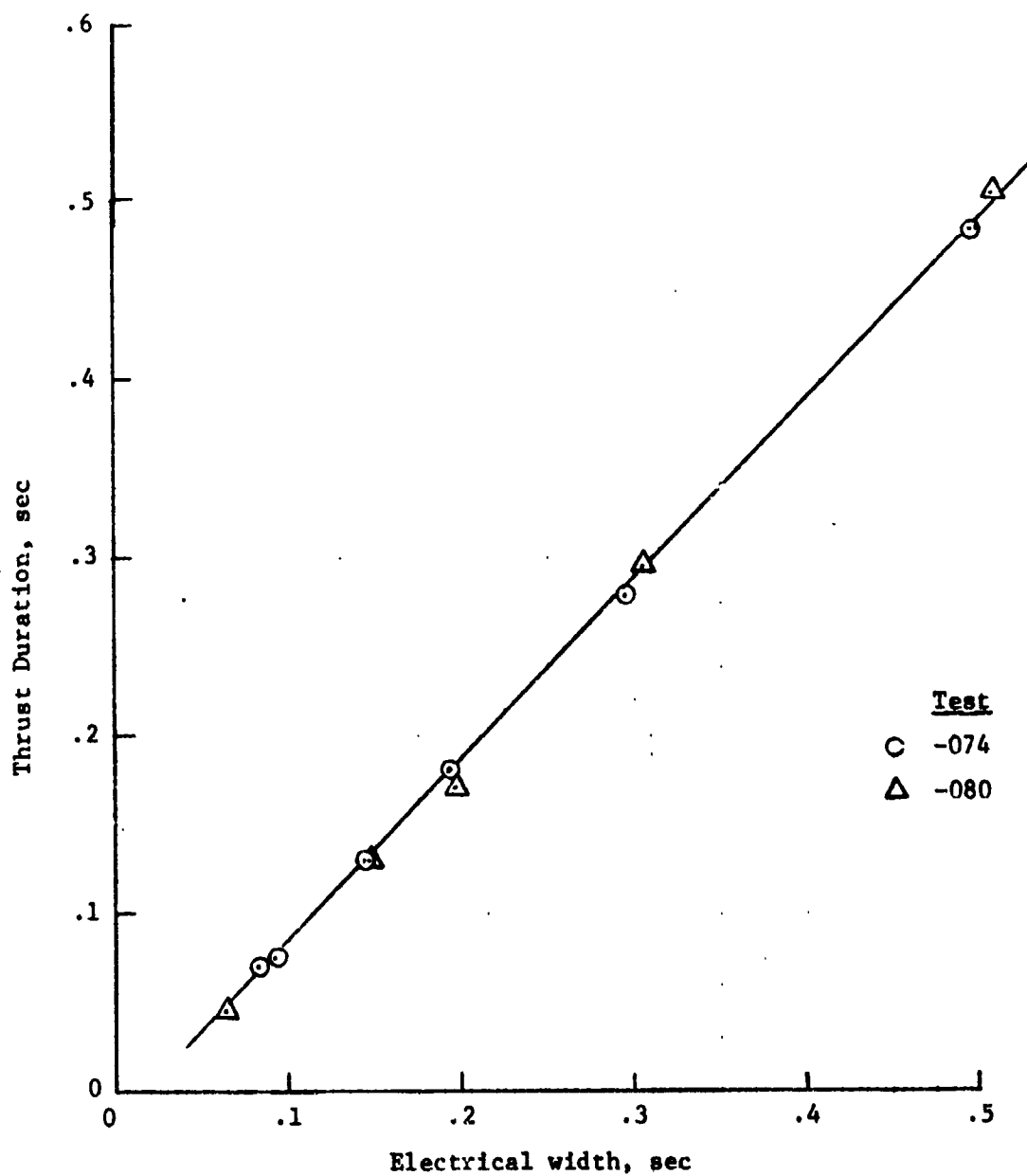
Figure 145. Pulse Width vs. On Time
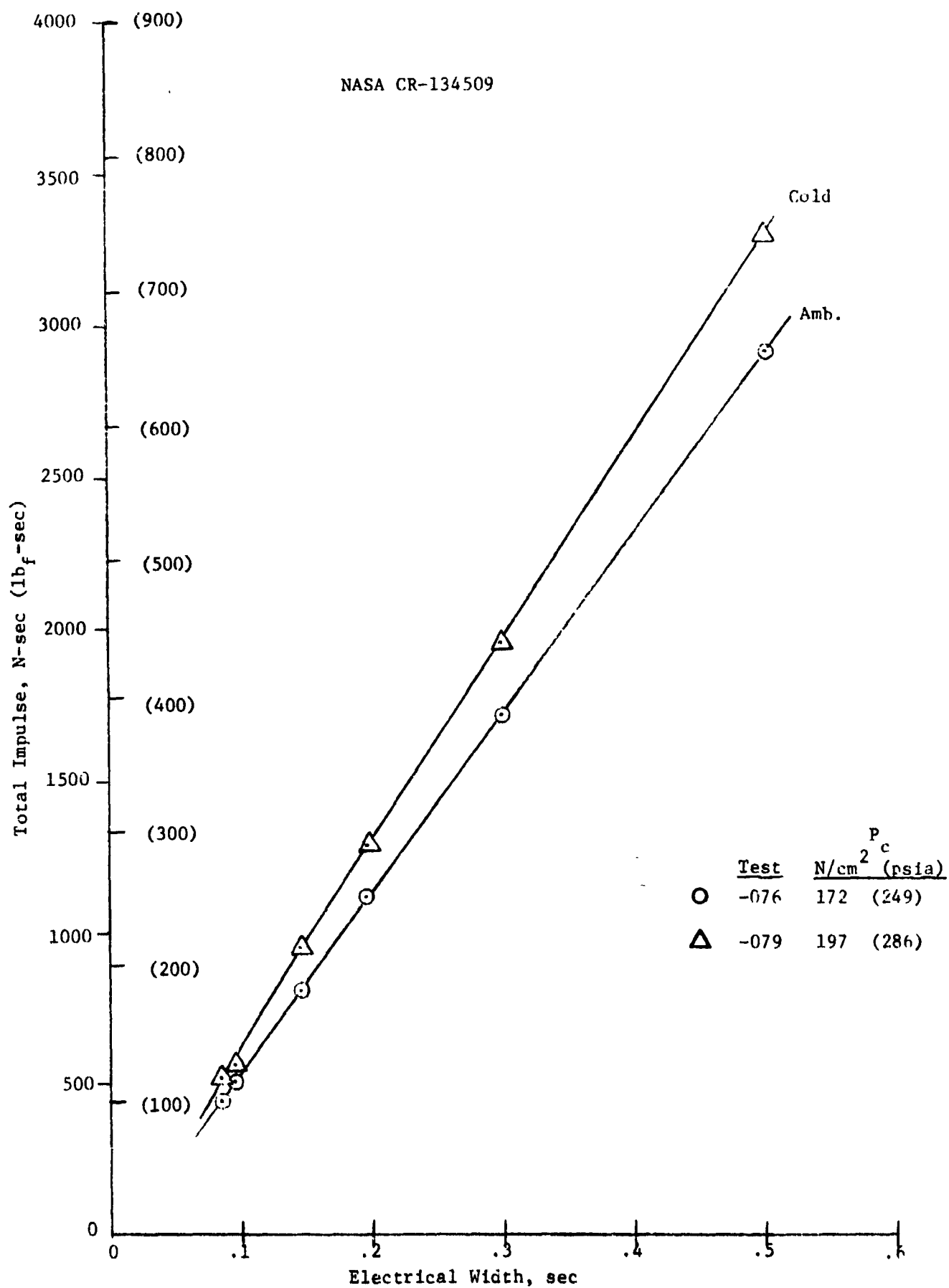
Figure 146.   Total Impulse vs. Electrical Width

Page 430
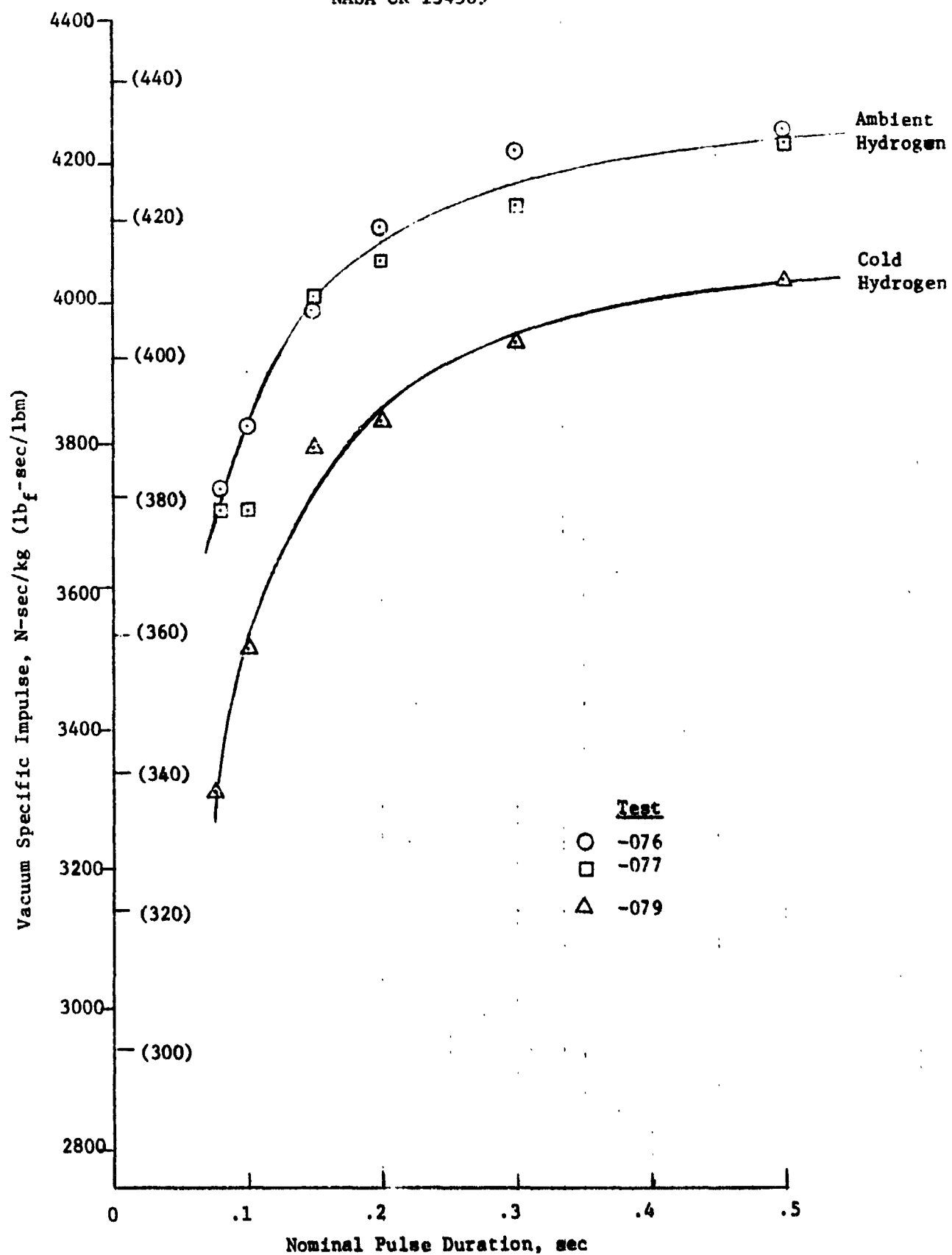
Figure 147. Effect of Propellant Temperature on Specific Impulse

4.5, Data Analysis (cont.)

206°K (371°R) during Test -079. The oxidizer temperature was 214°K (385°R)
during Test -080 and the performance was comparable to Tests -076 and -077
(ambient) rather than Test -079 (cold).

Figure 148 is a plot of the performance (averaged over
several pulses) versus impulse bit. The scatter in the data is due to valve
sequencing which, although never optimum, was significantly better on some tests
than others. Even the longest pulses were 19 N-sec/kg (2 lb_f-sec/lbm) lower in
specific impulse than the steady state performance. At the minimum demonstrated
impulse bit, the average specific impulse was 3609 N-sec/kg (368 lb_f-sec/lbm).
However, as shown in Figure 143, performance on some pulses was as high as
3825 N-sec/kg (390 lb_f-sec/lbm).

The main propellant valve sequencing had a strong influence
on performance as shown in Figure 149. This figure demonstrates the importance
of reacting all the oxidizer. A zero ox lead on start up meant the oxidizer was
reacted when it started to flow. Likewise, a 20 msec fuel lag on shutdown resulted
in good performance because hydrogen was present for combustion during the slower
blowdown of the oxygen. A longer fuel lag reduced performance because fuel was
being spent when no oxidizer was present.

In Figure 148, the Test -069 performance is low for two
reasons. First, the mixture ratio was high (6 to 7) and the sequencing was not
optimum (5 msec ox lead on startup and simultaneous valve closing on shutdown).
Much of the performance data from Tests -081 thru -085 were low because the tests
were made with a 10 msec ox lead on start up and little or no fuel lag on shutdown.

Test -071 was made with simultaneous valve opening times
and a slight fuel lag on closing. Approximately 78 N-sec/kg (8 lb_f-sec/lbm)
increase in performance could have been realized by delaying the fuel valve closing.
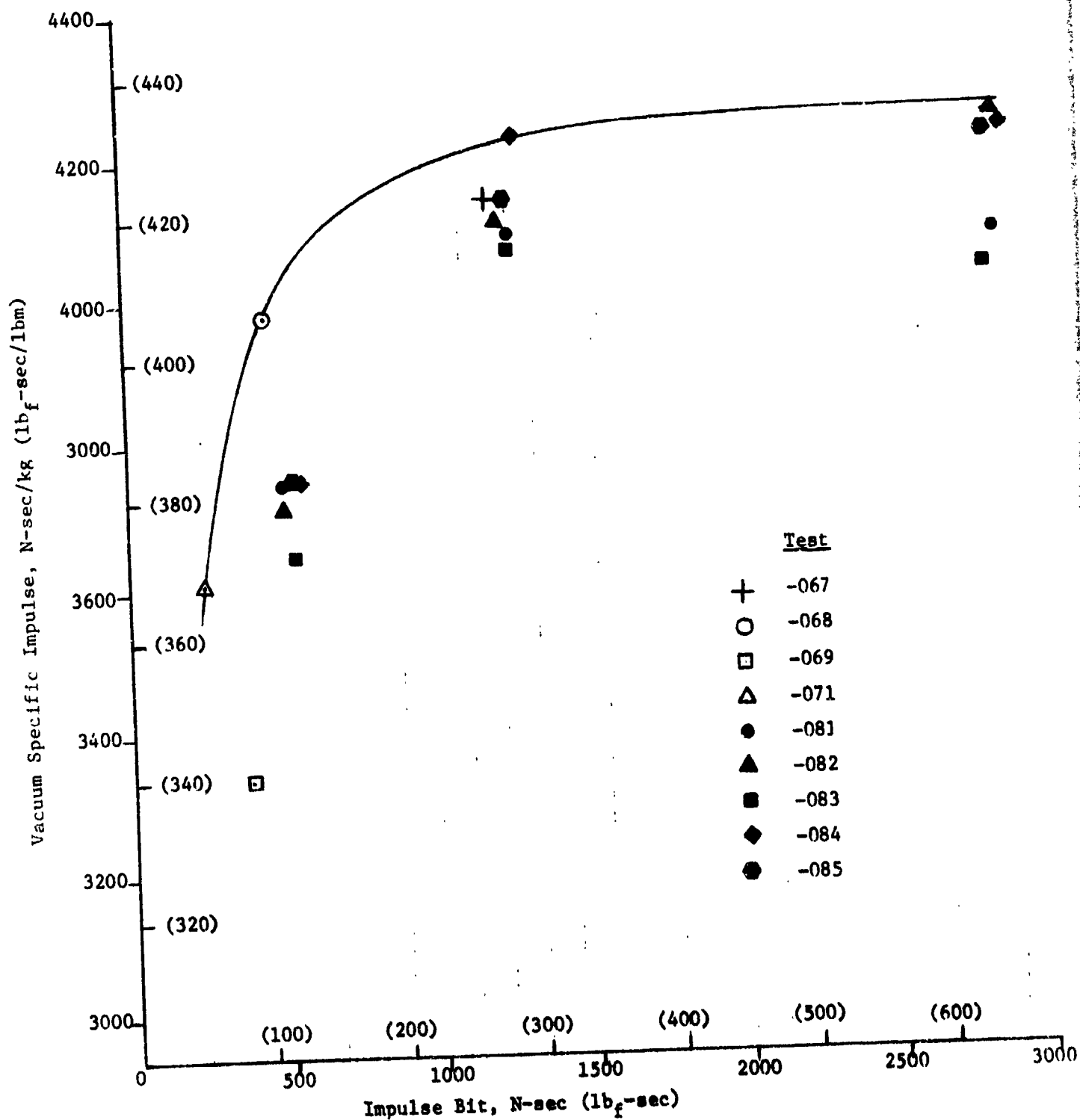
Figure 148. Specific Impulse vs. Total Impulse
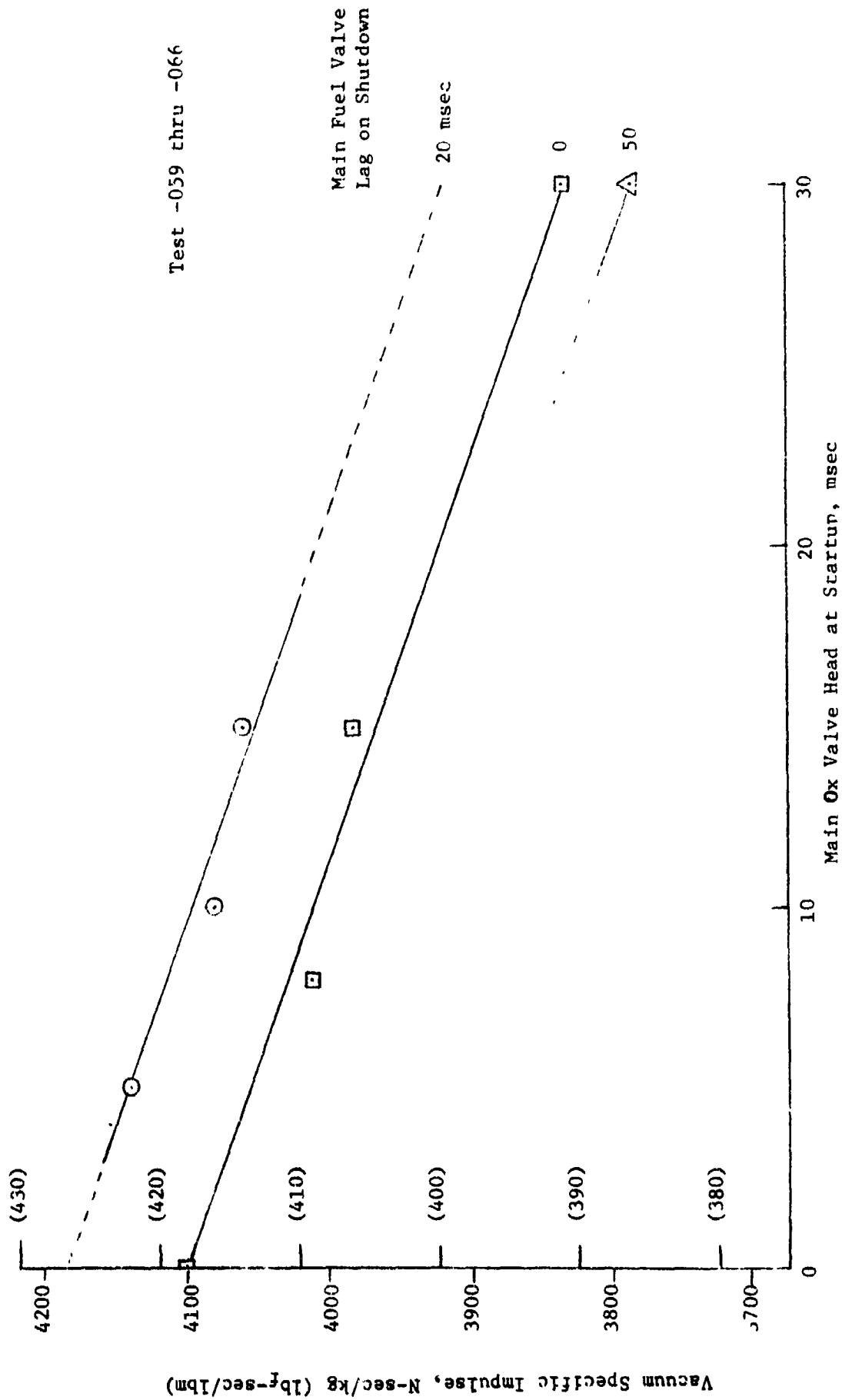
Figure 149. Effect of Valve Sequencing on Performance

4.5, Data Analysis (cont.)

This would result in a 267 N-sec (60 lb_f-sec) minimum impulse bit with a 3688 to 3903 N-sec/kg (376 to 398 lb_f-sec/lbm) performance.

4.5.5 Structural Analysis

On the basis of the temperature data obtained during the igniter checkout testing and the ITA testing, the following conclusions were drawn relative to the structural adequacy of the ITA.

1. The strength analysis summarized in Table XV is valid. There was an adequate factor of safety for all components.

2. With the exception of the throat of the ITA, the fatigue and life analysis summarized in Table XVI is valid.

a. Igniter temperature measurements were limited, but concur with in-house and Contract NAS 3-14354 (Ref. 3) experience that actual temperatures were less than those used in the design analysis. The igniter thermal fatigue analysis was conservative.

b. The injector and chamber regen section temperatures agreed with or were less than those used in the design analysis. The life shown for these components in Table XVI is not altered.

c. Based on the temperatures measured upstream and downstream of the critical location in the dump cooled section, the ffc injection location after thruster SN 001 and SN 002 testing, there is no reason to change the life prediction for this component from that shown in Table XVI.

d. Temperatures in the nozzle extension were less than those used in the creep analysis; therefore, the results shown in Table XVI for the nozzle extension are conservative.

4.5, Data Analysis (cont.)

3.   The measured thro..: temperature was 111°C (200°F)
higher on the average than those used in the design analysis. As a result, the
transient ΔT through the wall would be increased from 189°C (340°F) to 211°C
(380°F). The higher ΔT increases the thermal strain from .21 to .235%,
and reduces the thermal cycle life from 100,000 cycles to 65,000 which is in
excess of the 50,000 design requirement.

Some of the test experience points up the ..act that
there needs to be better protection of high cycle life components during fabri-
cation and testing. All of the small incidents that required repair of chamber
SN 002 occurred under circumstances that invalidate the high cycle life design.

The pin hole leak in the torus and the cracks in the fuel
inlet line-to-torus weld (Figure 91) at 5621 cycles should have been precluded
by better inspection. As much care must be taken to make the "as built" part
conform to the design as is in taken in design for fatigue or else greater
allowance must be made in design for the "as built" conditions that will occur.
This does suggest, for example, that the designer should have cycle to failure
curves based on welded (EB & TIG) fatigue specimens both annealed and not
annealed. It is also recommended that components be proofed to set flaws.

The crack in the Haynes throat section to nozzle extension
weld (Figure 90) was clearly caused by mechanical damage. The fact that once
repaired there were no further problems, shows that the basic design and
hardware were satisfactory.

The crack that occurred in the torus at 30,049 cycles
illustrates the necessity for hardware protection. It was probably caused by
stresses resulting from distortion of the torus due to mechanical damage.
Pressing a tool against the torus hard enough to scratch the surface (Figure 96)
to the extent that occurred could have caused the distortion. The crack

4.5, Data Analysis (cont.)

occurred in the heat affected zone adjacent to the weld. There were residual
stress since, for example, the outside of the torus shell on SN 004 expanded
during welding to the point that there was a discontinuity (Figure 53). Annealing
the torus after welding might have precluded the problem inspite of the mechanical
damage.

The crack at 34,594 was expected. Once extensive welding
was done on the torus, it was anticipated that the shrinkage would set up stresses
that would cause other cracks.

There are some observations that can be made relative to
the inlet line rupture. There was a scratch on the weld seam on the inside
radius of the fuel line. It was deep enough that if it were on the line itself,
it probably would have penetrated the thin wall. Secondly, the fuel line was
deflected to fit the test set up. In welding the fuel inlet line and torus to
the chamber of ITA SN 002, the alignment of the fuel inlet line flange to the valve
mounts was not identical to SN 001. In order to fit ITA SN 002 to the test
stand mounts that had been set up for ITA SN 001, two of the holes in the thrust
mounts and the two holes in the fuel valve mount were elongated. Additionally,
the fuel line was deflected approximately 1.3 mm (.050 in.) outward. This small
deflection may ve changed a low stress area into a high stress area.

In order to achieve high cycle life as much attention must
be payed to fabrication as the design and the components must be protected against
surface damage during fabrication and operation. Protection of the surface
applies to installation and use of the thruster in a Space Shuttle operation as
well as in testing.

REFERENCES

1. Ignition System for Space Shuttle APS, Contract NAS 3-14348, Final Report.

2. Space Shuttle APS Shutoff Valve, Contract NAS 3-14349, Final Report.

3. Hydrogen-Oxygen Auxiliary Propulsion for the Space Shuttle, Volume I: High Pressure Thrusters, Contract NAS 3-14354.

4. Integrated Thruster Assembly, Contract NAS 3-15850, Quarterly Progress Report 15850-Q-1, Appendix A and B.

5. S. S. Manson, "Avoidance, Control and Repair of Fatigue Damage," ASTM STP 495, American Society for Testing and Materials, 1971, pp. 254-346.

6. D. M. Campbell, "Finite Element Nonlinear Heat Transfer Analysis", Report No. SM-10, Vol. I and II, Structural Engineering Section, Applied Mechanics Department, ALRC dated 25 May 1971.

7. S. S. Manson, Thermal Stress and Low "Cycle Fatigue", McGraw-Hill, 1966.

8. Extended Temperature Range ACPS Thruster Investigation, Contract NAS 3-16775, Quarterly Progress Report 16775-Q-3, p. A-18.

9. Pieper, J. L., ICRPG Liquid Propellant Thrust Chamber Performance Evaluation Manual, Chemical Propulsion Information Agency, Report 178, September 1968.

10. McBride, B. and Gordon, S., "ICRPG One-Dimensional Equilibrium Reference Program," NASA LeRC, May 1969.

11. "Two-Dimensional Kinetic Nozzle Analysis Computer Program," ICRPG Performance Standardization Working Group, 30 July 1968 (available through CPIA), AD 841200.

12. "Turbulent Boundary Layer Nozzle Analysis Computer Program," ICRPG Performance Standardization Working Group (available through CPIA), AD 841202.

NASA CR-134509

APPENDIX A

TEST FACILITY

All static firing tests were conducted under simulated altitude conditions in a horizontal thrust configuration in the Test Stand J-3 of the altitude facility complex. The ALRC-owned altitude complex of which a flow schematic is shown in Figure A-1 consists of 9072 kg/hr (20,000 lb/hr), 335 N/cm^2 (500 psig) steam boilers, five steam accumulators capable of storing 20,412 kg (45,000 lbs) of steam at 286 N/cm^2 (400 psig) and 221°C (430°F). These accumulators are manifolded together and supply steam to the J-3 and J-4 ejector systems.

Test Stand J-3 is an 2.44 m (80ft) diameter by 39.62 m (130-ft) long altitude chamber in which the entire test setup (including the test article, firing fixtu.e, thrust calibration assembly, and flow measuring devices) was located inside the chamber and was subjected to the simulated altitude environment. The propellant supply tankage, heat exchangers, and ullage tanks are located adjacent to and outside of the vacuum chamber.

This stand was operated in several steam ejector configurations, depending on the desired altitude and engine mass flow conditions. The ejector configuration that yields the highest altitude and longest sustained duration is utilizing the three-stage ejector system located at the end of the altitude chamber. This configuration consumes approximately 14.5 kg/sec (32 lb/sec) of steam and will produce a maximum altitude, no flow, of 45.72 km (150,000 ft) for 2000 seconds. The sustaining altitude during engine flow conditions is not only dependent on the mass flow of the hardware and cell leakage but the resultant gas density. It can be seen on Figure A-2 that the test cell pressure is a function of both Pc and MR. As an example, a test with the Pc = 207 N/cm^2 (300 psia) and MR = 6.0, the ejector system will maintain approximately 25.9 km (85,000 ft) for 2000 sec of steady firing. Keeping everything the same and changing to a MR = 4.0, the altitude will change to 17.4 km (57,000 ft) in 12 seconds. To allow testing of this hardware through the entire range of conditions, a second ejector configuration was employed. This configuration utilized the second and third stage of the
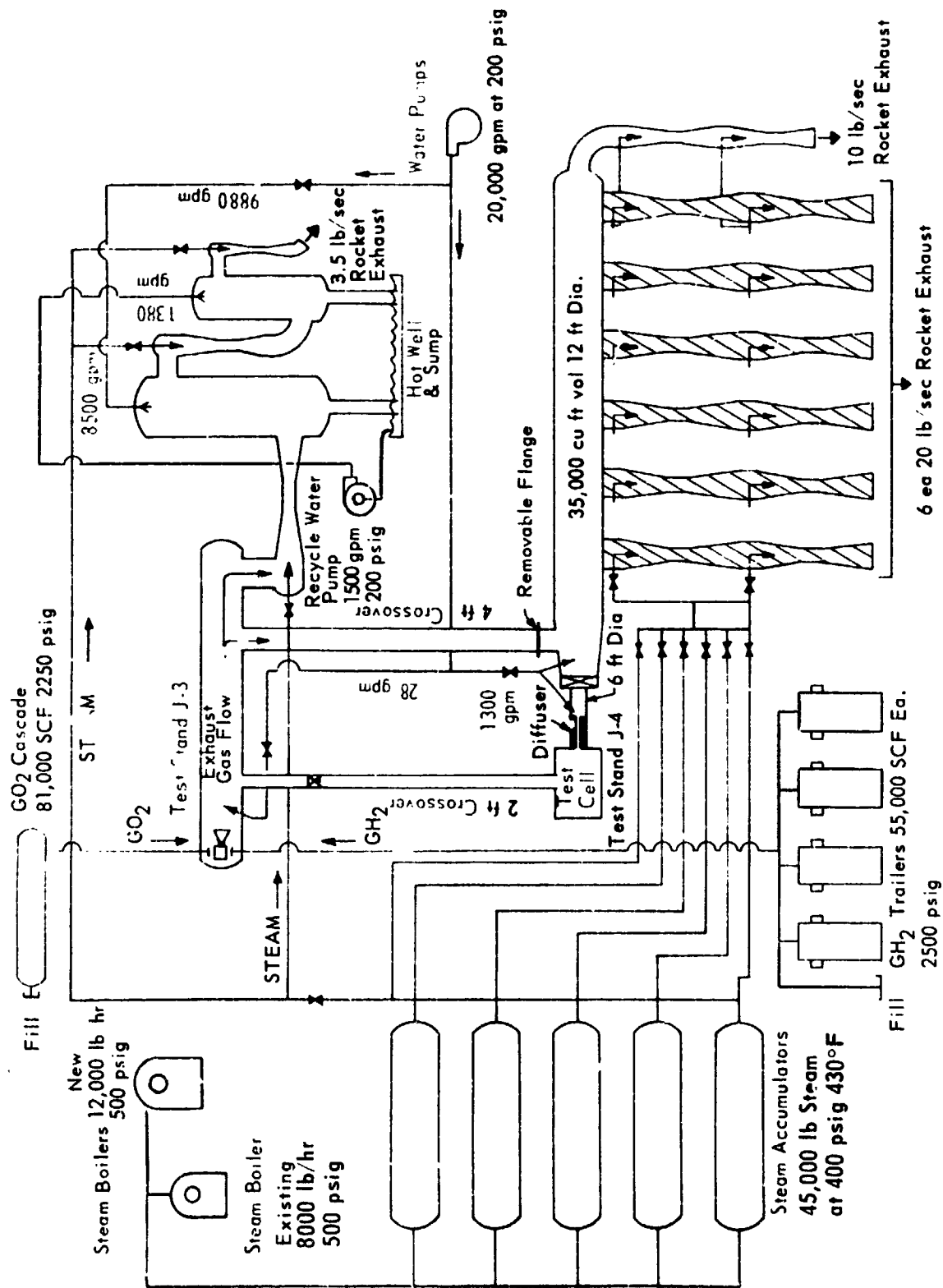
Figure A-1. N-Area Altitude Facility Flow Schematic
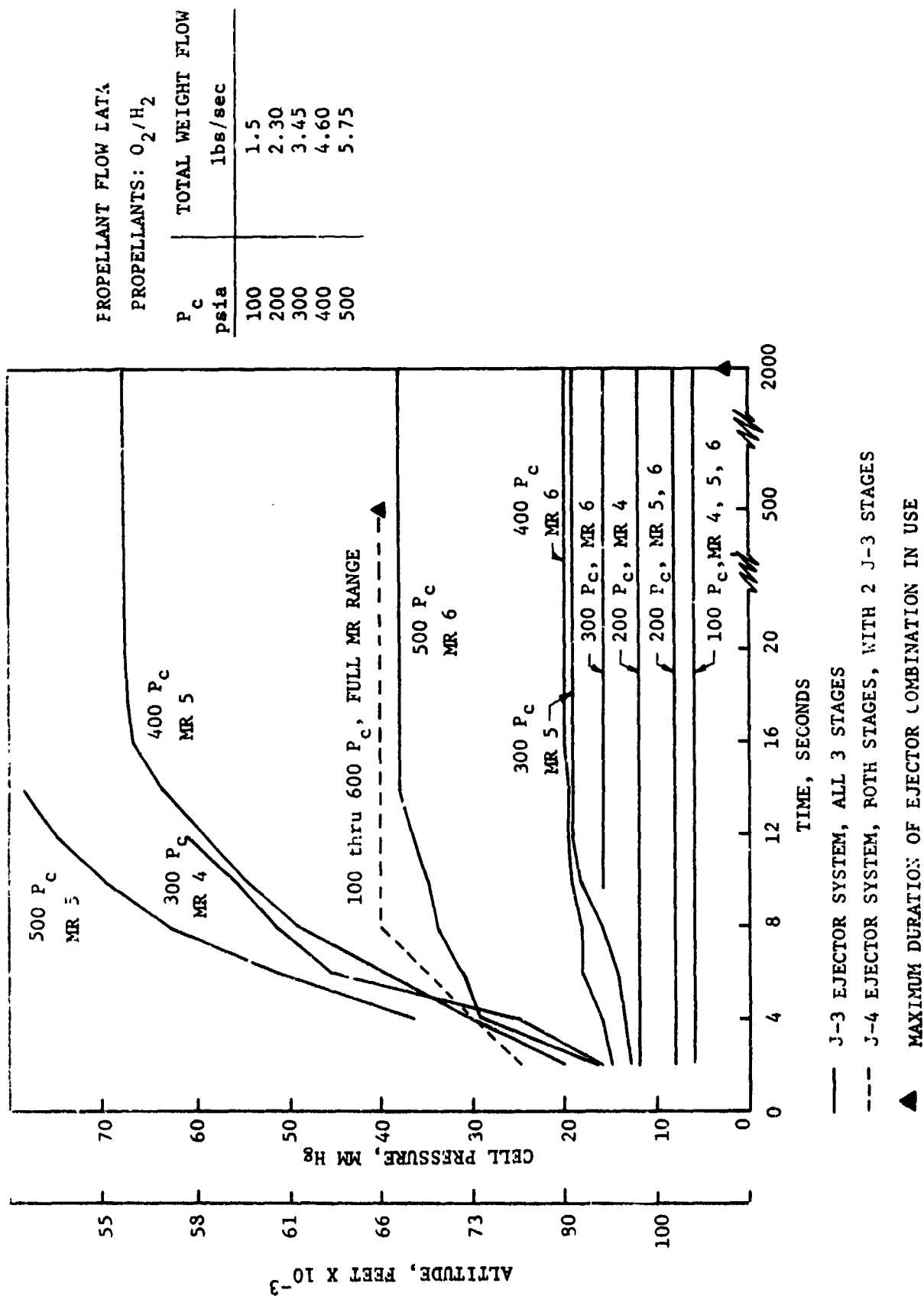
Figure A-2 Altitude System Performance Test Zone "J"

J-3 ejector system and a 4-ft-diameter crossover connection duct to a 4.536 kg/
sec (10 lb/sec) two-stage ejector on Test Stand J-4 (Figure A-1). This con-
figuration is capable of handling the entire range of flow and MR shown in
Figure A-2. However, its sustained altitude is approximately 20.1 km (66,000 ft)
which will provide full flow nozzle conditions for a duration of 500 seconds.

In both ejector configurations, the propellant bleed-in, temperature
stabilization, and in-place thrust calibrations were accomplished utilizing the
second and third stage ejectors which only consume 2.72 kg/sec (6 lb/sec) of
steam, allowing that entire operation to be conducted under a vacuum condition.
after the propellant bleed-in and the temperature throughout the system was
stable, the feed system was pressurized to the thrust chamber valves and a remote
thrust calibration was accomplished with the entire system under a vacuum en-
vironment. This in-place force stimulus calibration measured the system bias
caused by the propellant feed system growth as a result of both pressure and
temperature effects as well as any interaction introduced by the altitude
chamber to firing fixture movement caused by the low ambient pressure inside the
cell. The calibration was accomplished by physically pulling the fixture/ITA
on the centerline of thrust from zero up to 11,120 N (2500 lb_f) and then back
to zero in 2224 N (500-lb_f) steps. The thrust stand accuracy, over 75 calibra-
tions, yields a bias of -2.55% with an accuracy of +0.3% (95% confidence level)

The J-3 propellant system is designed to deliver GH_2 at 0.68 kg/sec (1.5
lb/sec) from "over the road", 2500 psig trailers and GO_2 at 1.81 kg/sec (4.0 lb/
sec) from a 229,366 sl (8100 scf), 1562 N/cm^2 (2250 psig) cascade to the test
hardware through 10µ stainless filters.

The steam and GH_2 propellant capacity were extended for this program to
provide an economical testing capability for meeting the 50,000 pulse, 5000
thermocycle life test goal, by installing an ALRC procured 5443 kg/hr (12,000
lb/hr) steam boiler, relocating an existing 5678 ℓ/min (1500 gpm) water recycle

pump and extending the GH_2 trailer manifold to accomodate a total of four 1,557,000 sl (55,000 scf), 1734 N/cm^2 (2500 psig) GH_2 trailers. The additions provided the capability of approximately six hours a day of continuous testing times under a pulse mode-type operation.

The 40,000 pulse, 4000 thermocycle life testing was accomplished by conducting 10 pulses while obtaining thermal equilibrium. At the end of the tenth pulse, the hardware was reutnred to ambient temperature by purging cold GH_2 through the injector. This pulse thermal cycle was repeated 4000 times and was automatically controlled by means of a computer located in the control room.

The facility contains heat exchangers in each of the propellant systems. The pool boiling type heat exchanger uses LN_2 for a cooling medium and the outlet temperature is determined by the level of LN_2 in the heat exchanger. The level is maintained by a remotely operated supply valve. The LN_2 source is a 49,209ℓ (13,000-gal) storage tank with a 455ℓ/min (120 gpm) pump. The heat exchangers are capable of delivering cold 111°K (200°R) conditioned propellants for an unlimited test duration. Test data have shown the fuel system starting with ambient propellant at the test hardware at a flow rate of .313 kg/sec (0.69 lb/sec) and in 9 seconds the GH_2 temperature at the test hardware was 139°K (250°R) and in 150 seconds the GH_2 temperature was 111°K (200°R). The oxidizer (GO_2) system was started at ambient temperature, flow rate of 1.25 kg/ sec (2.76 lb/sec), and the heat exchanger dry. Twenty-five seconds into the test, LN_2 was introduced into the heat exchanger and in 32 seconds the oxidizer was at 194°K (350°R) at the test hardware

Control of the propellant flow rates was accomplished by two Hammel-Dahl hydraulically operated flow control valve (fuel and oxidizer). The valves have a response time from full closed to full open of 0.075 seconds. Nominal operating range for the ITA program was approximately 20 to 50% open. The facility also contains an on-line EAI Pace TR-48 analog computer which controlled the engine

flow rates by monitoring the inlet pressure and temperature and adjusting the flow control valves accordingly through a feedback loop. The TR-48 is capable of using linear and nonlinear functions in calculating flow rate. The computer was programmed to provide several mixture ratio, combustion chamber pressures, and coolant system flow rates during a test. The changes were made from the control console on demand while the engine was firing. The computer is also capable of monitoring 16 pressures and temperatures and can terminate the test within 0.020-sec if values are not within a predetermined safe operating range. The safe operating range was determined after a failure mode analysis had been run on the test facility and a critical experiment review of the test program. Data obtained during this program indicates that computer shutdowns have prevented damage to the test hardware.

The facility is set up for two types of flow measurement: venturi flow-meters or meters such as constant temperature anemometers and ramapo meters. The venturi flowmeters were used for the initial steady-state testing and were located at the inlet to the test stand valves. The desired flow rate was maintained by sensing the inlet pressure and temperature. This information was converted to flow rate by the computer which, in turn, corrected the flow control valves for the desired output. There is a wide range of venturi sizes available for use in J-3 calibrated at Colorado Engineering Experimental Station, Inc., Boulder, Colorado. This is traceable to NBS through critical flow nozzles. The accuracy of the oxygen flow at 117°K (210°R) is 0.64% (95% confidence level) and for hydrogen flow at 111°K (200°R) is 0.93% (95% confidence level).

APPENDIX B

TEMPERATURE DATA

NASA CR-134509, APPENDIX B

STEADY STATE TEMPERATURE (°F) SUMMARY

Test	P_c (psia)	MR	Fuel Valve T_{FTCV} (°R)	Chamber Gas-Side TG 2B	Chamber Shell TC 2B	Fuel (Inj.) T_{FJ}	Convergent Section N1	N2	Throat N3	N4	Nozzle N5	N6	N7	N8	N9	Injector Face JF3	JF4	JF5
-008	195	4.12	237	425	-8	340	195	830	1130	1089	-	1590	1610	1620	1600	138	180	150
-010	209	4.07	556	630	242	199	683	1250	1490	1385	1615	1870	1890	1900	1850	485	480	500
-011	212	2.85	553	640	210	179	590	1030	1250	1150	1415	1590	1610	1600	1550	490	490	515
-012	210	3.48	311	468	50	-9	445	1000	1250	1180	1495	1605	1610	1560	1460	230	225	235
	205	3.48	302	553	5	-67	360	890	1170	1105	1470	1580	1580	1560	1550	197	204	255
	301	4.21	280	49.	-10	-95	405	1030	1005	1235	1620	1665	1630	1665	1640	197	220	404
	301	4.22	268	630	-8	-105	420	1070	1350	1265	1675	1650	1615	1635	1620	165	240	300
-013	200	3.87	288	412	-10	-53	310	880	1170	1100	1470	1540	1495	1510	1490	172	189	213
	303	3.66	300	500	-12	-55	355	885	1165	1090	1488	1535	1500	1515	1505	155	210	300
	300	4.48	293	550	-8	-60	434	1070	1375	1270	1670	1700	1660	1680	1680	170	240	300
	295	5.09	295	540	10	-55	490	1245	1495	1420	1800	1720	1630	1645	1640	180	230	290
	285	5.80	295	618	23	-46	545	139	1665	1555	1910	1853	1775	1790	1290	200	200	280
-014	250	4.07	230	360	0	-86	182	800	1100	1067	1414	1419	1360	1380	1390	210	285	226
	305	4.47	239	425	-10	-97	264	760	1056	1054	1412	1435	1386	1400	1409	180	240	170

Test	P (psia)	MR	Fuel Valve TFTCV (°R)	Chamber Gas-Side TG 2B	Chamber Shell TC 2B	Fuel (Inj.) TFJ	Conv. Sect. N1	N2	Throat N3	N3.5	N4	N5	Nozzle N6	N7	N8	N9	Inj. Face JF3	F4	JF5
-040	262	2.56	224	356	-122	-145	104	352	529	670	611	885	1010	1085	1121	1132	140	152	205
	308	3.03	230	390	-121	-137	136	540	743	739	816	1081	1140	1160	1165	1173	116	217	242
	326	5.70	224	620	-19	-113	426	1062	1265	1292	1300	1720	1445	1600	1560	1560	138	207	176
	394	4.34	217	513	-32	-126	272	768	1010	1010	1037	1403	1406	1552	1555	1541	99	248	167
	287	5.89	214	516	-5	-108	426	1032	1224	1310	1287	1674	1451	1635	1625	1617	123	140	172
	302	2.49	234	312	-130	-141	97	414	542	583	600	875	1016	1104	1150	1140	72	136	221
-041	248	3.98	488	624	163	125	623	1362	1399	1364	1364	1552	1497	1381	1347	1324	384	383	395
	257	4.10	429	585	117	71	575	1308	1350	1346	1475						314	311	320
	264	3.62	311	530	-10	-51	410	997	1065	1091	1173	1412	1425	1400	1370	1320	191	243	172
	271	3.64	270	478	-52	-98	310	600	920	1007	1030	807	946	1010	1034	1018	166	218	409
	254	2.31	270	304	-97	-117	107	380	518	633	385	1320	1390	1407	1386	1380	121	221	312
	275	3.73	258	378	-53	-108	364	711	910	898	980	1549	1538	1520	1513	1500	203	194	299
-042	278	4.13	280	597	-18	-79	400	993	1104	1115	1175	1650	1600	1600	1590	1590	172	268	183
	282	4.49	301	573	9	-57	450	1090	1208	1268	1267						189	256	245
	260	3.48	272	457	-47	-86	250	726	872	897	948						146	205	189
	296	4.54	253	542	-32	-89	410	1100	1185	1191	1260						147	191	157
-043	288	4.31	230	719	-1	-28	366	1477	1556	1603	1570	1772	1752	1625	1540	1405	328	297	273
	287	2.46	232	250	-134	-147	90	750	522	552	534	740	885	965	1010	1025	62	130	174
	307	4.38	214	485	-87	-130	329	857	1157	1041	1113	1532	1027	1652	1636	1580	92	173	102
	350	5.42	222	434	-81	-133	313	803	1100	1005	1103	1547	1672	1700	1670	1620	93	173	109
	281	2.40	225	389	-142	-148	106	858	610	590	580	855	995	1060	1220	1235	72	148	181
	230	2.66	227	321	-138	-142	108	564	800	717	691	1005	1080	1095	1175	1145	60	154	255
	187	2.42	225	289	-118	-135	110	640	813	499	720	935	1025	1095	1145	1120	92	256	116
	172	5.27	220	335	23	-93	290	1005	1300	1315	1245	1610	1690	1680	1600	1305	180	207	123
	180	6.60	217	481	37	-76	502	1260	1546	1597	1485	1680	1645	1615	1620	1625	199	224	156
	200	3.68	227	369	-47	-110	190	675	963	1014	960	1235	1330	1405	1395	1415	333	219	202
	218	4.51	234	346	-41	-66	315	870	1174	1068	1135	1465	1415	1435	1390	1425	217	189	203
	228	5.12	240	482	-10	-73	455	1135	1414	1328	1350	1635	1540	1510	1500	1515	229	274	320
	245	3.37	254	456	-33	-91	230	730	1011	948	955	1325	1360	1540	1405	1440	230	305	516
	290	5.52	261	550	-13	-66	500	1255	1521	1344	1410	1725	1570	1570	1495	1510	272	186	125
	293	5.74	263	586	5	-60	530	1315	1585	1410	1495	1720	1610	1550	1515	1580	248	196	114
	295	5.88	262	587	-5	-60	550	1420	1580	1463	1560	1805	1615	1550	1550	1565	222	202	128

NASA CR-134509, APPENDIX B

Test	P_c (psia)	MR	Fuel Valve T_{FTCV} (°R)	Chamber Gas-Side TG 2B	Chamber Shell TC 2B	Fuel (Inj.) T_{FJ}	Convergent Section T_{N1}	T_{N2}	Throat T_{N3}	$T_{N3.5}$	T_{N4}	Nozzle T_{N5}	T_{N6}	T_{N7}	T_{N8}	T_{N9}	Injector Face T_{JF3}	T_{JF4}	T_{JF5}
-044	438	3.44	243	480	-109	-103	280	730	1015	903	923						132	180	150
	482	4.69	243	786	-47	-96	445	745	1525	1366	1310	1765	1680	1575	1660	1680	242	272	318
	473	4.78	245	858	-44	-94	440	620	1450	1243	1280	1653	1590	1530	1585	1570	201	233	105
	434	6.42	255	824	0	-71	555	725	1670	1370	1490	1700	1640	1605	1645	1605	168	191	169
	342	3.25	274	372	-76	-82	315	535	970	868	873	1170	1220	1265	1280	1330	142	220	148
	283	4.12	280	444	-40	-64	390	675	1220	1165	1063	1415	1390	1360	1370	1380	164	125	185
	250	5.24	276	444	-11	-54	445	725	1385	1290	1198	1480	1440	1395	1405	1400	245	145	203
	265	5.71	279	541	12	-44	535	930	1645	1500	1453	1600	1540	1485	1505	1480	234	166	412
-045	198	4.16	541	597	219	190	715	665	1695	1505	1525	1643	1785	1570	1535	1465	462	480	470
	197	4.53	543	600	221	190	720	715	1685	1510	1475		1715	1535	1655	1620	460	480	463
	186	3.61	544	580	210	185	665	490	1490	1395	1238	1503	1570	1445	1560	1540	463	488	478
-046	213	4.27	546	624	225	194	730	510	1730	1550	1498	1570	1605	1475	1570	1550	462	472	460
	214	3.44	545	604	202	180	630	645	1390	1275	1225	1505	1620	1525	1510	1443	465	478	470
-047	302	4.16	545	701	212	174	710	980	1630	1480	1413	1705	1655	1560	1635	1620	461	461	447
	308	4.96	230	545	-60	-103	395	870	1180	1155	1100	1500	1550	1490	1580	1565	247	284	217
	305	4.99	250	523	-42	-79	460	915	1215	1200	1133	1550	1600	1525	1510	1585	183	251	327
	309	5.63	282	584	10	-38	530	1225	1535	1410	1353	1755	1707	1610	1705	1705	230	738	590
	306	5.73		642	25	-32	570	1320	1635	1490	1418	1800	1725	1625	1715	1720	230	396	483
	290	5.08		631	30	-32	580	1325	1635	1490	1395	1765	1650	1575	1650	1660	226	212	485
	240	4.24		551	28	-30	505	1110	1395	1300	1195	1564	1540	1460	1520	1530	218	260	477
	19?	5.17		497	65	-29	595	1355	1615	1495	1405	1680	1685	1585	1650	1650	193	245	380

APPENDIX C

PERFORMANCE DATA

11TA:427024.1.50

NOMENCLATURE LIST

7 JAN 74   22:10:29

PARAMATER	DEFINITION	UNITS
BLL	BOUNDARY LAYER LOSS	LBSF-SEC/LBSM
CSTAR	MEASURE CHARACTERISTIC EXHAUST VELOCITY	FT/SEC
C*	CHARACTERISTIC EXHAUST VELOCITY	FT/SEC
DATE	TEST DATE	----
DL	CURVATURE-DIVERGENCE LOSS	LBSF-SEC/LBSM
DP	DATA PERIOD	----
DT1	DATA TIME START	SEC.
DT2	DATA TIME END	SEC.
ERE	ENERGY RELEASE EFFICIENCY	PERCENT
ERL	ENERGY RELEASE LOSS	LBSF-SEC/LBSM
FCL	FILM COOLING LOSS	LBSF-SEC/LBSM
FVAC	VACUUM THRUST	LBSF
IST	THEORETICAL VACUUM SPECIFIC IMPULSE	LBSF-SEC/LBSM
ISV	MEASURED VACUUM SPECIFIC IMPULSE	LBSF-SEC/LBSM
KL	KINETICS LOSS	LBSF-SEC/LBSM
MR	OVERALL MIXTURE RATIO	----
MRU	CORE MIXTURE RATIO	----
MRD	IGNITER MIXTURE RATIO DISTRIBUTION LOSS	LBSF-SEC/LBSM
PA	ALTITUDE PRESSURE	PSIA
PC	CHAMBER PRESSURE	PSIA
TEST NUMBER	REFERENCE TEST SERIES AND NUMBER	----
TH2	HYDROGEN TEMPERATURE	DEG. RANKINE
TH2C	FILM COOLANT INLET TEMPERATURE	DEG RANKINE
TH2I	REGEN COOLANT INLET TEMPERATURE	DEG RANKINE
TH2OT	REGEN COOLANT OUTLET TEMPERATURE	DEG RANKINE
TO2	OXYGEN TEMPERATURE	DEG. RANKINE
WH	HYDROGEN MASS FLOWRATE	LBSM/SEC
WHC	FUEL COOLANT MASS FLOWRATE	LBSM/SEC
WHI	IGNITER HYDROGEN MASS FLOWRATE	LBSM/SEC
WO	OXYGEN MASS FLOWRATE	LBSM/SEC
WOI	IGNITER OXYGEN MASS FLOWRATE	LBSM/SEC
WT	TOTAL THRUSTER MASS FLOWRATE	LBSM/SEC
%C*	PERCENT CHARACTERISTIC EXHAUST VELOCITY	PERCENT
%FC	PERCENT OF TOTAL FUEL AS COOLANT	PERCENT
%IG	PERCENT OF TOTAL FLOW THROUGH IGNITER	PERCENT
%IS	PERCENT VACUUM SPECIFIC IMPULSE	PERCENT

1ITA-~27n24,1,5.

7 JAN 74   22:10:29   PAGE   18

7 JAN 74

FILM COOLED CHAMBER

11A TEST SUMMARY AND PERFORMANCE DATA

Column headers: TEST NUMBER | INJ | DATE | DTI | LT2 | PC | TO2 | TH2 | V2 | MRC | %FC | %C* | %IS | C* | TST | TSV | XL | MRD | RLL | DL | FCL | FRL | ORE

FILM COOLED CHAMBER

TEST SUMMARY AND PERFORMANCE DATA

TEST PROGRAM	TEST	DATE	PT1	PT2	PC	TO2	THO	VR	MRL	%FC	%C*	%IS	C*	IST	PSV	KL	MRD	RLL	CL	FCL	ERL	FRF
	13	07-03-73	231.0	225.0	283.8	394.0	293.0	5.0	6.4	21.0	96.2	96.4	7576.9	464.2	447.6	5.8	.8	6.3	3.5	15.4	-15.2	107.3
	13	07-03-73	235.0	237.0	283.4	394.0	293.0	5.3	6.8	21.0	95.6	95.2	7450.9	462.9	440.6	6.6	.9	6.2	3.5	17.5	-12.4	102.7
	13	07-03-73	239.0	241.0	241.0	393.0	293.0	5.5	7.1	21.0	95.3	94.6	7363.8	461.7	436.5	7.2	1.0	6.2	3.4	14.0	-11.8	100.5
	13	07-03-73	242.0	245.0	277.9	393.0	292.0	5.7	7.5	21.0	95.4	94.9	7330.7	460.8	437.3	7.7	1.0	6.1	3.4	19.8	-14.5	103.2
	13	07-03-73	246.0	247.0	276.5	393.0	292.0	5.8	7.5	21.0	95.3	94.9	7276.4	459.7	435.8	8.1	1.0	6.1	3.4	20.8	-15.5	103.4
	14	07-10-73	7.9	0.0	139.9	478.0	309.0	3.0	4.0	21.0	96.5	96.1	7883.4	465.5	447.2	4.0	.3	6.7	3.5	6.0	-7.1	100.7

14 FEB 74   09:16:22   PAGE   2n

14 FEB 74   09:16:45

117A,427063.1.50

FILM COOLED CHAMBER

ITA TEST SUMMARY AND PERFORMANCE DATA

TEST NUMBER	ID	DATE	DT1	DT2	PC	TO2	TH2	MR	MRL	WFC	WC*	%TS	C*	IST	TSV	KL	MRD	ALL CL	FCL	FRL FRE

```
      1ITA.427063.1.50                                      14 FEB 74   09:16:22   PAGE   21
                                                                                      14 FEB 74          09:16:45

                                                 FILM COOLED CHAMBER
              ITA TEST SUMMARY AND PERFORMANCE DATA

TEST NUMBER    INJ  DATE    DT1   DT2    PC    TO2    TH2   MR  MRC  %FC   %C*  %IS    C*     IST    TSV   KL  MRD ALL  DL   FCL   FRL  FRF

1972-001-0A- 43 5 09-06-73123.0125.0 343.8 329.1 219.5 5.4 7.0 21.0 91.1 89.0 7062.0 460.7 410.0 5.5 1.0 5.6 3.2 18.2 17.2 96.3
1972-001-0A- 43 5 09-06-73155.0156.0 226.7 318.5 226.7 2.7 3.4 21.0 97.6 94.3 7932.3 452.6 427.0  .9  .3 6.0 3.4  5.0 10.0 97.8
1972-001-0A- 43 5 09-06-73294.0296.0 214.3 342.4 234.9 4.5 5.2 21.0 93.2 90.1 7409.2 463.4 417.5 6.2  .6 6.4 3.3 13.1 16.3 96.5
1972-001-0A- 43 5 09-06-73322.0325.0 240.5 348.2 254.2 3.4 4.3 21.0 94.3 91.2 7693.0 461.6 420.9 2.5  .3 6.2 3.3  5.4 23.1 95.0
1972-001-0A- 43 5 09-06-73336.0338.0 272.5 356.0 259.8 4.6 6.1 21.0 91.6 89.1 7241.7 463.7 413.0 5.5  .7 6.0 3.2 14.4 20.9 95.5
1972-001-0A- 43 5 09-06-73340.0342.0 284.[illegible] 359.7 261.2 5.5 7.1 21.0 90.6 87.7 6993.4 461.0 404.1 7.0 1.0 5.8 3.2 18.8 21.1 95.4
1972-001-0A- 43 5 09-06-73343.0346.0 289.3 362.0 262.5 5.9 7.5 21.0 90.3 87.3 6881.7 458.7 400.3 7.8 1.0 5.7 3.1 21.3 19.5 95.7
1972-001-0A- 43 5 09-06-73349.5350.0 267.7 361.6 263.2 5.7 7.4 21.0 90.1 87.0 6898.3 459.7 400.1 7.5 1.0 5.7 3.1 20.3 21.9 95.2
1972-001-0A- 43 5 09-06-73 74.0 83.0 308.0 330.7 224.7 5.0 6.4 21.0 92.6 91.8 7277.9 462.3 424.4 5.1  .8 5.9 3.3 15.4  7.4 98.4
1972-001-0A- 43 5 09-06-73 89.0103.0 296.0 325.6 216.9 4.5 5.8 21.0 93.0 90.7 7401.0 463.0 420.2 4.5  .6 6.0 3.3 12.7 15.9 96.6
1972-001-0A- 43 5 09-06-73106.0117.0 328.1 327.9 219.6 4.5 5.8 21.0 92.5 90.8 7372.4 463.2 420.8 4.0  .5 5.8 3.3 12.2 16.5 96.4
1972-001-0A- 43 5 09-06-73133.0140.0 275.6 320.6 225.0 2.4 3.1 21.0 97.0 93.0 7855.4 448.2 416.6  .4  .3 5.5 3.3  5.5 16.5 96.3
1972-001-0A- 43 5 09-06-73144.0155.0 230.7 317.4 224.4 2.4 3.1 21.0 98.1 94.8 7940.7 447.9 424.6  .5  .4 5.8 3.3  5.8  7.6 98.3
1972-001-0A- 43 5 09-06-73164.0165.0 184.1 319.9 224.6 2.4 3.1 21.0 99.2 95.5 8038.5 448.5 428.3  .6  .4 6.2 3.4  5.9  3.8 99.1
1972-001-0A- 43 5 09-06-73198.0222.0 169.6 327.5 219.9 5.3 6.8 21.0 94.3 87.8 7297.0 460.4 404.1 9.9 1.0 6.7 3.2 17.7 17.9 96.1
1972-001-0A- 43 5 09-06-73243.0255.0 176.3 332.5 216.0 6.5 8.4 21.0 92.8 66.1 6850.1 450.5 397.712.9 1.1 6.3 3.0 25.7 13.7 97.0
1972-001-0A- 43 5 09-06-73296.0317.0 224.0 345.8 240.3 5.2 6.7 21.0 92.1 87.5 7173.1 461.7 403.8 7.7  .9 6.2 3.2 17.0 22.9 95.1
1972-001-0A- 43 5 09-06-73161.0162.0 179.4 313.8 220.8 2.3 3.0 21.0100.0 95.8 8079.4 446.0 427.4  .4  .4 6.2 3.4  6.4  1.8 99.6
1972-001-0A- 43 5 09-06-73170.0171.0 183.8 319.1 224.4 2.4 3.1 21.0 99.0 95.2 8025.2 448.8 427.3  .6  .4 6.2 3.4  5.8  5.2 98.8
1972-001-0A- 43 5 09-06-73184.0186.0 184.6 322.3 225.3 2.4 3.1 21.0 99.2 95.4 8033.3 448.6 427.8  .6  .4 6.2 3.4  5.1  4.4 99.0
1972-001-0A- 43 5 09-06-73201.0203.0 177.4 333.8 217.0 6.7 8.6 21.0 92.5 85.9 6793.6 449.1 385.613.2 1.1 6.2 3.0 26.7 13.3 97.0
1972-001-0A- 44 5 09-07-73  5.0  6.0 364.7 384.9 234.6 2.6 3.3 21.0100.0101.8 8132.4 451.9 460.0  .5  .3 5.6 3.6  4.6-22.6105.0
1972-001-0A- 44 5 09-07-73 16.0 20.0 420.5 338.5 236.8 3.4 4.4 21.0 94.5 95.6 7704.1 461.2 441.2 1.4  .2 5.5 3.5  4.4  5.0 98.9
1972-001-0A- 44 5 09-07-73 36.0 40.0 458.7 323.0 246.2 4.6 5.9 21.0 92.4 93.6 7366.1 463.9 434.1 2.9  .6 5.5 3.4 12.4  5.1 98.9
1972-001-0A- 44 5 09-07-73 78.0 80.0 466.5 332.0 244.8 5.1 6.6 21.0 91.3 92.0 7175.6 462.6 425.5 3.5  .8 5.3 3.3 15.6  8.6 98.1
1972-001-0A- 44 5 09-07-73123.0125.0 445.2 351.0 247.0 5.7 7.4 21.0 90.0 89.4 6926.0 460.2 411.5 4.7 1.0 5.2 3.2 20.0 14.5 96.9
1972-001-0A- 44 5 09-07-73155.0157.0 425.2 364.6 255.0 6.4 8.3 21.0 89.4 88.7 6710.0 454.8 403.2 6.3 1.1 5.1 3.2 25.3 10.7 97.6
1972-001-0A- 44 5 09-07-73173.0175.0 344.3 352.6 274.2 3.2 4.2 21.0 92.7 92.1 7588.3 461.6 425.3 1.6  .2 5.6 3.3  4.4 21.1 95.4
1972-001-0A- 44 5 09-07-73201.0203.0 277.4 356.2 278.6 4.1 5.3 21.0 92.2 89.9 7435.8 464.9 418.2 4.2  .4 6.0 3.3  9.7 23.2 95.0
1972-001-0A- 44 5 09-07-73237.0239.0 269.5 371.2 279.2 5.7 7.3 21.0 91.0 88.0 6975.1 460.0 404.7 8.2 1.0 5.9 3.2 20.1 16.9 96.3
1972-001-0A- 44 5 09-07-73269.0270.0 251.5 374.9 285.2 5.1 6.6 21.0 91.0 88.7 7120.8 463.2 410.7 6.9  .9 6.0 3.2 16.5 19.2 95.9
1972-001-0A- 44 5 09-07-73  1.7  2.0 342.3 415.3 261.1 2.4 3.1 21.0100.2103.0 8161.0 451.5 465.1  .5  .3 5.6 3.7  5.2-28.8106.4
1972-001-0A- 45 5 09-10-73  1.0  2.0 176.4 544.1 541.1 3.4 4.3 21.0 94.6 95.5 7879.3 473.0 452.4 4.2  .3 6.7 3.6  6.1  -.3100.1
1972-001-0A- 45 5 09-10-73 16.0 20.0 195.9 549.2 542.5 4.2 5.3 21.0 94.4 95.0 7705.8 473.3 449.8 6.8  .4 6.7 3.5 10.7 -4.7101.0
1972-001-0A- 45 5 09-10-73 74.0 76.0 184.2 532.5 543.5 3.6 4.6 21.0 95.3 95.6 7895.7 473.4 452.4 5.0  .3 6.8 3.6  7.0 -1.7100.4
1972-001-0A- 45 5 09-10-73 76.1 77.0 210.5 537.7 546.3 4.3 5.5 21.0 94.3 94.8 7667.7 473.2 448.4 6.7  .5 6.6 3.5 11.4 -3.9100.8
1972-001-0A- 45 5 09-10-73 49.0 75.0 184.2 533.4 543.3 3.6 4.6 21.0 95.3 95.4 7892.0 473.4 451.7 5.0  .3 6.8 3.6  7.0 -1.0100.2
1972-001-0A- 45 5 09-10-73 76.5 79.0 212.4 538.6 546.5 4.4 5.6 21.0 94.1 94.5 7632.2 472.9 446.9 6.9  .5 6.6 3.5 12.1 -3.6100.8
1972-001-0A- 46 5 09-10-73  1.5  2.0 198.9 541.5 542.4 3.1 3.9 21.0 95.9 97.2 8029.4 471.7 458.6 2.9  .2 6.6 3.6  5.3 -5.5102.2
1972-001-0A- 46 5 09-10-73 18.0 20.0 211.6 540.2 544.9 3.4 4.4 21.0 96.4 97.2 8029.8 473.1 459.8 3.8  .3 6.7 3.6  5.8 -6.7101.4
1972-001-0A- 46 5 09-10-73 38.0 40.0 223.8 538.4 545.9 3.8 4.9 21.0 95.6 96.9 7904.0 473.7 458.8 5.0  .3 6.6 3.6  7.9 -8.6101.8
1972-001-0A- 46 5 09-10-73 58.0 60.0 231.8 533.8 548.5 3.6 4.7 21.0 96.3 97.5 7982.6 473.6 461.7 4.3  .3 6.6 3.6  6.6 -4.5102.0
1972-001-0A- 46 5 09-10-73 96.0100.0 261.5 535.9 547.9 3.9 5.1 21.0 97.9 95.2 8050.0 473.7 450.8 4.7  .4 6.6 3.5  8.6  -.9100.2
1972-001-0A- 46 5 09-10-73118.0120.0 264.7 532.1 547.5 4.0 5.2 21.0 98.1 95.1 8055.2 473.7 450.5 4.9  .4 6.6 3.5  9.0 -1.2101.3
1972-001-0A- 46 5 09-10-73138.0140.0 267.8 528.9 547.4 4.0 5.1 21.0 97.7 95.3 8028.6 473.7 451.5 4.7  .4 6.6 3.5  9.7 -1.7100.4
```

LITA-A47063.1.5L

14 FEB 74   09:16:22   PAGE   22

14 FEB 74   09:16:45

FILM COOLED CHAMBER

IIA TEST SUMMARY AND PERFORMANCE DATA

TEST NUMBER	T.D. DATE	OT1	OT2	PC	TO2	TH2	VO	MRC	%FC	%C*	%IS	C*	IST	TSV	KL	MRD	ALL DI	FCL	FGL	FDF

7 JAN 74   22:10:29   PAGE   23

7 JAN 74   22:10:49A

1ITA=427,,34,1.50

IIA TEST CORRLLATION PARAMETERS

FILM COOLED CHAMBER

TEST NUMBER	VO	VF	VFC	MO	MF	MFC	VR	MMR	VDIFF	MDIFF	RUPEL	RUPEC	RUPF	VRC	VDIFFC	VRF
1972-001-0A- 3	367.5	2232.6	353.4	607.1	1104.7	52.5	6.1	1.8	497.5	1865.0	.05	.24	2.42	.20	1865.0	101.5
1972-001-0A- 3	372.1	2298.1	802.8	616.1	1137.0	107.2	6.1	1.8	520.9	1921.0	.04	.23	2.46	.39	1921.0	100.7
1972-001-0A- 4	290.9	1275.1	920.1	777.2	635.7	123.7	4.4	.8	-141.5	984.2	.44	.84	1.08	.84	984.2	101.4
1972-001-0A- 6	309.9	1299.5	1334.9	839.8	644.3	179.1	4.2	.8	-195.5	984.6	.40	.87	1.02	.74	984.6	101.0
1972-001-0A- 6	330.3	1605.4	2236.8	516.9	736.9	277.1	4.9	1.4	220.0	1275.1	.10	.43	1.90	1.09	1275.1	101.0
1972-001-0A- 6	264.5	1452.7	2779.7	486.2	786.6	406.3	5.1	1.6	306.3	1168.1	.07	.32	2.15	1.32	1168.1	102.1
1972-001-0A- 6	272.4	1434.6	3184.0	469.3	796.9	477.4	5.3	1.7	327.6	1162.3	.06	.29	2.24	1.52	1162.3	100.2
1972-001-0A- 6	259.8	1367.7	3560.4	470.5	765.0	508.3	5.3	1.6	294.5	1107.9	.07	.32	2.17	1.66	1107.9	96.0
1972-001-0A- 6	306.0	986.0	2906.9	621.2	389.8	110.1	3.2	.6	-231.4	679.9	.66	.93	.84	1.59	679.9	88.1
1972-001-0A- 6	322.4	971.0	3178.3	603.0	350.8	309.8	2.9	.6	-253.0	641.6	.72	.96	.77	1.72	641.4	
1972-001-0A- 8	322.4	901.7	3490.3	613.7	314.4	328.2	2.7	.5	-299.3	569.4	.80	.96	.58	1.89	569.2	104.0
1972-001-0A- 10	290.2	1210.2	4150.8	767.6	694.8	633.8	4.1	.9	-82.8	912.0	.37	.73	1.10	2.15	912.0	90.2
1972-001-0A- 10	367.0	2693.3	6565.6	520.0	1434.4	942.8	7.3	2.8	914.4	2325.5	.07	.03	1.67	3.11	2207.5	00.1
1972-001-0A- 10	370.0	2667.7	6905.3	532.0	1418.6	990.1	7.2	2.7	886.6	2297.1	.01	.05	3.55	3.33	2207.1	00.5
1972-001-0A- 10	370.3	2671.5	7319.8	531.2	1422.8	1050.5	7.2	2.7	891.5	2301.3	.01	.05	3.57	3.53	2301.1	00.7
1972-001-0A- 10	450.2	1755.2	511.3	989.3	688.8	547.3	3.7	.7	-301.1	1276.2	.58	.91	.95	2.52	1276.2	05.7
1972-001-0A- 10	473.0	1774.0	5566.3	473.3	695.0	587.8	3.7	.7	-278.6	1300.0	.56	.90	.97	2.04	1300.0	66.5
1972-001-0A- 10	406.3	1777.4	5957.3	455.0	697.8	630.4	3.8	.7	-257.1	1311.1	.54	.90	.95	3.76	1411.1	66.0
1972-001-0A- 11	342.5	1187.5	7640.9	684.9	1065.1	1604.1	5.6	1.6	341.5	1794.4	.08	.30	2.07	4.00	1794.4	103.1
1972-001-0A- 11	340.5	2144.0	8070.0	682.6	1066.1	1061.5	5.6	1.6	383.5	1793.5	.08	.35	2.08	4.30	1793.6	103.5
1972-001-0A- 11	335.2	2168.8	8423.7	681.4	1056.0	1106.1	5.6	1.6	375.5	1786.6	.08	.35	2.07	4.38	1786.6	103.5
1972-001-0A- 11	357.4	2156.0	8773.2	720.7	1047.2	1148.2	5.0	1.2	366.0	1703.8	.08	.37	1.57	4.30	1465.7	102.6
1972-001-0A- 12	390.4	1568.9	8010.3	681.2	849.2	1054.0	4.7	.9	128.6	1462.7	.18	.72	1.23	4.71	1161.4	101.0
1972-001-0A- 12	405.1	1568.9	8347.0	746.9	690.5	1049.0	3.9	.8	-55.4	1161.8	.34	.77	1.08	4.86	1161.5	101.0
1972-001-0A- 12	356.7	1420.6	9072.2	752.6	610.6	1051.3	3.5	.8	-142.0	1011.5	.45	.84	1.04	2.01	101.0	00.0
1972-001-0A- 12	335.2	1201.2	9363.5	645.0	511.5	1040.0	3.5	.8	-133.5	890.0	.47	.85	1.06	5.22	6.30	100.2
1972-001-0A- 12	326.1	1147.0	9705.0	612.1	488.5	1064.4	3.6	.8	-123.6	865.0	.46	.85	.93	5.12	85.3	101.2
1972-001-0A- 12	321.5	1147.0	905c.2	924.7	542.6	1334.6	3.7	.7	-282.1	856.3	.58	.90	.93	5.49	825.3	100.2
1972-001-A- 12	321.5	1136.3	4933.3	948.0	620.7	1361.4	3.6	.7	-325.8	825.2	.63	.92	.47	5.49	816.8	102.2
1972-001-0A- 12	323.2	1118.2	9663.5	934.8	611.4	1401.3	3.5	.7	-322.9	810.8	.63	.92	.47	5.01	726.7	100.5
1972-001-A- 13	330.5	1119.7	10001.4	932.1	599.3	1446.1	3.5	.6	-332.8	794.7	.64	.92	.86	5.01	767.3	00.5
1972-001-0A- 13	329.7	1111.6	10401.1	933.9	601.0	1500.3	3.5	.6	-331.9	797.3	.64	.92	.86	6.10	768.3	00.5
1972-001-0A- 13	314.9	1111.6	10735.6	939.1	595.8	1551.0	3.4	.6	-343.4	788.3	.66	.91	.84	6.07	1162.0	101.1
1972-001-0A- 13	356.8	1521.7	12551.4	723.2	647.6	1441.0	3.8	.9	-75.6	1122.9	.36	.73	1.10	1.01	746.9	101.1
1972-001-0A- 13	349.2	1385.5	12747.5	755.9	572.0	1419.0	3.4	.8	-183.9	978.9	.51	.87	1.01	6.06	746.9	100.0
1972-001-0A- 13	336.7	1096.2	12650.8	645.2	413.0	1261.2	3.1	.8	-232.2	746.0	.65	.92	.45	7.15	751.0	100.2
1972-001-0A- 13	529.7	1673.0	13025.8	616.4	396.9	1264.6	3.2	.6	-219.5	737.2	.44	.95	.86	7.43	745.0	102.0
1972-001-0A- 13	349.2	1281.0	13025.3	554.5	332.5	1289.0	2.4	.9	-267.1	578.3	.51	.72	.74	7.02	846.0	101.0
1972-001-0A- 13	310.0	1281.0	14047.0	828.3	740.3	2190.6	4.1	.8	-87.9	965.9	.36	.82	1.19	7.01	917.6	102.5
1972-001-0A- 13	314.2	1257.7	14540.2	954.8	721.9	2175.3	4.0	.8	-132.8	944.6	.41	.91	1.17	7.49	773.3	102.0
1972-001-0A- 13	326.3	1143.9	15070.3	945.4	589.7	1820.6	3.5	.6	-355.7	815.4	.47	.91	.87	7.01	772.3	101.3
1972-001-0A- 13	326.0	1140.6	13497.7	943.5	594.0	1885.1	3.5	.6	-347.8	821.4	.66	.64	.84	4.16		101.3
1972-001-0A- 13	331.4	1096.0	13584.7	943.5	550.7	1841.0	3.4	.9	-192.7	772.5	.72	.91	.70			
1972-001-0A- 13	295.1	1224.4	15923.7	721.6	643.0	2258.0	4.1	.9	-78.6	922.1	.57	.71	1.19			
1972-001-0A- 13	342.7	1011.3	1325u.4	1053.0	470.8	1663.5	3.0	.4	-582.2	660.0	.47	.91	.60			

IIIA.427.63.1.50

14 FEB 74   09:16:22   PAGE   74

14 FFB 74   09:16:45

FILM COOLED CHAMBER

IIIA TEST CORRELATION PARAMETERS

TEST NUMBER	JC	VF	VFC	"O	MF	MFC	VR	WMF	VDIFF	MDIFF	RMPEL	MMPEC	RMPF	VPC	VDIFFC	FRF
1972-001-04- 13	535.2	1022.2	13615.8	980.4	468.6	1710.5	3.0	.5	-611.8	687.0	.84	.97	.64	8.36	687.0	103.7
1972-001-04- 15	544.4	984.3	13674.7	1034.0	435.0	1628.6	2.9	.4	-600.0	634.8	.40	.94	.56	8.41	679.2	102.7
1972-001-04- 13	56.3	946.1	13711.7	1061.1	406.7	1580.1	2.7	.4	-652.9	604.1	.92	.91	.51	9.51	604.1	102.5
1972-001-04- 15	62.3	936.6	13645.5	1067.1	362.4	1551.3	2.7	.4	-678.7	563.7	.93	.91	.48	8.66	583.7	103.2
1972-001-04- 15	57.3	926.3	13604.9	1186.5	373.7	1534.4	2.6	.3	-712.9	563.3	.94	.91	.96	8.79	543.3	102.4
1922-001-04- 11	57.7	1195.5	13617.7	665.1	480.3	2115.4	3.3	.7	-204.8	827.8	.57	.90	.95	10.63	827.8	100.7

11TA-427063.150

14 FEB 74   09:16:22   PAGE   25

14 FEB 74   00:16:45

FILM COOLED CHAMBER

AIA TEST CORRELATION PARAMETERS

TEST NUMBER	LO	VF	VFL	WO	WF	WFL	VR	MIX	VDIFF	WDIFF	R1PFL	R1PFC	R1PF	VPC	VDIFF	FRE

FILM COOLED CHAMBER

FILM TEST CORRELATION PARAMETERS

TEST NUMBER	TF	VF	VFC	TC	MF	MFC	VR	VMP	VDIFF	MDIFF	PIPEL	RVPFC	RVPF	VRC	VDIFFC	EFF

FILM COOLED CHAMBER

31A TEST CORRELATION PARAMETERS

TEST NUMBER	VO	VF	VFC	MO	MF	MFC	VR	MMR	VDIFF	MDIFF	RMFEL	RMRFC	RMRF	VPC	VDIFFC	FRF
1972-U01-UA-46	407.9	1771.8	49560.4	1058.2	900.1	6794.1	4.3	.9	-158.0	1363.9	.41	.82	1.13	28.59	1363.9	101.0
1972-U02-UA-46	411.9	1767.0	49809.7	1132.2	928.0	7012.0	4.3	.8	-203.8	1355.0	.44	.84	1.09	28.54	1355.0	101.3
1972-U01-UA-46	413.1	1771.7	49803.8	1160.4	947.0	7190.2	4.3	.8	-212.6	1358.5	.44	.84	1.09	28.71	1358.5	101.2
1972-U03-UA-46	416.7	1753.8	49634.1	1188.6	935.4	7144.5	4.2	.8	-253.2	1337.1	.47	.8_	1.05	28.73	1337.1	101.0
1972-U03-UA-47	399.3	1384.4	54495.9	888.3	92_	7333.1	4.7	1.0	34.9	1485.1	.25	.69	1.38	30.68	1485.1	101.5
1972-U03-UA-47	410.7	1777.7	51162.7	1118.5	92	7276.8	4.3	.8	-181.5	1367.1	.47	.83	1.17	29.50	1367.1	101.2
1972-U03-UA-47	320.0	1463.2	54022.1	898.6	912.5	8100.1	4.5	.9	-86.1	1136.4	.36	.79	1.20	30.20	1136.4	102.3
1972-U01-UA-47	296.4	1190.6	53060.7	846.7	645.9	7774.1	4.0	.8	-200.8	892.2	.50	.87	1.02	29.79	892.2	101.4
1972-U04-UA-47	269.0	1042.4	52400.0	827.2	562.4	7363.0	3.8	.7	-258.8	802.8	.59	.91	.92	29.47	802.8	100.2
1972-U01-UA-47	278.5	1021.4	47701.7	590.6	325.1	4097.3	3.7	.6	-265.5	742.9	.76	.95	.73	27.82	742.9	96.8
1972-U01-UA-47	278.1	1023.7	48216.1	588.6	326.6	4151.8	3.7	.6	-262.0	745.6	.75	.95	.74	28.00	745.6	99.7
1972-U01-UA-47	270.0	1025.5	52332.5	799.4	514.0	7084.5	3.7	.6	-285.4	746.7	.64	.92	.86	29.73	746.7	99.4
1972-U01-UA-47	286.5	423.2	46292.0	924.3	454.6	6392.7	3.2	.5	-469.7	641.7	.82	.97	.66	28.50	641.7	98.1
1972-U01-UA-47	295.5	732.1	49234.9	965.0	468.3	6686.2	3.2	.5	-496.7	636.6	.83	.97	.65	28.33	636.6	98.0
1972-U01-UA-47	304.5	415.4	50375.7	985.2	478.7	6895.7	5.1	.5	-506.4	640.0	.83	.97	.65	29.00	640.0	97.5
1972-U01-UA-77	310.1	957.1	51104.6	998.3	485.4	7006.1	3.1	.5	-512.9	616.9	.93	.97	.65	29.56	686.0	97.2
1972-U01-UA-77	308.7	977.1	50600.4	1002.1	488.7	6856.2	3.2	.5	-114.0	668.2	.83	.97	.64	29.47	668.2	97.5
1972-U01-UA-77	305.2	985.0	50174.1	1004.9	484.9	6674.1	3.2	.5	-519.9	680.7	.83	.97	.63	29.19	680.7	97.2
1972-U01-UA-77	296.0	965.4	44951.6	1004.0	477.5	6354.2	3.3	.5	-530.5	688.8	.84	.97	.62	29.10	688.8	97.2
1972-U01-UA-77	292.5	985.2	48401.1	1004.9	467.9	6217.8	3.4	.5	-537.0	492.9	.84	.97	.63	29.10	622.9	97.2
1972-U01-UA-77	291.0	1013.6	44455.5	1004.3	473.4	6113.5	5.5	.5	-530.9	721.8	.84	.97	.62	29.10	721.8	97.2
1972-U01-UA-77	257.0	1163.4	57887.7	623.1	509.3	6807.4	4.5	.8	-113.8	911.6	.44	.84	1.00	32.31	911.6	96.4
1972-U01-UA-77	260.0	1176.3	57869.6	632.5	508.6	6755.6	4.5	.8	-123.9	915.7	.45	.85	1.07	32.33	915.7	96.0
1972-U01-UA-77	262.3	1174.3	57790.0	638.2	505.1	6684.5	4.5	.8	-135.1	912.0	.47	.86	1.05	32.46	912.0	96.8
1972-U01-UA-77	276.1	1029.1	53164.2	589.4	324.6	4566.5	3.7	.6	-264.8	742.0	.76	.95	.73	31.01	742.0	94.7

IITA,427,24,1,5L

7 JAN 74   22:10:29   PAGE   28

7 JAN 74

22:10:48

ITA TEST DATA INPUT

FILM COOLED CHAMBER

TEST NUMBER	MR	MRC	WO	WF	WFC	WOI	WFI	MT	FR2	TH2IN	TH2OT	TH2C	PC	PA	FVAC	CSTAR	ISP	%IG	%FC

IITA.427..63.1.50

FILM COOLED CHAMBER

IITA TEST DATA INPUT

TEST NUMBER	WR	WRC	WO	WF	WFC	WOI	WFI	WT	To2	TH2IN	TH2OT	TH2C	PC	PA	FVAC	CSTAR	ISP	WIG	WFC
1972-001-0A-15	5.13	6.60	3.07	.47	.13	.00	.01	3.67	396.0	294.0	478.4	5793.0	293.0	.1	1631.7	7488.7	444.5	.20	21.0
1972-001-0A-15	4.76	6.38	2.93	.46	.12	.00	.01	3.51	394.0	293.0	475.7	5950.7	283.8	.1	1573.2	7576.0	447.6	.21	21.0
1972-001-0A-15	5.29	6.01	3.09	.44	.12	.00	.01	3.57	394.0	293.0	475.5	6114.3	283.4	.2	1572.6	7450.7	440.6	.20	21.0
1972-001-0A-15	5.53	7.11	3.93	.73	.12	.00	.01	3.58	392.0	293.0	474.3	6262.3	281.0	.2	1564.1	7363.6	436.8	.19	21.0
1972-001-0A-13	5.27	7.29	3.02	.71	.11	.00	.01	3.56	393.0	292.0	471.7	6453.6	277.0	.2	1555.6	7330.7	437.3	.19	21.0
1972-001-0A-13	5.35	7.50	3.04	.41	.11	.00	.01	3.57	393.0	292.0	471.0	6627.0	276.5	.2	1553.7	7276.4	435.6	.18	21.0
1972-001-0A-14	5.01	4.64	1.46	.40	.11	.00	.01	2.38	478.0	309.0	447.1	6763.9	199.9	.1	1064.0	7843.4	447.2	.25	21.0

14 FEB 74   09:16:25   PAGE

14 FEB 74

FILM COOLED CHAMBER

```
                                        FILM COOLED CHAMBER

        [illegible] TEST DATA INPUT

TEST NUMBER       MR  MRC   WC   WF  WFC   WOI  WFI  WT    TO2   TH2IN TH2OT TH2C     PC     PA   FVAC  CSTAR   ISP  %IG  %FC

1972-001-UA- 43 4.38 5.64 3.10 .55 .15   .00 .01 3.80 324.5 215.9 407.1******* 300.7   .2 1598.3 7416.9 420.1 .24 21.0
1972-001-UA- 43 5.42 6.97 3.86 .55 .15   .00 .01 4.57 329.1 219.5 432.3******* 343.8   .2 1873.1 7062.1 410.0 .20 21.0
1972-001-UA- 43 2.66 3.42 1.95 .57 .15   .00 .01 2.68 318.5 226.7 379.2******* 226.7   .1 1145.1 7932.3 427.0 .34 21.0
1972-001-UA- 43 4.51 5.80 2.22 .58 .10   .00 .01 2.71 342.4 234.9 381.0******* 214.3   .1 1133.0 7409.2 417.5 .23 21.0
1972-001-UA- 43 3.37 4.33 2.26 .52 .14   .00 .01 2.94 348.2 254.2 414.3******* 240.8   .1 1236.1 7693.0 420.9 .29 21.0
1972-001-UA- 43 4.79 6.15 2.92 .47 .13   .00 .01 3.53 356.0 259.8 436.6******* 272.5   .1 1458.1 7241.7 413.0 .22 21.0
1972-001-UA- 43 5.51 7.09 3.23 .46 .12   .00 .01 3.81 359.7 261.2 444.0******* 284.0   .1 1540.0 6993.4 404.1 .20 21.0
1972-001-UA- 43 5.98 7.57 3.37 .45 .12   .00 .01 3.94 362.0 262.5 448.0******* 289.3   .1 1578.9 6881.7 400.3 .19 21.0
1972-001-UA- 43 5.74 7.39 3.33 .45 .12   .00 .01 3.91 361.8 263.2 447.9******* 287.7   .2 1565.8 6898.3 400.1 .19 21.0
1972-001-UA- 43 4.96 6.39 3.30 .52 .14   .00 .01 3.97 336.7 224.7 419.6******* 308.0   .2 1685.5 7277.9 424.4 .22 21.0
1972-001-UA- 43 4.32 5.62 3.07 .53 .14   .00 .01 3.75 325.6 216.9 405.7******* 296.0   .2 1576.8 7401.0 420.2 .24 21.0
1972-001-UA- 43 4.43 5.78 3.42 .59 .16   .00 .01 4.18 327.9 219.6 424.5******* 328.1   .2 1757.2 7372.4 420.8 .24 21.0
1972-001-UA- 43 2.40 3.09 2.33 .75 .20   .00 .01 3.29 320.8 225.0 403.1******* 275.6   .1 1371.6 7855.1 416.6 .36 21.0
1972-001-UA- 43 2.39 3.08 1.92 .62 .17   .00 .01 2.73 317.4 224.4 379.0******* 230.7   .1 1157.4 7940.7 424.6 .37 21.0
1972-001-UA- 43 2.42 3.11 1.52 .49 .13   .00 .01 2.15 319.9 224.6 353.8******* 184.1   .1  920.4 8038.5 428.3 .37 21.0
1972-001-UA- 43 5.27 6.79 1.83 .27 .07   .00 .00 2.18 327.5 219.9 341.3******* 169.6   .1  881.3 7297.0 404.1 .21 21.0
1972-001-UA- 43 [illegible] 6.42 2.09 .25 .07   .00 .00 2.41 332.5 216.0 341.4******* 176.3   .1  936.2 6850.1 387.7 .18 21.0
1972-001-UA- 43 [illegible] 6.66 2.46 .37 .10   .00 .01 2.93 345.8 240.3 391.7******* 224.0   .1 1183.2 7173.1 403.9 .21 21.0
1972-001-UA- 43 2.30 2.96 1.45 .49 .13   .00 .01 2.08 317.8 220.8 347.3******* 179.4   .1  890.5 8079.4 427.4 .38 21.0
1972-001-UA- 43 2.44 3.13 1.52 .49 .13   .00 .01 2.15 319.1 224.4 353.4******* 183.8   .1  918.2 8025.2 427.3 .36 21.0
1972-001-UA- 43 2.42 3.11 1.53 .49 .13   .00 .01 2.16 322.3 225.3 354.8******* 184.6   .1  922.5 8033.3 427.0 .37 21.0
1972-001-UA- 43 6.07 [illegible] 2.13 .25 .07   .00 .00 2.45 333.8 217.0 343.0******* 177.4   .1  944.8 6793.5 386.6 .17 21.0
1972-001-UA- 44 2.90 3.70 3.03 .92 .25   .00 .01 4.21 384.9 234.6 457.3******* 364.7   .2 1935.5 8132.4 460.0 .35 21.0
1972-001-UA- 44 3.46 4.38 3.98 .90 .24   .00 .01 5.12 338.5 236.6 486.4******* 420.6   .2 2260.0 7704.1 441.2 .29 21.0
1972-001-UA- 44 4.60 5.92 4.80 .61 .22   .00 .01 5.64 323.0 246.2 513.8******* 458.7   .2 2536.6 7366.1 434.1 .23 21.0
1972-001-UA- 44 5.10 6.56 5.10 .78 .21   .00 .01 6.10 332.0 244.8 516.1******* 466.5   .2 2595.9 7175.6 425.5 .22 21.0
1972-001-UA- 44 5.72 7.36 5.13 .70 .19   .00 .01 6.03 351.0 247.0 508.4******* 445.2   .2 2482.1 6976.0 411.5 .20 21.0
1972-001-UA- 44 6.42 8.26 5.14 .62 .17   .00 .01 5.95 354.6 255.0 507.1******* 425.2   .2 2397.3 6710.0 403.2 .18 21.0
1972-001-UA- 44 3.25 4.18 3.16 .76 .20   .00 .01 4.13 352.6 274.2 482.0******* 334.3   .2 1757.9 7588.3 425.7 .30 21.0
1972-001-UA- 44 4.12 5.30 2.82 .53 .14   .00 .01 3.50 358.2 278.6 457.9******* 277.4   .2 1463.8 7435.1 418.2 .25 21.0
1972-001-UA- 44 5.71 7.35 2.98 .41 .11   .00 .01 3.50 371.2 279.2 449.9******* 260.5   .1 1418.4 6975.1 404.7 .19 21.0
1972-001-UA- 44 5.11 6.57 2.77 .42 .11   .00 .01 3.31 374.9 285.2 451.1******* 251.5   .1 1360.9 7120.3 410.7 .21 21.0
1972-001-UA- 44 2.45 3.15 2.79 .89 .24   .00 .01 3.94 415.3 261.1 472.8******* 342.3   .6 1830.5 8161.0 465.1 .34 21.0
1972-001-UA- 45 3.36 4.32 1.62 .37 .10   .00 .01 2.10 544.1 541.1 666.1******* 176.4   .1  950.3 7879.3 452.4 .26 21.0
1972-001-UA- 45 4.16 5.35 1.92 .36 .10   .00 .01 2.39 549.2 542.5 678.5******* 195.9   .1 1073.0 7705.8 449.8 .22 21.0
1972-001-UA- 45 3.51 4.53 1.71 .37 .10   .00 .01 2.19 532.5 543.5 672.9******* 184.2   .1  990.3 7895.7 452.4 .25 21.0
1972-001-UA- 45 4.27 5.49 2.09 .36 .10   .00 .01 2.58 537.7 546.3 690.3******* 210.5   .1 1155.0 7667.7 448.4 .22 21.0
1972-001-UA- 45 3.51 4.53 1.71 .37 .10   .00 .01 2.19 533.4 543.3 672.7******* 184.2   .1  989.3 7892.0 451.7 .25 21.0
1972-001-UA- 45 4.36 5.62 2.13 .38 .10   .00 .01 2.61 539.6 546.5 691.5******* 212.4   .1 1167.0 7632.2 446.9 .22 21.0
1972-001-UA- 46 3.07 3.94 1.75 .44 .12   .00 .01 2.32 541.5 542.4 679.9******* 198.9   .1 1066.0 8029.4 458.8 .28 21.0
1972-001-UA- 46 3.39 4.35 1.91 .44 .12   .00 .01 2.48 540.2 544.9 689.5******* 211.8   .1 1138.0 8029.1 454.6 .26  1.0
1972-001-UA- 46 3.81 4.89 2.10 .43 .12   .00 .01 2.66 538.4 543.9 697.0******* 223.8   .1 1219.0 7904.1 458.8 .24   .0
1972-001-UA- 46 3.63 4.66 2.14 .46 .12   .00 .01 2.72 533.8 548.5 703.9******* 231.8   .1 1258.0 7982.5 461.7 .25   .0
1972-001-UA- 46 3.95 5.07 2.43 .46 .13   .00 .01 3.05 535.9 547.9 719.0******* 261.5   .3 1374.0 8050.0 450.8 .24   .0
```

FILM COOLED CHAMBER

14 FEH 74

TEST				TC2	TM2IN	TM2OT	TH2C	PC	PC	FVAC	CSTAR	ISP	*IG	OFC

APPENDIX D

LIFE CYCLE DESIGN ANALYSIS

I.   LIFE CYCLE ANALYSIS

The thermal data from the initial ITA test firings were reviewed to upgrade the life cycle prediction in light of actual operating characteristics and in connection with the definition of a duty cycle for the 50,000 pulse life test.

A.   HAYNES 188 THROAT

The basis for evaluation of throat life is the fatigue life curve shown in Figure 49 of the main text (ε = .21%, η_f = 1 x 10^5). The basis for the .21% strain is the temperature gradient through the wall shown in Figure 45 (axial station 6) of the main text.

The thermal data that were used were taken from Test -009. This test was selected because the hardware had been prechilled and startup was made with the fuel at approximately the nominal temperature, 139°K (250°R). The data from thermocouple TN-3,   shown in Figure 1-D, was used in the analysis.

The maximum strain in the throat is a result of the temperature gradient through the wall. The maximum temperature gradient (ΔT) occurs during the startup transient.

No gas side temperature measurements were made in the throat. Therefore, a simple analytical model was used to predict the throat temperature transients. A flat plate model was used with the exterior insulated and the interior face convectively heated. The gas side heat transfer coefficient was taken from Contract NAS 3-14354 data (Ref. 3).

Figure 2-D shows the throat startup temperature transient. The wall temperature has been initialized. that is the initial temperature subtracted out, so that the results from this program can be compared to NAS 3-14354 data.

INTEGRATED THRUSTER ASSEMBLY (I.T.A.)
NOZZLE TEMPERATURES UPSTREAM OF THROAT
TEST NO. 1972-CC1-04-009
TEST STAND J-3
TEST DATE: 03 JULY 1973

STARTUP TRANSIEN TIME (SECONDS)

1	TN-1	DEG.F
2	TN-2	DEG.F
3	TN-3	DEG.F
4	TN-4	DEG.F
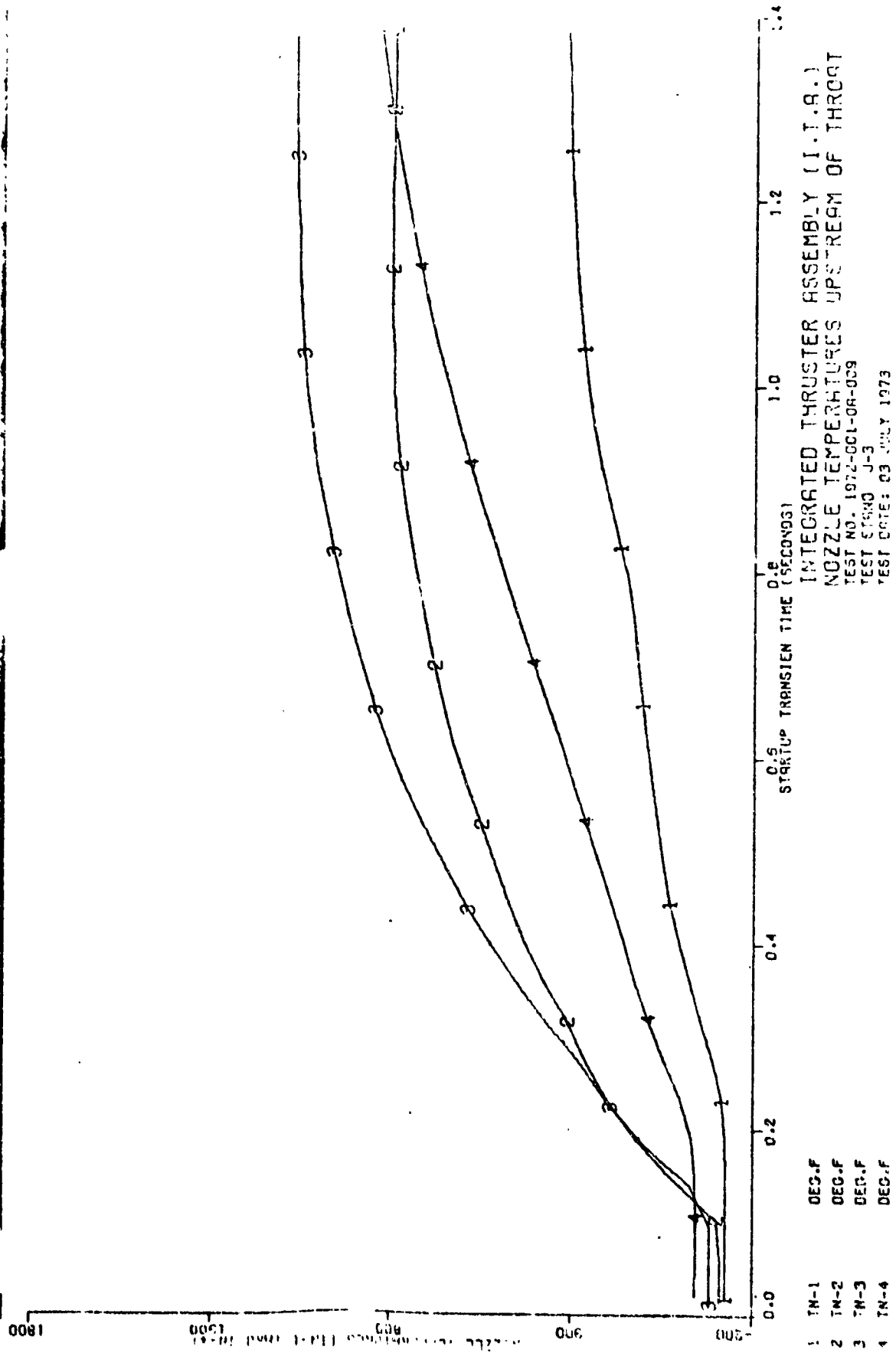
Figure 1-D

I.A. Haynes 188 Throat (cont.)

Shown in Figure 2-D are: the gas-side and exterior transient temperature predicti.
for this program, the exterior temperature data from Test -009 (correlation with
model), and for comparison, the exterior and gas-side temperature transient from
Figure VI-13 of Ref. 3.

The following conclusions can be drawn from the results shown in
Figure 2-D:

1.   The correlation of the analytical model with the data is
satisfactory.

2.   The maximum ΔT occurs .15 second after the initiation of
the transient.

3.   Although the steady state temperature measured on TN-3 is at
least 56°C (100°F) higher than the Contract NAS 3-14354 data, the transients are
very similar and the maximum ΔT, 200°C (360°F), is only 20° higher than at the ΔT,
189°C (340°F), on which the life analysis is based.

The effect of the duty cycle (cumulative damage) on the throat
thermal cycle life was analyzed as follows:

1.   On the basis of prior analysis, it is known that a ΔT of
189°C (340°F) produces a total strain of .21%.

2.   The strain is assumed proportional to the ΔT.

3.   The ΔT is the gas-side temperature minus the exterior
temperature as predicted by the model.
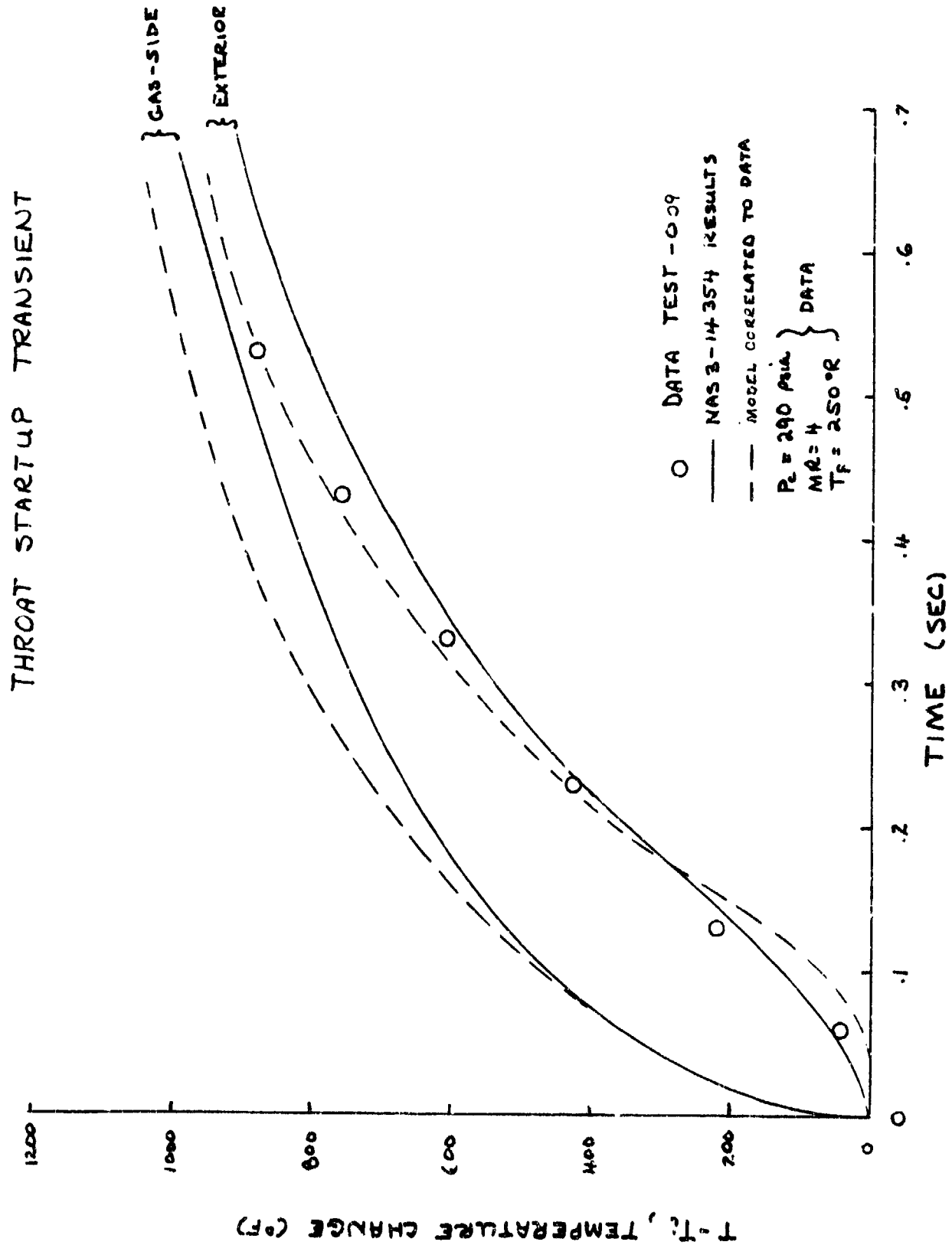
Figure 2-D

I,A, Haynes   188 Throat (cont.)

4.   The strain occurs with no hold time. Thus, any firing duration that produces a transient of .15 sec or longer will result in the maximum strain even though the final ΔT is less than the maximum.

5.   The average wall temperature after a firing is the arithmetic average of the interior and exterior surface temperatures (assumes linear temperature gradient).

6.   There will be a hardware chilldown every 10th pulse. Thus, 50,000 pulses give 5000 repeats of the basic 10 pulse train.

7.   Cumulative damage is defined as

$$5000 \left(\sum_{1}^{10} \frac{1}{\eta_f} \right)$$

where: η_f is the number of cycles to failure for a given pulse in the basic repetitive 10 pulse train.

8.   The initial conditions correspond to Test -009.

Initial uniform wall temperature = -62°C (-80°F).
Adiabatic wall temperature = 577°C (1070°F).
Driving ΔT = 577 - (-62) = 639°C (1150°F).

Using the thermal model, the maximum ΔT (gradient through the wall) and final average temperature were calculated for series of pulses of various durations. The average wall temperature from one pulse was used as the initial wall temperature for the next pulse. The cumulative damage was evaluated for:

1.   A series of .050 sec pulses

2.   A series of .100 sec pulses

I,A, Haynes 188 Throat (cont.)

3.   A series of .150 sec pulses

4.   A series of .180 sec pulses

5.   A .180 sec pulse followed by .100 sec pulses

6.   A .180 sec pulse followed by .150 sec pulses

7.   A .3 sec pulse followed by a .150 sec pulse

The calculations were generally made for only a few pulses since the contribution
to cumulative damage becomes negligible as the wall warms up (as the initial
temperature increases the driving ΔT and, therefore, the maximum ΔT decreases).
Figure 1 was used to determine the cycle life for each strain condition (this
neglects the effect of temperature on the strain versus life relationship). The
results are tabulated in Table I-D.

The following conclusions were made relative to throat life:

1.   The program design and test requirements do not permit throat
life to be evaluated. A 25,000 thermal cycle life requirement coupled with a 5000
thermal cycle test requirement represents only a 20% cumulative damage.

2.   The more the design exceeds the cycle life requirement, the
more difficult it becomes to test the throat to the life limit. For a predicted
life of .8 x 10^5 thermal cycles [ΔT = 200°C (360°F)], 5000 thermal cycles (test
requirement) constitutes only 6.25% cumulative damage.

3.   Unless cooldown of the hardware is employed more often than
every 10th pulse (number of full thermal cycles increased beyond 5000) the most
limiting combination of pulses will result in only approximately 8% cumulative
damage to the throat.

TABLE I-D

CUMULATIVE EFFECT OF PULSE WIDTH ON THROAT LIFE

577 (1070)

Pulse	Initial Temp °C (°F)	Pulse Dur. (sec)	Final Temperature Inside °C (°F)	Final Temperature Outside °C (°F)	Final Temperature Avg. °C (°F)	Max. ΔT °C (°F)	Strain ε (%)	Cycles to Fail	Cum. Damage (%)
1	621(1150)	.05	99(210)	-18(0)	40.5(105)	117(210)	.13	5.2×10^5	.96
2	518(965)	.05	177(350)	76.7(170)	127(260)	100(180)	.11	9×10^5	.56
3	432(810)	.05	241(465)	157(315)	199(390)	83(150)	.0925	15×10^5	.33
4	360(680)	.05	295(563)	227(440)	260(500)	69(125)	.077	–	
									1.85%
1	621(1150)	.10	1-9(390)	21(70)	110(230)	178(320)	.198	1.2×10^5	4.15
2	449(840)	.10	302(575)	171(340)	238(460)	131(235)	.145	3.7×10^5	1.35
3	321(610)	.10	377(710)	282(540)	329(625)	94(170)	.105	11×10^5	0.45
									5.95%
1	621(1150)	.15	246(475)	57.2(135)	152(305)	200(360)	.222	$.8 \times 10^5$	6.25
2	407(765)	.15	366(690)	323(450)	299(570)	133(240)	.148	3.4×10^5	1.47
3	260(500)	.15	438(820)	346(655)	393(740)	86.1(155)	.096	4×10^5	0.36
									8.08%
1	621(1150)	.180	285(545)	107(225)	196(385)	200(360)	.222	$.8 \times 10^5$	6.25
2	363(685)	.180	404(760)	296(565)	349(660)	108(195)	.1205	7×10^5	0.72
3	210(410)	.180	474(885)	410(770)	442(828)	63.9(115)	.071	–	
									6.97%
1	621(1150)	.180	285(545)	107(225)	196(385)	200(360)	.222	$.8 \times 10^5$	6.25
2	363(685)	.10	352(665)	246(475)	299(570)	106(190)	.1175	7.5×10^5	0.67
3	260(500)	.10	413(775)	335(635)	374(705)	77.7(140)	.0865	20×10^5	0.25
									7.17%
1	621(1150)	.180	285(545)	107(225)	196(385)	200(360)	.22	$.8 \times 10^5$	6.25
2	363(685)	.150	391(735)	268(515)	327(620)	119(215)	.133	4.8×10^5	1.04
3	232(450)	.150	452(845)	374(705)	413(775)	77.7(140)	.0865	20×10^5	0.25
									7.5
1	621(1150)	.3			610	360	.222	$.8 \times 10^5$	6.25
2	238(460)	.15				195	.12	6×10^5	0.35
									7.0

I,A, Haynes 188 Throat (cont.)

4.   Pulses of .150 sec result in the most cumulative damage to
the throat. Pulses of less than .100 sec result in significantly less cumulative
damage.

5.   The higher than predicted throat temperatures reduce the
predicted life from 1×10^5 to $.8 \times 10^5$ thermal cycles. (Design requirement is
$.25 \times 10^5$ thermal cycles.)

6.   As long as the first pulse is at least .15 sec in duration,
the duration of subsequent pulses is not very significant. The first pulse ($\leq$ .15
sec) will result in 6.25% cumulative damage. The maximum additional damage that can
result from subsequent pulses is only about 1.75%. (This values may increase due
to the fact that subsequent pulses occur at a higher temperature which reduces
fatigue life.)

B.   FFC TIP (ZrCu)

The most limiting location in the chamber is the ZuCr liner at the
location of the ffc injection (hereafter called the ffc tip). The thermal cycle
life of the ffc tip is similar to the throat since the maximum strain (maximum ΔT)
occurs during the startup transient. Cumulative damage calculations were not made
for the ffc tip since the results would be similar to those obtained for the throat
(most damage occurs on first pulse and small increase in cumulative damage with
succeeding pulses because initial wall temperature increases with each pulse). In-
stead, the analysis was directed at finding the minimum firing duration at which
the maximum or near maximum ΔT through the wall is produced. This was done so that
the duty cycle that was selected to produce maximum cumulative damage to the throat
would also produce the maximum cumulative damage in the ffc tip.

I,B, FFC Tip (ZrCu) (cont.)

.

Since the chamber exterior temperatures measured on this program
agree with the Contract NAS3-14354 data, the ffc temperature transient (which was
the basis for design prediction) shown in Figure 47 of the main text was assumed
to apply. A simple flat plate thermal model correlated to the results shown in
Figure 47 was used to predict the exterior and gas-side temperature transient for
the initial conditions of Test -009. The results are shown in Figure 3-D. The
gradient through the wall is shown in Figure 4-D as a function of the firing
duration.

The following conclusions were made relative to the cycle life of
the ffc tip:

1.   The chamber exterior thermocouple data agree with the NAS 3-
14354 data and, therefore, the design analysis is applicable.

$$\text{Final gas-side temperature} = 271°C \ (520°F)$$
$$\text{Max } \Delta T = 100°C \ (180°F)$$
$$\varepsilon = .325\%$$
$$\eta = 56,000 \ (\text{thermal cycles})$$

2.   Although the maximum ΔT does occur at about 0.18 sec into
the transient as shown in Figure VIII-7 of Reference 1, there is very little differ-
ence in the maximum ΔT for times in the transient of .1 to .3 seconds.

t (sec)	ΔT °C (°F)
.1	132(269)
.2	137(278)
.3	135(275)
.4	127(360)

FFC TIP TEMPERATURES AS A FUNCTION OF FIRING DURATION

INITIAL CONDITION
BASED ON TEST -009
FINAL TEMP. = 520°F

Figure 3-D

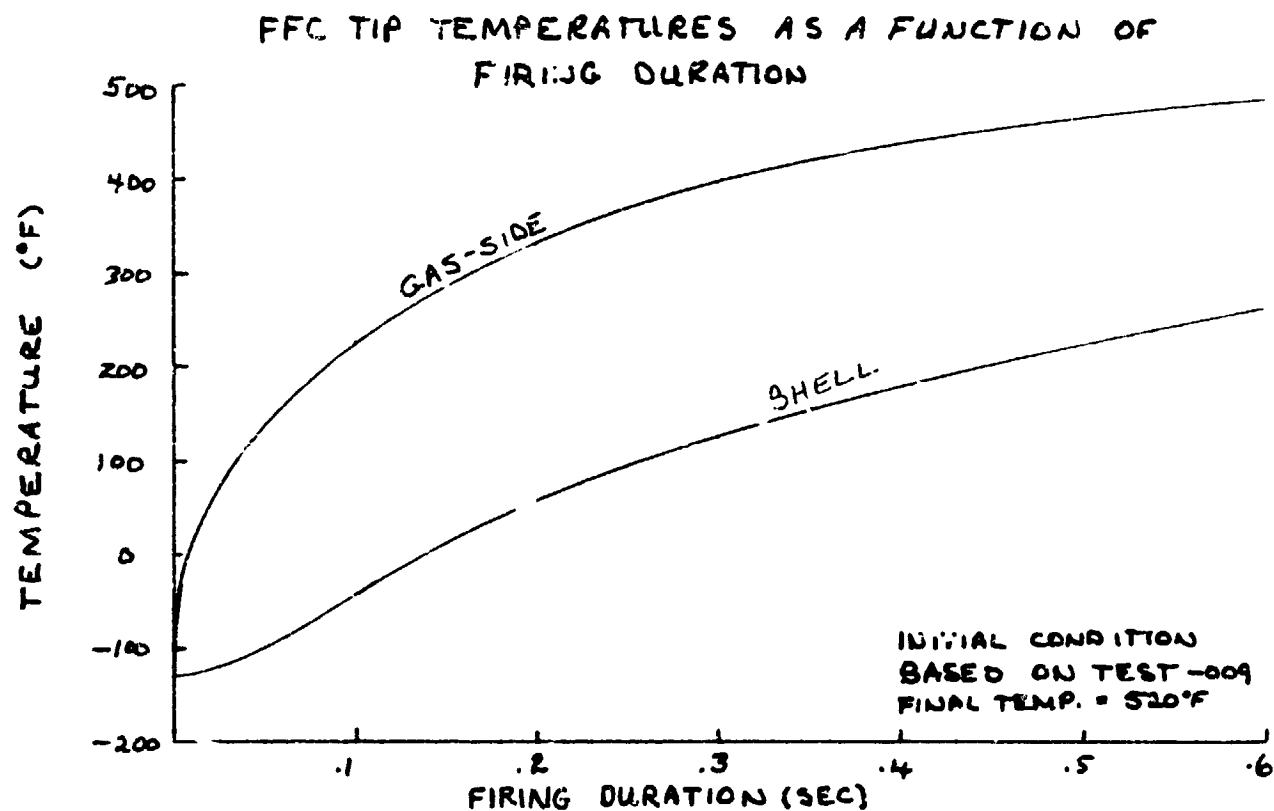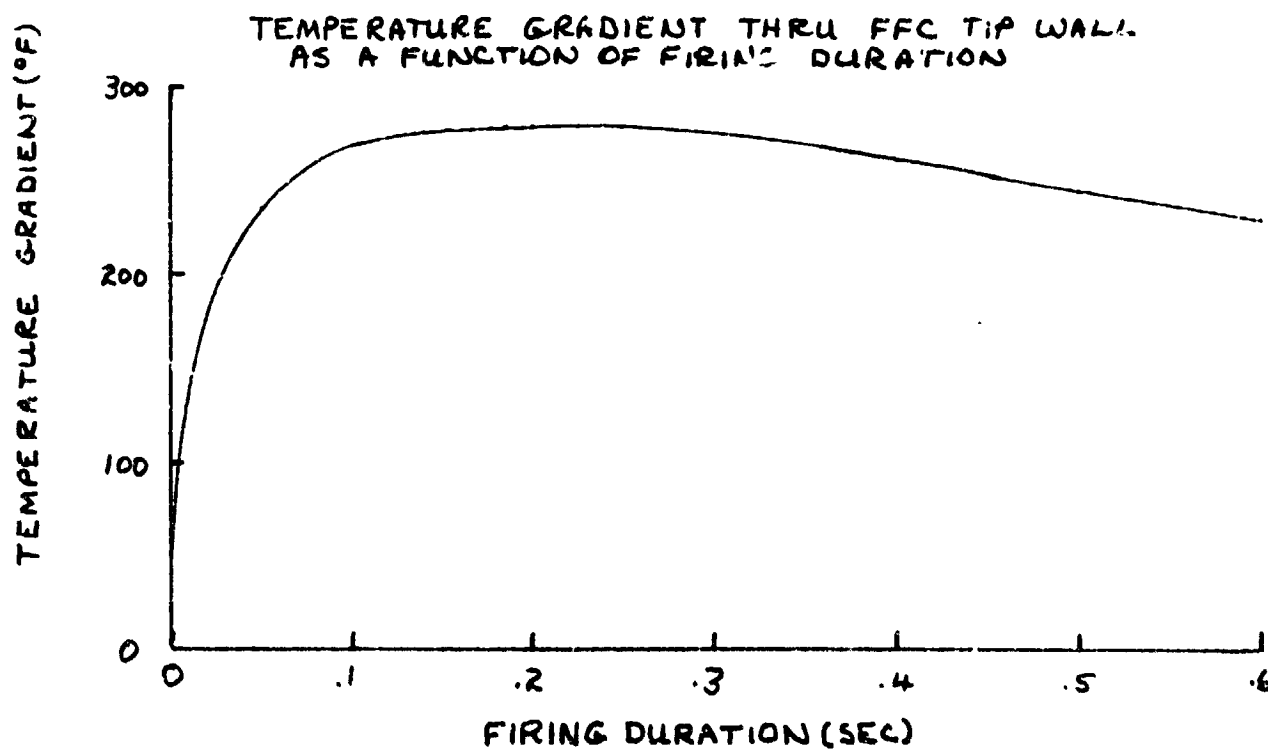# TEMPERATURE GRADIENT THRU FFC TIP WALL AS A FUNCTION OF FIRING DURATION

Figure 4-D

L,B, FFC Tip (ZrCu) (cont.)

       3.   Any pulse in excess of .1 sec duration will produce the maximum ΔT. This conclusion should be checked at other initial temperatures since the initial temperature 36.7 vs. -90°C (80 vs. -130°F), affects the maximum ΔT, 100 vs 154°C (180 vs. 278°F).

       4.   Two or three pulses of .1 sec will probably do the maximum damage to the ffc tip as is the case for the throat.

       5.   A duty cycle starting with .15 sec pulses in addition to doing maximum damage to the throat will probably produce a near maximum cumulative damage to the ffc tip.

       C.   ZrCu CHAMBER

       The regen-cooled section of the chamber, unlike the throat and ffc tip, reaches its maximum ΔT (maximum strain) in steady state.

       The key to the duty cycle requirements of the chamber are (1) time to reach steady state, (2) time to equilibrate after shutdown, and (3) average temperature on shutdown.

       The time required for the chamber to reach steady state is needed for comparison to the throat duty cycle requirements to determine if the duty cycle that maximizes damage to the throat is compatible with the one that maximizes damage to the chamber.

       Time required for the gas-side and chamber exterior temperatures to equilibrate after shutdown is important for determining whether coast times are a factor in the cumulative damage to the chamber.

I,C, ZrCu Chamber (cont.)

The average temperature or equilibration temperature after shutdown is important in determining initial temperature conditions for successive pulses.

The thermocouple data from Test -014 were selected for qualitative evaluation of pulsing on cumulative thermal cycle life damage to the regen section of the chamber. On Test -014 the propellant valves were closed with a very short fuel lag. On almost every other test there is an appreciable lag in the fuel TCV closing with the ensuing hardware cooldown.

In Figure 5-D, the data from one gas-side thermocouple and the corresponding exterior thermocouple have been plotted versus time to provide an overview of the test. The areas of concern are the startup and shutdown. Both the gas-side and exterior temperatures go through a maximum in the first second of test because the pre-test chilldown only to the accumulators means the lines downstream of the accumulator and the thruster are warm and therefore the temperature of the propellants will initially be near ambient due to transfer of sensible heat from the feed system and engine.

The temperature rise to the initial peak, which is represented very crudely in Figure 5-D due to scale difficulties, is shown in detail in Figure 6-D. It takes approximately .4 sec for the chamber to reach steady state (in agreement with Contract NAS3-14354 results). The rise rate of thermocouple TG-2B in the first 0.2 sec appears to be faster than would be predicted on the basis of Contract NAS3-14354 data (see Figure VIII-7, mid-region, Ref. 3). This is consistent with the previously stated observation (Section 4.5.3) that this thermocouple is reading high because it protrudes from the wall into the gas boundary layer.

There are two important facts demonstrated in the shutdown temperature transients shown in Figure 7-D. The gas-side and exterior thermocuples are
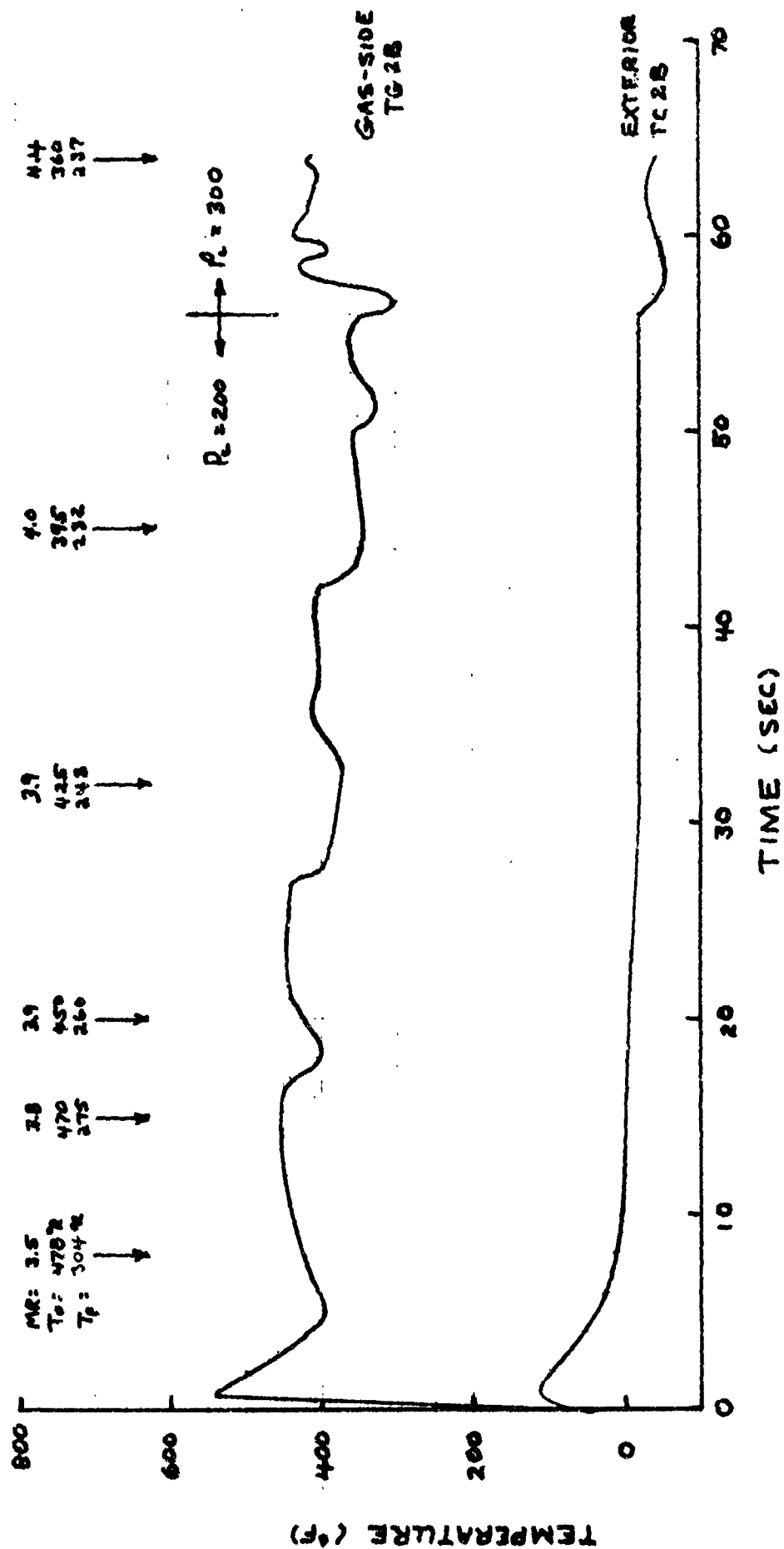
CHAMBER TEMPERATURES
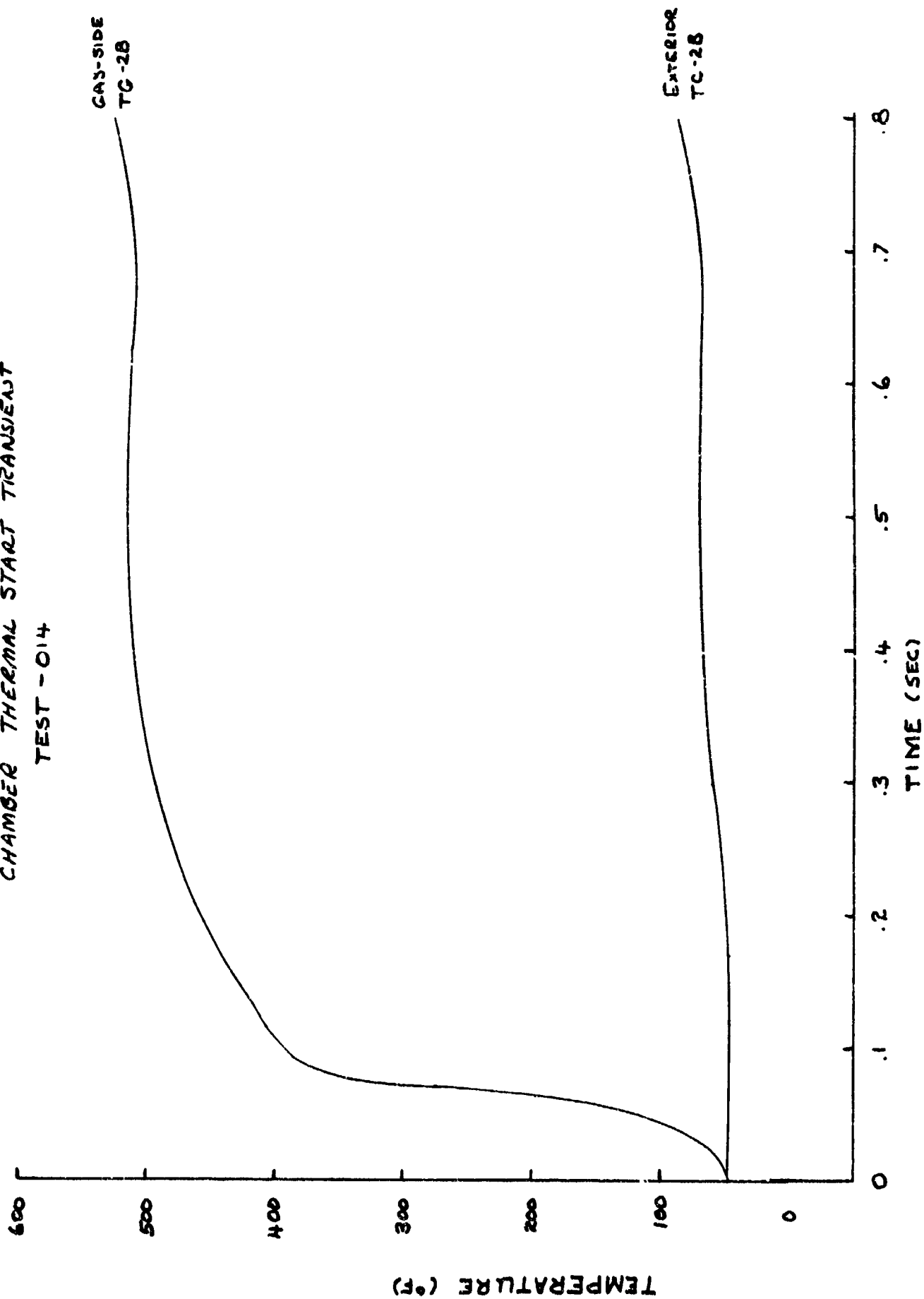TEST -014

Figure 5-D

CHAMBER THERMAL START TRANSIENT
TEST-014

Figure 6-D

GAS-SIDE
TG-28

EXTERIOR
TC-28

TIME (SEC)

TEMPERATURE (°F)
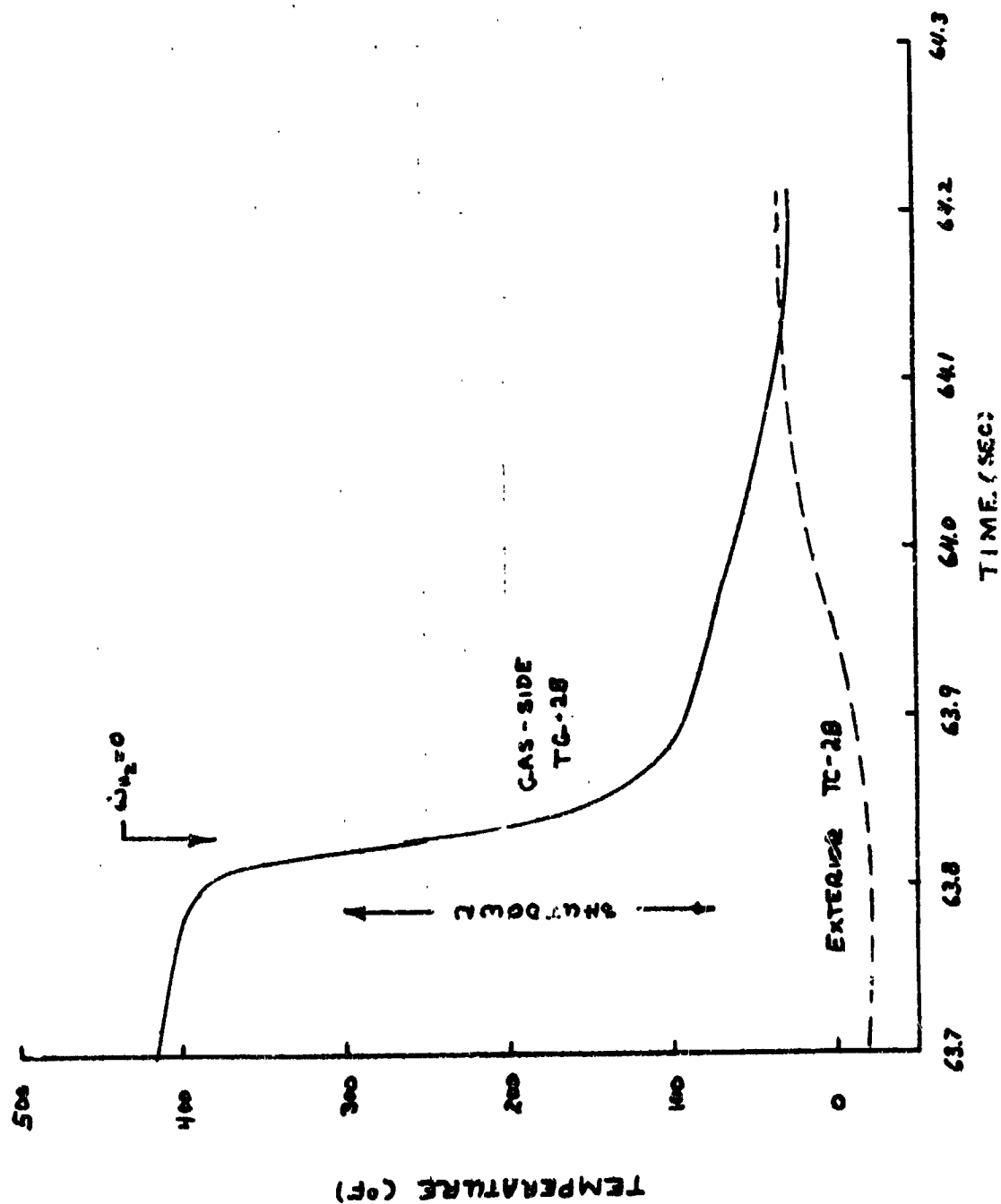
CHAMBER THERMAL TRANSIENT AT SHUTDOWN
TEST -014

Figure 7-D

I.C. ZrCu Chamber (cont.)

fully equilibrated in less than .3 sec after shutdown. This means that long coast periods are not required. Secondly, the chamber equilibrates to the initial temperature. Thus, pulsing will not "pump up" the average temperature as occurs in the throat and ffc tip. Each pulse will result in a ΔT that is dependent only on the firing duration and not on any residual temperature effects from the pulse that preceeded it

The following conclusions were drawn relative to the chamber:

1. The maximum ΔT and therefore the maximum strain and damage occur during steady state.

2. The firing duration must be .4 sec or longer to reach steady state.

3. All pulses will result in cumulative damage (unlike transient ΔT cases); the longer the pulse (up to .4 sec) the more the damage.

4. In a ten pulse sequence followed by a cooldown, a full thermal cycle can be achieved by a .4 sec firing whether it is the first or last pulse of the sequence.

D. INJECTOR FACE

Since injector face temperatures from this program agree with the NAS3-14354 data as discussed in Section 4.5.3, the design analysis is considered valid. The maximum ΔT and strain occur during steady state. Approximately 0.3 sec is required to reach the maximum ΔT. Thus, the pulse that results in a full thermal cycle on the chamber will result in one on the injector.

I, Life Cycle Analysis (cont.)

    E.   RECOMMENDED DUTY CYCLE

        The following conclusions were drawn from the life cycle analysis:

        1.   The more the margin in the design, the more difficult it is to conduct tests that result in appreciable damage within the constraints of time, propellant costs, etc.

        2.   The ALRC test method (cooldown every 10th pulse) will not result in significant thermal cycle cumulative damage to the ffc tip or Haynes throat.

        3.   The ALRC test method can best be used to explore the design life limits of the chamber and injector face.

        4.   The NASA test method (4th ITA) is probably better suited to testing the ffc tip and throat because it results in a cooldown between each pulse (full thermal cycle).

        5.   A firing duration of at least 0.15 sec is required to produce a full thermal cycle in the throat and ffc tip; a firing duration of at least 0.3 sec is required to produce a full thermal cycle in the injector face; a firing duration of 0.4 sec is required to produce a full thermal cycle in the chamber. A firing longer than the minimum will produce the full thermal cycle.

        6.   Longer firing durations (approaching 0.4 sec) with more frequent cooldowns (vs. one every 10th pulse) will produce a full thermal cycle in every component. The frequency of the cooldown can be varied to give one full thermal cycle for every 10 pulses (ALRC method) to one full thermal cycle for every pulse (cooldown after each pulse).

I,E, Recommended Duty Cycle (cont.)

7.   The first pulse following cooldown must be .15 sec or longer duration to produce a full thermal cycle in the throat and ffc tip.

The following is the recommended duty cycle:

Pulse No.	1	2	3	4	5	6	7	8	9	10	11
On (sec)	.15	.15	.15	.15	.4	.05/.1	.05/.1	.05/.1	.05/.1	.05/.1	.3*
Off (sec)	.3	.3	.3	.3	.6	.1	.1	.1	.1	2	24.3

* Fuel valve only opened to cool down hardware.

The duty cycle is the same length as that originally proposed, but requires approximately 30% more propellant. The rationale' for its selection is as follows:

1.   The four .15 sec pulses produce maximum cumulative thermal cycle damage to the throat and ffc tip. The .4 sec pulse provides a full thermal cycle for the chamber and injector face. The final pulses will be at the MIB (.05 to .1 sec) and will pressure cycle components while they are hot.

2.   The duty cycle meets the program requirements of 50,000 pulses and 5000 thermal cycles.

3.   The duty cycle provides a demonstration of 10 year life and therefore is a worthwhile goal. This demonstration should be made before testing to destruction to evaluate design limits.

4.   The chamber can be tested to failure after the demonstration test.

5.   The important aspect of the analysis described above will be refinement of the analysis coupled with the thermal data so that the cumulative damage to each component is known. Thus, if and when a component is tested to failure, its life history and strain conditions are known.

REFERENCES

1.   Hydrogen-Oxygen Auxiliary Propulsion for the Space Shuttle, Volume I:
      High Pressure Thrusters; Contract NAS 3-14354, 30 January 1973, NASA-
      CR-120895.